①

REPORT DOCUMENTATION PAGE

Public reporting burden for this collection of information is estimated to average 1 hour per response, including the time for reviewing instructions, searching existing data sources, gathering and maintaining the data needed, and reviewing the collection of information. Send comments regarding this burden estimate or any other aspect of this collection of information, including suggestions for reducing this burden, to Washington Headquarters Services, Directorate for Information Operations and Reports, 1215 Jefferson Davis Highway, Suite 1204, Arlington, VA 22202-4302, and to the Office of Information and Regulatory Affairs, Office of Management and Budget, Washington DC 20503.

1. AGENCY USE ONLY (Leave Blank)	2. REPORT DATE 6 May 1991	3. REPORT TYPE AND DATES COVERED Final Ph.D. Dissertation 1 June 1988 - 6 May 1991

4. TITLE AND SUBTITLE

Structural and Acidic Properties of Niobia-Silica
and Niobia-Alumina Aerogels

5. FUNDING NUMBERS

6. AUTHOR(S)

Scott M. Maurer

7. PERFORMING ORGANIZATION NAME(S) AND ADDRESS(ES)

Carnegie Mellon University
Chemical Engineering Dept.
5000 Forbes Ave.
Pittsburgh, PA 15213

8. PERFORMING ORGANIZATION REPORT NUMBER

9. SPONSORING/MONITORING AGENCY NAME(S) AND ADDRESS(ES)

Department of the Army

10. SPONSORING/MONITORING AGENCY REPORT NUMBER

11. SUPPLEMENTARY NOTES

12a. DISTRIBUTION/AVAILABILITY STATEMENT

Releasable and available to the general public

12b. DISTRIBUTION CODE

13. ABSTRACT (Maximum 200 words)

This study used a variety of techniques to establish the structural-chemical property relationships over niobia, niobia-silica, and niobia-alumina binary oxide aerogels. The objective is to develop a comparative set of samples of known structure for chemical characterization. Bulk oxide aerogels of niobia, alumina, and silica were prepared as base oxides by the sol-gel method followed by supercritical extraction to dry the solvent-ladened gel. The niobia aerogel was calcined at 500 °C and yielded the highest surface area, 190 m^2/g, ever reported for bulk niobia. Niobia/silica and niobia/alumina mixed oxide aerogels (containing 25 weight % niobia) were synthesized to form a set of binary oxides with which to investigate structural-chemical relationships. Along with these mixed oxide aerogels, a set of silica and alumina aerogel supported niobia samples were synthesized in order to complement the study on binary oxides. These results establish the relationship between the chemical properties and the developed structures caused by thermal treatment or increased concentration of niobia on the silica and alumina aerogel supports. This work also shows that there is a similarity between the mixed and surface oxide systems in that the structures of niobia fundamentally determine the strength and type of surface acidity.

14. SUBJECT TERMS

Niobia, Aerogel, Niobia-Silica, Niobia-Alumina,
Acidity, High-Surface Area, Oxide, Catalyst

15. NUMBER OF PAGES

478

16. PRICE CODE

17. SECURITY CLASSIFICATION OF REPORT	18. SECURITY CLASSIFICATION OF THIS PAGE	19. SECURITY CLASSIFICATION OF ABSTRACT	20. LIMITATION OF ABSTRACT
UNCLASSIFIED, UNLIMITED	UNCLASSIFIED, UNLIMITED	UNCLASSIFIED, UNLIMITED	UNCLASSIFIED, UNLIMITED

10 May 1991

7752 Carrleigh Pkwy
Springfield, VA 22152

Defense Technical Information Center
ATTN: Reference Services Branch (DTIC-FD)
Building 5, Cameron Station
Alexandria, VA 22304-6145

Dear Sirs,

Enclosed please find the following documents: one 478 page Ph.D. Thesis, one DTIC Form 50, and one Standard Form 298. I realize that I was supposed to enclose two copies of my thesis, but due to extenuating circumstances of not being able to reproduce any more original photogrpahs and the fact that I am leaving in one week make it impossible for me to send any more original copies. I will not have access to reproduce any more copies once I leave because all materials must stay at the school. It is possible at your end to make a duplicate of the thesis if it is mandatory to have two copies. I hope I have not inconvenienced you and that you will be able to get by with only one copy of the thesis.

Sincerely,

Scott M. Maurer
CPT, CM

Carnegie
Mellon

Carnegie Mellon University

CARNEGIE INSTITUTE OF TECHNOLOGY

THESIS

SUBMITTED IN PARTIAL FULFILLMENT OF THE REQUIREMENTS FOR THE DEGREE OF

DOCTOR OF PHILOSOPHY

TITLE: Structural and Acidic Properties of Niobia-Silica and Niobia-Alumina Aerogels

PRESENTED BY: Scott M. Maurer

ACCEPTED BY THE DEPARTMENT OF CHEMICAL ENGINEERING

Edmond I. Ko _____   _May 6, 1991_ _____
Edmond I. Ko, Advisor   Date

John L. Anderson _____   _May 6, 1991_ _____
John L. Anderson, Department Head   Date

APPROVED BY THE COLLEGE COUNCIL

_____   _____
Paul Wynblatt, Associate Dean   Date

STRUCTURAL AND ACIDIC PROPERTIES OF NIOBIA-SILICA AND NIOBIA-ALUMINA AEROGELS

Submitted in Partial Fulfillment of the
Requirements for the Degree of

Doctor of Philosophy

in

Chemical Engineering

by

SCOTT M. MAURER

Department of Chemical Engineering
Carnegie Mellon University
Pittsburgh, Pennsylvania

May 1991

ACKNOWLEDGEMENTS

ABSTRACT

This study used a variety of techniques to establish the structural-chemical property relationships over niobia, niobia-silica, and niobia-alumina binary oxide aerogels. The objective is to develop a comparative set of samples of known structure for chemical characterization.

Bulk oxide aerogels of niobia, alumina, and silica were prepared as base oxides by the sol-gel method followed by supercritical extraction to dry the solvent-ladened gel. The synthesis of the bulk niobia aerogel was followed by a 500 °C calcination and yielded the highest surface area, 190 m^2/g, ever reported for bulk niobia. Other physical properties of the aerogel of niobia such as total pore volume and average pore diameter were significantly higher than found previously for conventionally prepared niobia. Laser Raman Spectroscopy (LRS) and pyridine adsorption experiments were used to investigate the structural and chemical properties of the niobia aerogel as a function of heat treatment. From these structural/chemical studies it was established that the origins of high acid strength (~ 30 kcal/mol) and acidity for the niobia aerogel were due to highly distorted NbO$_6$ groups that contained Nb=O bonds, while the more conventionally prepared niobia had acid strength (~ 22 kcal/mol) and acidity attributed primarily to slightly distorted NbO$_6$ species which possessed Nb-O bonds. Heat treating the niobia aerogels to temperatures greater than 500 °C induced crystallization. At the same time, the surface concentration of terminal Nb=O bonds decreased and lowered the acid strength of these oxides.

Niobia/silica (A-NS25w) and niobia/alumina (A-NA25w) mixed oxide aerogels (containing 25 weight % niobia) were synthesized to form a set of binary oxides with which to investigate structural-chemical relationships, and were also compared to conventionally prepared co-precipitated samples. Along with these mixed oxide aerogels, a set of silica and alumina aerogel supported niobia samples were synthesized in order to complement the study on binary oxides and further our understanding of the chemical-structural relationships. High acid strengths (~ 40 kcal/mol) and acidity were found on the niobia-silica binary oxides, which was attributable to highly distorted niobia tetrahedral species containing Nb=O bonds. The tetrahedral niobia species in the niobia/silica mixed oxide aerogel had primarily strong Lewis acid sites as well as some weak Brønsted acidity. The silica aerogel supported niobia samples also had strong Lewis acidity as well as strong

Brønsted acidity which was due to hydroxyl groups, -OH, adjacent to the doubly bonded oxygen. Niobia was found to be stabilized against reduction when it crystallized out of A-NS25w or the silica aerogel supported niobia because of the formation of a distorted octahedral niobia-rigid silica interface. Isomerization of 1-butene confirmed the existence of Brønsted acidity for both niobia-silica binary oxide systems after a standard calcination; however, heat treating these materials induced a change in the bonding environment of niobia to one which is primarily octahedral (distorted) and produced active catalysts for 1-butene isomerization as shown by a 3-fold increase in activity.

Similar behavior for the niobia-silica system was also found for the niobia-alumina binary oxides. The niobia/alumina mixed oxide aerogel exhibited moderate acid strength (~24 kcal/mol) and acidity that was simliar to the low surface coverage of niobia on the supported oxide, and was attributed to highly distorted groups containing terminal Nb=O bonds. The mixed oxide of niobia/alumina showed strong Lewis acidity with little to no Brønsted acid sites, similar to bulk alumina and the supported oxide at low niobia coverages. The sample containing a quarter monolayer of surface niobia showed increased acid strength of the supported oxide while also developing weak Brønsted acidity and new Lewis acid sites. These new Brønsted acid sites were found to weakly catalyze 1-butene isomerization. Heat treating these niobia-alumina binary oxides resulted in the formation of $NbAlO_4$ and a loss in acid strength and acidity.

These results establish the relationship between the chemical properties and the developed structures caused by the thermal treatment or increased concentration of niobia on the silica and alumina aerogel supports. This work also shows that there is a similarity between the mixed and surface oxide systems in that the structures of niobia fundamentally determine the strength and type of surface acidity.

NOMENCLATURE

Acronym	Meaning
B.E.T.	Brunauer-Emmet-Teller, used in reference to surface area
DRIFT	Diffuse Reflectance Infrared Spectroscopy, used in examining molecualr vibrational states
DTA	Differential Thermal Analysis, used to examine endo- and exothermic changes in samples
EDS	Energy Dispersive Spectroscopy, used for elemental mapping and quantitative composition analysis
EXAFS	Extended X-Ray Absorption Fine Structure, used to detect surface species and valence, with bonding distance information
FTIR	Fourier Transform Infrared Spectroscopy, used to examine molecular vibrational states
HRTEM	High Resolution Electron Microscopy, used in imaging samples with a resolution of approximately 1.6Å
LRS	Laser Raman Spectroscopy, used to examine the vibrational states of molecules
SEM	Scanning Electron Microscopy, used to observe morphological changes in samples on a microscopic scale
TG	Thermogravimetry, used to measure sample weight changes in controlled thermal environments
TOS	Time On Stream, used to denote reaction time for 1-Butene isomerization
XANES	X-Ray Absorbtion Near Edge Spectroscopy, used to determine coordination of atoms in molecular structures
XRD	X-Ray Diffraction, used to measure intensity of diffracted X-ray radiation from powder samples

TABLE OF CONTENTS

LIST OF TABLES

LIST OF FIGURES

Chapter 1

INTRODUCTION

1.1 Scope of Thesis

Bulk transition metal oxides are important materials that have many technological applications. In the chemical industry alone, these oxides are used as functional catalysts in a large number of processes to convert hydrocarbons to other useful chemical products. Many of the processes require a high selectivity for a particular product; in fact, selective oxidation, ammoxidation, and selective dehydrogenation constitute probably the most important catalytic uses of transition metal oxides.

When transition metal oxides are combined with another oxide as a binary or multicomponent oxide, materials are developed which often have physical and chemical properties which are different from and often superior to the separate component oxides. These binary oxides allow one to possibly tailor an even more selective catalyst than the bulk transition oxide by using *the correct concentrations of the appropriate metal oxide* components. Although certain reasons for this type of behavior have been given, a general lack in understanding of the oxide-oxide interactions developed in these systems makes the design of catalysts impractical. It is the goal of this research to examine the bulk oxide system of niobia, and the binary oxide systems of niobia-silica and niobia-alumina, in order to study *the effects of preparation on the structure* of these oxides and to advance the understanding of how structure is related to the physical and chemical properties of these oxide systems.

There are two basic types of binary oxides, mixed oxides and supported oxides as shown in Figure 1-1, which are of great importance to a number of industrial processes. In a mixed oxide the two oxide components are homogeneously mixed on an atomic level in the bulk. These binary mixed oxides are well known for their acidic properties and used primarily as acid catalysts or as bifunctional supports. For example while SiO_2 is non-acidic and Al_2O_3 or TiO_2 are acidic only in certain forms, their combinations into amorphous mixed oxides of SiO_2/Al_2O_3 and SiO_2/TiO_2 are very acidic and used in catalytic cracking, isomerization, and acid-catalyzed dehydration reactions.[1, 2, 3, 4] The second type of binary oxide is a surface phase oxide. We use this term to refer to materials formed when one metal oxide phase is dispersed on a second metal oxide substrate. Supported oxides are used as catalysts to control reaction selectivity in petroleum and chemical industries and are usually employed with the hope of improving the desirable catalysis of the pure oxide, whether through a stabilization or oxide interaction with the substrate. For example, TiO_2-supported MoO_3 is a very selective catalyst for the photo-oxidation of methanol to dimethoxymethanol, while bulk titania forms several other products.[5] Another classic example is the well-studied TiO_2-supported V_2O_5 system which is a very selective catalyst for the oxidation of o-xylene to phthalic anhydride, while bulk vanadia is less effective.[6, 7, 8] The formation of a surface monolayer of these supported species has been found to be responsible for the catalytic behavior.[6] Thus, these supported oxides can have properties very different from those of the pure oxide because of interactions with the support. Clearly, these examples show that the properties of the supported and mixed oxides are dependent on the chemistry of the interaction between their component oxides. The supported and mixed oxide systems have been generally treated separately despite their similarities. Not until recently, when Connell and Dumesic, and Bernholc et al. demonstrated that supported oxides have commercially important uses and can serve as model acids, did there begin an understanding of the origin of acidity from a structural point of view on these binary oxide systems.[9, 10, 11, 12] These studies showed that

Figure 1-1: SCHEMATIC OF BINARY OXIDE SYSTEMS: SUPPORTED AND MIXED OXIDES
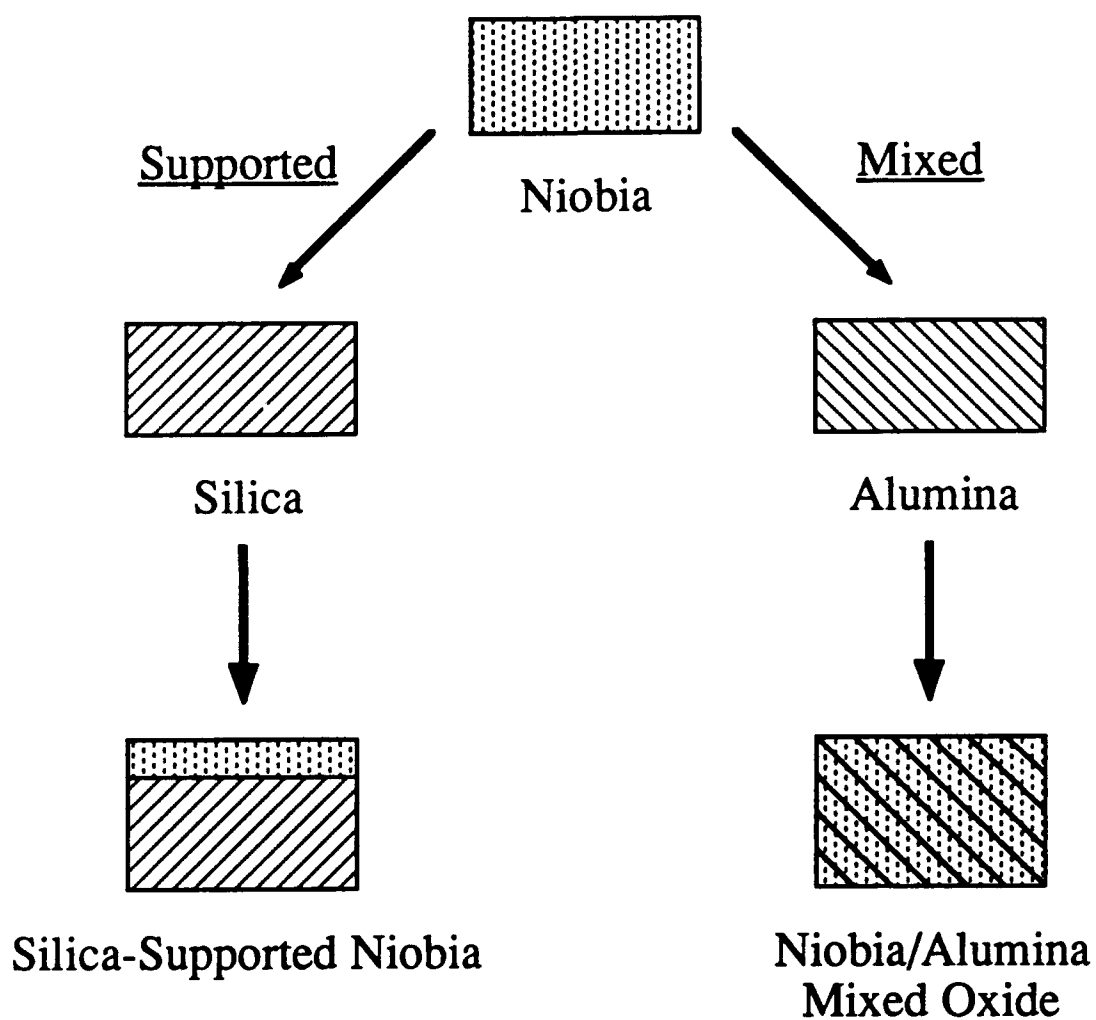
supported and mixed oxides are similar systems and that one can begin to develop binary oxide catalysts by understanding the structural aspects as well as the oxide-oxide interactions inherent in these binary systems.

A lack of understanding associated with binary oxides can be viewed as stemming from uncertainty inherent in the interfacial interaction between the two component oxides. Many oxide systems are complicated for study because these oxides form stable solid-state compounds upon heating to low temperatures. Niobia and silica are two oxides which are immiscible even to high temperatures in excess of their melting points.[13] Thus, the niobia-silica system is ideal for the study of interfacial interactions as any properties which develop other than the properties of the pure components can be attributed to this oxide-oxide interaction. Silica is amorphous to high temperatures, while niobia undergoes a series of phase transformations with the same heating schedule; therefore, the stabilizing effect of silica should easily be discernible by monitoring the crystallization pattern of niobia with temperature as well as the reduction behavior of niobia (since silica is very stable and will not reduce except under severe conditions). Niobia and alumina, unlike niobia and silica, form niobium aluminate ($NbAlO_4$) upon high temperature treatments.[14] This niobia-alumina binary oxide is amorphous at low temperatures (< 800 °C) and only forms compounds at high temperatures (> 1000 °C), thus this system is ideal for the study of interfacial effects at low temperatures since the properties arising outside of those for the pure components can be attributed to interfacial interactions. This system is also useful in comparing the interfacial effects between niobia and silica versus niobia and alumina.

To examine the structural effects in these materials several niobia-silica and niobia-alumina binary oxide systems will be examined. These binary oxides consist of various partial coverages of niobia on silica or alumina to determine the effect of dispersion on these supported oxides, as well as mixed oxides of niobia/silica and niobia/alumina in which niobia was the minor oxide. These samples were subjected to various heat treatments to determine the stability of niobia in these systems as well as to create similar

interfaces between the supported and mixed oxide systems so that a direct comparison of interfacial interactions could be made. By determining similarities and differences in the acidic properties, reduction behavior, and catalytic activities of these binary oxides, we aim at developing an understanding of the structural aspects important to their physical and chemical properties.

This dissertation consists of 7 chapters, with the first discussing the general scope and pertinent background literature. Chapter 2 gives an overview of the equipment and procedures used to synthesize, characterize, and analyze the oxide samples in this study. Chapter 3 deals with the characterization of the bulk oxides, in particular the physical and chemical properties of niobia. This chapter lays the foundation on how structure relates to the properties of niobia. Chapter 4 discusses the properties of the mixed oxides of niobia/silica and niobia/alumina and how they are similar or different from one another. Comparisons are made on mixed oxides prepared by different methods as well as investigating how heat treatment affects the structure and ensuing properties of these mixed oxide systems. Chapter 5 investigates the properties of supported oxides for niobia supported on silica and alumina. Interfacial interactions were investigated in both these binary oxides by varying surface coverages, as well as heat-treating both systems. Structure-acidity relationships were developed from the results in these chapters based upon the structures and properties of the bulk and binary oxides, and are presented in Chapter 6. These are presented according to current theories of acidity and help to draw a line between the understanding of surface and mixed oxides by determining the relationship between chemical properties and structure. Finally, Chapter 7 summarizes the thesis and gives some guidance for future work to be done in the field.

1.2 Background

Some background information is important for the understanding of the scope of this thesis. First of all, the structural and thermal characteristics of the pure oxides: silica, alumina, and niobia, must be discussed for later comparison with the binary oxides. Next, the current understanding of the structures of mixed and surface oxides with respect to preparation and thermal treatment will be mentioned. In light of this discussion, it is important to go into detail on the sol-gel synthesis used to prepare the oxides in this study, as well as the supercritical extraction step used to prepare the final oxide aerogels. Next, we will briefly discuss the current theories of acidity in binary oxides and the relevant information on the acidity of surface and mixed oxides. Together with this background information will be the most current work related to the niobia-silica and niobia-alumina surface and mixed systems.

1.3 Individual Oxide Materials

Since one of the main goals of this research is to understand the oxide-oxide interactions inherent between niobia-silica and niobia-alumina, and how these interactions in turn relate to the properties of these materials, it is important to first understand the bulk oxides that make up these binary oxide systems. The following is a brief overview of the properties of silica, alumina, and niobia. The crystalline phases of niobia are discussed in some detail, because the crystallization of this oxide from both the mixed and surface oxides is one of the parameters used to understand the stability behavior of these binary oxides.

1.3.1 The Structure and Properties of Silica

The preparations, mechanisms, and properties of silica have been well studied by Iler.[15, 16] Some of the general findings are listed below. Gelation of a silica sol is most rapid at a neutral pH.[16] The average pore diameter of the primary particles in silica gel are typically around 3 - 6 nm although some particles range upwards to 30 nm.[17] The silica gels have a highly porous structure as synthesized and when supercritically extracted, maintain this open structure since no vapor-liquid interface forms to collapse the structure by the forces of surface tension, and lead to high surface area materials.[4] High surface area, amorphous silica is difficult to crystallize at temperatures less than 1000 °C unless heated on the order of weeks.[15, 18] The crystallization of amorphous silica is also inhibited by the presence of certain oxides such as alumina.[19] Therefore, when niobia is a secondary oxide with silica as in the mixed oxide, it is unlikely that enhancement of silica crystallization will be seen; on the contrary, it would be more likely that niobia will have no effect or at the very least suppress its crystallization. Therefore, the silica synthesized in this study is likely to remain amorphous in the temperature range of interest.

1.3.2 The Structure and Properties of Alumina

The structural chemistry of alumina is complicated by the existence of different phases, as well as by the effects of various methods of preparation.[17] When a precipitate is formed from an aqueous aluminum solution, the nature of the precipitate, i.e. whether it is an amorphous hydrogel or whether it is crystalline, is determined by the precipitation conditions such as temperature, speed, and pH. If the initial precipitate is a hydrogel (prepared with water as the major constituent), an amorphous structure is never retained (except transiently) on dehydration. Conversion of the precipitate to a crystalline form will also occur when left in an aqueous environment. Such aging has been described by a change in morphology in which an amorphous alumina hydrogel, characterized by

spherical particles of diameter 2 - 5 nm, is gradually converted via gelatinous boehmite to bayerite, characterized by fibrils of length around 10 nm.[17]

The above study concentrated on the hydro- or aquagels formed by precipitation in an aqueous medium. This study used alcohol as its solvent and thus different structures and properties would be expected when compared to the aqueous environment. There are currently two main ways of preparing alumina as an aerogel via the sol-gel process, the most common way is by using the method developed by Yoldas.[20, 21, 22, 23] This method consisted of 4 basic steps. First of all, the hydrolysis of an alkoxide must occur in a large excess of water (mol H_2O/mol Al^{3+} ~ 100) at a temperature above 80 °C. Next peptization of the crystalline monohydroxide into a clear sol is accomplished by the addition of a critical amount of a certain acid (usually HNO_3 or HCl). Gel formation occurs by concentration of the alumina solution by evaporation at elevated temperatures. One specific step for this process to work is the hot water hydrolysis of the alumina alkoxide at temperatures above 80 °C. Cold water hydrolysis leads to the formation of the crystalline β-aluminum trihydrate (bayerite) which can not undergo further peptization with the addition of acid. Teichner et al. used a procedure similar to that of Yoldas.[24] The main difference between the two methods is the fact that a stoichiometric amount of water to hydrolyze the aluminum alkoxide (mol H_2O/mol Al^{3+} = 3.0) is used instead of the large excess of water. In Teichner's study of alumina aerogels, it was determined that water in excess of the stoichiometric amount was detrimental to the textural characteristics of alumina aerogels in terms of high surface area, high pore volume, and the resulting amorphous state of alumina.[24] Increased crystallinity was observed in the alumina as the water concentration was increased above the stoichiometric amount. Thus, since the Yoldas process is primarily used to process transparent porous membranes and also used as a method in preparing porous ceramic alumina instead of catalyst supports, the method advanced by Teichner was used in this study. Similar conditions were used in this work and should yield the same high surface area, amorphous alumina as shown earlier. This is

exactly what we found with our alumina having surface areas around 600 - 700 m^2/g, and which are amorphous up to calcination temperatures of 800 °C. Although both methods as discussed above are expected to produce the β-aluminum trihydrate (bayerite) it is in a very distorted form as shown by our amorphous X-ray diffraction (XRD) patterns.

A number of dehydration products have been characterized that depend on starting materials, reaction conditions, and heating schedule, and ultimate impurity contents. These all play some role in determining what phase of alumina is present at any given time. This situation is further complicated because a number of the alumina dehydration products are not thermodynamically distinct and stable phases, and because many of the structures are closely related, XRD scans are difficult to analyze unless the product is very distinct in its diffraction pattern. However, under all conditions, α-alumina (corundum) is the final stable high temperature dehydration product. All of the other aluminas result form lower temperature dehydrations and approximate to a greater or lesser extent a model in which the oxygens are arranged in a spinel, but which not all the cation positions are occupied, and in which there are varying degrees of cation disorder.[25, 26] These other forms of dehydrated alumina, other than the stable end product, have been termed transition aluminas and are labeled as γ, η, δ, χ, κ, and Θ. These dehydration sequences, as summarized by Lippens and Steggerda[27], are shown in Figure 1-2.

Both γ- and η- Al_2O_3 possess defect spinel lattices which are tetragonally distorted from cubic symmetry, this distortion being more pronounced in the γ-phase.[25] Both of these products have cation disorder, particularly on the tetrahedral sites, and in addition η-Al_2O_3 has a stacking disorder.[17] χ-Al_2O_3 as well as γ- and η-Al_2O_3 are known as a low temperature alumina dehydration product and is rhombohedrally distorted with a substantial stacking disorder. The κ- and Θ-Al_2O_3 products are the higher temperature dehydration products which readily convert to the stable α-phase with time. Θ-Al_2O_3 is monoclinically distorted with the cations occupying mainly tetrahedral positions, and κ-Al_2O_3 is rhombohedrally distorted, again with stacking disorders. These alumina products are often

Figure 1-2: TRANSITION ALUMINA PHASE TRANSFORMATION FROM HYDRATES VS HEATING SCHEDULE

Gibbsite $\longrightarrow \chi \longrightarrow \kappa \longrightarrow \alpha$

Boehmite $\longrightarrow \gamma \longrightarrow \delta \longrightarrow \Theta \longrightarrow \alpha$

Bayerite $\longrightarrow \eta \longrightarrow \Theta \longrightarrow \alpha$

Temperature (°C)

0   200   400   600   800   1000
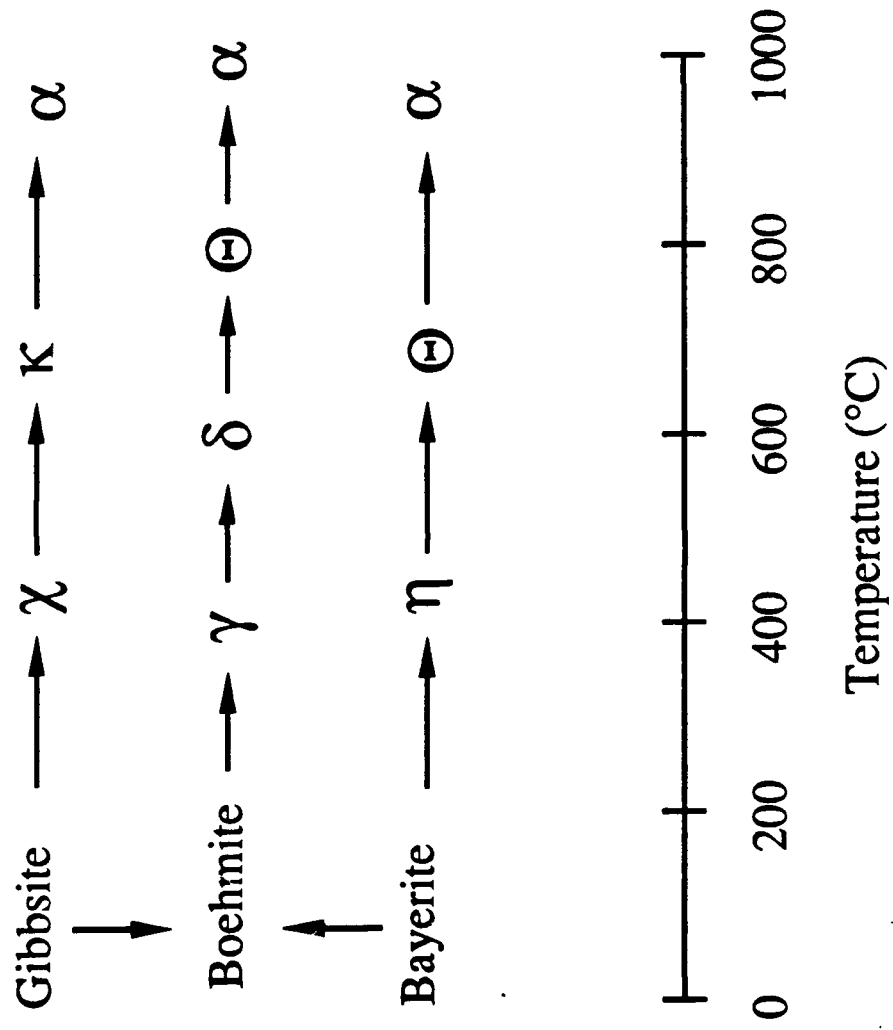
difficult to isolate because of their transitory metastable states that usually readily form α-Al_2O_3 after being formed themselves. These examples show the complicated nature of alumina and how the products of dehydration depend on starting materials, heating schedules, and environment.

Studies done on the surface area of alumina show that the maximum area is attained at a temperature of around 300 - 400 °C. Upon higher temperature treatments to 500 - 600 °C this surface area declines by approximately 30% due to the elimination of water by reactions of hydroxyl groups on the surface. The thermal stability of alumina, γ-Al_2O_3 in particular, may be enhanced by the addition of small amounts of another oxide such as silica. Thus, in this research, the surface area decline of alumina would not be expected to be enhanced by the addition of niobia; on the contrary, it should be attenuated, except at high enough temperatures at which point compounds form. Except when the high temperature form of alumina, α-Al_2O_3, is formed, all aluminas prepared by dehydration contain residual water in the range of a few tenths to ~ 5% with the amount of water decreasing with increasing temperature. Upon exposure to atmospheric moisture these aluminas may take on additional water by a surface reaction with any exposed unsaturated alumina cations. The conversion of hydroxyl groups to water on heating the alumina hydroxides or other alumina products, leaves behind a structure with exposed aluminum atoms that behave like Lewis acids because of the electron accepting nature of the coordinatively unsaturated aluminum cation. The intrinsic acidity of these surfaces may be enhanced by addition of impurity ions such as chlorine or fluorine, but since this study did not deal with any types of impurities we expect to see no enhancement of acidity. This section on the background of alumina shows the complicated nature of this material, and we will use the structural information of the various phases of alumina to determine the overall stabilizing effect that niobia has on this oxide and vice versa.

1.3.3 The Structures and Properties of Niobia

Niobium pentoxide (Nb_2O_5) is a very complex material that has many different phase transformations, with some of the observed structures being well documented. There has been a good deal of work done on the phase behavior of niobia and along with it, a great deal of confusion as to how to designate the differing phases. Bauer[28] originally named just three modifications by their temperature of formation: low (T), medium (M), and high (H). Along the way a number of other researchers began to use a new set of nomenclature using greek letters to designate different phases. However, it was not until Schafer et al.[29] did a comprehensive review of the phases and nomenclature of niobia, that the standard notation (similar to that used by Bauer) became firmly entrenched. The modification of niobia are named after either the range of temperature in which they are formed, or by the abbreviation of the shape the crystalline modification forms. This nomenclature will be used throughout this dissertation.[29, 30]

There are three modifications of niobia that are stable in the temperature range of interest (500 - 1000 °C): T, B, and H.[31] These stable modifications can be formed reversibly with each other. There are also a few other metastable modifications of Nb_2O_5: TT, M, N, P, and R. These modifications will form into a stable form given sufficient time at the temperature range of interest for their formation. Their formation can also be pathway dependent. The dependence of a pathway means that the formation of these modifications of niobia is dependent on a number of factors: starting materials of niobia, the method of preparation, and the temperatures and pressures used.[29] These metastable modifications of niobia have also been thought of as being stabilized by impurities, hence their formation can also be impurity dependent.[29, 32, 33]

For the purpose of this work, the phase behavior can be greatly simplified by the elimination of phases that would be unlikely to form under the conditions used in this study. N-, P-, and R- are rare and are not expected to form in the conditions of this study. These three forms are also stabilized by impurities (F^- ions) which are not found here,

hence the observation of these phases in this work is unlikely. The remaining phases: TT, T, M, B, and H can be divided into two groups, low temperature niobia and high temperature niobia. T-Nb_2O_5 is a stable, low temperature phase of niobia and TT-Nb_2O_5 is thought to be merely a less ordered precursor to the stable T-form.[29] H-Nb_2O_5 is the stable, high temperature phase of niobia and the form which all niobia will attain provided sufficient temperature and time is supplied. M-Nb_2O_5 is thought to be a less ordered metastable precursor to this high temperature form of niobia in much the same way as TT-Nb_2O_5 is the less ordered precursor to T-Nb_2O_5. B-Nb_2O_5 is unlikely to be found in this study as well because it is not an operationally stable phase.[34] Long heating times as well as sufficient pressures (on the order of 50 kilobars) are needed to attain this modification which has a structure very much unlike any other form as described above (rutile-like ribbons of edge-sharing NbO_6 octahedra).[35] We feel that the observation of this unique phase is unlikely in this research. The simplified structural behavior of niobia in this work is outlined in Figure 1-3.

The crystal structure of niobia is complicated; however the basic building block of these forms is a niobium atom in 6-fold coordination with oxygen atoms in an octahedral configuration. There are many fashions in which to arrange these octahedra in order to achieve an overall stoichiometry of O/Nb=2.5, hence the many different stable or metastable forms of niobia.[29] The stoichiometry is controlled largely by the number of octahedra (and therefore oxygens) that share edges and corners and by the number of octahedra that each oxygen is associated with, that is 1, 2, or 3 octahedra. It is these differing niobium and oxygen sites that occur that define the crystal structure of niobia, because the relative amount of oxygen sharing between octahedra varies from one octahedron to another. For example, suppose a octahedron shares 2 edges (3 oxygen atoms) and 3 corners with other octahedra. The edge oxygens belong to 3 octahedra while the corners are shared among 2 octahedra, therefore the stoichiometry becomes $NbO_{3/2}O_{3/3}$, or $NbO_{2.5}$.

Figure 1-3: Nb_2O_5 PHASE MODIFICATION AS A FUNCTION OF TEMPERATURE

Temperature	Modification
1200	H
	↑
1000	M
	↑
800	T
	↑
600	TT
	↑
400	Amorphous

These different phases of niobia will be investigated to determine how their properties change with structure. In this investigation it is important to be able to identify the distinct phases of niobia in order to understand how the effects of structure are related to different properties such as acidity, support effects, reducibility, and interactions with silica or alumina. These properties are all important, as is the effect of preparation of the niobia aerogel and the binary oxide aerogels that are prepared as amorphous materials by the sol-gel method.

1.4 The Structure of Binary Oxides

This section gives a review of the binary oxides, supported and mixed oxides, which have relevance and are closely related to the niobia-silica and niobia-alumina systems. This section will also cover some of the unique chemistry-structure relationships used in order to prepare these binary oxides and will later go into depth of the different preparations found in the current literature in order to synthesize silica-supported niobia and alumina-supported niobia as well as the mixed oxides thereof. Acidity models used to explain the results of the binary oxides will be discussed in later sections.

1.4.1 Supported Oxides

Supported metal oxides are prepared when one metal oxide phase is dispersed on a second metal oxide substrate. There are a number of reasons to use supported oxides instead of bulk, unsupported ones. One reason is to increase the effective surface area. Often times bulk oxides, especially transition oxides such as niobia, are prepared by a relatively high temperature calcination that results in significant sintering or crystallization and loss of surface area. A suitable supporting oxide can help reduce this sintering and reduction of area by imparting thermal stability to the supported oxide. Another very important reason for preparing supported oxides is to modify the chemical properties of the

bulk unsupported oxides by the formation of a surface oxide phase. These surface oxide properties can often be quite different from those found in the bulk unsupported phase of the oxide. The catalytic behavior of these supported oxides is closely related to the structure of the surface phase oxide.[36, 37] An understanding of the formation of surface layers and their interaction with the substrate has therefore become increasingly important since supported oxides are commercially used as oxidation, isomerization, dehydrogenation, and dehydration catalysts.[5, 38]

As mentioned above, it has recently been discovered that supporting an oxide on another oxide may lead to more desirable properties than that of the oxide in bulk form.[5] An example of this is that V_2O_5 supported on TiO_2 (anatase) selectively oxidizes o-xylene to phthalic anhydride much more readily than unsupported V_2O_5.[6, 7, 8] Also, MoO_3 supported on either SiO_2, TiO_2, or Al_2O_3 is both more active and selective in the photo-oxidation of hydrocarbons than bulk MoO_3.[5, 39] Forming a surface monolayer of these supported species was found to be responsible for the catalytic behavior.[6, 39] Thus, by simply dispersing the oxide in the form of a complete monolayer, one can convert a support with undesirable chemistry into a useful and catalytically active material. Although a large number of supported oxide systems have been examined, a review of only those supported systems relevant to Nb_2O_5-SiO_2 will be discussed which will help give a general understanding of the effects of supporting an oxide on molecular structure.

Of the many supported oxide systems studied in the literature V_2O_5-TiO_2, TiO_2 supported V_2O_5, is a good starting point in understanding these systems because of the extensive data available. Recent studies indicated that the surface vanadium oxide has two terminal and two bridging bonds to surface oxygens, and exhibits intrinsic disorder below monolayer coverage.[40] This type of tetrahedral environment with terminal double-bonded oxygen atoms, $V=O$, has been confirmed by other researchers.[6, 41] Above monolayer coverages, small crystallites of V_2O_5 are present on the TiO_2 support in addition to the monolayer of the surface vanadium species. These small V_2O_5 crystallites are also

somewhat distorted in comparison to bulk, unsupported V_2O_5.[6] Evidence by Gasior and Machej[42] showed that the (010) crystallographic plane of V_2O_5, the plane containing exposed V=O bonds, is more active and selective than other V_2O_5 planes for the oxidation of o-xylene to phthalic anhydride. The same type of V=O bond exposed on the vanadia surface oxide monolayer on TiO_2 is the reason for the superior oxidation chemistry of this catalyst. This bond for the surface vanadia species has also been found to be easily reducible during reaction conditions and is related to the vanadia-support interaction.[43, 44] Most workers have agreed that different preparation techniques yield surface vanadia species which are independent of the method, but are intrinsic to the vanadia-titania interaction, thus showing that V_2O_5 strongly interacts with TiO_2.[6, 40, 45, 46]

The study of V_2O_5-TiO_2 has led to the study of V_2O_5 supported on other oxides such as SiO_2, and Al_2O_3.[40, 41, 47] V_2O_5 supported on Al_2O_3 has been well studied using a variety of techniques.[41, 47] For a 5 wt.% V_2O_5-Al_2O_3, Raman features were found in the spectra that corresponded to the presence of both monovanadate (VO_4), and divanadate (V_2O_7) species.[47] Upon increasing the vanadia content on alumina to coverages beyond 5 wt.% (10 to 20 wt.%), a new distinct species with a different coordination began to appear. This species was similar to highly distorted (containing a V=O bond) vanadia, suggesting that octahedral VO_6 groups were forming with this material.[41] On silica, the behavior of the supported vanadia species was slightly different. A 5 wt.% V_2O_5-SiO_2 sample exhibited Raman bands characteristic of micro-crystalline V_2O_5 since the bulk V_2O_5 phase was just beginning to form. The crystalline V_2O_5 bands, with stonger intensities, overshadow the presence of any weak surface vanadate Raman bands. The formation of crystalline V_2O_5 in the V_2O_5-SiO_2 system reflects the weaker interaction of vanadium oxide with the silica support relative to the Al_2O_3 and TiO_2 supports. At coverages below 5 wt.% (onset of crystallization) the silica supported vanadium oxide phases have been found to be present as tetrahedral mono-oxo vanadate species and polymeric tetrahedral metavanadate species.[47] Hydrating these vanadium oxide species on SiO_2 converts the

tetrahedral mono-oxo vanadates into an octahedral polymeric vanadate structure, while both hydrated and dehydrated vanadium oxide species on Al_2O_3 possess isolated tetrahedral vanadate structures at low coverages.[48]

Another system that has been well studied is Al_2O_3-supported MoO_3. This system, which is commercially very important to the petrochemical industry in terms of its ability for hydrodesulfurization and hydrotreating, will be discussed in terms of the structures that have been characterized as forming on the alumina support as well as the effect that preparation has on the formation of these structures. Structural models have been proposed by several researchers.[49, 50, 51, 52, 53] Isolated dioxo monomolybdate, MO_4, as well as dimerized molybdate, M_2O_7, species that are tetrahedrally coordinated, are believed to be formed primarily at low coverages of MoO_3. This behavior is nearly identical as seen previously for V_2O_5-Al_2O_3. Polymeric molybdate in an octahedral environment increases with increasing loading of MoO_3 at the expense of tetrahedral molybdate structures.[50, 54, 55] Further increase in loading of MoO_3 results in crystalline MoO_3 because of the extra mobility of MoO_3.

The study of the MoO_3-Al_2O_3 surface oxide has led to the study of supported MoO_3 systems on other oxides.[39, 56, 57, 58, 59] Similar to V_2O_5-TiO_2 supported oxides, MoO_3-TiO_2 surface oxides were found to be strongly interacting and similar structures were found on these supports regardless of preparation.[58, 60, 61] Surface structures on MoO_3-Al_2O_3 supported oxides have shown discrepancies in the literature and this is probably attributed to the different preparation techniques used by the different research groups in synthesizing these materials. Therefore, the preparation method used to bond MoO_3 to Al_2O_3 has an effect on the final structure of MoO_3-Al_2O_3. On SiO_2, MoO_3-SiO_2 surface oxides were found to be poorly interacting as shown by the poor dispersion of MoO_3 crystallites on the surface.[58, 62, 63] Because of these findings of weak interactions with the silica substrate, several researchers have investigated different preparation methods to try to disperse MoO_3 over SiO_2. The results of these findings show that effects of

preparation do necessarily affect the final surface oxide of MoO_3-SiO_2.[39, 56, 59] Below is a brief discussion on the role of preparation of these supported oxides and how their resulting surface oxide structures are influenced by the different methods.

Supported oxides are synthesized by grafting one oxide onto the surface of a second supporting oxide. The technique most commonly used to prepare these materials is that of impregnation, although several other methods are used such as vapor phase reactions using organometallic precursors or solid-surface diffusion of the supported oxides.[64] The technique of impregnation typically involves filling the pores of the supporting oxide with a solution containing the precursor for the supported oxide. When the solvent is water and the dissolved species is in the aqueous phase, the technique is usually termed as aqueous impregnation, while if the solvent is a dehydrated hydrocarbon solution the method is called non-aqueous incipient wetness impregnation. There are typically two types of precursors that are used, a complexed oxide which can be dissolved in a solution such as $(NH_4)_6Mo_7O_{24} \cdot 4H_2O$, or organometallic precursors such as $Mo(\eta^3-C_3H_5)_4$ or $[Mo(OC_2H_5)_5]_2$. For preparations in an aqueous environment the former precursor is typically used and it has been found that pH has a direct effect on the reaction between the precursor and supporting oxide.[53, 65] The equilibrium of this reaction is given as:[66]

$$7MoO_4^{2-} + 8H^+ \rightleftharpoons Mo_7O_{24}^{6-} + 4H_2O \qquad (1.1)$$
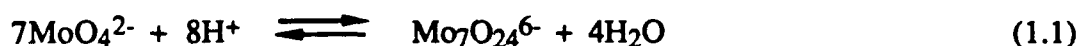
This equilibrium is shifted to the right at low pH (~ 1) at which point the $Mo_7O_{24}^{6-}$ solution species can react with the surface hydroxyls because of a net positive charge associated with the surface.[53] Since the species reacted with the surface is already polymeric in nature, this preparation leads to polymeric molybdate species on the surface. At the other end of the pH scale, at high pH (~ 9), MoO_4^{2-} is the prominent solution species but because the surface is now negatively charged, the surface hydroxyls are unreactive

because of the electrical repulsions and MoO_4^{2-} is simply dispersed over the surface, but can later react with the supporting oxide during calcination as the impregnating solution is driven away.[53] This preparation can also lead to polymeric molybdate species because of the non-reactivity of the surface during the preparation step which leads to greater mobility of the active molybdate species.[53] When organometallic precursors are used, the preparation is usually performed as an incipient wetness impregnation using a dehydrated hydrocarbon as the solvent, such as hexane or benzene. In this preparation it is usually believed that the surface hydroxyl group reacts with the electropositive metal atom in the organometallic compound thus grafting the supported oxide as shown in Equation 1.2.

$$\equiv Si\text{-}O\text{-}H + Mo(OC_2H_5)_5 \rightleftharpoons \equiv Si\text{-}O\text{-}Mo(OC_2H_5)_4 + C_2H_5\text{-}OH \qquad (1.2)$$
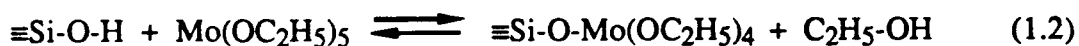
There are several reasons as to why the preparation method influences the structure of silica supported oxides more so than the other discussed oxides of TiO_2 and Al_2O_3. The main reason is probably attributed to different isoelectric points (IEP) of these oxides. Silica has the lower IEP at a pH = ~ 2, while titania and alumina have IEP's of 5-6 and 8-9, respectively.[67] These various points determine at which point anions (pH < IEP) or cations (pH > IEP) will be adsorbed onto the surface of the supporting oxide. Unless a pH of about 1 is used in preparing MoO_3-SiO_2 from $(NH_4)_6Mo_7O_{24}\cdot 4H_2O$ the surface molybdate species will not be well dispersed and crystalline MoO_3 will readily form upon calcination, as when a pH of around 6 is typically used.[65] This explains why well dispersed surface molybdate species are readily seen with the TiO_2 and Al_2O_3 supports, under these typical conditions of pH ~ 6, because this pH is lower than the IEP's for both these oxides and will allow the molybdate to bond to the positively charged surfaces. Organometallic precursors like $Mo(\eta^3\text{-}C_3H_5)_4$ are more effective in dispersing tetrahedral molybdate species over oxides (silica in particular) than when $(NH_4)_6Mo_7O_{24}\cdot 4H_2O$ is used.[39, 68, 69] The different types of organometallic species also lead to differences in the

final structure of the silica supported oxide, because of the different bonding environments afforded by the organometallic precursor. Other reasons for the differing surface oxide structures for silica over other oxides is that silica typically has a much larger surface area than other oxides (typically 2 to 10 times higher) which makes problems such as steric effects in the pores and capillary wetting (possible solvent differences) more pronounced. These differences are believed to be responsible for the influence of preparation method used.[39, 59, 65]

Other supported oxide systems which have been investigated display similar features to those discussed above for the supported V_2O_5 and supported MoO_3 systems.[47] The interactions of several transion metal oxides (rhenium oxide, chromium oxide, and tungsten oxide) show the strong interaction of the metal oxides with the Al_2O_3 and TiO_2 supports as indicated by the formation of atomically dispersed surface metal oxide phases. The much weaker interaction of the metal oxides with the SiO_2 support results in the formation of both atomically dispersed surface metal oxide phases as well as metal oxide crystallites. From the work by Wachs' group it is generally assumed that silica is a less interacting support than other oxides, which basically means that an effective reaction to chemically bond the supported oxide precursor to silica has not taken place.[47] When silica supported systems are effectively formed, i.e. observation of well-dispersed tetrahedral or octahedral species, strong interactions in terms of chemical properties of the supported oxides are generally seen.[59, 70, 71, 72, 73] Thus, understanding the interactions of the oxide support and supported oxide is crucial to understanding the supported oxide system. With this background on general surface oxides, we will now concentrate our efforts in discussing the current literature of silica and alumina supported niobia.

1.4.1.1 Silica-Supported Niobia (Nb_2O_5-SiO_2)

This section is a brief discussion of background information on the structure of silica-supported niobia. This review consists of work recently done by our group as well

as detailed structural information that has been compiled by other researchers. The first research on silica-supported niobia systems was done six years ago by Ko et al.[74] In this work, three niobia-silica supports were prepared using incipient wetness impregnation of a hexane solution onto a high surface area silica support. These three supported oxides consisted of one, two, and three monolayers of Nb_2O_5 grafted onto silica and were designated as NSI, NSII, and NSIII, respectively. All three samples were found to be XRD amorphous after a standard calcination at 500 °C for 2 hours and were thus considered stable, since pure niobia crystallizes to $TT-Nb_2O_5$ after these same thermal treatments. After heat treatment to 600 °C for 2 hours, NSII and NSIII sintered and crystallized into $T-Nb_2O_5$ while the monolayer sample remained amorphous, as shown by XRD. These results suggest that niobia-silica surface oxides are stable after a 2 hour, 500 °C calcination, but only the monolayer is stable after further heat treatment to 600 °C. This initial study brought up many interesting questions that needed to be addressed. First, does the initial layer at the silica surface of NSII and NSIII remain stable after crystallization at 600 °C or do these layers fully dewet the silica surface and sinter the first layer as well? Secondly, is NSI, the silica-supported niobia monolayer, actually stable or are there microcrystalline particles or amorphous niobia aggregates that are forming? To help answer these questions, a study was performed on model thin films of niobia to aid in a further examination of the niobia-silica supported oxide structural morphology. This research constituted the Ph.D. thesis of J.G. Weissmann.[75]

The results of the model thin films will be discussed along with the previous study on the high surface area oxides to determine if there is a relation between the structural interactions of these oxides and their chemical properties.[75, 76, 77, 78, 79] The model thin films (one-, two-, and three- atomic layers of niobia on silica) gave significantly different results than those of the high surface area oxides. Niobia on the model thin films crystallized to $T-Nb_2O_5$ after calcination at 500 °C and to either all $H-Nb_2O_5$ or to H- and $T-Nb_2O_5$ after the heat treatment to 600 °C, depending on the method of preparing the

niobia layers and duration of the thermal treatment. Recall that the high surface area counterparts after this same thermal schedule were amorphous, for the monolayer sample NSI, or crystallized to TT-Nb_2O_5, for the multilayer samples of NSII and NSIII. While these model thin film samples do not correspond directly to their high surface area counterparts, important observations were made concerning these systems. First, when H- and T-Nb_2O_5 were found together, the H-Nb_2O_5 crystals were found to be large and well ordered, while the T-Nb_2O_5 crystals were smaller and flatter. In fact, for the multilayer thin film samples, T-Nb_2O_5 crystallites were found to lie below the larger H-Nb_2O_5 crystals. The more surface reactive niobia preparation technique led to higher proportions of T-Nb_2O_5 to H-Nb_2O_5 after the 600 °C treatment. These observations led to the conclusion that T-Nb_2O_5 crystallites are stabilized by niobia strongly interacting with the silica surface. Thus, T-Nb_2O_5 crystallites are indicative of regions were niobia is stabilized by the surface, while the H-Nb_2O_5 crystals occur in areas where niobia is destabilized.

The difference in the behavior between the high surface area (HSA) samples and the thin film (TF) samples has been attributed to different extents of support interaction, which can be related to the concentration of surface -OH groups on the support. On the HSA supports, the surface contains a large concentration of -OH groups on the surface, and the niobia monolayer, NSI, is stabilized by Nb-O-Si linkages from the surface reaction with the -OH groups; however, on the TF supports, there is a much lower concentration of -OH groups, thus only a partial coverage of the support can stabilize the niobia monolayer.[79] The remaining niobia dewets the surface and crystallizes. In the HSA samples, niobia above a stabilized monolayer forms T-Nb_2O_5 crystals upon higher heat treatment to 600 °C, while on the TF samples, only a partial stabilization occurs, as seen by the increased amount of crystallization to T- and H-Nb_2O_5. Reduction studies on these high surface area samples confirm that the interfacial interaction which stabilizes niobia as a surface phase in this system also makes niobia more difficult to reduce. These reduction results also showed that if niobia is allowed to crystallize first in a non-reducing environment, then the

crystalline phase is stabilized and reduces at a higher temperature than bulk niobia; however, if sufficient niobia loading is used on the sample, niobia located far enough away from the stable niobia-silica interface reduces similarly to bulk Nb_2O_5. These studies provided information on the interaction chemistry between niobia and silica, but not until recently has the structural chemistry of these niobia overlayers been investigated.

Several researchers have recently done considerable studies on silica-supported niobia.[67, 80-90] In the first paper by Iwasawa[81] the structure of a one-atomic monolayer of niobia attached to silica, prepared in a similar fashion as previously mentioned by Ko[74], was probed using a variety of techniques including Extended X-ray Absorption Fine Structure (EXAFS), and High Resolution Electron Microscopy (HRTEM). From this work they determined that niobia was amorphous after calcination at 500 °C in oxygen and that Nb exists in a pentavalent state and also that the Nb-O-Nb and Nb-O bond distances were shorter for the attached niobia monolayer than those found in $T-Nb_2O_5$. Correspondingly, shorter Nb-O bonds for the surface phase imply stronger Nb-O bonds.[91, 92] The presence of Nb-O-Si bonds were also detected confirming the existence of niobia attached to silica (see Figure 1-4). It was also determined in this study from the Nb-O-Nb distance, that the relative portion of edge-shared to corner-shared structures in the one-atomic monolayer catalyst is much larger when compared with $T-Nb_2O_5$. These results indicated that niobia is indeed structurally different from $T-Nb_2O_5$ when supported on silica at a monolayer coverage.

Papers reporting the structure of niobia supported on silica at low coverages, below monolayer, have recently been published.[80, 84, 86, 88, 90] Using a variety of sensitive spectroscopic techniques including Laser Raman and Infrared Spectroscopy, EXAFS, and X-ray Photoelectron Spectroscopy (XPS), researchers have identified the surface structures of supported niobia. There exists some controversy over exactly what types of structures exist on silica so a review of the most current literature on the subject is in order.

Figure 1-4: STRUCTURE OF Nb_2O_5 MONOLAYER ON SiO_2 [84]
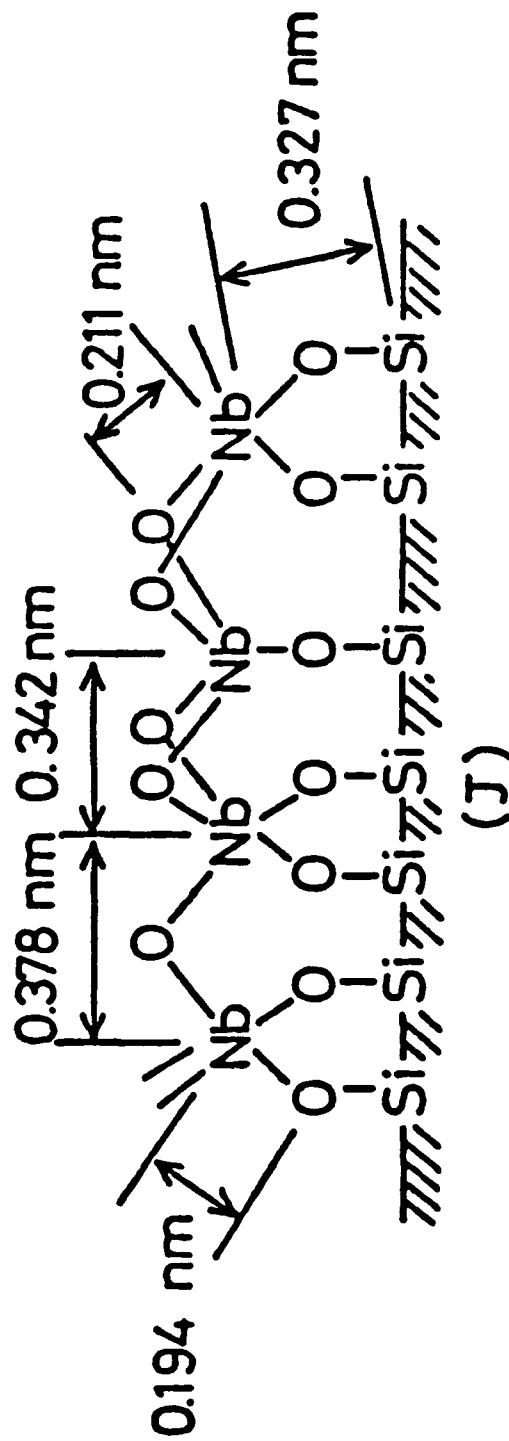
Nishimura[80] determined that the structure of the low coverage niobia supported oxide consisted of a tetrahedral dioxo structure that was bridged to the silica substrate as shown in Figure 1-5(A).

The niobia structures with niobium oxygen double bonds were confirmed by EXAFS, and Raman spectroscopy was used to conclude that the structure was tetrahedral. EXAFS also showed the presence of Nb-O-Si surface bonds indicating the linkage of the monomer unit to the support, and no Nb-O-Nb interactions were detected by EXAFS showing that these species are isolated on the surface as well. These monomers were grafted onto the surface of the silica support by a reaction between an organometallic precursor, $Nb(\eta^3-C_3H_5)_4$, and the hydroxyl groups of SiO_2, which was pretreated at 400 °C under vacuum to control the surface -OH concentration at 2 OH/nm^2.[80, 84] Iwasawa[84] has recently expanded research of the monomer species to a dimer niobia species on silica. These were prepared in a similar fashion to above; however, the organometallic precursor, $[Nb(\eta^5-C_5H_5)H-\mu-(\eta^5,\eta^1C_5H_4)]_2$ was different. The loading on the support was kept low to a value of about 1.0 wt.%. The local structure of the dimer was not drastically different when compared to the Nb monomer [see Figure 1-5(B)]. A tetrahedral environment was noted in the dimer of niobia, and the only profound difference seen is the Nb-O-Nb interaction with the bridging oxygen atom. Again Nb-O-Si bonds were detected confirming the existence of a grafted niobia species to the support.

Other researchers including our group have suggested slightly different environments for niobia when it is bonded to silica at less than monolayer coverage. Burke and Ko suggested that the basic building block at low coverages is a tetrahedral species with one doubly bonded oxygen and two hydroxyl groups attached to the niobium atom which is then anchored to the silica support through a single bond as shown in Figure 1-6(A). Using EXAFS and X-Ray Absorbtion Near Edge Spectroscopy (XANES), Yoshida et al.[86], also concluded that at low loadings, the surface phase of niobia exists as a highly dispersed phase and is tetrahedral with a single Nb=O double bond. Other than the

Figure 1-5: A) STRUCTURE FOR NIOBIA MONOMERS ON SILICA AND B) STRUCTURE FOR NIOBIA DIMERS ON SILICA[84]

A) Nb_2O_5-monomer on SiO_2
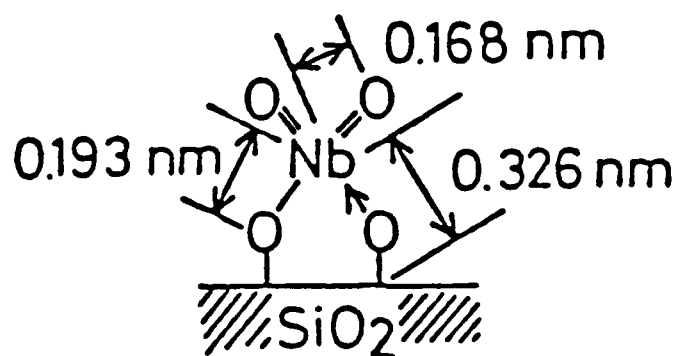
B) Nb_2O_5-dimer on SiO_2
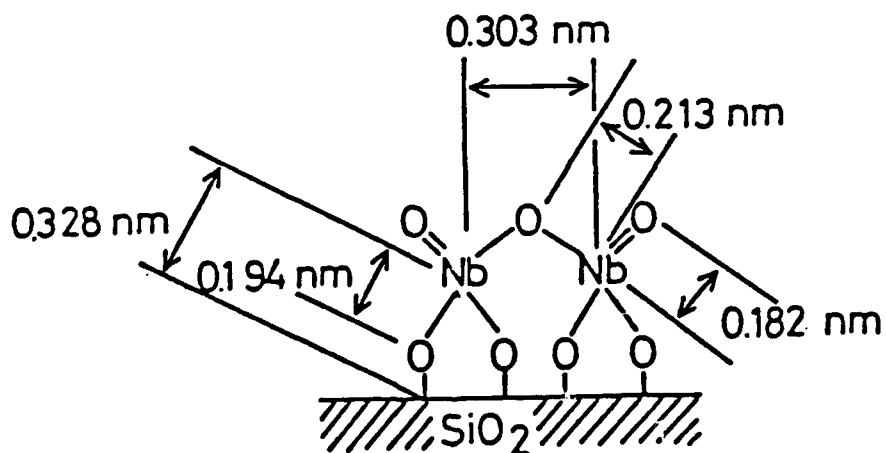
Figure 1-6: A) STRUCTURE FOR LESS THAN MONOLAYER COVERAGE OF NIOBIA ON SILICA[90] AND B) PROPOSED QUANTUM MECHANICAL STRUCTURE OF LOW COVERAGE FOR NIOBIA ON SILICA[93]

A) Nb_2O_5-SiO_2 (<< Monolayer Coverage)
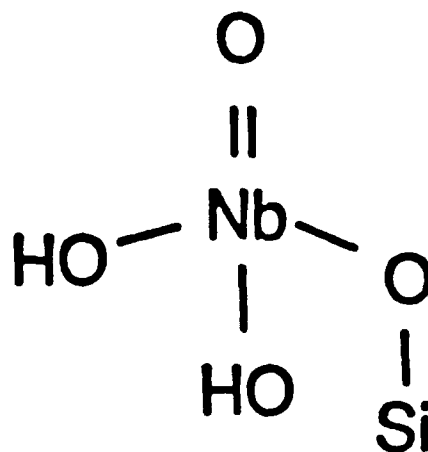
B) Nb_2O_5-SiO_2 (Quantum Mechanical Determination, M = Nb atom)
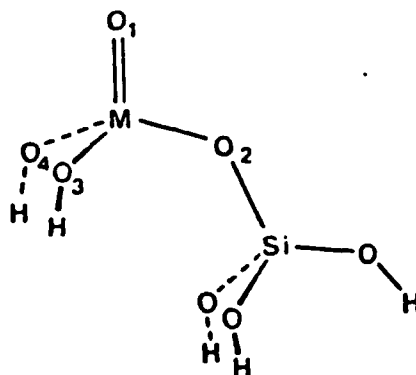
experimental evidence cited above, the quantum chemical calculation of Kobayashi[93] also showed this to be a stable structure. From these calculations, the preferred structure of isolated niobia-silica is tetrahedral [see Figure 1-6(B)], with one Nb=O double bond along with adjacent hydroxyl groups - similar to the structure proposed by Bernholc et al.[12] for niobia-alumina as will be discussed later. In these calculations the number of Nb-O-Si bonds was assumed to be fixed at one.

At higher loadings of niobia on the silica support, Yoshida et al.[86] reported that square pyramidal species occur in an aggregated state. Figure 1-7(A) represents such a structure which is also referred to as a highly distorted octahedron by Jehng and Wachs.[67, 94] Jehng and Wachs also showed that Nb_2O_5 aggregated on SiO_2 at a concentration above 2 wt.% into slightly distorted octahedra as shown in Figure 1-7(B). Thus, Burke and Ko[90] used these results to suggest a model of their NS(0.25) and NSI samples, based also on experimental results for the heats of adsorption of pyridine. With increasing Nb_2O_5 concentration, the shift from tetrahedral to octahedral niobia as the dominant species was proposed. Even though these studies differed slightly in the support and precursor used as well as the experimental techniques used to extract structural information, they all have given a better perspective on the structure of the surface phase of silica-supported niobia. This background information on the structure of niobia when it is supported on silica, shows that the structure changes with niobia coverage and that these structures differ significantly from that of bulk niobia. Next we will discuss the available literature information on alumina supported niobia, Nb_2O_5-Al_2O_3.

1.4.1.2 Alumina-Supported Niobia (Nb_2O_5-Al_2O_3)

There is considerable information on the commercial importance of Nb_2O_5-Al_2O_3 supported oxides as acid catalysts.[12, 38, 95, 96, 97] However, there is a general lack of understanding on the origin of acidity of these materials. Not until recently has there been

Figure 1-7: A) HIGHLY DISTORTED NIOBIA STRUCTURE FOR NIOBIA ON SILICA AND B) SLIGHTLY DISTORTED NIOBIA STRUCTURE FOR NIOBIA ON SILICA[90]

A) Highly Distorted NbO_6 Octahedra
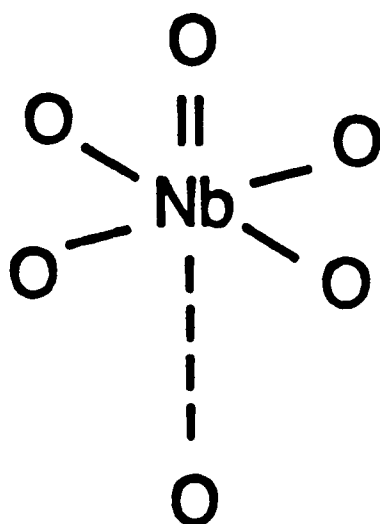
B) Slightly Distorted NbO_6 Octahedra
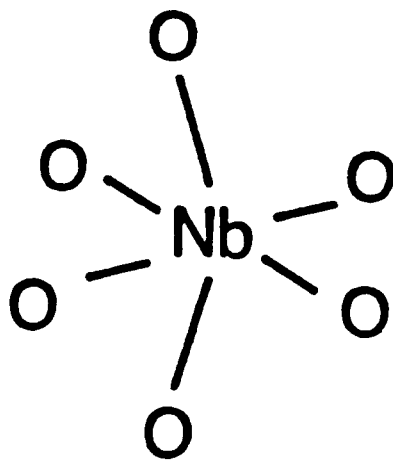
any kind of research done on the structural basis of these binary oxides, but even with this preliminary work, there exists controversies over their actual structures.

The first work of alumina-supported niobia was published approximately 5 years by Japanese researchers.[80] The supported catalysts were prepared by the reaction of an organometallic $Nb(\eta^3-C_3H_5)_4$ and -OH groups of Al_2O_3. This material was then treated with H_2 and O_2 to yield the structure shown in Figure 1-8. XANES work found the Nb atom to be tetrahedral. The niobia monomers were also determined to be distributed as isolated species since no observance of Nb-O-Nb bonds were found.

Another model for the structure of alumina supported niobia comes about by a two-fold compilation of experimental data and quantum mechanical calculations.[12] These structures were proposed in order to explain the trends and origins of Brønsted acidity on dispersed γ-alumina - supported transition metal oxides. The main feature in this model structure was the double bonded oxygens, as determined by Laser Raman Spectroscopy, that give these materials their high acid strength. The proposed acid structure along with the conjugate base of the acid cluster is shown in Figure 1-9. The doubly bonded oxygens can help distribute or delocalize the negative charge that is associated with the donation of a proton. The support was also found to play an "inductive" role by allowing the negative charge to spread into the oxide support network, and in so doing lowered the proton removal energy thus making a stronger Brønsted acid. $WO_3-Al_2O_3$ was also investigated in this study and found to have an even greater Brønsted acid strength than $Nb_2O_5-Al_2O_3$. This extra strength was attributed to the additional electron withdrawing action of two doubly bonded oxygens on the tungsta species as opposed to niobia which only has one doubly bonded oxygen. $Nb_2O_5-Al_2O_3$ was believed to be much more stable than $WO_3-Al_2O_3$, because of the two Nb-O-Al bonds which anchor the niobia surface species to the alumina support, while the tungsta had only one W-O-Al bond. Overall, both $WO_3-Al_2O_3$ and $Nb_2O_5-Al_2O_3$ had high Brønsted acid strength, while $WO_3-Al_2O_3$ was considered to

Figure 1-8: STRUCTURE OF NIOBIA SURFACE OXIDE ON ALUMINA (<< MONO-
LAYER COVERAGE)[80]
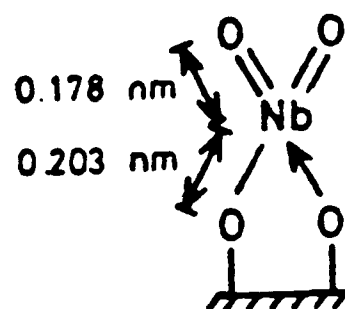
Figure 1-9: A) STRUCTURE OF ALUMINA-SUPPORTED NIOBIA (BRØNSTED ACID) AND B) RESULTING STRUCTURE OF CONJUGATE BASE OF NIOBIA-ALUMINA[12]

A) Nb_2O_5-Al_2O_3 (Brønsted Acid)
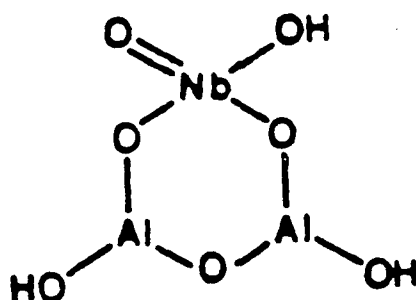
B) Nb_2O_5-Al_2O_3 (Conjugate Base)
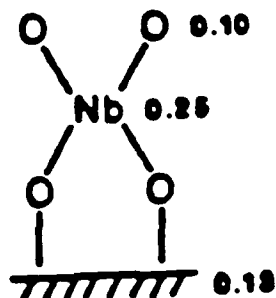
be a slightly stronger acid because of the extra delocalization effect of the two doubly bonded oxygens.[12, 38, 95, 96]

Another study similar to that of Bernholc was undertaken by Kobayashi et al. to explain the interaction of niobia on alumina by quantum mechanical calculations of model clusters.[93] Calculations of silica-supported niobia were mentioned earlier; however, results for the alumina-supported niobia are similar. The results actually show that a tetrahedral dioxo structure is the most stable structure for niobia supported on alumina; however, these findings are somewhat skewed by the calculations and proposed model which favor a stabilizing effect by the formation of a 4-membered ring, with the electronegative oxygen atom bonding to the electropositive aluminum atom. This is an unlikely structure because of the truncation of the alumina support used to simplify their calculations. A similar study of this same dioxo structure on silica showed it to be highly unstable. Therefore, the model suggested by their findings is a tetrahedral mono-oxo structure with one Nb-O-Al bond to anchor the moiety to the support as shown in Figure 1-10. In these calculations the number of bonds to the support was fixed at one. Further calculations need to be explored to determine whether an increased number of bonds to the support actually stabilizes the niobia cluster. Although the previously mentioned studies differ somewhat in the support, precursor, or technique used to analyze the alumina-supported niobia, they all have similar features. The most striking observation is that all of the proposed models feature at least one Nb=O bond. Also all of the structures are tetrahedral in nature. The last structure proposed by Kobayashi looks remarkably similar to that proposed by Bernholc if there was another surface bond accounted for in the calculation.

Within the past few years there has been research done from Wachs' group that has led to proposed structures on these systems.[67, 85, 92, 94, 98] These studies have primarily concentrated on experimental results of Raman Spectroscopy as well as theoretical calculations. These researchers have come to the same conclusions as those previously

Figure 1-10: A) PROPOSED QUANTUM MECHANICAL STRUCTURE OF
ALUMINA-SUPPORTED NIOBIA (<< MONOLAYER COVERAGE)[93]
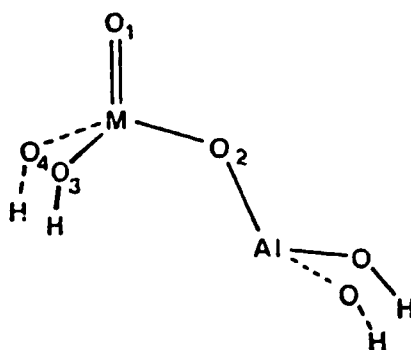
mentioned in that the supported niobia systems on alumina contains a niobium oxygen double bond, Nb=O. Their proposed structure for this system is a highly distorted NbO_6 octahedra as shown in Figure 1-11(A).[67, 94, 98] However, in recent papers, they have suggested that a mono-oxo tetrahedral structure could also not be ruled out. See Figure 1-11(B) for the mono-oxo structure proposed by Hardcastle.[85, 92] In general the highly distorted mono-oxo NbO_6 species is more probable in light of the structural chemistry of niobium oxide, i.e. the fact that tetrahedrally coordinated niobate species are rare, and NbO_4 tetrahedra appear under extreme circumstances.

These past few sections introduced the current background information on supported oxides and more specifically, those supported systems directly applicable to this study. We will now focus attention on the lesser known systems of mixed binary oxides containing niobia.

1.4.2 Mixed Oxides

In the field of catalysis, mixed oxides are important because of their strong acidic properties. These oxides cover a large array of forms and structures and can be used either as catalysts or catalyst supports. Research on mixed oxides using different starting materials, preparation steps, and composition of components, has shown that these catalysts can be crystalline, glassy, amorphous, or heterogeneous materials.[1, 11] Currently, the role of structure in relationship to the properties of these catalysts is not well understood. There are a number of ways to synthesize mixed oxides, as reviewed by Courty.[99] There has also been an interest in preparing these materials through a sol-gel process which is then followed by a supercritical extraction of the solvent ladened gel. The preparation techniques used in this study involve the co-precipitation and sol-gelling of mixed oxides. The first part of this section will discuss combinations of mixed oxides which help shed some light into these systems and will subsequently be followed by a discussion of the relevant binary oxide systems of niobia/silica and niobia/alumina.

Figure 1-11: A) HIGHLY DISTORTED MONO-OXO NbO_6 OCTAHEDRA AND B)
HIGHLY DISTORTED MONO-OXO NbO_4 TETRAHEDRA

A)

B)
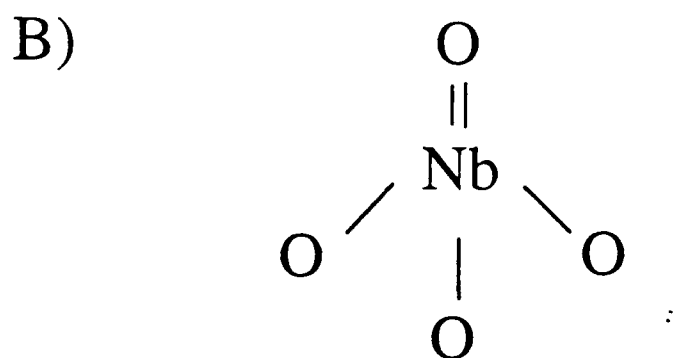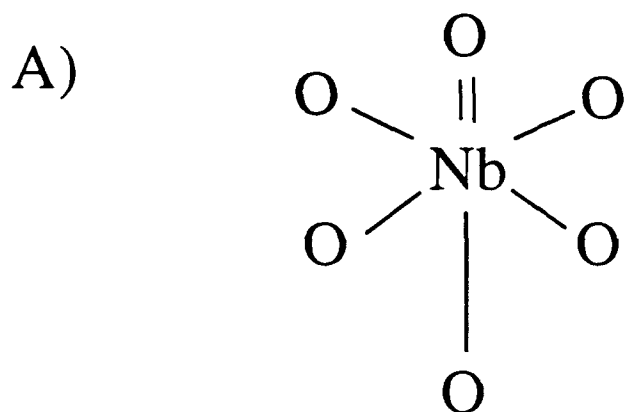
There is very little information on both the niobia/silica and niobia/alumina mixed oxide systems. Ibraihm and Bright[13] studied niobia/silica at temperatures above 1300 °C. Their results showed that silica and niobia are completely immiscible, even in their liquid phases. Layden[14] has also studied the niobia/alumina system at elevated temperatures and found that these two oxides readily undergo a solid-state reaction to form the compound of $NbAlO_4$ ($Nb_2O_5 \cdot Al_2O_3$) Another study which showed a compound formation was for the niobia/germania system which formed a compound of stoichiometry $9Nb_2O_5 \cdot GeO_2$.[100, 101] The structure of this compound is very different from those phases of niobia which typically appear in the same temperature range. Also, it was observed that niobia crystallized into the TT- and T-Nb_2O_5 phases from a high temperature melt of niobia/germania.[100] Normally M- or H-Nb_2O_5 are the stable forms of niobia in this temperature range of crystallization from a melt.[29] This suggests that TT- and T-Nb_2O_5 could be stabilized by germania through the compound formation mentioned earlier, but whether GeO_2 is actually incorporated into TT- and T- Nb_2O_5 is unknown.

Another mixed oxide that has been investigated is TiO_2/SiO_2.[3, 102-108] These mixed oxides, prepared by co-precipitation and sol-gel methods, showed interesting mixed oxide behavior that is similar to the Nb_2O_5/SiO_2 system. First of all, the TiO_2/SiO_2 system has one component (TiO_2) that crystallizes readily, while the other oxide component (SiO_2) does not. This is identical to the Nb_2O_5/SiO_2 system where Nb_2O_5 crystallizes at low temperature, and SiO_2 does not crystallize below 1000 °C.[16] Another similarity between these two systems is that both binary mixed oxides are highly acidic.[2, 3, 88] Amorphous silica appeared to inhibit the crystallization of TiO_2, i.e. as TiO_2 content increased, the crystallization tendency of the mixed oxides became more and more pronounced.[108] At low concentration of TiO_2 in the TiO_2/SiO_2 mixed oxide system EXAFS and XANES experiments have identified the coordination geometry of the Ti^{4+} ion.[106, 109] It was determined that the geometry is primarily a four-fold coordination.[106, 109] This result is somewhat surprising since tetrahedral titanium compounds are rare. The compound

Ba_2TiO_4 (4-fold Ti bearing compound) has Ti-O separations which are short ranged and confirm the above assignments for tetrahedral coordination of titania.[110] Increasing the concentration of TiO_2 increased the number of 6-fold coordination Ti^{4+} sites and decreased the number of 4-fold sites until at high concentrations of TiO_2 (above 50 wt.%) the coordination of titanium was primarily octahedral.[106, 109] Along these same lines of reasoning, Chen found that the most acidic compounds of TiO_2/SiO_2 were the ones with low concentrations of titania (~ 25 wt.%). This same concentration was found to have a large proportion of tetrahedrally coordinated titania. Only at very high temperatures was it found that crystobalite crystallized from these mixed oxides with Ti in a substitutional solid solution.[111] Now we will concentrate our attention on the mixed oxide systems of Nb_2O_5/SiO_2 and Nb_2O_5/Al_2O_3.

1.4.2.1 Nb_2O_5/SiO_2 Mixed Oxide

Little to no structural information is available for niobia/silica mixed oxides. Ibraihm and Bright[13] studied niobia/silica at temperatures above 1300 °C and found that the two component oxides are immiscible even in liquid form, thus no driving force for compound formation exists. It therefore makes an ideal system for studying interfacial interactions between niobia and silica, to determine if niobia is actually stabilized by silica and vice versa. Recently a study by Burke[88, 90] and Sivade et al.[112, 113] found that silica inhibits the crystallization of niobia. Laser Raman studies also indicated that for NS25w (25 wt.% Nb_2O_5), a broad peak existed which could be assigned to a combination of tetrahedral and highly distorted octahedral species.[88] Upon heat treating this sample to 1000 °C crystallization of TT-Nb_2O_5 ensued and a conversion from tetrahedral to octahedral niobia was found by Raman studies.[88] Increasing the concentration of niobia in the niobia/silica mixed oxide also showed a conversion of tetrahedral to octahedral niobia, similar to the effect the 1000 °C heat treatment had on NS25w.[88] Acidity studies were performed and showed high heats of adsorption similar to those of silica supported niobia,

thus Burke and Ko proposed the dominant structure to be a tetrahedral species as shown in Figure 1-12.[90] This proposed structure did not have any terminal -OH groups, which explained the lack of any strong Brønsted acid sites. The heat treated (1000 °C) NS25w sample was found to have a significantly lower heat of adsorption than the untreated, calcined sample. Thus, a decrease in acid strength accompanied the tetrahedral to octahedral conversion in the mixed oxide. These niobia/silica mixed oxides were also found to be more difficult to reduce than bulk niobia showing the oxide-oxide interactions inherent in this system influence its physical and chemical properties.

1.4.2.2 Nb_2O_5/Al_2O_3 Mixed Oxide

Little work has been done on the niobia/alumina mixed oxide system. Layden showed that these two components readily underwent a solid-state reaction to form $NbAlO_4$.[14] Recent research from our group confirmed this compound formation upon heating the mixed oxide to 1000 °C; however, this work also showed that these materials were all amorphous after a standard calcination at 500 °C.[114] The niobia/alumina mixed oxides also showed great acidity and acid strength as the concentration of niobia was lowered in the mixed oxide. Jehng and Wachs showed that $NbAlO_4$ is formed at high calcination temperatures and high niobia concentrations, but low concentrations of surface niobium oxide phases are stable to high heat treatments.[85] Although Jehng and Wachs' work is not directly applicable to the mixed oxide analysis, it does show that there is a strong oxide-oxide interaction between niobia and alumina. These past few examples of mixed oxide systems and surface oxide systems show that oxide-oxide interactions play a significant role in the crystallization of one oxide in the presence of a second oxide. The strength of these interactions is often such that the structure or surface properties of these binary oxides are significantly different from either of the bulk oxide starting materials.

The work previously mentioned was performed primarily on samples prepared by a standard co-precipitation technique. This thesis will deal almost entirely with samples

Figure 1-12: PROPOSED TETRAHEDRAL NIOBIA STRUCTURE IN Nb_2O_5/SiO_2
MIXED OXIDE[90]
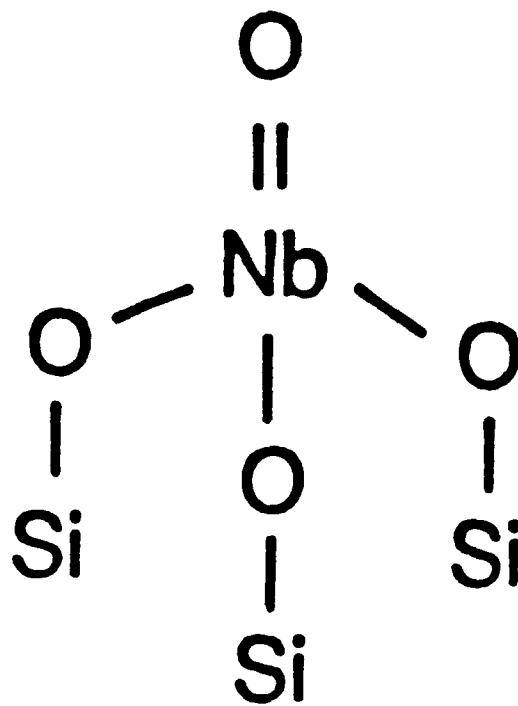
(aerogels) prepared via the sol-gel method, followed by a supercritical extraction. The next few sections will discuss in detail the method of preparation used in this thesis and give examples of samples that have been utilized as catalysts or catalyst supports.

1.5 Sol-Gel Method of Preparation for Aerogels

The main method used in this work for the preparation of the mixed and bulk oxides was the sol-gel technique followed by a supercritical extraction of the solvent from the gel.[4, 17, 24,115-121] These materials were first made by Kistler in the 1930's and were termed aerogels.[117, 118, 119] The metal oxide aerogels are suitable for a variety of applications such as ceramics, adsorbents, and insulators.[115-119, 122, 123] The very high surface areas and pore volumes of aerogels make them especially attractive for reaction catalysts or catalyst supports.[124] Not until recently though have aerogels been utilized as supports and catalysts.[24, 115, 124, 125] Reasons for the long time delay between development and application are probably due to the early difficulties in preparing the gel that often took weeks to synthesize.

The sol-gel method and its importance to the ceramic and glass industry has been well documented.[123, 126, 127] The sol-gel process using metal alkoxides $[M(OR)_n]$ is basically a three step process.[122, 123, 128] The first step involves adding the alkoxide(s) to the solvent, which results in a homogeneous solution. The second and third steps involve the hydrolysis and polycondensation of the alkoxide(s):[128, 129]

- **Hydrolysis:**

$$-M-OR \quad + \quad H_2O \quad \longrightarrow \quad -M-OH \quad + \quad ROH \qquad (1.3)$$

- **Polycondensation:**

$$-M-OH \quad + \quad HO-M- \quad \longrightarrow \quad -M-O-M- \quad + \quad H_2O \qquad \text{(dehydration)} \qquad (1.4)$$

$$-M-OH \quad + \quad RO-M- \quad \longrightarrow \quad -M-O-M- \quad + \quad ROH \qquad \text{(dealcoholation)} \qquad (1.5)$$
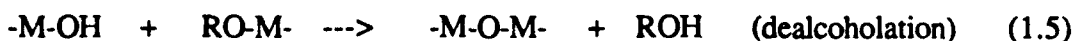
All of the above reactions tend to occur simultaneously.[128] It appears that an S_N2 type mechanism is the most probable, with the electronegative oxygen atom attacking the more positive metal atom, releasing either water (1.4) or alcohol (1.5).[129] In general, the ease of replacement of the alkoxy group decreases from tertiary to secondary to primary.[122, 128, 130] Gelation of this material can be brought about by: (1) removing the solvent, thus, bringing the polymer species into closer proximity and increasing the probability of crosslinking; (2) allowing the system to age and bringing about further dehydration and hydrolysis reactions; (3) adding more water; (4) increasing the alkoxide solution concentration; or (5) changing the pH of the solution.[122, 128] Upon gelation the resulting metalloxane chain (-M-O-M-O-M-) forms covalent macromolecules which will form giant coordination polymers with each other.[129, 131] One difficulty with this process is the fact that the reaction variables: type of solvent, system dilution, order of addition of reactants, rate of addition, rate of mixing, amount and type of catalyst (acid or base), amount of water, reaction temperature and time, all effect the rate of the competing hydrolysis and polymerization reactions, and these parameters are not well studied for most solutions.[131, 132] The main advantages of the sol-gel process over most precipitation reactions are that one may obtain a material with high purity (no contaminating ions like Cl⁻) and homogeneity at a microscopic scale. This briefly covers the sol-gel process itself, now we can discuss the preparation of the aerogel.

An inorganic hydrated oxide which is precipitated or sol-gelled from a solution, washed, and then dried in air is often obtained as a *relatively* porous gel and is given the term "xerogel".[24, 130] Extracting the solvent from a wet gel under hypercritical conditions in an autoclave yields an *extremely* porous material which is called, "aerogel".[116, 117, 130] Xerogels tend to have macropores while aerogels usually maintain more of a microporous structure and develop much larger surface areas and pore volumes. This is a result of the supercritical extraction process described below. Kistler knew that as liquid begins to evaporate from a gel, surface tension creates concave menisci in the gels pores (see Figure

1-13).[133] As evaporation continues, the menisci come into the gel body, resulting in a contraction due to the compressive forces around the pore perimeter. The surface tension eventually causes the collapse of the gel body, which results in a poor structure in terms of surface area and pore volume. In order to prevent this surface tension from destroying the gel structure, Kistler dried the gel in an autoclave.[117, 118, 119] When the liquid is raised above its critical pressure and temperature, it becomes a "supercritical" fluid in which there is no liquid-vapor interface.[133] Without the menisci, the gel retains its structure and original size and shape.

Kistler originally converted the solvent into the supercritical fluid to do the extraction. His original gels were prepared primarily in aqueous environments in which the colloidal material was dispersed in a liquid water phase. These gelled materials are termed "aquagels" if the liquid phase is water, or "alcogels" if the liquid phase is an alcohol.[124] Kistler encountered problems in trying to extract his aquagels because of the solubility of the metal oxides at temperatures approaching the critical point of water (T_c = 374 °C, P_c = 3204 psia). When the water was exchanged with a miscible alcohol such as ethanol (T_c = 243 °C, P_c = 927 psia), forming an alcogel, success was achieved in the supercritical extraction of the alcohol.[117, 118, 119] Since Kistler's efforts in 1932, considerable effort has been used on developing and/or refining supercritical drying technology with the goals of scaling up the process (for commercial use), simplifying the procedure, and improving safety aspects. Below is a brief review of these efforts and describes the evolution of the technique used in this thesis.

For several years, workers had tried to refine Kistler's original process, but it was not until 1968 that Nicolaon and Teichner[134, 135] reported on the preparation of inorganic alcogels by hydrolyzing metal alkoxides using a minimum amount of water. This technique was a major breakthrough from Kistler's work because it eliminated the salt removal and solvent exchange steps; however, one drawback was that the raw materials (alkoxides) were more expensive than the salts used in the early work. Nicolaon and

Figure 1-13: SCHEMATIC OF FORMATION OF MENISCI IN PORES OF A GEL AS RESULT OF SURFACE TENSION[133]
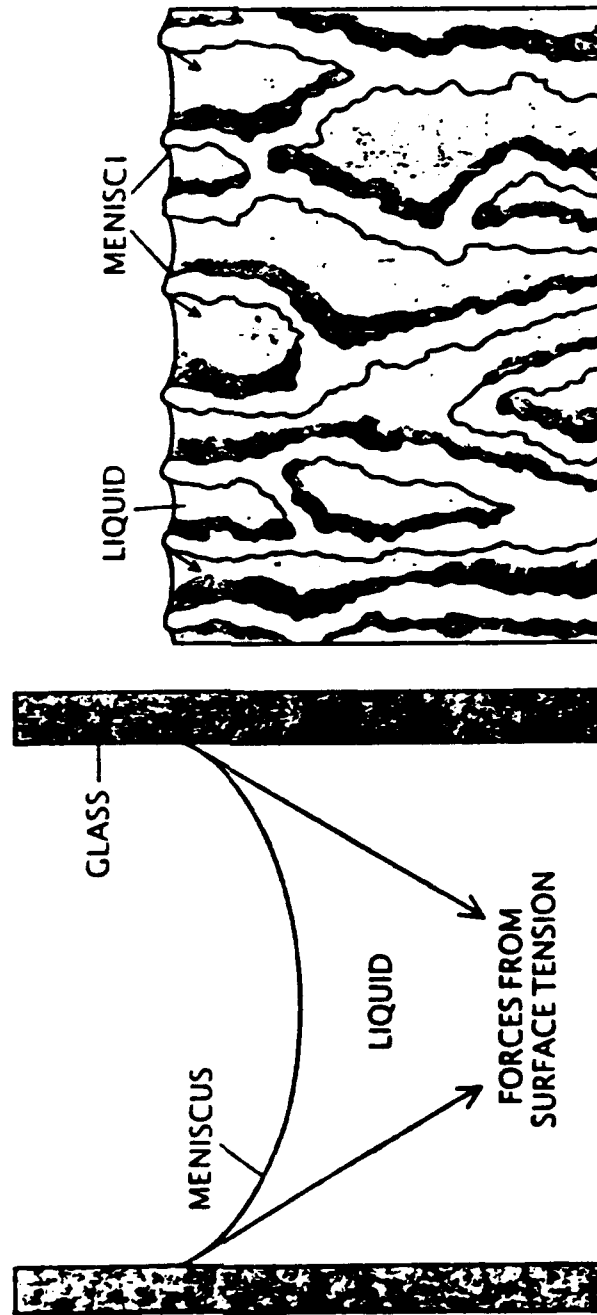
Teichner set up an essentially water-free system by hydrolyzing silicon alkoxides with an amount of water corresponding from one to five times the stoichiometric requirement.[134, 135] They also investigated volume ratios of alkoxide to alcohol and determined that 10% gave the best results; in fact, this is roughly the same ratio used in the synthesis of gels prepared in this thesis. The resulting gels were extracted in an autoclave at temperatures and pressures above their critical values. The solvent vapor was evacuated and the autoclave was then flushed with an inert gas to rid all traces of alcohol vapors. This process took only approximately half a day versus the "few weeks" needed in Kistler's original process. This work was extended to the preparation of other inorganic bulk oxides such as alumina, titania, zirconia, as well as mixed oxides of zirconia/magnesia.[24] The aerogel oxides exhibited unusually high surface areas and pore volumes as compared to their conventional xerogel counterparts.

The next significant improvement was not noted until 1985 by Tewari et al.[136, 137] This work centered around the same procedure as used by Teichner et al.[24, 134, 135]; however, before extracting the alcogel, the alcohol in the gel pores was replaced by liquid carbon dioxide. This process was motivated by the fact that CO_2 has a much lower critical temperature and pressure ($T_c = 31.1$ °C, $P_c = 1073$ psia) than the standard solvent of methanol ($T_c = 240$ °C, $P_c = 1155$ psia). The incentive for the lowering of these parameters by choosing CO_2 as the supercritical solvent is obvious from both an economic as well as a safety viewpoint. This work was a precursor for the ensuing research to follow, as well as the technique used in this thesis.

The next major contribution in the synthesis of inorganic oxide aerogels was developed by Iacobucci et al. in 1986 at the Stauffer Chemical Company.[115] This work discussed the semi-continuous supercritical carbon dioxide extraction procedure for preparing aerogel powders. The process begins with the preparation of a gel through the sol-gel process similar to that of Teichner et al.[24, 134, 135, 138] The resulting alcogel (prepared using an organic solvent, water for the hydrolysis/condensation reactions, and

catalyst for above reactions) is ready for the supercritical extraction step. A schematic of the apparatus is shown later in Figure 2-2. The CO_2 compressor delivers CO_2 at approximately 3500 psig to the extraction vessel which is heated to maintain a temperature above 40 °C. The CO_2 passes through the gel, thus extracting the alcohol. The pressure of the CO_2/alcohol exiting stream, which has a single supercritical phase, is reduced to atmospheric across the micro-metering valve, which results in the formation of liquid alcohol and CO_2 in the gas phase. This mixture is subsequently separated in the separator vessel, with the flowrate of CO_2 being monitored downstream by a rotameter. The alcogel is supercritically extracted at a desired pressure of approximately 3500 psig with a constant flow of CO_2, until no further alcohol is observed to be extracted from the separator vessel. After the extraction, the alcogel is dried at a temperature of 80 - 100 °C to remove surface water. As prepared, the metal oxide aerogels were white fluffy powders.[115, 124]

Using supercritical CO_2 as the extraction fluid in the extraction of alcohol from the alcogel is advantageous for a number of reasons. Carbon dioxide is inert to metal oxides, it is a good solvent for low molecular weight alcohols, it has a much lower critical pressure and temperature than alcohols, it is nonflammable, and it is relatively inexpensive. Iacobucci et al. mentioned that it is important to maintain the density of the supercritical CO_2 at about the same value as the density of the solvent being removed, since a small difference minimizes the surface tension acting on the walls and preserves a product with maximum surface area.[115] By varying the temperature and pressure in the extraction step, it is possible to vary the pore size and surface area of the resulting aerogels as shown in Figure 1-14.[124] In this research an intermediate pressure (~ 3000 psig) was used because high surface areas were produced with this pressure as shown previously, and also safety reasons prevented the use of higher pressures.

Silica and alumina aerogels have been shown to be quite stable to high temperature heat treatments.[24, 118] Also, typical results on heating from 500 °C to 1000 °C, showed that aerogels suffer area reductions of about 20%, while a xerogel suffers a corresponding

Figure 1-14: EFFECT OF EXTRACTION PRESSURE ON SURFACE AREA OF SILICA AEROGELS[124]
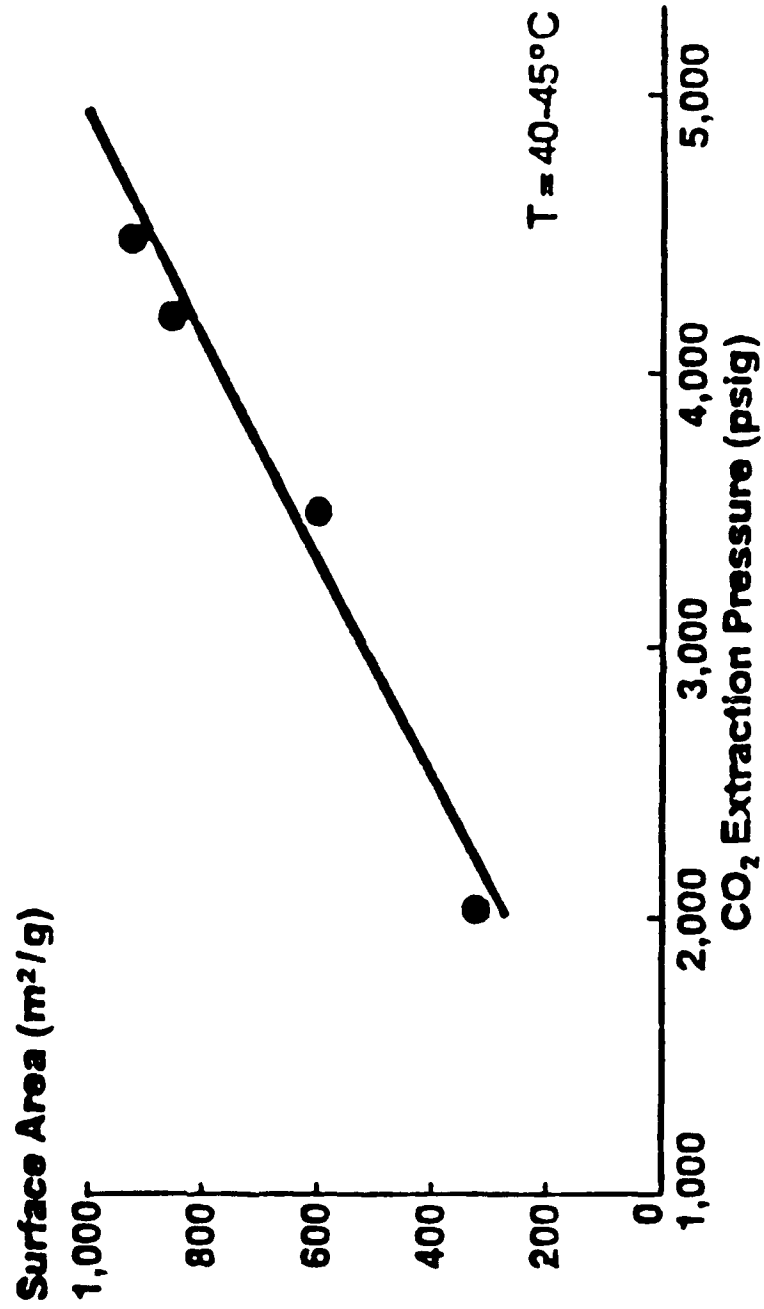
reduction of around 65%.[17] This stability is generally thought to arise from the rigid polymeric network that is maintained after the supercritical extraction.[118] It has recently been shown that mixed oxide aerogels can be prepared in very much the same fashion as the single oxide aerogels, since the sol-gel process allows practically any multicomponent material to be produced as long as the alkoxide precursors are soluble in an alcoholic solvent.[22, 24, 108, 112, 113, 115, 131] Better textural characteristics were also found for the mixed aerogels as compared with those of pure oxide aerogels.[24]

1.5.1 Aerogels as Catalysts

The very high surface areas and pore volumes of aerogels make them suitable candidates for catalysts and catalyst supports. Kistler had mentioned in his early work in the 1930's the possible applications of aerogels as catalysts.[117, 118] It was not until nearly 50 years later that their viability as catalysts or supports has actually taken hold.[24, 115, 125, 138, 139] Reasons for such a delay can only be explained by the great difficulty in first preparing these materials; however, current techniques as reviewed above make the synthesis of aerogels much easier.

One example of the use of a supported oxide aerogel is that for silica aerogel supported iron oxide (Fe_2O_3-SiO_2) and alumina aerogel supported iron oxide (Fe_2O_3-Al_2O_3).[139] These binary oxides are important catalysts for the Fisher-Tropsch process which is based on the hydrogenation of carbon monoxide over a reduced iron catalyst and yields a broad range of hydrocarbons from methane to gasoline and diesel oil fractions. These catalysts are even more important currently because of the search for secondary energy sources and the need to be self-sufficient in fuel. It was shown that iron oxide supported on silica or alumina aerogels exhibited activities for the above reaction two to three orders of magnitude greater than a conventionally reduced iron oxide catalyst on a per mass basis.[139] Also, the aerogel catalysts do not deactivate with time on stream. A palladium on alumina aerogel catalyst was also shown by Armor et al.[125] to be effective in

promoting the hydrogenation of nitrobenzene to aniline. These examples show the viability of aerogels to the current research of oxide catalysts. The next sections will discuss solid acids in general as well as the current theories of acidity.

1.6 Acid Strength and Acidity

Solid acids have been extensively used and studied as catalysts or catalyst carriers in the petroleum industry and organic syntheses for the past 50 years. Currently, acid catalyzed reactions are by far the most commercially important and include a wide range of reactions such as catalytic cracking, polymerization, alkylation, and isomerization.[4, 140] The use of solid acid catalysts provides the following advantages compared with the use of liquid acid catalysts:[1]

- High catalytic activity and selectivity are frequently observed;
- Corrosion in reactor vessels is minimal;
- Repeated use of the catalyst is possible;
- Separation of solid acid catalyst from reaction mixture is easy;
- Disposal of spent catalyst offers no environmental problems.

The importance of solid acids as catalysts has caused an extensive study of the acidic properties on catalyst surfaces, the structure of acid sites, and their catalytic action. For example, Rodenas et al. studied the surface and catalytic properties of TiO_2/Al_2O_3 and proposed hypotheses as to the structure of the acid sites.[141] Even more recently has it been found that niobia is a strong solid acid with a very high activity and selectivity in ethylene hydration as well as many other reactions.[142, 143, 144, 145] The study undertaken has also focused mainly on the acidic and catalytic properties of the materials and the nature of the surface acid sites.

A solid acid may be understood in simple terms as a solid which changes the color of a basic indicator, or as a solid on which a base is chemically adsorbed. More

specifically there are two types of acid sites found on solid acids. Brønsted acid sites have tendencies to donate protons, while Lewis acid sites accept electron pairs. The distinction between the two sites is important because the catalytic and acidic properties of these acid sites can be very different.

The properties of a solid acid can be described by the distribution of its acid strengths and acidity for each type of acid on the surface, Brønsted or Lewis. Walling defined the acid strength of a solid surface as the ability of the surface to convert an adsorbed neutral base to its conjugate acid.[146] The weaker the base, the stronger the acid must be to adsorb it. The number of acid sites on a solid surface (loosely referred to as acidity) is usually expressed in millimoles of acid sites per unit weight or surface area of the solid, and is obtained by measuring the amount of base which is required to neutralize the solid acid.[1, 147] In this research, the acidity of these materials was measured by n-butylamine titration with Hammett indicators following the procedure of Benesi.[148] To fully characterize a solid acid, the distribution of acid strengths and acidity for each type of acid sites, Brønsted and Lewis, must be known.[2]

1.7 Models of Acidity in Mixed Oxides

Most binary oxides are known to have surface acidities that are greater than the sum of the single component oxides which make up the chemical mixture. This generation of or synergistic effect in acidity can be explained in terms of Pauling's electrostatic valence rule.[149] This rule states that the local charge imbalances that result from the mixing of the oxides, are the reason that acidity develops in the mixture. Publications by Tanabe, Kung, and Seiyama have proposed predictive models for the formation of acid sites and acid types in mixed oxides which are extensions of Pauling's rule.[1, 150, 151] It is obvious that acidity can be predicted theoretically if the structure of the binary oxide is known. The structure determines the local coordination numbers and valences for the metal and oxygen ions and

thus the electrostatic charge distribution. Once one imposes bonding rules, the presence or absence of acidity can be predicted. These models will be separately discussed for clarity.

1.7.1 Tanabe's Model

Tanabe et al. developed a model which predicts what kinds of binary oxides will form acid sites and whether they will be of the Brønsted or Lewis type.[1] The acidity generation is caused by an excess of positive or negative charge in a model binary oxide structure. Excessive positive charge will produce Lewis acids through the creation of electron pair acceptor sites. Excessive negative charge will generate Brønsted acids through the association of protons with oxygens to neutralize the electronic charges. Tanabe's model structure has the following constraints:

- The coordination numbers (and valences) of both the major metal ion and minor metal ion components are maintained even when mixed.

- The coordination number (and valence) for the oxygen ion of the major metal ion component is retained for all the oxygen ions in the binary oxide.

Even with the above restrictions, Tanabe's hypothesis correctly predicted acidity generation in 90% of the chemically mixed oxides studied.[1]

An example of the application of this theory is demonstrated for the Nb_2O_5/Al_2O_3 mixed oxides. In pure niobia, the coordination numbers for oxygen and niobium are 2.4 and 6, respectively. In alumina, the coordination numbers for oxygen and aluminum are 4 and 6, respectively.[10] The charge distribution from each metal ion to the surrounding oxygens is assumed to be even and is thus equal to the total charge of the metal ion divided by its coordination number. Figures 1-15(A) and 1-15(B) show the cases when Nb_2O_5 is the major oxide, and when Al_2O_3 is the major oxide respectively. In the Nb_2O_5-rich environment, the three positive charges of aluminum are distributed to the 6 bonds, while the two negative charges of the oxygen atom are distributed to 2.4 bonds. Therefore, the charge difference at one bond is given by $(+3 / 6) + (-2 / 2.4) = -0.33$, and accounting for

Figure 1-15: TANABE'S ACIDITY MODEL FOR Nb_2O_5/Al_2O_3

A) Nb_2O_5 is the Major Oxide:

+2.0

(proton donor)

Brønsted Acid
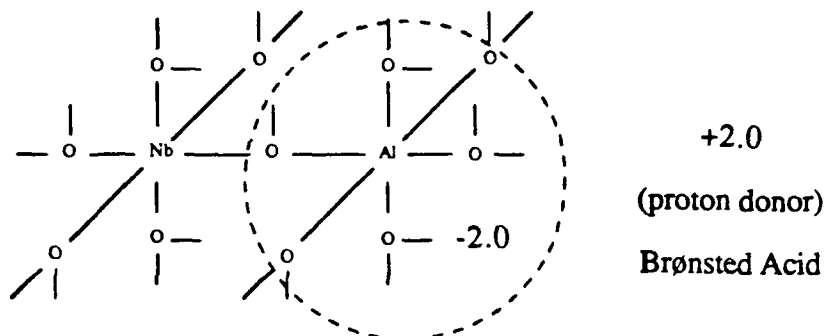
Coordination Numbers

O:	2.4
Nb:	6
Al:	6

Charge Difference Between Al - O: $(+3/6) + (-2/2.4) = -0.33$

Total Charge Difference Per Unit: $(-0.33) \times 6 = -2.0$

B) Al_2O_3 is the Major Oxide:

-2.0

(electron acceptor)

Lewis Acid
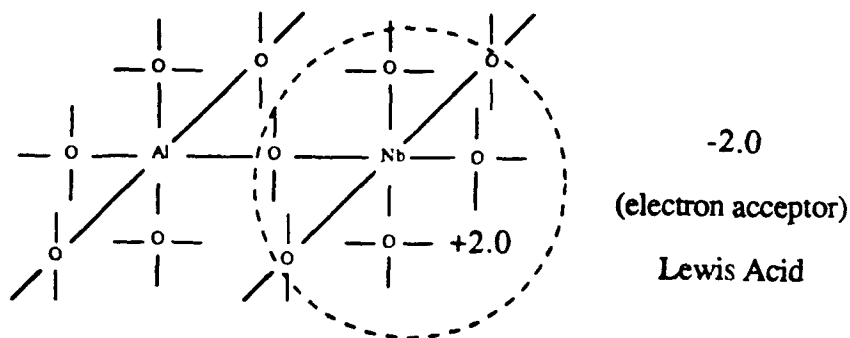
Coordination Number:

O:	4
Nb:	6
Al:	6

Charge Difference Between Nb - O: $(+5/6) + (-2/4) = +0.33$

Total Charge Difference Per Unit: $(+0.33) \times 6 = +2.0$

all bonds gives (-0.33) x 6 = -2.0 in excess. This excess of negative charge should result in Brønsted acidity, because protons are considered to associate with the oxygens in order to maintain charge neutrality. In the Al_2O_3-rich environment, the five positive charges of the niobium atom are distributed to 6 bonds, while the two negative charges of the oxygen atom are distributed to 4 bonds. Therefore, the charge difference for each bond is (+5 / 6) + (-2 / 4) = +0.33, and accounting for all 6 bonds gives (+0.33) x 6 = +2.0 in excess. In this case, the large excess of positive charge should result in Lewis acidity. As will be shown later, this Nb_2O_5/Al_2O_3 mixed oxide did indeed exhibit a very high acidity and acid strength, as well as Lewis acidity in particular.

1.7.2 Kung's Model

Kung has recently developed a predictive model for the acidity in dilute binary oxides by examining the effects of substituting a cation A into the matrix of an oxide BO_z.[150] The first effect deals with the substitutional A cation, and results from a different electrostatic potential for the A cation in the BO_z oxide matrix from that found for A in its pure oxide, AO_Y. When a substituted cation experiences a more negative potential than is found in its own lattice, the cation will become more electron deficient in its own matrix. Hence, it will be more likely to accept electrons and act as a Lewis acid. When there is a relatively positive potential surrounding the substituting ion, Kung's model predicts no local acidity.

The second effect deals with the differences in formal oxidation states between the substituting and the major oxide component cations. This difference in cation oxidation states creates charge imbalances in the mixed oxide matrix and in order to achieve neutrality, defects are created which can result in acidity. The substituting cation is assumed to have the same coordination number as the major component. When the oxidation state of A is less than that of B ($Y<Z$), a net negative charge results, and in order to balance this excess charge, a proton may be adsorbed onto an oxygen to form a Brønsted

acid. When the oxidation state of A is greater than that of B (Y>Z) a positive charge results which can be balanced by a cation vacancy, thus a Lewis acid site may be formed because cation vacancies are electron deficient.

When Kung's model is applied to the Nb_2O_5/Al_2O_3 system, Brønsted acidity is predicted in the matrix when niobia is the major oxide and Lewis acidity is possible at the alumina sites; however, Lewis acidity is predicted in the matrix when alumina is the major oxide (see Table 1-1). These predictions match almost identically with those of Tanabe's except that Lewis acidity is possible as well as Brønsted acidity when niobia is the major component. Kung's model also does equally well as Tanabe's at predicting acidity in other oxide systems. This is really not a surprise since both are based on Pauling's electrostatic valence rule. One downfall of Kung's model is that it is only applicable in the limit of dilute solution when substituting ions are far apart for the approximation of electrostatic potentials.

Table 1-1: KUNG'S ACIDITY MODEL FOR Nb_2O_5/Al_2O_3

Matrix Oxide BO_Z	Substituting Oxide AO_Y	CASE	Type of Acid Site At Substituting Ion	In Matrix
$NbO_{2.5}$	$AlO_{1.5}$	Y<Z	Lewis	Brønsted (maybe Lewis)
$AlO_{1.5}$	$NbO_{2.5}$	Y>Z	None	maybe Lewis

1.7.3 Seiyama's Model

Seiyama has presented a slightly different model for the generation of acidity in binary mixed oxides.[151] He assumed that acid sites form at the boundaries where two oxides come into contact. The assumptions he made are listed below:

- The coordination numbers (and valences) of each metal ion are maintained as that of the pure oxide.

- The coordination number (and valence) of each oxygen atom depends on the type of metal ion that oxygen is associated with. If the oxygen is associated with a single metal ion, it retains the coordination number found in that metal oxide. If oxygen is shared between different metal ions, then its coordination number is 2 (it must be on a phase boundary). See Figure 1-16.

Figure 1-16 SEIYAMA'S MODEL FOR ACIDITY GENERATION

charge difference: [(+5)/6 + (+3)/6] - 2 = -0.67
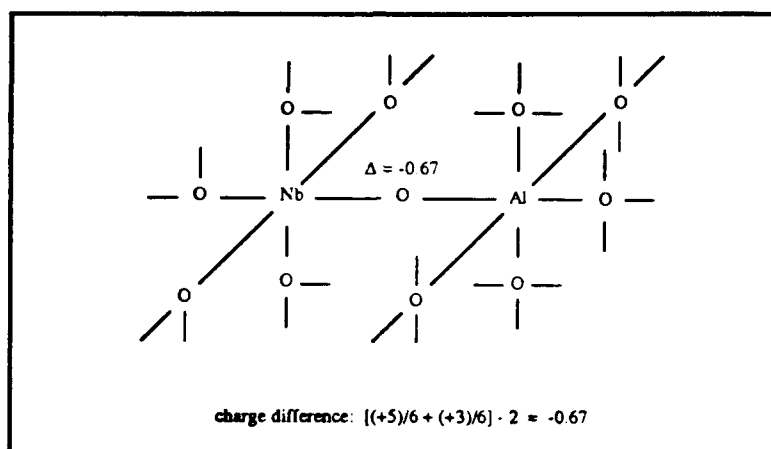
The Nb_2O_5/Al_2O_3 mixed oxide will contain an excessive negative charge of -0.67. The +5/6 charge of Nb and +3/6 charge of Al are distributed to the boundary oxygen which has 2 negative charges; therefore, the charge difference around the oxygen becomes -0.67, and Brønsted acidity is expected. This theory is limited to cases where phase boundaries comprise a large percentage of the binary oxide, while Tanabe's model can be applied to all amorphous binary oxides.

All three of the models mentioned above have their limitations. These models do not directly apply to surface properties; however, they do predict acidity from the bulk structures. Also, the assumptions made in the models in defining the structure are greatly simplified. There may be strains in the oxide lattices when a metal cation substitution takes place that may not allow configurations defined by Kung and Tanabe. These models work well, although they are simple, to offer a fundamental understanding of acidity.

1.8 Models of Acidity in Supported Oxides

1.8.1 Connell and Dumesic's Models

Connell and Dumesic's model is used to predict Lewis acid sites in the limit of dilute binary oxides where the major component controls the oxide structure and the dopant surface concentration controls the number of acid sites.[10] They used silica as the major oxide component and a variety of dopant cations for their study on Lewis acid generation. This model as well as all of the previous ones mentioned was based on Pauling's electrostatic valence rule. This model is subject to the following constraints:

- The local structure for the major component (oxide) is not dramatically altered by the addition of a minor component (oxide). The coordination numbers (and valences) of the major component metal ions and all oxygen ions are retained from those of the pure major component.
- The valence of the substituting metal ion is retained from that of the pure oxide.
- The doping cation can not easily form a solid solution or a crystalline mixed oxide, and also the doping cation must be bonded to the host oxide sufficiently strongly so that it does not sinter into particles of its own oxide.
- The host oxide must be acidic or at least not strongly basic.

The proposed model for Lewis acidity that gives the criterion for the existence of coordinatively unsaturated cations on the surface is as follows. One merely calculates the number of bonds required by the dopant cation to be electrically neutral in the host oxide. If this number is less than 4, Lewis acidity is predicted for the dopant cations that are on the surface of the oxide.[10] Thus, for example, oxygen has a coordination number of two in silica. The charge transfer along each cation to anion bond according to Pauling's rule is 2/2 or 1. Therefore, for a +2 cation on the silica surface, two bonds are required for charge neutrality, and this sample would be predicted to have Lewis acidity. For a +5 cation, such as Nb^{+5}, the number of bonds increases to five, and this material would not be predicted to have Lewis acidity, in contrast to what has been found.[88] This model does not predict Lewis acid strengths, but only predicts the existence of Lewis acids. Also, it merely states

that the *probability* of forming acid sites becomes greater as the predicted coordination number decreases.[10] This model only involves valence and coordination numbers of the metal cations on the silica surface, in accord with Pauling's electrostatic bond strength rules. Despite the simplicity of this model, it successfully predicted that all seven singly supported oxides studied by their group would generate Lewis acidity.[11] The predicted generation of Brønsted acid sites for supported oxides on silica was the subject of a second model. This model predicts ionic Brønsted acid sites only for +3 cations occupying a tetrahedral site on the surface of silica.[11] Pauling's electrostatic bonding model predicts the generation of a -1 charge with this structure, which might be balanced (for charge neutrality) by a proton, thus creating a Brønsted acid site. The model works well for the systems they studied and also for systems where the cation is easily incorporated into the tetrahedral structure as a result of its charge, size, and bonding characteristics.[11] However, many supported oxide systems can not meet these requirements and acidity is incorrectly predicted not to occur. Kataoka and Dumesic addressed these issues in another model designed to better predict Brønsted acidity.

1.8.2 Kataoka and Dumesic's Model

The model by Kataoka and Dumesic is developed around the fact that it is the coordinatively undersaturated oxygens in oxides which serve as Brønsted acid sites.[152] The authors applied the concepts developed in Pauling's electrostatic bonding rule to locate oxygens that would fall into a certain range of undersaturation, in terms of Pauling's valence units (v.u.) or electron charges. Oxygens which fall in the range of undersaturation of 0.1 to 0.4 v.u. can serve as Brønsted acid sites. Their model will be illustrated for silica-supported alumina, in which the coordination number of Al is 4. For alumina in this coordination, the valence units per bond is equal to +3 cation charge divided by 4, or 0.75. For silica the valence units per bond are +4/4, or 1. Thus, with this model a Al-O-Si bond will have an undersaturation of -[+1 (silica) + 0.75 (alumina) + (-2)

(oxygen)] = 0.25. Their model states that an undersaturated oxygen in the range of 0.1 to 0.4 will act as a Brønsted site, and thus predicts that a hydrogen atom will bond with the oxygen on a Al-O-Si bond to become a Brønsted acid site. Also, hydrogen at the terminal hydroxyl groups, Al-O-H, will be undersaturated with a valence unit undersaturation of -(-2 + 0.75) = 1.25, hence these hydrogens will be strongly bonded to the oxygens in this arrangement. This model was extended and used to analyze the undersaturation of oxygens in pure oxides, vanadia and molybdena in particular. From their calculations and experimental findings, they attributed the origins of Brønsted acidity in both of these pure bulk oxides to the undersaturated oxygen-metal double bonds.

1.8.3 Burke's Model

The model by Burke is developed with the aid of Pauling's electrostatic bond rules.[88] It allows the incorporation of doubly bonded oxygens and predicts enhanced *Lewis acidity for dispersed oxides on silica*. Unlike Connell and Dumesic's model, which predicts Lewis acidity if the coordination number of the cation is less than 4, Burke's model is used for supported oxide systems of coordination numbers greater than 4.[88] Basically, his model states that enhanced Lewis acidity is predicted if the pure oxide already has Lewis acidity and its structure is distorted by the supporting oxide, which is almost always the case if the oxide is dispersed evenly at a coverage of a monolayer or less. The reason behind this model is that the *distorted structure* of the supported oxide creates a more accessible cation. In accord with the other models discussed, certain guidelines must be followed. In addition, certain rules are issued which help screen for unrealistic structures:[88]

- Coordination numbers of the supported cations are even, as is required for most stable bonding environments.
- Coordination numbers of the supported oxide is never greater than the valence of the cation + 1 (not applicable to complex surface structures, which are not considered disperse). This criterion accounts for charge neutrality as prescribed

by Pauling's rules, unrealistic separation of charge, and unrealistic oxygen bonding.

- No change in coordination number of the supported oxide cation can occur with proton donation (Brønsted acid) as such a complicated process is unlikely.
- The number of surface linkages per supported oxide cation must be at least 1 and not greater than 3, for geometric reasons.

The appearance of Lewis acidity for supported transition metal oxides of coordination 4 or higher which have intrinsic acidity (Nb, Ta, Cr, Mo, and W) is predicted as likely, and is predicted as possible for amphoteric oxides (Ti, Zr, Al, V, Co).[153] An example of this model will be given for a +6 supported cation with coordination 4 (see Figure 1-17). Hydroxyl groups and silica linkages each provide a formal charge of -1 to the cation, while doubly bonded oxygens supply -2. To satisfy charge neutrality the system must have 2 doubly bonded oxygens and either 2 silica linkages or one silica linkage and one hydroxyl group. With a coordination of 4, the cation should be accessible and function as a Lewis acid. The second figure which has a hydroxyl group adjacent to 2 doubly bonded oxygens should be a strong Brønsted acid, as outlined by Bernholc et al.[12] This Brønsted acidity comes about because the doubly bonded oxygens act to distribute the negative charge associated with the donation of a proton from the hydroxyl group. The number of surface linkages can vary from 1 to 3 without significant changes in structure other than the distortions in the supported oxide species, and the electron withdrawing effects of the silica support increase with more surface linkages. The larger the number of surface bonds, the greater the possible enhancement in Lewis acidity, i.e. the more distortion that is possible.

This model can be applied to the current system being studied, i.e. supported niobia binary oxides. It is proposed that at low coverages, 0.25 and 0.50 monolayers, niobia on silica predominantly contains niobium in a tetrahedral environment.[80, 84, 88, 90, 93] From Burke's model, for a +5 cation with a coordination number of 4, enhanced Lewis acidity is expected and Brønsted acidity should result due to the doubly bonded oxygen adjacent to the hydroxyl [see Figure 1-18(A)]. This is exactly what was found experimentally.[84, 88] For niobia on alumina at low coverages, it is also proposed that the niobium cations are

Figure 1-17: POSSIBLE STRUCTURES FOR A +6 CATION HAVING A
COORDINATION NUMBER OF 4

2 Surface Linkages   1 Surface Linkage
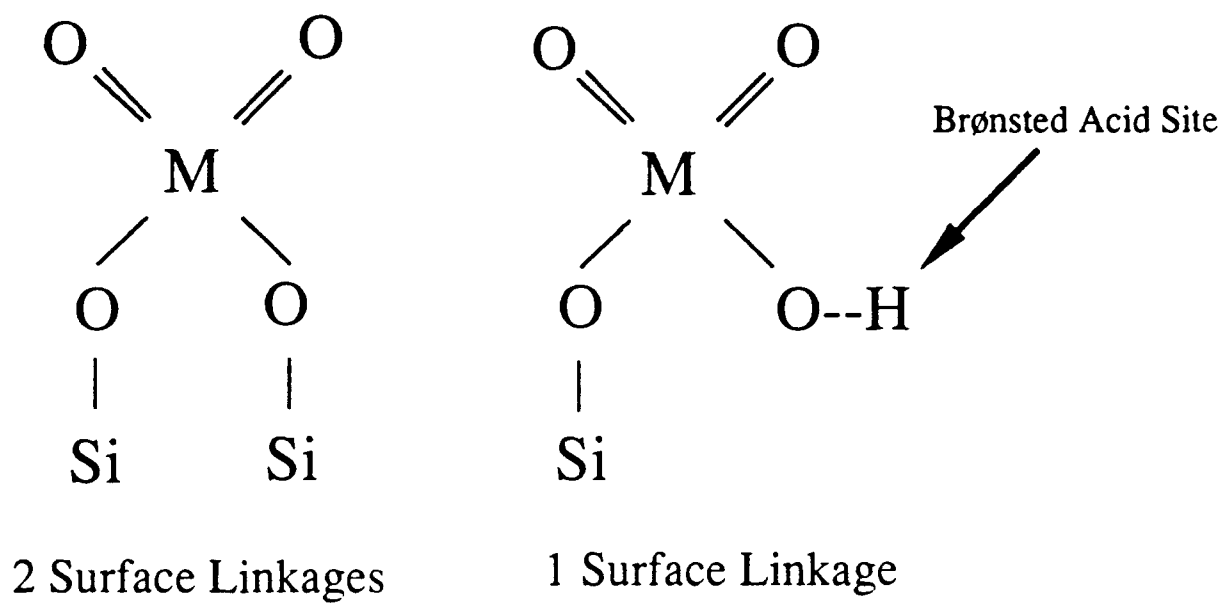
Figure 1-18: A) POSSIBLE STRUCTURE FOR NIOBIA ON SILICA (BRØNSTED
ACIDITY) AND B) POSSIBLE STRUCTURE FOR NIOBIA ON
ALUMINA (ENHANCED LEWIS ACIDITY)
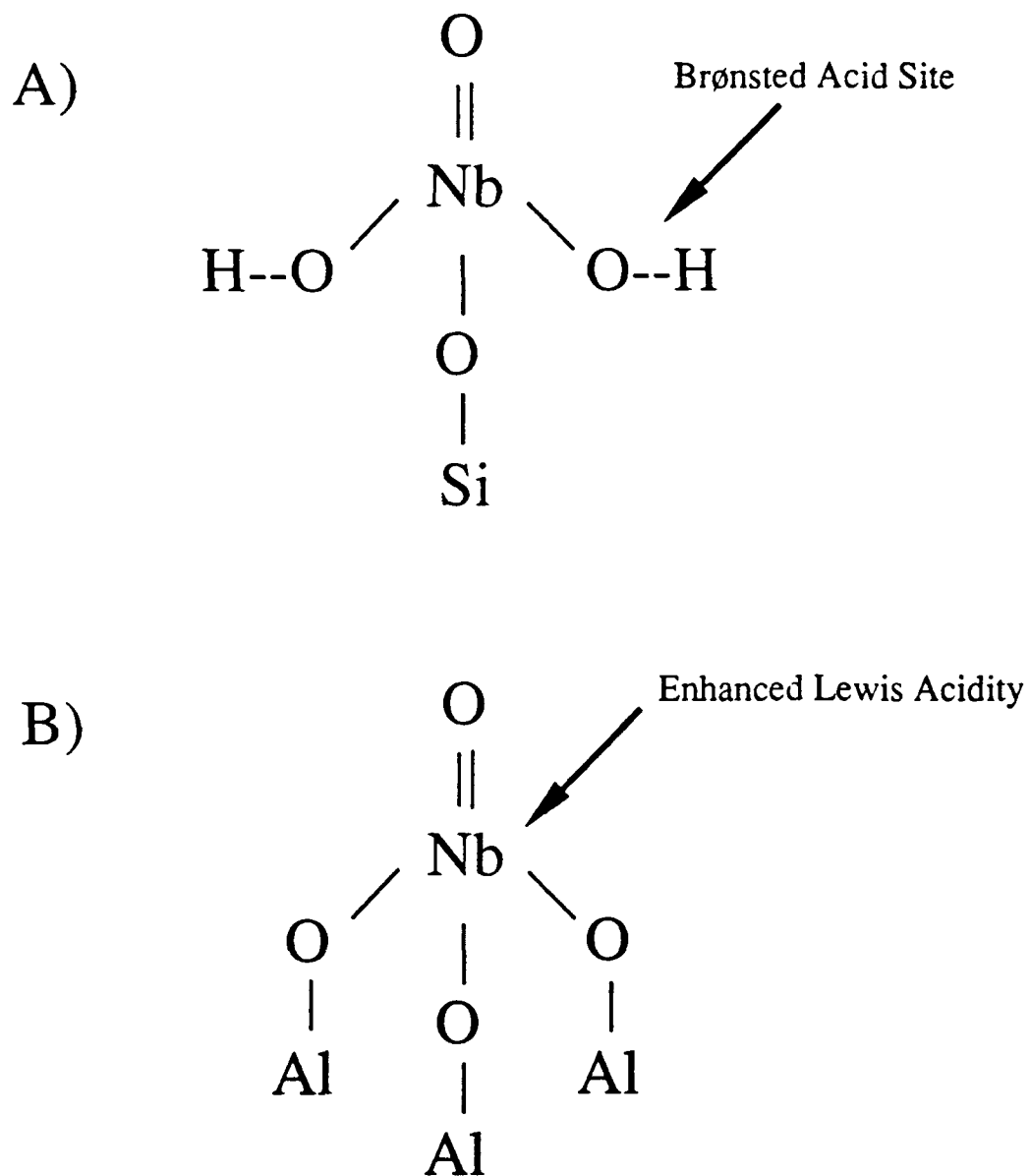
predominantly in a tetrahedral environment.[80, 92, 93] For a +5 cation with a coordination number of 4, enhanced Lewis acidity is predicted as explained above. This sample has indeed been found to possess only Lewis acidity at these low coverages with no Brønsted acidity. Thus, no terminal OH groups are in this structure which must lead to three Nb-O-Al bonds anchoring this niobia species to the alumina surface as shown in Figure 1-18(B). This structure should lead to even greater enhancement of Lewis acidity, because of the extra distortion involved in the extra surface linkages.

1.9 Summary

The goal of this thesis is to examine the mixed and supported binary oxide systems containing niobia. This work will explore how the structures of the binary oxides affect the chemical properties of these materials. The first part of the thesis concentrates particularly on the structure/property relationships of niobia. The preparation of niobia aerogels and their properties as a function of changing niobium cation environment are closely monitored and compared to those of more conventionally prepared niobia. This is the focus of Chapter 3. With this basic understanding of niobia, the chemical/physical properties and structures of binary oxides are examined for two different oxides as the major component, silica and alumina. The mixed oxide aerogels of niobia/silica and niobia/alumina are compared to their more conventionally prepared counterparts. Their physical properties were closely examined as a function of structure by inducing crystallization or compound formation with different heat treatments, and are discussed in Chapter 4. Various probe molecules were also used to determine acid strength, acidity, and distribution of acid sites for the binary oxides. Chapter 5 discusses the silica or alumina aerogel supported niobia binary oxides. These materials were investigated to determine the level of dispersion in these oxides and to monitor how the structure of the surface phase oxide evolves with increasing coverage of niobia. These various structural modifications were also studied as

a function of temperature and correlated to their physico-chemical properties. Chapter 6 discusses the proposed structures of these two binary oxide systems and attempts to bridge the gap in the understanding of these materials that will lead to further development of catalysts through a better understanding of oxide-oxide interactions. Thus, this thesis will offer a unique perspective on the role and evolution of structure and how this structure in turn relates to the key physical and chemical properties in binary oxide aerogels containing niobia.

Chapter 2

EXPERIMENTAL

This chapter deals with the procedures and experimental equipment used to carry out the research presented in this thesis. The first part of this chapter concentrates on the preparation of the oxide catalysts. The second part presents an overview of the experimental techniques and procedures used to characterize the structures and chemical properties of these oxides.

2.1 Preparation of Bulk Oxide Aerogels

The synthesis of aerogels was undertaken for the bulk oxides of Nb_2O_5, SiO_2, and Al_2O_3. Whatever the desired material, there are generally two major steps that must be accomplished in order to produce a good aerogel. First, one must be able to hydrolyze the appropriate precursor to a sol which then forms a gel, and second, one must supercritically extract the solvent-ladened gel. Figure 2-1 shows the various steps in a typical sol-gel process with inorganic metal alkoxides as precursors. Even though the same procedure can be used to prepare single and binary component oxides, the process parameters necessary to gel these materials are often different and need to be established empirically. The preparations for single oxide aerogels will be discussed in this section.

Figure 2-1: THE SOL-GEL PROCESS SHOWN FOR A TWO-COMPONENT SYSTEM

$$M(OR)_n + M'(OR')_{n'}$$

solvent (additives)

Heterometallic alkoxide
(homogeneous solution)

H_2O
(hydrolysis/polymerization)

Sol

destabilization

Gelled Mass (porous)

Conventional Drying
"Xerogel"

Supercritical Extraction
"Aerogel"
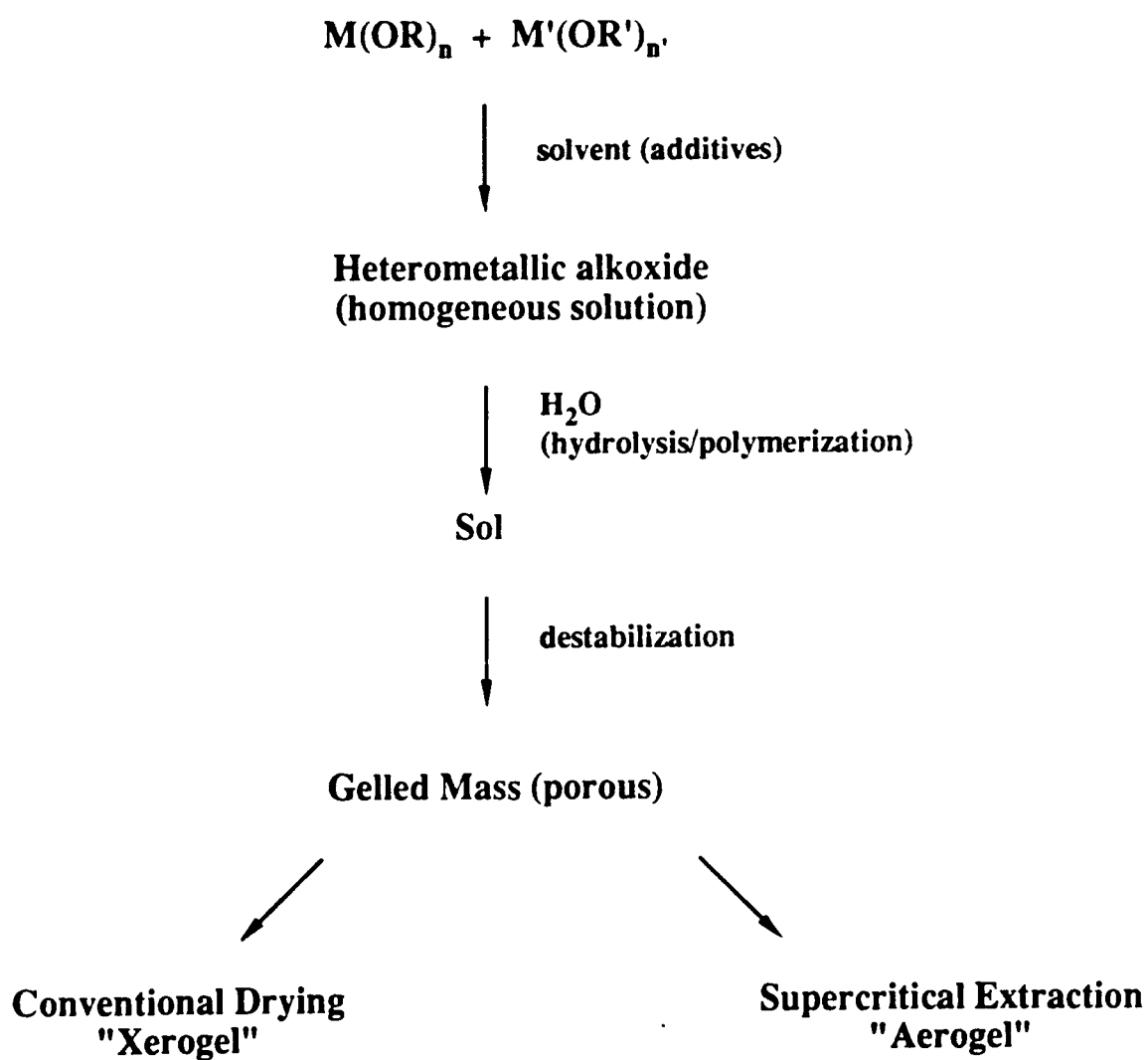
2.1.1 Niobia Aerogel

Niobia aerogels were prepared by dissolving the precursor, niobium(V) ethoxide [Nb(OC$_2$H$_5$)$_5$, Alfa], in either s-butyl alcohol (99+% anhydrous, Aldrich) or methyl alcohol (99.9% anhydrous, Fisher). This solution was then quickly added to a well mixed solution of s-butyl alcohol or methyl alcohol, respectively, doubly deionized water (enough added to insure complete molar stoichiometric hydrolysis), and nitric acid (70%, Fisher) to catalyze the hydrolysis and condensation reactions.[114] The resulting solution gelled within a range of seconds to minutes depending on the concentrations and conditions used. See Table 2-1 for the exact procedure and conditions used in the niobia sol-gel process. Initial estimates for the gelation conditions were derived on the basis of literature data.[129]

Once the niobia gel had been prepared, the second major step was to supercritically extract the solvent from the gelled mass in a standard autoclave (Autoclave Engineers, model #08U-06-60FS).[154] A schematic for this apparatus is shown in Figure 2-2. Basically, the solvent-ladened gel was placed in the extractor vessel and contacted by CO_2 (with syphon tube, Airco) above its critical temperature and pressure (T_c = 31 °C, P_c = 1070 psi).[155] This supercritical fluid was then allowed to flow through the sample until the solvent was no longer being extracted with the supercritical CO_2. This was determined by the lack of collection (over a 30 minute period) of the alcohol phase from the separator vessel. The extractor vessel temperature used was 70 °C and the pressure was 3000 psi, both well above the critical values for CO_2. The CO_2 flowrate through the system was 0.05 SCFM. The normal duration of the extraction process was approximately 3 hours to insure that no alcohol or excess water was contained in the niobia aerogel. After the extraction was complete, the unit was depressurized isothermally at approximately 100 psi/min while maintaining the temperature (70 °C) above the critical value for the CO_2. This was done to insure that the supercritical fluid would change over to a gas in the solid matrix and not a liquid, so as to avoid any vapor-liquid interfaces in the oxide aerogel which may possibly collapse the network. The resulting inorganic material produced was a

Table 2-1: EXPERIMENTAL PROCEDURE AND CONDITIONS FOR NIOBIA
AEROGEL AND XEROGEL SYNTHESIS

NIOBIA GELATION CONDITIONS: $[Nb(OC_2H_5)_5]$

	Molar Ratios		
Nb^{5+} (mmole Nb/50 ml s-BuOH)	H_2O/Nb^{5+}	HNO_3/Nb^{5+}	Result
0.5	10.0	0.8	Gelled upon addition of H_2O and HNO_3

PROCESS	STEPS AND CONDITIONS OF PROCEDURE
DISSOLUTION	1. Add required amount of niobium (V) ethoxide to 25 ml of s-BuOH or MeOH 2. Add required amount of deionized H_2O and HNO_3 to a second 25 ml of s-BuOH or MeOH 3. Stir both beakers for 10 minutes to homogenize
REACTION	1. Let both beakers stir under constant mechanical agitation 2. Add acidified water/alcohol to niobia solution (niobia sol) 3. Let hydrolyze and polymerize over time
AGING	1. Allow to set into firm gel that will not flow 2. Typical setting times are on the order of 1 hour
DRYING	1. Supercritically extract using CO_2 at T=70 °C, P=3000 psi, F=0.05 SCFM for 3 hours (Aerogel) 2. OR Heat in vacuum oven for 3 hours at 110 °C (Xerogel)
CALCINING	1. Heat in N_2 (300 cc/min) at 400 °C for 2 hours 2. Heat in O_2 (300 cc/min) at 500 °C for 2 hours

Figure 2-2: SCHEMATIC OF SUPERCRITICAL EXTRACTION UNIT

Flow Meter

Vent

Liquid Phase

Separator Vessel

Heat Source

Critical Phase

Extractor Vessel

Back Pressure Regulator

Pump

Vent

CO$_2$ Cylinder

Autoclave Engineers, Inc.
Model #: 08U-06-60FS
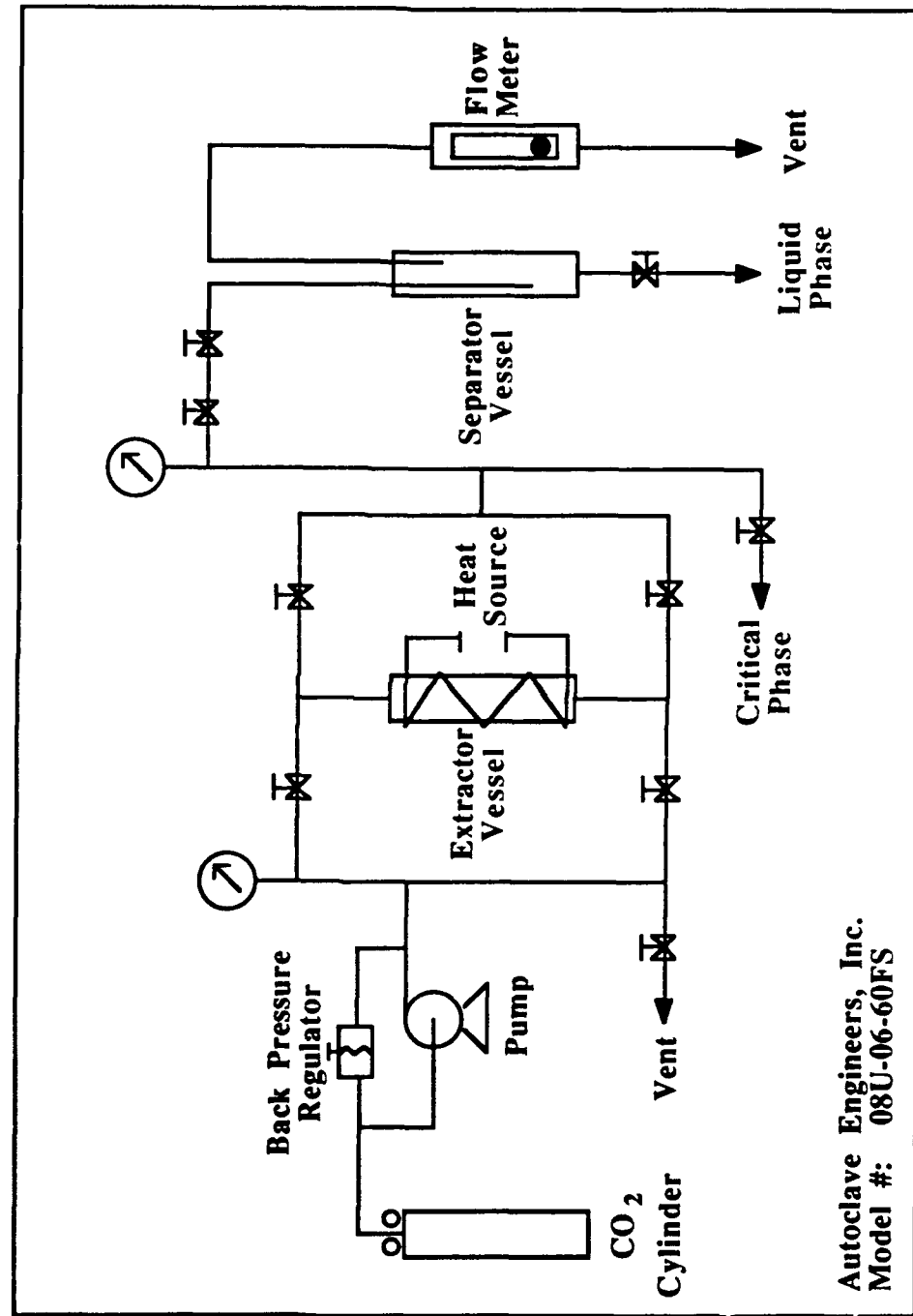
solid, dry, extremely light and granular material that was easily sifted into a mesh size >100. This material was then subjected to the standard calcination procedure which consisted of heating the niobia aerogel in N_2 (300 cc/min) at 400 °C for 2 hours to decompose any impurities that may be present, and then calcined in O_2 (300 cc/min) at 500 °C for 2 hours to fully oxidize the sample. The resulting oxide was cooled to room temperature, with no hold at 500 °C, under a reduced O_2 flow (50 cc/min), and then placed in vials, labelled, and stored in a dessicator for future experiments. These niobia aerogel samples are denoted as A-Nb_2O_5 (see Table 2-2 for nomenclature).

Two other conventional Nb_2O_5 samples were prepared for comparison with the aerogel. A precipitated sample, denoted as P-Nb_2O_5, was made by adding ammonium hydroxide (28 wt.% NH_3, Fisher) dropwise to a methanolic solution of niobium(V) ethoxide. The precipitate was washed and filtered to remove any impurities. The resulting filter cake was dried in a vacuum oven at 110 °C for 3 hours (see Table 2-3 for procedure). A xerogel, denoted as X-Nb_2O_5, was made by bypassing the supercritical extraction step in the synthesis of the aerogel. This gel was dried by heating in a vacuum oven at 110 °C for 3 hours (see Table 2-1 for procedure). Both of these materials, P-Nb_2O_5 and X-Nb_2O_5, were ground to a mesh >100 and subjected to the standard calcination procedure as mentioned above.

2.1.2 Silica Aerogel

Silica prepared by the sol-gel technique, is one of the most widely studied gelation reactions.[15, 16, 24, 115, 117-119, 124, 134, 135, 137, 139, 156] Its slow rate of polymerization makes it amenable to kinetic study, and it is easily gelled by either of three mechanisms: acid catalyzed condensation, base catalyzed condensation, or a 2-step acid-base catalyzed reaction.[16, 156] This work used the last mechanism for its flexibility in establishing gelation times and rates. The silica precursor, $Si(OC_2H_5)_4$ (Aldrich), was initially dissolved in sec-butyl alcohol. This solution was then added slowly to a well-stirred

Table 2-2: NOMENCLATURE USED TO DESCRIBE SYNTHESIZED BULK
OXIDES

BULK OXIDES

Notation	Description
A-Nb_2O_5	Aerogel-Bulk Niobia
X-Nb_2O_5	Xerogel-Bulk Niobia
P-Nb_2O_5	Precipitated-Bulk Niobia
A-SiO_2	Aerogel-Bulk Silica
X-SiO_2	Xerogel-Bulk Silica
A-Al_2O_3	Aerogel-Bulk Alumina

Table 2-3: EXPERIMENTAL PROCEDURE FOR PRECIPITATED NIOBIA

PROCESS	STEPS AND CONDITIONS OF PROCEDURE
DISSOLUTION	1. Add 75 grams niobium (V) ethoxide to 2000 ml MeOH 2. Stir for 10 minutes to homogenize
REACTION	1. Let beaker stir under constant mechanical agitation 2. Add NH_4OH dropwize until solution pH=7 3. Let precipitate settle overnight
FILTERING	1. Decant excess methanol 2. Use mechanical pump to aid in filter process
WASHING	1. Wash with deionized water 2. Agitate filter cake until a homogeneous solution results and repeat filter process 4 - 5 times
DRYING	1. Heat in vacuum oven for 3 hrs at 110 °C
CALCINING	1. Heat in N_2 (300 cc/min) at 400 °C for 2 hours 2. Heat in O_2 (300 cc/min) at 500 °C for 2 hours

mixture of sec-butyl alcohol, doubly deionized water (enough added for complete molar stoichiometric hydrolysis to occur), and a catalytic amount of acid, HNO_3, to promote the hydrolysis reactions. Note that without the addition of HNO_3 in this step, a gel would form, but it would require a longer time (~ 3 months). Then NH_4OH (~ 1.4 ml) was added to this well mixed solution until a neutral pH of 7 was reached - resulting in a gelled material that could not be stirred (see Table 2-4).[157, 158] It was at this point (pH = 7) where the condensation reactions proceeded the fastest and thus gelled the silica in a shorter time (~ 10 minutes).[16, 130, 156] Table 2-4 gives the exact conditions and concentrations used in the synthesis.

Next as with the niobia aerogel, the solvent was extracted supercritically from the rubbery silica gel. The extraction temperature (T = 70 °C), pressure (P = 3000 psi), and flowrate (F = 0.05 SCFM) for silica aerogels were identical to those for the niobia aerogels. The extraction process took about 2 hours to completely remove all liquid from the gel network, and the resulting dry inorganic solid that emerged was a light (slight bluish tint), granular material that was easily ground into a mesh >100. The silica aerogel was calcined in a similar fashion as above.

2.1.3 Alumina Aerogel

The preparation of alumina gels can proceed by a number of methods, most of which are as well known as those used in preparing silica.[24, 117, 159, 160] Within the past twenty years a very promising new procedure, pioneered by Yoldas, has emerged that makes it possible to obtain clear homogeneous gels.[20, 21, 22, 23, 161] This method basically consisted of hydrolyzing an aluminum alkoxide, $Al(OR)_3$, normally aluminum sec-butoxide, in a large excess of water at 80 - 100 °C, resulting in the precipitation of fibrillar boehmite, which was then followed by peptization with HNO_3, yielding a stable particulate sol. Gelation was achieved by concentration of the sol by evaporation.[21] These materials, however, tend to have low surface areas. Thus, the method employed in this

Table 2-4: EXPERIMENTAL PROCEDURE AND CONDITIONS FOR SILICA
AEROGEL AND XEROGEL SYNTHESIS

SILICA GELATION CONDITIONS: [$Si(OC_2H_5)_4$]

Molar Ratios

Si^{4+} (mmole Si/50 ml s-BuOH)	H_2O/Si^{4+}	HNO_3/Si^{4+}	Result
1.0	4.0	0.15	Gelled upon addition of NH_4OH

PROCESS	STEPS AND CONDITIONS OF PROCEDURE
DISSOLUTION	1. Add required amount of $Si(OC_2H_5)_4$ to 30 ml s-butanol 2. Add required amount of deionized H_2O and HNO_3 to another 20 ml s-butanol 3. Let both solutions stir separately to homogenize
HYDROLYSIS	1. Mix the two solutions to start hydrolysis reactions 2. Allow 10 minutes to equilibrate
CONDENSATION	1. Add NH_4OH to polymerize silica sol 2. Add until solution pH is 7
AGING	1. Allow sol to continue stirring while gellation occurs (typically ~ 5 min) 2. Set aside to form visco-elastic gel (typically ~ 1 hour)
DRYING	1. Supercritically extract using CO_2 at T=70 °C, P=3000 psi, F=0.05 SCFM for 2 hours (Aerogel) 2. OR Heat in vacuum oven for 3 hours at 110 °C (Xerogel)
CALCINING	1. Heat in N_2 (300 cc/min) at 400 °C for 2 hours 2. Heat in O_2 (300 cc/min) at 500 °C for 2 hours

research was that of Teichner.[24, 120, 160] The alumina precursor, $Al(OC_4H_9)_3$ (Alfa), was dissolved in sec-butyl alcohol. This solution was added very slowly to a well mixed amount of sec-butanol, doubly deionized water (enough added for complete molar stoichiometric hydrolysis to occur), and a catalytic amount of acid, HNO_3, to promote the condensation reactions. This procedure resulted in the formation of a soft gel. See Table 2-5 for exact conditions of the gelation parameters.

Next, this gel was supercritically extracted in a similar fashion to the other synthesized aerogels. The extraction temperature (150 °C) was higher than in other runs in order to facilitate the extraction process. The length of the extraction run was extended to 3 and sometimes even 4 hours to insure all liquid had been extracted. The time for the extraction was longer because of the difficulty in extracting the alumina gel and also to insure that the resulting aerogel was completely dry. The resulting dry white powdery solid was easily ground to a mesh >100. This alumina aerogel was then subjected to the standard calcination procedure.

2.2 Preparation of Binary Oxides

A binary oxide is an oxide resulting from the combination of two pure oxides. There are two primary ways of combining two different oxides: first, mixing the two oxides in the bulk resulting in a homogeneous mixed oxide, and second, grafting the second oxide onto the surface of a supporting oxide. The next few sections describe the procedure used to synthesize these materials.

2.2.1 Niobia/Silica and Niobia/Alumina Mixed Oxide Aerogels

The precursors used to prepare the mixed oxide aerogels were the same materials used in preparing the individual bulk oxides. The two mixed oxide aerogels will be separately discussed since they were synthesized in slightly different fashions.

76

Table 2-5: EXPERIMENTAL PROCEDURE AND CONDITIONS FOR ALUMINA
AEROGEL SYNTHESIS

ALUMINA GELATION CONDITIONS: [Al-s-(OC$_4$H$_9$)$_3$]

	Molar Ratio		
Al^{3+} (mmole Al/50 ml s-BuOH)	H$_2$O/Al^{3+}	HNO$_3$/Al^{3+}	Result
1.0	3.0	0.04	Gelled upon addition of Al-s-(OC$_4$H$_9$)$_3$

PROCESS	STEPS AND CONDITIONS OF PROCEDURE
DISSOLUTION	1. Add required amount of Al(OC$_4$H$_9$)$_3$ to 35 ml s-butanol 2. Add required amount of deionized H$_2$O and HNO$_3$ to 15 ml s-butanol 3. Let both solutions stir separately to homogenize
REACTION	1. Add the Al-s-(OC$_4$H$_9$)$_3$ solution dropwize to the acidified deionized water solution 2. Continue adding until a soft gel results
AGING	1. Allow to set into viscous gel that will not easily flow 2. Typical setting times were one hour
DRYING	1. Supercritically extract using CO$_2$ at T=150 °C, P=3000 psi, and F=0.05 SCFM for 3 hours
CALCINING	1. Heat in N$_2$ (300 cc/min) at 400 °C for 2 hours 2. Heat in O$_2$ (300 cc/min) at 500 °C for 2 hours

For the niobia/silica mixed oxide the silica precursor, $Si(OC_2H_5)_4$, was diluted with MeOH and added to a methanolic solution of doubly deionized water and nitric acid and allowed to hydrolyze. This solution was titrated with NH_4OH until the pH of the clear solution was 6 in order to increase the rate of the condensation reactions.[22, 156] Next, the niobia precursor, $Nb(OC_2H_5)_5$, was diluted with methanol and added to a methanolic solution of deionized water and nitric acid. This niobia sol was then quickly added to the titrated silica sol, resulting in a light clear-yellow niobia/silica sol. To this mixed oxide sol, diluted NH_4OH in MeOH (1/10 parts by volume) was added until the solution pH was 7. The resulting solution was allowed to sit for about 10 minutes at which point a firm gel was obtained (see Table 2-6 for detailed procedure). This gel was subsequently extracted supercritically with the standard operating conditions ($T = 70\ °C$, $P = 3000$ psi, $F = 0.05$ SCFM). The resulting aerogel was ground to a mesh >100 and calcined with the standard procedure as above. Table 2-7 shows the exact conditions used in the gelation of this material.

For the niobia/alumina mixed oxide, the procedure was slightly different from the above method since the condensation rate of the silica was increased for the niobia/silica system, whereas for the niobia/alumina system the polymerization rate of the niobia was increased. In both of these procedures the slowest hydrolyzing alkoxide was first rendered to an active polymerizing species, while the fast hydrolyzing alkoxide is kept in its original form so that self polymerization cannot occur.[22] This procedure results in greater homogeneity of the gel.[22] In the preparation of the niobia/alumina mixed oxide the niobia precursor, $Nb(OC_2H_5)_5$, was diluted with sec-butanol and added to a solution of sec-butanol, doubly deionized water, and nitric acid. This niobia sol was allowed to stir for 10 minutes (in order to allow partial hydrolysis to occur) at which point the alumina precursor, $Al(OC_4H_9)_3$, diluted with sec-butanol, was added to this solution. This niobia/alumina sol stirred for 10 minutes, and then deionized water was added for the completion of the alumina hydrolysis reactions. After 1 minute, the sol condensed into a thick gel that did not

Table 2-6: EXPERIMENTAL PROCEDURE FOR NIOBIA/SILICA MIXED OXIDE
AEROGEL (A-NS25w) SYNTHESIS

PROCESS	STEPS AND CONDITIONS OF PROCEDURE
DISSOLUTION	1. Add required amount of $Si(OC_2H_5)_4$ to 35 ml MeOH 2. Add required amount of $Nb(OC_2H_5)_5$ to 10 ml MeOH 3. Add required amount of deionized water and HNO_3 (for the niobia hydrolysis reaction) to 5 ml MeOH 4. Allow all three solutions to stir for 10 minutes
HYDROLYSIS	1. Add required amount of deionized water and HNO_3 to silica solution 2. Let stir for 10 minutes 3. Add NH_4OH to this solution until pH=6 (silica sol) 4. Mix acidified water (for niobia hydrolysis) into the niobia solution (niobia sol) 5. Quickly mix the niobia sol into the silica sol under vigorous stirring (niobia/silica sol)
CONDENSATION	1. Add diluted NH_4OH to the mixed niobia/silica sol until solution pH=7 2. Continue vigorous agitation after addition
AGING	1. Mixed sol will gel after approximately 10 minutes 2. Set aside to form visco-elastic gel (typically ~ 1 hr)
DRYING	1. Supercritically extract using CO_2 at T=70 °C, P=3000 psi, F=0.05 SCFM for 2 hours (Aerogel)
CALCINING	1. Heat in N_2 (300 cc/min) at 400 °C for 2 hours 2. Heat in O_2 (300 cc/min) at 500 °C for 2 hours

Table 2-7: GELATION CONDITIONS USED IN THE SOL-GEL PROCESS FOR THE MIXED BINARY OXIDES OF NIOBIA/SILICA AND NIOBIA/ALUMINA

NIOBIA/SILICA (NS25w): [Nb(OC$_2$H$_5$)$_5$ and Si(OC$_2$H$_5$)$_4$]

(mmole/50 ml MeOH)		Molar Ratio		
Nb^{5+}	Si^{4+}	H$_2$O/(Nb+Si)	HNO$_3$/(Nb+Si)	Result
0.15	1.0	4.1	0.40	Gelled upon addition of NH$_4$OH

NIOBIA/ALUMINA (NA25w): [Nb(OC$_2$H$_5$)$_5$ and Al-s-(OC$_4$H$_9$)$_3$]

(mmole/50 ml s-BuOH)		Molar Ratio		
Nb^{5+}	Al^{3+}	H$_2$O/(Nb+Al)	HNO$_3$/(Nb+Al)	Result
0.15	1.2	2.1	0.28	Gelled upon addition of H$_2$O

flow (see Table 2-7 for conditions and Table 2-8 for procedure). As with all previous gels, this niobia/alumina gel was supercritically extracted with the standard pressure (P = 3000 psi) and flow (F = 0.05 SCFM) conditions, but with a higher temperature (T = 150 °C) in order to facilitate the extraction process. The extraction typically lasted 3 hours resulting in a dry aerogel which was easily ground to a mesh >100, and calcined according to the standard procedure as above.

2.2.2 Precipitated Niobia/Silica and Niobia/Alumina Mixed Oxides

Conventionally prepared mixed oxides (precipitated) were prepared for later comparisons with the mixed oxide aerogels. The procedure for forming a homogeneous oxide (atomically mixed) of niobia/silica has been previously described.[3] Briefly the procedure consisted of titrating a methanolic solution of niobium(V) chloride (Alfa) and silicon(IV) chloride (Alfa) with ammonium hydroxide to a pH of 7. The relative proportions of niobia and silica being determined by the relative concentrations of the precursors. The resulting precipitate is filtered and washed repeatedly until no chloride ions are detected by precipitation with silver nitrate in the filtrate. The precipitate is dried overnight at 110 °C and then subjected to the standard calcination procedure.

Precipitated niobia/alumina mixed oxides were produced in a similar fashion. This method involved titrating a sec-butanol solution of niobium(V) ethoxide and aluminum(III) sec-butoxide with ammonium hydroxide until a pH of 7 was attained. The mixed hydroxide precipitate was washed and filtered to remove any impurities that may be present. The precipitate is dried overnight at 110 °C and then subjected to the standard calcination as above. The mixed oxides prepared in this study as well as their nomenclature are listed in Table 2-9.

Table 2-8: EXPERIMENTAL PROCEDURE FOR NIOBIA/ALUMINA MIXED
OXIDE AEROGEL (A-NA25w) SYNTHESIS

PROCESS	STEPS AND CONDITIONS OF PROCEDURE
DISSOLUTION	1. Add required amount of $Nb(OC_2H_5)_5$ to 10 ml s-butanol
	2. Add required amount of deionized water and HNO_3 (for the niobia hydrolysis reaction) to 10 ml s-butanol
	3. Add required amount of $Al(OC_4H_9)_3$ to 30 ml s-butanol
	4. Allow all three solutions to stir 10 minutes to homogenize
HYDROLYSIS	1. Mix acidified water (for niobia hydrolysis) into the niobia solution (niobia sol)
	2. Let stir for 10 minutes to hydrolyze
	3. Mix niobia sol into the alumina solution (niobia/alumina sol)
	5. Let stir 10 minutes to homogenize
CONDENSATION	1. Add required amount of deionized water (for alumina hydrolysis) to niobia/alumina sol
	2. Let stir for about 1 minute to obtain gel
	3. Allow gel to sit for 1 hour to firm before extracting
DRYING	1. Supercritically extract using CO_2 at T=150 °C, P=3000 psi, F=0.05 SCFM for 3 hours (Aerogel)
CALCINING	1. Heat in N_2 (300 cc/min) at 400 °C for 2 hours
	2. Heat in O_2 (300 cc/min) at 500 °C for 2 hours

Table 2-9: NOMENCLATURE USED TO DESCRIBE SYNTHESIZED BINARY MIXED OXIDES NIOBIA/SILICA AND NIOBIA/ALUMINA

BINARY MIXED OXIDES

Notation	Wght.% Niobia	Mol.% Niobia	Description
A-NS25w	25	7.0	Mixed Oxide Aerogel of 25 weight % Nb_2O_5 75 weight % SiO_2
NS25w	25	7.0	Mixed Oxide (ppt.) of 25 weight % Nb_2O_5 75 weight % SiO_2
A-NA25w	25	11.3	Mixed Oxide Aerogel of 25 weight % Nb_2O_5 75 weight % Al_2O_3
NA25w	25	11.3	Mixed Oxide (ppt.) of 25 weight % Nb_2O_5 75 weight % Al_2O_3

2.2.3 Silica-Supported Niobia and Alumina-Supported Niobia

A surface oxide consists of one oxide supported and/or grafted onto the surface of another oxide. In this work we investigated two surface oxides: silica aerogel-supported niobia and alumina aerogel-supported niobia. The procedures for preparing them were identical. A detailed description of the initial silica-supported niobia preparation is presented elsewhere.[74] Briefly, niobia is placed onto the silica or alumina aerogel support (or Davison 952 Silica) using incipient wetness impregnation with a hexane-niobium(V) ethoxide solution. In this technique, the pores and the outside area of the solid are filled and coated with solution. The incipient wetness points were experimentally determined to be 2.8 ml/g SiO_2 for the silica aerogel and 2.0 ml/g Al_2O_3 for the alumina aerogel. The niobium ethoxide solution was added dropwise to the supports and distributed homogeneously throughout the mixture by using a mortar and pestle. After impregnation, these samples were dried by heating overnight under vacuum at 110 °C. The materials were then calcined according to the standard procedure. Several surface coverages for each material were made to determine dispersion of the niobia phase, varying from 2.5 to 25% monolayer (fully coated silica or alumina surface with one atomic layer of niobia) coverage. These coverages of niobia were controlled by the amount of niobium(V) ethoxide present in the solution and assuming the area of one molecule of $NbO_{2.5}$ occupies an area of 16 $Å^2$.[74, 81] A table of the surface oxides prepared as well as their niobia loadings and associated nomenclature is given in Table 2-10.

All of the above samples were subjected to various thermal treatments for different times and temperatures to study the interactive effects of these oxides. A sample with heat treatments beyond the standard calcination, 500 °C for 2 hours, will be denoted by brackets which contain the temperature, time, and treatment gas; i.e. a material heated at 800 °C for 2 hours in O_2 is labelled as (800,2) O_2.

Table 2-10: NOMENCLATURE USED TO DESCRIBE SYNTHESIZED BINARY
SURFACE OXIDES

BINARY SURFACE OXIDES

Notation	Wght.% Niobia	Mol.% Niobia	Description
A-NS(.25)	23.7	6.6	25% monolayer of Nb_2O_5 on SiO_2 (Aerogel)
NS(.25)	9.1	2.2	25% monolayer of Nb_2O_5 on SiO_2 (Davison 952)
A-NS(.10)	9.6	2.3	10% monolayer of Nb_2O_5 on SiO_2 (Aerogel)
A-NS(.05)	5.2	1.2	5% monolayer of Nb_2O_5 on SiO_2 (Aerogel)
A-NS(.025)	3.1	0.72	2.5% monolayer of Nb_2O_5 on SiO_2 (Aerogel)
A-NA(.25)	16.7	7.1	25% monolayer of Nb_2O_5 on Al_2O_3 (Aerogel)
A-NA(.10)	7.7	3.1	10% monolayer of Nb_2O_5 on Al_2O_3 (Aerogel)
A-NA(.05)	4.0	1.6	5% monolayer of Nb_2O_5 on Al_2O_3 (Aerogel)

2.3 Characterization of Physical Properties

This section discusses the equipment and procedures used to characterize the physical properties of the oxide catalysts in this thesis. Some of the newer or modified techniques will be discussed in full detail; however, those procedures which are common will have a more cursory discussion.

2.3.1 B.E.T. Surface Area

The total surface areas of all mixed and surface oxides were determined with a commercial Quantasorb unit (Quantachrome Corporation).[162] The system included a thermal conductivity detector with two filaments: one filament was located upstream as a reference and the other filament was set downstream from the sample. The difference in thermal conductivity of the two gas streams was measured and integrated with respect to time to give the amount of nitrogen adsorbed on the oxide sample. Because adsorption signals usually led to non-Gaussian distributions that were difficult to integrate, the desorption signals were the preferred runs. A known volume of adsorbate gas was injected into the system after each run for calibration purposes. A mixture of 30% nitrogen (balance helium) (Grade 5, Airco) was used as the carrier gas in these experiments. The single point-BET method was used, and the calculations for the surface areas can be found in the Quantasorb manual with the computer program for the calculation located in Appendix A. Because of the high surface areas of the samples studied, only 0.1 to 0.2 grams of sample were used. A gas volume of 10 cc was used for calibration purposes.

2.3.2 Pore Size Distribution and Pore Volume Analysis

Pore size distribution and pore volume analyses were done by Porous Materials, Inc. (PMI). Desorption isotherms (volume desorbed versus relative pressure) were constructed from which pore size distribution information for pores in the range of 10 - 400 Å could be obtained. The desorption isotherm was determined by making 100

measurements in the relative pressure (p/p_o) range of 0.05 to 0.95. The desorption data was then used to calculate cumulative pore volume as a function of pore radius. The relationship between the pore radius and relative pressure is given by the modified Kelvin equation (see Equation 2.1):

$$a - \delta = \frac{-2\sigma V_l \cos\Theta}{R_g T \ln(p/p_o)}$$

(2.1)

where a = pore radius, δ = adsorbed layer thickness, V_l = molar volume of the condensed liquid, σ = surface tension, Θ = contact angle between surface and adsorbate (= 0° for nitrogen), R_g = gas constant, T= absolute temperature, p = adsorbate gas pressure at equilibrium in the pore (vapor pressure over curved surface), p_o = saturation pressure of adsorbate gas at equilibrium (normal vapor pressure over planar liquid surface). The thickness of adsorbed nitrogen on the pore wall, δ, is related to the relative pressure by Equation 2.2 by Wheeler[163]:

$$\delta(\text{Å}) = 9.52 \left(\log\frac{p_o}{p}\right)^{-1/3}$$

(2.2)

Cumulative pore volume versus pore size curves were constructed and then differentiated with respect to diameter from which distributions of pore volumes, and average pore diameters were determined. Total pore volume is determined when capillary condensation is complete, $p/p_o \rightarrow 1.0$, and all pores are filled with condensed nitrogen. Multipoint B.E.T. surface area analyses were also performed by PMI using the nitrogen relative pressure (p/p_o) range of 0.05 $\rightarrow$ 0.35.

2.3.3 X-Ray Diffraction (XRD)

Powder X-ray diffraction (XRD) experiments were performed on a Rigaku Geigerflex D/Max series diffractometer with a $\Theta-2\Theta$ goniometer, model number CN2155D5, using a Mo radiation source. These experiments were used to observe and determine whether any chemical changes or phase transformations occurred on the samples during the heat treatments. XRD samples were prepared by suspending the oxide powder in a colloidion solution (2/3 amyl acetate and 1/3 colloidion) on one side of a microscope slide and allowing the solution to dry by evaporation. Scanning diffraction angles (2Θ) ranged from 5 to 35 degrees, and were scanned at 2 degrees/min. Crystalline patterns were indexed by measuring d-spacings from the spectra and compared to known d-spacings for various niobia phases, alumina phases, and niobia/aluminia compounds.[164-174]

Powder XRD experiments were also performed using a Rigaku Geigerflex D/Max series diffractometer with a $\Theta-\Theta$ goniometer, model number CN2182D5, with a Mo radiation source as above. The apparatus was also equipped with a platinum hot-stage (high temperature X-Ray diffractometer attachment for a $\Theta-\Theta$ goniometer). This equipment was interfaced to a Macintosh SE/40 computer to facilitate data acquisition. Experiments were performed to determine at which point the low temperature form of niobia, $TT-Nb_2O_5$, was formed from the amorphous, calcined niobia aerogel. From previous XRD experiments, it was found that a heat treatment of (600,2) O_2 induced the niobia sample into the crystalline phase of $TT-Nb_2O_5$; hence, a 10 °C ramp from 25 to 600 °C with a hold of 15 minutes at 600 °C was used in this investigation. The sample was then subsequently cooled to room temperature. The experiment was performed by locking onto the 100% intensity peak (2Θ = 12.80°) associated with $TT-Nb_2O_5$ and following its intensity as a function of time and temperature. Scans were taken and recorded every second with the dedicated computer system.

2.3.4 Differential Thermal Analysis (DTA)

Differential thermal analysis was used to study the heat effects of crystalline formation of the bulk and binary oxides when heated in He. The DTA experiments were performed on a Perkin-Elmer DTA Model 1700 High Temperature Differential Thermal Analyzer. Approximately 30 milligrams of sample were analyzed by heating from 25 - 1000 °C at 10 °C/min in an inert atmosphere of helium flowing at 50 cc/min.

2.3.5 Scanning Electron Microscopy (SEM)

A JEOL Ltd. CAMSCAN Scanning Electron Microscope (SEM), equipped with an X-Ray detector manufactured by Princeton/Gamma-Tech for Energy Dispersive Spectroscopy (EDS), was used for elemental mapping and quantitative elemental composition analysis on the binary oxide aerogels. Sample preparation consisted of taking the catalyst powder of interest, and depositing it on a carbon paste covered 0.5 inch aluminum holder. An additional step of depositing a thin conductive layer of gold on the surface was used in order to prevent surface charging during analysis.

2.3.6 Laser Raman Spectroscopy (LRS)

Laser Raman Spectroscopy (LRS) is used to examine the vibrational modes of molecules. The Raman scattering effect arises when an incident photon interacts with a molecule and induces the molecule to go from a lower to a higher level of vibrational energy.[175] In order for a molecular vibration to be Raman active, the vibration must be accompanied by a change in the polarizability of the molecule.[176, 177] This is in contrast to an infrared spectrum which results from vibrationally induced changes in the dipole moments of the molecules. Since the Raman scattering is also highly dependent on the ordering of the sample, a well-ordered material will be much more Raman active than a disordered sample.[175] Thus, LRS will be expected to give different information than IR, and has generally been found to be useful in the low frequency ranges of 200 - 1000 cm^{-1}

(corresponding to first order molecular vibrations in oxides) since many oxide materials are not IR transparent in this region.[176]

LRS spectra were taken primarily at the Zettlemoyer Center for Surface Studies at Lehigh University with the help of Jih-Mirn Jehng and I.E. Wachs, and also at Carnegie Mellon University with the supervision of Bob Winters and W.S. Hammack. The Raman spectra taken at Lehigh University were obtained with a Spectra-Physics Ar+ laser delivering 1 - 100 mW of incident radiation measured at the sample, with the excitation line at 514.5 nm. The scattered radiation was then directed into a Spex Triplemate Spectrometer (Model 1877) coupled to a Princeton Applied Research OMA III optical multichannel analyzer (Model 1463) with an intensified photodiode array cooled thermoelectrically to -30 °C. Most Raman data were obtained at room temperature and under ambient conditions.

In-situ Raman spectra were taken at Lehigh University with a specially designed Raman cell on a few select samples. The sample holder was made from a quartz glass, and the sample disk was held by a stationary slot in the sample holder. The sample was heated by a cylindrical heating coil surrounding the quartz cell, and the temperature was measured with an internal thermocouple. The cell was designed for operation temperatures up to 600 °C. Reaction-gas mixtures were introduced into the cell from a manifold at a rate of 50 to 500 cm^3/min with a delivery pressure of 150 - 200 Torr. These materials were analyzed in order to investigate the Raman spectral changes on dehydration of the binary oxides containing niobia.

2.3.7 Diffuse Reflectance Infrared Spectroscopy (DRIFT)

Infrared spectroscopy (IR), like Laser Raman Spectroscopy (LRS), examines the vibrational energies of molecules, but whereas LRS is a scattering process, IR is an absorptive process. IR spectra occur when a photon of infrared radiation is absorbed causing a vibration which in turn must cause a change in the dipole moment of the

molecule. It can be shown that the infrared absorption band is proportional to the square of the change in the dipole moment.

Structural information of solids is difficult to obtain when IR is run in the transmission mode, because the low frequencies which contain this necessary information are often opaque to the IR radiation. An alternative method is Diffuse Reflectance Infrared Spectroscopy (DRIFT). DRIFT spectra are often complicated by particle size scattering effects which can produce erroneous results. For the surface phase oxides, little to no change in particle size results from the grafting of niobia on the silica or alumina support, and these will be the samples examined.

Spectra were taken using an IBM DRIFT Accessory, part #A6106640, and an IBM 98 FTIR spectrometer, which ran at 0.5 cm^{-1} resolution. The FTIR system also included a dedicated Aspect 3000 computer system, and CMD-CDC disk drive assembly.

2.4 Characterization of Chemical Properties

This section discusses how various chemical probes (bases including n-butylamine and pyridine) were used to examine the acidic properties of the prepared oxides. New or modified procedures are discussed at length while those similar to previous studies are given a brief discussion.

2.4.1 Acid Strength and Acidity using n-Butylamine Titration

2.4.1.1 Acid Strength

The acid sites on various oxide surfaces differ in amount and strength. Some oxides may have a large number of acid sites with a low acid strength, while others may have only a few acid sites which have a high acid strength.[2] The Benesi titration method with Hammett indicators was used to measure the number and strength of acid sites over

the oxides in this study.[178] Table 2-11(A) shows these indicators and their pKa values along with the equivalent acidity in terms of percent H_2SO_4. The method of determining acid strength was made by placing approximately 40 milligrams of sample into a ground test tube, adding 1-2 ml of benzene and then 3 drops of indicator (0.1 wt.% in benzene), and then shaking briefly. Adsorption proceeded very rapidly, if it occurred at all, with a striking change in color between the basic and acidic forms of the indicator.[1] It should also be noted that the lower the pKa value of the indicator, the greater the acid strength of the solid.

In order to test for superacidity of the bulk and binary oxides three separate indicators were prepared in a similar fashion to above [see Table 2-11(B)]. These indicators are called super-acidic because their acid strengths are higher than the acid strength of 100% H_2SO_4. Because of the hygroscopic nature of these catalyst powders, heat treatments were done in a dry glove box purged with nitrogen, and equipped with a furnace and dedicated temperature controller. After heat treating the samples to 450 °C for 2 hours and allowing them to cool to room temperature, 3 drops of indicator were addded to a small amount of sample placed in aluminum pans to determine if the solid would turn the indicator to its acidic form.

In a simliar test to determine basicity of the oxides, two basic indicators were prepared in a similar fashion to above [see Table 2-11(C)]. This test was performed to determine the basic strength of a solid surface; i.e. the ability of a surface to convert an adsorbed neutral acid to its conjugate base, or more simply, the ability of the surface to donate an electron pair to an adsorbed acid. Because of the hygroscopic nature of the catalyst powders, the same heat treatment and procedure used for the superacidity measurements above was used on these samples as well.

Table 2-11: INDICATORS USED FOR ACID-BASE STRENGTH
MEASUREMENTS: A) ACID DISTRIBUTION INDICATORS, B)
SUPERACIDIC INDICATORS, AND C) BASIC INDICATORS

A) Acid Distribution Indicators

INDICATORS	Color BASE	ACID	pKa	wt.% H$_2$SO$_4$
Methyl Red	yellow	red	+4.8	5 x 10^{-5}
Dimethyl Yellow	yellow	red	+3.3	3 x 10^{-4}
4(Phenylazo)-Diphenylamine	yellow	purple	+1.5	2 x 10^{-2}
Dicinnamalacetone	yellow	red	-3.0	48
Benzalacetophenone	colorless	yellow	-5.6	71
Anthraquinone	colorless	yellow	-8.2	90

B) Superacidic Indicators (> 100 % H$_2$SO$_4$)

INDICATORS	Color BASE	ACID	pKa
p-Nitrotoluene	colorless	yellow	-11.35
p-Nitrochlorobenzene	colorless	yellow	-12.70
2,4-Dinitrotoluene	colorless	yellow	-13.75

C) Basic Indicators

INDICATORS	Color BASE	ACID	pKa
Phenolphthalein	colorless	red	+9.30
2,4-Dinitroaniline	yellow	violet	+15.0

2.4.1.2 Acidity Distribution

The amount of acid sites (or acidity) of a solid acid was measured by n-butylamine titration immediately after a determination of acid strength by the Benesi method.[148] The method consisted of titrating a solid acid suspended in benzene with 0.05 N n-butylamine, using a range of various indicators. The indicator changes color into its acidic form when adsorbed onto a solid acid. Therefore, the titres of n-butylamine required to restore the color of its basic form give a measure of the number of acid sites on the surface.

The use of various indicators with different pKa values, as noted above, allows one to determine a distribution of acidity at various acid strengths by amine titration. Great precautions were taken to prevent effects from titration time, powder size, volume of added indicator, and moisture on the measured acid amounts. All samples used were >100 mesh particles, the same amount of indicator was added to each sample, and the titration times for the oxides all spanned a period of no more than 1 day. The greatest precaution taken was against moisture. Since many of the acid sites studied were of a very strong nature and since water is amphoteric (able to possess both acidic and basic properties), all titration experiments were performed in a dry box purged with nitrogen to prevent poisoning of the acid sites. All indicators were mixed with benzene (99.9%, Aldrich), which had been further dried with molecular sieves, and stored in a dessicator which was also located in the glove box. The oxide samples were weighed out in vials and heated, with caps and stirring bars, in a vacuum oven at 110 °C for one hour to free the surface of any physisorbed water. The ground vials were then coated with teflon tape to prevent any evaporation that occurred with the added benzene. Also, all titrations were carried out using a digital pipette (4710 Eppendorf) which facilitated the use of small volumes of base, 10 - 100 μl, to be added to the samples, which were stirred with micromagnetic bars to insure equilibrium between the solution and surface was established. This method gave the sum of both Lewis and Brønsted sites since the nitrogen on the amine and the indicator can react equally with both sites.

2.4.2 Pyridine Adsorption Studies

In order to determine the acid strength - acid type distribution of the binary oxides, pyridine adsorption experiments were performed which consisted of Thermogravimetry (TG) and Fourier Transform Infrared Spectroscopy (FTIR). Thermogravimetric analysis studies were used to extract the heat of adsorption of pyridine as a function of pyridine coverage. Infrared studies were used to determine the type of acid sites (Lewis or Brønsted) on the surface of these binary oxides.

2.4.2.1 Thermogravimetry: Heat of Adsorption Measurement

The original procedure for determining the heat of pyridine adsorption versus coverage has been published elsewhere.[179] In this work, the original procedure was slightly modified in order to better accommodate our needs.

Details concerning the experimental procedure can be found elsewhere.[88] To briefly outline the procedure, a sample is first heat treated and weighed free of adsorbed pyridine. Pyridine is admitted into the system until equilibrium is achieved at room temperature, then the weight is monitored as a function of temperature and time at a constant pyridine pressure. This measurement is repeated for different pyridine pressures until a family of plots is generated for the weight of adsorbed pyridine as a function of temperature, at various pyridine vapor pressures. Using this plot, the heat of adsorption (ΔH_{ads}) can be determined using the Clausius-Clapeyron equation (see Equation 2.3):

$$\frac{\Delta H_{ads}}{R} = - \frac{d\ln(P_{eq})}{d(1/T)} \bigg|_{\Theta}$$

(2.3)

where ΔH_{ads} is the heat of adsorption, P_{eq} is the pyridine equilibrium vapor pressure, Θ is the pyridine coverage, T is the sample temperature (absolute), and R is the gas constant.

(1) Experimental Equipment:

The apparatus (see Figure 2-3)[88] for these experiments was constructed of glass for cleanliness, and was connected to a diffusion pump with heating tapes on all glassware for ease of removal of pyridine. The pretreatment gas side and pyridine gas side were separated to prevent contamination of pyridine throughout the entire system. Temperature programs and thermal treatments were done using a Cahn 113 Thermogravimetry Microbalance, and the weight was electronically processed with a Cahn 2000 Recording Electrobalance and recorded using a Bascom Turner Model 4000 computer. A constant temperature bath [ethylene glycol/water (60/40)] was used for maintaining a constant pyridine vapor pressure. The bath temperature was maintained using a Polyscience 730 immersion circulator/heater (temperature controller) and a model KR80A Immersion Cooler.

(2) Experimental Procedure:

The following procedure was used because of the extremely small weights involved (~ 10 mg). To avoid pyridine contamination of the microbalance, helium was flowed through the microbalance at 100 cc/min in all flow situations to act as a purge line.

1. **Purge system** for pyridine removal with all tapes on for at least 3 hours and a helium flow of 40 cc/min (using a helium purge flow of 100 cc/min).

2. **Pump system** for pyridine removal with heating tapes on for 3 hours. The vacuum reached should be $2 - 6 \times 10^{-7}$ Torr.

3. **Zero empty basket** for calibration using a reactor temperature of 250 °C and a helium flow of 40 cc/min - heating tapes on (using a helium purge flow of 100 cc/min).

4. **Load sample and pretreat in O_2** to 450 °C and hold for 3 hours to minimize problems of catalyst aging and contamination (using a helium purge flow of 100 cc/min).

5. **Purge in helium** for 30 min and pump for 30 min to a vacuum of $2 - 6 \times 10^{-7}$ Torr.

Figure 2-3: TG SYSTEM FOR PYRIDINE ADSORPTION[88]

Symbol	Description
⊗	On/off stopcock(glass)
○	3-way stopcock(glass)
aux	auxiliary trap
C1,2,3	gas cylinders
cb	circulating temperature bath
exhaust	exhaust stream (to hood)
furnace	microbalance furnace
Hg mon	mercury monometer
HgT	mercury trap
H/C	heater/temperature controller
KOH	Potasium-hyroxide trap
mb	Cahn 113 microbalance
ms	molecular sieve trap
NV1,2,3	needle valves
purge	helium purge stream
pyrid	pyridine trap
R1,2,3	rotameters
ref	refrigeration unit
s	sample and sample basket
T	thermocouple

6. Pretreat sample in helium to 450 °C and hold for 1 hour with a helium flowrate of 40 cc/min. (If sample reduces easily as is the case with niobia, then pretreat sample only at 300 °C and hold for 1 hour with above helium flowrates.) The final weight of this run is taken as the sample weight free of adsorbed base.

7. Flow pyridine at a constant pressure with a helium carrier gas flow of 40 cc/min and helium purge flow of 100 cc/min after sample cools to below 100 °C from above pretreatment. Wait for sample to equilibrate with pyridine (3 - 8 hours).

8. Measure weight versus temperature with the dedicated Cahn 113 microbalance at 11 different temperatures (100 - 350 °C, at 25 °C intervals) at constant pyridine vapor pressure until no weight change was seen (1 - 2 hours) (see Figure 2-4).

9. Zero runs were performed to compensate for temperature buoyancy effects as well as any weight added due to pyridine adsorption on the basket, stirrup-holder, or wire. For each zero run, the same procedure as noted above was run for each experiment without sample in order to determine a baseline.

(3) Data Analysis:

The data was analyzed by first subtracting the zero run weights from the weight of the adsorbed pyridine. Next, a family of pyridine coverage versus 1/T plots were generated for different runs at constant pyridine vapor pressure (see Figure 2-5). These plots were then manipulated in order to generate $\ln(P_{eq})$ versus 1/T plots at constant coverage (see Figure 2-6). The heats of adsorption, ΔH_{ads}, were taken from the slopes of these lines by least squares fit to the data. Samples with large surface areas that were not very acidic (low amounts of adsorbed pyridine) gave the largest errors. For these samples, multiple runs were taken at the same or slightly different pyridine pressure in order to get statistically meaningful results. The number of points per line ranged from 3 to 6. A computer program used in the analysis of the data is listed in Appendix F.

2.4.2.2 Fourier Transform Infrared Spectroscopy: Acid Type

Infrared spectra of pyridine adsorbed on a solid acid can readily be used to distinguish between adsorbed pyridine species: bonded to a Brønsted acid site as a pyridinium ion (BPY), bonded to a Lewis acid site (LPY), or weakly hydrogen bonded to the surface (HPY).[180]

Figure 2-4: TG DATA OF WEIGHT OF ADSORBED PYRIDINE VS. TEMPERATURE (AT CONSTANT PYRIDINE PRESSURE)
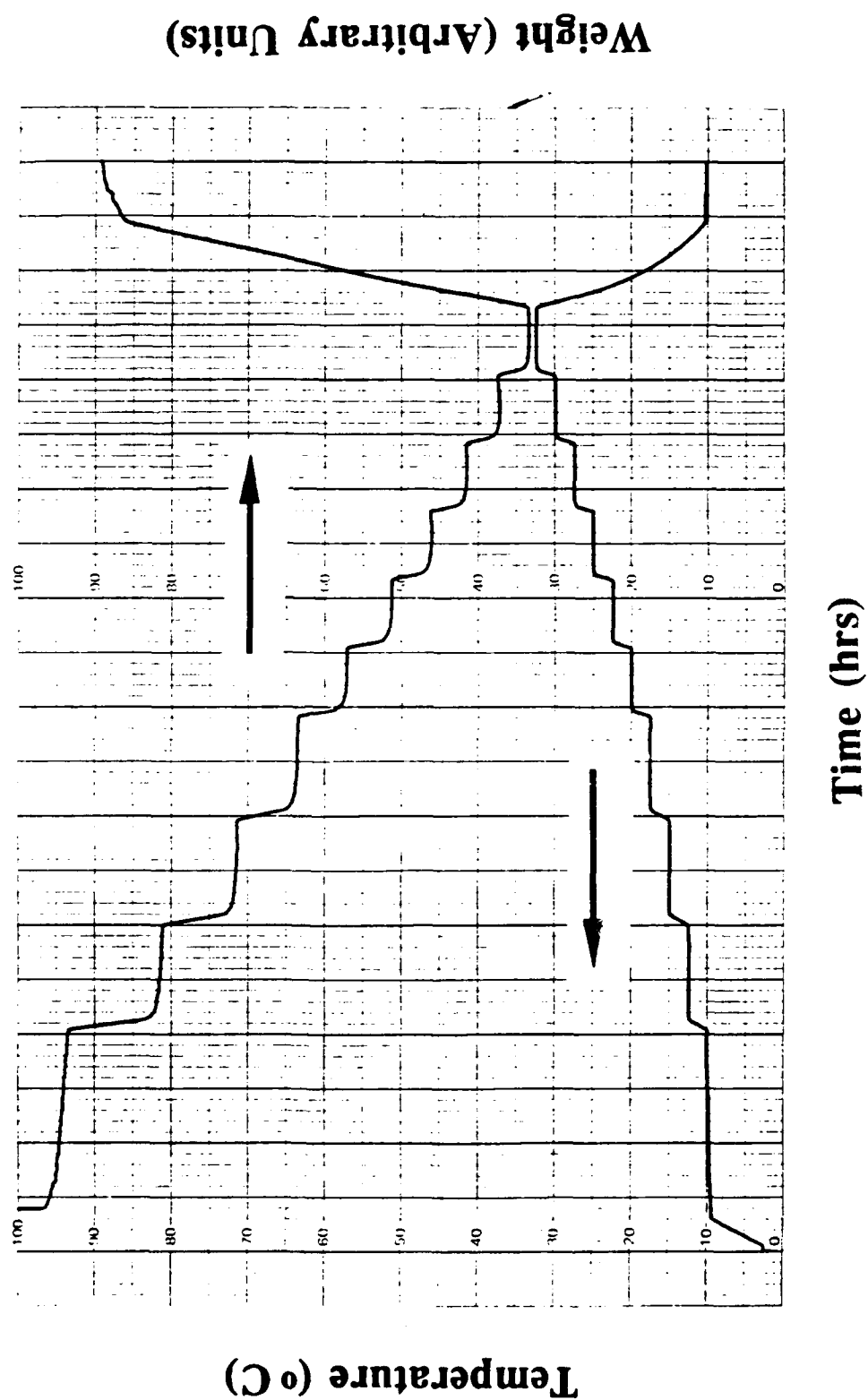
Figure 2-5: TG DATA OF LN(Θ) VS. 1/T (AT CONSTANT PYRIDINE COVERAGE)
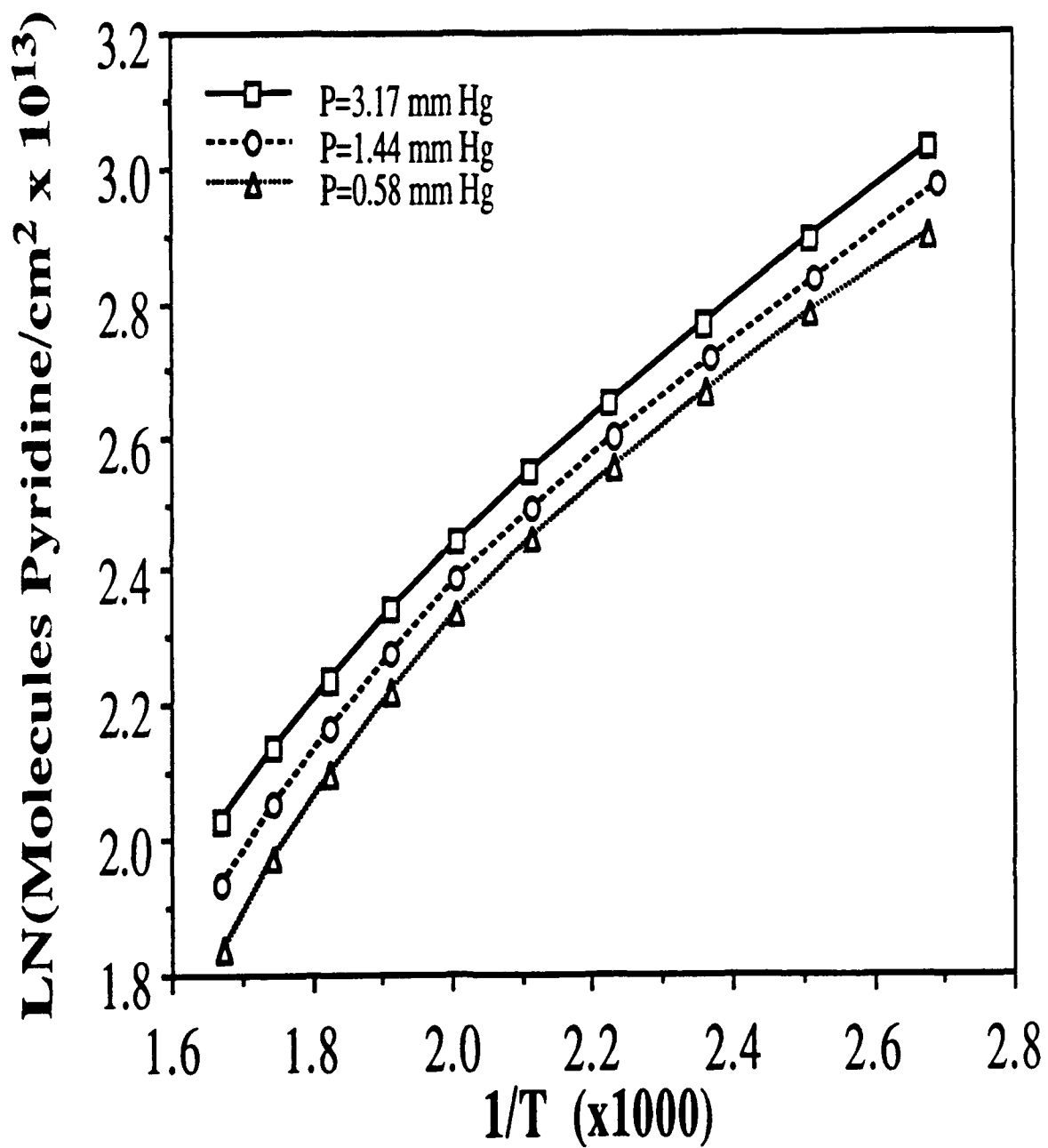
Figure 2-6: TG DATA LN(P$_{eq}$) VS. 1/T (FOR CONSTANT PYRIDINE COVERAGE)
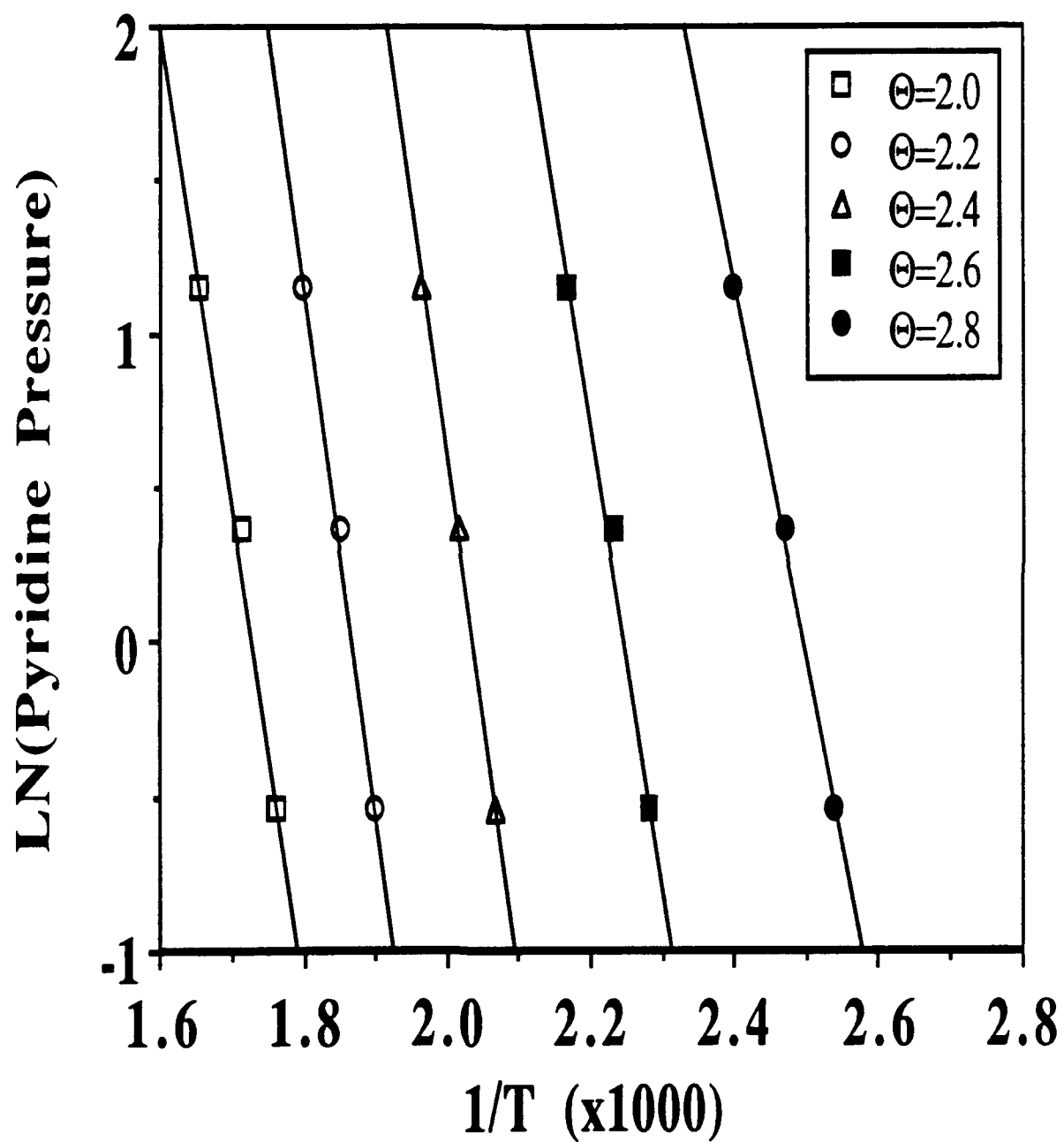
(1) Experimental Equipment:

IR spectra were obtained using an IBM 98 FTIR spectrometer. This research was facilitated by the use of infrared cells and a gas handling system designed and constructed by co-workers in our group. The IR cell design is shown in Figure 2-7.[88] The IR cell allows samples to be heat treated up to 500 °C in a controlled flow of helium or oxygen, or in vacuum (approximately 10^{-4} to 10^{-6} Torr) with the sample temperatures directly recorded using a type K thermocouple. The outer seals and lid allow the cell to be used with the IBM FTIR sample chamber (under evacuation) for data acquisition. The gas handling system (see Figure 2-8)[88] was constructed with stainless steel Nupro high vacuum valves, mounted and arranged on a 3/8" thick aluminum plate for flow through one pyridine trap and for vacuum to 2 IR cells. The gas handling system was mounted on a cart for mobility, to which a Barbara Coleman 570 temperature controller with 470 A/C power supply, CVC Products VMF-20 diffusion pump, Sargent Welch Model 1400 mechanical pump, and a glass pyridine bubbler trap were also mounted.

(2) Experimental Procedure:

1. **Press** a sample disk from catalyst powder using a pressure of 4000 psi and load into IR cell with the thermocouple touching the sample.

2. **Purge** IR cell in helium at 50 cc/min for 15 min.

3. **Pump** IR cell to 10^{-4} Torr with the diffusion pump and heat sample to 450 °C at 10 °C/min and hold for 1 hour. (For samples that reduced easily, like niobia, only heat to 300 °C and hold for 1 hour.) Final vacuum should be approximately 10^{-5} Torr.

4. **Cool** sample to room temperature and load IR cell in sample chamber and take average of 500 FTIR spectra at 0.5 cm^{-1} resolution.

5. **Pressurize** cell to one atmosphere very slowly in helium and expose sample to pyridine for 15 minutes.

6. **Purge** in helium for 3 hours after turning pyridine off.

7. **Pump** at room temperature (with heating tapes on) for 3 hours and take average of 500 spectra.(Room temperature scan with adsorbed pyridine).

8. **Continue to pump** and heat treat to 100 °C and hold for 3 hours.

Figure 2-7: INFRARED SPECTROSCOPY CELL FOR PYRIDINE STUDIES: A) SIDE-VIEW AND B) FRONT-VIEW[88]

A) Side-view of IR Cell for pyridine studies:
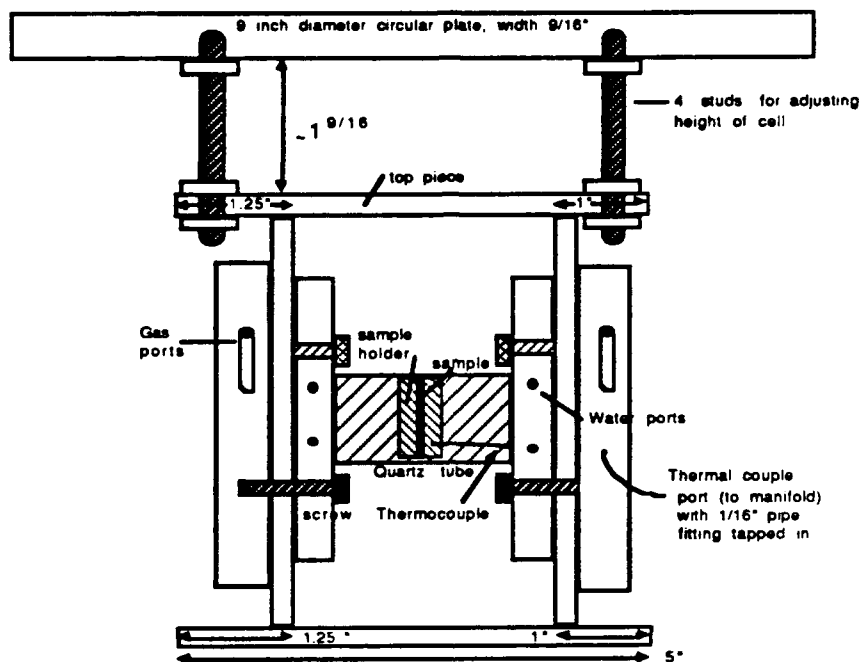
B) Front-view of IR Cell for pyridine studies:
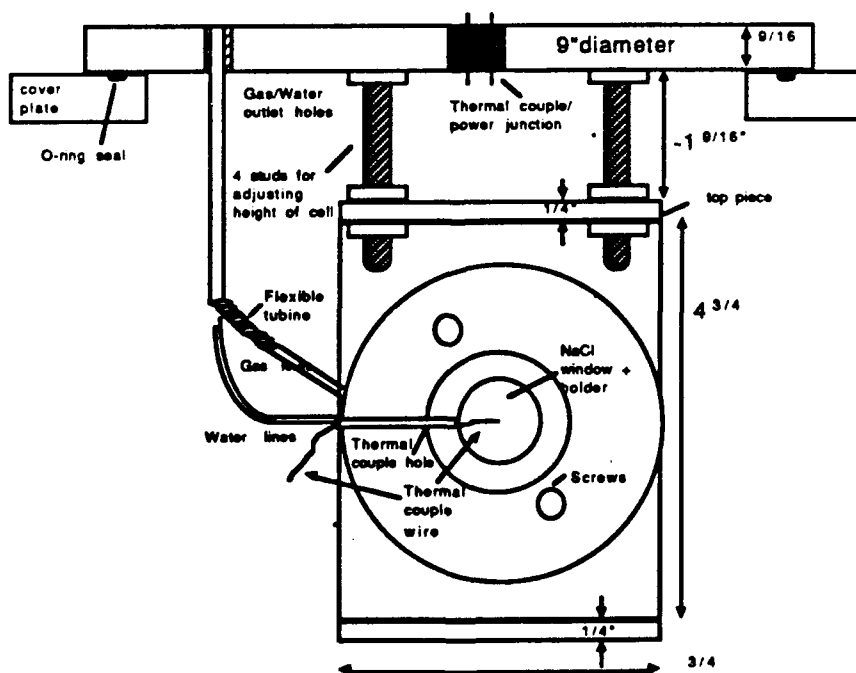
Figure 2-8: PORTABLE GAS HANDLING SYSTEM FOR PYRIDINE INFRARED SPECTROSCOPY STUDIES[88]
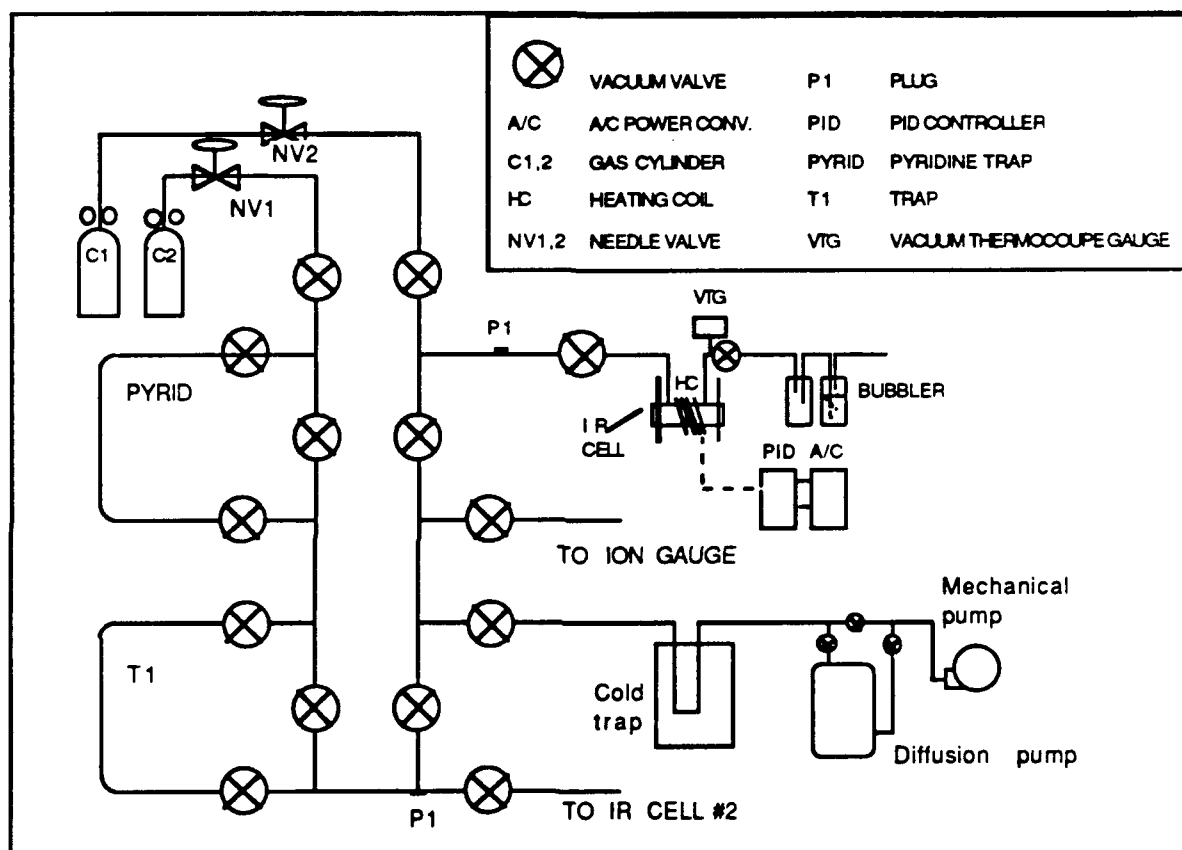
9. Cool sample to room temperature and take average of 500 spectra.

10. Repeat steps 8 and 9 with temperatures of first 200 °C and then 300 °C, remembering to take IR cell out of FTIR each time a heat treatment was performed.

(3) Data Analysis:

The above procedure allows one to generate an IR spectrum of adsorbed pyridine as shown in Figure 2-9, which will be discussd later. The ratio of Lewis to Brønsted sites can be calculated using the procedure of Basila and Kantner.[181] This method uses the relative integrated absorbance of the 1450 and 1490 cm^{-1} pyridine absorption peaks of Lewis and Brønsted sites. The relative ratio of extinction coefficients of the 1490 and 1450 cm^{-1} peaks was determined to be 0.205 from a sample free of Brønsted acidity.[88] This value was then used to calculate the Lewis/Brønsted ratios at the different treatment temperatures. A sample calculation is shown in Appendix F.

2.4.3 Reduction Studies

Reduction studies of the bulk and binary oxides were done using a Cahn 113 Thermogravimetry Analysis (TGA) unit. The weight was measured and processed electronically with a Cahn 2000 Recording Electrobalance. The signal from this unit was then sent to a Bascom Turner Model 4000 computer which monitored the weight loss as a function of temperature and time. Reduction studies were performed by heating the oxide sample to 1000 °C at 10 °C/min in flowing hydrogen (50 cc/min) and holding at 1000 °C for 2 hours. Direct reduction experiments, as previously mentioned, are often complicated by the desorption of water, and more importantly by the crystallization of niobia during the heat treatment. Therefore, in order to overcome these complications, a second series of reduction experiments was performed in which the oxide sample was first heated in flowing helium (40 cc/min) to 1000 °C at 10 °C/min and then cooled to room temperature. The sample was subsequently reduced in flowing hydrogen following the direct reduction procedure as above.

Figure 2-9: INFRARED SPECTRUM OF PYRIDINE ADSORBED ON A-Nb₂O₅ AT 100 °C (EVACUATED)
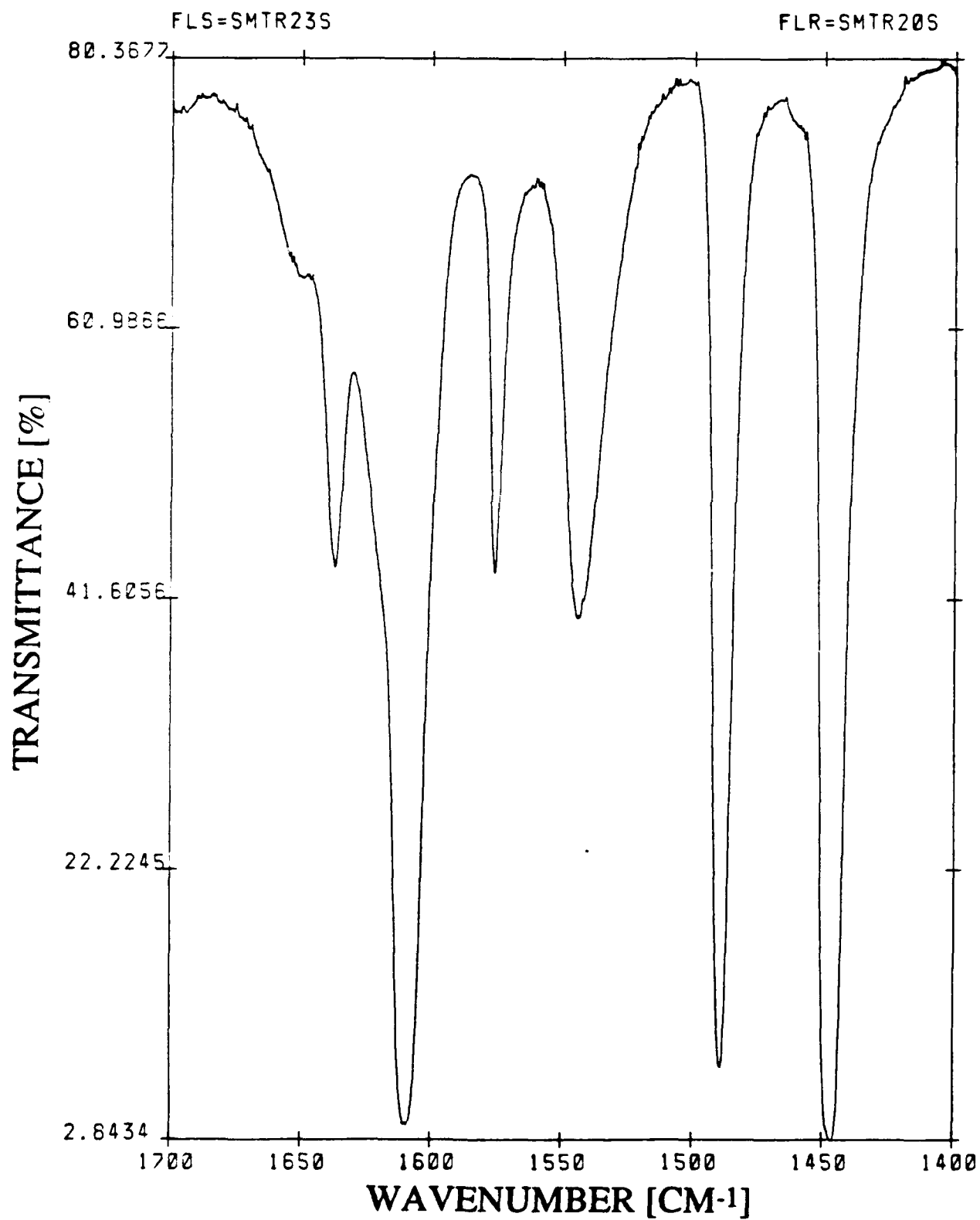
2.4.4 1-Butene ($1\text{-}C_4H_8$) Isomerization

The catalytic activities of the bulk and binary oxides were studied with the isomerization of 1-butene in a continuous flow micro-reactor shown schematically in Figure 2-10.[3] This system had a feedback control system for the gas flow rates, a reactor with a temperature controller, and gas analysis system, all attached to a control panel.

(1) Experimental Equipment:

The gas handling system consisted of molecular sieve purifiers (Linde 4A), filters (Swagelok), on/off solenoid valves (General Valve Co.), proportional control valves (Brooks Instrument Co.), orifices and pressure transducers, and three-way valves (General Valve Co.) for both of the feed lines. The $1\text{-}C_4H_8$ gas flowed directly to the reactor, while the He gas passed through the molecular sieve trap before entering the reactor as a carrier gas. Helium (Grade 5, Airco) was used as a carrier gas for the research grade $1\text{-}C_4H_8$ (99.8%, Matheson). The two gases were well mixed before entering the reaction chamber.

The micro-reactor consisted of a 1.5 cm O.D. vertical tube (316 stainless steel) equipped with a fritted disk to support the catalyst bed. The reactor was heated by a tubular ceramic heating element. The temperature of the furnace was sensed by a K-type thermocouple and controlled by a PID programmable temperature controller (Series CN-2010, Omega Engineering Co.). The bed was located in the middle of the furnace and had a height of 1 cm. The reactor temperature was also measured by a K-type thermocouple located in the center of the catalyst bed and was displayed with a digital temperature indicator (400B, Omega Engineering Co.).

The gaseous reactants were fed through the top of the reactor and reacted over the catalyst sample. The product gas was diverted through a 4-way valve to a vent or a gas chromatograph (GC) for analysis.

Figure 2-10: 1-BUTENE ISOMERIZATION REACTION SYSTEM[3]

LEGEND

A,B: fixed-bed flow reactor
C : gas cylinder
CV : proportional control valve
D : Deoxo purifier
DR : Drierite purifier
F : gas filter
FIC: flow rate controller
GC : Caw-Mac GC
IP : injection port
M : molecular sieve
O : orifice
R : bubble meter (25 ml)
S : solenoid valve
TI : temperature indicator
TIC: temperature controller
V : 4-way valve

cylinder	C_2H_6/H_2	$1-C_4H_8$ Isomer.
C1	H_2	-
C2	He	-
C3	C_2H_6	$1-C_4H_8$
C4	-	-

The outlet gas from the reactor was connected to a programmable GC (Series 550P, Gow Mac) where the gaseous products were analyzed using a stainless steel 2m x 1/8" column containing 0.19 wt.% picric acid on 80/100 mesh Carbopack C packing (Supelco, Inc.). A manual valve was used to inject samples. A 40 °C isothermal program was used for all experiments. The output signal of the GC was analyzed with an HP 3390A integrator. The operating conditions for both GC and integrator are included in Appendix E. Some of the mixed oxides which had been heat treated with a 1000 °C ramp gave results which were difficult to integrate because of the low surface areas and distorted (non-Gaussian) peaks. These results were handled by a special integrator program which can also be found in Appendix E.

(2) Experimental Procedure:

A 100 to 200 milligram sample was used in all experiments. The conversion was maintained as low as possible to eliminate transport limitations. Reactions were carried out at 150 °C and 1 atmosphere in the micro-reactor. Gas products from the reaction were taken every 12 minutes using a manual sampling valve and analyzed by the gas chromatograph. Helium was used as the carrier gas and a total flowrate of 100 SCCM (Standard Cubic Centimeters per Minute) was maintained. The flow of 1-butene was kept at 5 SCCM.

In order to maintain consistency, the same pretreatment conditions were used on all oxide samples. All samples were treated at 25 °C under He gas at 50 SCCM for 2-3 hours (overnight preferably) until no background 1-butene was detected. Then, the samples were pretreated at 200 °C for 1 hour under He gas at 50 SCCM. The reactor was then cooled to 150 °C and conditioned for 2 hours with the reaction mixture. An analysis was performed on the isomerization products every 12 minutes until the activity of the catalyst was steady.

(3) Data Analysis:

Under the conditions listed, no iso-butene was detected in the product stream. Therefore, since cis- and trans-2-butene were the only two products of interest, the reaction rate was calculated as follows and recorded at different times.

$$X_{C_4} = (1 - \frac{S_{C_4}A_{C_4}}{\sum_{i=1}^{n} S_i A_i}) \times 100 \tag{2.4}$$

$$r_{C_4} = (\frac{X_{C_4}}{100}) \times (C_4 \frac{cc}{min}) \times (\frac{1}{22400 \text{ cc/mol}}) \times (\frac{1}{W(g)}) \times (\frac{60 \text{ min}}{hr}) \times (\frac{1}{S.A.(m^2/g)}) \tag{2.5}$$

where C_4 : 1-Butene

X_{C4}: Mole% conversion of 1-C_4H_8

S: RRM values (see Appendix E)

A: GC Area (counts)

i: Component of 1-C_4H_8, cis- and trans-2-butene

n: Total number of C_4H_8 isomers

r_{C4}: Reaction rate of 1-C_4H_8 (mol/hr-m^2)

W: Weight of catalyst (g)

S.A.: Surface area of catalyst (m^2/g)

The flowrates were all calculated at standard conditions (STP). The selectivity (cis-/trans-2-butene) were calculated as the ratio of the two products analyzed by the GC. A basic program is included in Appendix E for calculations of the activities and selectivities.

Chapter 3

BULK OXIDE AEROGELS

3.1 Introduction

This chapter discusses the results used to physically and chemically characterize the bulk oxide aerogels synthesized in this study. The focus here will first be on the characterization of niobia aerogels. A variety of techniques were used to establish both the microscopic and macroscopic details of these samples with the objective of developing a comparative set of samples of known structure for chemical characterization. These results were used as a guide and base in establishing the chemical-structural relationship found in bulk niobia. This foundation will be built upon later to determine how the oxide-oxide interaction of binary materials affects structure and in turn their chemical properties. This discussion will next concentrate on the results for both silica and alumina aerogels. These bulk aerogels were examined to establish their behavior in the absence of any interactions, and to determine their suitability as oxide supports for the subsequent introduction of niobia. Results in this chapter are presented separately, for clarity, depending on the specific technique used.

3.2 Physical Property Characterization of Niobia Aerogels

3.2.1 Surface Area and Physical Property Data

Niobium pentoxide aerogels were synthesized via the sol-gel route, followed by a supercritical extraction of the solvent-ladened gel. This technique has led to the formation of niobium pentoxide with the highest surface area, 190 m^2/g, ever reported for a sample calcined at 500 °C.[182] There are very few references in the literature on the synthesis of niobium pentoxide gels; however, one group, using Extended X-ray Absorption Fine Structure (EXAFS), has determined that the hydrolysis of niobium ethoxide (precursor for Nb_2O_5 gels) yields primarily corner-sharing NbO_6 octahedra, instead of edge-sharing octahedra, and an open 3-dimensional structure.[183, 184] With this developed 3-dimensional structure now built into the gels, one can believe that supercritically extracting the solvent from this material will preserve the integrity of the network, hence leading to extremely large surface areas. This has indeed been our finding with all aerogels, especially niobia, investigated in this study.

In light of the above result, and the fact that very little information can be found in the literature about niobia gels, we undertook a study to understand the effect of three parameters on the gelation of niobium pentoxide. These parameters were the concentration of precursor, the concentration of water, and the type of solvent. Table 3-1 reveals how these parameters affect gelation time, and Table 3-2 shows the physical property data of the corresponding aerogels. It is clear from Table 3-1 that for both methanol and s-butanol, as the concentration of niobium ethoxide precursor increases, the gel time (time it takes for the solution to not flow) goes down significantly. A similar effect with water concentration is seen, i.e. as the concentration of water goes up, the time for gelation goes down. Also shown in Table 3-1 is a comparison of our Single-Point B.E.T. measurements and Multi-Point B.E.T. surface area measurements. It is seen that the difference in the two

Table 3-1: GELATION PARAMETERS AND TIMES FOR Nb_2O_5 AEROGELS

MeOH AS SOLVENT

(Conc.[1]	H_2O[2]	HNO_3[3])	Gel Time	Surface Area[4] (Single Point)	Surface Area[5] (Multi Point)	Percent Difference
(0.62	5.0	0.25)	60 sec	235	222.0	5.8
(0.50	5.0	0.25)	10 min	220	200.3	9.8
(0.31	5.0	0.25)	2 days	230	215.2	6.9
(Conc.	H_2O	HNO_3)	Gel Time	(Single Point)	(Multi Point)	Difference
(0.62	10.0	0.25)	60 sec	205	195.5	4.8
(0.50	10.0	0.25)	5 min	205	193.9	5.7
(0.31	10.0	0.25)	1 hr	220	218.3	0.8

s-BuOH AS SOLVENT

(Conc.	H_2O	HNO_3)	Gel Time	(Single Point)	(Multi Point)	Difference
(0.62	5.0	0.80)	30 sec	150	151.4	0.9
(0.50	5.0	0.80)	2 min	115	132.6	13.3
(0.31	5.0	0.80)	30 min	80	91.4	12.5
(Conc.	H_2O	HNO_3)	Gel Time	(Single Point)	(Multi Point)	Difference
(0.62	10.0	0.80)	5 sec	160	166.1	3.7
(0.50	10.0	0.80)	10 sec	190	196.3	3.2
(0.31	10.0	0.80)	60 sec	165	165.1	0.1

[1] Concentration of Niobium Ethoxide Precursor (mmoles Nb^{5+}/ml alcohol)

[2] Molar concentration of water (moles H_2O/moles Nb^{5+})

[3] Molar concentration of nitric acid (moles HNO_3/molesNb^{5+})

[4] Total Surface Area, Single-Point B.E.T. (m^2/g)

[5] Total Surface Area, Multi-Point B.E.T. (m^2/g)

Table 3-2: PHYSICAL PROPERTY DATA OF Nb_2O_5 AEROGELS

MeOH as SOLVENT

(Conc.[1]	H_2O[2]	HNO_3[3])	Surface Area[4] (Multi Point)	Total Pore Volume[5]	Avg. Pore Diameter[6]
(0.62	5.0	0.25)	222.0	0.677	121.9
(0.50	5.0	0.25)	200.3	0.661	132.0
(0.31	5.0	0.25)	215.2	0.702	130.6
			avg=212.5	avg=0.680	avg=128.2

(Conc.	H_2O	HNO_3)	(Multi Point)	Total Pore Volume	Avg. Pore Diameter
(0.62	10.0	0.25)	195.5	0.812	166.1
(0.50	10.0	0.25)	193.9	1.028	212.1
(0.31	10.0	0.25)	218.3	0.905	165.7
			avg=202.5	avg=0.915	avg=181.3

s-BuOH as SOLVENT

(Conc.	H_2O	HNO_3)	(Multi Point)	Total Pore Volume	Avg. Pore Diameter
(0.62	5.0	0.80)	151.4	0.811	214.3
(0.50	5.0	0.80)	132.6	0.598	180.5
(0.31	5.0	0.80)	91.4	0.381	166.8
			avg=125.1	avg=0.597	avg=187.1

(Conc.	H_2O	HNO_3)	(Multi Point)	Total Pore Volume	Avg. Pore Diameter
(0.62	10.0	0.80)	166.1	1.276	307.4
(0.50	10.0	0.80)	196.3	1.280	260.9
(0.31	10.0	0.80)	165.1	1.627	394.2
			avg=175.8	avg=1.394	avg=320.8

1	Concentration of Niobium Ethoxide Precursor (mmoles Nb^{5+}/ml alcohol)
2	Molar concentration of water (moles H_2O/moles Nb^{5+})
3	Molar concentration of nitric acid (moles HNO_3/molesNb^{5+})
4	Multi-Point B.E.T. Surface Area (m^2/g)
5	Total Pore Volume (cm^3/g)
6	Average Pore Diameter , 4V/S, (Å)

techniques is in most cases only 5 - 10%, showing that our single-point surface area measurements are quite accurate.

Table 3-2 gives the physical properties of the prepared niobia aerogels. It is apparent that the main determining factor in the physical properties of niobia aerogels stems from the concentration of water. The higher water concentrations in both solvents appear to yield the larger pore diameters and pore volumes. This could possibly be due to the fact that the hydrolysis reactions predominate over the condensation reactions, because of the higher water content, resulting in a partial precipitation of $Nb(OH)_5$ in the gel. This leads to the porosity existing on two length scales: microporosity within the hydroxide clusters, and meso- or macroporosity between clusters.[156] This difference is more apparent in the gels prepared with the s-butanol than with methanol, and could be due to the limited solubility of water in this secondary alcohol or the increased acid content in these gels. One last observation was the clarity among the gels prepared in the different solvents. The niobium pentoxide gels prepared with methanol were nearly always transparent with a golden tinge due to the niobium ethoxide precursor, while those prepared with s-butanol were mostly opaque along with some amber transparency. This indicates that the gels prepared in methanol were probably more homogeneous than those prepared in s-butanol, because of the precipitation reactions that had occurred with s-butanol, according to the above visual observation. This can also be verified by the nearly constant surface area of these prepared samples in methanol. The gelation times in methanol are also higher than those in s-butanol (usually by at least an order of magnitude) and could be explained by the rapid hydrolysis reactions that occur in the latter alcohol. These rates of gelation depend on a number of factors, with the solubility of the parent alcohol and the various other reactants and products (partially hydrolyzed alkoxides) obviously being important. It is beyond the scope of this study to investigate and explain all interactions of the gelation process as a whole. The above observations have helped to suggest possible mechanisms, but there is obviously more work that needs to be done in order to expand in this area.

The niobia aerogel used in this investigation was prepared in s-butanol, with a precursor concentration of 0.5 mmoles Nb^{5+}/ml alcohol, a water concentration of 10.0 moles H_2O/moles Nb^{5+} to insure that all alkoxy groups had been hydrolyzed, and an acid concentration of 0.80 moles HNO_3/moles Nb^{5+} in order to catalyze the condensation reaction. This aerogel was compared to other more conventionally prepared niobia (see Chapter 2 for details): $X-Nb_2O_5$ (xerogel), $P-Nb_2O_5$ (precipitated), and niobic acid [uncalcined-hydrated niobia, commercial catalyst (NPC)]. Table 3-3 shows the physical property data of these four niobia after a standard calcination (500,2) in O_2. It is apparent from this table that the surface area of the niobia aerogel is greater than the other niobia by a factor of 2, but even more striking is the pore volume of the aerogel. The niobia aerogel pore volume, 1.28 cm^3/g, is an order of magnitude greater than the pore volumes of the more conventionally prepared niobia samples, 0.15 cm^3/g, and corresponds to an aerogel having an average pore diameter 3 times larger than the other niobia samples. As stated in the experimental section, the only difference between $A-Nb_2O_5$ and $X-Nb_2O_5$ is the fact that the aerogel was supercritically dried in an autoclave, while the xerogel was conventionally dried in a vacuum oven. The above data indicate that the extraction step does indeed maintain the porosity of the initial gel in its pre-extracted condition, with that of the supercritically dried aerogel in its final state. Conventionally drying the gel collapses the structure as is shown with the xerogel of niobia.

Table 3-4 lists the surface area of the synthesized niobium pentoxide after various thermal heat treatments, and Figure 3-1 shows this tabulated surface area decline as a function of temperature. Close examination of Figure 3-1 indicates the superior surface area of the aerogel over that of the conventionally prepared samples after both the 500 °C and 600 °C calcinations. It is also seen that this superior edge in surface area for the aerogel is lost at the higher calcination temperatures of 800 °C and 1000 °C. We will later see that this collapse is due to the oxide undergoing a phase transformation and attaining a more ordered state.

Table 3-3: PHYSICAL PROPERTY DATA OF Nb_2O_5 AFTER STANDARD CALCINATION (500,2)

Name	Total B.E.T. Surface Area[1]	Total Pore Volume[2]	Avg. Pore Diameter[3]
A-Nb_2O_5	196.3	1.2802	260.9
X-Nb_2O_5	77.0	0.1841	95.7
P-Nb_2O_5	85.6	0.1532	71.5
Niobic Acid[4] ($Nb_2O_5 \cdot nH_2O$)	95.7	0.1292	54.0

[1] Total Surface Area, Multi-Point B.E.T. (m^2/g)

[2] Total Pore Volume (cm^3/g)

[3] Average Pore Diameter, 4V/S, (Å)

[4] Commercial Niobic Acid (HY340) calcined

Table 3-4: SURFACE AREA OF NIOBIA AEROGEL AND CONVENTIONALLY PREPARED NIOBIA WITH THERMAL TREATMENTS

| Heat Treatment | Total Surface Area (m^2/g)* | | | |
| | Samples | | | |
[Temp.(°C),Time(hr)]	A-Nb$_2$O$_5$	X-Nb$_2$O$_5$	P-Nb$_2$O$_5$	Niobic Acid
(500,2)	190	100	85	100
(600,2)	60	35	30	25
(800,2)	5	4	4	3.5
(1000,-)	1	1	1	0.5

* Surface Areas measured using Single-Point B.E.T. method; (500,2) samples agree with those measured using Multi-Point B.E.T. method.

Figure 3-1: SURFACE AREA STABILIZATION OF NIOBIA AEROGEL AND CONVENTIONALLY PREPARED NIOBIA
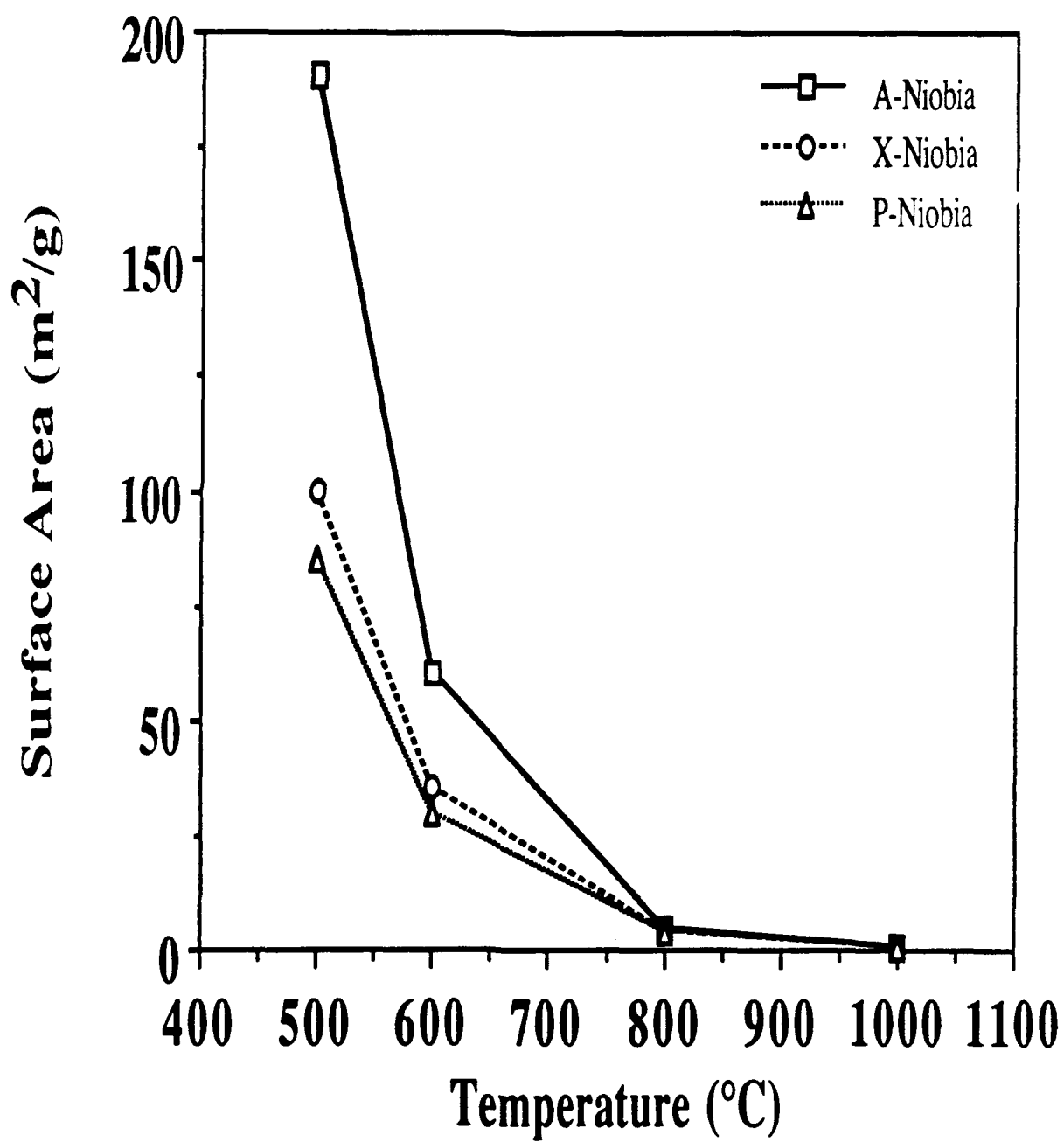
3.2.2 X-ray Diffraction (XRD)

In order to elucidate the surface area collapse, we used X-ray diffraction (XRD) to examine the calcined samples. Table 3-5 shows the phases of niobia after various heat treatments ranging from (500,2) to (1000,48). At (500,2) the niobia aerogel is amorphous, possibly due to its 3-dimensional inorganic polymer network set in from the supercritical extraction which appears to be unperturbed with this low temperature calcination. The other niobia samples and even niobic acid (hydrated niobia) all form the lowest ordered phase of niobia (TT-Nb_2O_5) after the (500,2) calcination. The actual XRD diffraction patterns are shown in Figure 3-2. This figure clearly shows the amorphous nature of the niobia aerogel as indicated by a lack of diffraction peaks, whereas the conventional niobia samples have XRD patterns indexed as TT-Nb_2O_5. Upon heat treatment to (600,2), all niobia samples were indexed to TT-Nb_2O_5. In order to examine at which temperature this transformation to TT-Nb_2O_5 occurred, in-situ XRD work was done with a platinum hot stage. The experiment was performed by locking onto the angle corresponding to the main d-spacing of TT-Nb_2O_5 [(d=3.13Å), corresponding to $2\Theta = 12.80°$ after accounting for thermal broadening of the crystal lattice] and measuring this intensity as a function of both temperature and time with a heating rate of $10°$/min. Results of this study are shown in Figure 3-3. It is seen from this figure that the crystalline phase of TT-Nb_2O_5 quickly emerges from the niobia aerogel at a temperature of 600 °C. No further increase in intensity was seen after holding this temperature for 15 minutes. The intensity was also unchanged upon cooling the sample to a temperature of 100 °C. An XRD scan taken of this sample after cooling to room temperature confirmed the phase transformation to TT-Nb_2O_5. This method gave a good estimate on the temperature at which the phase transformation occurred; however, one should recall that XRD can only detect crystallites which are larger than 3 nm. Thus, it is possible that smaller crystallites could be growing at lower temperatures without being detected.

Table 3-5: XRD PHASES OF NIOBIA AEROGEL AND CONVENTIONALLY PREPARED NIOBIA WITH THERMAL TREATMENTS

Heat Treatment [Temp.(°C),Time(hr)]	X-Ray Diffraction Phases Samples			
	A-Nb$_2$O$_5$	X-Nb$_2$O$_5$	P-Nb$_2$O$_5$	Niobic Acid
(500,2)	A	TT	TT	TT$_{PC}$
(600,2)	TT	TT	TT	TT
(800,2)	T	T	T	T
(1000,-)	M	M	T + M	T + M
(1000,2)	M + H	H	H	M
(1000,48)	H	H	H	H + M

A=Amorphous; TT,T,M, and H refer to the phases of niobia; PC=poorly crystalline

Figure 3-2: XRD OF CALCINED Nb_2O_5 (500,2): A) A-Nb_2O_5, B) P-Nb_2O_5, AND C) X-Nb_2O_5 (NIOBIA PHASE IN BRACKETS)
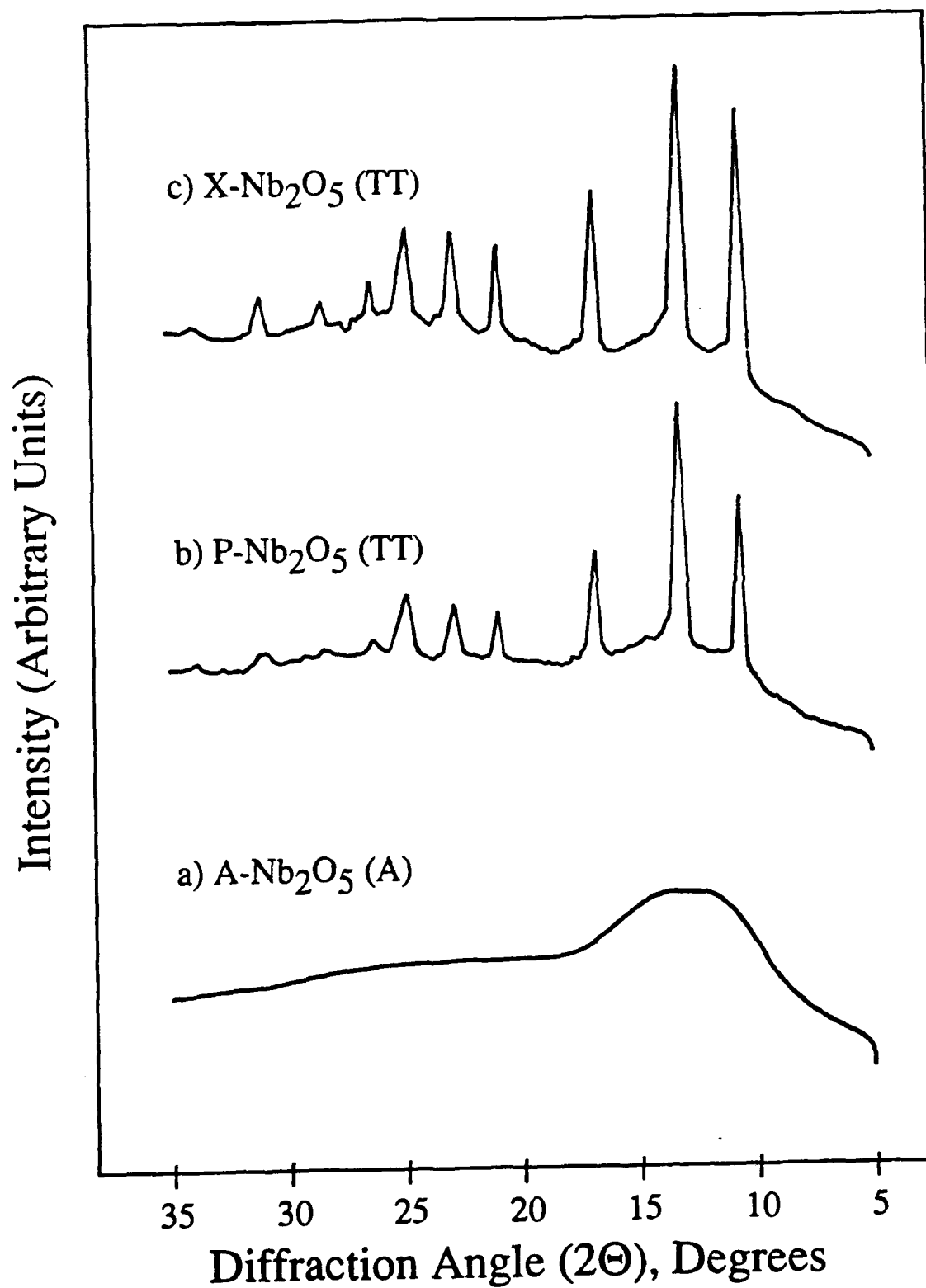
Figure 3-3: AMORPHOUS TO TT-Nb_2O_5 TRANSITION OF CALCINED A-Nb_2O_5 USING PLATINUM HOTSTAGE
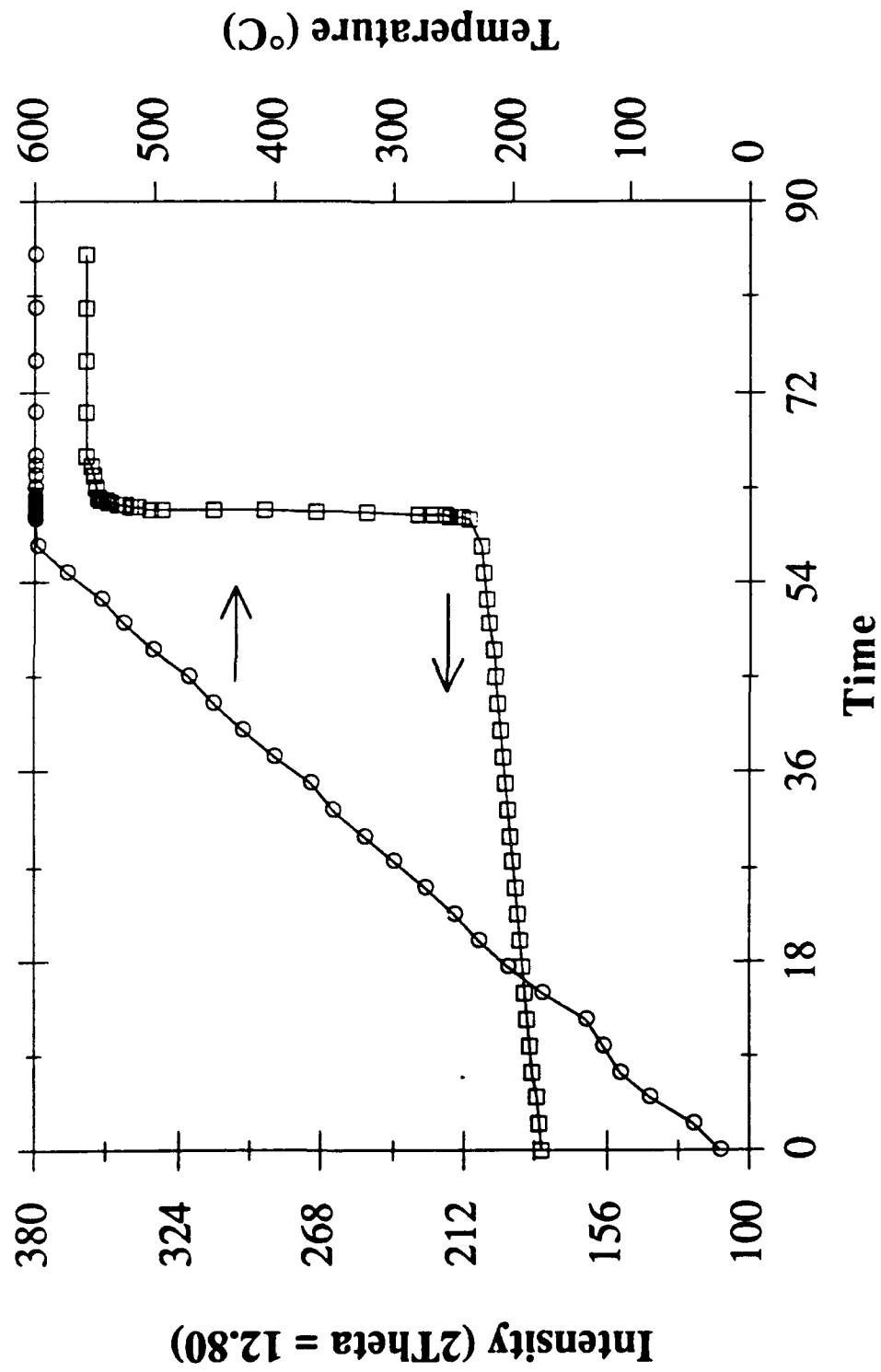
After the (600,2) and (800,2) heat treatments, identical results in XRD phases were seen for all prepared niobia samples as revealed in Table 3-5. Figures 3-4 and 3-5 show XRD scans of the low temperature and high temperature forms of Nb_2O_5, respectively, of the heat treated aerogel of niobia. After the (1000,-) heat treatment, the samples prepared by precipitation (P-Nb_2O_5 and Niobic Acid) all showed T-Nb_2O_5 along with M-Nb_2O_5. This could be due to a stablilizing effect of an impurity, while the niobia prepared through the sol-gel technique were readily transformed to M-Nb_2O_5 only.[29, 75] Upon longer holding times at 1000 °C, one sees that at (1000,2) the niobia aerogel is slower at totally transforming into H-Nb_2O_5 than the two conventionally prepared niobia. This could be due to a disordered nature of the aerogel which has not fully or completely organized into the highly ordered and stable H-Nb_2O_5.[78, 87, 185, 186] The niobic acid is even slower at organizing into the H-Nb_2O_5 phase and does not even attain this structure until heating to (1000,48). It still has XRD peaks attributed to M-Nb_2O_5 in the sample, even at this high thermal treatment. As stated before, this is probably due to impurities used in the commercial process to manufacture this material. In this study we found that the overall modification of Nb_2O_5 as a function of temperature is very similar to what has been reported earlier.[29, 87]

3.2.3 Differential Thermal Analysis (DTA)

DTA scans were performed on A-Nb_2O_5, X-Nb_2O_5, and P-Nb_2O_5 and the results are shown in Figure 3-6. The first feature in all three of these scans is the broad endothermic peak around 100 - 200 °C which is due to the evolution of physically bonded water from the niobium oxide surface. Niobic acid shows an even stronger endothermic peak at this same region due also to the evolution of water from this hydrated form of niobia. The next salient features of these scans are the sharp exothermic peaks around 550 - 600 °C. The peak temperatures for the three scans are 591 °C for A-Nb_2O_5, and 568 °C for both X-Nb_2O_5 and P-Nb_2O_5. Niobic acid also shows an exothermic peak temperature

Figure 3-4: XRD OF A-Nb_2O_5 AFTER HEAT TREATMENT: A) (500,2) [A], B) (600,2) [TT], AND C) (800,2) [T] (NIOBIA PHASE IN BRACKETS)
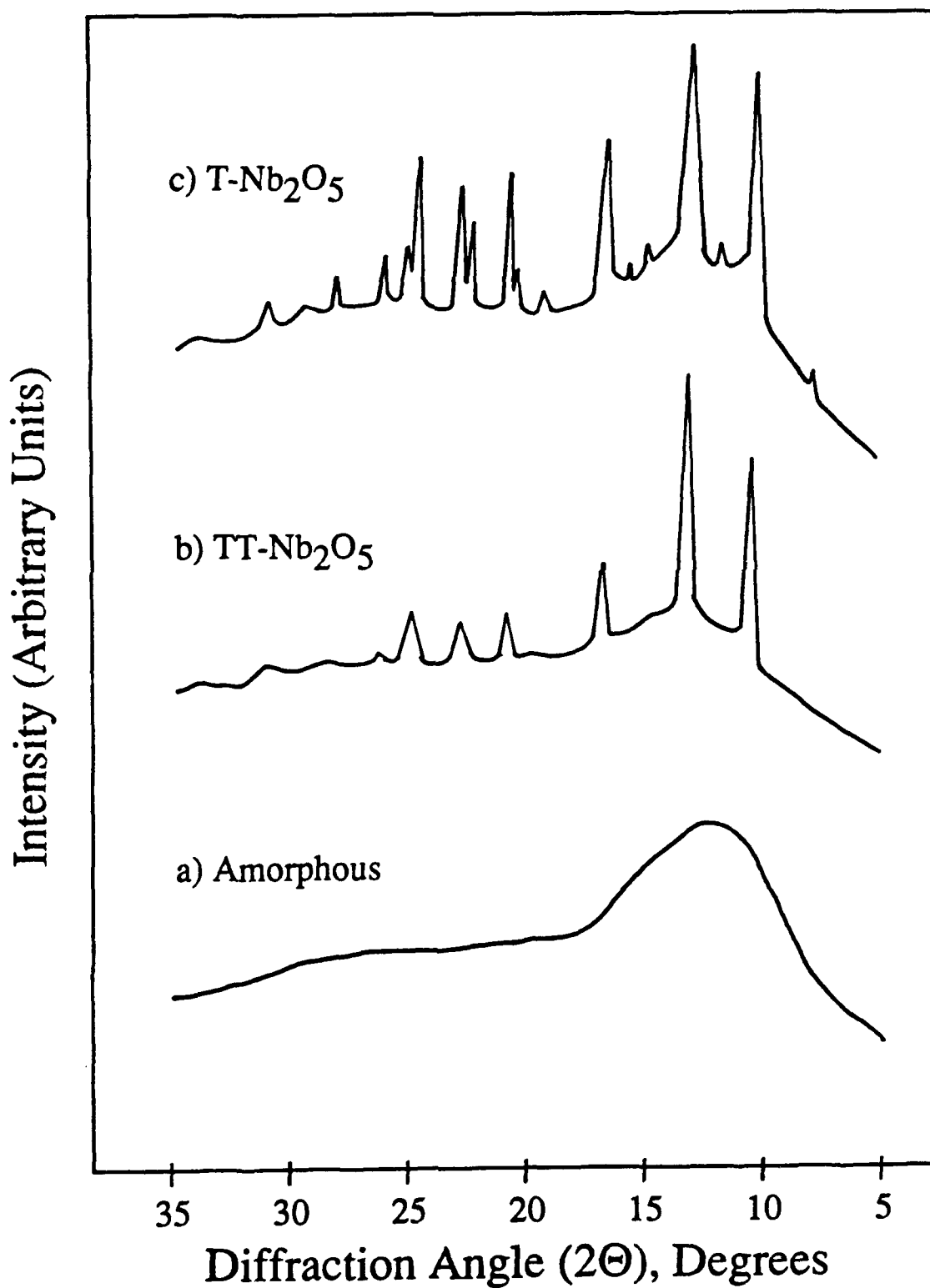
Figure 3-5: XRD OF A-Nb$_2$O$_5$ AFTER HEAT TREATMENT: A) (800,2) [T], B) (1000,-) [M], AND C) (1000,8) [H] (NIOBIA PHASE IN BRACKETS)

126
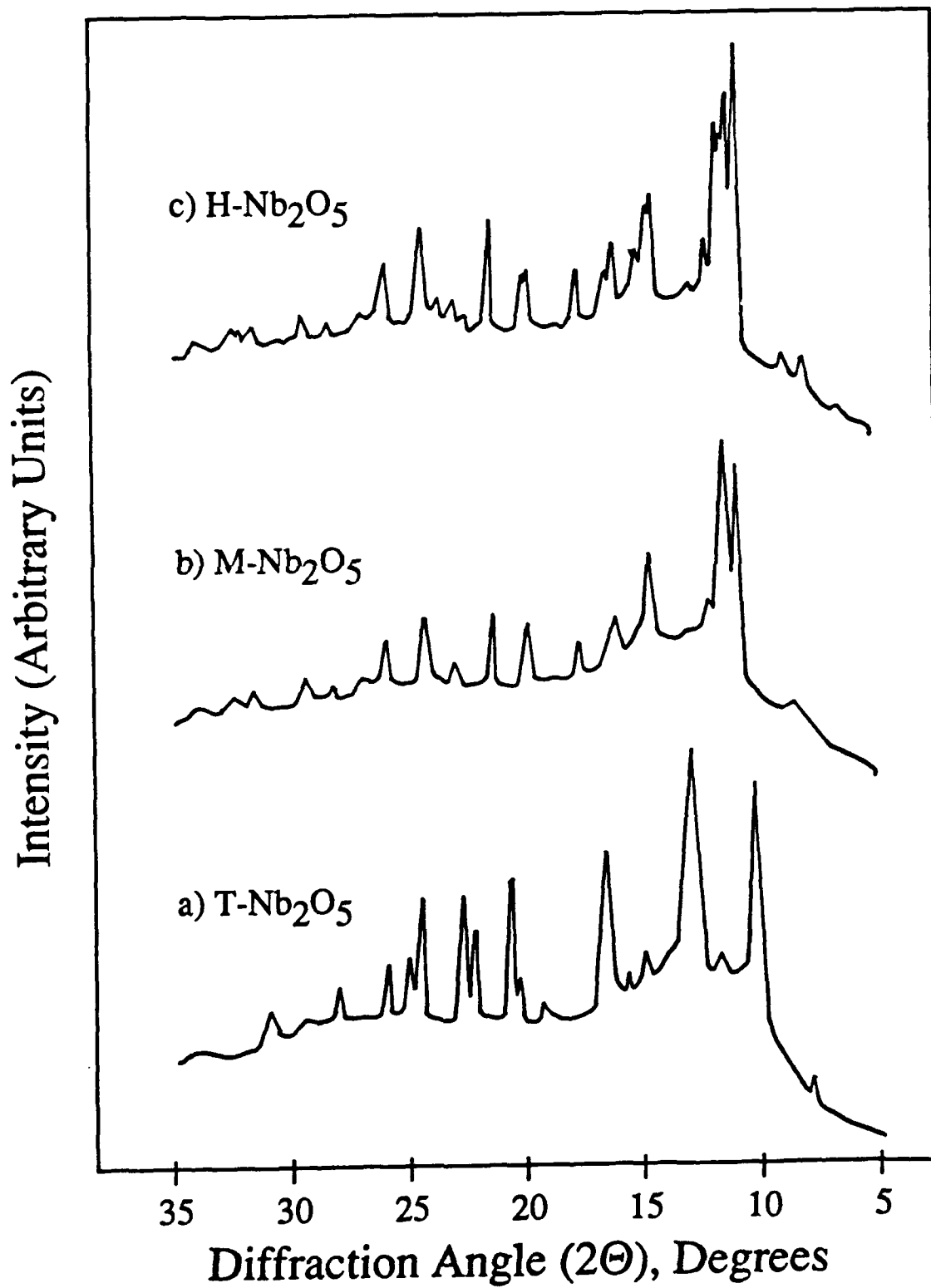
Figure 3-6: DTA SCANS OF A-Nb$_2$O$_5$, X-Nb$_2$O$_5$, AND P-Nb$_2$O$_5$ (FROM TOP TO BOTTOM)
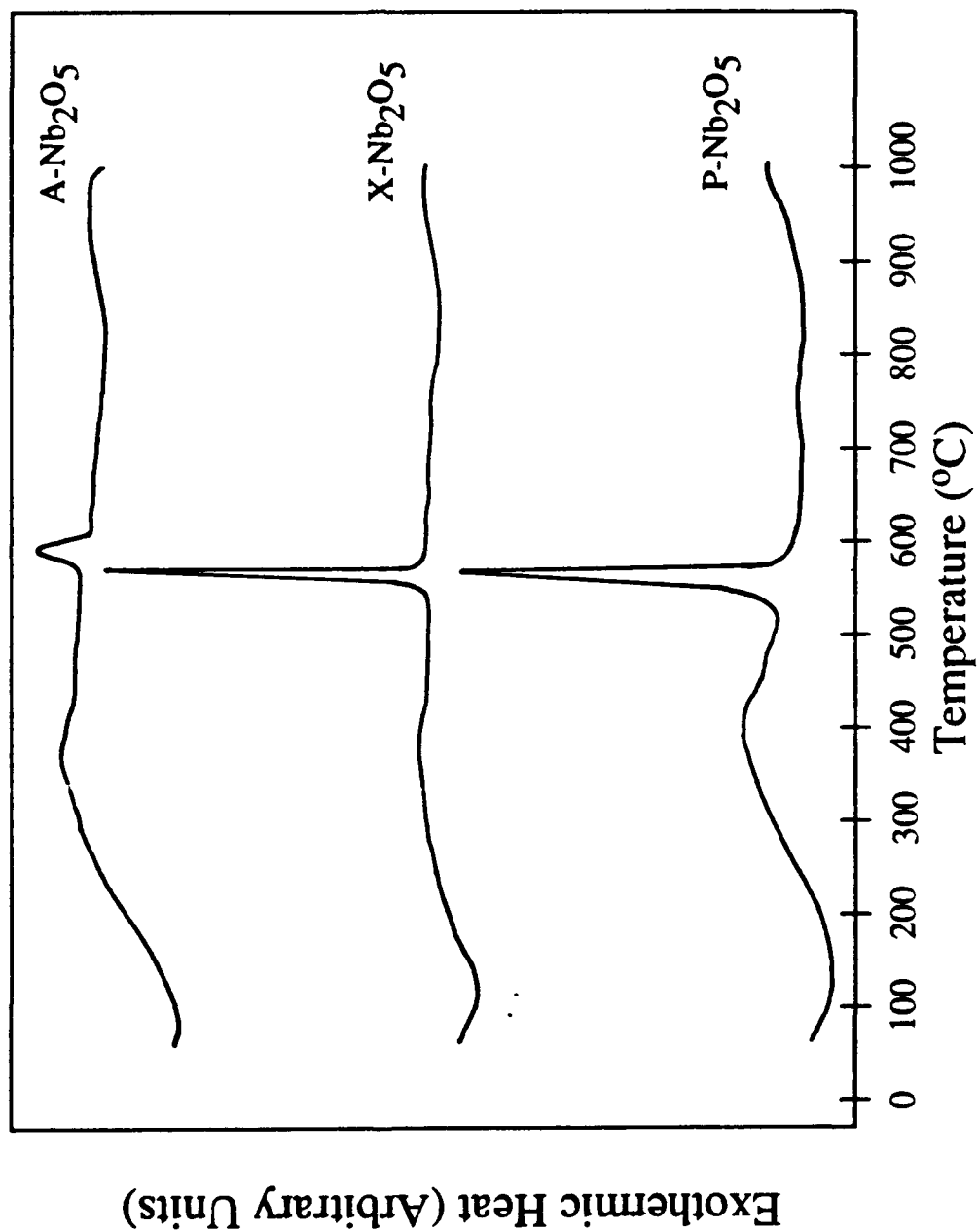
of 569 °C which is nearly identical to the other conventionally prepared niobia samples. This exothermic peak has been assigned to the amorphous to TT-Nb_2O_5 transformation.[143] Indeed all XRD scans, including the *in-situ* work with the platinum hot stage, indicated that TT-Nb_2O_5 formed after heat treatment to 600 °C. The lower transformation temperature for the conventionally prepared niobia indicates that the ordering to attain the crystalline phase of TT-Nb_2O_5 is easier; possibly due to the samples being more dense (lower pore volume), thus the atoms have smaller distances to move to attain order, or maybe because a seed of TT-Nb_2O_5 is already in place and it is easier for the remaining amorphous niobia in the sample to form the TT-Nb_2O_5 phase and sinter. The higher transformation temperature (~ 20 °C higher) of the niobia aerogel indicates that it is more difficult to attain order with this sample, and the fact that the peak is broader than the others suggests a more heterogeneous environment in this material, due possibly to its much larger pore volume and smaller bulk density.

3.2.4 Scanning Electron Microscopy (SEM)

Scanning electron microscopy (SEM) was used to examine morphological differences among the prepared niobia samples. Figures 3-7, 3-8, 3-9, and 3-10 show SEM micrographs of A-Nb_2O_5 which was subjected to various heat treatments: (500,2), (600,2), (800,2), and (1000,-), respectively. After the standard (500,2) calcination, the aerogel of niobia appears as a "fluffy" mass of particles as shown in Figure 3-7. The same morphology is maintained even after the heat treatment at (600,2) as seen in Figure 3-8. Not until the (800,2) thermal treatment do we see an agglomeration of particles that appear to have attained an ordered state of platelets as shown in the lower right corner of Figure 3-9. The morphology of platelets existing throughout the sample is not seen until heat treatment at (1000,-) as shown in Figure 3-10. Figure 3-11 and Figure 3-12 show SEM micrographs of the calcined, (500,2), samples of X-Nb_2O_5 and P-Nb_2O_5. It is apparent that for these two samples the platelets already appear. The platelets are a sign of ordering

Figure 3-7: SEM MICROGRAPH OF CALCINED A-Nb_2O_5 (500,2)

No. #1 250X   100μ
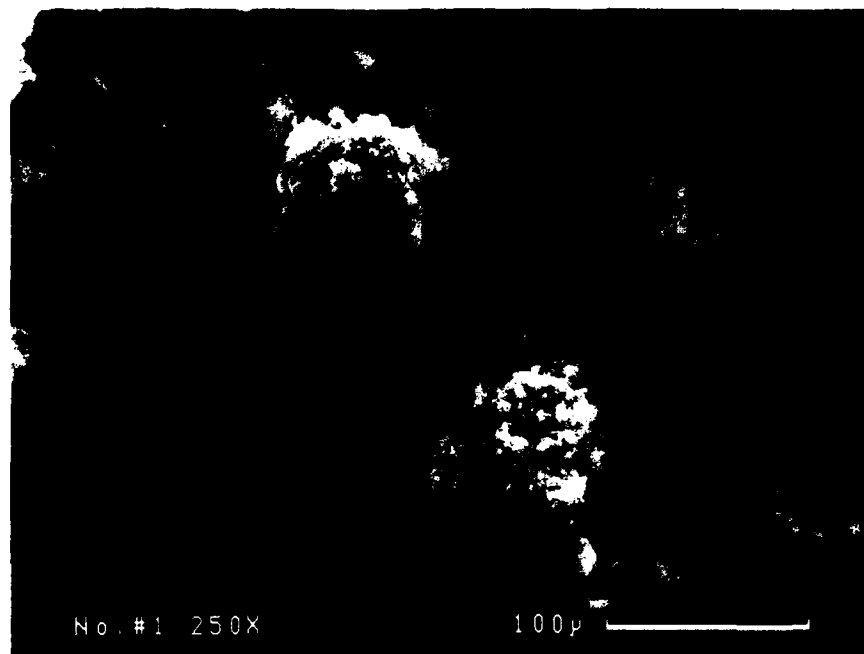
Figure 3-8: SEM MICROGRAPH OF HEAT TREATED A-Nb_2O_5 (600,2)

NO. #8 250X   100μ
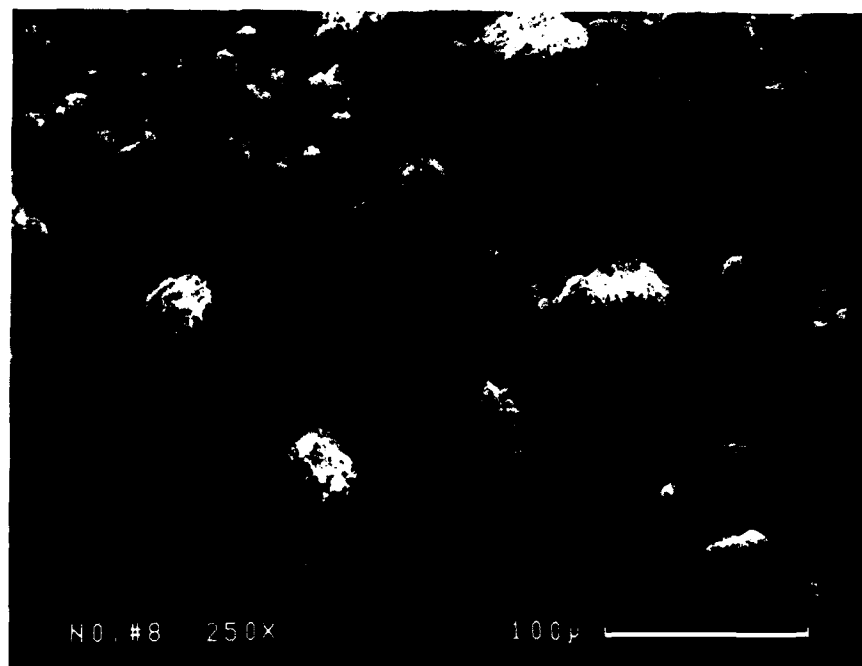
Figure 3-9: SEM MICROGRAPH OF HEAT TREATED A-Nb$_2$O$_5$ (800,2)
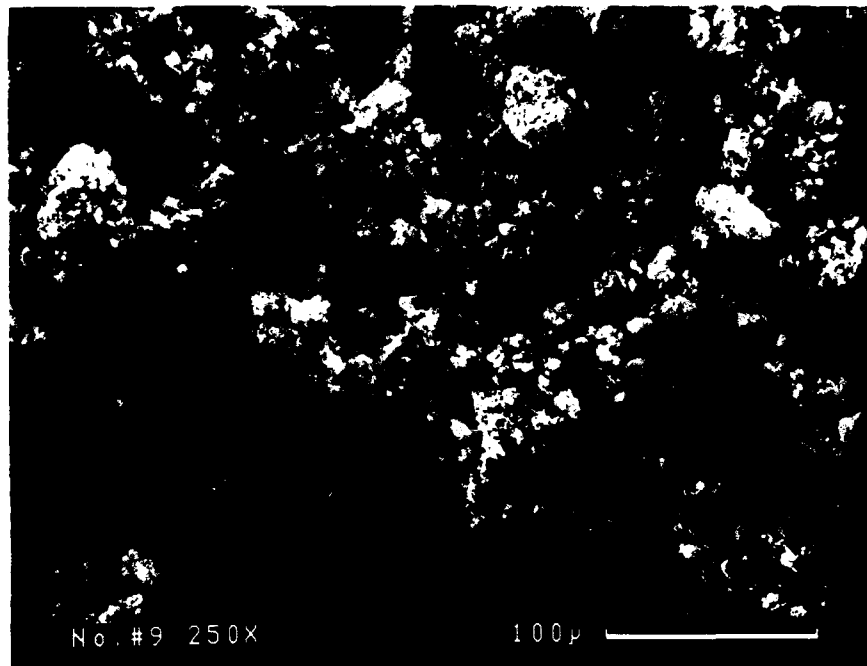
Figure 3-10: SEM MICROGRAPH OF HEAT TREATED A-Nb$_2$O$_5$ (1000,-)
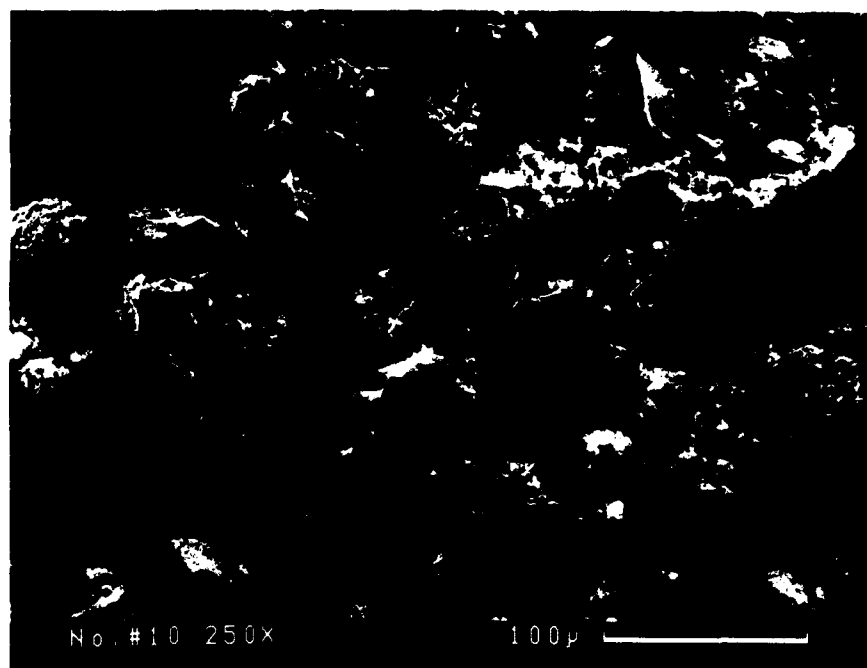
Figure 3-11: SEM MICROGRAPH OF CALCINED X-Nb$_2$O$_5$ (500,2)
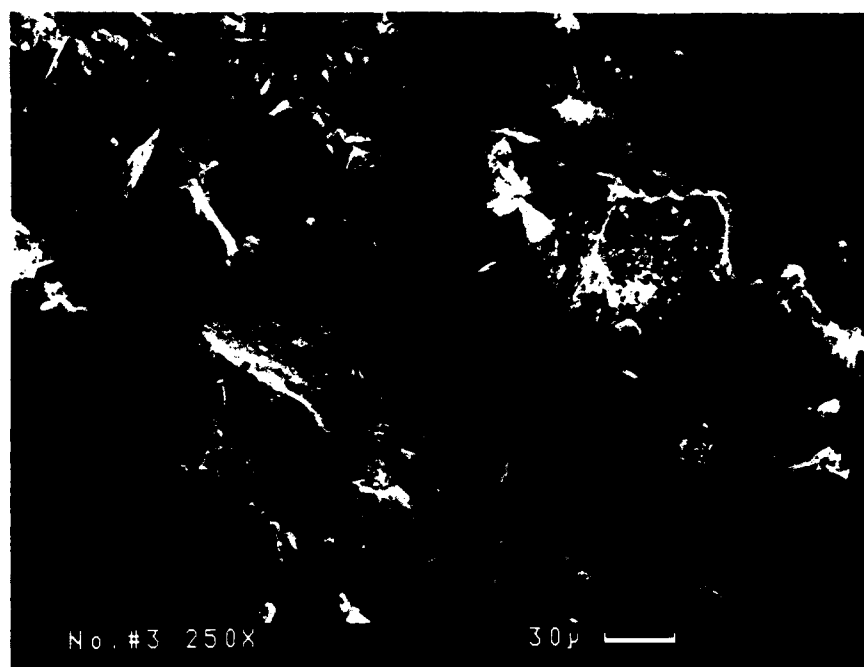
Figure 3-12: SEM MICROGRAPH OF CALCINED P-Nb$_2$O$_5$ (500,2)
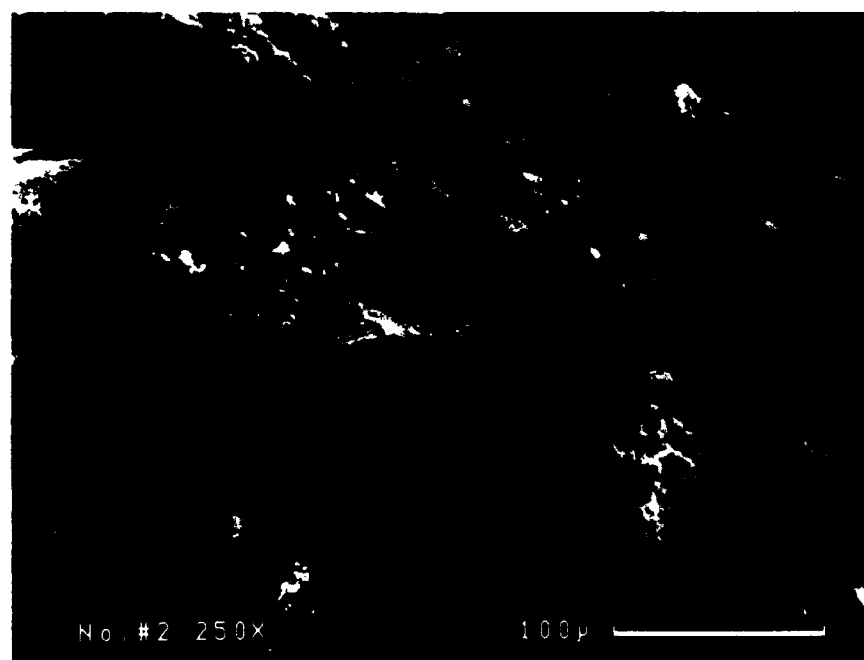
that has begun to take place with the conventional niobia, while the aerogel of niobia has a disorganized and possibly distorted structure as seen by its random particle appearance. These findings are further confirmed by the XRD studies mentioned previously which indicated the presence of $TT\text{-}Nb_2O_5$ in the conventionally prepared niobia.

3.2.5 Laser Raman Spectroscopy (LRS)

Laser Raman Spectroscopy (LRS) was used to analyze the vibrational modes of molecules. The spectra presented here and in the subsequent chapters will be interpreted by comparison with reference niobium oxide compounds.[67, 187] LRS spectra for the niobia aerogel heat treated at low temperatures [(500,2), (600,2), and (800,2)] are shown in Figure 3-13. These spectra correspond to the amorphous, TT-, and $T\text{-}Nb_2O_5$ structures respectively. Figure 3-14 shows the LRS spectra for samples treated at higher temperatures [(800,2), (1000,-) and (1000,8)]. These spectra correspond to T-, M-, and $H\text{-}Nb_2O_5$ respectively as indicated by our previous XRD studies (see Table 3-5). Our Raman spectrum for $H\text{-}Nb_2O_5$ agrees well with that found by other researchers.[88, 94, 187]

Table 3-6 shows McConnell's frequency assignments for $H\text{-}Nb_2O_5$.[187] The vibrational modes at 995 cm^{-1} (S) and 883 cm^{-1} (W) have been assigned to symmetric stretches of edge and corner sharing NbO_6 octahedra, respectively, and the mode at 850 cm^{-1} (W) to an NbO_4 tetrahedron. The bending modes of NbO_6 octahedra (signature bands for bulk niobia) have been assigned to 625 - 670 cm^{-1} (S). Below 550 cm^{-1} (W and S) are located various lower vibrational modes of NbO_6 octahedra and NbO_4 tetrahedra. Recently, Jehng and Wachs have related reference niobium oxide structures to Raman frequencies.[67, 94] They have determined that highly distorted NbO_6 octahedra (usually in possession of at least one Nb=O bond) have Raman bands in the range of 850 - 1000 cm^{-1} depending on the distortion. Slightly distorted NbO_6 (also NbO_7 and NbO_8) units (not possessing Nb=O bonds) have Raman bands in the 500 - 700 cm^{-1} range; these units exist in the TT- or T- forms of bulk niobia. Tetrahedral species were shown to have stretching

Figure 3-13: LRS SPECTRA OF A-Nb_2O_5 AFTER HEAT TREATMENT: (500,2) [A], (600,2) [TT], AND (800,2) [T] (FROM BOTTOM TO TOP)
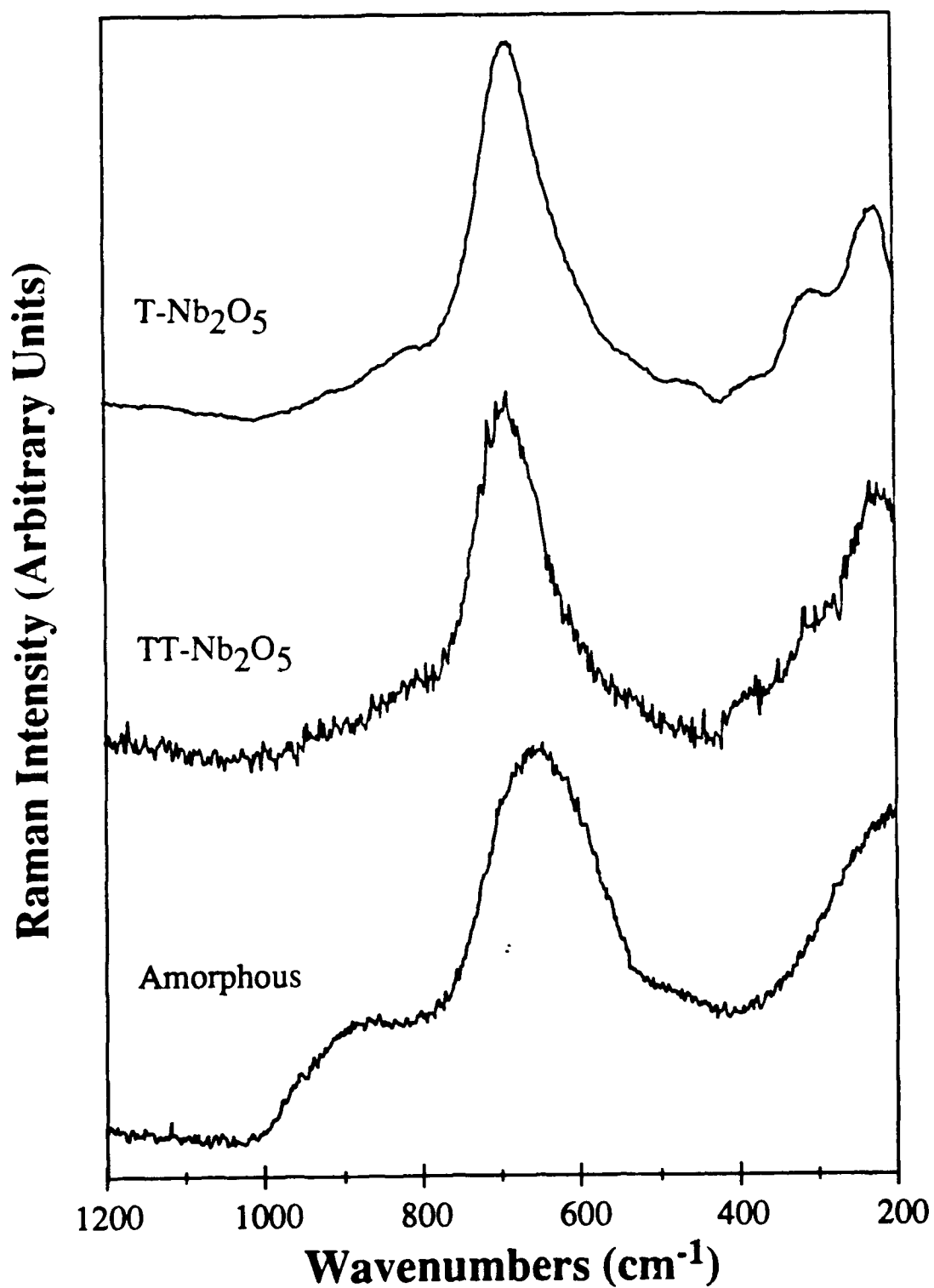
Figure 3-14: LRS SPECTRA OF A-Nb$_2$O$_5$ AFTER HEAT TREATMENT: (800,2) [T], (1000,-) [M], AND (1000,8) [H] (FROM BOTTOM TO TOP)
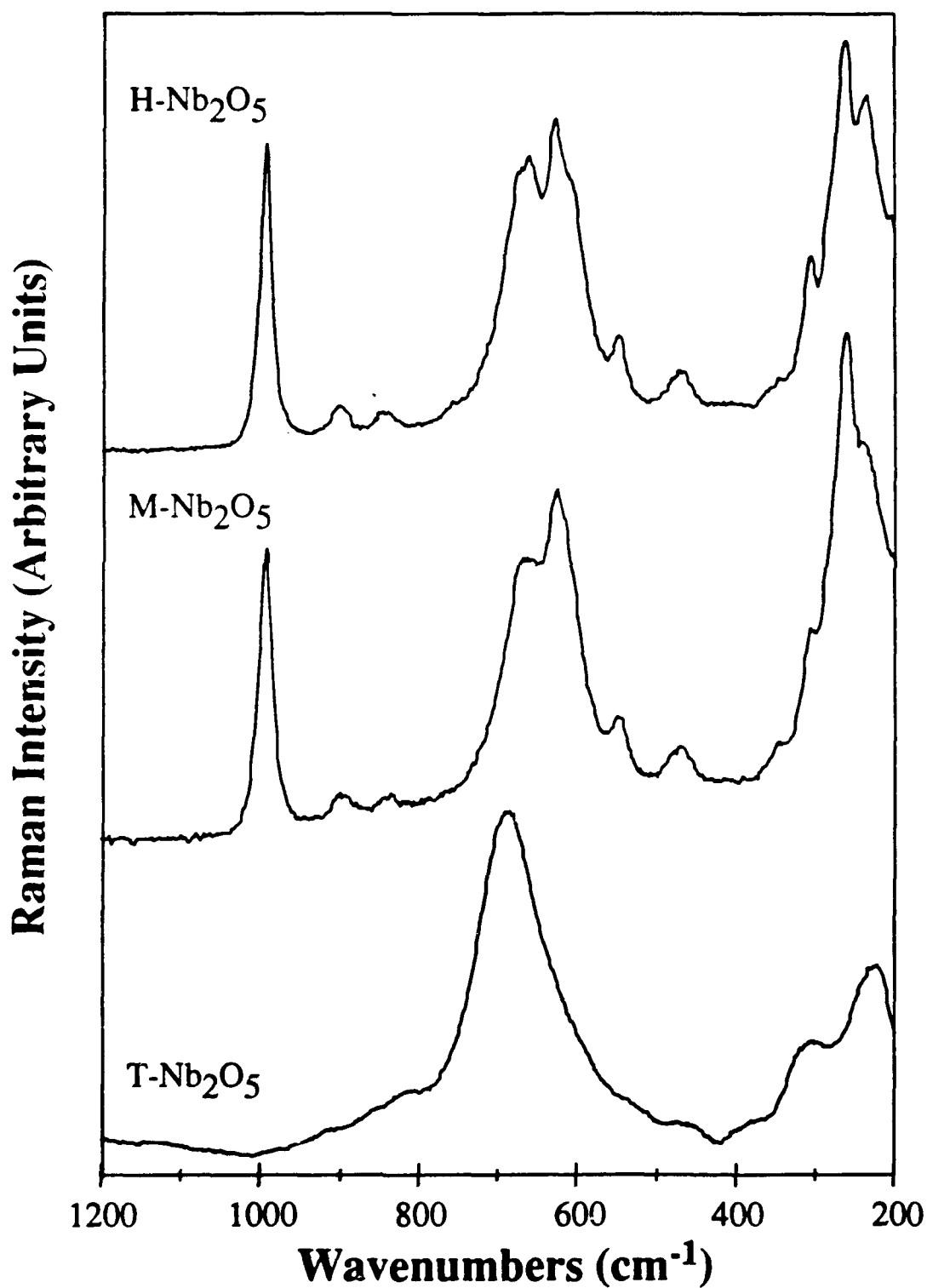
Table 3-6: ASSIGNMENTS OF MAJOR RAMAN BANDS FOR $H\text{-}Nb_2O_5$[187]

Vibrational Mode	Wavenumber cm^{-1}	Assignment
ν_1	995(S)	Symmetric stretch of edge sharing NbO_6
ν_1	883(W)	Symmetric stretch of corner sharing NbO_6
ν_1	850(W)	NbO_4 tetrahedron
ν_2	670(S)	Bending modes of NbO_6
ν_2	625(S)	Bending modes of NbO_6
ν_{5+6}	<550(W+S)	Lower vibrational modes of NbO_6

frequencies in the range of 790 - 830 cm^{-1}, closely matching the frequency assignment for tetrahedra found in H-Nb$_2$O$_5$. An interesting study on Nb-O bond distances and bond orders by Raman Spectroscopy recently has shown that Raman frequencies strongly depend on the bond order of the niobium oxide structure.[92] The higher the niobium oxygen bond order, corresponding to a shorter Nb-O distance, the higher is the corresponding Raman wavenumber.

The low-temperature forms of niobia (amorphous, TT-, and T-Nb$_2$O$_5$) have features that are similar, but different in certain ways (see Figure 3-13). The amorphous niobia aerogel has a large noticeable shoulder around 900 cm^{-1} that disappears upon higher heat treatment and formation of TT-Nb$_2$O$_5$. A shift in the bending modes of the NbO$_6$ octahedra from ~ 650 cm^{-1} to 690 cm^{-1} is seen for the amorphous to TT-Nb$_2$O$_5$ phase transition. The main difference between TT- and T-Nb$_2$O$_5$ appears to occur in the lower frequency range, with peaks beginning to sharpen at 307 and 230 cm^{-1} for T-Nb$_2$O$_5$. The bending mode for T-Nb$_2$O$_5$ does not shift at 690 cm^{-1}. Since TT- and T-Nb$_2$O$_5$ have been considered to be nearly identical in structure, and it has been stated that T-Nb$_2$O$_5$ is simply a better ordered TT-Nb$_2$O$_5$ with more long range order, the bands below 400 cm^{-1} can be attributed to this difference in long range order.[18, 29, 78]

The features of the high-temperature forms of niobia: T-, M- and H-Nb$_2$O$_5$ are shown in Figure 3-14. Drastic changes in the LRS spectra are seen between T- and M-Nb$_2$O$_5$. This is not surprising considering the drastic changes in structure that have occurred to obtain the well-ordered M-Nb$_2$O$_5$.[29, 87] Two very noticeable peaks new to M- over T-Nb$_2$O$_5$ are the 995 and 850 cm^{-1} frequencies corresponding to the edge sharing NbO$_6$ octahedra and the NbO$_4$ tetrahedra, respectively. The LRS spectra between M- and H-Nb$_2$O$_5$ (H having the more distinct features) look similar and this would be expected since High Resolution Electron Microscopy (HRTEM) data show these two phases to be nearly indistinguishable.[87] In fact, it has been reported that the nature of M-Nb$_2$O$_5$ can best be explained by assuming that M-Nb$_2$O$_5$ is simply a disordered H-Nb$_2$O$_5$ structure.[78,

[87, 185, 186] From our XRD finding that M-Nb_2O_5 readily transforms exclusively into H-Nb_2O_5, the likely explanation is indeed that M-Nb_2O_5 is a poorly crystallized H-Nb_2O_5 precursor, in similar fashion as TT-Nb_2O_5 is the disordered precursor to the more ordered T-Nb_2O_5.

3.2.5.1 In-situ LRS (Dehydrated)

In-situ LRS studies were performed on the calcined (500,2) niobia aerogel to provide additional discrimination between surface and bulk functionalities in this high surface area oxide, because moisture has been found to only coordinate to surface functionalities.[188] The Raman features resulting from a dehydration treatment are then identified as surface functionalities. The process is reversed by readsorbing water vapor onto these surface groups. The *in-situ* Raman experiment for A-Nb_2O_5 is shown in Figure 3-15 for various dehydration temperatures and also for the aerogel sample in its hydrated form. This figure demonstrates that the broad and weak Raman bands at ~ 900 cm^{-1} shift to higher frequencies due to the thermal desorption of the adsorbed moisture. After (100,1) there is no shift in frequencies indicating that water is still physically bound to the sample. Upon higher dehydration heat treatments, (200,1) and (500,1), we observe two new Raman bands at ~ 930 cm^{-1} and ~ 990 cm^{-1} which are characteristic of two different highly distorted Nb=O surface sites, and no phase transformations occur during these heat treatments since the Raman features of the bulk amorphous niobium oxide remain unchanged (no shift from 650 cm^{-1} to 690 cm^{-1} due to increasing bond order of the NbO_6 octahedra).[94] Rehydrating this sample with adsorbed moisture returns the bulk niobia aerogel to its former state with one broad peak around 900 cm^{-1} (see Figure 3-15). This peak shift is nearly identical to what has been found by *in-situ* Raman studies with commercial niobic acid; however, the peak intensities are attenuated, especially at the 990 cm^{-1} frequency.[94] After a (600,1) heat treatment of the niobia aerogel, *in-situ* Raman reveals features at 990 cm^{-1} and 930 cm^{-1} but both are weak and severely attenuated due to

Figure 3-15: IN-SITU LRS SPECTRA OF HYDRATED AND DEHYDRATED A-Nb$_2$O$_5$ AFTER VARIOUS EVACUATION TEMPERATURES: (100,1), (200,1), AND (500,1) (FROM BOTTOM TO TOP)
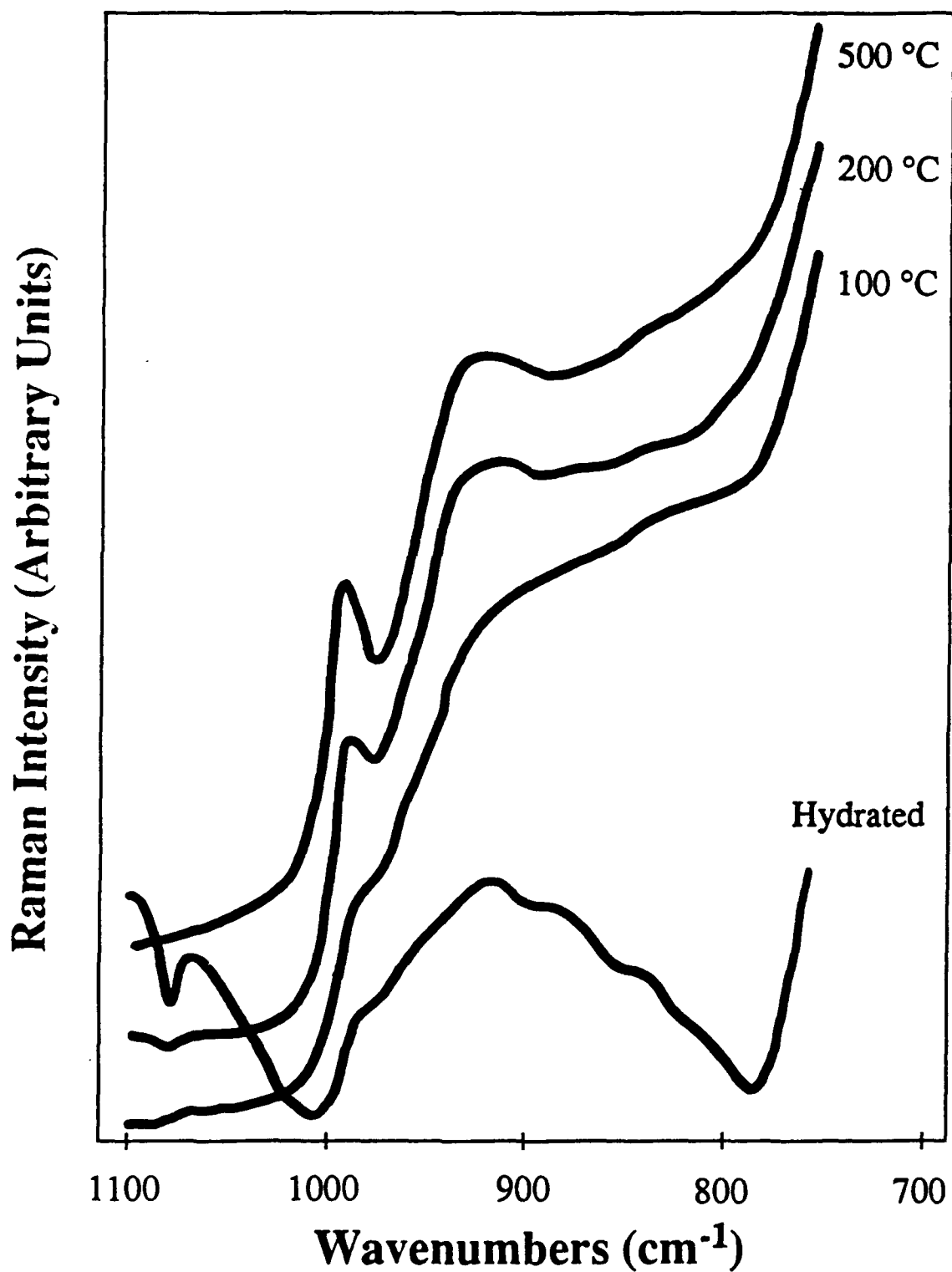
the heat treatment. We also noticed a shift from 650 cm^{-1} to 690 cm^{-1}, indicating a phase transformation had occurred.[94] The results reveal that the concentration of Nb=O terminal sites on A-Nb$_2$O$_5$ (600,2) is small and can probably be eliminated all together by higher thermal treatments to decrease the surface area and increase the order of the sample. Thus, to summarize the *in-situ* Raman studies, it is evident that terminal Nb=O surface species are present in amorphous niobia and the Raman band (hydrated) at ~ 900 cm^{-1} is assigned to these terminal Nb=O sites. Higher thermal treatments reduce the number of these terminal sites significantly.[94]

3.2.6 Diffuse Reflectance Infrared Spectroscopy (DRIFT)

Diffuse Reflectance Infrared Spectroscopy (DRIFT) was attempted in this study to observe the Nb=O feature; however, due to the low throughput of the infrared signal and the complications of adsorbed water, as seen with the previous LRS spectra, we were unable to get meaningful data in this range (< 1200 cm^{-1}). We were able to study the hydroxyl stretching region of the niobia aerogel as a function of heat treatment. One interesting result of this study on the hydroxyl region was the formation of a second hydroxyl group on the hydrated niobia aerogel that is not observed on the other heat treated forms of niobia. This data is compiled in Appendix C along with data for all other aerogel samples studied, and is discussed along with data for the transmission spectra of the oxides prior to and after treatment with pyridine in Section 3.5.2.2.

3.3 Chemical Property Characterization of Niobia Aerogels

3.3.1 Acid Strength/Acidity with n-Butylamine Titration

The acid strength (pKa) and corresponding acidity in terms of a per gram and per surface area basis for the uncalcined and calcined niobia are shown in Table 3-7, and those for the heat treated niobia are listed in Table 3-8. All samples were pretreated in air under

Table 3-7: ACID STRENGTH OF Nb_2O_5: A) ACIDITY (MMOLES/G) AND B) ACIDITY (MMOLES/M^2) VERSUS pKa

A) Acid Strength of Nb_2O_5 [Acidity (mmoles/g)]

	Acidity (mmoles/g)					
	pKa					
Sample	+4.8	+3.3	+1.5	-3.0	-5.6	-8.2
A-Nb_2O_5 (500,2)	0.74	0.52	0.47	0.45	0.45	0.26
Niobic Acid Uncalc.	0.57	0.47	0.44	0.40	0.32	0.058
P-Nb_2O_5 (500,2)	0.18	0.15	0.15	0.12	0.12	0.036
X-Nb_2O_5 (500,2)	0.063	0.038	0.038	0.037	0.021	0.00

B) Acid Strength of Nb_2O_5 [Acidity (mmoles/m^2)]

	Acidity (mmoles/m^2) x 10^4					
	pKa					
Sample	+4.8	+3.3	+1.5	-3.0	-5.6	-8.2
A-Nb_2O_5 (500,2)	37.9	26.7	24.2	23.1	22.9	13.2
Niobic Acid Uncalc.	37.9	31.5	29.4	26.4	21.3	3.9
P-Nb_2O_5 (500,2)	19.2	15.4	15.3	12.6	12.6	3.8
X-Nb_2O_5 (500,2)	9.0	5.4	5.4	5.2	3.0	0.0

Table 3-8:   ACID STRENGTH OF HEAT TREATED Nb_2O_5: A) ACIDITY
(MMOLES/G) AND B) ACIDITY (MMOLES/M^2) VERSUS pKa

A) Acid Strength of Heat Treated Nb_2O_5 [Acidity (mmoles/g)]

	Acidity (mmoles/g)					
	pKa					
Sample	+4.8	+3.3	+1.5	-3.0	-5.6	-8.2
A-Nb_2O_5 (500,2)	0.74	0.52	0.47	0.45	0.45	0.26
Niobic Acid Uncalc.	0.57	0.47	0.44	0.40	0.32	0.058
Niobic Acid (500,2)	0.27	0.17	0.16	0.11	0.069	0.007
P-Nb_2O_5 (500,2)	0.18	0.15	0.15	0.12	0.12	0.036
A-Nb_2O_5 (600,2)	0.27	0.18	0.12	0.10	0.099	0.00
X-Nb_2O_5 (500,2)	0.063	0.038	0.038	0.037	0.021	0.00
Niobic Acid (600,2)	0.077	0.026	0.023	0.014	0.008	0.00

B) Acid Strength of Heat Treated Nb_2O_5 [Acidity (mmoles/m^2)]

	Acidity (mmoles/m^2) x 10^4					
	pKa					
Sample	+4.8	+3.3	+1.5	-3.0	-5.6	-8.2
A-Nb_2O_5 (500,2)	37.9	26.7	24.2	23.1	22.9	13.2
Niobic Acid Uncalc.	37.9	31.5	29.4	26.4	21.3	3.9
Niobic Acid (500,2)	27.1	17.4	16.1	11.0	6.9	0.7
P-Nb_2O_5 (500,2)	19.2	15.4	15.3	12.6	12.6	3.8
A-Nb_2O_5 (600,2)	44.0	30.4	19.3	16.7	16.4	0.0
X-Nb_2O_5 (500,2)	9.0	5.4	5.4	5.2	3.0	0.0
Niobic Acid (600,2)	29.8	9.8	9.0	5.3	2.9	0.0

vacuum at 110 °C for 1 hour, after the calcinations, and then transferred immediately to the dry glove box while still hot to eliminate or minimize physisorbed water on the sample surface. Figures 3-16(A) and(B) show the acidity of these samples in terms of millimoles (n-butylamine) per gram and per area of sample, respectively, versus acid strength (pKa). The calcined (500,2) niobia aerogel and uncalcined niobic acid show much greater acidity on a per gram (an average of 5 times as much) over the entire range of acid strength than the conventionally prepared niobia; however, on a surface area basis, the acidity is approximately twice as much. The corresponding XRD and LRS data show that the two samples with the greater acidity were amorphous, while the two samples whose acidity was much lower contained TT-Nb_2O_5 (the least ordered structure of niobia). Figures 3-17(A) and (B) show the acidity per gram and per area, respectively, versus acid strength of various heat treated niobia samples. Notice the two fairly distinct regions in the figure. The upper portion, as noted earlier, corresponds to amorphous niobia and the lower portion corresponds to more ordered crystalline niobia that has a somewhat distorted appearance due to the nature of the TT-Nb_2O_5 structure, and is confirmed by XRD and LRS studies on these materials. These regions appear in both figures for acidity on both a per gram and per surface area basis which shows that the crystalline structure of niobia is playing a role in the acidity of these materials.

The acid strength and corresponding acidity for the heat treated aerogels of niobia are listed in Table 3-9(A) and (B) for acidity on a per gram and per area basis, respectively. Note that A-Nb_2O_5 (400,2) is merely the niobia aerogel calcined at a lower temperature (400 °C). Table 3-10(A) and (B) shows the same information for heat treated niobic acid. Figures 3-18(A) and (B) and 3-19(A) and (B) show plots of the tabulated heat treated niobia aerogel and niobic acid data, respectively. Notice in Figure 3-18 that again one can chart the crystallinity and ordering of the niobia aerogel as a function of temperature by measuring its marked acidity (per gram) decrease from the amorphous upper portion, to the slightly distorted TT-Nb_2O_5 (middle portion), to the longer ranged order of T-Nb_2O_5

Figure 3-16: A) NIOBIA ACIDITY (MMOLES/G) AND B) NIOBIA ACIDITY (MMOLES/M^2) VS. pKa

A) Niobia Acidity (mmoles/g)
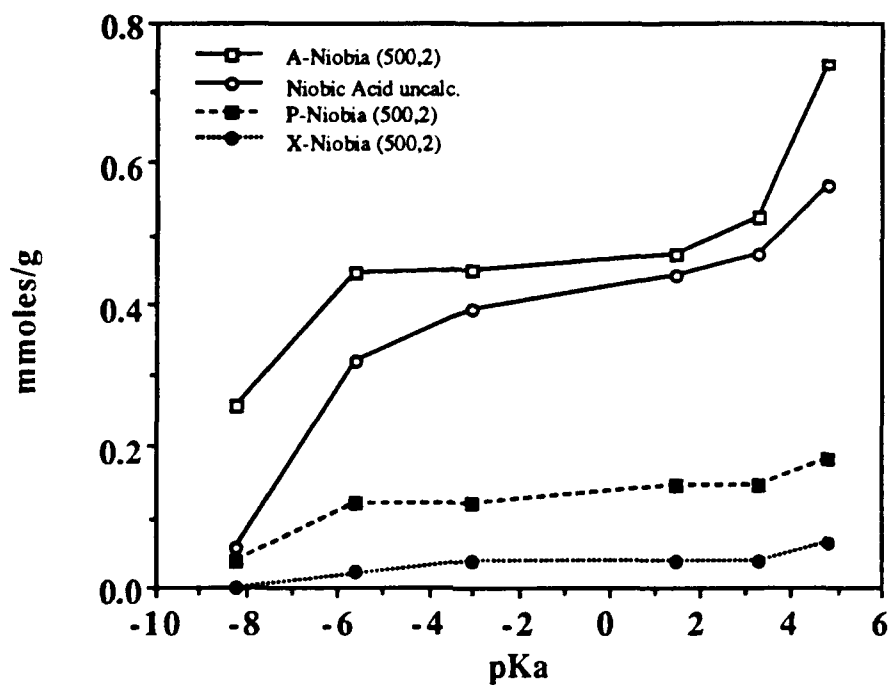
B) Niobia Acidity (mmoles/m^2)
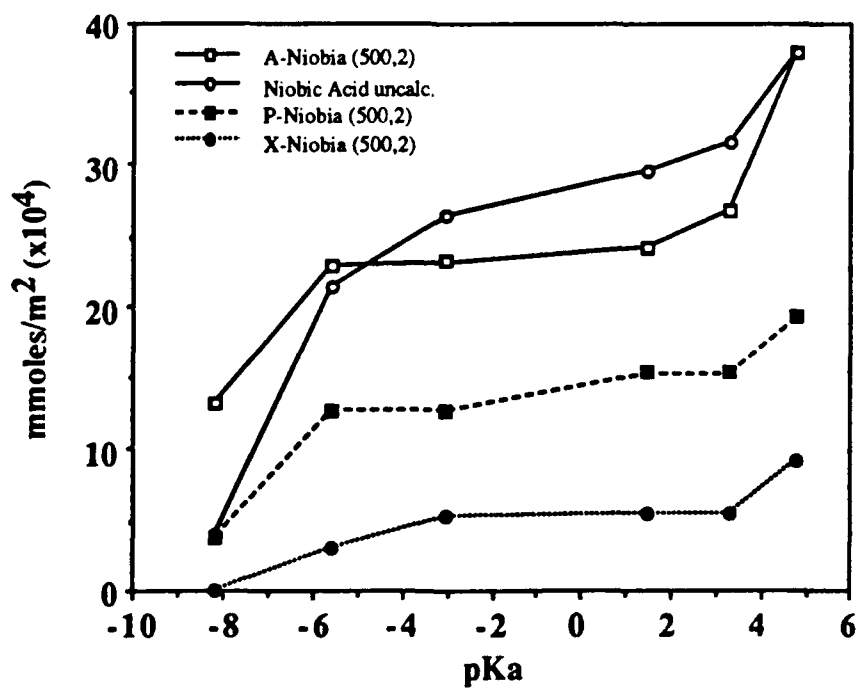
Figure 3-17: A) HEAT TREATED NIOBIA ACIDITY (MMOLES/G) AND B) HEAT
TREATED NIOBIA ACIDITY (MMOLES/M^2) VS. pKa

A) Heat Treated Niobia Acidity (mmoles/g)
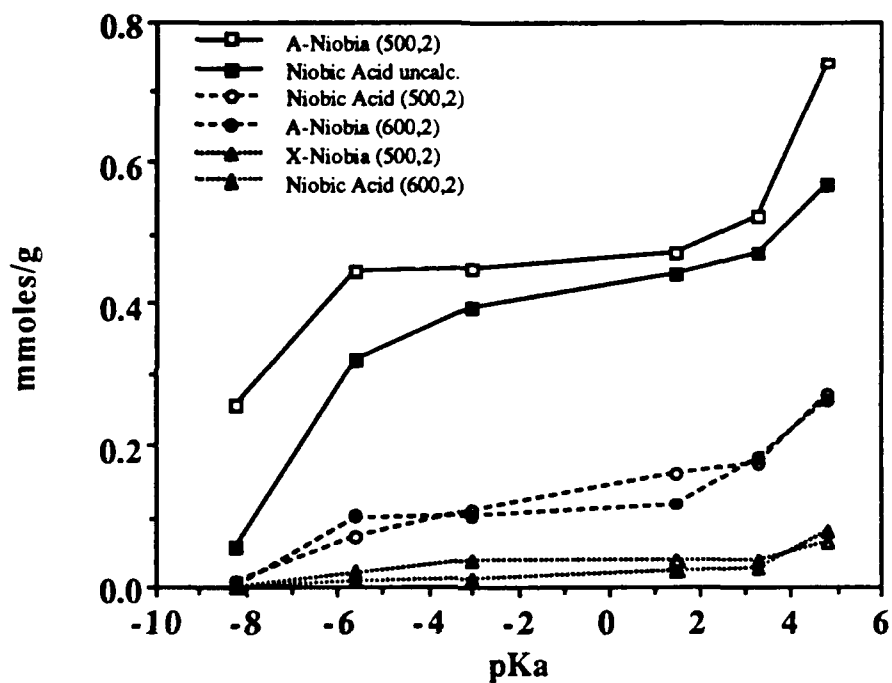
B) Heat Treated Niobia Acidity (mmoles/m^2)
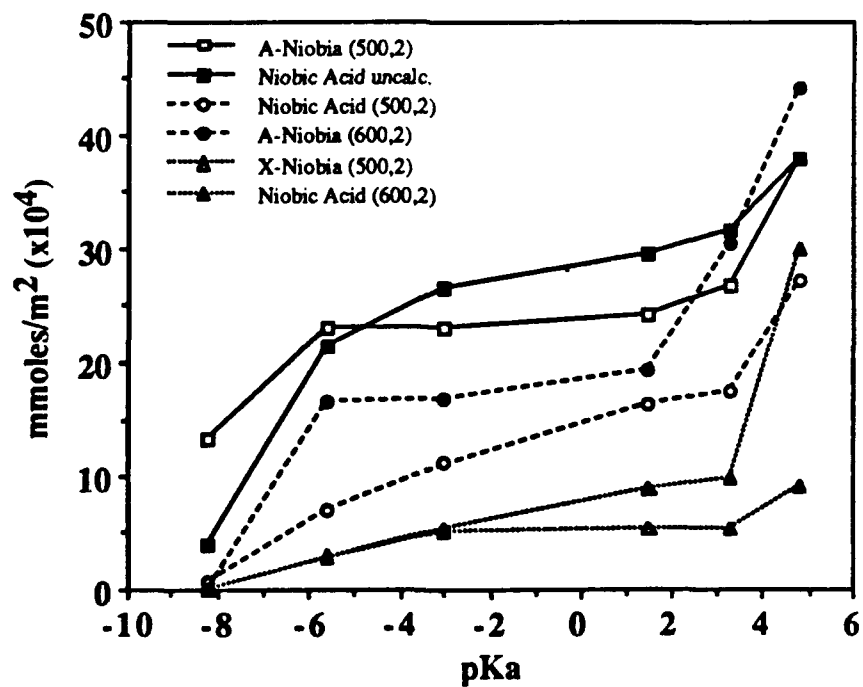
Table 3-9: ACID STRENGTH OF HEAT TREATED A-Nb$_2$O$_5$: A) ACIDITY (MMOLES/G) AND B) ACIDITY (MMOLES/M^2) VERSUS pKa

A) Acid Strength of Heat Treated A-Nb$_2$O$_5$ [Acidity (mmoles/g)]

	Acidity (mmoles/g)					
			pKa			
Sample	+4.8	+3.3	+1.5	-3.0	-5.6	-8.2
A-Nb$_2$O$_5$ (400,2)	0.81	0.66	0.66	0.57	0.53	0.28
A-Nb$_2$O$_5$ (500,2)	0.74	0.52	0.47	0.45	0.45	0.26
A-Nb$_2$O$_5$ (600,2)	0.26	0.18	0.12	0.10	0.099	0.00
A-Nb$_2$O$_5$ (800,2)	0.012	0.0060	0.00	0.00	0.00	0.00

B) Acid Strength of Heat Treated A-Nb$_2$O$_5$ [Acidity (mmoles/m^2)]

	Acidity (mmoles/m^2) x 10^4					
			pKa			
Sample	+4.8	+3.3	+1.5	-3.0	-5.6	-8.2
A-Nb$_2$O$_5$ (400,2)	34.5	28.3	28.3	24.2	22.7	12.0
A-Nb$_2$O$_5$ (500,2)	37.9	26.7	24.2	23.1	22.9	13.2
A-Nb$_2$O$_5$ (600,2)	44.0	30.4	19.3	16.7	16.4	0.0
A-Nb$_2$O$_5$ (800,2)	23.3	12.1	0.0	0.0	0.0	0.0

Table 3-10: ACID STRENGTH OF HEAT TREATED NIOBIC ACID: A) ACIDITY (MMOLES/G) AND B) ACIDITY (MMOLES/M^2) VERSUS pKa

A) Acid Strength of Heat Treated Niobic Acid [Acidity (mmoles/g)]

	Acidity (mmoles/g)					
	pKa					
Sample	+4.8	+3.3	+1.5	-3.0	-5.6	-8.2
Niobic Acid Uncalc.	0.57	0.47	0.44	0.40	0.32	0.058
Niobic Acid (400,2)	0.41	0.26	0.23	0.15	0.13	0.011
Niobic Acid (500,2)	0.27	0.17	0.16	0.11	0.069	0.007
Niobic Acid (600,2)	0.077	0.026	0.023	0.014	0.008	0.00

B) Acid Strength of Heat Treated Niobic Acid [Acidity (mmoles/m^2)]

	Acidity (mmoles/m^2) x 10^4					
	pKa					
Sample	+4.8	+3.3	+1.5	-3.0	-5.6	-8.2
Niobic Acid Uncalc.	37.9	31.5	29.4	26.4	21.3	3.9
Niobic Acid (400,2)	25.4	16.4	14.4	9.7	8.4	0.7
Niobic Acid (500,2)	27.1	17.4	16.2	11.0	6.98	0.7
Niobic Acid (600,2)	29.8	9.8	9.0	5.3	2.9	0.0

Figure 3-18: HEAT TREATED A-Nb$_2$O$_5$: A) ACIDITY (MMOLES/G) AND B)
ACIDITY (MMOLES/M^2) VS. pKa

A) Heat Treated A-Nb$_2$O$_5$ Acidity (mmoles/g)
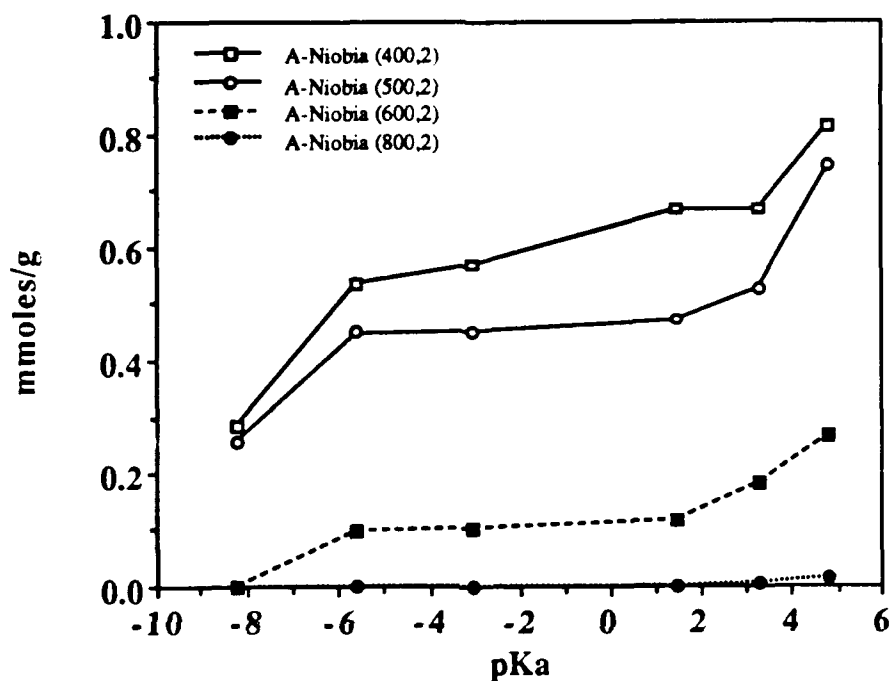
B) Heat Treated A-Nb$_2$O$_5$ Acidity (mmoles/m^2)
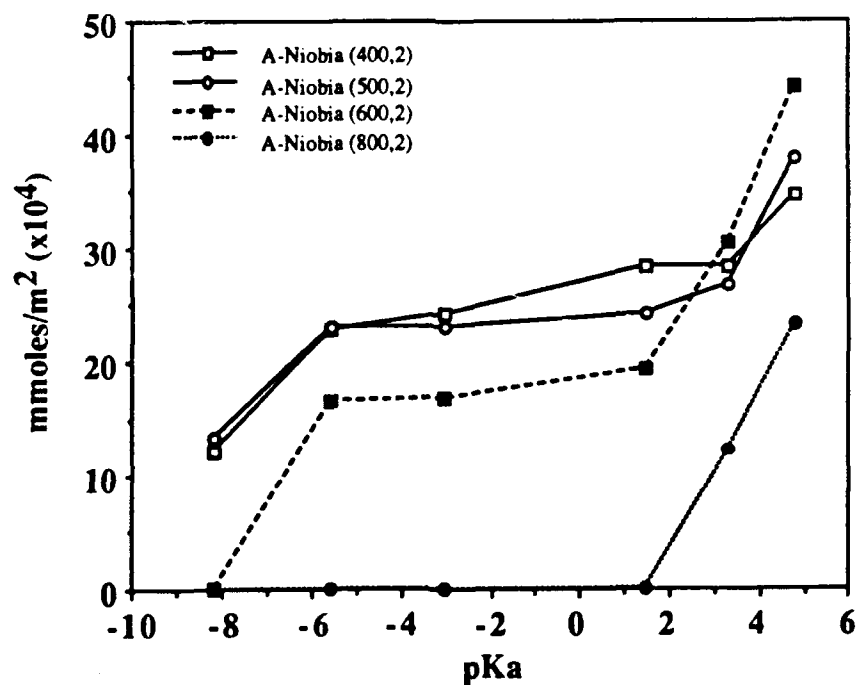
Figure 3-19: HEAT TREATED NIOBIC ACID: A) ACIDITY (MMOLES/G) AND B) ACIDITY (MMOLES/M^2) VS. pKa

A) Heat Treated Niobic Acid Acidity (mmoles/g)
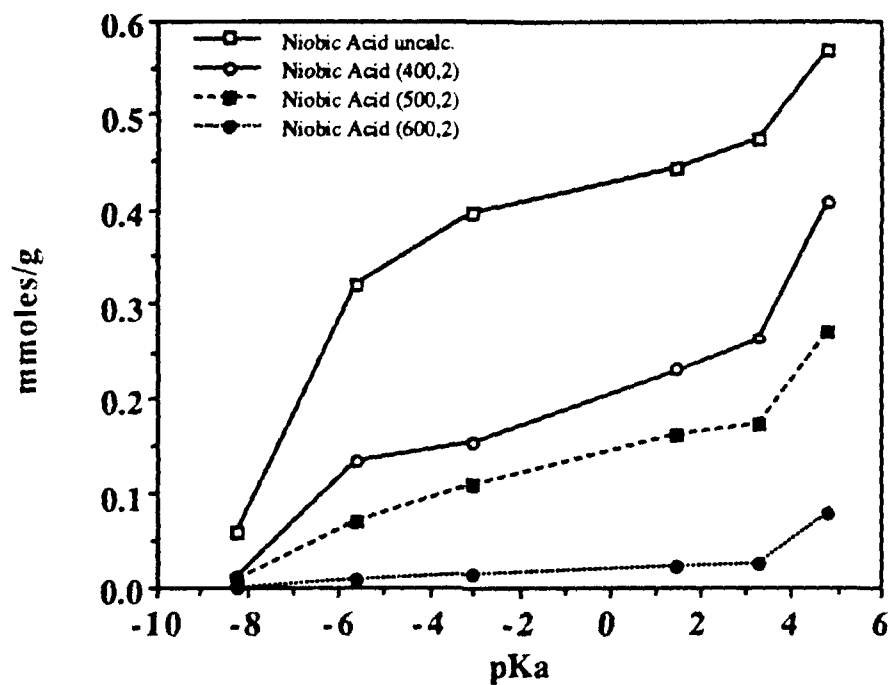
B) Heat Treated Niobic Acid Acidity (mmoles/m^2)
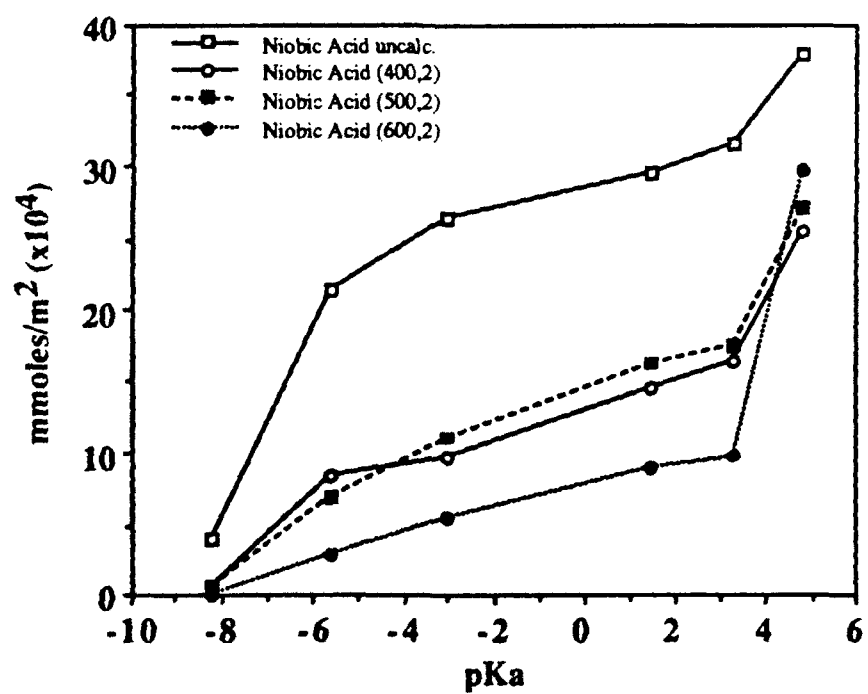
(bottom portion). It is hypothesized that because of the high thermal treatment at (800,2) on this aerogel, little to no Nb=O terminal groups exist because of the dramatic decrease in surface area, hence the absence of any strong acidity. Figure 3-18(B) shows the acidity of the heat treated niobia aerogel normalized with respect to surface area. Notice that there is still significant acidity on the oxide after the (600,2) heat treatment, but no acidity at the pKa = -8.2 indicator. This sample as will be shown later has superacidity, and hence should show acidity at this indicator, but this heat treated niobia aerogel was also seen to strongly adsorb water (see Appendix C), which could be poisoning these strongest sites. Even after the (800,2) heat treatment we observe some significant acidity when it is normalized with respect to surface area; however, it is only at the weakest acid sites where this acidity is found.

Figures 3-19(A) and (B) basically show the same information as Figures 3-18(A) and (B), but for niobic acid. One sees that the uncalcined niobic acid has acidity comparable to that of A-Nb_2O_5 [(400,2) and (500,2)]. After heat treatment to (400,2), the niobic acid, although still XRD amorphous, has obviously begun to lose acidity and attain an ordered crystalline structure. This order is attained at (500,2) as evidenced by XRD indicating the formation of TT-Nb_2O_5, and is followed by a corresponding loss in acidity as seen in Figure 3-19(A). Heat treating niobic acid to (600,2) results in an even greater loss in acidity as seen in Figure 3-19(A) and can be correlated to the majority of the sample attaining the TT-Nb_2O_5 phase as determined by XRD and DTA studies. Figure 3-19(B) shows the acidity for niobic acid normalized with respect to surface area. The uncalcined niobic acid shows an acidity ($/m^2$) approximately twice as high as the heat treated niobic acid; this was similar to what we found earlier for the various heat treated niobia in Figure 3-16(B). The (600,2) heat treatment on niobic acid decreases the acidity across most acid strengths; however, significant acidity is still prevalent at the lowest acid strength indicator, pKa = +4.8.

One interesting observation with acidity studies on these two materials is the apparent stability of the niobia aerogel over that of niobic acid. The heat treatments that give similar corresponding acidities appear staggered. For instance, the acidity for uncalcined niobic acid matches that of A-Nb_2O_5 (500,2). Notice that the acidity for niobic acid after (500,2) matches up with A-Nb_2O_5 (600,2) and not A-Nb_2O_5 (500,2). This same observation is seen for the acidity of niobic acid (600,2) matching with A-Nb_2O_5 (800,2), not A-Nb_2O_5 (600,2). This could possibly be a result of the distorted nature of the niobia aerogel over that of niobic acid.

3.3.2 Superacidity and Basicity

Table 3-11 shows the qualitative results of the superacidity (> 100% H_2SO_4) and basicity of the niobia aerogel as subjected to various heat treatments. These tests were performed by adding drops of indicator (see Table 2-11) onto a powder sample which had been heat treated for 2 hours at 450 °C in a dry N_2 purged glove box. After the standard calcination, (500,2), it appears that the aerogel possesses very strong acid sites as noted by the positive signal of the pKa = -13.75 indicator. This material also seems to possess strong basic sites as seen by the positive indication with the pKa = +15.0 indicator. This basicity could possibly be a test for Nb=O on the surface of the aerogel since the oxygen in this bond is very electronegative and may be willing to donate an electron pair (basic strength).[189] Upon heat treating the aerogel of niobia to (600,2) we see that it still appears to be superacidic; however, a negative indication was noted on the most acidic indicator, meaning that this material has lost some of its very acidic properties. A positive sign was also seen with the basic indicators of this sample possibly leading to a conclusion that Nb=O are still accessible and prevalent on this material. Further heat treatment to (800,2) and (1000,-) destroys the superacidic nature (and basic property) of this niobia aerogel, due to the ordering and restructuring of the oxide as a whole.

Table 3-11: SUPERACIDITY AND BASICITY OF HEAT TREATED NIOBIA AEROGELS

Sample	Acid Strength (pKa)			Basic Strength (pKa)	
	-11.35	-12.40	-13.75	+9.3	+15.0
A-Nb$_2$O$_5$ (500,2)	++	++	++	++	+
A-Nb$_2$O$_5$ (600,2)	+	+	-	+	+/-
A-Nb$_2$O$_5$ (800,2)	-	-	-	-	-
A-Nb$_2$O$_5$ (1000,-)	-	-	-	-	-

++	(Very Positive Acid or Basic Indication)
+	(Positive Acid or Basic Indication)
+/-	(Positive and/or Negative Indication)
-	(Negative Acid or Basic Indication)

3.3.3 Pyridine Adsorption Studies

3.3.3.1 Heat of Adsorption (ΔH_{ads}): TG Study

Pyridine adsorption experiments were performed using thermogravimetry (TG) to determine the acid strength-coverage dependence of the prepared niobia samples. These experiments were done in order to obtain a better understanding of the relationships between acid strength and structure. The pyridine heats of adsorption versus coverage for the bulk oxides are summarized in Table 3-12. Figure 3-20 shows ΔH_{ads} versus coverage for both the niobia aerogel and precipitated niobia after the standard calcination. P-Nb_2O_5 shows ΔH_{ads} ranged from approximately 24 to 19 kcal/mol for coverages of 10.0 to 16.4 x 10^{13} molecules/cm^2, respectively. A-Nb_2O_5, on the other hand, shows ΔH_{ads} ranged from approximately 33 to 24 kcal/mol for pyridine coverages of 7.4 to 18.2 x 10^{13} molecules/cm^2, respectively. This data seems to fit a Temkin isotherm since there appears to be a linear relationship between the heat of adsorption and coverage. The heat of adsorption for A-Nb_2O_5 is on average about 8 kcal/mol higher than that for P-Nb_2O_5. It was noted earlier that precipitated niobia and niobic acid showed TT-Nb_2O_5 crystallites while the niobia aerogel was amorphous according to our XRD study. From the *in-situ* LRS study on the aerogel of niobia, it was also determined that this material contained a large number of distorted Nb=O bonds. Niobic acid heat treated to (500,2) and studied by *in-situ* LRS was found to contain very little if any distorted Nb=O bonds.[94] This calcined niobic acid and precipitated niobia showed similar acidity distributions using the n-butylamine titration method, hence we would expect the precipitated nobia to have similar results to the niobic acid above, with respect to the *in-situ* LRS study, i.e. very little if any distorted Nb=O. Using this information we can infer that the strength of the acid sites in the aerogel is dependent on the ability of the surface to maintain doubly bonded oxygens. This strength stems from the ability of the Nb=O to delocalize the negative charge

Table 3-12: ΔH_{ads} VERSUS PYRIDINE COVERAGE FOR BULK AEROGELS

Pyridine Coverage (Θ) (Molecules/cm^2 x 10^{13})	ΔH_{ads}(kcal/mol)			
	A-Nb$_2$O$_5$	P-Nb$_2$O$_5$	A-Al$_2$O$_3$	SiO$_2$
1.0				12.6
1.3				13.7
1.8				15.0
2.5				15.0
4.1			23.6	
4.9			22.6	
6.1			23.8	
7.4	31.1		22.4	
8.2	32.4			
9.0	33.5		22.6	
10.0	33.5	24.0		
11.0	32.8	23.7	21.3	
12.2	31.0	22.9		
13.5	29.6	22.3	20.4	
14.9	27.2	20.5		
16.4	24.1	18.9		
18.2	24.3			

Figure 3-20: ΔH_{ads} VERSUS PYRIDINE COVERAGE FOR BULK AEROGELS
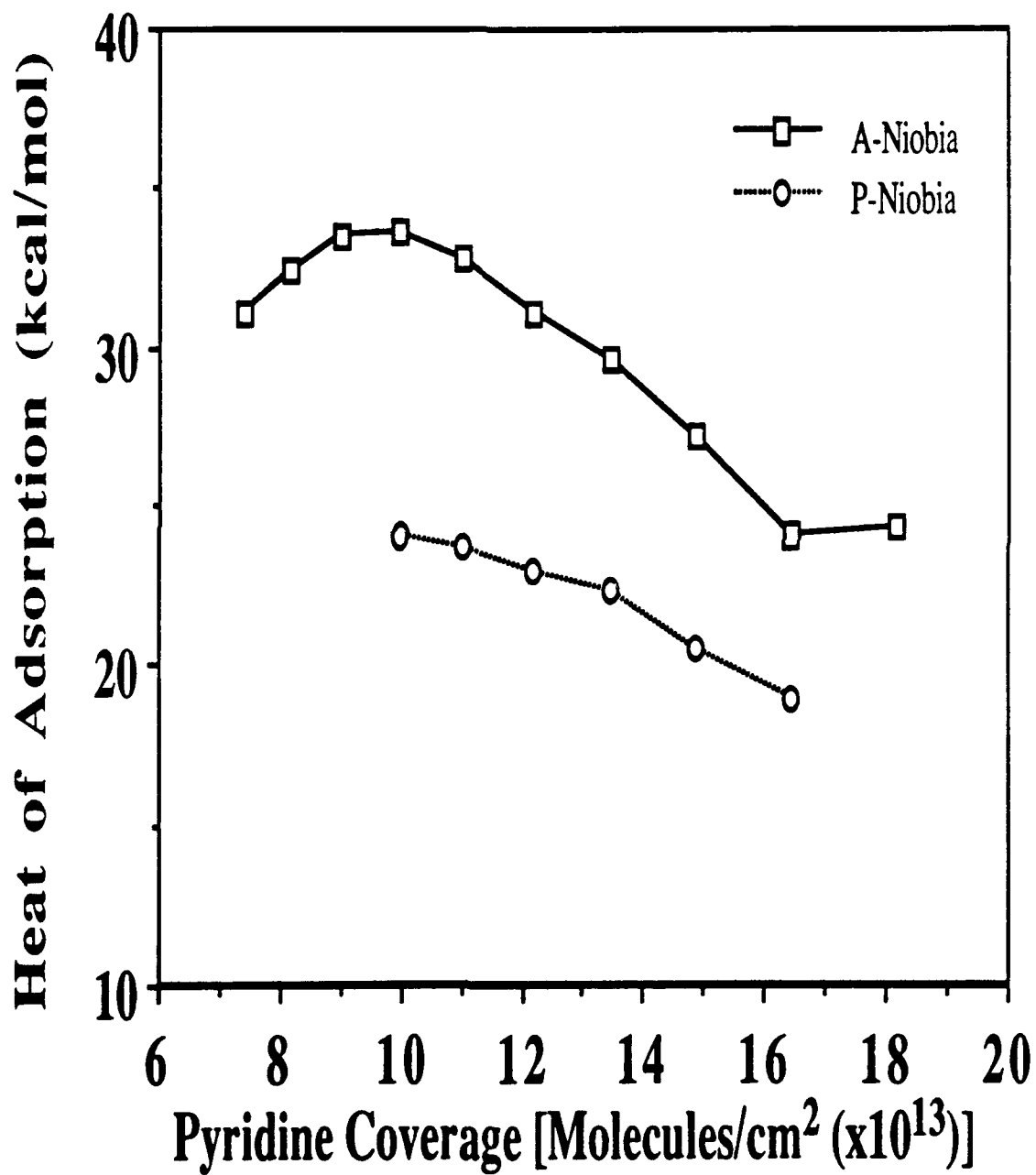
associated with the acceptance of an electron pair, and/or with the donation of a proton as the terminal oxygen acts to better distribute the charge.

3.3.3.2 Acid Type: FTIR Study

Pyridine adsorption studies using Fourier Transform Infrared Spectroscopy (FTIR) were performed to examine the nature of the acid sites on the oxides. FTIR can be used to determine the ratio of Lewis (electron pair acceptor) to Brønsted (proton donor) acid sites as well as yielding some information about relative acid strengths. FTIR spectra were taken for niobia after pretreatment at 300 °C for 1 hour, and after exposure to pyridine (upon cooling) and constant pumping at 25, 100, 200, and 300 °C. The data from these experiments were designed to extract the relative strengths of the Lewis to Brønsted sites (L/B) by examining changes in the ratio with thermal treatment, and also possibly the participation of different cation species as Lewis acid sites by noting shifts in the absorption frequency of pyridine at ~ 1600 cm^{-1}.

Table 3-13 summarizes the characteristic infrared absorption frequencies for pyridine adsorbed on Lewis and Brønsted acid sites in the 1400 - 1700 cm^{-1} region.[190, 191, 192] Due to the large number of spectra, only figures which directly aid in the results and discussion of these materials will be shown in the main text. All hydroxyl region data, as well as the low intensity spectra of the 300 °C heat treated samples, are shown in Appendix C along with a complete discussion of them and DRIFT spectra.

Figure 3-21 shows pyridine adsorption on A-Nb$_2$O$_5$. The characteristic frequencies for the Lewis acid sites are between 1450 - 1460 cm^{-1} and 1600 - 1630 cm^{-1}, and for the Brønsted sites, at around 1540 - 1545 cm^{-1}. It is obvious from Figure 3-21 that A-Nb$_2$O$_5$ shows both Lewis and Brønsted sites. Similar results have been found with conventionally prepared niobia.[88, 143, 144, 145] Table 3-14 summarizes the peak absorption shifts of the bulk oxide aerogels for the 19b (~ 1450 cm^{-1}) and 8a (~ 1610 cm^{-1}) frequencies. The shifts in absorption frequency with increasing temperature were about 2

Table 3-13: INFRARED ABSORPTION BANDS FOR PYRIDINE ADSORBED ON ACID SITES IN THE 1400-1700 cm^{-1} REGION[190, 191, 192]

Vibrational Mode	Hydrogen Bonded (HPY)	Coordinately Bonded Lewis Acid (LPY)	Pyridinium Ion Brønsted Acid (BPY)
8a	1580-1600(S)*	1600-1633(VS)	1620,1640(S)
19a	1485-1490(W)	1488-1503(S)	1485-1500(VS)
19b	1400-1447(VS)	1447-1460(VS)*	1540-1547(S)*

* Characteristic or unique frequency of the acid type

Figure 3-21: FTIR SPECTRA OF PYRIDINE ADSORBED ON A-Nb$_2$O$_5$ AFTER HEAT TREATMENTS AT 300, 200, 100, AND 25 °C (TOP TO BOTTOM)
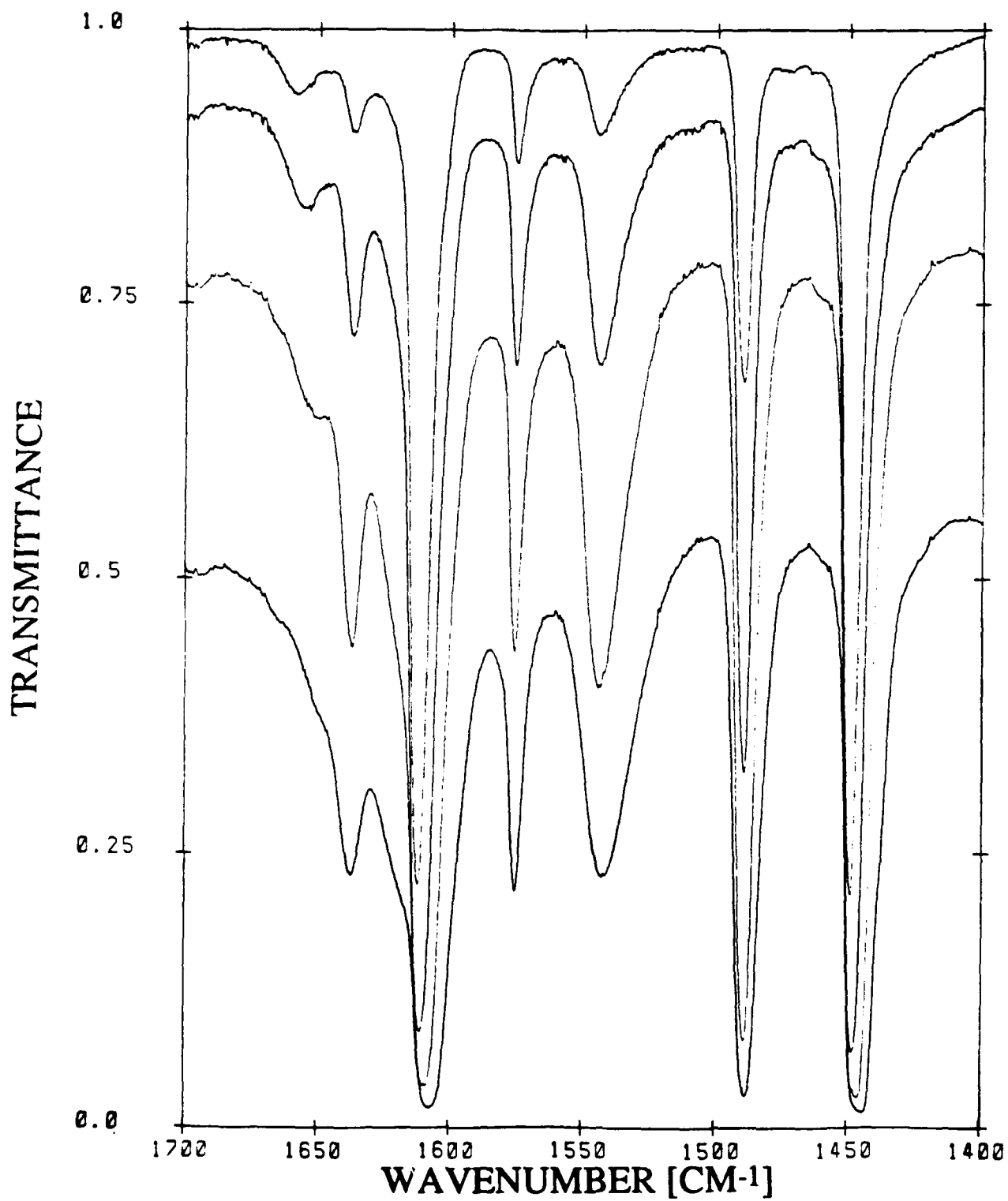
Table 3-14: LEWIS ACID PYRIDINE ABSORPTION FREQUENCIES FOR BULK OXIDES

	Lewis Acid Pyridine Absorption Frequencies					
	19b Frequency (cm⁻¹)			8a Frequency (cm⁻¹)		
Sample	Heat Treatment			Heat Treatment		
	100 °C	200 °C	300 °C	100 °C	200 °C	300 °C
A-Nb₂O₅	1446.3	1448.5	1449.4	1609.5	1611.4	1612.4
P-Nb₂O₅	1447.3	1448.6	1449.4	1609.3	1611.0	1611.9
A-Al₂O₃	1450.1	1452.8	1453.3	1616.0	1621.1	1622.5

Table 3-15: LEWIS/BRØNSTED RATIO FOR BULK OXIDES

| | Lewis/Brønsted Ratio | | |
| Sample | Heat Treatment | | |
	100 °C	200 °C	300 °C
A-Nb₂O₅	3.3	7.7	25.0
P-Nb₂O₅	3.8	7.1	20.0
A-Al₂O₃	8.4	40.4	675.8

to 2.5 cm⁻¹ for the precipitated niobia for the 19b and 8a frequencies, respectively; while upward shifts for A-Nb₂O₅ of approximately 3 cm⁻¹ indicated higher Lewis acid strengths with decreasing coverage. Table 3-15 shows the Lewis/Brønsted ratio as a function of heat treatment of the bulk oxides. Both the aerogel and precipitated niobia exhibited nearly identical L/B ratios ranging from ~ 4 to ~ 20 with increasing temperature, which indicates that pyridine is preferentially desorbed from Brønsted sites with increasing temperature. This result shows that Brønsted sites are weaker than Lewis acid sites on niobia regardless of the preparation method.

3.3.4 Reduction Studies

Reduction was performed by heating the calcined sample to 1000 °C at 10 °C/min and holding for 2 hours at 1000 °C in pure flowing hydrogen. In some instances a second series of TG reduction experiments were performed in which all samples were first pretreated in flowing helium to 1000 °C at 10 °C/min as a ramp or held there for various times (1, 2, or 8 hours), and then reduced following the above temperature schedule in hydrogen. These experiments were performed to minimize the complications induced by the desorption of water, and the crystallization of niobia during the heat treatment. Figure 3-22 shows the direct reduction of the niobia aerogel, precipitated niobia, and niobic acid. The peak reduction temperatures are listed in Table 3-16. This table and figure show that the aerogel reduces at a lower temperature (~ 800 °C) by approximately 60 °C over the other samples. The peak reduction temperature of precipitated niobia (~ 850 °C) is in agreement to earlier results from our group.[88] Figure 3-23 shows the TG reduction data for the same group of niobia after a pretreatment of (1000,2) in helium. The corresponding peaks are listed in Table 3-17. We see that even after this severe heat treatment, the niobia aerogel still reduces at a lower temperature (~ 920 °C) by approximately 60 °C. Figure 3-24 shows the effect of pretreatment temperature on the reducibility of A-Nb₂O₅. The corresponding peak shifts are shown in Table 3-18. This data shows that the longer pretreatments at 1000

Figure 3-22: TG DIRECT REDUCTION DATA FOR Nb_2O_5
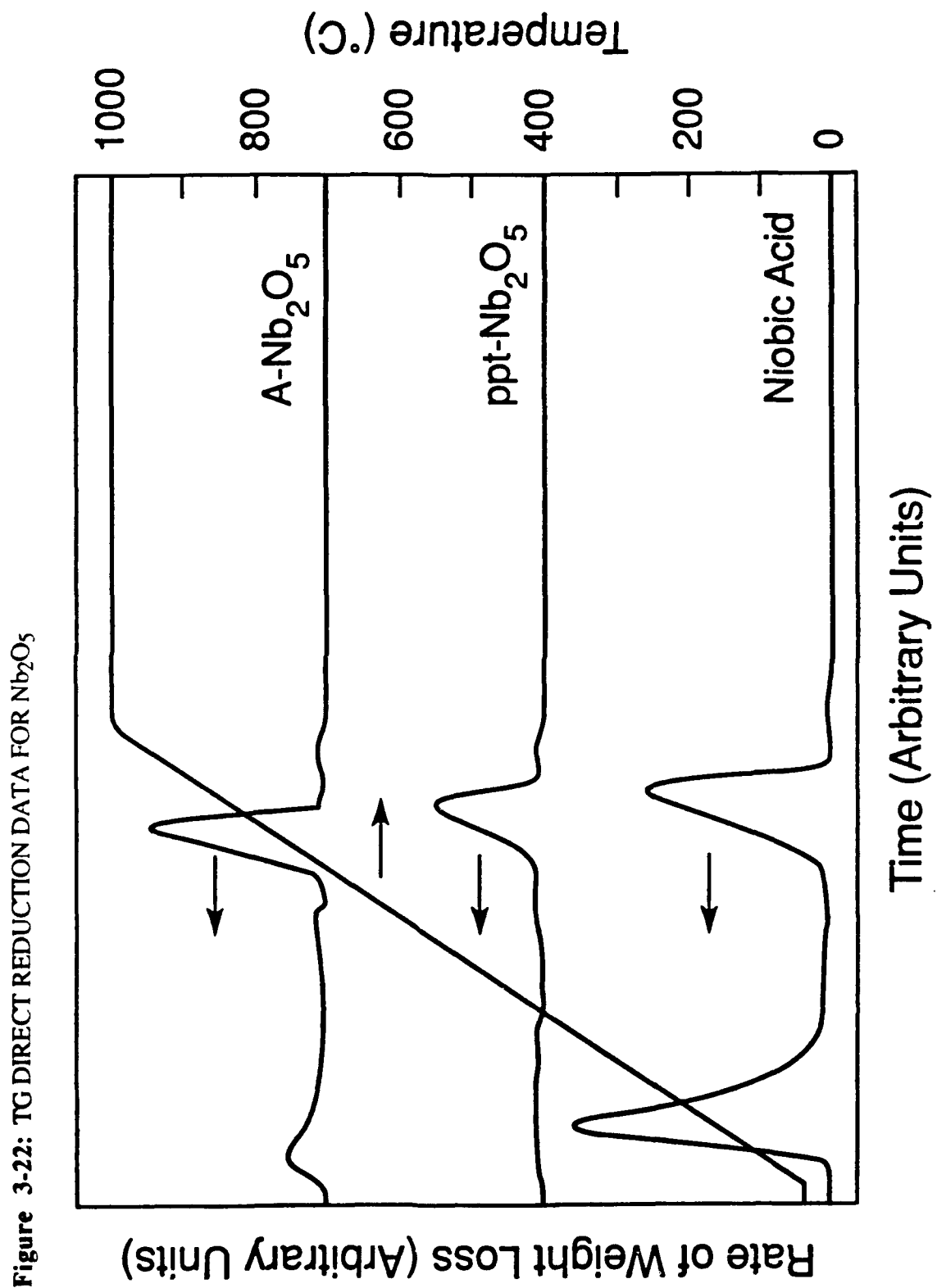
Table 3-16: PEAK TEMPERATURES FOR TG DIRECT REDUCTION DATA OF Nb_2O_5

Sample	Heat Treatment	Peak Temperature (°C)
A-Nb_2O_5	(500,2)	797
P-Nb_2O_5	(500,2)	844
X-Nb_2O_5	(500,2)	900
Niobic Acid	(500,2)	878

Table 3-17: PEAK TEMPERATURES FOR TG REDUCTION DATA OF HEAT TREATED Nb_2O_5

Sample	Heat Treatment	Peak Temperature (°C)
A-Nb_2O_5	(1000,2)	920
P-Nb_2O_5	(1000,2)	988
Niobic Acid	(1000,2)	978

Table 3-18: PEAK TEMPERATURES FOR TG REDUCTION DATA OF HEAT TREATED A-Nb_2O_5

Sample	Heat Treatment	Peak Temperature (°C)
A-Nb_2O_5	(500,2)	797
A-Nb_2O_5	(1000,-)	900
A-Nb_2O_5	(1000,2)	920
A-Nb_2O_5	(1000,8)	930
A-Nb_2O_5	(1000,48)	980

Figure 3-23: TG REDUCTION DATA FOR PRETREATED [(1000,2) He] Nb_2O_5

162
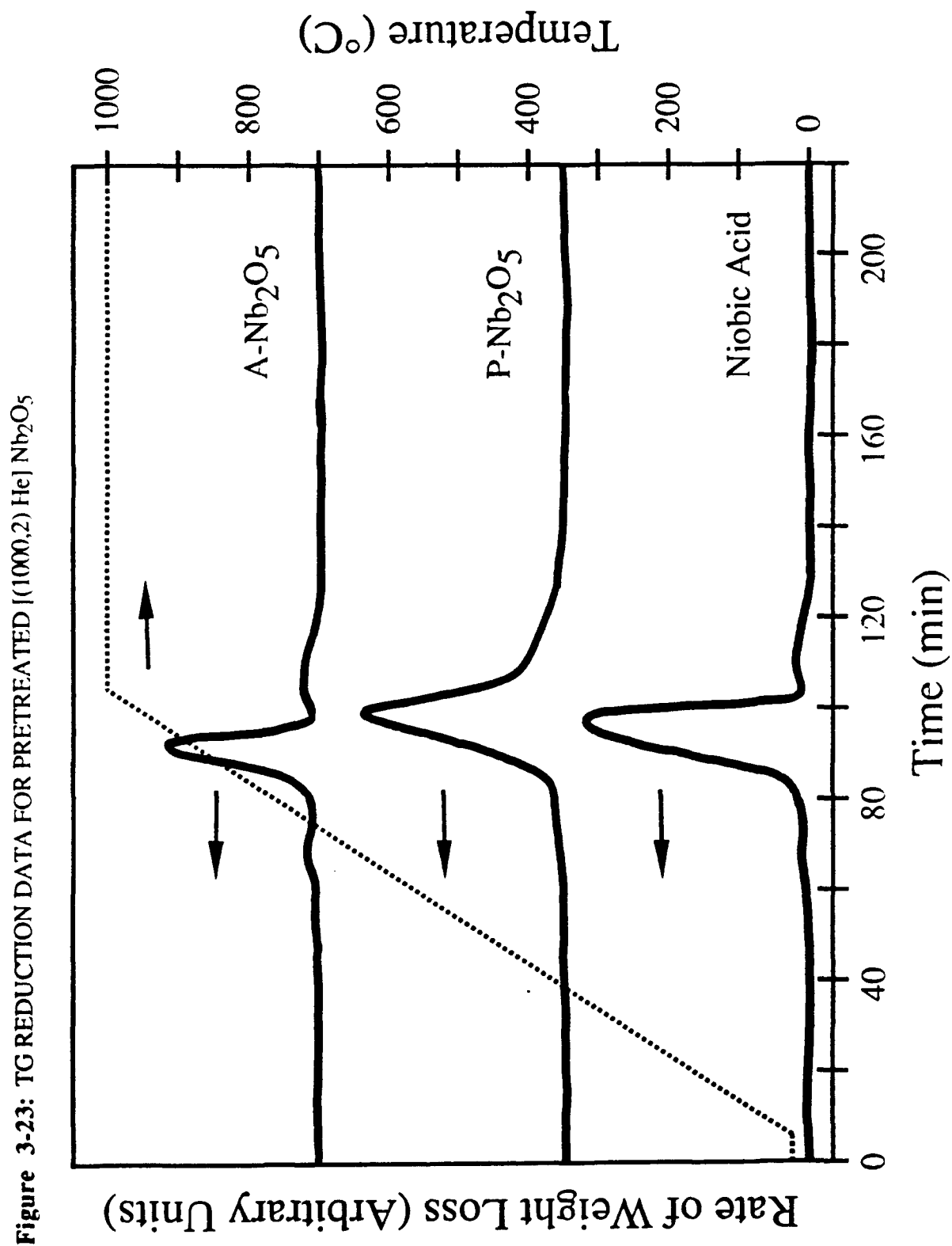
Figure 3-24: TG REDUCTION DATA FOR PRETREATED A-Nb₂O₅: A) (500,2), B) (1000,-), C) (1000,2), AND D) (1000,8)
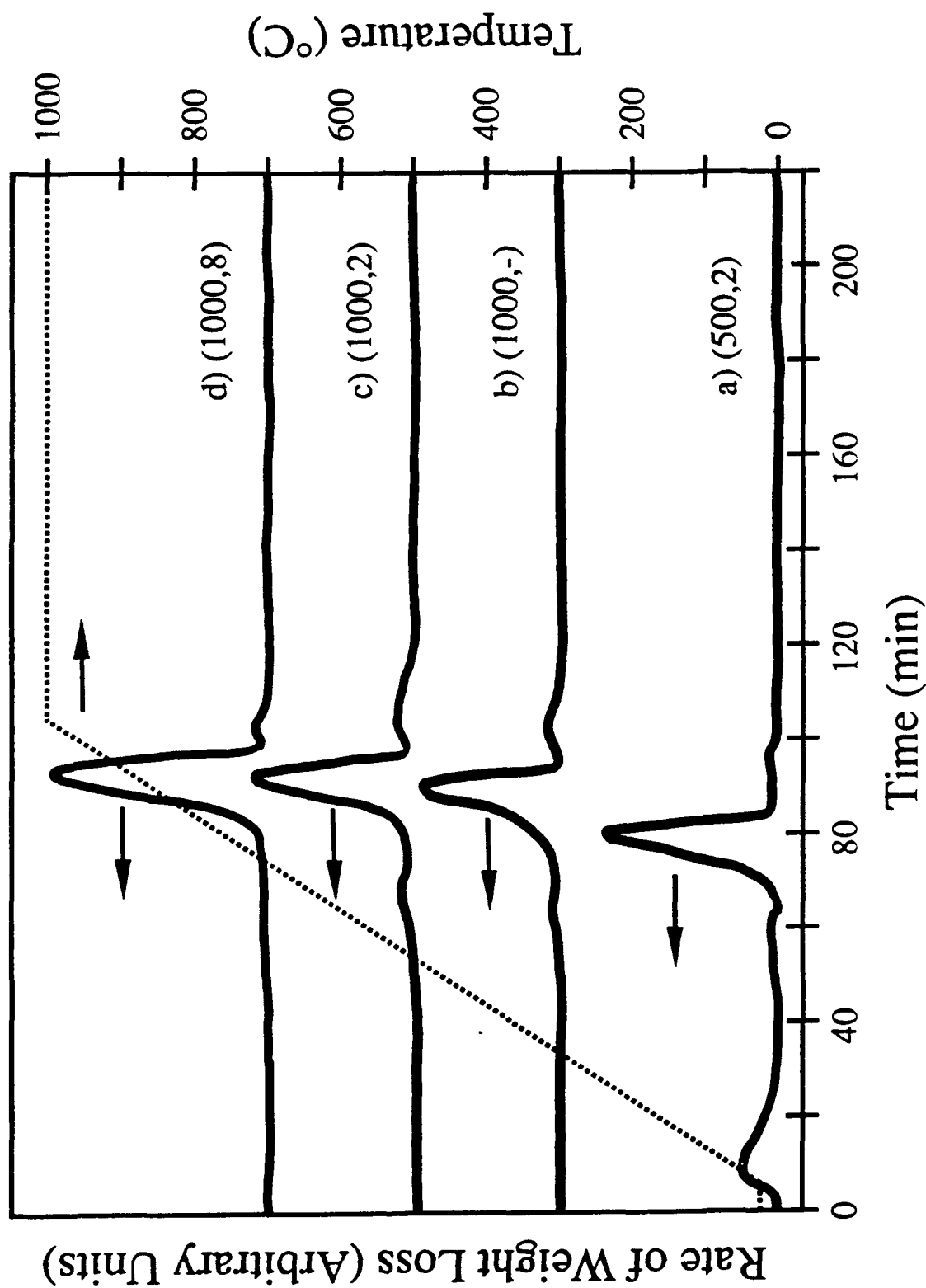
°C gradually shift the reduction peak to higher temperatures. H-Niobia was found to reduce at ~ 990 °C from a previous study.[88] The precipitated niobia (~ 990 °C) and niobic acid (~ 980 °C) show a reduction peak at about the same temperature and correspond to H- and M-Niobia, respectively. This shows the difficulty in reducing these well ordered structures of H-Niobia and its distorted precursor M-Niobia. The aerogel of niobia reduces at a significantly lower temperature (~ 930 °C) than M- or H-Niobia after the (1000,8) pretreatment, even though it has been indexed as H-Niobia by XRD. This could be due to H-Niobia crystallizing out of the niobia aerogel which has not completely attained a well-ordered structure throughout the entire material. We indeed see a shift towards higher peak temperatures as the length of the 1000 °C pretreatment is increased, indicating increasing ordering in the sample. Recent results on the reduction of A-Nb_2O_5 after a (1000,48) pretreatment show this sample to reduce at ~ 980 °C, comparable to that found for H-Nb_2O_5 and our conventionally pretreated, (1000,2), niobia samples. There exists a possibility too, that the more open structure of the niobia aerogel (as indicated by the pore volume data) leads to a material that has an oxygen atom that is different and which is easier to be extracted (suggesting the existence of Nb=O) than the conventional niobia. This is especially true of the directly reduced niobia samples.

3.3.5 1-Butene Isomerization

The goal of this section is to show the viability of the synthesized niobia as a catalyst. 1-Butene isomerization will be used as the reaction to test the activity of these oxides. Figure 3-25 shows the isomerization rate of 1-butene (mol/hr-g) versus time on stream (TOS) for the four niobia samples investigated in this study. All samples were subjected to a 1 hour pretreatment in helium at 200 °C to remove any physisorbed surface water. Notice in Figure 3-25 that the niobia can be split into two groups as we saw with the acidity measurements of these materials. The upper portion corresponds to amorphous niobia and has a steady-state activity around 1.4 x 10^{-2} mol/hr-g, and the lower portion

Figure 3-25: 1-BUTENE ISOMERIZATION ACTIVITY OVER NIOBIA (/G)
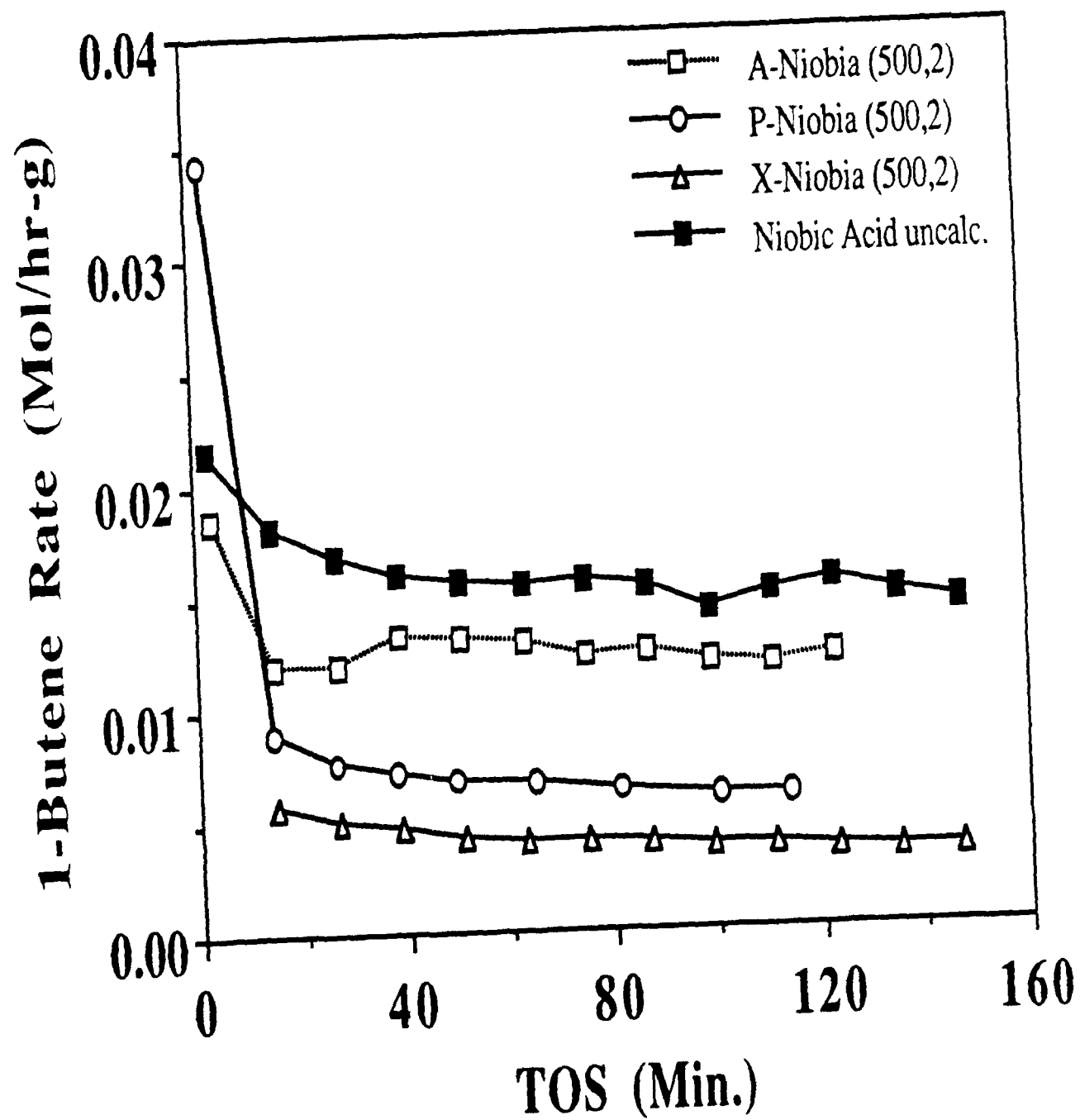
relates to a crystalline niobia (TT-Nb_2O_5) and has an average steady-state activity of 0.47 x 10^{-2} mol/hr-g (about 3 times less). Figure 3-26 shows the 1-butene rate normalized with respect to surface area. This figure shows that the steady state activity (~ 0.7 x 10^{-4} mol/hr-m^2) on a surface area basis is invariant to the niobia sample studied. Earlier results show that the niobia aerogel has stronger acid sites than the precipitated niobia from ΔH_{ads} measurements, and that P-Nb_2O_5 as well as X-Nb_2O_5 have TT-Nb_2O_5 crystallites. Thus, it appears from our interpretation and previous results that the active site for 1-butene isomerization can be assigned to weak acid sites. Table 3-19 lists the steady-state activities and cis/trans-2-butene (C/T) ratio for the synthesized bulk oxides of this study. It has been established from many previous studies that 1-butene isomerizes via a highly reactive carbonium ion. The ion can be formed by a number of methods, but the simplest is by abstracting a proton from a Brønsted acid site to the 1-butene molecule.[193] This reactive intermediate is predicted to yield C/T ratios of about 1 because of energetically equal and probable pathways to forming the final cis and trans isomers.[193] Results from Table 3-19 show that the niobia C/T ratios are all approximately 1. With our above hypothesis of the reaction being catalyzed by weak acids and the fact that C/T ~ 1 for niobia, we can conclude that the most probable active site on these materials is a weak Brønsted acid.

Figure 3-27 shows the 1-butene rate (/g) versus TOS for heat treated niobia aerogels. One sees from this figure the steady decline in activity with the higher thermal treatment, which corresponds to the formation of various crystalline forms of niobia: TT-, T-, and M-Nb_2O_5, respectively. This same data normalized with respect to surface area is shown in Figure 3-28. The steady state activity (~ 0.7 x 10^{-4} mol/hr-m^2) is unchanged with heat treatment to the aerogel. A similar result was seen with the other prepared niobia samples in Figure 3-26. These activity results are compiled in Table 3-20 along with the C/T ratios of these materials. All of the C/T ratios for the heat treated samples were around 1, even for the sample heat treated at (1000,-), whose very low surface area made its activity normalized on a per area basis uncertain. The niobia aerogel heat treated to (800,2)

Figure 3-26: 1-BUTENE ISOMERIZATION ACTIVITY OVER NIOBIA (/M²)
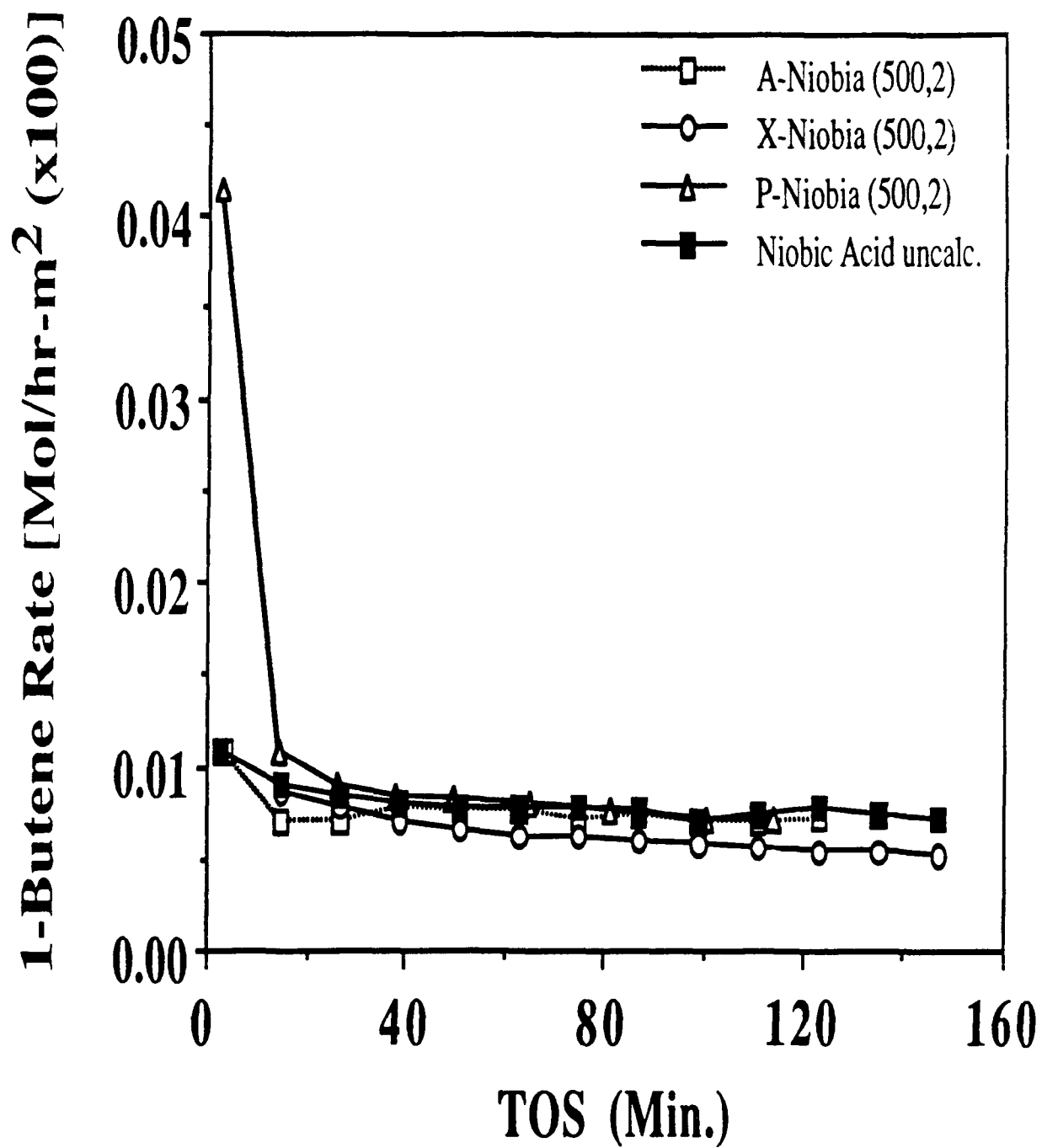
Table 3-19: 1-BUTENE ISOMERIZATION ACTIVITY BULK OXIDES (CALCINED)

	Steady-State Activity (mol/hr-) [x100]			
Sample	(/g)	(/g Nb$_2$O$_5$)	(/m^2 x100)	C/T*
A-Nb$_2$O$_5$	1.2	1.2	0.71	1.6
P-Nb$_2$O$_5$	0.59	0.59	0.71	1.4
X-Nb$_2$O$_5$	0.34	0.34	0.53	0.7
Niobic Acid uncal.	1.5	1.5	0.74	0.7
SiO$_2$ (Davison)	0.006	-	0.0019	0.0
A-Al$_2$O$_3$	0.027	-	0.0045	0.4

* C/T = Cis/Trans-2-butene ratio

Figure 3-27: 1-BUTENE ISOMERIZATION ACTIVITY OVER HEAT TREATED A-Nb$_2$O$_5$ (/G)
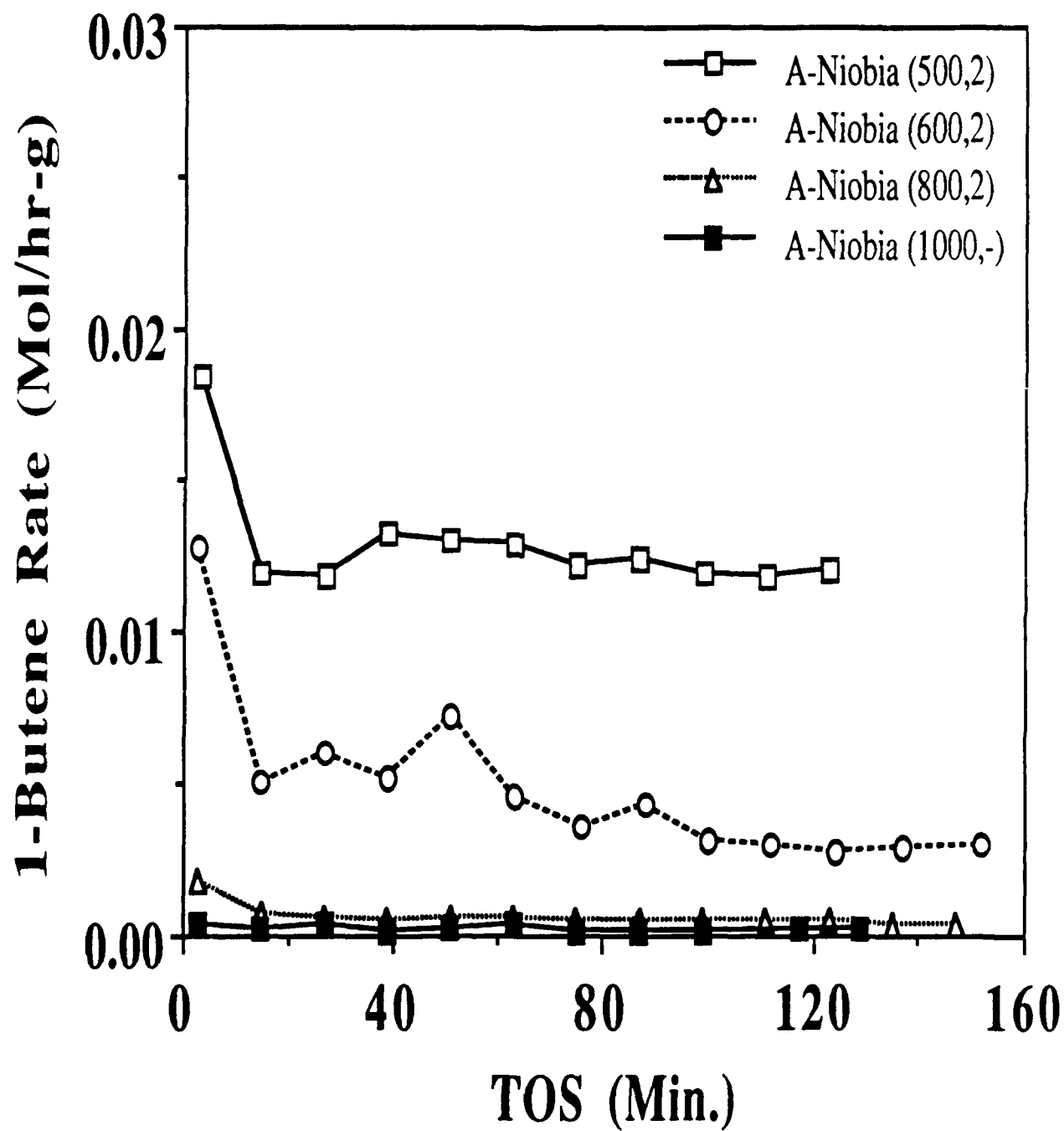
Figure 3-28: 1-BUTENE ISOMERIZATION ACTIVITY OVER HEAT TREATED A-Nb_2O_5 ($/M^2$)
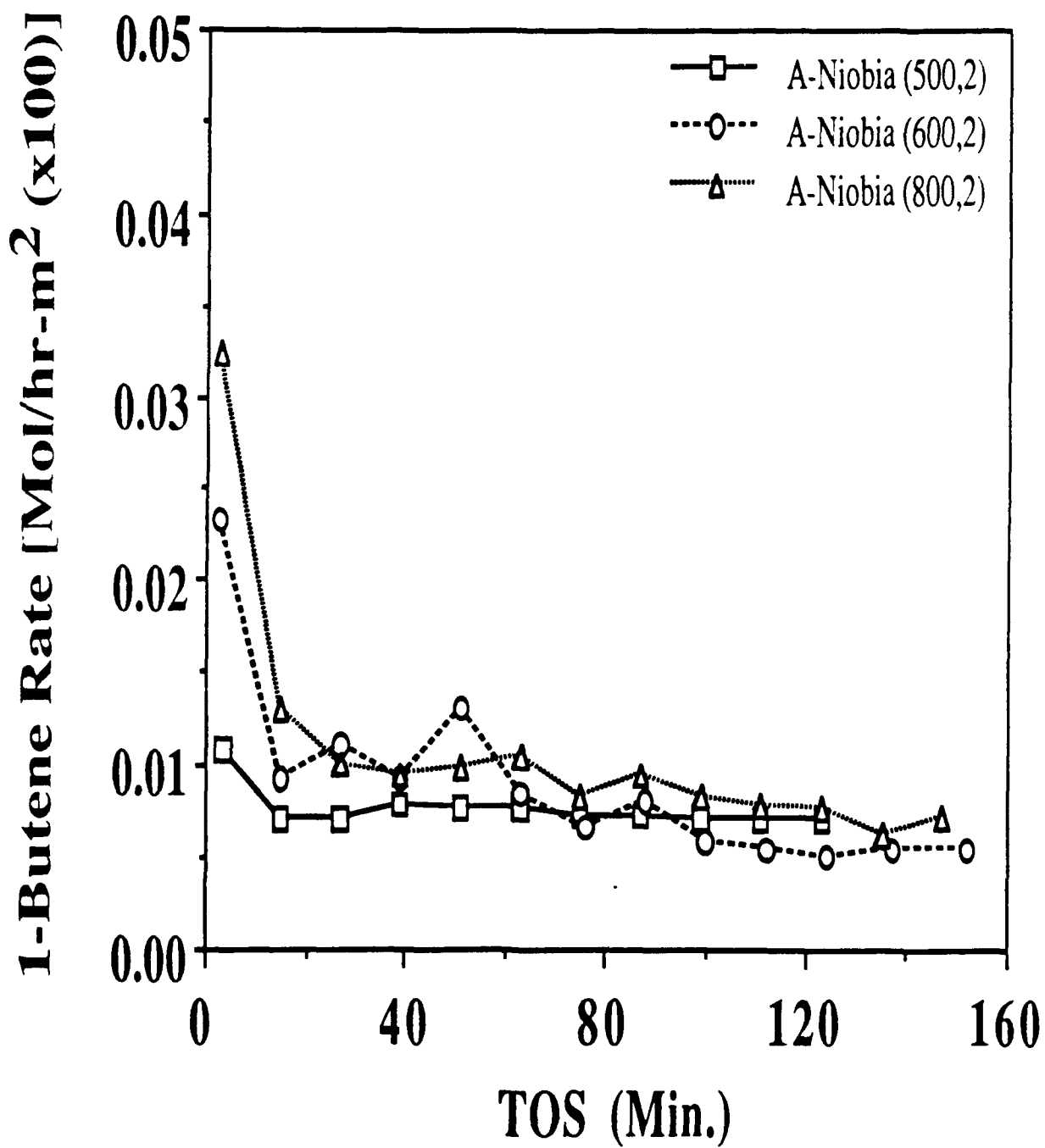
Table 3-20: 1-BUTENE ISOMERIZATION ACTIVITY OF HEAT TREATED A-Nb_2O_5

Sample	Steady-State Activity (mol/hr-) [x100]			
	(/g)	(/g Nb_2O_5)	(/m^2 x100)	C/T*
A-Nb_2O_5 (500,2)	1.2	1.2	0.71	1.6
P-Nb_2O_5 (500,2)	0.59	0.59	0.71	1.4
A-Nb_2O_5 (600,2)	0.29	0.29	0.53	1.3
A-Nb_2O_5 (800,2)	0.04	0.04	0.73	1.1
A-Nb_2O_5 (1000,-)	0.02	0.02	2.0	0.5

* C/T = Cis/Trans-2-butene ratio

showed very weak acidity (only able to turn pKa = +1.5 to its acidic form) as did the (1000,-) niobia aerogel, but both of these samples showed comparable 1-butene activity. Hence along with the observation of C/T ~ 1, we can conclude as before that a weak Brønsted acid is the active site for the 1-butene isomerization reaction.

3.4 Physical Characterization of Silica and Alumina Aerogels

This section focuses on the properties of the silica and alumina aerogels prepared in this study. Much less attention will be focused on these materials than was reported for the aerogel of niobia, because the primary goal of studying these oxides was to determine whether they were viable as supports for niobia. Intrinsic properties of the bulk silica and alumina aerogels were also examined to determine what effect the addition of niobia to these oxides has in the newly formed binary oxides.

3.4.1 Surface Area and Physical Property Data

Silica and alumina aerogels were synthesized using metal alkoxide precursors via the sol-gel route, followed by a subsequent supercritical extraction. All aerogels produced had very high surface areas, pore volumes, and pore diameters. A study of the effect of solvents, methanol and s-butanol, on the physical property data of silica aerogels is shown in Table 3-21. The total multi-point B.E.T. surface areas of these two aerogels of silica are 989 and 908 m^2/g in s-butanol and methanol, respectively. The total pore volume and average pore diameter are 2.7 cm^3/g and 110 Å (average values) for both solvents. Note that because most of the adsorption occurs near p/p_0 ~ 1, pore volumes and pore size distributions may be inaccurate for aerogels.[156] Pore volume and pore size distribution data for all aerogels investigated can be found in Appendix B.

Bulk oxide aerogel physical property data using s-butanol as the solvent can be found in Table 3-22. Notice in this table the larger pore volumes and average pore

Table 3-21: EFFECT OF SOLVENT ON THE SURFACE AREA, PORE VOLUME, AND PORE DIAMETER OF A-SiO$_2$

Solvent	Total B.E.T. Surface Area[1]	Total Pore Volume[2]	Avg. Pore Diameter[3]
sec-Butanol	989.0	2.4023	97.16
Methanol	908.0	2.9317	129.14

Table 3-22: BULK OXIDES SURFACE AREA, PORE VOLUME AND AVERAGE PORE DIAMETER WITH sec-BuOH AS THE SOLVENT

Solvent	Total B.E.T. Surface Area[1]	Total Pore Volume[2]	Avg. Pore Diameter[3]
A-Nb$_2$O$_5$	196.3	1.2802	260.9
A-SiO$_2$	989.0	2.4023	97.2
X-SiO$_2$	1094.8	0.9514	34.8
A-Al$_2$O$_3$	552.3	1.4893	107.9

[1]   Total Surface Area, Multi-Point B.E.T. (m^2/g)

[2]   Total Pore Volume (cm^3/g)

[3]   Average Pore Diameter, 4V/S, (Å)

diameters of the aerogels when compared to that of X-SiO_2. The only difference in A-SiO_2 and X-SiO_2 is that the aerogel had been supercritically extracted, while the xerogel was dried in a vacuum oven. Surface tension forces created in the xerogel of silica during solvent removal cause the network to collapse as the coordination of the particles is increased.[15, 16] Porosity in this material develops when, due to additional crosslinking, the gel network becomes sufficiently strengthened to resist the compressive forces of surface tension. Thus, the dried xerogel will be a densely-contracted and distorted version of the structure originally formed in solution. The aerogel on the other hand was dried by removal of a solvent above its critical point; the absence of liquid-vapor interfaces eliminated the capillary pressure which destabilized the network structure in the xerogel. Thus, in the aerogel, there is a greatly reduced driving force for shrinkage, and as a direct result of this, aerogels are expanded structures that are more closely related to the structure that was formed at the gel point.[156] The large surface area for the xerogel (~ 1100 m^2/g) is not surprising when one considers that the silica network is a very rigid structure due to the strong covalent bonding of Si-O-Si throughout the material. Even though the drying of the xerogel densifies this sample by a factor of 3 over that of the aerogel, the rigid network is still very intact and leads to its skeletal and porous phases.[156] This enhancement in surface area for the silica xerogel over that of the silica aerogel has been noted elsewhere.[156] The surface area of the alumina aerogel is around 550 m^2/g and this high surface area is attributed to its amorphous nature in preparation. The aerogel of alumina also has a large average pore diameter, as does the silica aerogel, which makes it ideal for later surface oxide impregnation with niobia. This alumina aerogel has a surface area and pore volume nearly identical to that found by Teichner et al.[24] (530 m^2/g and 1.18 cm^3/g respectively). The surface area of the alumina aerogel was about 2 to 3 times that of many commercial Al_2O_3.[4]

An interesting effect of surface area collapse as a function of time over uncalcined silica aerogels is noted in Appendix D. The overall findings are that the supercritical

process can not totally remove all water and/or ammonium hydroxide (used for condensation reaction), and that an additional step of vacuum drying, 110 °C for 3 hrs, is necessary to totally rid the aerogel of physisorbed water-ammonia.[15, 16, 115] After this additional drying step, the surface areas for the silica aerogels were found to be stable for up to 4 months with little more than a 1 or 2% decrease in surface area. Note, in this study all silica aerogels reported and used as surface oxide supports were gelled, extracted, and calcined all in one 12-hr day, in order to prevent or minimize the aforementioned phenomenon. One last point was that calcined alumina aerogels had a tendency to have large decreases in surface area (~ 30%) unless precautions were taken to keep the samples extremely dry. This decrease in surface area was noted in another study using amorphous alumina prepared from precipitated aluminum chloride.[194]

3.4.2 XRD, DTA, and SEM Studies

Table 3-23 reveals the surface area and XRD patterns of the prepared aerogels of silica and alumina as well as a commercial grade silica (Davison 952) for comparison. The surface area of the silica aerogel is on average about 2.5 times as large as the commercial silica throughout most of the temperature range tabulated. The aerogel of silica retains nearly 80% of its high surface area up to a temperature of 1000 °C, whereas the commercial silica maintains approximately 90% of its area under the same conditions. Figure 3-29 shows the normalized surface area of the silica aerogel and commercial SiO_2 (Davison). The expanded scale merely accentuates the difference of surface area retention in these materials; however, it can be seen that both samples exhibit great stability over a large temperature range. This ability to retain surface area and the inert nature inherent to silica makes this aerogel an ideal choice as a support. Only prolonged periods of time at severe heat treatments cause collapse of the aerogel structure, possibly due to the silica becoming mobile and undergoing severe dehydroxylation to sinter this material. The silica samples remain amorphous as found by XRD, despite these severe heat treatments.

Table 3-23: SiO$_2$ AND Al$_2$O$_3$ SURFACE AREA AND XRD AS A FUNCTION OF HEAT TREATMENT

	A-SiO$_2$		SiO$_2$[3]		A-Al$_2$O$_3$	
Heat Treatment [Temp.(°C),Time(hr)]	B.E.T S.A.[1]	XRD[2]	B.E.T S.A.	XRD	B.E.T S.A.	XRD
(500,2)	920	A	345	A	580	A
(600,2)	825	A	340	A	470	A
(800,2)	750	A	325	A	390	γ-Al$_2$O$_3$
(1000,-)	700	A	310	A	190	γ-Al$_2$O$_3$
(1000,48)	290	A	260	A	60	α-Al$_2$O$_3$

[1] Total Surface Area, Single Point B.E.T. (m^2/g)

[2] X-Ray Diffraction with Molybdenum Radiation, A = Amorphous

[3] SiO$_2$ [Davison Chemical, (952)]

Figure 3-29: SiO₂ NORMALIZED SURFACE AREA VERSUS CALCINATION
TEMPERATURE
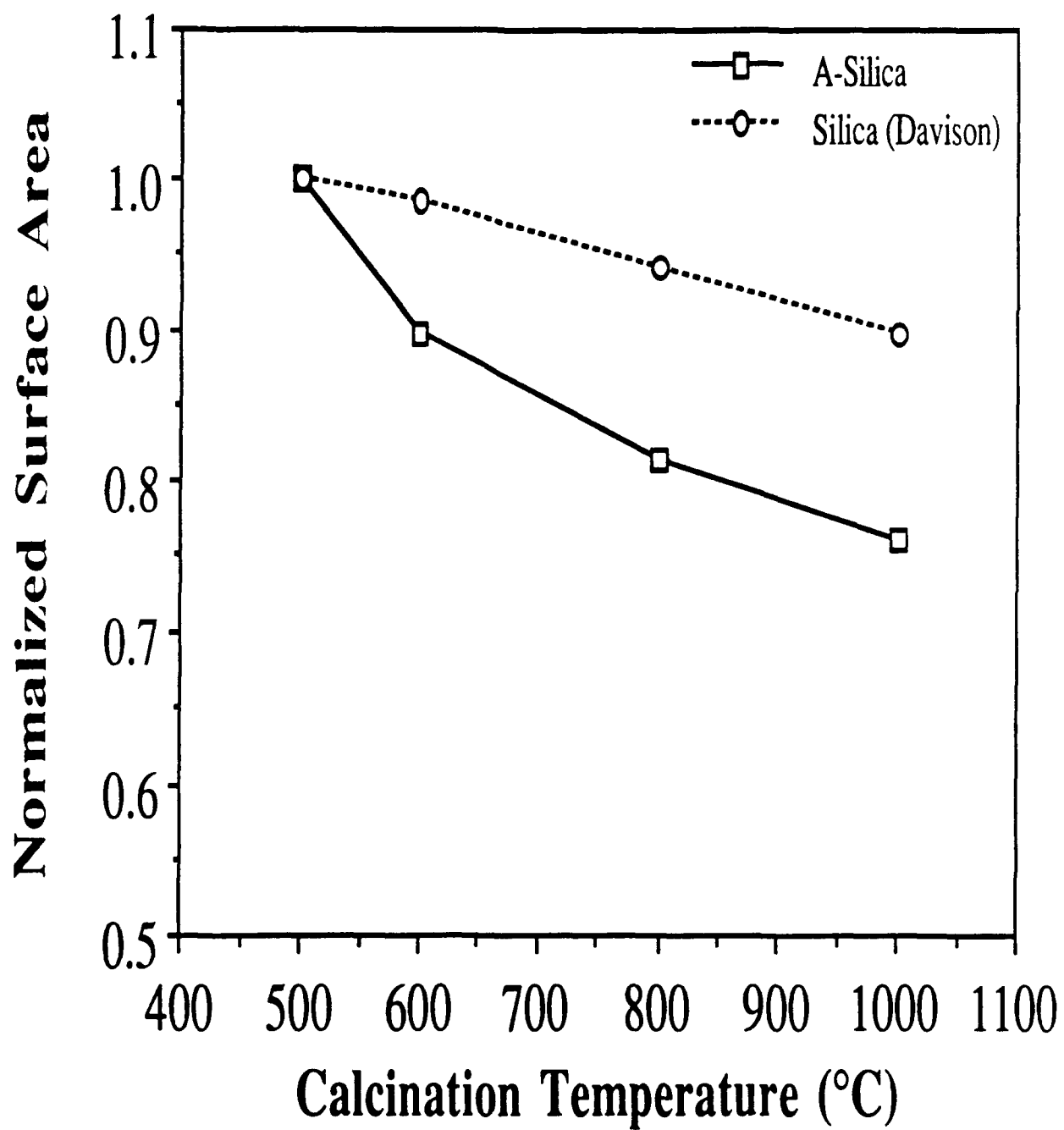
The alumina aerogel surface area, like that for the silica aerogel, is on average about 2 - 3 times greater than many commercial alumina.[4] A-Al_2O_3 maintains nearly 70% of its surface area up to temperatures of 800 °C. This stability is lost upon higher thermal treatment to 1000 °C due to the aerogel undergoing a phase transformation to form γ-Al_2O_3. The surface area at this point drops to a level of approximately one third (~ 190 m^2/g) of its original value, comparable to that of commercial alumina.[4] A severe thermal treatment at 1000 °C (1000,48) causes the aerogel of alumina to undergo further restructuring by transforming into the stable phase of α-Al_2O_3. The collapse of surface area to 60 m^2/g, a mere 10% of its original area, is due to this phase transformation.

Figure 3-30 shows the XRD scan of A-Al_2O_3 as a function of heat treatment. This figure indicates the transformation from amorphous to γ-Al_2O_3, and finally to α-Al_2O_3. The XRD amorphous background in the crystalline scans of both γ-Al_2O_3 and α-Al_2O_3 indicates that the alumina aerogel has not reached an entirely structured state, and that crystallites of these phases are probably just growing out of the aerogel. No data for A-SiO_2 is shown because it was found to be XRD amorphous at all thermal treatments.

No DTA scans are shown in this chapter for either A-SiO_2 and A-Al_2O_3 because no compound formation or phase transformations could be observed in the collected scans. The silica aerogel showed a flat profile for the entire scanned range of 25 - 1000 °C indicating no measureable physisorbed water or transformations occurred. The alumina aerogel had a broad measureable endothermic valley up to 300 °C indicating physisorbed and possibly chemisorbed water was on the surface of this material. Appendix C shows the hydroxyl region from FTIR and DRIFT studies for both the silica and alumina aerogels and confirms that the alumina aerogel strongly chemisorbs water.

SEM was not employed to examine the silica and alumina aerogels as large differences were not expected from the examined aerogels of niobia, A-NS25w, and A-NA25w, which all showed a "fluffy" mass of randomly distributed particles (see Chapters 3 and 4). The surface oxides of silica aerogel-supported niobia [A-NS(.25)] and alumina

Figure 3-30: XRD OF A-Al$_2$O$_3$ AFTER HEAT TREATMENT: A) (500,2) [A], B)
(1000,-) [γ], AND C) (1000,48) [α] (ALUMINA PHASE IN BRACKETS)
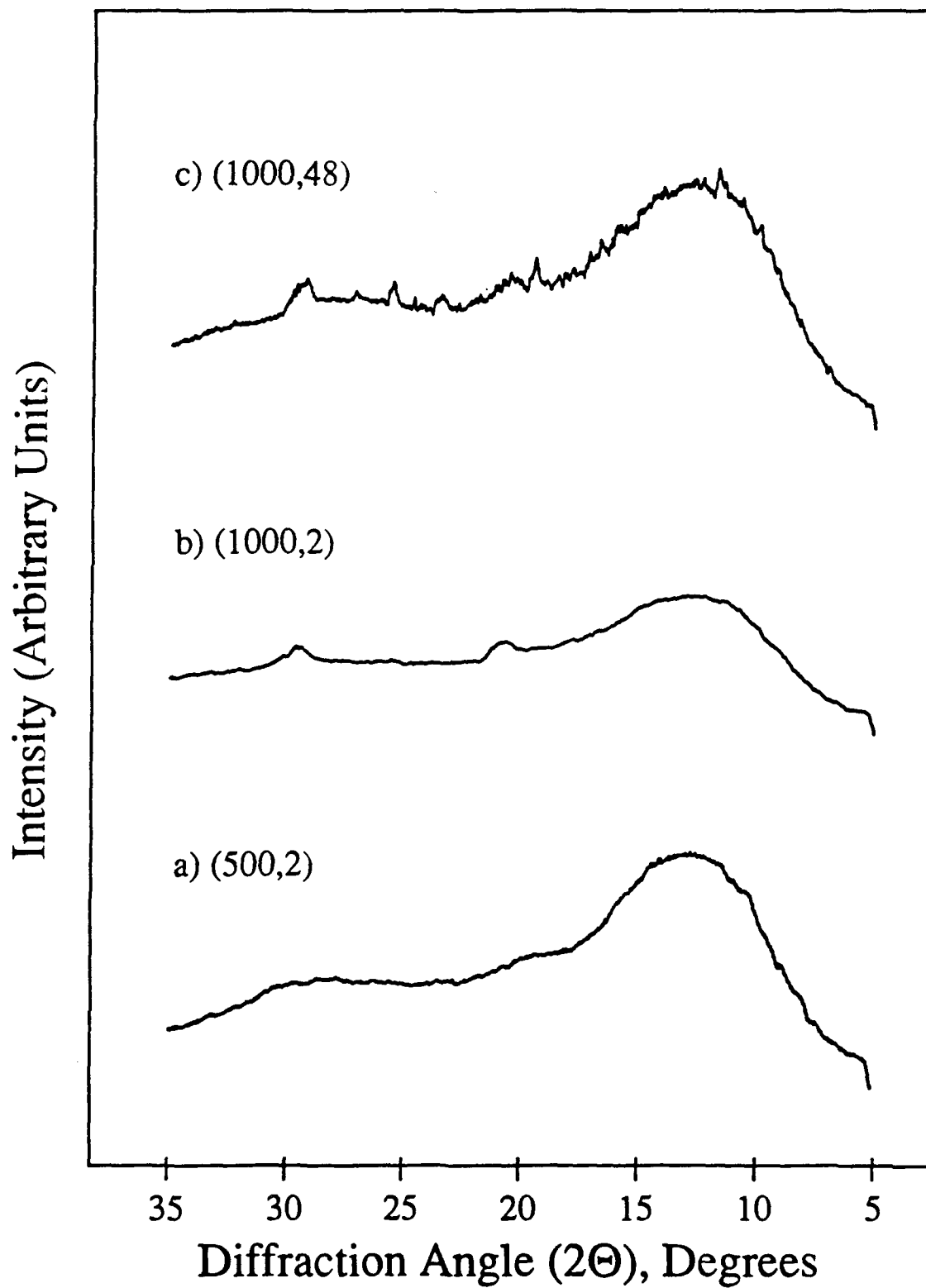
aerogel-supported niobia [A-NA(.25)] are shown later in Chapter 5 after calcination to have the "fluffy" morphology. This same appearance is expected of the bulk silica and alumina aerogels, because these materials are the supports for the surface oxides.

3.4.3 LRS and DRIFT Studies

Laser Raman Spectroscopy (LRS) employed on the calcined samples of silica and alumina yields no useful spectra as both materials fluoresce strongly, and any information contained in the samples are obscured by the large background. Higher thermal treatments to (600,2) are used to minimize this fluorescing problem in most surface oxides which have as their major component, the supporting oxide aerogel. This is later seen in the surface oxide results of Chapter 5. All DRIFT spectra, and other FTIR spectra, of the hydroxyl region for the silica and alumina aerogels can be found in Appendix C. A brief discussion of these spectra is also contained in that part of the dissertation. The main results of that section show that the silica aerogel has only one hydroxyl peak while the aerogel of alumina has three distinct hydroxyl stretches. The alumina aerogel was found to strongly chemisorb water while the aerogel of silica was shown to also adsorb water.

3.5 Chemical Property Characterization of Silica and Alumina Aerogels

3.5.1 Acid Strength/Acidity with n-Butylamine Titration and Superacidity/Basicity

Silica is an oxide which has been well documented as a weak acid.[2, 88, 180] Our study of A-SiO$_2$ has confirmed the above findings. Acid strength measurements of the silica aerogel indicate that it can only turn the pKa = +4.8 indicator to its red acidic form and has an acidity of 0.28 mmoles/g, nearly identical to that found with commercial silica (0.30 mmoles/g). Superacidity and basicity experiments, again using indicators for only qualitative analysis of silica aerogel, were performed as a baseline, to see if this sample turned any of the indicators to their acidic forms. Table 3-24 shows results of this analysis

Table 3-24: SUPERACIDITY AND BASICITY OF HEAT TREATED BULK
AEROGELS

Sample Name	Acid Strength (pKa)			Basic Strength (pKa)	
	-11.35	-12.40	-13.75	+9.3	+15.0
A-Nb$_2$O$_5$ (500,2)	++	++	++	++	+
A-Nb$_2$O$_5$ (1000,-) He	-	-	-	-	-
A-Al$_2$O$_3$ (500,2)	+	+	+	++	++
A-Al$_2$O$_3$ (1000,-) He	-	-	-	+	-
A-SiO$_2$ (500,2)	-	-	-	-	-
A-SiO$_2$ (1000,-) He	-	-	-	-	-

++   (Very Positive Acid or Basic Indication)

+   (Positive Acid or Basic Indication)

+/-   (Positive and/or Negative Indication)

-      (Negative Acid or Basic Indication)

for calcined and heat treated A-SiO$_2$. One clearly sees that the observations are all negative as expected for this weak acid.

Alumina is an oxide which has been shown to contain strong surface acidity when heated to temperatures above 470 °C in vacuum.[2] Our results on the study of A-Al$_2$O$_3$ using n-butylamine titration did not show any acidity for this material after (500,2), in conflict with what was shown previously. However, this negative result for alumina was also seen in experiments conducted by two independent researchers, Walling[146] and Benesi.[195] Superacidity and basicity tests were then done on the calcined and heat treated A-Al$_2$O$_3$ to see if water was effectively poisoning the acid sites. These experiments for A-Al$_2$O$_3$ were performed in a dry glove box in which the sample was heated in-situ at 450 °C for 2 hrs, and the following results are revealed in Table 3-24. One immediately notices the fact that the aerogel of alumina has very strong acidity, in sharp contrast to what was shown by the n-butylamine titration; and it also possesses strong basicity as noted by the very positive indication of the basic strength indicators, much like that of calcined A-Nb$_2$O$_5$. Heat treating the alumina aerogel to (1000,-) destroys its superacidic properties as indicated by the negative observations at these acid strengths, but it still contains some basicity as noted by the positive indication at pKa = +9.3. Results by FTIR will later show that the calcined alumina aerogel is indeed a very strong Lewis acid. The results above show that A-Al$_2$O$_3$ is a strong acid; however, n-butylamine titration fails to confirm this fact. One explanation for this negative indication of acidity could possibly be attributed to alumina being such a strong Lewis acid, that physi- and/or chemisorbed water on the sample surface is not totally removed at the 110 °C vacuum oven pretreatment for the n-butylamine titrations. This adsorbed water layer could poison or even act as a shield to the acid sites of the alumina aerogel. DTA, DRIFT, and FTIR measurements all indicate that the alumina aerogel has water strongly adsorbed to its surface.

3.5.2 Pyridine Adsorption Studies

3.5.2.1 ΔH_{ads}: TG Study

Pyridine adsorption experiments were performed on silica and the aerogel of alumina to determine the strength of acid sites versus pyridine coverage. These experiments were performed to better understand the acidity inherent in these two materials, and to better clarify any conflicts that were noted in the previous section. Data for silica (Davison), A-Al$_2$O$_3$, P-Nb$_2$O$_5$, and A-Nb$_2$O$_5$ are shown in Figure 3-31. These bulk oxide results can be found in Table 3-12. Figure 3-31 shows heats of adsorption data for silica with values of ΔH_{ads} ranging from 12.6 to 15 kcal/mol at low coverages of 1.0 to 2.5 x 10^{13} molecules/cm^2 and an average value of 14.1 kcal/mol. This data again confirms that silica is indeed a weak acid and that very little pyridine adsorbs to the surface in the range of our experimental conditions. This measured value corresponds well with other findings of ΔH_{ads} = 12.4 kcal/mol for silica.[196]

The heat of adsorption for the alumina aerogel is also found in Figure 3-31. We see that ΔH_{ads} is 20.4 to 23.6 kcal/mol at coverages of 13.5 to 4.1 x 10^{13} molecules/cm^2, which corresponds closely to literature findings for an acidic alumina.[179] This acidic alumina sample studied by Deeba and Hall[179] was 98.4 wt.% Al$_2$O$_3$ (other 1.6 wt.% SiO$_2$) and had a ΔH_{ads} ranging from 20 to 28 kcal/mol for coverages of 10.0 to 5.1 x 10^{13} molecules/cm^2. The aerogel of alumina also reveals an acid strength comparable to that of precipitated niobic acid, which shows that the alumina aerogel possesses moderately strong acid sites.

3.5.2.2 Acid Type: FTIR Study

Pyridine adsorption on acid sites was examined for the silica and alumina aerogels in the 1400 - 1700 cm^{-1} range. Figure 3-32 shows the pyridine adsorbed on A-SiO$_2$ after evacuation temperatures of 25, 100, 200, and 300 °C. This figure confirms that silica has

Figure 3-31: ΔH_{ads} VERSUS PYRIDINE COVERAGE FOR BULK AEROGELS
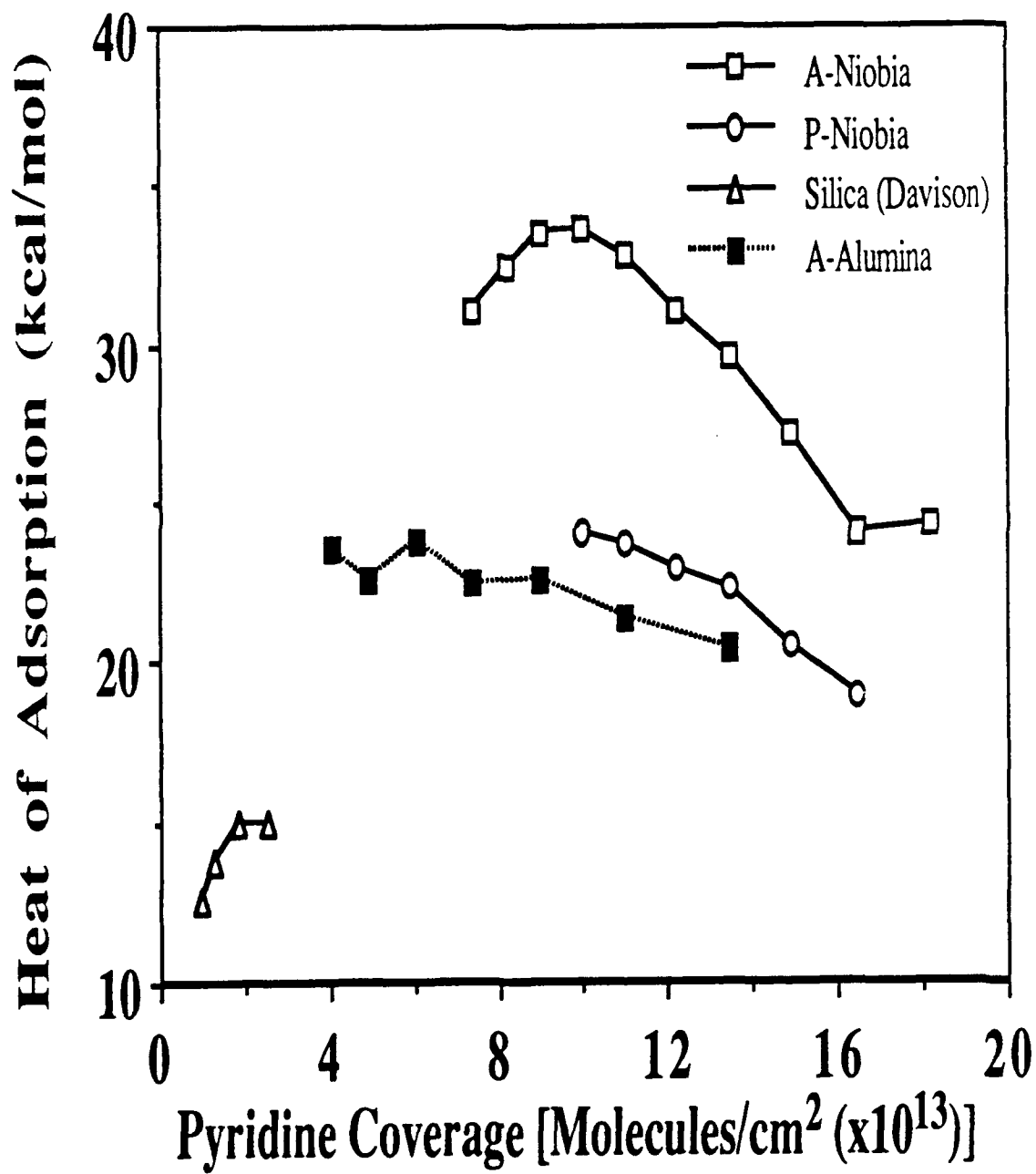
Figure 3-32: FTIR SPECTRA OF PYRIDINE ADSORBED ON A-SiO$_2$ AFTER HEAT TREATMENTS AT 300, 200, 100, AND 25 °C (TOP TO BOTTOM)
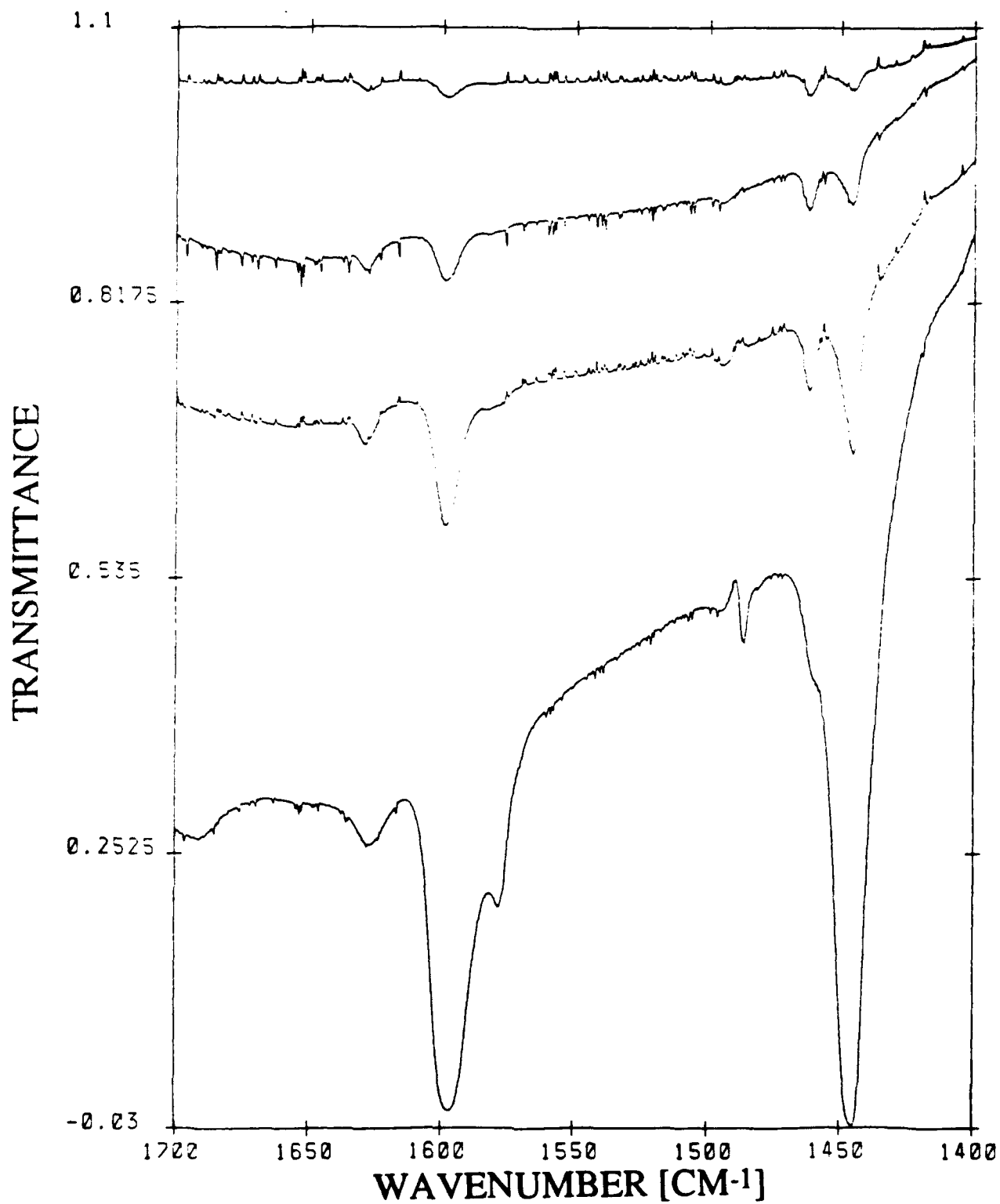
weak acidity as noted by the severe attenuation in peaks after only a 100 °C thermal treatment. Very little absorption is observed in the spectrum after the 300 °C treatment, which indicates that little pyridine adsorbs on silica after temperatures higher than 100 °C; in other words, silica primarily physisorbs and hydrogen bonds with pyridine.[180]

Results for pyridine adsorption on the calcined alumina aerogel can be found in Figure 3-33. Table 3-14 lists the Lewis pyridine absorption frequency for the 19b and 8a bands respectively. The absorption spectra by other researchers of pyridine adsorbed on dehydrated (450 °C and 500 °C) η-Al_2O_3 are similar to the spectra observed for pyridine on the aerogel of alumina.[180, 197, 198] The infrared bands of pyridine adsorbed on these aluminas and those of A-Al_2O_3 provide very convincing evidence that the alumina acid sites are of the Lewis type. The retention of pyridine after a 300 °C heat treatment, as shown by the large absorption bands - frequency shift of the 1450.1 cm^{-1} band to 1453.3 cm^{-1} (Δ = 3.2 cm^{-1}), and the large frequency shift of 1616 cm^{-1} to 1622.5 cm^{-1} (Δ = 6.5 cm^{-1}) indicate that the alumina aerogel is a very strong Lewis acid, since increasing wavenumber in these vibrational modes corresponds to increasing coordination bond strength.[180, 198] Also, the absence of a band at 1540 cm^{-1} indicates that there are no Brønsted acid sites on the surface strong enough to react with pyridine. The Lewis to Brønsted (L/B) acid ratio as shown in Table 3-15 increases from 8.4 to 40.4 to 675.8 as the evacuation temperature is increased from 100 to 200 to 300 °C, respectively. This L/B ratio of 675.8 and even 40.4 for that matter may basically be thought of as infinity, i.e. no Brønsted acid sites, since integrating the 1490 cm^{-1} and 1450 cm^{-1} peaks becomes difficult when no Brønsted acidity is detected. See Appendix F for sample calculations of this ratio.

3.5.3 1-Butene Isomerization

The 1-butene isomerization reaction was used to test the activity of the silica and alumina aerogels. Results of the activity (mol/hr-g) versus TOS can be found in Figure 3-34. It is quite evident from this figure that the aerogels of silica and alumina do not catalyze

Figure 3-33: FTIR SPECTRA OF PYRIDINE ADSORBED ON A-Al₂O₃ AFTER HEAT TREATMENTS AT 300, 200, 100, AND 25 °C (TOP TO BOTTOM)
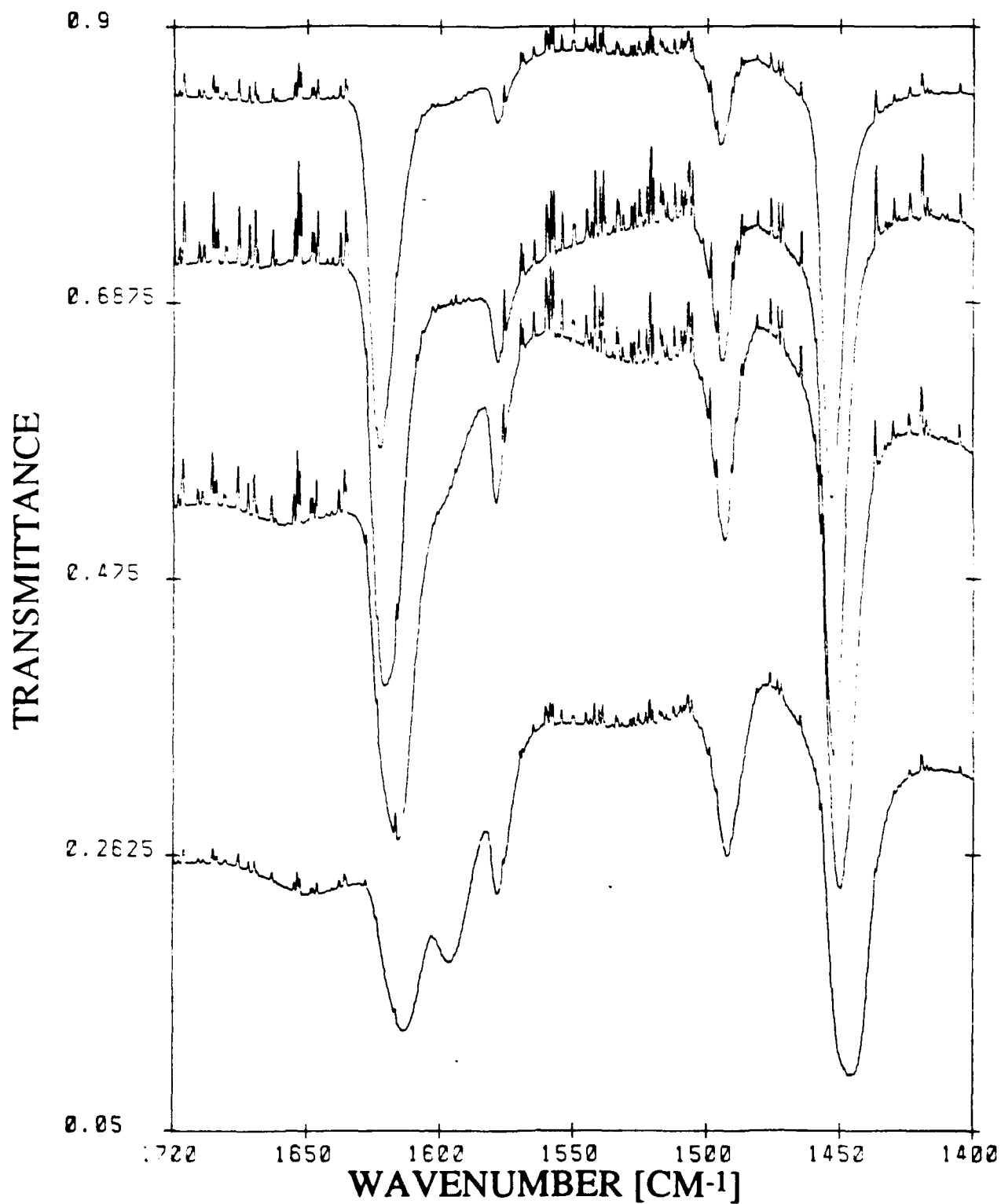
Figure 3-34: 1-BUTENE ISOMERIZATION ACTIVITY OVER BULK OXIDES
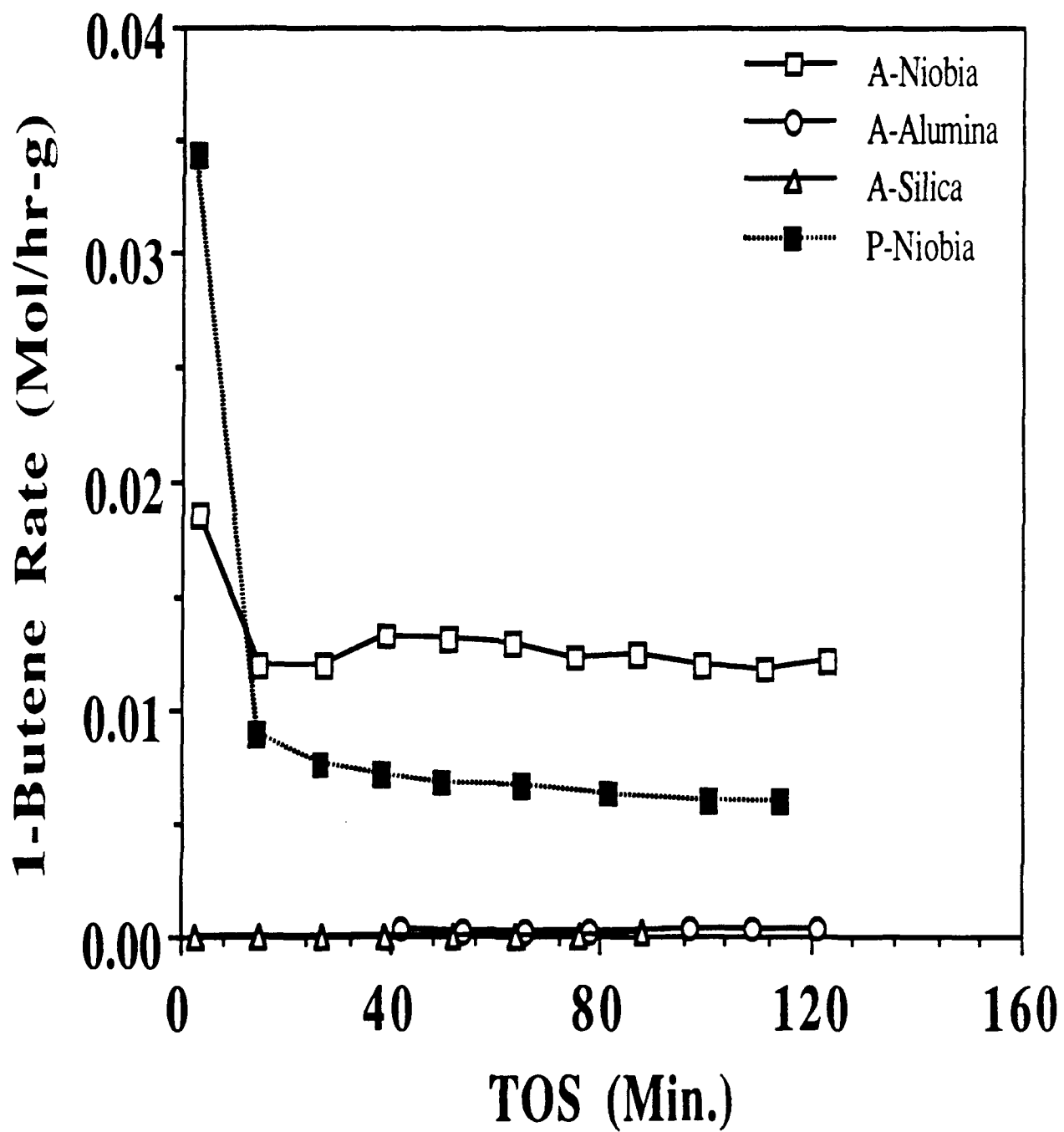
this reaction well (see Table 3-19). This is not surprising since 1-butene isomerization has been well known to be catalyzed primarily by weak Brønsted sites, of which silica has none. It has been documented and shown in this study that the alumina aerogel has very strong Lewis acidity, and little or no Brønsted acidity, hence the small activity of the oxide in this reaction. The aerogel of niobia as well as the precipitated niobia are shown for comparison in Figure 3-34. These results lead to the conclusion that any activity with respect to this reaction from distributing niobia either in silica or alumina as a mixed oxide, or on silica or alumina as a supported oxide may be related to the incorporation of niobia in these materials. These studies will be investigated in the two subsequent chapters.

3.6 Summary

This chapter summarizes both the physical and chemical properties of the bulk oxide aerogels of niobia, silica, and alumina, while also going into detail comparing conventionally prepared niobia samples with the niobia aerogel. With these niobia samples it was established that the origin of both acid strength and acidity for the niobia aerogel stemmed from very distorted terminal Nb=O groups, while the conventionally prepared niobia samples acidity and acid strength was attributed to distorted Nb-O bonds. Acidity measurements concluded that ordering of the bulk niobia crystal lattice was detrimental to the unique acid properties of these niobia samples. The silica aerogel was found to be a very weak acid with little to no Lewis or Brønsted acidity, and was shown to be quite inert and stable in retention of surface area over a large temperature range. The alumina aerogel had strong Lewis acidity as indicated by IR and TG measurements of pyridine adsorption. This aerogel of alumina, like the silica aerogel, was inactive for 1-butene isomerization, and was found to be moderately stable in terms of surface area retention and phase transformation. Thus, both of these oxides, silica aerogel and alumina aerogel, make suitable choices as oxide supports for this study.

Chapter 4

MIXED OXIDE AEROGELS

4.1 Introduction

This chapter contains characterization results of the mixed oxide aerogels prepared in this study. Techniques employed to examine the structural and chemical properties of these binary oxides were used as an aid to better understand the oxide-oxide interaction through structural observations, and to help elucidate the chemical-structural relationship inherent in these materials. This chapter will build upon those results presented for niobia in the previous chapter. It will later be supplemented with results in Chapter 5, the supported oxides, in establishing a model to explain the oxide-oxide interactions in these materials.

4.2 Physical Property Characterization of Mixed Oxide Aerogels

4.2.1 Surface Area and Physical Property Data

Niobia/silica (A-NS25w) and niobia/alumina (A-NA25w) mixed oxide aerogels were prepared via the sol-gel route, using metal alkoxides, followed by a semi-continuous supercritical extraction with CO_2. Mixed oxides of these same materials were prepared by a standard co-precipitation of metal chlorides (NS25w) and metal alkoxides (NA25w). The gelation conditions for both binary oxide aerogels were empirically determined. Exact conditions of these materials may be found in Chapter 2. Table 4-1 shows the physical

Table 4-1: PHYSICAL PROPERTY DATA OF NIOBIA/SILICA AND
NIOBIA/ALUMINA MIXED OXIDES

Sample	Total B.E.T. Surface Area[1]	Total Pore Volume[2]	Avg. Pore Diameter[3]
A-NS25w	639.8	1.9960	124.8
NS25w	440.8	0.4812	43.7
A-NA25w	454.1	1.0795	95.1
NA25w	339.3	0.4470	52.7

[1]   Total Surface Area, Multi-Point B.E.T. (m^2/g)

[2]   Total Pore Volume (cm^3/g)

[3]   Average Pore Diameter, 4V/S, (Å)

property data for the mixed oxides synthesized in this study. As with the other prepared aerogels of niobia, silica, and alumina, the niobia/silica and niobia/alumina aerogels show surface areas which are significantly larger (1.5 times larger) than their conventionally prepared counterparts. Other similar characteristics with these aerogels and those examined previously are the extremely large pore volumes (as measured by nitrogen adsorption), 0.48 vs. 2.00 cm^3/g and 0.45 vs. 1.08 cm^3/g, and large average pore diameters, 43.7 vs. 124.8 Å and 52.7 vs. 95.1 Å, for NS25w vs. A-NS25w and NA25w vs. A-NA25w, respectively. These characteristics of very large pore volumes and large average pore diameters are what distinguish aerogels from xerogels and other more commonly prepared oxides.[156] The large surface area for both aerogels and the co-precipitated samples, can be explained by the fact that both mixed oxides are rigid due to the covalent bonding of the networks: Si-O-Si, Si-O-Nb, Al-O-Al, and Al-O-Nb.[199] This rigidity, upon drying, leads to a retention of most of the mixed oxide network and its skeletal and porous phase, thus giving a large surface area, but the surface area of the precipitated sample is at the expense of a smaller pore volume which densifies the material.[156]

The surface area of the NS25w mixed oxides after various thermal treatments are shown in Table 4-2. The aerogels of niobia and silica are also included for comparison. Both of the niobia/silica mixed oxide samples retain nearly 50% of their surface areas after ramping to 1000 °C, from 670 to 315 m^2/g and from 480 to 205 m^2/g for the aerogel and precipitated samples, respectively. At this temperature the aerogel of niobia has nearly totally collapsed to a surface area of ~ 1 m^2/g after undergoing a transformation to M-Nb_2O_5. Heating longer at 1000 °C causes further collapse in surface area for both A-NS25w and NS25w.

These surface area declines with respect to temperature are shown in Figure 4-1. Notice that the total surface area of the niobia/silica aerogel is greater than the precipitated sample over the entire range of heat treatment, but follows the same general form as shown by the normalized data in Figure 4-2. These two curves superimpose on each other, within

Table 4-2: SURFACE AREAS OF A-NS25w AND NS25w MIXED OXIDES WITH THERMAL TREATMENTS

| Heat Treatment | Total Surface Area $(m^2/g)^*$ | | | |
| | Samples | | | |
[Temp.(°C).Time(hr)]	A-NS25w	NS25w	A-Nb$_2$O$_5$	A-SiO$_2$
(500,2)	670	480	190	920
(600,2)	600	455	60	825
(800,2)	390	225	5	750
(1000,-)	315	205	1	700
(1000,4)	155	60	-	N/A
(1000,48)	100	45	-	290

Table 4-3: SURFACE AREAS OF A-NA25w AND NA25w MIXED OXIDES WITH THERMAL TREATMENTS

| Heat Treatment | Total Surface Area $(m^2/g)^*$ | | | |
| | Samples | | | |
[Temp.(°C).Time(hr)]	A-NA25w	NA25w	A-Nb$_2$O$_5$	A-Al$_2$O$_3$
(500,2)	530	400	190	580
(1000,-)	130	110	1	190
(1000,48)	27.5	15	-	60

* Surface Areas measured using Single-Point B.E.T. method; (500,2) samples agree with those measured using Multi-Point B.E.T. method.

Figure 4-1: A-NS25W AND NS25W TOTAL SURFACE AREA VERSUS HEAT
TREATMENT
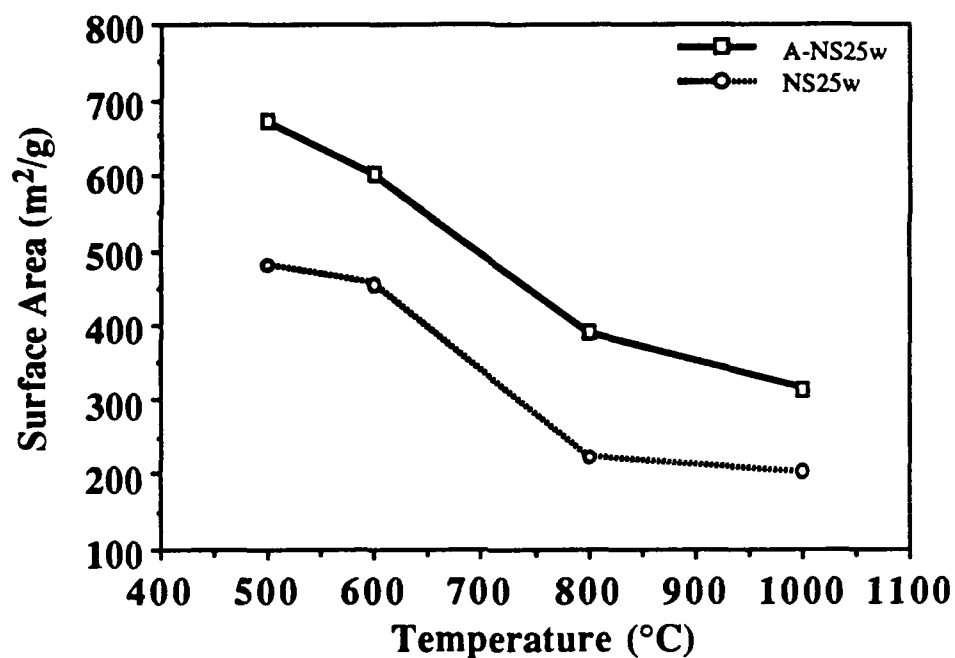
Figure 4-2: A-NS25W AND NS25W NORMALIZED SURFACE AREA VERSUS
HEAT TREATMENT
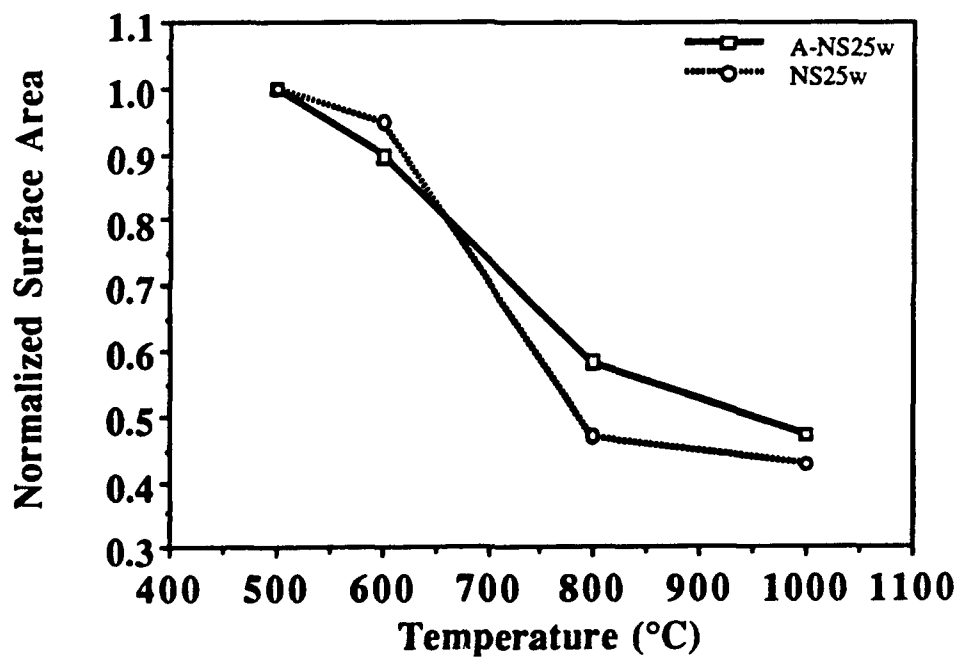
experimental error, throughout the entire temperature range. Thus, proportionally the two mixed oxides follow the same trend of surface area decline.

Table 4-3 shows the surface areas of the two niobia/alumina mixed oxides along with the two bulk oxide aerogels in this system. The surface areas of both A-NA25w and NA25w collapse at 1000 °C, (1000,-), to values which are roughly 25% of original calcined surface areas. We will see later that this can be explained by the compound formation of poorly crystalline $NbAlO_4$ and phase transformation of alumina to γ-Al_2O_3. The ensuing surface area collapse to levels which are approximately 5% of the original areas after (1000,48) is caused by further crystallization to $NbAlO_4$. The alumina and niobia aerogels after this severe thermal treatment of (1000,48), have surface areas of 60 m^2/g and near zero (negligible uptake on niobia), respectively, due to phase transformation into the most stable forms for these bulk oxides, α-Al_2O_3 and H-Nb_2O_5.

4.2.2 X-Ray Diffraction (XRD)

Figure 4-3 shows the XRD patterns of the niobia/silica mixed oxide aerogel after heat treatment. Similar results are found for the precipitated niobia/silica over the same temperature range. One can see the emergence of the 1 or 2 major peaks indexed to TT-Nb_2O_5 or T-Nb_2O_5 from the mixed oxide aerogel as the temperatures and holding times are increased. Table 4-4 shows the indexed phases of both niobia/silica mixed oxides and niobia aerogel after different heat treatments ranging from (500,2) to (1000,48). One sees only poorly crystalline TT-Nb_2O_5 forms from either A-NS25w or NS25w, even after a severe thermal treatment, (1000,48), while the bulk niobia aerogel forms the stable H-Nb_2O_5 after these same conditions. This shows that by mixing niobia into silica as a binary oxide, one can stabilize niobia from crystallization and subsequent phase transformations beyond TT-Nb_2O_5.[113, 200] From this data and other results from our group, it appears that niobia adjacent to a developing niobia/silica interface remains stabilized to TT-Nb_2O_5.[87, 88, 200] The fact that the surface areas of these niobia/silica

Figure 4-3: XRD OF A-NS25w AFTER HEAT TREATMENT: A) (800,2), B) (1000,-),
C) (1000,4), AND D) (1000,48)

d) (1000,48)

c) (1000,4)

b) (1000,-)

a) (800,2)

Intensity (Arbitrary Units)

Diffraction Angle (2Θ), Degrees
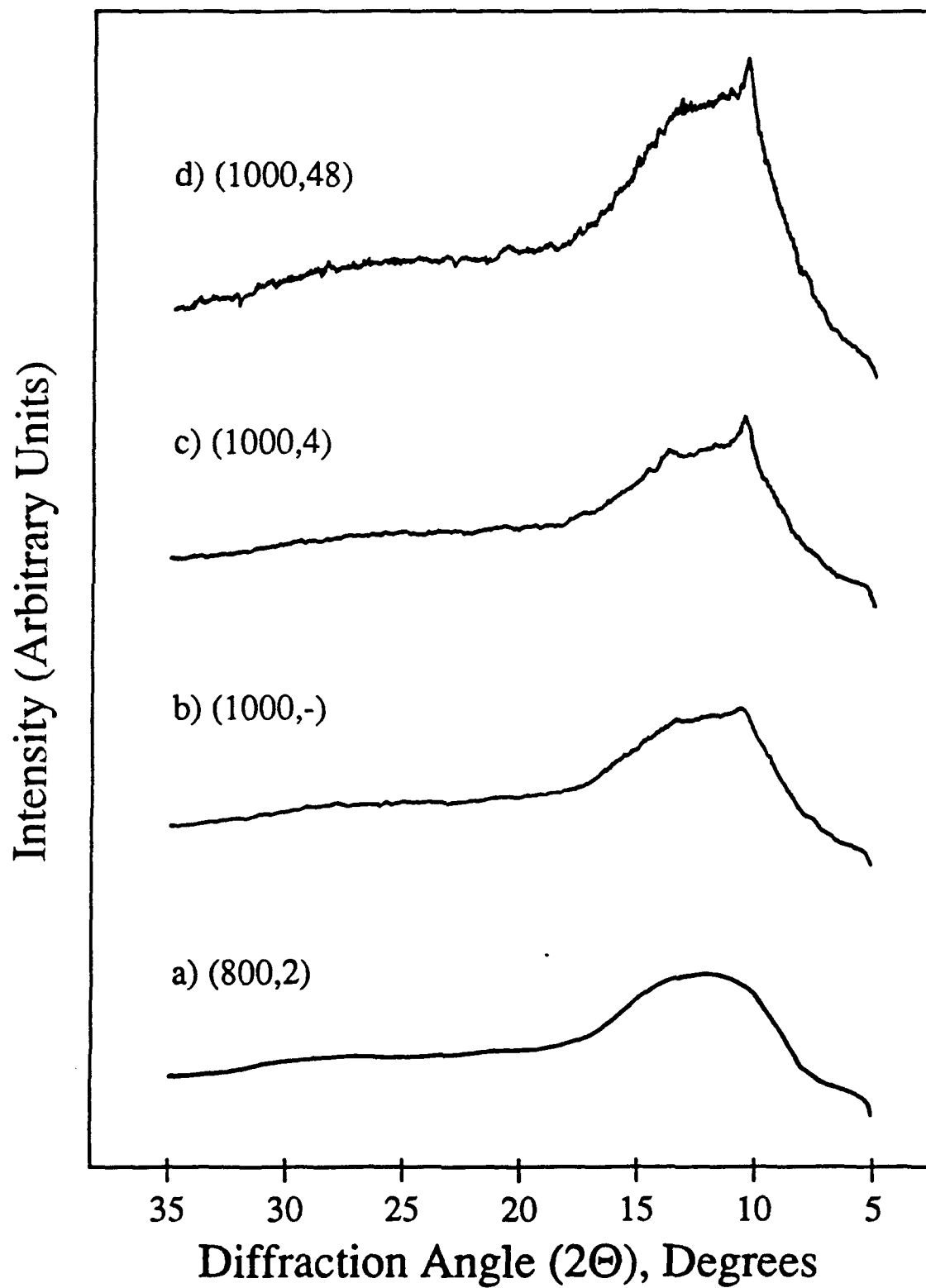
Table 4-4: PHASES OF A-NS25w MIXED OXIDE AEROGEL AND NS25w
PRECIPITATED MIXED OXIDE WITH THERMAL TREATMENTS

	X-Ray Diffraction Phases		
Heat Treatment [Temp.(°C),Time(hr)]	**Samples** A-NS25w	NS25w	A-Nb₂O₅
(500,2)	A	A	A
(600,2)	A	A	TT
(800,2)	A	A	T
(1000,-)	TT VPC	TT VPC	M
(1000,4)	TT VPC	TT VPC	H + M
(1000,48)	TT PC	TT PC	H

A=Amorphous; TT,T,M, and H refer to the phases of niobia; V, PC=very, poorly crystalline

mixed oxides have not totally collapsed, indicates that the oxide structure is stabilized and there is insufficient mobility for forming the high-temperature forms of niobia.

The XRD patterns for A-NA25w and NA25w after thermal treatments are shown in Figures 4-4 and 4-5, respectively. In both of these mixed oxides, after (500,2), XRD detected no diffraction peaks. The niobia/alumina aerogel (A-NA25w) diffraction pattern after (1000,-) shows weak peaks which were indexed to poorly crystalline $NbAlO_4$, as well as other broad peaks assigned to γ-Al_2O_3. More severe thermal treatment, (1000,48), on the niobia/alumina aerogel merely sharpens the peaks assigned to both $NbAlO_4$ and γ-Al_2O_3. The precipitated niobia/alumina (NA25w) diffraction pattern after (1000,-) shows sharp peaks indexed to $NbAlO_4$ and larger and broader peaks ($2\Theta = \sim 21°$ and $29°$) attributed to γ-Al_2O_3. The more severe heat treatment of (1000,48) causes increased sharpening of the $NbAlO_4$ peaks, but the one striking difference between the diffraction patterns for NA25w and A-NA25w are the sharp peaks indexed to α-Al_2O_3 in the NA25w scan. These results for the niobia/alumina mixed oxides and aerogels of bulk niobia and alumina are listed in Table 4-5. Note that the aerogel of alumina forms the stable phase of α-Al_2O_3 after (1000,48). The fact that this bulk oxide of alumina readily transforms into α-Al_2O_3 reveals the stabilizing interaction when niobia is introduced into the alumina matrix, as shown by A-NA25w after (1000,48). This mixed oxide aerogel shows the $NbAlO_4$ compound formation in addition to the alumina phase, γ-Al_2O_3. NA25w, after the same severe thermal treatment at 1000 °C, reveals no such stabilizing interaction, as evidenced by the phase transformation to α-Al_2O_3, the same as with the bulk alumina aerogel. These results reveal a large difference inherent in these niobia/alumina mixed oxides that can be traced back to the different preparations of these two materials. The aerogel of niobia/alumina was prepared via the sol-gel technique which produced a binary oxide that was atomically mixed on a microscopic scale with Nb-O-Al linkages built into the network of the inorganic oxide gel. The subsequent supercritical extraction preserved the integrity of the network and this structure. The precipitated niobia/alumina mixed oxide

Figure 4-4: XRD OF A-NA25w AFTER HEAT TREATMENT: A) (500,2), B) (1000,-), AND C) (1000,48)
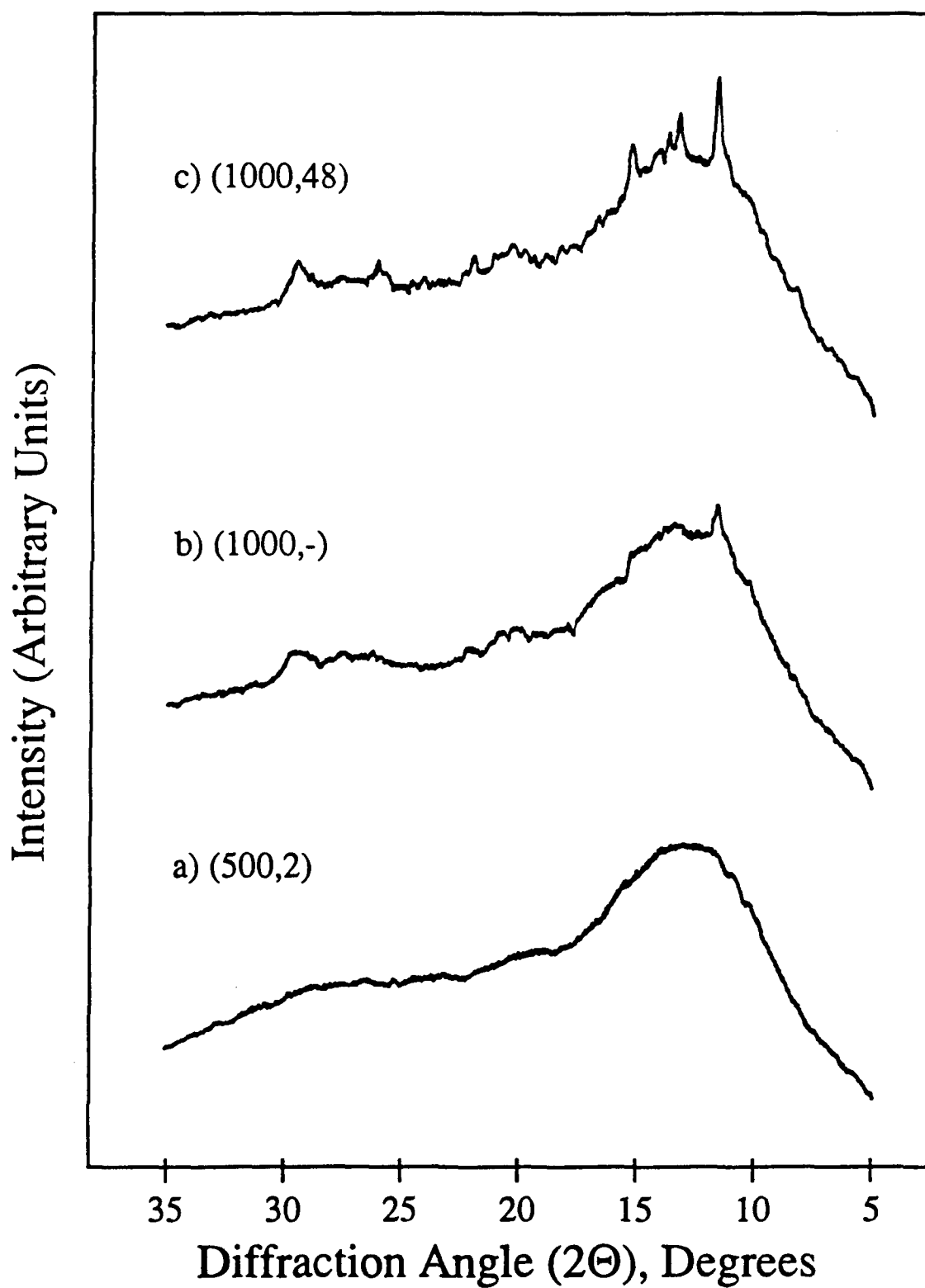
Figure 4-5: XRD OF NA25w AFTER HEAT TREATMENT: A) (500,2), B) (1000,-), AND C) (1000,48)
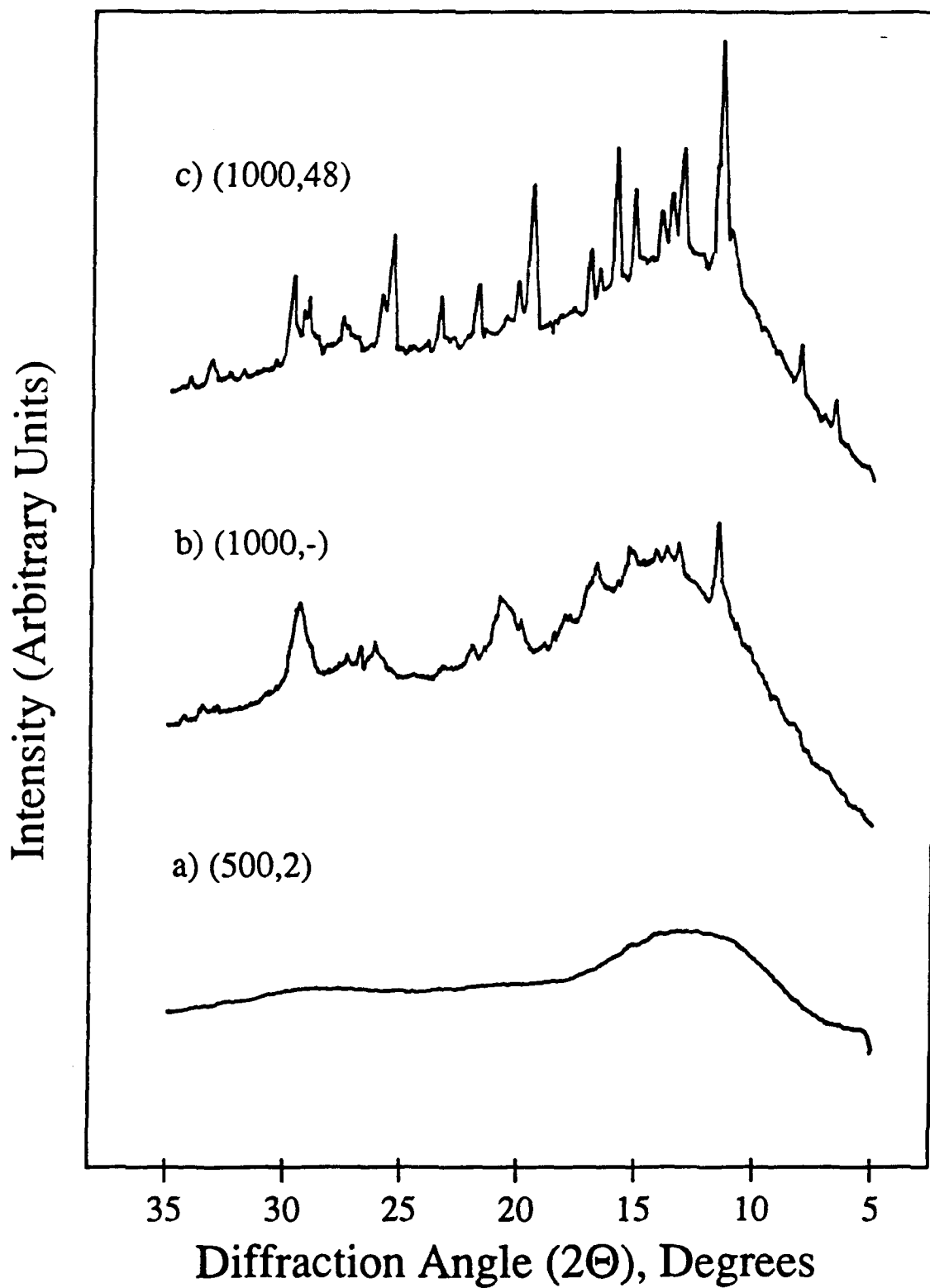
Table 4-5: PHASES OF A-NA25w MIXED OXIDE AEROGEL AND NA25w PRECIPITATED MIXED OXIDE WITH THERMAL TREATMENTS

| Heat Treatment | X-Ray Diffraction Phases | | | |
| | Samples | | | |
[Temp.(°C),Time(hr)]	A-NA25w	NA25w	A-Nb$_2$O$_5$	A-Al$_2$O$_3$
(500,2)	A	A	A	A
(1000,-)	γ-Al$_2$O$_3$, NbAlO$_4$ PC	γ-Al$_2$O$_3$, NbAlO$_4$	M	γ-Al$_2$O$_3$
(1000,2)	γ-Al$_2$O$_3$, NbAlO$_4$ PC	γ-Al$_2$O$_3$, NbAlO$_4$	H + M	γ-Al$_2$O$_3$
(1000,48)	γ-Al$_2$O$_3$, NbAlO$_4$	α-Al$_2$O$_3$, NbAlO$_4$	H	α-Al$_2$O$_3$

A=Amorphous; TT,T,M, and H refer to the phases of niobia; PC=poorly crystalline

:

was synthesized via a standard co-precipitation procedure.[1, 2, 64, 114] This technique leads to inhomogeneities in the final mixed oxide unless the rates of precipitation are identical for both precursors.[22] Empirical findings in this study qualitatively revealed a much faster rate of hydrolysis and precipitation in s-butanol for the alumina precursor, aluminum s-butoxide, than the niobia precursor, niobium ethoxide. This was thought to be due to the better leaving group on the aluminum atom, s-butoxy, than the ethoxy group on the niobium atom.[122] Thus, with this knowledge we believe that domains of alumina will be built into this precipitated mixed oxide, far enough from any kind of niobia-alumina interface, that upon severe thermal treatments the alumina is destabilized and transformed into α-Al_2O_3. This is analogous to a similar interpretation by our group for the niobia/silica system.[76, 88] As niobia (similar to alumina in niobia/alumina) crystallizes from niobia/silica, some niobia crystallizes to a high temperature phase of niobia (M-Nb_2O_5) in regions far enough removed from the niobia-silica interface.[76, 88] Niobia adjacent to the developing niobia-silica interface remains stabilized to the lower temperature phase, T-Nb_2O_5. In an analagous fashion, alumina in A-NA25w only undergoes a phase transformation to γ-Al_2O_3, i.e. it is stabilized to this low temperature phase in much the same way as niobia is stabilized to T-Nb_2O_5 in niobia/silica mixed oxides. One difference between the two systems is that whereas niobia and silica are immiscible, niobia reacts with alumina to form $NbAlO_4$.[13, 14]

4.2.3 Differential Thermal Analysis (DTA)

DTA scans were performed on all four prepared binary mixed oxides after the standard calcination. Figure 4-6 shows the data for both A-NS25w and NS25w. Both scans show a broad endothermic peak around 80 - 100 °C due to the evolution of physisorbed water from the binary oxide surface. The remaining parts of this scan are featureless and show no noticeable peaks which would indicate a phase transition. Thus, it appears from this data that the silica matrix has imparted stability to niobia from undergoing

Figure 4-6: DTA SCANS OF A-NS25w AND NS25w
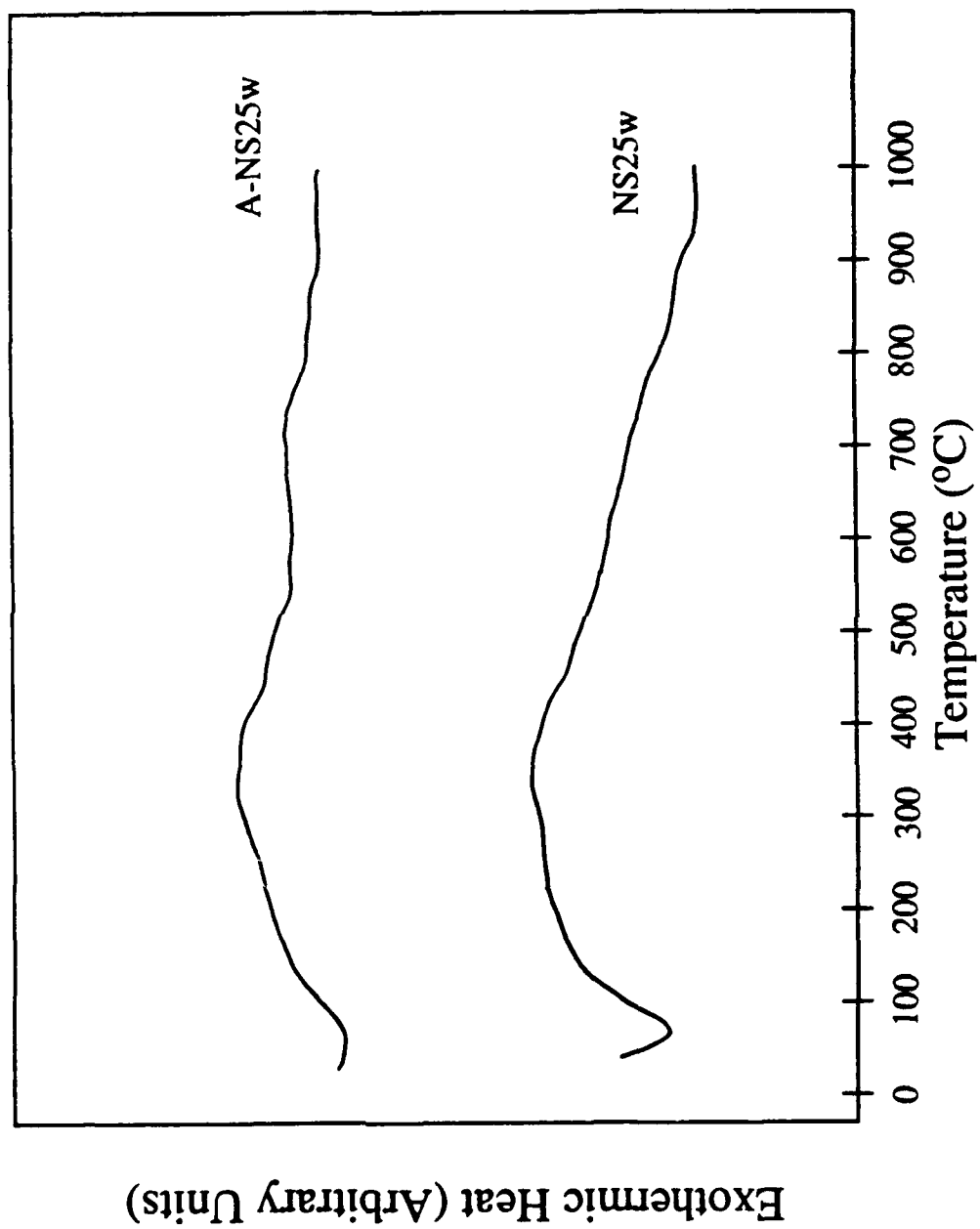
an ordered phase transition to TT-Nb$_2$O$_5$. Figure 4-7 shows the DTA scans for A-NA25w and NA25w. A very shallow and broad enothermic peak from 25 - 300 °C can be seen for both materials and may be attributed to chemisorbed water (see Appendix C for FTIR and DRIFT spectra). The aerogel of niobia/alumina shows an exothermic peak at ~ 860 °C which is attributed to the compound formation of NbAlO$_4$ as seen by XRD. NA25w (precipitated) does not show a peak in the scan as the aerogel, but it does appear to have a broad rise from 850 - 950 °C possibly indicating the formation of NbAlO$_4$. The broadness and low heat evolved through the compound formation indicate that the niobium aluminate forms slowly. This could be due to the different procedures used in synthesizing these two niobia/alumina mixed oxides, as explained previously.

4.2.4 Scanning Electron Microscopy (SEM)

SEM was used to examine any morphological similarities or differences in the niobia/silica mixed oxides. Figure 4-8 and Figure 4-9 show SEM micrographs of calcined, (500,2), A-NS25w and NS25w, respectively. Both micrographs indicate the "fluffy" particle appearance as was seen with the aerogel of niobia in Chapter 3. The only difference in the two micrographs appears to be the smaller particle sizes for NS25w. Both materials were originally ground to a mesh > 100; however, this size of particle was too large for the precipitated NS25w because of the massive cracking observed in the thin conductive gold layer applied to this SEM sample. Thus, to remedy this problem, the NS25w particles were ground to roughly about half the size, 10-20 μm, with an atomizer.

The scanning electron microscope was equipped with an X-ray detector for Energy Dispersive Spectroscopy (EDS), and was used for elemental mapping and quantitative elemental composition analysis of the binary oxide aerogels. Figures 4-10, 4-11, and 4-12 show the SEM micrographs and elemental dot maps for the calcined A-NS25w. One can see that the elemental niobium dot map in Figure 4-11 reveals a good dispersion of niobium atoms in the mixed oxide. SEM micrographs and elemental dot maps for the calcined A-

Figure 4-7: DTA SCANS OF A-NA25w AND NA25w
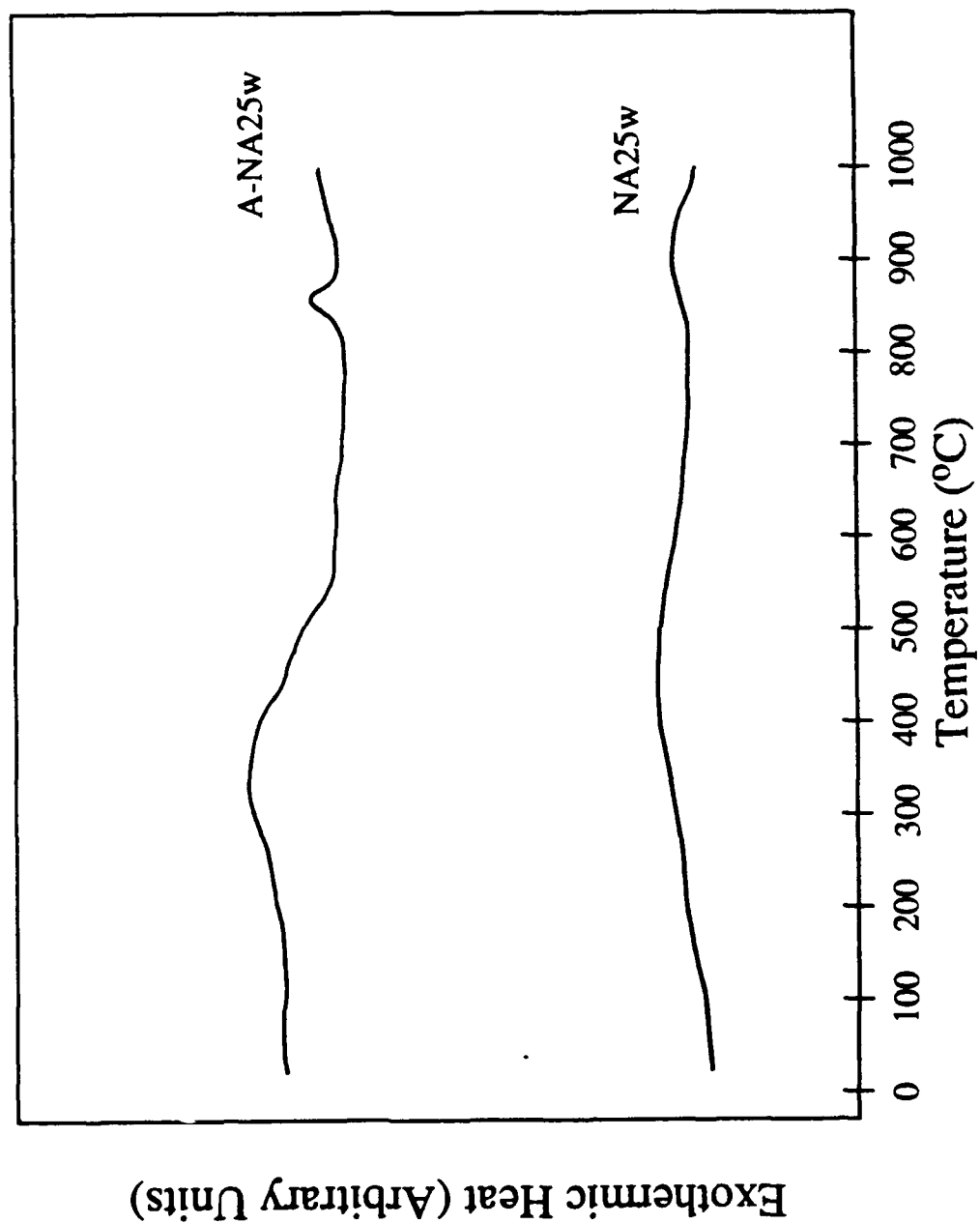
Figure 4-8: SEM MICROGRAPH OF CALCINED A-NS25w (500,2)
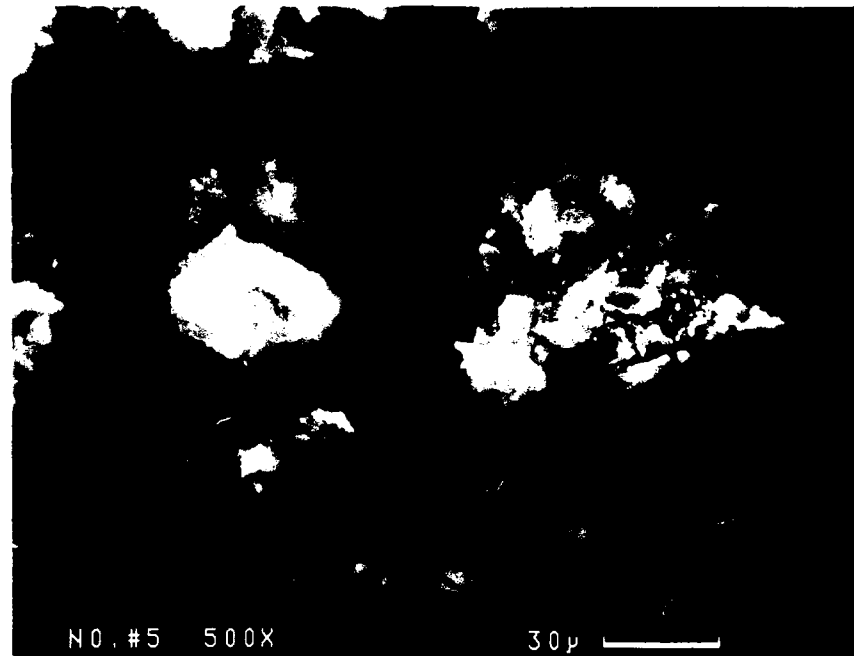
Figure 4-9: SEM MICROGRAPH OF CALCINED NS25w (500,2)
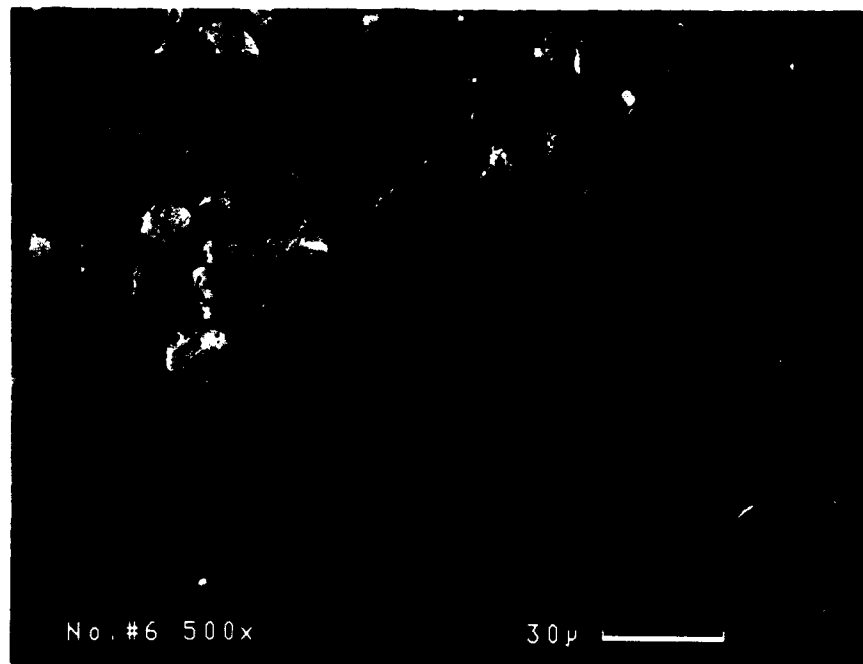
Figure 4-10: SEM MICROGRAPH OF A-NS25w (500,2) OVER WHICH
ELEMENTAL DOT MAPS WERE GENERATED
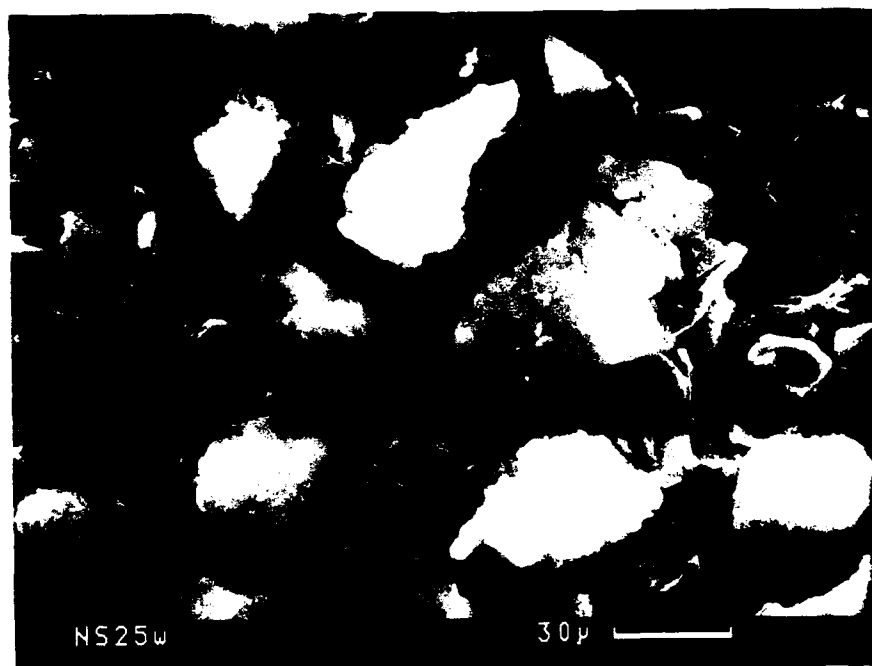
Figure 4-11: NIOBIUM DOT MAP FOR A-NS25w (500,2)
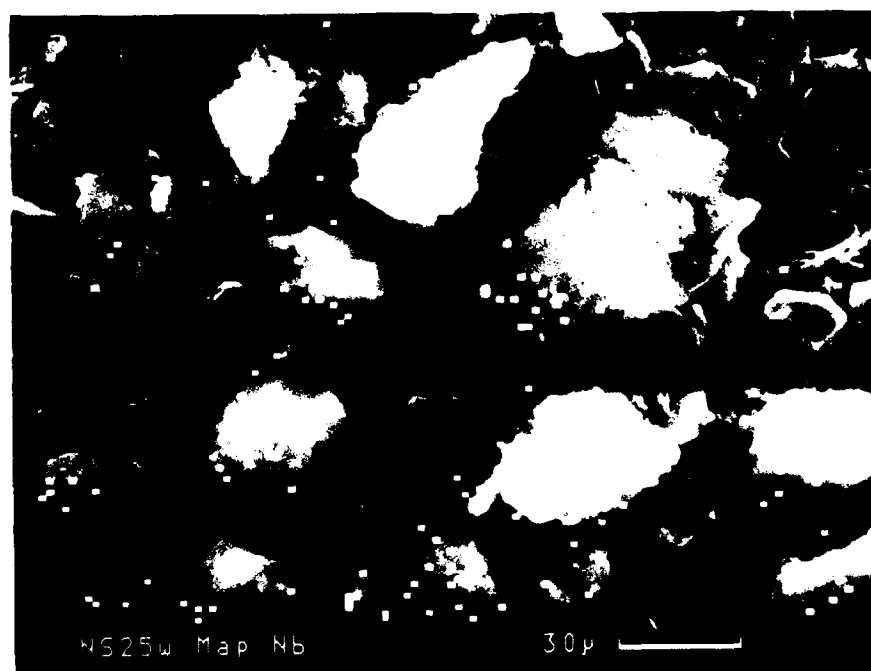
Figure 4-12: SILICON DOT MAP FOR A-NS25w (500,2)
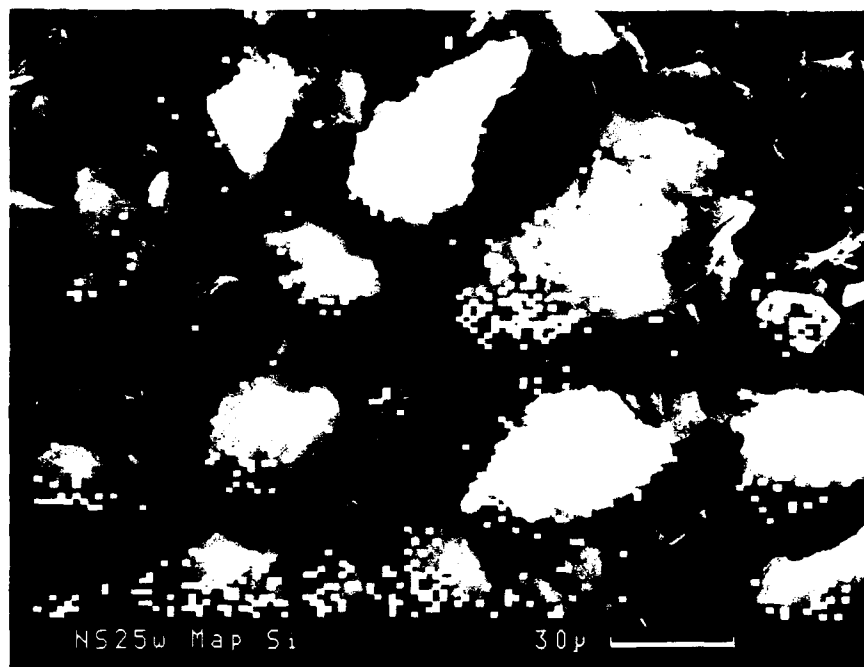
NA25w are shown in Figures 4-13, 4-14, and 4-15. As with A-NS25w, we see a good dispersion of niobia in the mixed oxide of A-NA25w as revealed by the dot map for niobium atoms in Figure 4-14. These figures show that the aerogels synthesized through the sol-gel process contain homogeneously distributed niobia. Table 4-6 lists the results of the EDS elemental analysis for the binary oxide aerogels of A-NS25w and A-NA25w. Converting the elemental composition to an actual oxide content yields very good results with those of the predicted oxide content. For A-NS25w, the actual niobium oxide content by EDS gives 24.3 wt.% or a difference from the predicted value of only 2.8%. The actual niobia content for A-NA25w was 22.7 wt.% or a difference from the predicted value of 9.2%. These close values of actual and predicted niobia contents, assuming the micrograph and EDS analyses are representative of the entire mixed oxide, lead us to conclude that we have successfully synthesized well-dispersed mixed oxides of A-NS25w and A-NA25w.

4.2.5 Laser Raman Spectroscopy (LRS)

LRS was used to examine the vibrational modes of molecules in the mixed oxides of niobia/silica and niobia/alumina. The spectra presented here will be interpreted by comparison with reference niobium oxide compounds.[67, 94, 187] LRS spectra of A-NS25w after various thermal treatments are shown in Figure 4-16. The (500,2) sample is not included because of fluorescing problems encountered with A-NS25w. A-NS25w (600,2) does not show any noticeable spectral features characteristic of regular NbO_6 octahedra, but does have a small and broad peak centered at ~ 930 cm^{-1}. Upon heat treating to (800,2) we see a sudden increase in intensity for the characteristic Nb-O stretch of NbO_6 octahedra (distorted) at ~ 710 cm^{-1}, as well as a broad peak at ~ 930 cm^{-1}. No major differences are seen upon heat treatment to (1000,-) from (800,2). These spectra indicate that while remaining XRD amorphous until 1000 °C, niobia in A-NS25w is structurally close to $TT\text{-}Nb_2O_5$ at only (800,2). The band at ~ 710 cm^{-1} can be assigned to

Figure 4-13: SEM MICROGRAPH OF A-NA25w (500,2) OVER WHICH
ELEMENTAL DOT MAPS WERE GENERATED
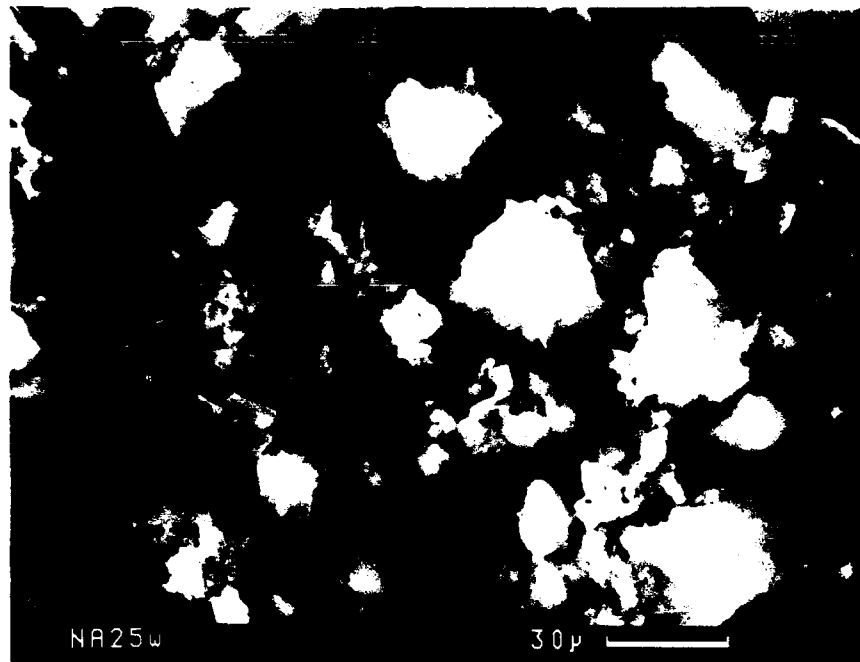
Figure 4-14: NIOBIUM DOT MAP FOR A-NA25w (500,2)
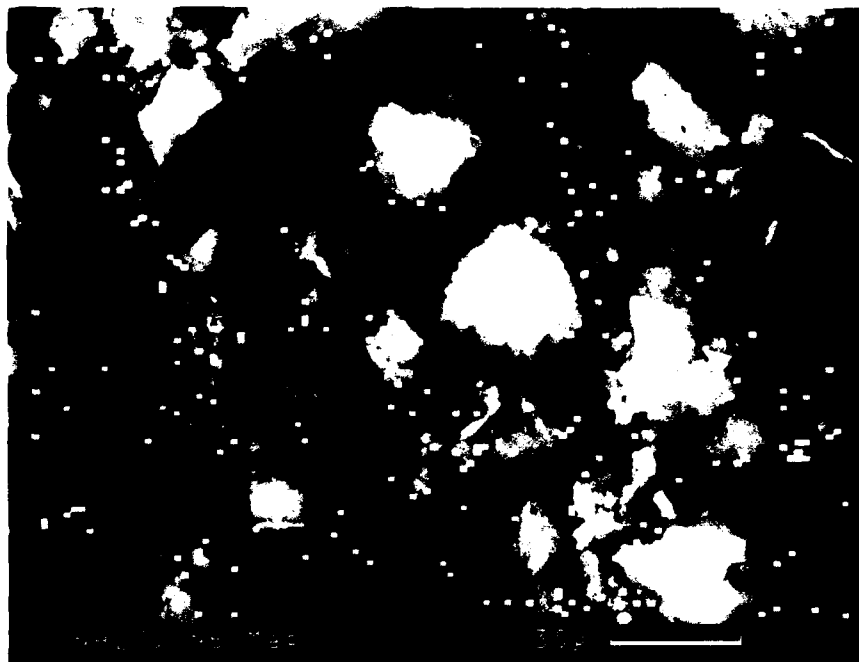
Figure 4-15: ALUMINUM DOT MAP FOR A-NA25w (500,2)
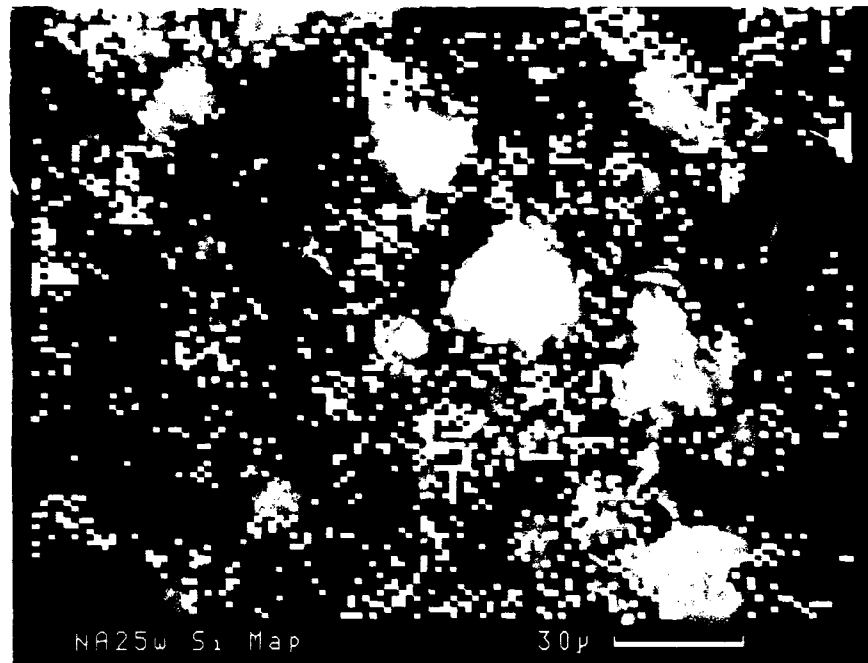
Table 4-6: RESULTS OF EDS ELEMENTAL ANALYSIS FOR MIXED OXIDE AEROGELS: A) A-NS25w, AND B) A-NA25w

A) A-NS25w (500,2)

Sample	EDS Elemental Analysis		Actual Oxide Content		Predicted Oxide Content	
	Si wt%	Nb wt%	SiO_2 wt%	Nb_2O_5 wt%	SiO_2 wt%	Nb_2O_5 wt%
A NS25w	67.6	32.4	75.7	24.3	75.0	25.0

B) A-NA25w (500,2)

Sample	EDS Elemental Analysis		Actual Oxide Content		Predicted Oxide Content	
	Al wt%	Nb wt%	Al_2O_3 wt%	Nb_2O_5 wt%	Al_2O_3 wt%	Nb_2O_5 wt%
A-NA25w	72.1	27.9	77.3	22.7	75.0	25.0

Figure 4-16: LRS SPECTRA OF A-NS25w AFTER HEAT TREATMENT: A) (600,2), B) (800,2), AND C) (1000,-)
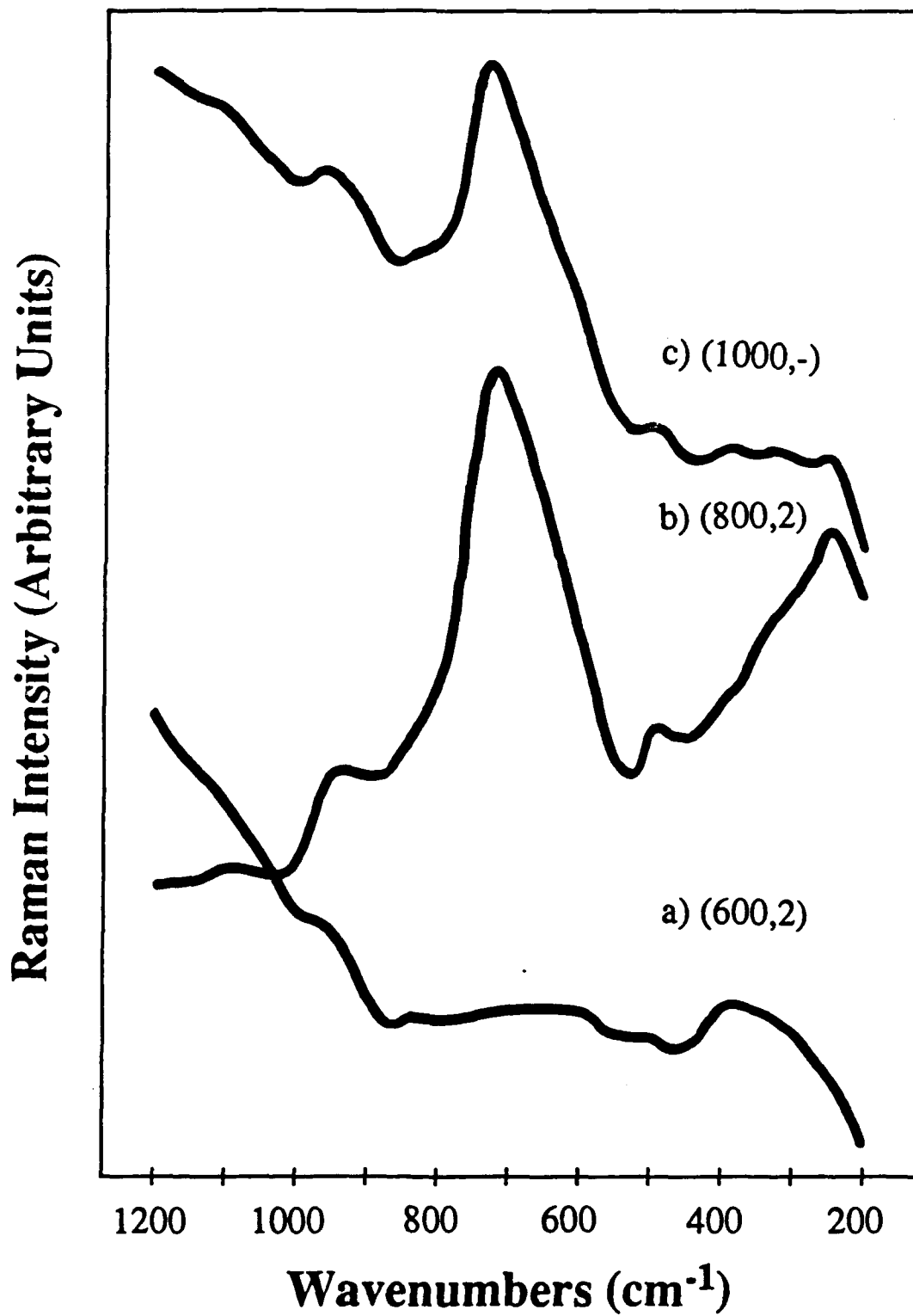
slightly distorted NbO_6 (or NbO_7) octahedra, similar to those found for TT- and T-Nb_2O_5. The broad peak at ~ 940 cm^{-1} indicates a stronger Nb-O bond and possibly a highly distorted tetrahedral structure as will be shown later with the *in-situ* Raman study.

Figure 4-17 shows LRS spectra of A-NA25w after various thermal treatments. Information about the aerogel of niobia/alumina after calcination, (500,2), is obscured by the fluorescing background of alumina in this sample. Heating to (600,2) reveals 3 peaks and a shoulder at ~ 235, 620, 915, and 960 cm^{-1}, respectively. The bending mode at ~ 235 cm^{-1} is characteristic of Nb-O-Nb linkages, while the symmetric stretch at ~ 600 - 650 cm^{-1} match that found in amorphous and TT-Nb_2O_5 for slightly distorted NbO_6 octahedral units.[47, 67, 94] The vibrations at 915 and 960 cm^{-1} are indications of a stronger Nb-O bond than at the lower 620 cm^{-1} frequency, and could possibly be attributed to very distorted tetrahedral or octahedral species, and will be investigated later with *in-situ* Laser Raman Spectroscopy.[67, 92, 94] Upon further heat treatment to (1000,-) we know that A-NA25w undergoes a solid state reaction to form crystalline $NbAlO_4$ from our previous XRD study. The structure of $NbAlO_4$ consists of highly distorted NbO_6 and AlO_6 octahedra, the structural unit of which consists of 2 NbO_6 units and 2 AlO_6 units sharing edges and linked to the next adjacent unit by sharing 2 corners.[201] The Nb-O bond which links to the adjacent unit cell by sharing the 2 corners, possesses the shortest bond length (1.74 Å), and has been assigned the Raman band at ~ 930 cm^{-1} which is characteristic of very distorted Nb-O bonds.[67, 94] The various Raman bands in the 400 - 800 cm^{-1} region are assigned to the symmetric and antisymmetric stretching modes of Nb-O, and the associated bending modes of the Nb-O-Nb linkages appear in the low wavenumber region of 200 - 300 cm^{-1}. This Raman spectrum for the (1000,-) heat treatment of A-NA25w can be found in Figure 4-17, and matches identically with the spectrum found for pure $NbAlO_4$.[94]

Figure 4-17: LRS SPECTRA OF A-NA25w AFTER HEAT TREATMENT: A) (500,2), B) (600,2), AND C) (1000,-)
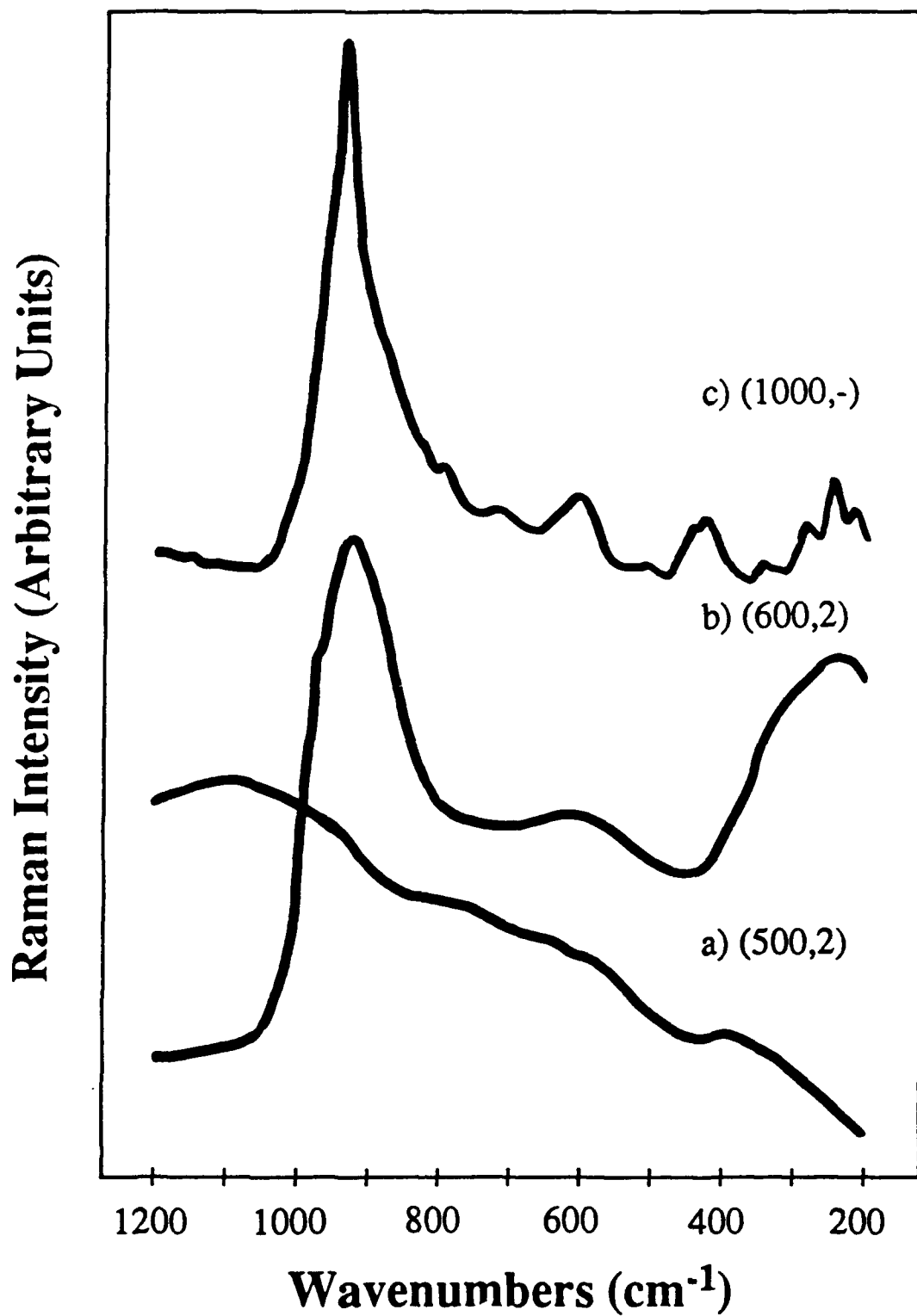
4.2.5.1 In-situ LRS (Dehydrated)

In-situ Raman studies were done on both mixed oxide aerogels of A-NS25w and A-NA25w. Figure 4-18 shows Raman spectra for hydrated and dehydrated (450 °C, 30 min) A-NS25w after (600,2). The higher temperature of (600,2) was used because of the fluorescing problems of alumina and silica at the lower calcination of (500,2) in both mixed oxide aerogels. The hydrated niobia/silica mixed oxide has a broad peak centered around 930 cm^{-1}. Upon dehydration, this peak splits into two distinct frequencies with the higher one located as a sharp peak at ~ 985 cm^{-1} and the lower one at ~ 930 cm^{-1}. The shifts of these bands and high frequencies of the vibration, indicate coordination of moisture to surface functionalities, and possibly highly distorted NbO_4 tetrahedra or NbO_6 octahedra.[67, 94, 188] The observations of these high frequencies as mentioned previously revealed very distorted environments, and have led researchers to assign these frequencies to terminal Nb=O bonds.[67, 92, 94, 202] In an attempt to relate bond order to Raman frequency, Hardcastle and Wachs concluded that higher bond orders, Nb--O $\rightarrow$ Nb-O $\rightarrow$ Nb=O, led to higher Raman shifts in frequency.[92] They also examined Nb=O bonds in distorted tetrahedral and octahedral environments and found that they vibrated at similar frequencies for either structure and that the frequency was primarily dependent on the bond length of the terminal Nb=O. Thus, we can possibly assign this high frequency peak at ~985 cm^{-1} to a highly distorted tetrahedral environment and not a distorted octahedral environment. Since silica, the major component in this mixed oxide, has a strongly covalent and very rigid tetrahedral structure, doping the silica network with niobia would probably force the niobium cation into a tetrahedral environment. The absence of peaks in the hydrated form of A-NS25w at ~ 700 cm^{-1} shows the lack of slightly distorted NbO_6 octahedra and that the niobia in this mixed oxide is well dispersed and possibly in an environment other than octahedral.[67]

Figure 4-19 shows the *in-situ* LRS spectra of A-NA25w (600,2) in both hydrated and dehydrated (450 °C, 30 min) conditions. The hydrated niobia/alumina mixed oxide

Figure 4-18: IN-SITU LRS SPECTRA OF A-NS25w (600,2): A) HYDRATED AND
B) DEHYDRATED (450,30 min)
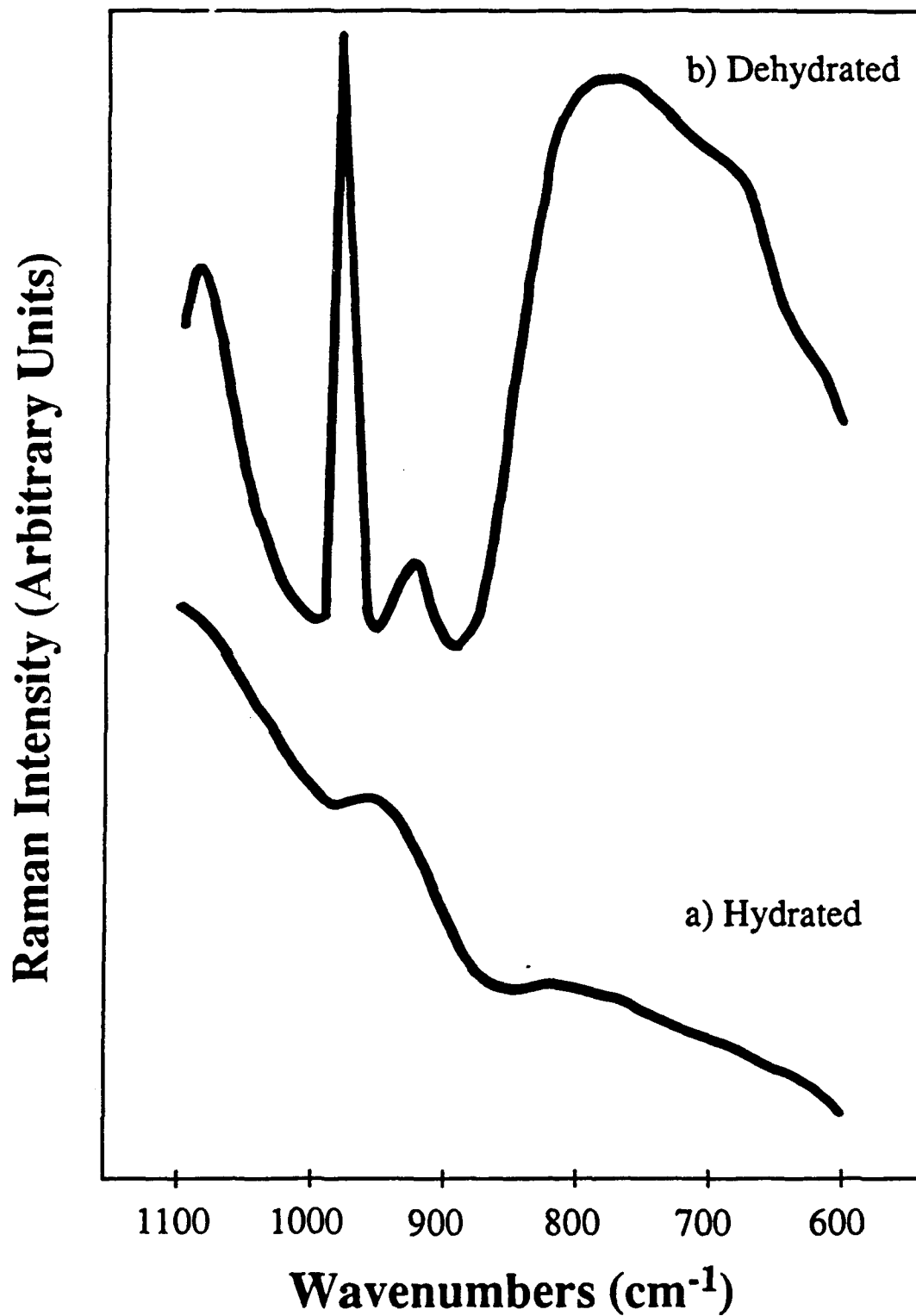
Figure 4-19: IN-SITU LRS SPECTRA OF A-NA25w (600,2): A) HYDRATED AND B) DEHYDRATED (450,30 min)
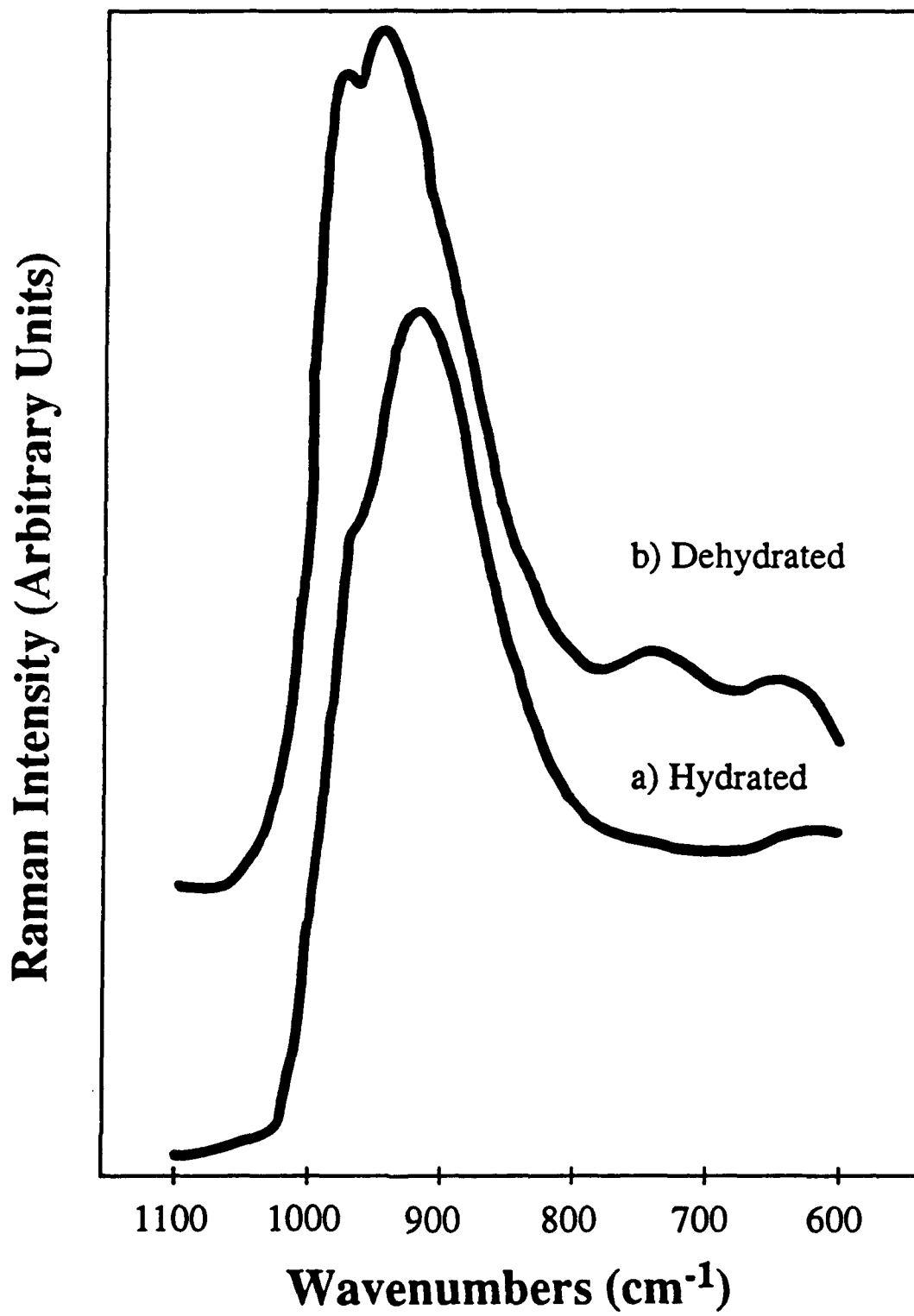
aerogel shows 2 bands around 960 and 915 cm^{-1} indicating the existence of two different highly distorted NbO_6 octahedra or NbO_4 tetrahedra. The lower frequency can be assigned to a longer Nb=O bond.[92] Dehydrating this mixed oxide shifts the peaks by approximately 25 cm^{-1} to new positions at ~ 985 cm^{-1} and ~ 945 cm^{-1}, respectively. This shows that water is indeed coordinated to the available surface species. The fact that alumina can assume either tetrahedral or octahedral environments makes this network slightly less rigid than the silica matrix.[10, 25] Thus, it is unclear whether these Nb=O bonds belong primarily to highly distorted octahedra or tetrahedra. The bands at ~ 745 cm^{-1} and ~ 645 cm^{-1} in the dehydrated sample coincide with Raman bands of slightly distorted octahedra as found in a high loading of Nb_2O_5 on Al_2O_3 (19 wt.%).[98] We will see similar results later when we discuss the dehydration effects on the surface oxides.

4.2.6 Diffuse Reflectance Infrared Spectroscopy (DRIFT)

DRIFT was utilized in an attempt to observe the terminal Nb=O bond in the mixed oxides, but the complication of strongly adsorbed water made this task untractable. However, we were able to study the hydroxyl region of the niobia/silica mixed oxide aerogel in its hydrated state with DRIFT. The main result from this spectrum was that the sample strongly chemisorbed water. This data along with those for all aerogels studied are compiled in Appendix C, and discussed along with the transmission spectra of the hydroxyl region for the oxides after treatment with pyridine.

4.3 Chemical Property Characterization of Mixed Oxide Aerogels

4.3.1 Acid Strength/Acidity with n-Butylamine Titration

The acid strength and corresponding acidity for all calcined mixed oxides are shown in Table 4-7(A) mmoles/g and (B) mmoles/m^2, and in Table 4-8 (mmoles/g Nb_2O_5). These data are compiled into acidity plots in Figures 4-20(A) mmoles/g Nb_2O_5, (B)

Table 4-7: ACID STRENGTH OF MIXED OXIDES: A) ACIDITY (MMOLES/G) AND B) ACIDITY (MMOLES/M^2) VERSUS pKa

A) Acid Strength of Mixed Oxides [Acidity (mmoles/g)]

	Acidity (mmoles/g)					
	pKa					
Sample	+4.8	+3.3	+1.5	-3.0	-5.6	-8.2
A-NS25w (500,2)	1.02	0.60	0.51	0.48	0.45	0.34
NS25w (500,2)	0.69	0.44	0.43	0.43	0.41	0.40
A-NA25w (500,2)	0.41	0.35	0.28	0.27	0.26	0.21
NA25w (500,2)	0.46	0.39	0.34	0.29	0.28	0.19

B) Acid Strength of Mixed Oxides [Acidity (mmoles/m^2)]

	Acidity (mmoles/m^2) x 10^4					
	pKa					
Sample	+4.8	+3.3	+1.5	-3.0	-5.6	-8.2
A-NS25w (500,2)	15.3	8.9	7.6	7.2	6.7	5.1
NS25w (500,2)	14.5	9.1	9.1	8.9	8.4	8.3
A-NA25w (500,2)	8.1	6.9	5.5	5.4	5.1	4.1
NA25w (500,2)	11.4	9.8	8.4	7.3	7.1	4.7

Table 4-8: ACID STRENGTH OF MIXED OXIDES: ACIDITY (MMOLES/g Nb_2O_5) VERSUS pKa

| | Acidity (mmoles/g Nb_2O_5) | | | | | |
| | pKa | | | | | |
Sample	+4.8	+3.3	+1.5	-3.0	-5.6	-8.2
A-NS25w (500,2)	4.09	2.39	2.03	1.93	1.78	1.37
NS25w (500,2)	2.77	1.74	1.74	1.71	1.62	1.60
A-NA25w (500,2)	1.65	1.40	1.11	1.10	1.04	0.83
NA25w (500,2)	1.83	1.56	1.35	1.17	1.13	0.76

Figure 4-20: A-NS25w AND NS25w ACIDITY: A) (MMOLES/g Nb_2O_5) AND B)
(MMOLES/M^2) VERSUS pKa

A) A-NS25w and NS25w Acidity (mmoles/g Nb_2O_5)
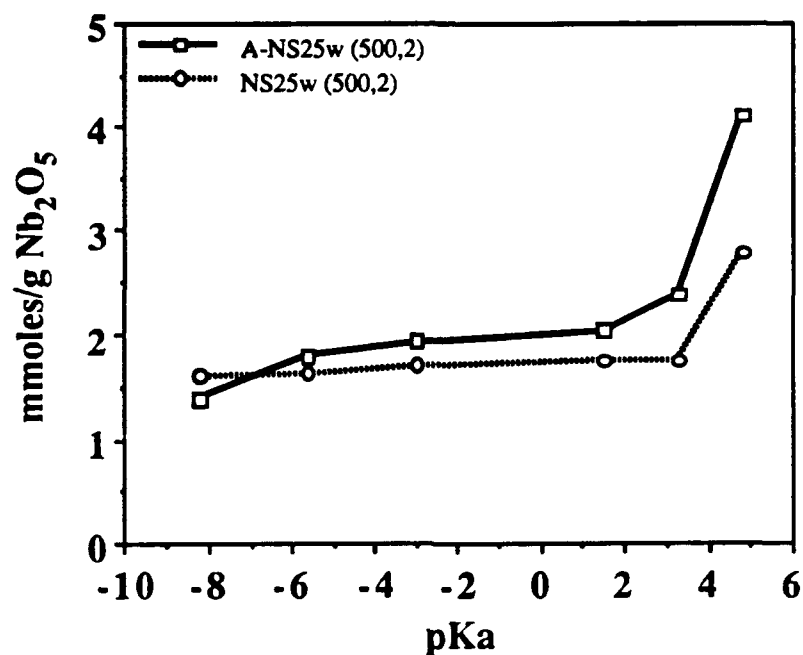
B) A-NS25w and NS25w Acidity (mmoles/m^2)
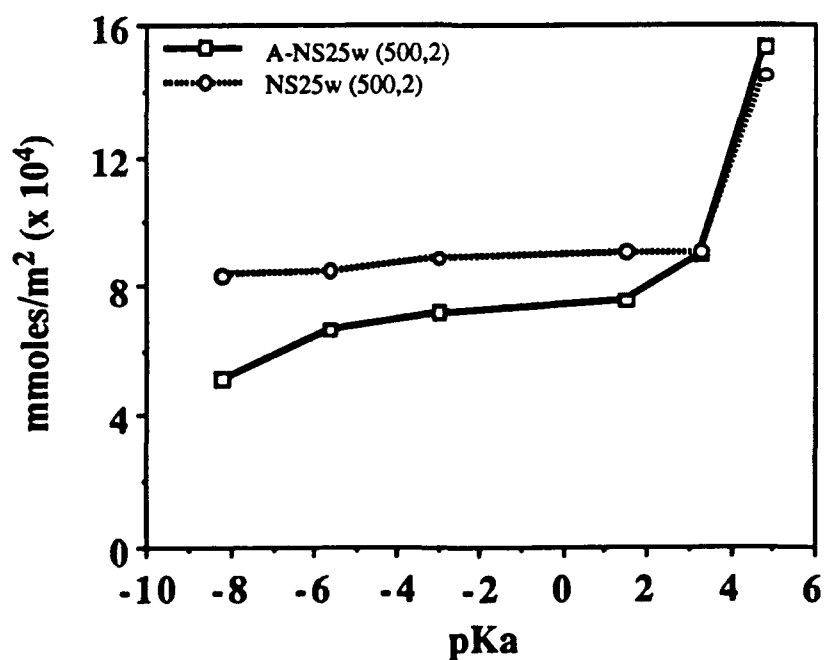
mmoles/m^2 and Figures 4-21(A) mmoles/g Nb$_2$O$_5$, (B) mmoles/m^2 for the mixed oxides of niobia/silica and niobia/alumina, respectively. These figures show that A-NS25w and NS25w, as well as A-NA25w and NA25w show similar acidity distributions on a per g Nb$_2$O$_5$ basis. Figure 4-20(B) and Figure 4-21(B) show the acidity distributions normalized with respect to surface area. The niobia/silica mixed oxides again show similar distributions, but the niobia/alumina mixed oxides appear significantly different. This could be due to the different methods of preparation used to synthesize these materials. In fact the co-precipitated niobia/alumina mixed oxide was expected to have regions of bulk alumina or bulk niobia because of the differing precipitation rates of the alkoxide precursor. Thus, the increase of acidity on a per area basis for the niobia/alumina mixed oxide, could possibly be due to more bulk-like niobia, since the niobia aerogel and uncalcined niobic acid were found to have a large acidity normalized with respect to area of ~ 2.5 x 10^{-3} mmoles/m^2.

The acidity distribution of A-NS25w, A-NA25w, and A-Nb$_2$O$_5$ are shown in Figures 4-22(A) mmoles/g Nb2O5 and (B) mmoles/m^2. From the previous chapter, we know that the aerogel of niobia (500,2) was acidic (and amorphous) as shown by comparison with other more crystalline niobia phases. Figure 4-22(A) reveals that A-NS25w and A-NA25w show more acidity (/g Nb$_2$O$_5$) over the entire acid strength range than bulk A-Nb$_2$O$_5$, with A-NS25w showing the highest acidity of all 3 oxides. From our previous acidity results we know that alumina does not turn any indicator to its acidic form, and silica only turns the lowest acid strength indicator (pKa = +4.8). Thus, any positive indication of acid strength/acidity is the result of the incorporation of niobia into either one of these oxide networks. The silica matrix appears to be better at dispersing niobia into a distorted environment than the alumina matrix, since normalizing with respect to Nb$_2$O$_5$ will tend to reveal the degree of this dispersion; i.e. individual molecules of niobia may be serving as acid sites on a 1:1 basis in a very disperse binary oxide, whereas clustering of niobia tends to lower this value depending on the size and crystal structure of the

Figure 4-21: A-NA25w AND NA25w ACIDITY: A) (MMOLES/g Nb₂O₅) AND B) (MMOLES/M²) VERSUS pKa

A) A-NA25w and NA25w Acidity (mmoles/g Nb₂O₅)
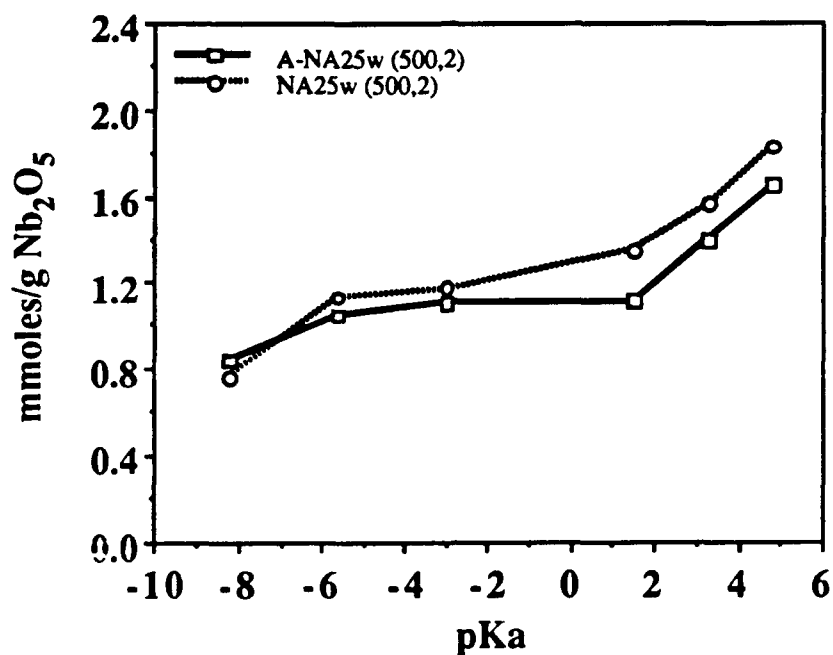
B) A-NA25w and NA25w Acidity (mmoles/m²)
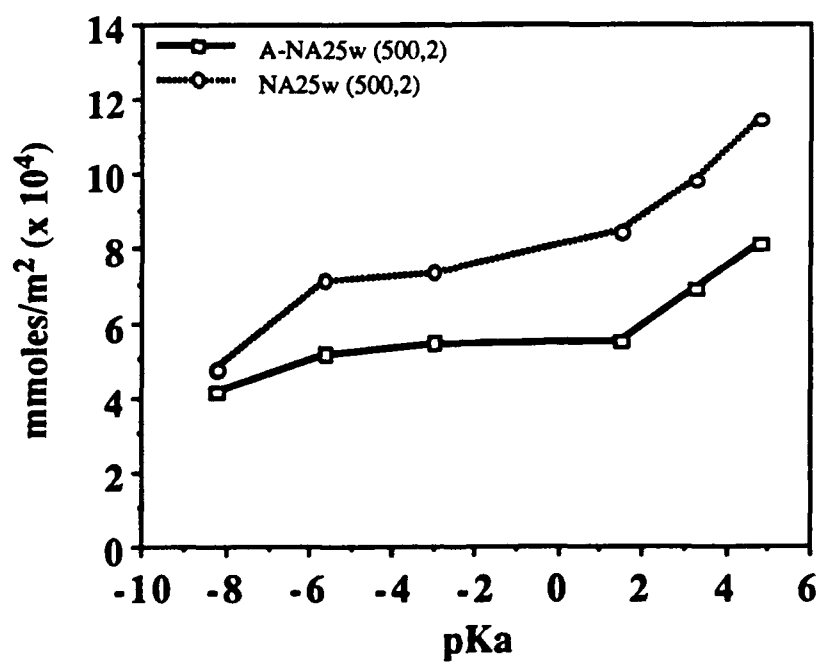
Figure 4-22: A-NS25w AND A-NA25w ACIDITY: A) (MMOLES/g Nb_2O_5) AND B) (MMOLES/M^2) VERSUS pKa

A) A-NS25w and A-NA25w Acidity (mmoles/g Nb_2O_5)
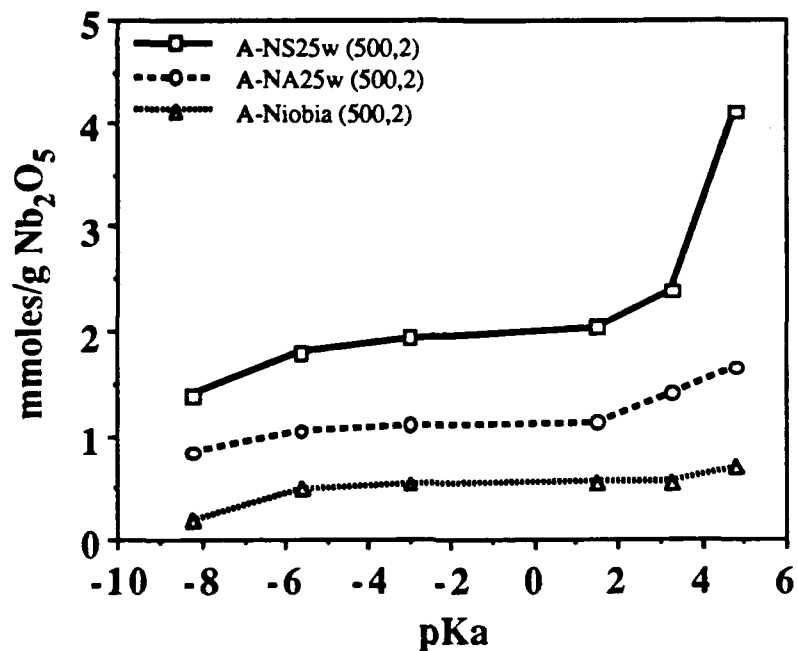
B) A-NS25w and A-NA25w Acidity (mmoles/m^2)
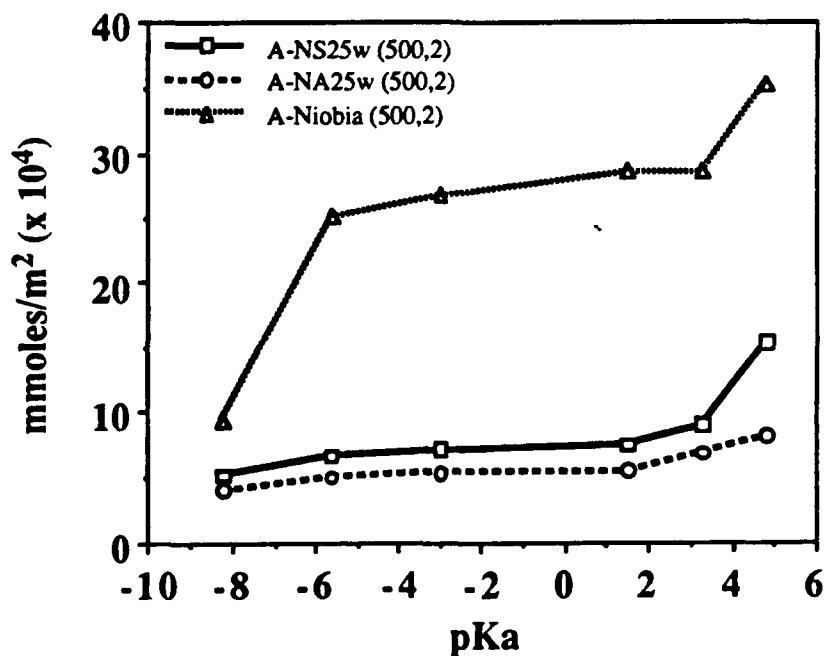
aggregates. With this knowledge, it appears possible that niobia is clustering in an amorphous environment in A-NA25w to slightly distorted and highly distorted NbO_6 octahedra. These results are consistent with the LRS results discussed previously. The fact that LRS did not detect slightly distorted NbO_6 groups for A-NS25w even after heat treatment at (600,2) shows that this material is indeed very disperse. The peak at ~ 930 cm^{-1} in the Raman spectrum was also taken to be an indication of highly distorted tetrahedral or octahedral species which should lead to significant acid strength and acidity, and appears to be true as shown in Figure 4-22(A). Figure 4-22(B) shows the acidity normalized with respect to surface area for A-NS25w, A-NA25, and A-Nb_2O_5. The aerogel of niobia is shown to have acidity ($/m^2$) which is approximately 4 times the amount of the binary mixed oxides over most of the acid strength range. The mixed oxide aerogels have approximately the same amount of acidity ($/m^2$) over this same acid strength range. Thus, although the niobia aerogel has a seemingly low acidity when normalized with respect to weight, the acidity normalized with respect to surface area shows that the surface functionalities of this oxide are highly acidic. Both A-NS25w and A-NA25w strongly adsorb water as indicated by DTA and IR Studies (see Appendix C), but this does not significantly affect the titration results as the 110 °C heat treatment in vacuum is apparently sufficient for the removal of most of the adsorbed water.

Table 4-9 and Table 4-10 list the acid strength and acidity, (mmoles/g Nb_2O_5) and (mmoles/m^2), respectively, for A-NS25w with various thermal treatments of (500,2) to (1000,-). Figure 4-23 shows the acidity (/g Nb_2O_5) versus acid strength of the niobia/silica mixed oxide aerogel as a function of heat treatment. The decrease in acidity (/g Nb_2O_5) as shown in Figure 4-23 with increasing temperature could be due to the niobia becoming less disperse, as indicated by LRS after (800,2) with the appearance of slightly distorted NbO_6 octahedra, or even crystallization of TT-Nb_2O_5 as shown by both the LRS and XRD studies at the higher temperature of 1000 °C, (1000,-). The acidities (/g Nb_2O_5) for A-NS25w after (500,2) and (600,2) appear to be nearly identical, indicating no

Table 4-9: ACID STRENGTH OF HEAT TREATED A-NS25w: ACIDITY (MMOLES/g Nb$_2$O$_5$) VERSUS pKa

| | Acidity (mmoles/g Nb$_2$O$_5$) | | | | | |
| | pKa | | | | | |
Sample	+4.8	+3.3	+1.5	-3.0	-5.6	-8.2
A-NS25w (500,2)	4.09	2.39	2.03	1.93	1.78	1.37
A-NS25w (600,2)	3.69	2.21	1.92	1.83	1.60	1.24
A-NS25w (800,2)	3.07	2.18	1.89	1.82	1.53	0.90
A-NS25w (1000,-)	2.52	1.51	1.47	1.24	1.13	0.73

Table 4-10: ACID STRENGTH OF HEAT TREATED A-NS25w: ACIDITY (MMOLES/M^2) VERSUS pKa

| | Acidity (mmoles/m^2) x10^4 | | | | | |
| | pKa | | | | | |
Sample	+4.8	+3.3	+1.5	-3.0	-5.6	-8.2
A-NS25w (500,2)	15.29	8.90	7.56	7.19	6.65	5.12
A-NS25w (600,2)	15.37	9.20	8.02	7.62	6.68	5.15
A-NS25w (800,2)	19.65	13.95	12.14	11.64	9.78	5.77
A-NS25w (1000,-)	19.98	11.96	11.65	9.86	8.96	5.79

Figure 4-23: A-NS25W HEAT TREATED ACIDITY (MMOLES/g Nb_2O_5) VS. pKa
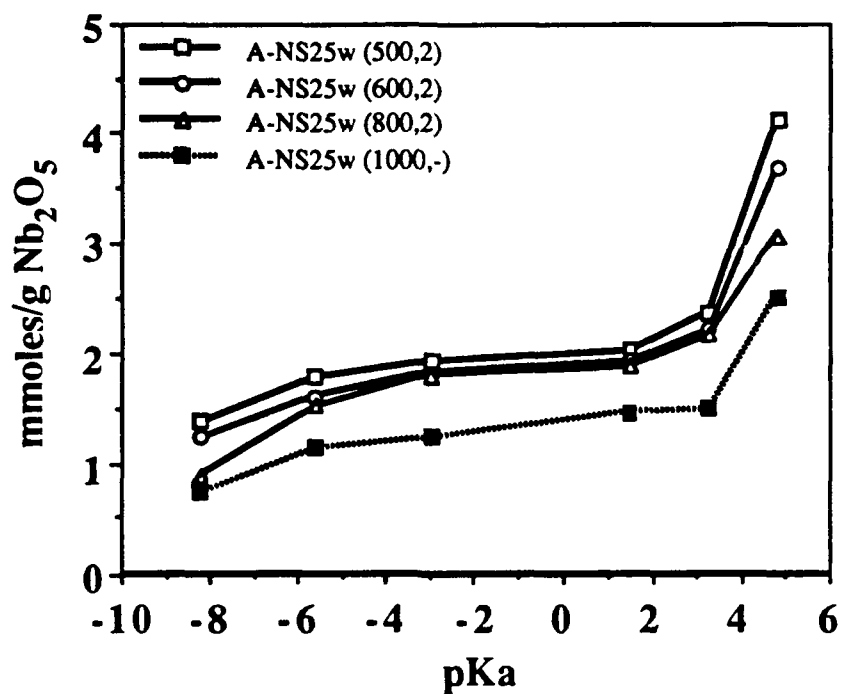
Figure 4-24: A-NS25W HEAT TREATED ACIDITY (MMOLES/M^2) VS. pKa
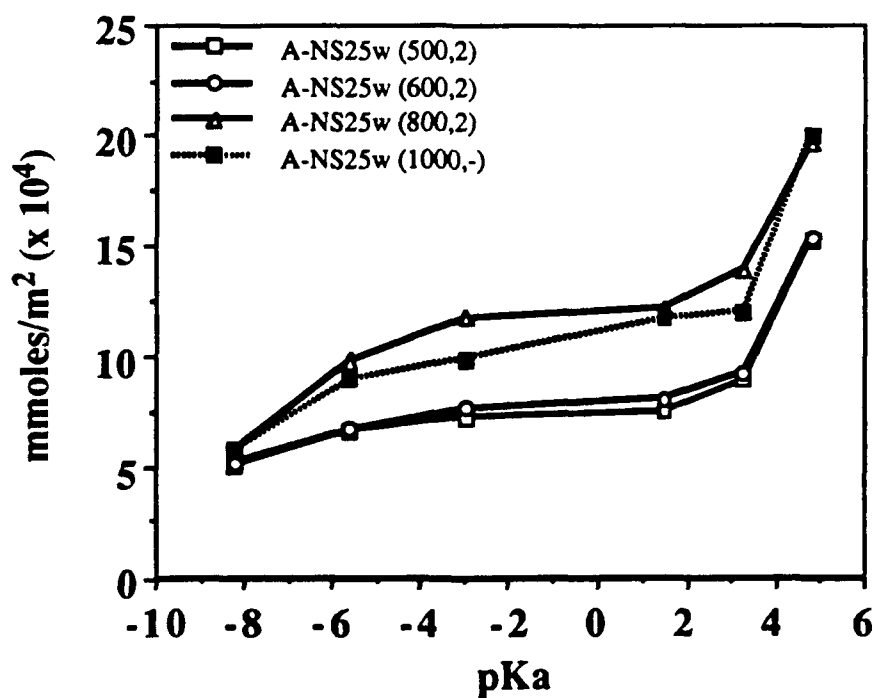
structural change in these systems; however, upon heat treating to (800,2), one sees a significant drop in the number of strongest acid sites at pKa = -8.2. This could be due to niobia transforming from highly distorted and highly acidic Nb=O tetrahedra into highly distorted octahedra as well as slightly distorted octahedra. After a (1000,-) heat treatment this transformation and loss in dispersity is even more apparent by the significant decline in acidity, and could be explained by the detection of ordered TT-Nb$_2$O$_5$ by XRD. Significant amounts of acidity in the highest acid strength, pKa = -8.2, are seen and may be attributed to the retention of highly distorted octahedra or tetrahedra as noted by the LRS study showing the vibration of the terminal Nb=O around 930 cm^{-1} in this sample. Figure 4-23 therefore shows the stabilizing effect of forcing niobia into a rigid silica matrix.

Figure 4-24 shows the acidity, normalized with respect to surface area, versus acid strength for A-NS25w as a function of thermal treatment. This figure presents the same data as above except the results are normalized with respect to surface area. We see exactly as one would expect in acidity after (500,2) and (600,2) with A-NS25w; i.e. no change at all since LRS detected similar structural bonding vibrations in these materials. However, upon heat treating to (800,2) we see a significant change in acidity, as revealed in Figure 4-24. This observed increase is associated with a drastic restructuring of the binary oxide material as indicated by LRS with A-NS25w heat treated to (800,2). This restructuring led to a significant drop in surface area [600 to 390 m^2/g, after (600,2) to (800,2) heat treatments, respectively], and formation of slightly distorted NbO$_6$ octahedra similar to those found in the niobia aerogel, from highly distorted octahedra or tetrahedra, which are still very acidic. Thus, since A-NS25w (800,2) appears to be restructuring into a material which has a significant amount of highly distorted and slightly distorted octahedra, similar to the aerogel of niobia, we would expect to see the acidity on a per surface area basis increase since the surface functionalities of niobia have been shown previously to be highly acidic. This is indeed what we find as shown in Figure 4-24. Since slightly distorted octahedra are acidic as well as the highly distorted Nb=O groups, one would expect that the

acidity ($/m^2$) would be attributed to a surface area effect since the concentration of these groups would be effectively greater on the surface. That is, the acidity for A-NS25w (800,2) would be 1.5 (600 m^2/g / 390 m^2/g) times higher than A-NS25w (600,2) over the entire acid strength range. This indeed is exactly our finding, in that the observed increase in acidity ($/m^2$) from (600,2) to (800,2) is due to a reduction of surface area. Heat treating A-NS25w to (1000,-) decreases the acidity from A-NS25w (800,2) and is ascribed to the formation of more crystalline TT-Nb_2O_5 as noted by LRS and XRD Studies. Again, there is still significant acidity at pKa = -8.2, and this may be due to the presence of highly distorted groups containing Nb=O terminal bonds. It has been shown with this heat treatment/acidity study that the silica matrix has a stabilizing effect of maintaining niobia in a distorted and highly acidic environment.

A similar study was performed with NS25w (precipitated) in order to determine if this binary oxide behaved as its aerogel counterpart, A-NS25w. The results of this heat treatment on acidity study are found in Tables 4-11 and 4-12 for acidity/g Nb_2O_5 and acidity/m^2, respectively. Figure 4-25 shows the acidity/g Nb_2O_5 versus acid strength for NS25w as a function of four different calcination temperatures. The trends in this figure are identical with those found for the niobia/silica aerogel, i.e. the acidity goes down with increasing thermal treatment on a per g Nb_2O_5 basis. Note errors are more significant for the precipitated mixed oxide because of the smaller surface areas and longer equilibration times for adsorption due to the smaller pore diameters and pore volumes.

Figure 4-26 shows the acidity/m^2 versus pKa for NS25w as a function of heat treatment. The same results as found for A-NS25w in Figure 4-24 are evident in this figure for NS25w. The large change after the (800,2) heat treatment corresponds to a restructuring of the binary oxide into a material that is structurally close to TT-Nb_2O_5 as evidenced by LRS, but is even more distorted as noted by the Nb-O frequency at ~ 710 cm^{-1}.[67] The (1000,-) heat treatment reduces the acidity slightly over (800,2) for NS25w, due to the ordering of the structure into less acidic TT-Nb_2O_5 crystallites as noted by XRD.

Table 4-11: ACID STRENGTH OF HEAT TREATED NS25w: ACIDITY (MMOLES/g Nb$_2$O$_5$) VERSUS pKa

| | Acidity (mmoles/g Nb$_2$O$_5$) | | | | | |
| | pKa | | | | | |
Sample	+4.8	+3.3	+1.5	-3.0	-5.6	-8.2
NS25w (500,2)	2.77	1.74	1.74	1.71	1.62	1.60
NS25w (600,2)	2.81	1.92	1.85	1.79	1.77	1.76
NS25w (800,2)	2.36	1.70	1.66	1.62	1.62	1.45
NS25w (1000,-)	2.13	1.35	1.32	1.31	1.25	1.23

Table 4-12: ACID STRENGTH OF HEAT TREATED NS25w: ACIDITY (MMOLES/M^2) VERSUS pKa

| | Acidity (mmoles/m^2) x10^4 | | | | | |
| | pKa | | | | | |
Sample	+4.8	+3.3	+1.5	-3.0	-5.6	-8.2
NS25w (500,2)	14.46	9.07	9.07	8.87	8.44	8.33
NS25w (600,2)	15.44	10.54	10.15	9.86	9.71	9.68
NS25w (800,2)	26.16	18.85	18.39	17.93	17.89	16.10
NS25w (1000,-)	26.04	16.46	16.13	16.00	15.24	14.95

Figure 4-25: NS25W HEAT TREATED ACIDITY (MMOLES/g Nb_2O_5) VS. pKa
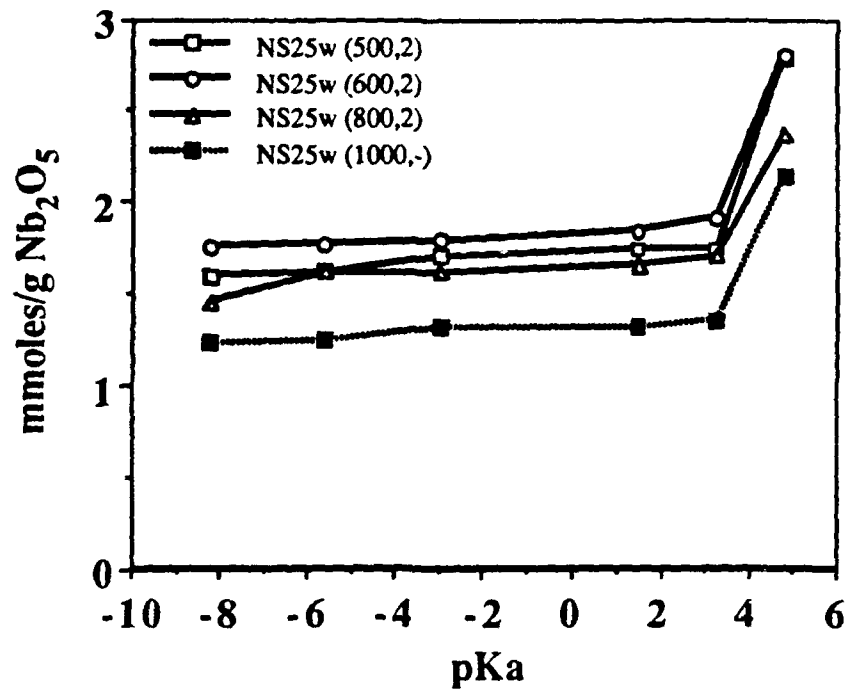
Figure 4-26: NS25W HEAT TREATED ACIDITY (MMOLES/M^2) VS. pKa
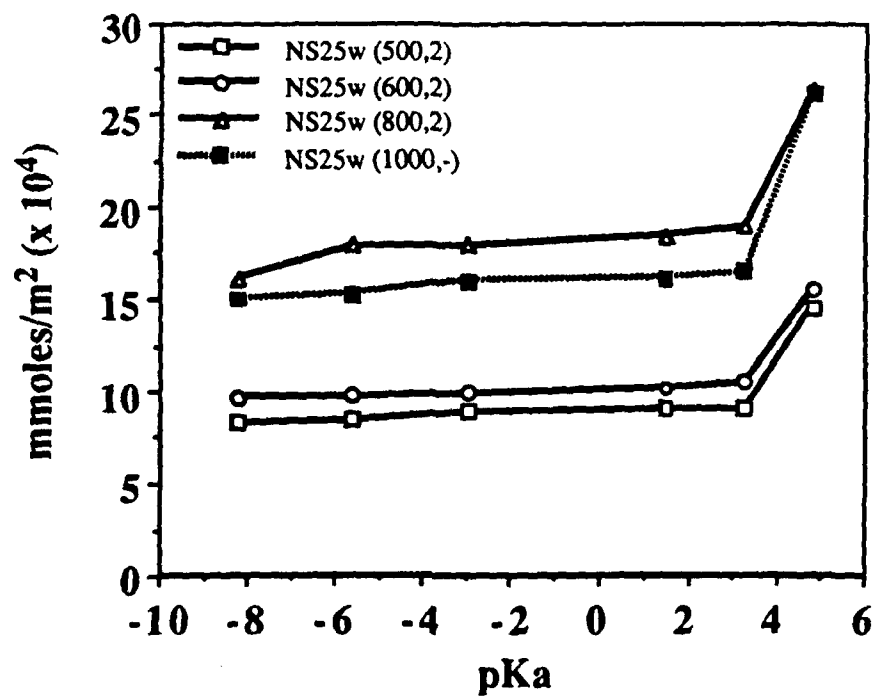
The acidity (mmoles/m^2) for NS25w shown in Figure 4-26 appears greater than A-NS25w in Figure 4-24 throughout the entire range. This apparently is due to a surface area effect between the two samples. Reducing the surface area preserves the same amount of active sites on the reduced area, therefore normalizing with respect to area gives an apparently larger specific acidity. This seems to be the case for all heat treatments on the NS25w (Figure 4-26) and A-NS25w (Figure 4-24) mixed oxides. If one takes an average offset of 1.5 in the two sample surface areas of these mixed oxides [surface area A-NS25w/surface area NS25w] over the entire heat treatment range, we notice that this is nearly identical to the offset of the specific acidity of these two figures. This is probably an inherent characteristic of the silica network being very rigid and preserving the acidity of the mixed oxide at lower surface areas; even though it is more dense at these lower areas, it has a more densely packed set of acid sites. The niobia/alumina mixed oxide aerogel, A-NA25w, and NA25w were not investigated with an acidity/heat treatment study because of the formation of NbAlO$_4$ at a temperature around 1000 °C which has been shown to contain very little if any detectable acidity by n-butylamine titration.[114]

4.3.2 Superacidity and Basicity

Table 4-13 reveals the superacidity and basicity of the mixed oxide aerogels after calcination (500,2) and a (1000,-) heat treatment on a purely qualitative basis (positive or negative indication). A-NS25w shows superacidity throughout the entire range, to a pKa = -13.75, and significantly strong basic sites also, pKa = +15.0. This basicity test could possibly be a test for Nb=O on the surface of the niobia/silica aerogel, indicating very distorted tetrahedral or octahedral environments. Upon heat treating the niobia/silica mixed oxide to (1000,-) we notice that the binary oxide still has superacidity as evidenced by the positive indication at pKa = -11.35. This heat-treated sample was also seen by LRS to still possess terminal Nb=O bonds, vibrational frequency at ~ 930 cm^{-1}, indicative of a highly distorted tetrahedral or octahedral environment. This sample also has a strong basic

Table 4-13: SUPERACIDITY AND BASICITY OF HEAT TREATED MIXED OXIDE AEROGELS

Sample Name	Acid Strength (pKa)			Basic Strength (pKa)	
	-11.35	-12.40	-13.75	+9.3	+15.0
A-NS25w (500,2)	++	+	+	+	+
A-NS25w (1000,-)	+	-	-	+	-
A-NA25w (500,2)	+	+	+	++	++
A-NA25w (1000,-)	-	-	-	-	-

++   (Very Positive Acid or Basic Indication)

+   (Positive Acid or Basic Indication)

+/-   (Positive and/or Negative Indication)

-     (Negative Acid or Basic Indication)

strength of pKa = +9.3 which was weaker than with the previous calcined sample, and indicates that this material is less likely to give up an electron pair, and could indicate the conversion of an Nb=O bond in a highly distorted tetrahedral NbO_4 unit to a Nb-O bond in a distorted octahedral group, NbO_6.

The aerogel of niobia/alumina (A-NA25w) shows results identical to those of the bulk alumina aerogel which makes it difficult to quantify the contribution due to Nb_2O_5. The heat treatment to (1000,-) was shown to cause the niobia/alumina to undergo a solid-state reaction to form the compound $NbAlO_4$ as evidenced by XRD and LRS. We confirmed a previous finding from our group that $NbAlO_4$ possesses little or no acidity by n-butylamine titration.[114] Heat-treated A-NA25w, (1000,-), revealed no superacidity or basicity on all indicators.

4.3.3 Pyridine Adsorption Studies

4.3.3.1 Heat of Adsorption (ΔH_{ads}): TG Study

Pyridine adsorption experiments were done using thermogravimetry (TG) to determine the heat of adsorption and its coverage dependence of the mixed oxide aerogels of A-NS25w and A-NA25w. The pyridine heats of adsorption versus coverage for the mixed oxides and aerogels of niobia and alumina are summarized in Table 4-14. Figure 4-27 shows ΔH_{ads} versus coverage for A-NS25w, SiO_2, and A-Nb_2O_5 all after the standard calcination. The ΔH_{ads} for A-NS25w (1.7 x 10^{14} Nb/cm^2) ranged from 40.1 to 18.8 kcal/mol for coverages of 1.6 to 9.5 x 10^{13} molecules/cm^2. The nearly linear relationship between heat of adsorption and coverage is indicative of a Temkin isotherm for which desorption and adsorption are influenced by other molecules on the surface. Since the more weakly bound pyridine will desorb at lower temperatures (higher coverages) easier than the more strongly held pyridine, which tend to be removed at higher temperatures (lower coverages), these data describe a distribution of acid sites. The heats of adsorption

Table 4-14: ΔH_{ads} VERSUS PYRIDINE COVERAGE FOR MIXED BINARY OXIDE AEROGELS

Pyridine Coverage (Θ) (Molecules/cm^2 x 10^{13})	ΔH_{ads}(kcal/mol)			
	A-Nb$_2$O$_5$	A-Al$_2$O$_3$	A-NA25w	A-NS25w
1.6				40.1
1.8				
2.0				
2.1				36.8
2.2				
2.5				
2.7				37.7
3.0				
3.3				
3.5				31.8
3.7			25.1	
4.1		23.6	26.4	
4.5				25.3
4.9		22.6	23.4	
5.8				23.3
6.1		23.8	23.8	
7.4	31.1	22.4	23.1	19.9
8.2	32.4			
9.0	33.5	22.6	22.0	
9.5				18.8
10.0	33.5			
11.0	32.8	21.3	21.2	
12.2	31.0			
13.5	29.6	20.4	22.0	
14.9	27.2			
16.4	24.1			
18.2	24.3			

Figure 4-27: ΔH_{ads} VERSUS PYRIDINE COVERAGE FOR A-NS25w
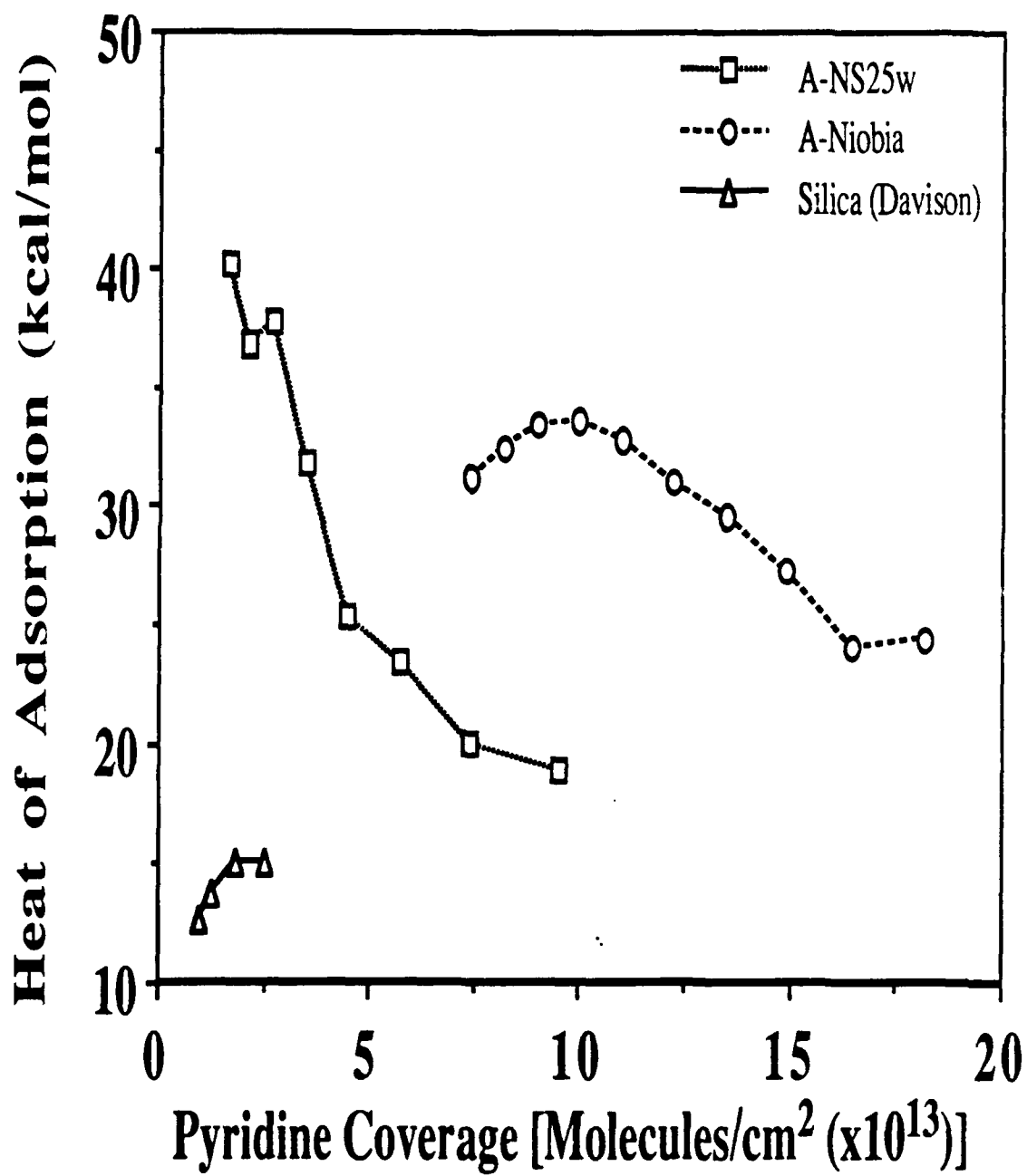
for A-NS25w are substantially higher than those for SiO_2 and are even higher than those for the aerogel of niobia at low coverages. The high acid strength for the aerogel of niobia was attributed to the highly distorted NbO_6 octahedra, and the terminal $Nb=O$ bonds that allow a better delocalization of electrons over the doubly bonded oxygen. This analogy can be related to the mixed oxide aerogel of niobia/silica. Ambient LRS as well as *in-situ* Raman studies indicate this sample also possesses terminal $Nb=O$ bonds that can be assigned to either highly distorted tetrahedral or octahedral sites. These groups have the potential to have high acid strength as shown above for A-Nb_2O_5, and appear to even exceed the strength of the acid sites on the aerogel of niobia. The acid sites on A-NS25w were some of the strongest observed in this study.

Figure 4-28 shows ΔH_{ads} versus pyridine coverage for A-NA25w, A-Nb_2O_5, and A-Al_2O_3, again following standard calcinations. This figure indicates the very strong acid strength of A-Nb_2O_5; however, the mixed oxide aerogel of niobia/alumina shows little acid *strength enhancement over that of the bulk alumina aerogel.* The heats of adsorption ranged from 26.4 to 22.0 kcal/mol for coverages of 3.7 to 13.5 x 10^{13} molecules/cm^2 for A-NA25w, and from 23.6 to 20.4 kcal/mol for corresponding coverages of 4.1 to 13.5 x 10^{13} molecules/cm^2 for A-Al_2O_3. The fact that the coverage shows no significant change and these materials have comparable acid strength, shows that alumina itself is an acidic oxide, and has a dominating effect in the acidity of the mixed oxide aerogel of niobia/alumina. This same acidity effect of alumina being the major or even minor *component and dominating the acid strength of the material has also been noted with* silica/alumina mixed oxides.[179] In our A-NA25w, we see a difference of about 3 kcal/mol in acid strength from that of the alumina at only the lowest coverages.

4.3.3.2 Acid Type: FTIR Study

FTIR of pyridine adsorption on the mixed oxides was used to examine the nature of Lewis or Brønsted acid sites on the oxides. The data from these experiments were used to

Figure 4-28: ΔH_{ads} VERSUS PYRIDINE COVERAGE FOR A-NA25w
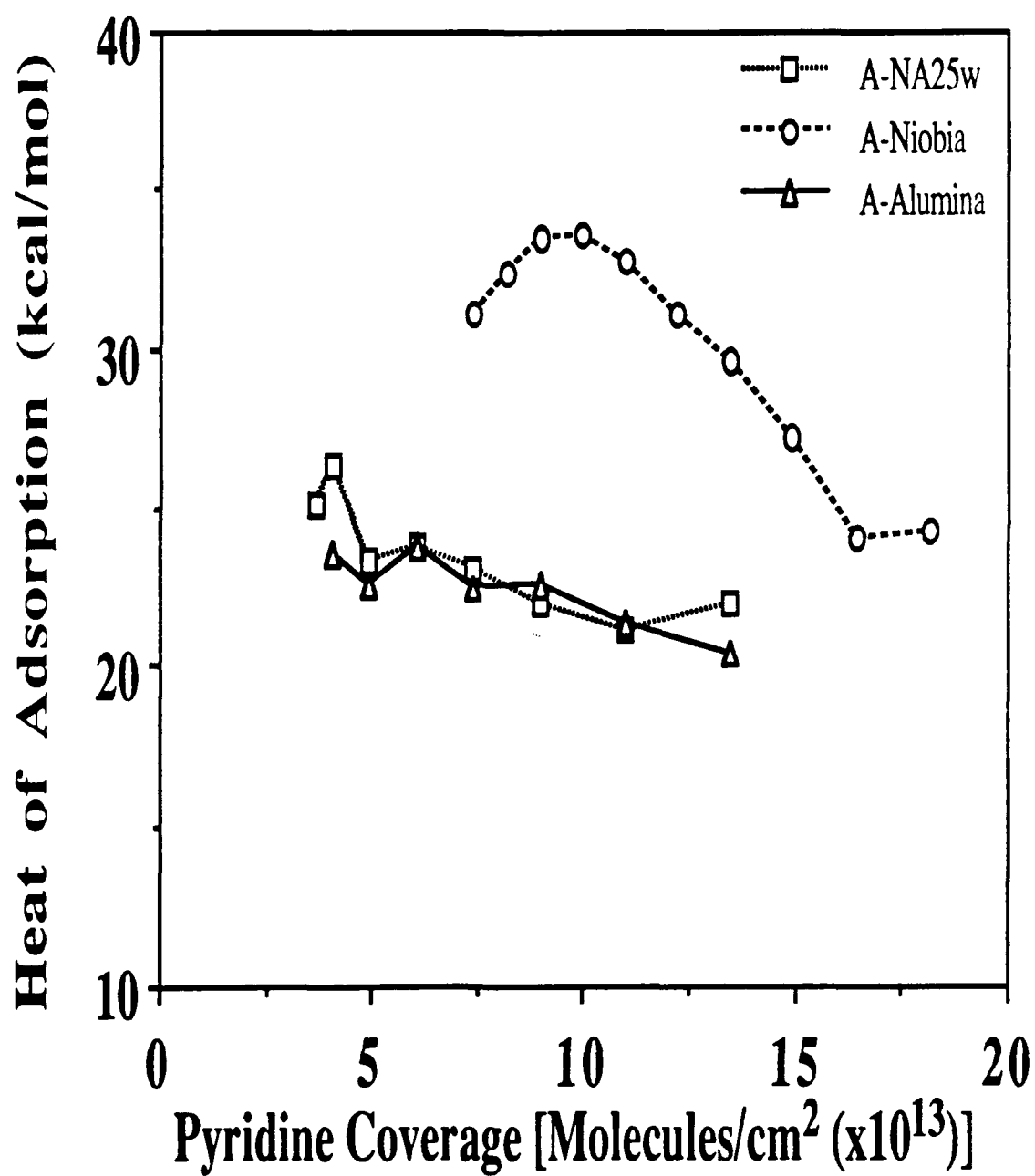
determine the strengths of the Lewis acid sites by noting shifts in the characteristic absorption frequencies, ~ 1450 and 1600 cm^{-1}, and were also designed to yield the relative strengths of the Lewis to Brønsted sites over various treatment temperatures by observing the change in the L/B ratio. This data has been summarized in Table 4-15 for the mixed oxide Lewis absorption frequencies, and in Table 4-16 to reveal the L/B ratios as a function of heat treatment. Only the absorption frequencies of the 1700 - 1400 cm^{-1} region are shown in the main text. All 300 °C heat treated infrared spectra because of the low intensity absorption signal, along with hydroxyl region data, 4000 - 2800 cm^{-1}, are shown in Appendix C.

Figure 4-29 shows FTIR spectra of pyridine adsorbed on A-NS25w. After evacuation at room temperature strong bands at ~ 1595 and 1445 cm^{-1} are apparent and have been assigned to physisorbed pyridine. These vibrational frequencies are eliminated upon heat treating the sample to 100 °C. The FTIR spectra reveal Brønsted acid sites on the mixed oxide as evidenced by the 19b peak at 1545 cm^{-1}. As treatment temperature increases the Brønsted acid site frequency appears to be attenuated, but a small portion of the 19b frequency peak can still be seen after the 300 °C heat treatment (see Appendix C for FTIR spectrum after 300 °C). These thermal treatments result in a large change in the L/B ratio from 2.6 to 27.2 after 100 and 300 °C, respectively. This is similar to results found for the precipitated NS25w where L/B varied from 8.1 to 21.0 over the same temperature range. The frequency shifts associated with the 19b and 8a Lewis acid sites after heat treatment are 1.5 and 1.2 cm^{-1} for A-NS25w, and 1.5 and 1.1 cm^{-1} for NS25w. These values of similar L/B ratios and peak shifts indicate that these materials are similar even down to a microscopic level, although the aerogel has a significantly larger surface area. The frequency shift for A-NS25w of around 1.5 cm^{-1} is lower than the shift found for A-Nb$_2$O$_5$ (~ 3 cm^{-1}) which indicates a more narrow distribution of Lewis acid sites on the niobia/silica mixed oxide than on the aerogel of niobia. The FTIR results for A-NS25w, in

Table 4-15: LEWIS ACID PYRIDINE ABSORPTION FREQUENCIES FOR MIXED OXIDES

	Lewis Acid Pyridine Absorption Frequencies					
	19b Frequency (cm^{-1})			8a Frequency (cm^{-1})		
	Heat Treatment			**Heat Treatment**		
Sample	100 °C	200 °C	300 °C	100 °C	200 °C	300 °C
A-NS25w	1448.7	1449.7	1449.9	1610.5	1611.4	1612.0
NS25w	1449.6	1450.0	1450.7	1611.0	1611.8	1612.5
A-NA25w	1447.6	1453.0	1453.8	1615.5(S)	1621.6(S)	1622.7(S)
				1609.8(S)	1612.8(W)	1613.3(W)
NA25w	1445.1	1448.2	1451.1	1610.0	1615.8(S)	1619.6(S)
					1609.8(W)	1612.6(W)

(S), Strong Absorption; (W), Weak Absorption

Table 4-16: LEWIS/BRØNSTED RATIO FOR MIXED OXIDES

| | Lewis/Brønsted Ratio | | |
| | **Heat Treatment** | | |
Sample	100 °C	200 °C	300 °C
A-NS25w	2.6	9.9	27.2
NS25w	8.1	16.0	21.0
A-NA25w	17.5	46.6	147.7
NA25w	10.0	63.5	143.5

Figure 4-29: FTIR SPECTRA OF PYRIDINE ADSORBED ON A-NS25w AFTER
HEAT TREATMENTS AT 300, 200, 100, AND 25 °C (TOP TO BOTTOM)
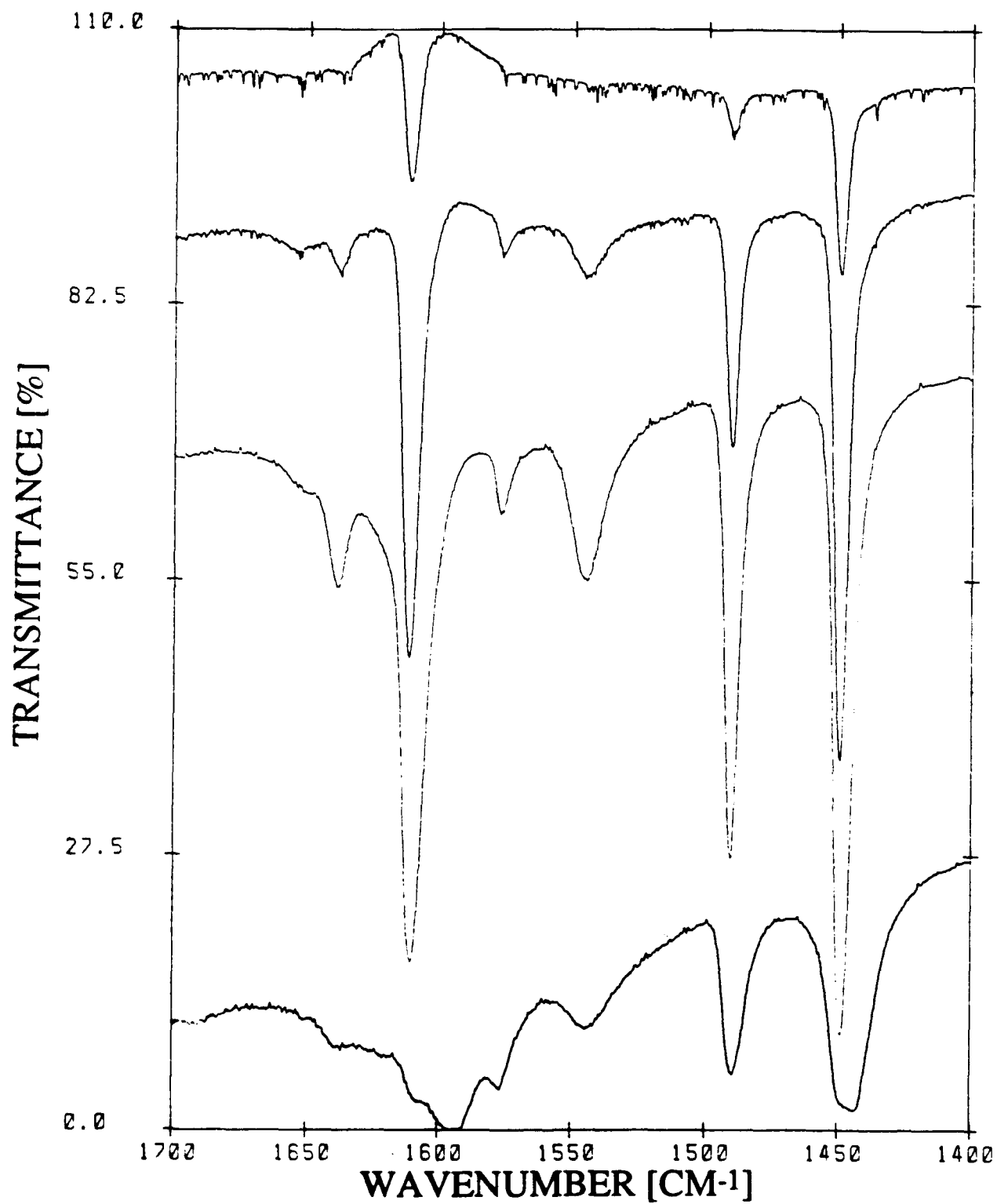
summary, reveal the presence of weak Brønsted acid sites and strong Lewis sites, and a narrow distribution of Lewis acid sites, as compared to that for A-Nb$_2$O$_5$.

Figures 4-30 and 4-31 show pyridine adsorption for A-NA25w and NA25w, after heat treatments of 100, 200, and 300 °C. One key observation in both sets of data, throughout all the heat treatments, is the noticeable absence of a 19b frequency peak (Brønsted acid site) which should be located at ~ 1540 cm^{-1} if any Brønsted acidity was on these mixed oxides of niobia/alumina. With this in mind, we would immediately expect high L/B ratios, because of the lack of any Brønsted acidity and the preponderance of Lewis acidity after the 300 °C heat treatment, and this is exactly what we found. Table 4-16 reveals L/B ratios of 17.5, 46.6, and 147.7 for A-NA25w, and 10.0, 63.5, and 143.5 for NA25w after heat treatments of 100, 200, and 300 °C, respectively. These ratios are nearly identical to A-Al$_2$O$_3$, which has already been seen to possess only very strong Lewis acidity (see Table 3-15).

Another observation that can be made about these niobia/alumina mixed oxides is in the 1600 - 1630 cm^{-1} region. We will look at the A-NA25w sample first, because of the clarity of the spectra. After the 100 °C heat treatment, there appears to be a doublet with a frequency at 1615.5 cm^{-1} which is attributable to the Lewis site of alumina and a new Lewis acid site at 1609.8 cm^{-1}, which is attributed to the incorporation of niobia into the alumina network.[180, 197, 198] This new frequency is possibly due to the highly distorted NbO$_6$ octahedra with the terminal Nb=O groups, as observed with the LRS study. The frequency shifts of the 8a frequency band attributed to alumina follow those found for the aerogel of alumina very closely. The 8a Lewis band shifts are 1615.5 to 1622.7 cm^{-1} (Δ = 7.2 cm-1) for A-NA25w, and 1616.0 to 1622.5 cm^{-1} (Δ = 6.5 cm^{-1}) for A-Al$_2$O$_3$ after heat treatment of 100 to 300 °C, respectively. This shows that A-NA25w has a slightly broader acid strength distribution than bulk alumina. The new 8a Lewis band shifts found in A-NA25w are 1609.8 to 1613.3 cm^{-1} (Δ = 3.5 cm^{-1}) after the same thermal treatments. This new frequency peak is seen as a definite shoulder throughout the entire temperature range.

Figure 4-30: FTIR SPECTRA OF PYRIDINE ADSORBED ON A-NA25w AFTER HEAT TREATMENTS AT 300, 200, AND 100 °C (TOP TO BOTTOM)
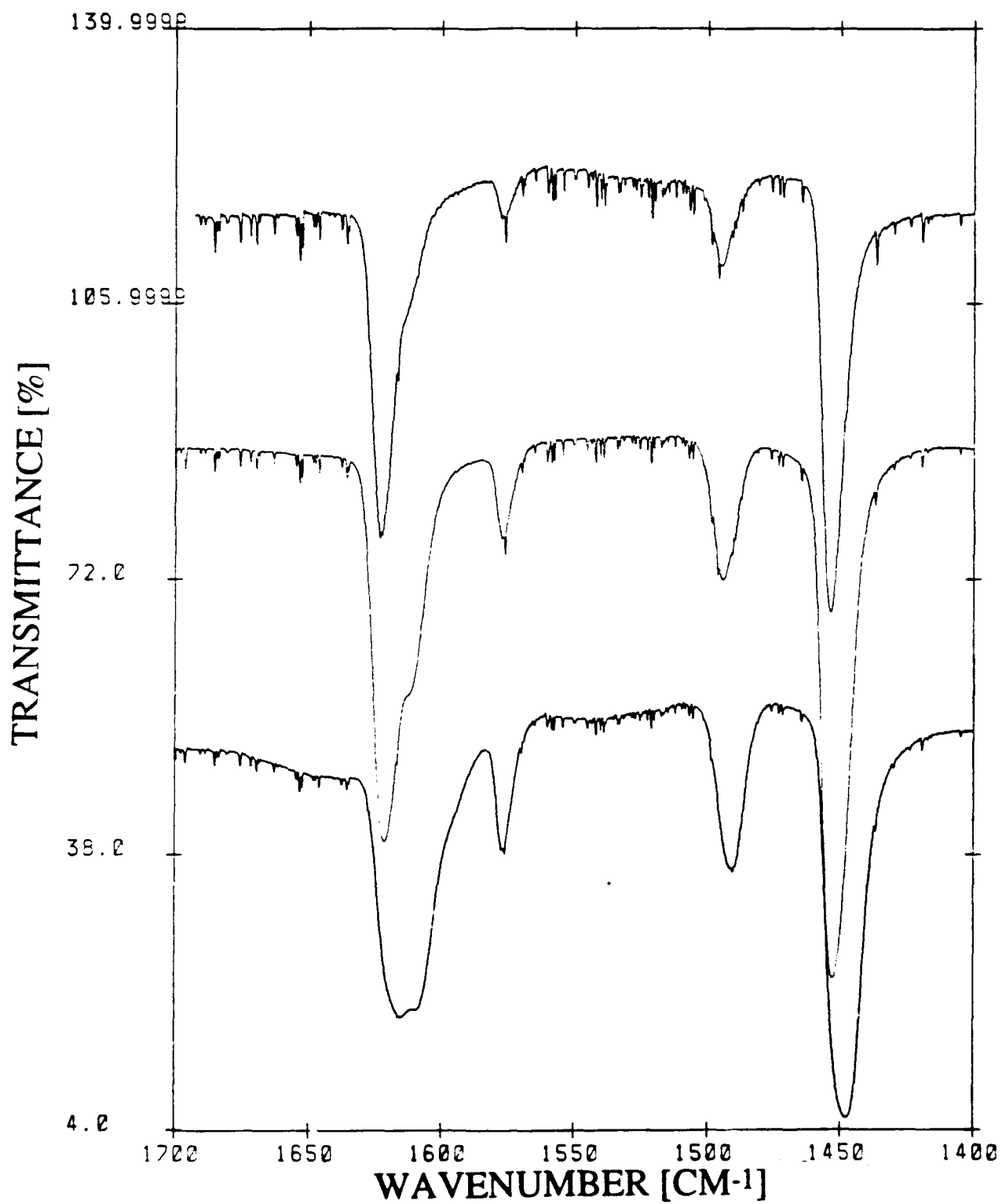
Figure 4-31: FTIR SPECTRA OF PYRIDINE ADSORBED ON NA25w AFTER HEAT TREATMENTS AT 300, 200, AND 100 °C (TOP TO BOTTOM)
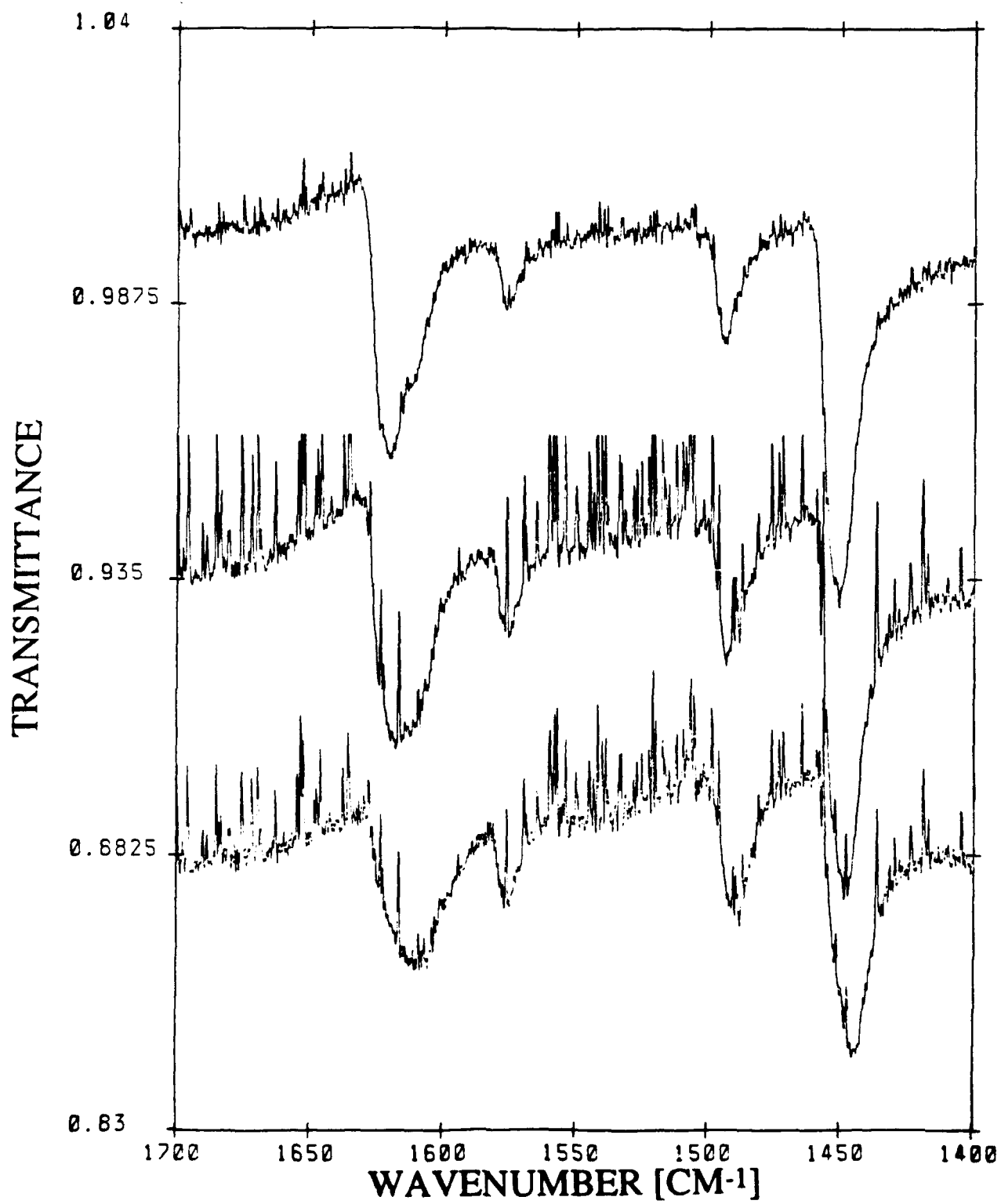
This large frequency shift indicates a slightly wider distribution of Lewis acid sites for A-NA25w than for $A-Nb_2O_5$ (total frequency shift, $\Delta = 3.0$ cm^{-1}). Thus, overall this new mixed oxide aerogel of niobia/alumina shows a larger distribution of Lewis acid sites and acid strength than the separate bulk oxide aerogels of niobia and alumina.

Figure 4-31 shows similar findings for the precipitated NA25w, but interpretation of the data is difficult because of the poor resolution of spectra after the lower heat treatments. The Lewis pyridine absorption frequencies are all downshifted by a few wavenumbers, which could be due to two main factors: first, the noisy spectra are leading to poor peak assignments, and second, water vapor could possibly be adsorbing (or still chemisorbed) on the sample surface and blocking or lowering the Lewis acid site vibrations. The general shape and distribution of the spectra for NA25w appear similar to A-NA25w, and the same L/B ratios were determined for both of these samples. No other conclusions can be drawn from the poorly resolved spectra. To summarize the results for A-NA25w, we know that these samples have very little if any Brønsted acid sites (L/B ~ very large), and also a peak is seen around 1610 cm^{-1} which can be assigned to a new Lewis site (results from the incorporation of niobia into the mixed oxide) which has a wide acid strength distribution as noted by the large shift in the 8a frequency. Placing niobia into the alumina matrix as in A-NA25w also results in larger Lewis acid site shifts than bulk alumina.

As an aside, the niobia/alumina mixed oxide (precipitated) shows a good deal of noise in these spectra which could possibly be due to the much lower pore volume and pore diameter which prevent the pyridine molecules from adsorbing into the oxide and thus lowers the effective surface area of this material. Low surface area samples have been shown in the past to yield poorly resolved spectra similar to those found for this sample.[88] Another possible and more likely explanation is that strongly chemisorbed water, which can be seen in the spectra in Appendix C, is effectively poisoning the acid sites. Higher

pretreatment temperatures might be necessary to desorb water from the sample surface; however, limitations with equipment prevented us from performing this experiment.

4.3.4 Reduction Studies

Direct reduction was performed by heating the calcined (500,2) mixed oxide aerogels to 1000 °C at 10 °C/min and holding for 2 hours at 1000 °C in pure flowing hydrogen. A second series of TG reduction experiments were done by pretreating the samples at 1000 °C for various times, followed by a subsequent reduction using the above temperature schedule in hydrogen. This was done to minimize compound formation effects or crystallization of niobia during the heat treatment. No noticeable peaks are noticed on the direct reduction of A-NS25w; therefore, the helium pretreated samples were examined in this study. Figure 4-32 shows the indirect reductions of A-NS25w along with A-Nb$_2$O$_5$ as a comparison. The peak reduction temperatures for A-NS25w are listed in Table 4-17 as a function of heat treatment.

It is seen from this table and figure that the mixed oxide of niobia/silica stabilizes the reduction of niobia. The peak reduction temperatures are 994 °C for both indirect reductions on pretreated A-NS25w, (1000,-) and (1000,4), while the pretreated bulk niobia aerogel reduces at a temperature of about 900 °C. This large temperature difference can possibly be explained by results from our group.[76, 88] A summary of these results suggest that if niobia is allowed to first crystallize in a non-reducing environment at a sufficiently high temperature, the crystalline phase is stabilized and reduces at a higher temperature than bulk niobia.[76, 88] XRD results confirm these findings by showing the formation of only TT-Nb$_2$O$_5$ at these severe thermal treatments. This indicates that niobia is indeed stabilized when it is adjacent to a rigid silica interface.

Figure 4-33 shows the direct and indirect reduction patterns for A-NA25w. The peak reduction temperatures are shown in Table 4-18. The direct reduction of A-NA25w as shown in Figure 4-33(a) shows two reduction peaks above 600 °C. The large and

Figure 4-32: TG REDUCTION DATA FOR PRETREATED A-NS25w: A) Nb_2O_5, B) A-NS25w (1000,-), AND C) A-NS25w (1000,4)
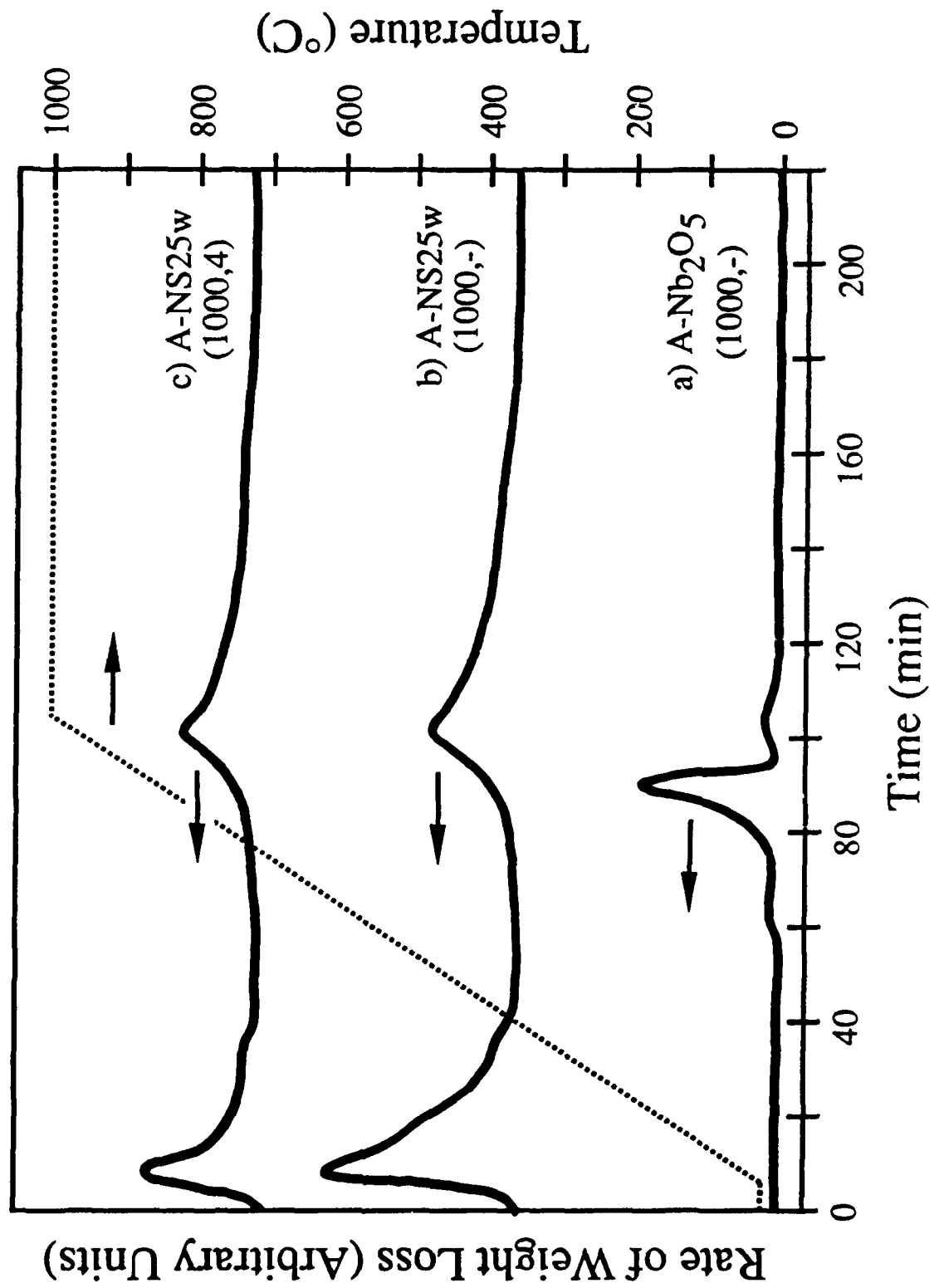
Table 4-17: PEAK TEMPERATURES FOR TG REDUCTION DATA OF HEAT TREATED A-NS25w AND A-Nb$_2$O$_5$

Sample	Heat Treatment	Peak Temperature (°C)
A-Nb$_2$O$_5$	(1000,-)	900
A-NS25w	(1000,-)	994
A-NS25w	(1000,4)	994

Table 4-18: PEAK TEMPERATURES FOR TG REDUCTION DATA OF HEAT TREATED A-NA25w

Sample	Heat Treatment	Peak Temperature (°C)
A-NA25w	(500,2)	893(B), 994
A-NA25w	(1000,-)	1000

B = Broad

Figure 4-33: TG REDUCTION DATA FOR PRETREATED A-NA25w: A) (500,2) AND B) (1000,-)
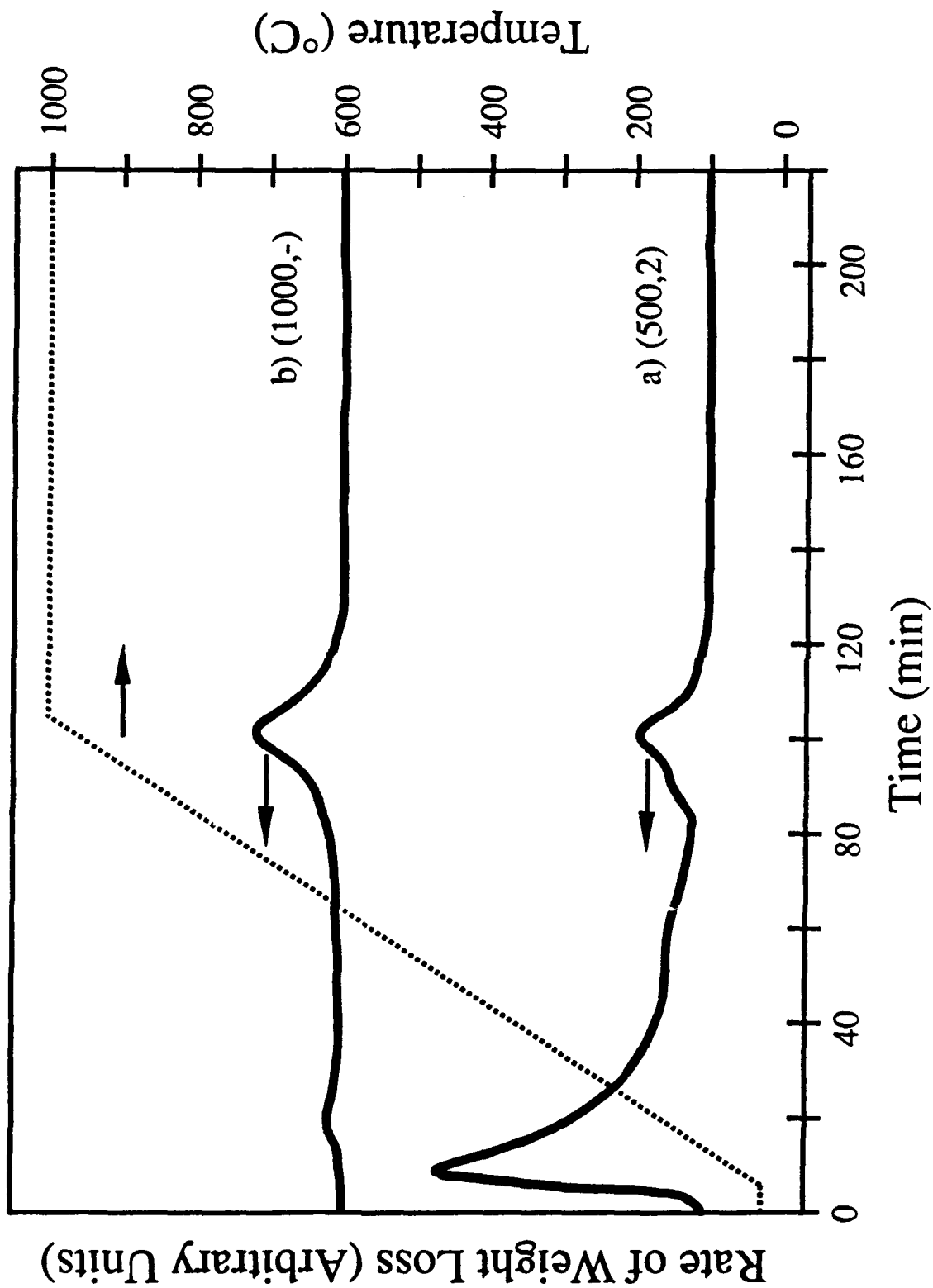
tailing peak from ~ 100 - 400 °C is due to the evolution of water from the surface. The reduction peak at ~ 890 °C is closely associated with the exothermic peak around ~ 860 °C in the DTA which we have assigned to formation of the compound NbAlO4. Thus, this peak is probably due to the restructuring of the oxide lattice needed to form this compound, which frees up niobia associated with the highly distorted octahedra and the Nb=O found in this material, or may be due to removal of water from a solid-state reaction between these two oxides. The higher reduction peak is due to the reduction of aluminum niobate, NbAlO4. The indirect reduction of A-NA25w is shown in Figure 4-33(b). We see that the peak at ~ 850 °C is missing in this (1000,-) pretreated sample, presumably because restructuring into NbAlO4 has already taken place and there are no longer any highly distorted octahedra containing Nb=O bonds, merely slightly distorted NbO6 groups and Nb-O bonds.[201] The peak has shifted slightly to ~ 1000 °C, from the direct reduction of the sample whose peak was at ~ 994 °C, but both peaks can be assigned to the reduction of NbAlO4.

4.3.5 1-Butene Isomerization

1-Butene isomerization is a reaction that is catalyzed by acidic materials, and will be used as the test for activity in these mixed oxide catalysts. Figure 4-34 shows the isomerization rate of 1-butene (mol/hr-g Nb_2O_5) for the mixed oxide aerogels as well as A-Nb_2O_5 for comparison. The A-NS25w and NS25w show the highest steady-state activities in the figure with a value of 5.4 and 3.4 x 10^{-2} mol/hr-g Nb_2O_5, while A-Nb_2O_5 only shows a value of 1.2 x 10^{-2} mol/hr-g Nb_2O_5. The lowest activity of all the mixed oxides was recorded by A-NA25w at 0.13 x 10^{-2} mol/hr-g Nb_2O_5. These results are not all that surprising when one considers the FTIR results in that the niobia/silica mixed oxide possessed Brønsted acidity, which was weak, and is thus an ideal catalyst for 1-butene isomerization. The high activity could also be a result of the good dispersion of niobia in silica so that nearly every surface niobium atom is acting as a separate acid site, as

Figure 4-34: 1-BUTENE ISOMERIZATION ACTIVITY (/g Nb_2O_5) OVER MIXED OXIDE AEROGELS
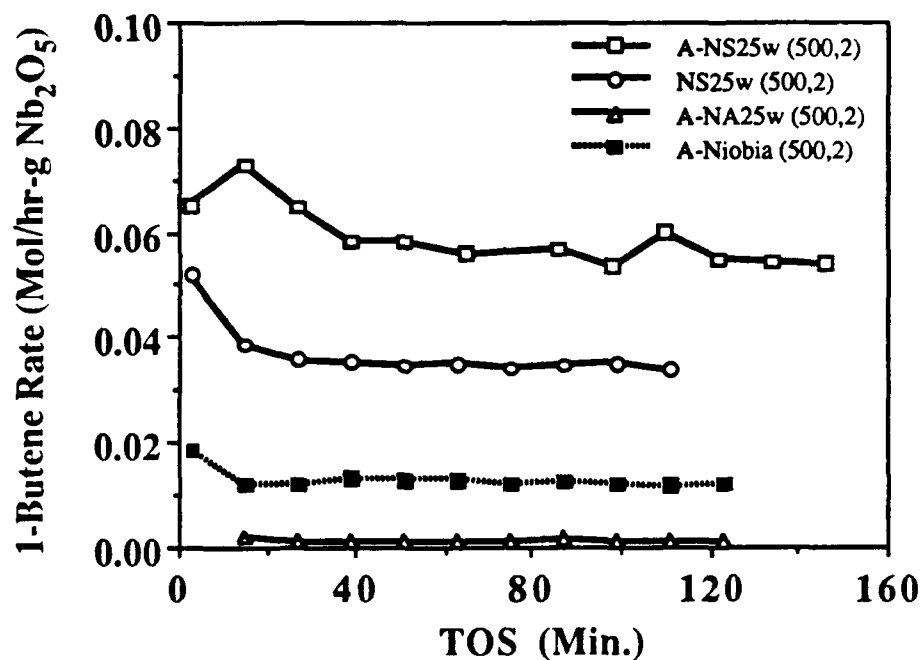
Figure 4-35: 1-BUTENE ISOMERIZATION ACTIVITY (/M^2) OVER MIXED OXIDE AEROGELS
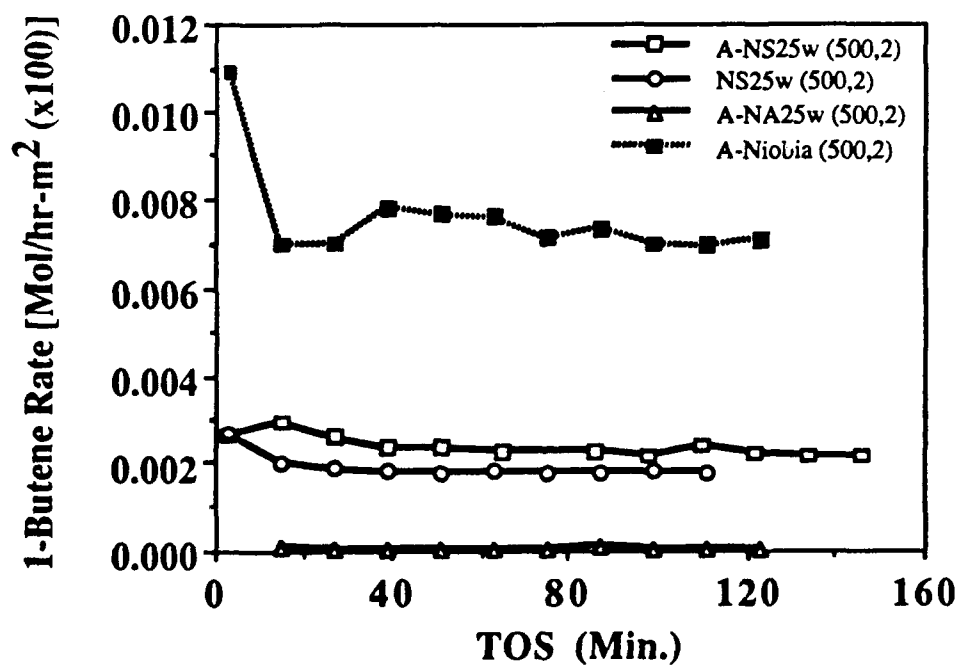
confirmed by our titrations. The niobia/alumina mixed oxide aerogel was seen by FTIR results of pyridine adsorption to possess very little if any Brønsted acidity, and showed primarily strong Lewis acidity. Our 1-butene results confirm this finding by the low activity associated with this reaction. Table 4-19 lists the activities of these mixed oxide samples normalized with different bases: (/g), (/g Nb_2O_5), and (/m^2), as well as showing C/T ratios for these catalysts. All mixed oxides showed C/T ratios of ~ 1 which indicates that the probable active site on these binary oxides is a weak Brønsted site, and indicates that A-NA25w must have water adsorbed onto a Lewis site to convert it to a weak Brønsted acid.

Figure 4-35 shows the activity of the mixed oxides normalized with respect to surface area. The niobia aerogel has the highest activity at 0.71×10^{-4} mol/hr-m^2, while the niobia/silica mixed oxides appeared to have the same average activity ~ 0.20×10^{-4} mol/hr-m^2. The large activity for the niobia aerogel is not surprising considering the weak Brønsted acidity found previously on this oxide. The surprising part comes from the fact that the titration results show the acidity for NS25w on a per m^2 basis to be higher by a factor of 1.5 over A-NS25w; however, the n-butylamine titration picked up all acid sites (even the strongest), while this reaction is catalyzed by only the weakest (Brønsted acids in particular). Thus, these findings show that the effective catalytic site distribution appears equal for both of these niobia/silica mixed oxides. A-NA25w shows little activity, due to the fact this material possesses primarily only very strong Lewis sites, with little to no Brønsted acidity.

Figure 4-36 shows the 1-butene activity (/g Nb_2O_5) for A-NS25w subjected to various thermal treatments. Table 4-20 lists the activities for these samples along with their respective C/T ratios. A-NS25w after the (500,2) and (600,2) heat treatments show similar activities and selectivities (C/T = 1.2). After (800,2) the activity goes down slightly because of the ordering that is occurring with this sample (loss of dispersion), as evidenced by the appearance of slightly distorted NbO_6 in the Raman spectra. This is similar to

Table 4-19: 1-BUTENE ISOMERIZATION ACTIVITY MIXED OXIDE AEROGELS (CALCINED)

	Steady-State Activity (mol/hr-) [x100]			
Sample	(/g)	(/g Nb$_2$O$_5$)	(/m^2 x100)	C/T*
A-NS25w (500,2)	1.4	5.4	0.22	1.2
NS25w (500,2)	0.86	3.4	0.18	1.2
A-NA25w (500,2)	0.032	0.13	0.0066	1.0
A-Nb$_2$O$_5$ (500,2)	1.2	1.2	0.71	1.6

* C/T = Cis/Trans-2-butene ratio

Table 4-20: 1-BUTENE ISOMERIZATION ACTIVITY HEAT TREATED A-NS25w

	Steady-State Activity (mol/hr-) [x100]			
Sample	(/g)	(/g Nb$_2$O$_5$)	(/m^2 x100)	C/T*
A-NS25w (500,2)	1.4	5.4	0.22	1.2
A-NS25w (600,2)	0.99	4.0	0.17	1.2
A-NS25w (800,2)	0.69	2.8	0.18	0.5
A-NS25w (1000,-)	3.1	12.4	1.0	0.05

* C/T = Cis/Trans-2-butene ratio

Figure 4-36: 1-BUTENE ISOMERIZATION ACTIVITY (/g Nb_2O_5) OVER HEAT TREATED A-NS25w
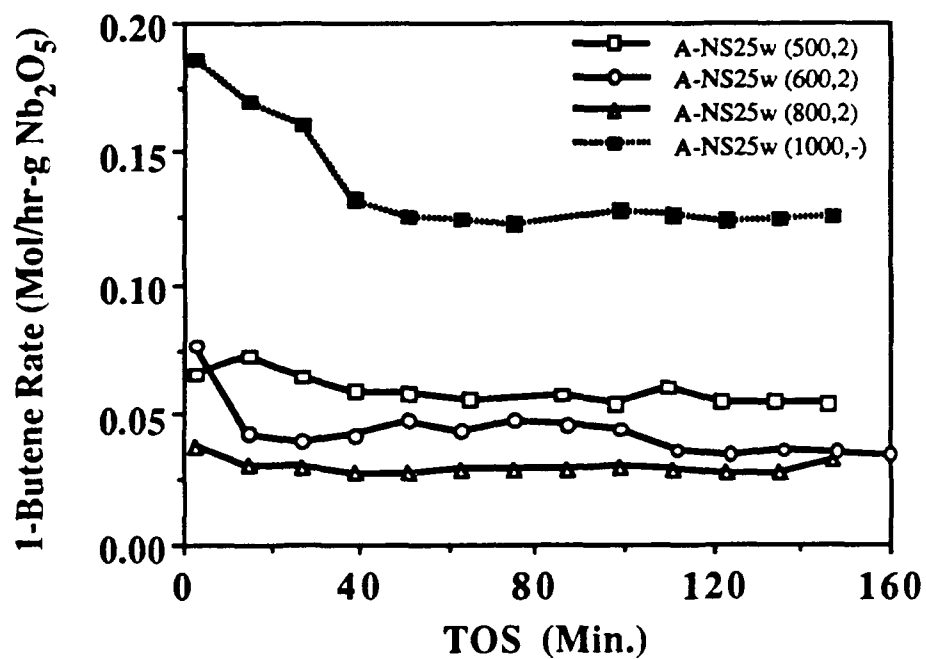
Figure 4-37: 1-BUTENE ISOMERIZATION ACTIVITY (/M^2) OVER HEAT TREATED A-NS25w
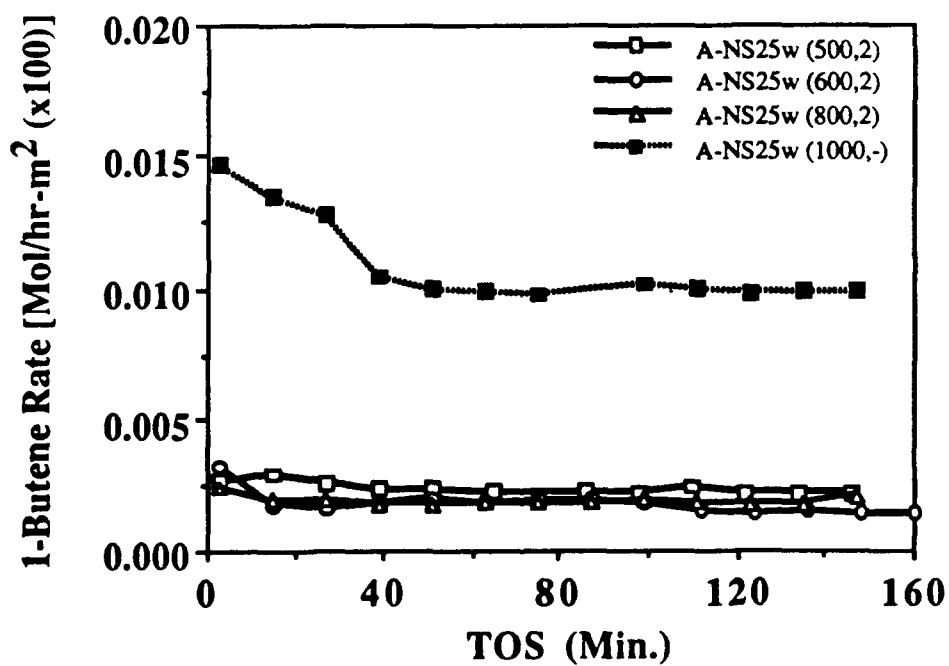
results from our titrations with this sample. The C/T ratio for the (800,2) sample is 0.5, which is still close enough to 1 to suggest weak Brønsted acid site catalysis. The major change in A-NS25w from the 1-butene reaction standpoint is after (1000,-). The activity increases greatly to 12.4 x 10^{-2} mol/hr-g Nb_2O_5 and the C/T ratio drops all the way to 0.05. Increased ordering of niobia is noticed with this sample by the shift of the 710 cm^{-1} peak in the LRS spectra, and XRD actually reveals TT-Nb_2O_5. This distorted niobia structure in A-NS25w (1000,-) shows great isomerization activity and is obviously related to the niobia coming out of its constrained environment in the silica matrix, in which it was highly distorted and showed great acid strength. The niobia after allowing to join other groups of slightly distorted niobia octahedra are still acidic and possess weak Brønsted acidity.[88] This Brønsted acidity for the (1000,-) heat treated sample is even weaker than that found on the calcined niobia/silica mixed oxide.[88] Some niobia is still locked into highly distorted environments within the silica matrix, but the majority of the niobia is in a new slightly distorted environment that is attached to a high surface area material and leads to great activity. The C/T ratio of 0.05 is much less than 1, the value assigned to Brønsted acid sites; however, Hall notes that this ratio may deviate largely from 1, for Brønsted acidity, if there was some kind of interaction with the surface which would create a larger energy barrier for the formation of trans-2-butene or cis-2-butene and then give a larger or smaller C/T ratio, respectively.[203] We believe this to be the case since this reaction is catalyzed by weak Brønsted sites, and A-NS25w (1000,-) has been shown to possess this type of acicity.[88]

Figure 4-37 shows the 1-butene activity for A-NS25w normalized with respect to surface area. The steady-state activities are listed in Table 4-20. The main features with this figure are the similarities in steady-state activity for all the heat-treated A-NS25w samples except for A-NS25w (1000,-). There seems to be an apparent rise (although very slight) in specific activity in the (800,2) over the (600,2) heat treatment, presumably because of the change of the highly distorted (strong Lewis acid sites) to slightly distorted

NbO$_6$ octahedra (Brønsted acid sites). As the heat treatment decreases the surface area, the density of acid sites should increase; therefore, we should expect to see a rise in activity on a normalized surface area basis. There is a slight increase with this increased heat treatment to (800,2), but the acid sites are still possibly too strong or distorted to effectively catalyze the reaction. Not until the (1000,-) treatment do we see a distinct jump which also indicates a change in the structure of this material as is evidenced by XRD as well as shifts in LRS frequencies. This high activity has been correlated to the existence of slightly distorted niobia octahedra adjacent to a rigid silica boundary.

4.4 Summary

This chapter presents the physical and chemical properties of the mixed oxide aerogels and their precipitated counterparts: A-NS25w, NS25w, A-NA25w, and NA25w. With all of these mixed oxides, it was determined that highly distorted groups containing terminal Nb=O were the basis for the origin of high acid strength and acidity. The samples of niobia/silica were found to contain strong Lewis acid sites as well as weak Brønsted acidity, while the niobia/alumina mixed oxides had primarily only Lewis acidity with little to no Brønsted acid sites. Several heat treatments revealed that the high acid strength and acidity was lost upon ordering of niobia into crystallites for niobia/silica, or compound formation into NbAlO$_4$ for niobia/alumina. Niobia is stabilized when it crystallizes out of A-NS25w because of the rigid niobia-silica interface, and forming the compound of NbAlO$_4$ from A-NA25w also stabilizes niobia because of the solid-state interaction. Results of 1-butene isomerization reveal that niobia/silica does possess catalytically active sites, but this activity may increase by a factor of three if the niobia is allowed to crystallize out and form slightly distorted octahedra instead of the highly distorted groups constrained in a silica matrix. Furthermore, niobia/alumina has little to no Brønsted acidity. The results from this chapter will be coupled with results of the following chapter on surface oxides, in order to form a model for these binary oxides in terms of oxide-oxide

interactions inherent to these systems, and to show how they relate to the structural and acidic properties of these oxides.

Chapter 5

SURFACE OXIDE AEROGELS

5.1 Introduction

This chapter discusses the results of the physical and chemical characterization of the supported niobia oxide aerogels synthesized in this research. Several techniques to probe the structural and chemical properties of these binary oxides were used to give additional insight into the oxide-oxide interactions within these materials. This chapter builds upon results presented earlier for the bulk and mixed oxides, and complements these findings by establishing a set of samples of known structure for chemical characterization. In so doing, an understanding of different oxide interactions, through structural observations, serves as a tool in forming a chemical-structural relationship found in this set of binary oxides. A model used to explain these findings will be presented in the next chapter.

5.2 Physical Property Characterization of Surface Oxide Aerogels

5.2.1 Surface Area and Physical Property Data

Silica aerogel supported niobia [A-NS(.)] and alumina aerogel supported niobia [A-NA(.)] were prepared by grafting niobia onto the surface of a silica and alumina aerogel, respectively. Several surface coverages for each supported oxide were made to determine dispersion of the niobia phase, varying from 2.5 to 25% (0.025 to 0.25) monolayer (fully

coated silica or alumina surface with one atomic layer of niobia) coverage. Table 2-10 shows the prepared surface oxides in terms of their respective niobia loadings and associated nomenclature.

Table 5-1(A) and (B) list the surface areas for the silica aerogel supported niobia samples as a function of various thermal treatment in terms of (m^2/g) and (m^2/g SiO_2), respectively. The bulk oxide aerogel of silica is shown for comparison. Figure 5-1(A) shows the total surface areas (m^2/g) versus calcination temperature for these supported oxides, while Figure 5-1(B) reveals the specific surface area (m^2/g SiO_2) with respect to the same heating schedule as above. Figure 5-2 shows these areas normalized with respect to the area after the standard calcination, (500,2), and plotted versus the same thermal treatments. These figures and tables show that A-NS(.05) and A-NS(.10) maintain approximately 75 to 80% of their surface area up to a heat treatment of 1000 °C (1000,-). This is identical to results found for the bulk aerogel of silica as shown in Figure 5-2, and shows the stability for these low loadings of surface oxides (5 and 10% monolayer coverages, respectively). At higher loadings of niobia, up to 25% monolayer, we notice that the surface area retention is only about 55 - 60% of the original calcined area after a (1000,-) thermal treatment. Thus, it appears that silica is stabilized better at the lower coverages than it is at the higher coverages of niobia supported on the aerogel of silica. This will later be explained as due to the crystallite formation of $TT-Nb_2O_5$ on A-NS(.25) after the (1000,-) heat treatment. When these oxides are subjected to more severe heat treatments, (1000,48), one notices a drastic decrease in surface area across the board for the silica aerogel supported niobia. These decreases range anywhere from 20 - 30% of their original calcined areas. Such a significant loss in surface area is indicative of a collapse in oxide structure as well as severe dehydroxylation, and can only occur when silica itself becomes mobile. As we have discussed earlier, the surface area of the silica aerogel itself drops to a level of approximately one third its original area, which is consistent with the above explanation and findings for the silica supported binary oxides.

Table 5-1: SURFACE AREA OF SILICA AEROGEL SUPPORTED NIOBIA WITH HEAT
TREATMENTS: A) TOTAL (M^2/G) AND B) NORMALIZED $(M^2/G \ SiO_2)$

A) Total Surface Area (m^2/g) of Silica Supported Niobia Aerogels

| Heat Treatment | Total Surface Area $(m^2/g)^*$ | | | | |
[Temp.(°C).Time(hr)]	A-SiO_2	A-NS(.025)	Samples A-NS(.05)	A-NS(.10)	A-NS(.25)
(500,2)	920	890	840	800	690
(600,2)	825	850	830	770	640
(800,2)	750	750	700	650	500
(1000,-)	700	660	630	600	390
(1000,48)	290	300	280	190	160

B) Normalized Surface Area $(m^2/g \ SiO_2)$ of Silica Supported Niobia Aerogels

| Heat Treatment | Normalized Surface Area $(m^2/g \ SiO_2)^*$ | | | | |
[Temp.(°C).Time(hr)]	A-SiO_2	A-NS(.025)	Samples A-NS(.05)	A-NS(.10)	A-NS(.25)
(500,2)	920	918	892	885	904
(600,2)	825	877	881	852	839
(800,2)	750	774	743	719	655
(1000,-)	700	681	669	664	511
(1000,48)	290	310	297	210	210

* Surface Areas measured using Single-Point B.E.T. method.

Figure 5-1: SILICA AEROGEL SUPPORTED NIOBIA SURFACE AREA: A) TOTAL (M^2/G) AND B) NORMALIZED (M^2/G SiO$_2$) VS. TEMPERATURE

A) Total Surface Area (m^2/g) of Silica Supported Niobia Aerogels
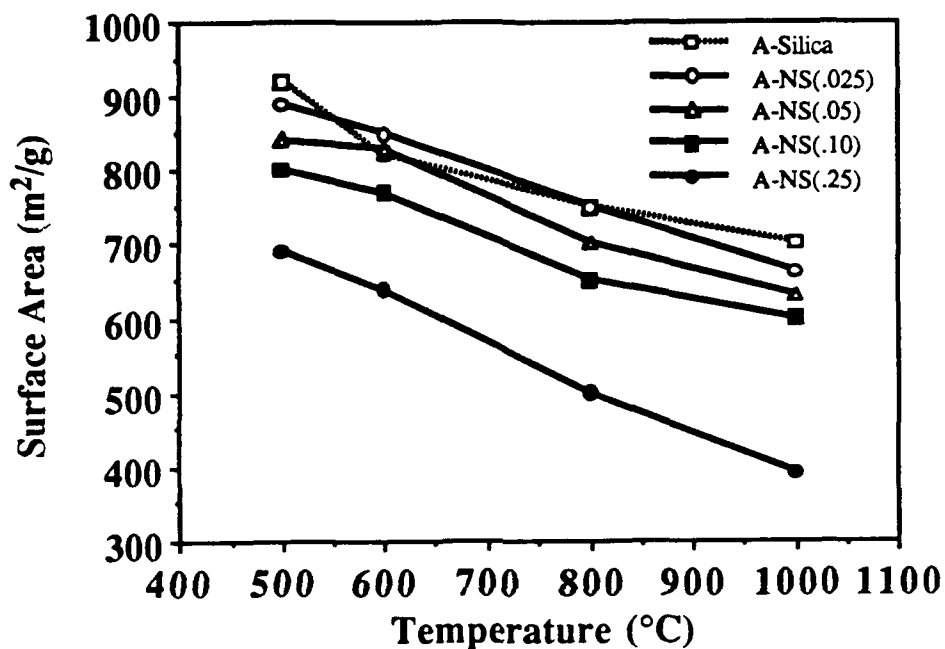
B) Normal Surface Area (m^2/g SiO$_2$) of Silica Supported Niobia Aerogels
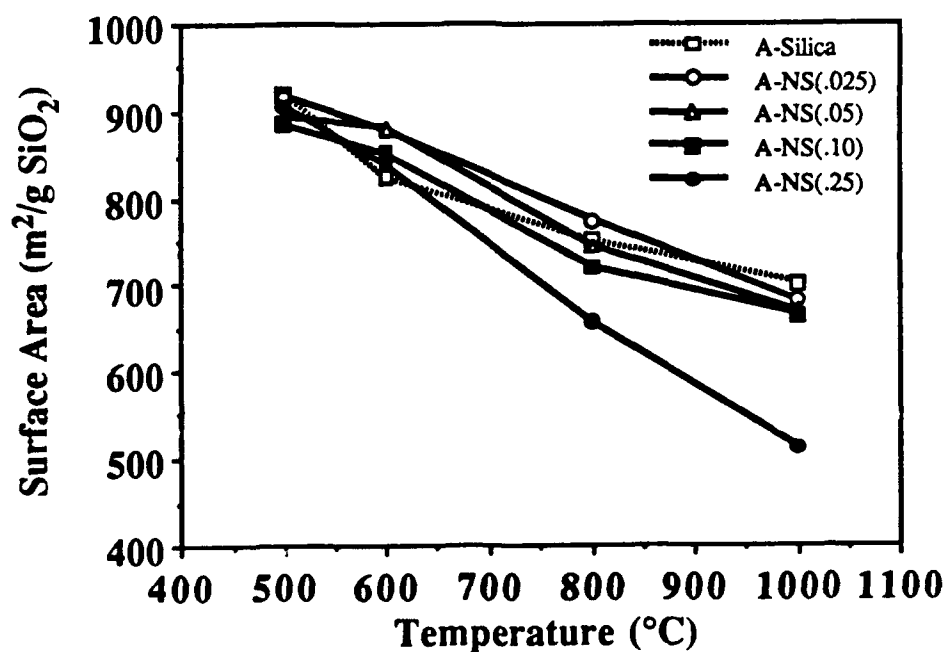
Figure 5-2: SILICA AEROGEL SUPPORTED NIOBIA NORMALIZED SURFACE AREA VS. TEMPERATURE
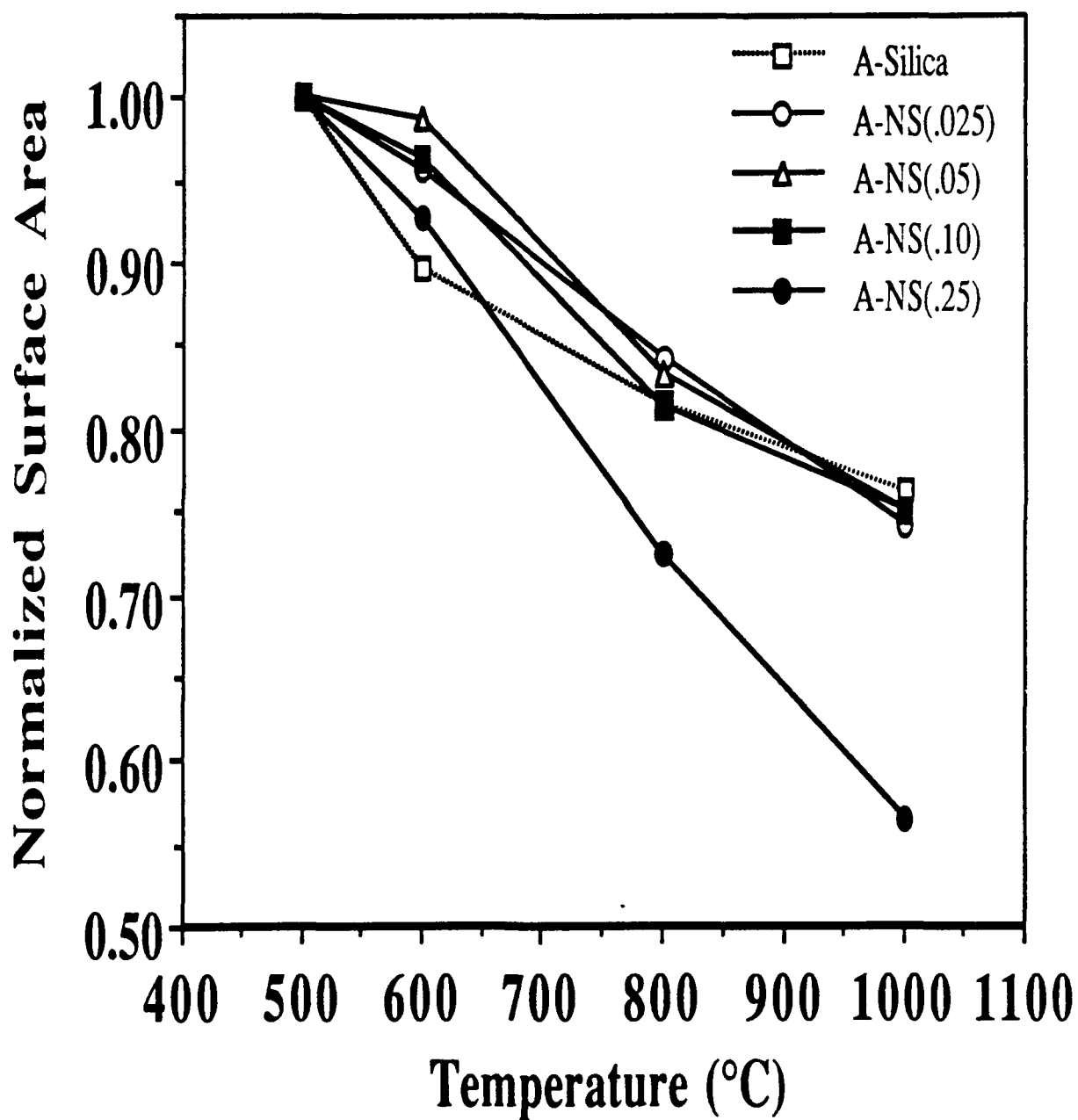
Table 5-2(A) and (B) show the total surface areas for the alumina aerogel supported niobia samples as a function of various heat treatments in terms of (m^2/g) and (m^2/g Al_2O_3), respectively. The bulk oxide aerogels of alumina and niobia are shown for comparison. Figures 5-3(A) and (B), and Figure 5-4 show the total surface area (m^2/g), (m^2/g Al_2O_3), and normalized surface area versus heat treatment, respectively. The normalized surface areas were calculated using the area after the standard calcination, (500,2), as the baseline. All of the alumina aerogel supported niobia maintained 60 - 70% of their surface area up to a thermal treatment of (800,2). This retention ability for surface area was mirrored by results for the bulk alumina aerogel as seen in Figure 5-4. Heat treating these alumina supported binary oxides to (1000,-) resulted in reductions of surface areas to approximately one third the original calcined values. This significant drop in surface area will later be seen as being attributed to the formation of γ-Al_2O_3 in all the alumina supported oxides (as well as bulk alumina), and also to $NbAlO_4$ formation in the higher niobia loading of A-NA(.25). All alumina supported oxides appear to follow the same rate of decrease as the alumina aerogel throughout the entire temperature as evidenced in Figure 5-4. The solid-state compound formation to $NbAlO_4$ after (1000,-) in A-NA(.25) does not seem to affect the surface area decline by more than about 5% over the alumina aerogel decrease. This shows that the alumina has the major influence in dictating how the alumina aerogel supported oxides behave with heat treatment.

5.2.2 X-Ray Diffraction (XRD)

Table 5-3 shows the XRD phases of silica aerogel supported niobia with various thermal treatments. The niobia aerogel has been included in this table as a reference to gauge the stability of the supported niobia oxide over the same range of heat treatment. Notice in this table that A-NS(.05) and A-NS(.10) are XRD amorphous to (1000,-), while A-NS(.25) has begun to form very poorly crystalline TT-Nb_2O_5. At this same heat treatment the bulk niobia aerogel has transformed into M-Nb_2O_5, a high temperature and

Table 5-2: SURFACE AREA OF ALUMINA AEROGEL SUPPORTED NIOBIA WITH TEMPERATURE: A) TOTAL (M^2/G) AND B) NORMALIZED (M^2/G Al_2O_3)

A) Total Surface Area (m^2/g) of Alumina Supported Niobia Aerogels

Heat Treatment	Total Surface Area (m^2/g)[*]				
			Samples		
[Temp.(°C).Time(hr)]	A-Al_2O_3	A-NA(.05)	A-NA(.10)	A-NA(.25)	A-Nb_2O_5
(500,2)	580	500	570	470	190
(600,2)	470	460	540	435	60
(800,2)	390	330	360	280	5
(1000,-)	190	190	170	130	1
(1000,48)	60	70	75	60	-

B) Normalized Area (m^2/g Al_2O_3) of Alumina Supported Niobia Aerogels

Heat Treatment	Normalized Surface Area (m^2/g Al_2O_3)[*]			
		Samples		
[Temp.(°C).Time(hr)]	A-Al_2O_3	A-NA(.05)	A-NA(.10)	A-NA(.25)
(500,2)	580	521	621	564
(600,2)	470	479	588	522
(800,2)	390	343	392	336
(1000,-)	190	198	185	156
(1000,48)	60	73	82	72

[*]   Surface Areas measured using Single-Point B.E.T. method.

Figure 5-3: ALUMINA AEROGEL SUPPORTED NIOBIA SURFACE AREA: A) TOTAL
(M^2/G) AND B) NORMALIZED (M^2/G Al$_2$O$_3$) VS. TEMPERATURE

A) Total Surface Area (m^2/g) of Alumina Supported Niobia Aerogels
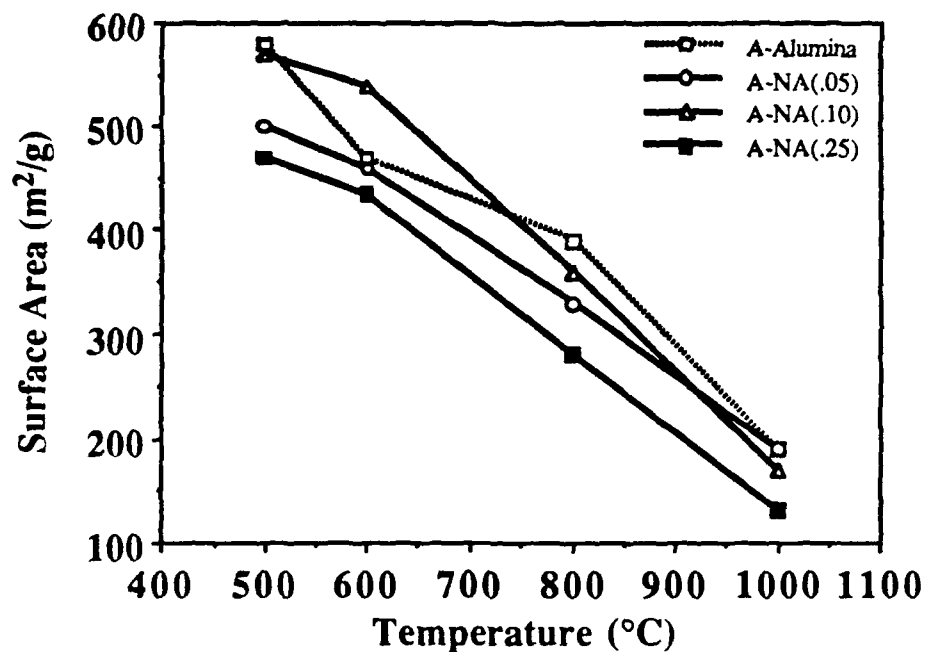
B) Normal Surface Area (m^2/g Al$_2$O$_3$) of Alumina Supported Niobia Aerogels
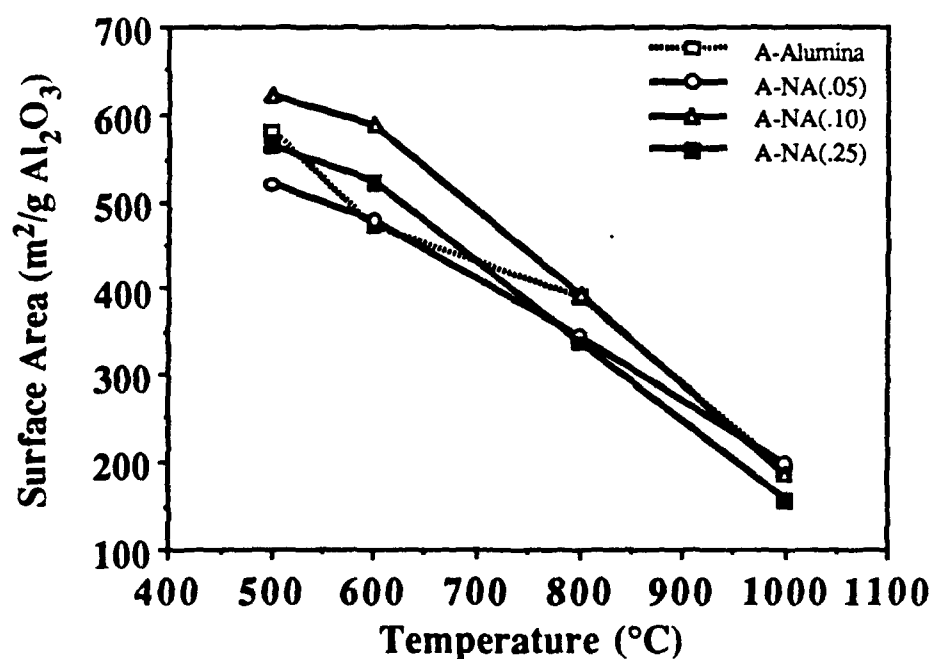
Figure 5-4: ALUMINA AEROGEL SUPPORTED NIOBIA NORMALIZED SURFACE
AREA VS. TEMPERATURE
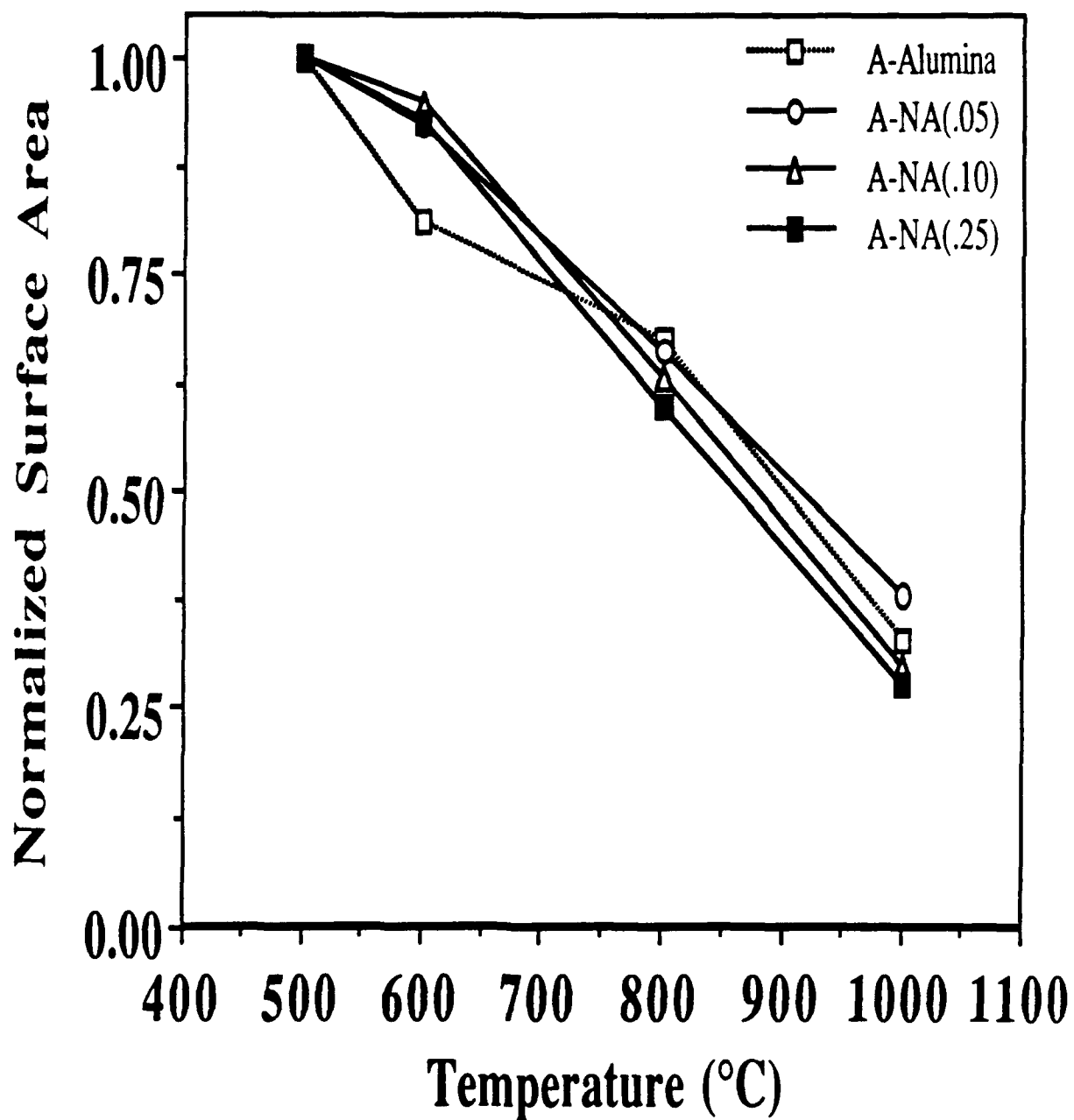
Table 5-3: PHASES OF SILICA AEROGEL SUPPORTED NIOBIA WITH THERMAL TREATMENTS

| Heat Treatment | X-Ray Diffraction Phases | | | |
| | Samples | | | |
[Temp.(°C),Time(hr)]	A-NS(.05)	A-NS(.10)	A-NS(.25)	A-Nb$_2$O$_5$
(500,2)	A	A	A	A
(600,2)	A	A	A	TT
(800,2)	A	A	A	T
(1000,-)	A	A	TT VPC	M
(1000,2)	A	A	TT PC	M + H
(1000,48)	A	TT VPC	T + M	H

A=Amorphous; TT,T,M, and H refer to the phases of niobia; VPC, PC=very-, poorly crystalline

ordered phase of niobia.[29] This indicates that the silica support is indeed interacting with the surface oxide overlayer of niobia. In fact, A-NS(.05) is XRD amorphous even after a severe heat treatment of (1000,48). This has a two-fold explanation: first, the covalent interaction of niobia with silica through the Si-O-Nb linkages built in by the grafting procedure acts as a stabilizing force in lowering the mobility of niobia; and second, the limited supply of niobia on the surface forces the oxide to diffuse over longer distances in order to link up with other groups, or form particles of TT-Nb_2O_5 that are beyond the detectable limits (< 3 nm) of the XRD apparatus. A-NS(.10) forms only very poorly crystalline TT-Nb_2O_5 when subjected to the severe thermal treatment of (1000,48), while A-NS(.25) has begun to show peaks of both T- and M-Nb_2O_5 over a mostly amorphous background (see Figure 5-5). At this same heat treatment, the aerogel of niobia has already transformed into H-Nb_2O_5. This well ordered and stable phase of H-Nb_2O_5 was seen on the niobia aerogel to appear with M-Nb_2O_5 after only (1000,2), and was indexed to entirely H-Nb_2O_5 after (1000,8) (see Chapter 2). The silica aerogel supported niobia with the highest loading (23.7 wt.% Nb_2O_5), A-NS(.25), was found to stabilize niobia to only TT-Nb_2O_5 after (1000,2), while bulk niobia was forming the high temperature phases of M- and H-Nb_2O_5. This indicates that silica is exerting a stabilizing influence on the niobia surface overlayer. The formation of M-Nb_2O_5 for A-NS(.25) after the severe (1000,48) thermal treatment was noted with a significant loss in surface area, indicating a collapse of the oxide structure and mobility of silica itself, which is apparently necessary for the sintering of M-Nb_2O_5 particles. The collapse of the silica structure effectively quadruples the amount of niobia on A-NS(.25), and hence makes it easier for this material to form the higher ordered M-Nb_2O_5 because of the added mobility caused by the silica collapse, and also the increased supply or concentration of niobia on the surface. Figure 5-5 traces the development of crystallinity in A-NS(.25) as a function of heat treatment. After (1000,-) there appears a very small peak at $2\Theta = \sim 10.5°$ attributable to TT-Nb_2O_5. After (1000,2) one can see the sharpening of this feature at $2\Theta = \sim 10.5°$, and after (1000,48) we see a

Figure 5-5: XRD OF A-NS(.25) AS A FUNCTION OF HEAT TREATMENT: A) (1000,-), B) (1000,2), AND C) (1000,48)
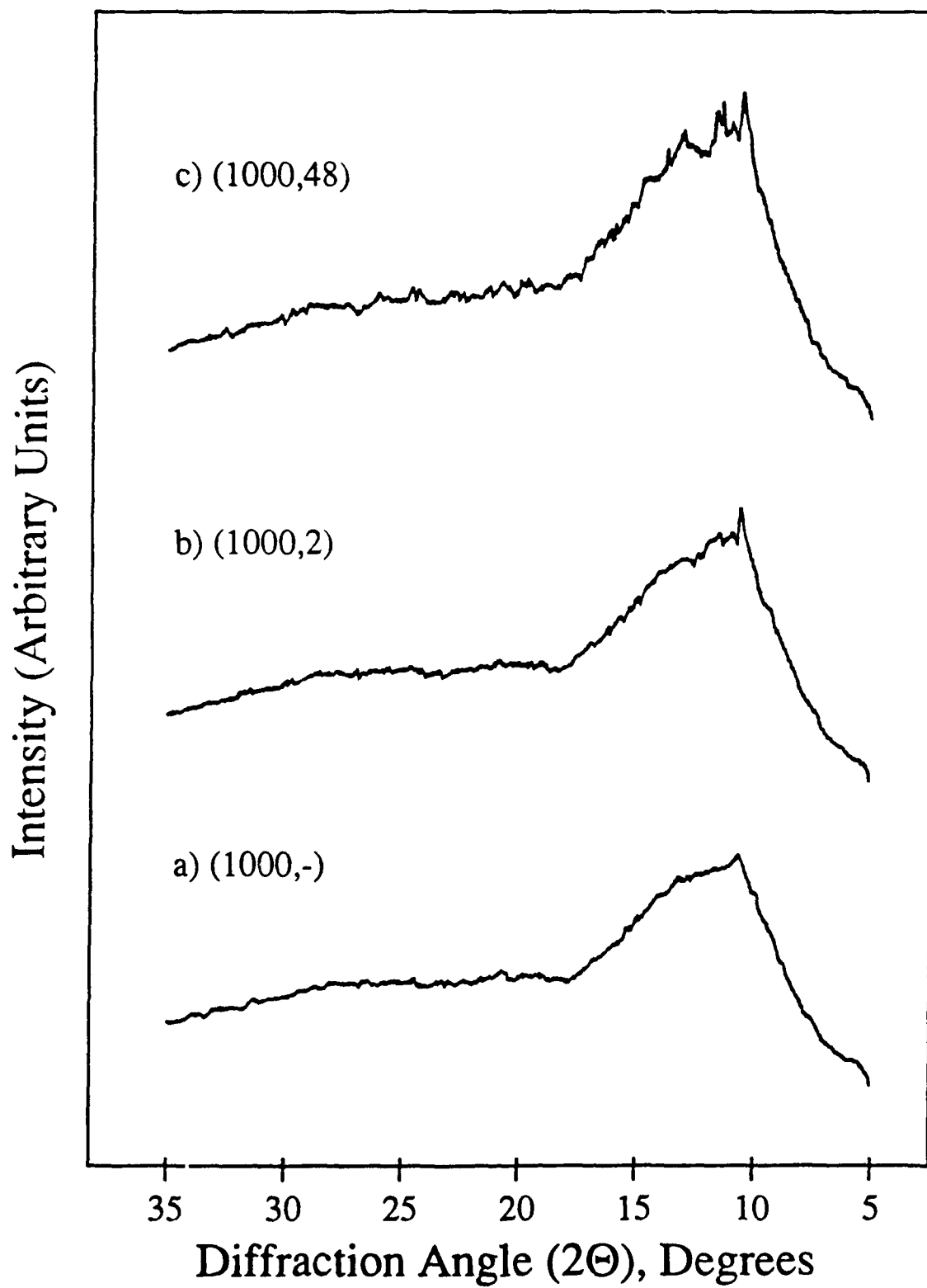
number of peaks which have been indexed, as mentioned previously, to both T- and M-Nb_2O_5. Notice also in these figures the amorphous background which is ascribed to the silica support. Figure 5-6 shows the development of crystallinity as a function of niobia coverage for the silica aerogel supported niobia after a thermal treatment of (1000,48). Notice that A-NS(.05) is XRD amorphous, A-NS(.10) begins to show small TT-Nb_2O_5 peaks, and A-NS(.25) shows sharp peaks indexed to both T- and M-Nb_2O_5. To summarize these findings, it appears that the silica aerogel stabilizes the niobia overlayer from forming the high temperature forms of M- and H-Nb_2O_5, except when sufficient loading and severe thermal treatment is used. These results agree with earlier findings from our group.[76, 88]

Table 5-4 lists the XRD phases found in the alumina aerogel supported niobia with thermal treatment. After the standard calcinations, all of the surface oxides are amorphous. Only the (1000,-) heat treatment induces a phase transformation to γ-Al_2O_3 for all of the alumina aerogel supported niobia as well as bulk alumina aerogel. Notice that the higher loading of niobia induces the compound formation of $NbAlO_4$ (very poorly crystalline). These compound formations and phase transitions are noted by the significant decreases in surface area from (800,2) to (1000,-). At the thermal treatment of (800,2) and lower calcination temperatures, alumina supported binary oxides were amorphous. The alumina aerogel itself, after the heat treatment at (800,2), was just beginning to show weak diffraction peaks indexed to γ-Al_2O_3. Longer holding times at 1000 °C induced the compound formation of $NbAlO_4$ to occur in all of the supported binary oxides of alumina. The lower loadings of niobia on alumina formed poorly crystalline structures at these severe thermal treatments as indicated by the broad peaks, while the higher loadings sharpened these peaks and was attributed to larger and more ordered $NbAlO_4$ crystallites. Notice in this table that the bulk alumina aerogel forms the most stable phase of alumina, α-Al_2O_3 at (1000,48); however, when niobia is present on the surface of alumina, it

Figure 5-6: XRD OF SILICA AEROGEL SUPPORTED NIOBIA AFTER (1000,48):
A) A-NS(.05), B) A-NS(.10), AND C) A-NS(.25)

c) A-NS(.25)

b) A-NS(.10)

a) A-NS(.05)

Intensity (Arbitrary Units)

Diffraction Angle (2Θ), Degrees
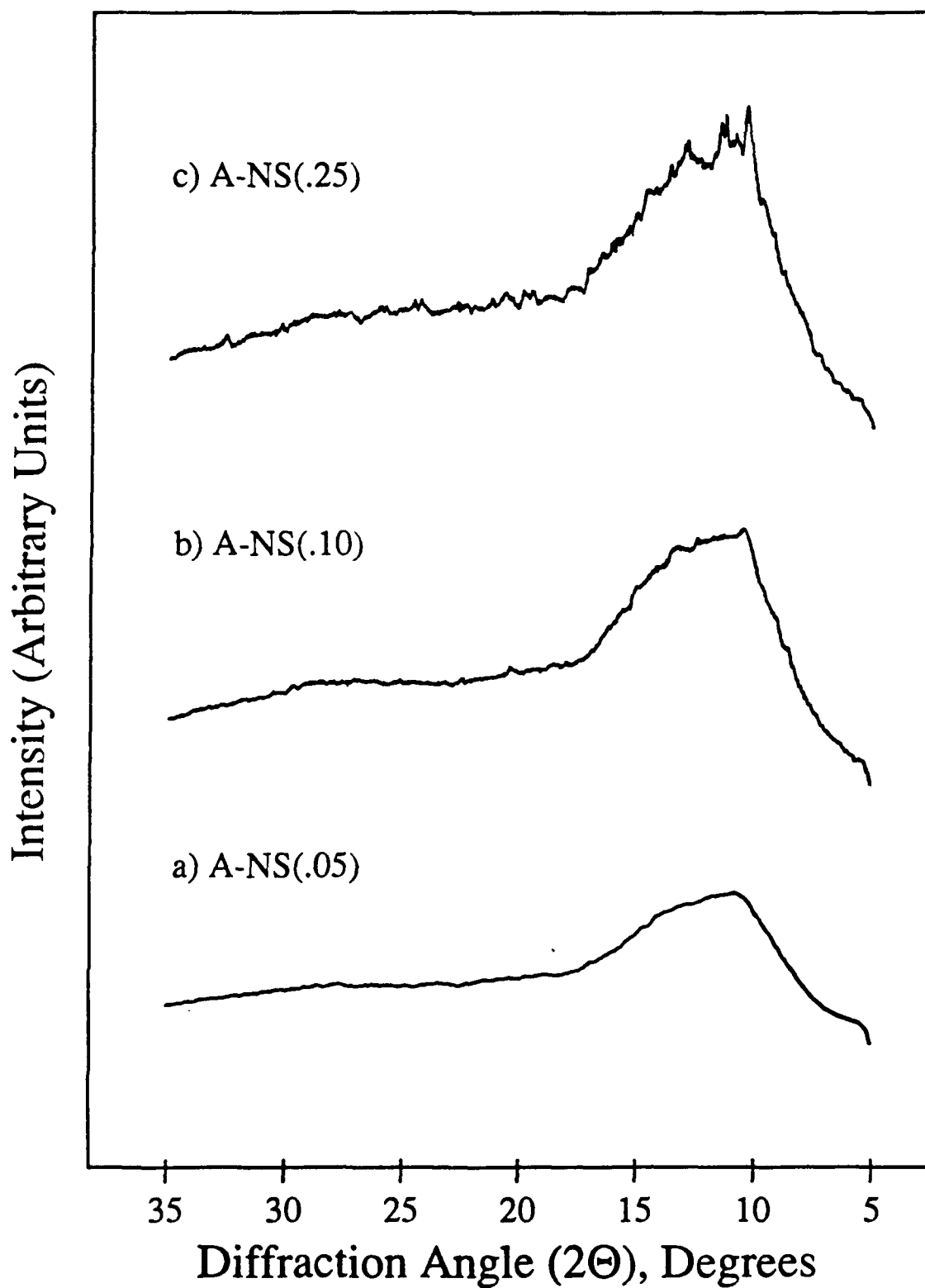
Table 5-4: PHASES OF ALUMINA AEROGEL SUPPORTED NIOBIA WITH
THERMAL TREATMENTS

	X-Ray Diffraction Phases			
Heat Treatment	**Samples**			
[Temp.(°C),Time(hr)]	A-Al$_2$O$_3$	A-NA(.05)	A-NA(.10)	A-NA(.25)
(500,2)	A	A	A	A
(1000,-)	γ-Al$_2$O$_3$	γ-Al$_2$O$_3$,	γ-Al$_2$O$_3$,	γ-Al$_2$O$_3$, NbAlO$_4$VPC
(1000,2)	γ-Al$_2$O$_3$	γ-Al$_2$O$_3$,	γ-Al$_2$O$_3$, NbAlO$_4$VPC	γ-Al$_2$O$_3$, NbAlO$_4$
(1000,48)	α-Al$_2$O$_3$	γ-Al$_2$O$_3$, NbAlO$_4$VPC	γ-Al$_2$O$_3$, NbAlO$_4$ PC	γ-Al$_2$O$_3$, NbAlO$_4$

A=Amorphous; VPC, PC=very poorly crystalline, poorly crystalline

suppresses the formation of α-Al_2O_3 by strongly interacting with the substrate. This suppression is indicated by the XRD identification of only γ-Al_2O_3 and $NbAlO_4$.

Figure 5-7 shows the XRD patterns of A-NA(.25) as a function of thermal treatment. After (1000,-) very broad peaks indicating γ-Al_2O_3 are seen at $2\Theta = \sim 21°$ and $\sim 29°$, and very small broad peaks indexed to $NbAlO_4$ are just forming, indicating that the crystallite size for this compound is small. Longer heating times at 1000 °C, (1000,2) and (1000,48), lead to the sharpening of the $NbAlO_4$ peaks as well as the peaks indexed to γ-Al_2O_3. The fact that no α-Al_2O_3 peaks were found in these scans shows the stabilizing effect of niobia on the alumina support. Figure 5-8 shows the XRD pattern of A-NA(.05), A-NA(.10), A-NA(.25) after the severe thermal treatment of (1000,48). The major XRD peaks assigned to γ-Al_2O_3 ($2\Theta = \sim 21°$ and $29°$) are readily seen in all of the scans. Notice also the sharpening of peaks indexed to $NbAlO_4$, especially the predominant feature (100% peak) at $2\Theta = 11.60°$ with the increasing coverage of niobia. The A-NA(.05) lacks any sharp features of this compound, but it does show small and broad peaks which indicate that it is on the detectable limits of the XRD equipment and suggest the size of the crystallites as ~ 3 nm or less.

5.2.3 DTA and SEM

DTA scans are not shown for the binary surface oxides because no compound formation or phase transformations could be observed in the collected scans. The silica aerogel supported niobia showed a flat profile for most of the entire range, but had a small noticeable endothermic valley around 50-100 °C indicating the evolution of water from the surface. The alumina aerogel supported niobia also showed a mostly flat scan indicative of no compound formation or phase transition; however, like the bulk alumina aerogel, the alumina supported oxides showed a broad endothermic valley from ~ 50 - 300 °C indicating that these samples chemisorbed water on the surface. Appendix C shows the hydroxyl

Figure 5-7: XRD OF A-NA(.25) AS A FUNCTION OF HEAT TREATMENT: A) (1000,-), B) (1000,2), AND C) (1000,48)

c) (1000,48)

b) (1000,2)

a) (1000,-)

Intensity (Arbitrary Units)

Diffraction Angle (2Θ), Degrees
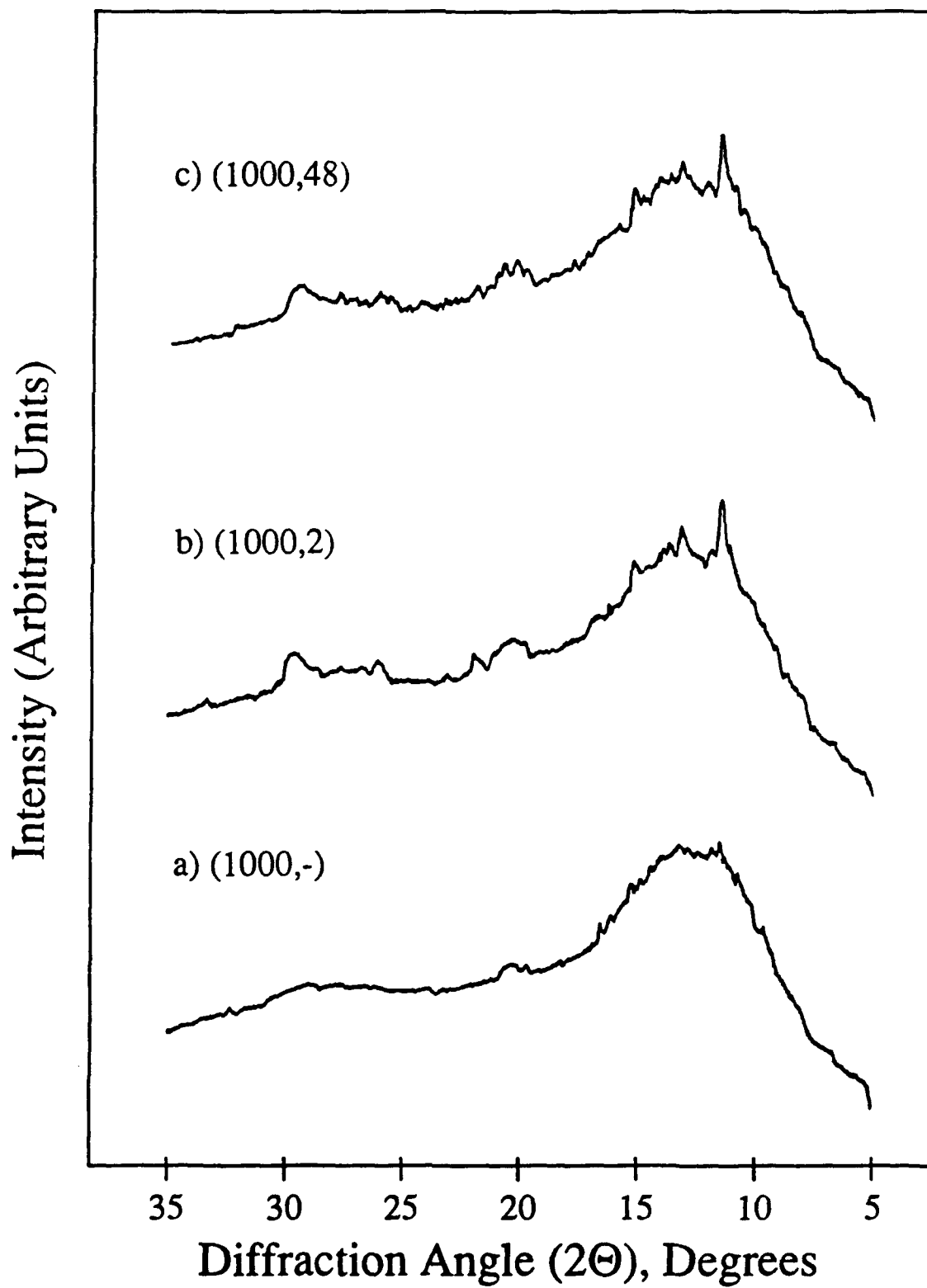
Figure 5-8: XRD OF ALUMINA AEROGEL SUPPORTED NIOBIA AFTER (1000,48): A) A-NA(.05), B) A-NA(.10), AND C) A-NA(.25)
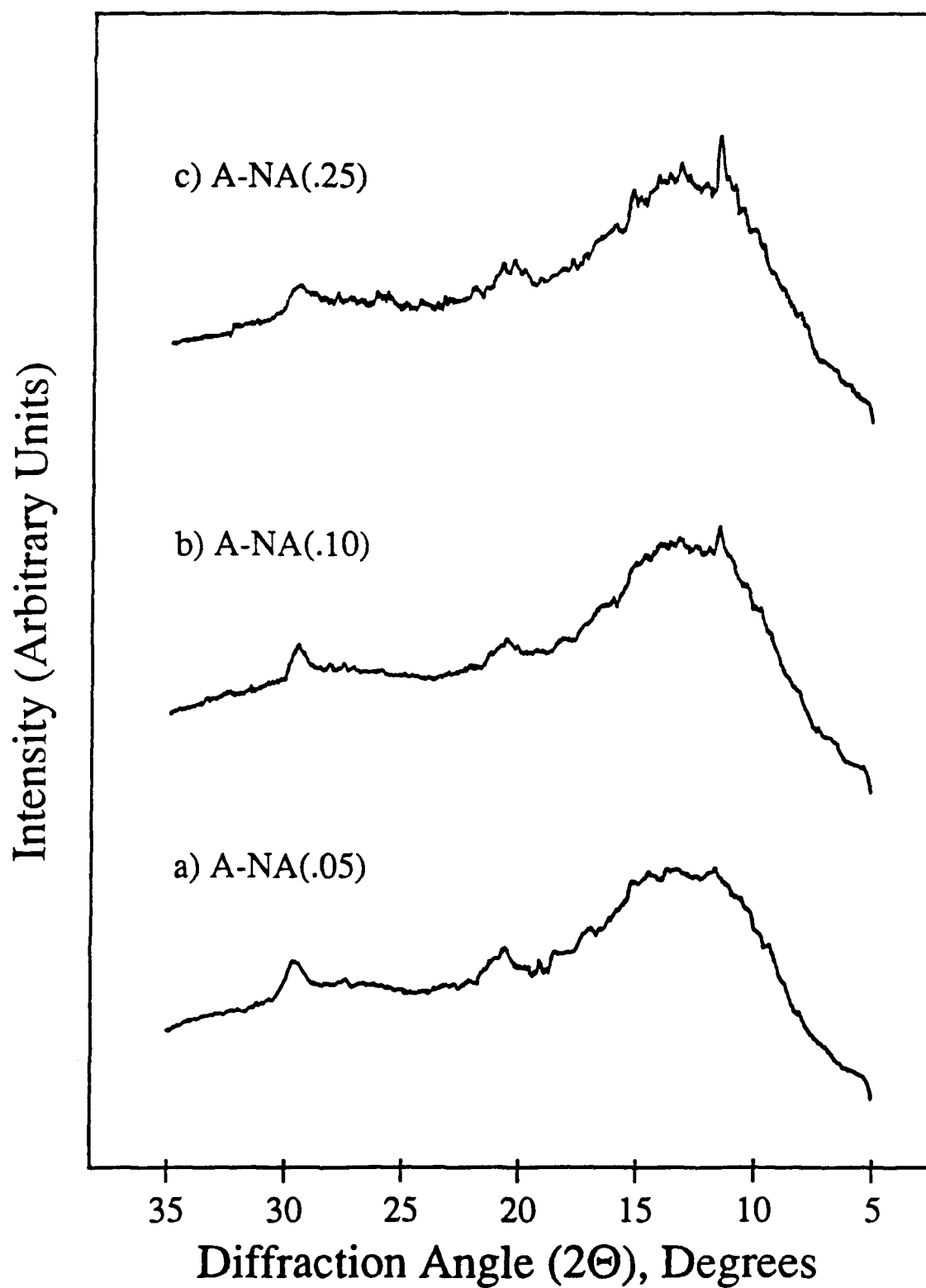
region of all supported oxides for both DRIFT and FTIR spectra and shows that the alumina supported oxides did indeed strongly chemisorb water.

SEM was employed to examine the morphology of the surface oxides, and was also used for elemental mapping and quantitative elemental composition analysis of the supported surface oxides. Figures 5-9, 5-10, and 5-11 show the SEM micrographs and elemental dot maps for the calcined A-NS(.25). Figure 5-9 shows that these particles have a "fluffy and sponge-like" morphology, similar to the other aerogels of niobia, A-NS25w and A-NA25w. The elemental niobium dot map in Figure 5-10 reveals a good dispersion of niobium atoms on the surface oxide. The silicon dot map does not show much information other than it is the major oxide because of its intensity (see Figure 5-11).

SEM micrographs and elemental dot maps for A-NA(.25) are shown in Figures 5-12, 5-13 and 5-14. As before with the silica aerogel supported niobia, A-NS(.25), we see a good dispersion for A-NA(.25) as revealed by the niobium atom dot map in Figure 5-13. The aluminum atom dot map in Figure 5-14 gives little information because of the intensity, but does show it is the major component in this supported oxide system. Both sets of these surface oxides reveal that niobia is dispersed when supported on either silica or alumina aerogels at a 25% monolayer coverage. Lower coverages of niobia would be expected to show even better dispersions. Table 5-5 lists the EDS elemental analysis results for the supported oxides of A-NS(.25) and A-NA(.25). Converting the elemental weight % composition into an actual oxide content yields values which are very close to those of the predicted oxide content. For A-NS(.25) the actual niobia content by EDS gives 25.5 wt.% or a difference from the predicted value of 7.6%; and the actual niobium oxide content for A-NA(.25) was 17.3 wt.% or a difference from the predicted value of only 3.6%. These small differences in actual to predicted oxide contents, assuming the micrograph and EDS analysis are representative of the entire surface oxide, lead us to conclude that we successfully synthesized well-dispersed niobia on silica and alumina aerogels to a coverage of 0.25 monolayer.

Figure 5-9: SEM MICROGRAPH OF A-NS(.25) (500,2) OVER WHICH
ELEMENTAL DOT MAPS WERE GENERATED
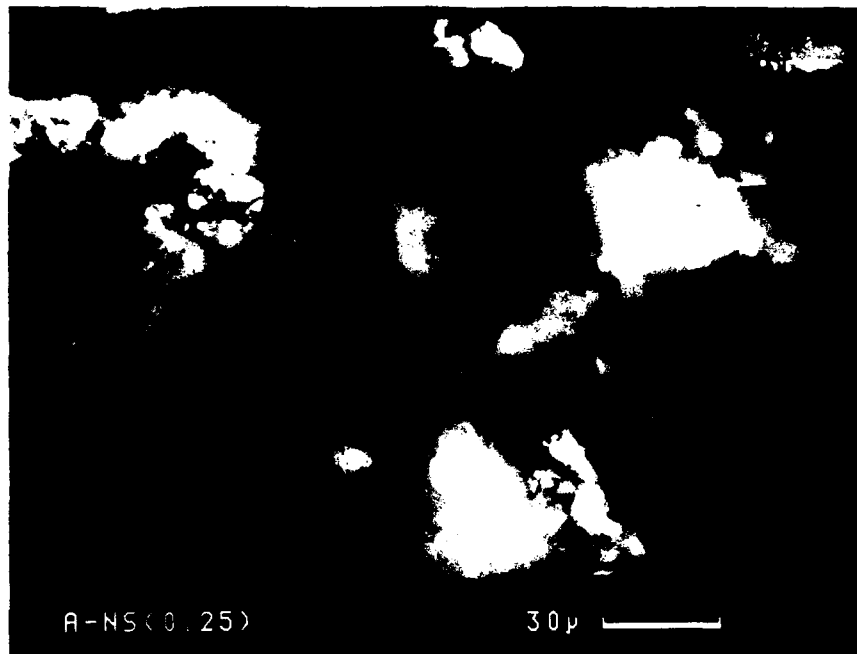
Figure 5-10: NIOBIUM DOT MAP FOR A-NS(.25) (500,2)
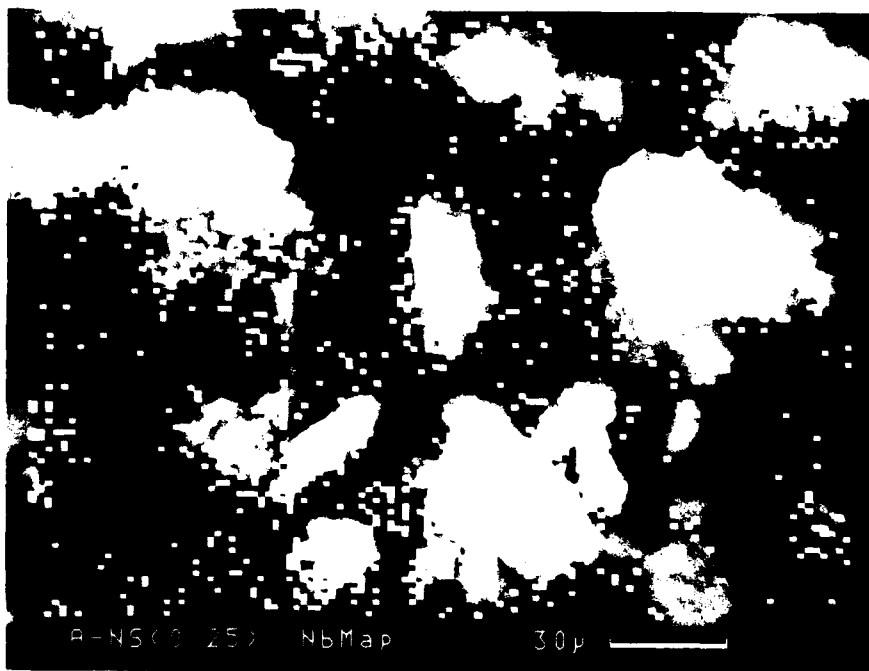
Figure 5-11: SILICON DOT MAP FOR A-NS(.25) (500,2)
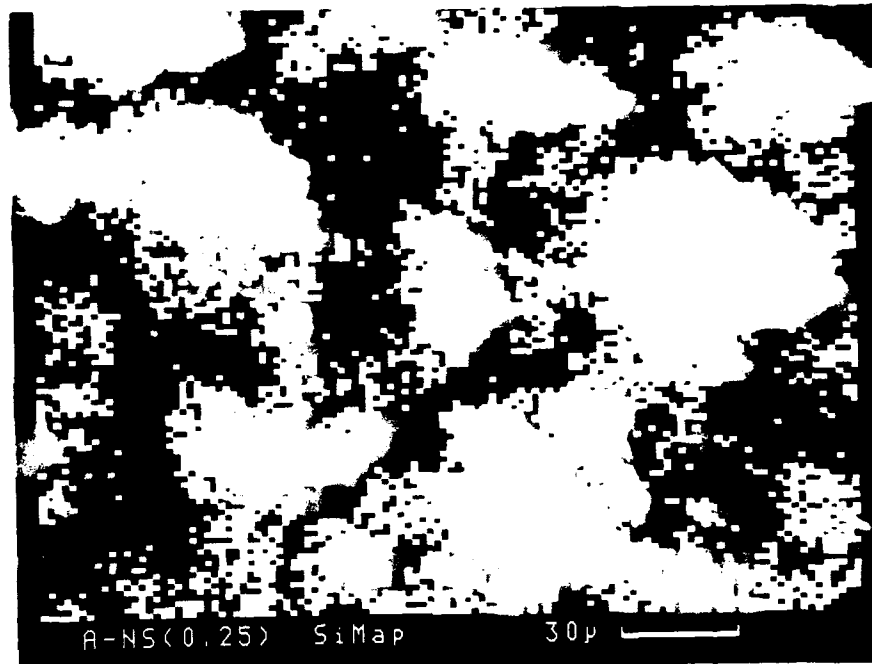
Figure 5-12: SEM MICROGRAPH OF A-NA(.25) (500,2) OVER WHICH
ELEMENTAL DOT MAPS WERE GENERATED
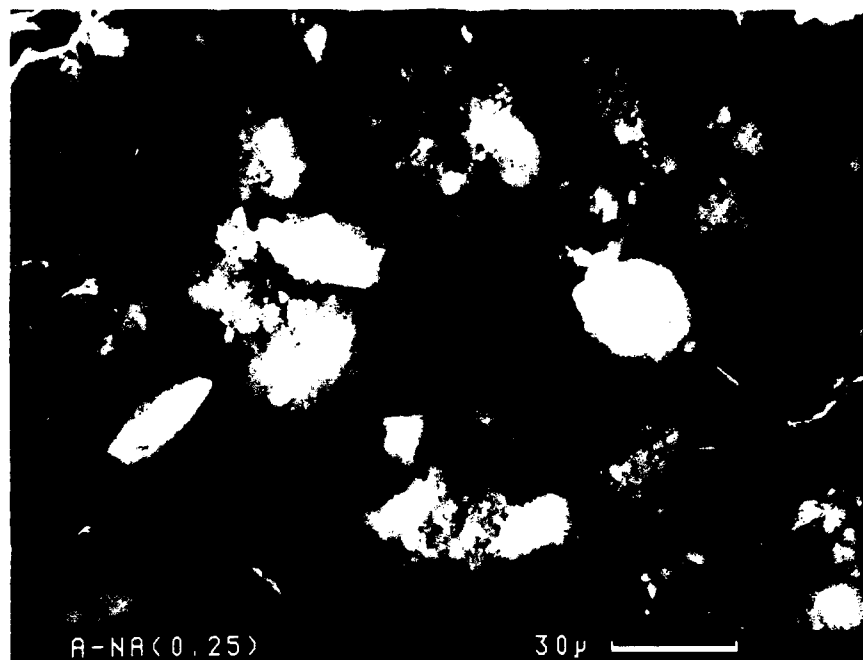
Figure 5-13: NIOBIUM DOT MAP FOR A-NA(.25) (500,2)
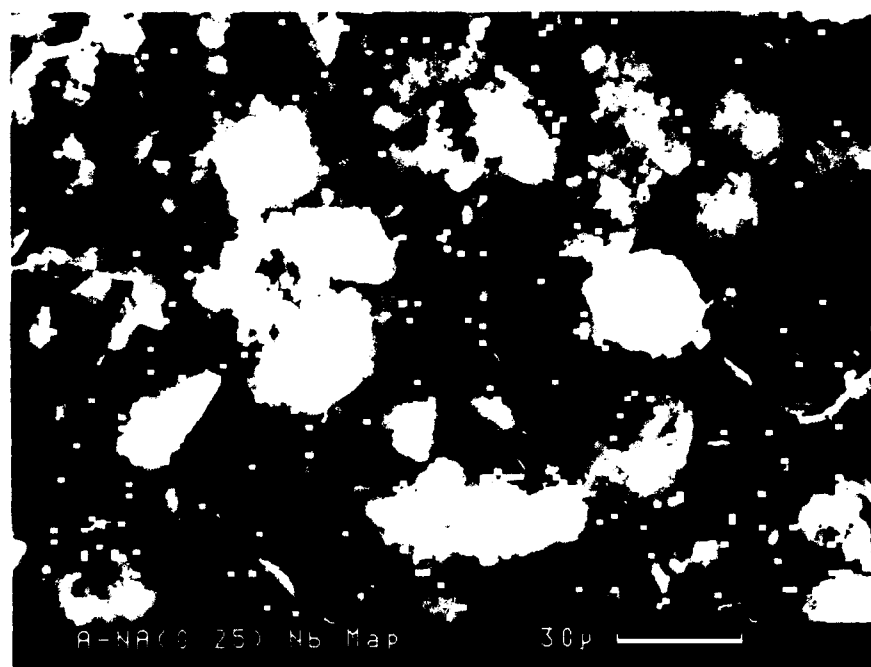
Figure 5-14: ALUMINUM DOT MAP FOR A-NA(.25) (500,2)

A-NA(0.25) Al Map   30μ
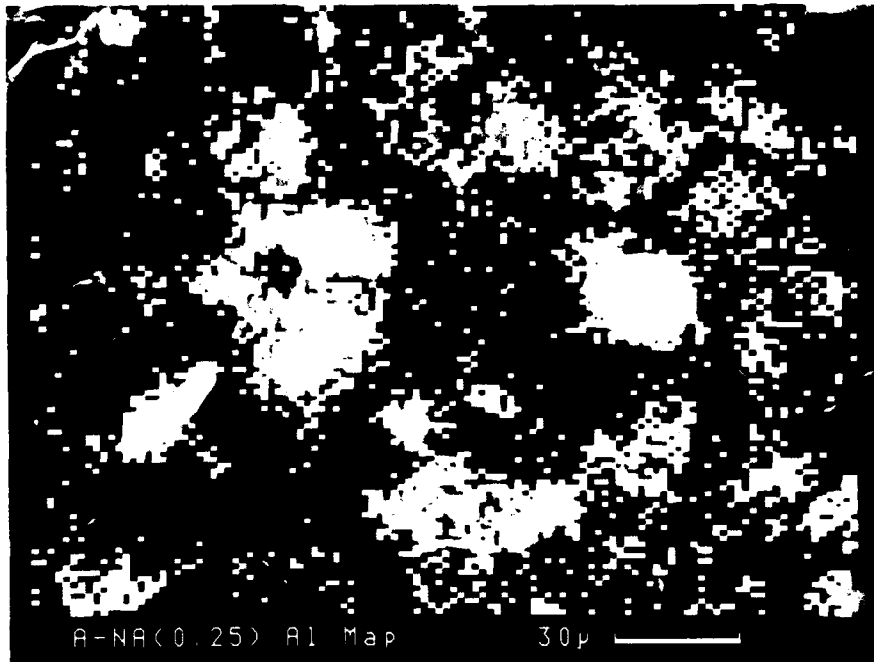
Table 5-5: RESULTS OF EDS ELEMENTAL ANALYSIS FOR SURFACE OXIDE
AEROGELS: A) A-NS(.25) AND B) A-NA(.25)

A) A-NS(.25) (500,2)

Sample	EDS Elemental Analysis		Actual Oxide Content		Predicted Oxide Content	
	Si wt%	Nb wt%	SiO_2 wt%	Nb_2O_5 wt%	SiO_2 wt%	Nb_2O_5 wt%
A-NS(.25)	66.2	33.8	74.5	25.5	76.3	23.7

B) A-NA(.25) (500,2)

Sample	EDS Elemental Analysis		Actual Oxide Content		Predicted Oxide Content	
	Al wt%	Nb wt%	Al_2O_3 wt%	Nb_2O_5 wt%	Al_2O_3 wt%	Nb_2O_5 wt%
A-NA(.25)	78.4	21.6	82.7	17.3	83.3	16.7

5.2.4 Laser Raman Spectroscopy (LRS)

LRS was used to examine the molecular vibration modes in the silica and alumina aerogel supported niobia samples. The spectra presented here will be interpreted, as in the previous chapters, by comparison with reference compounds of niobium oxide. Figure 5-15 shows LRS spectra of the silica aerogel supported niobia after a (600,2) heat treatment. No information is obtained after the (500,2) calcination due to the fluorescing background. All of these supported oxides: A-NS(.05), A-NS(.10), and A-NS(.25), show a small broad peak around 950 cm^{-1}. A-NS(.25) also shows a broad peak centered at ~ 680 cm^{-1} that is characteristic of the Nb-O stretch found in distorted NbO_6 octahedra. The sharper peaks in these spectra at ~ 605 cm^{-1} and ~ 490 cm^{-1} are characteristic of the SiO_2 support.[156, 204] The fact that no peaks around ~ 680 cm^{-1} are observed for A-NS(.05) and A-NS(.10), indicates that NbO_6 octahedra are not linking into units, and thus leads to the conclusion that these supported oxides are well dispersed. Figure 5-16 shows LRS spectra for A-NS(.25) after various thermal treatments. The heat treatment of (600,2) shows a small broad peak at ~ 950 cm^{-1} and a broad yet larger peak at ~ 680 cm^{-1}. These two peaks have been assigned to highly distorted (Nb=O) and slightly distorted octahedra (Nb-O), respectively.[67] The highly distorted band at ~ 930 cm^{-1}, which is also attributed to a surface phase of niobia, is still observed by LRS after the (1000,-) heat treatment. The peak attributable to slightly distorted NbO_6 octahedra sharpens and shifts by ~ 45 cm^{-1} to 725 cm^{-1}. This same type of shift is also seen when heat treating the niobia aerogel, by the ordering of the Nb-O stretches from an amorphous environment to a more crystalline structure of TT- or T-Nb_2O_5. We can also see the longer range of order being built in this surface oxide by the appearance of a peak at ~ 240 cm^{-1}.

Figure 5-17 shows the LRS spectra of the alumina aerogel supported niobia after a (600,2) heat treatment. No information is obtained after the (500,2) calcination due to the fluorescing background similar to that found for the silica aerogel supported oxides. A-

Figure 5-15: LRS SPECTRA OF SILICA AEROGEL SUPPORTED NIOBIA AFTER (600,2): A) A-NS(.05), B) A-NS(.10), AND C) A-NS(.25)
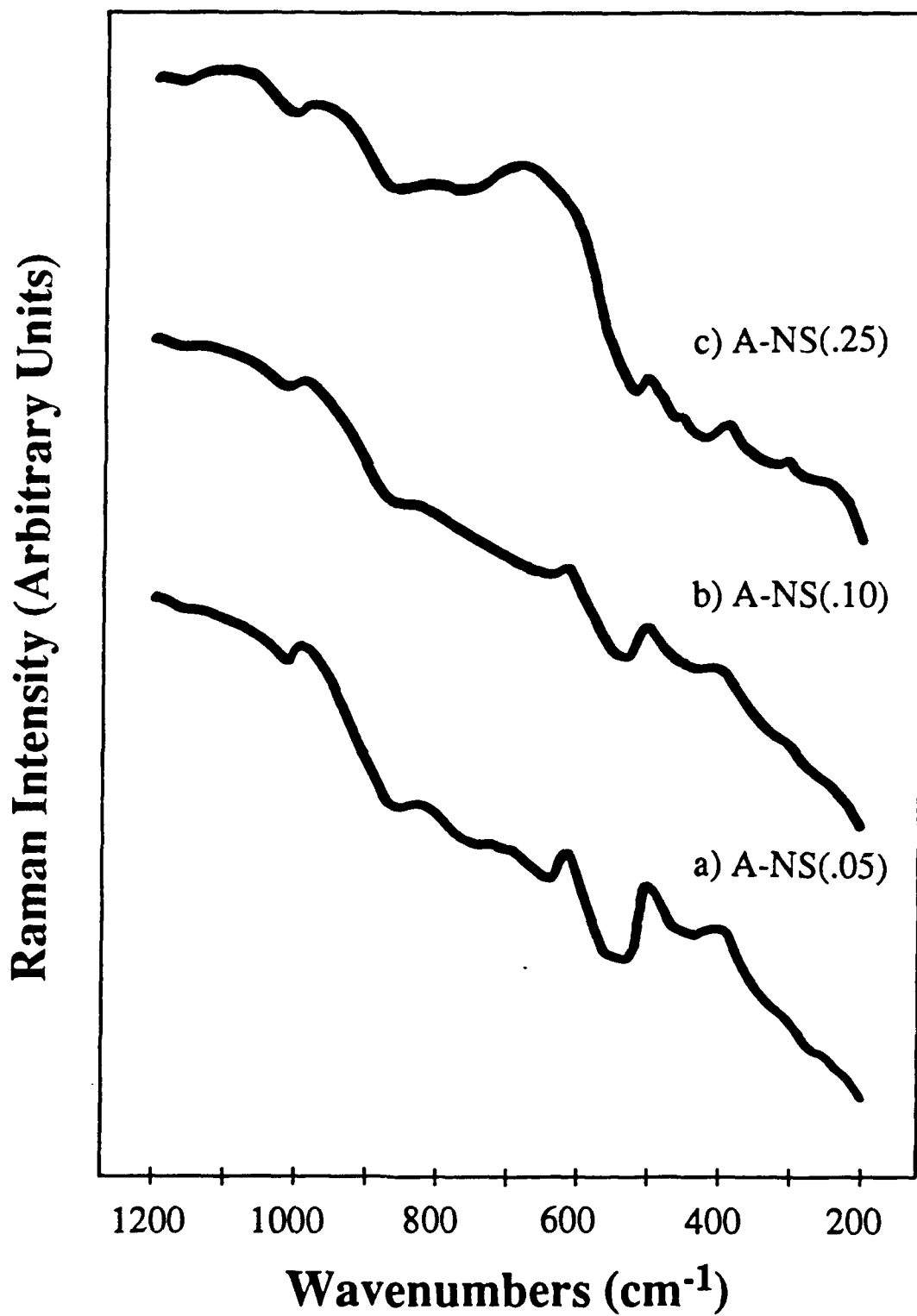
Figure 5-16: LRS SPECTRA OF A-NS(.25) AFTER HEAT TREATMENT: A) (500,2), B) (600,2), AND C) (1000,-)
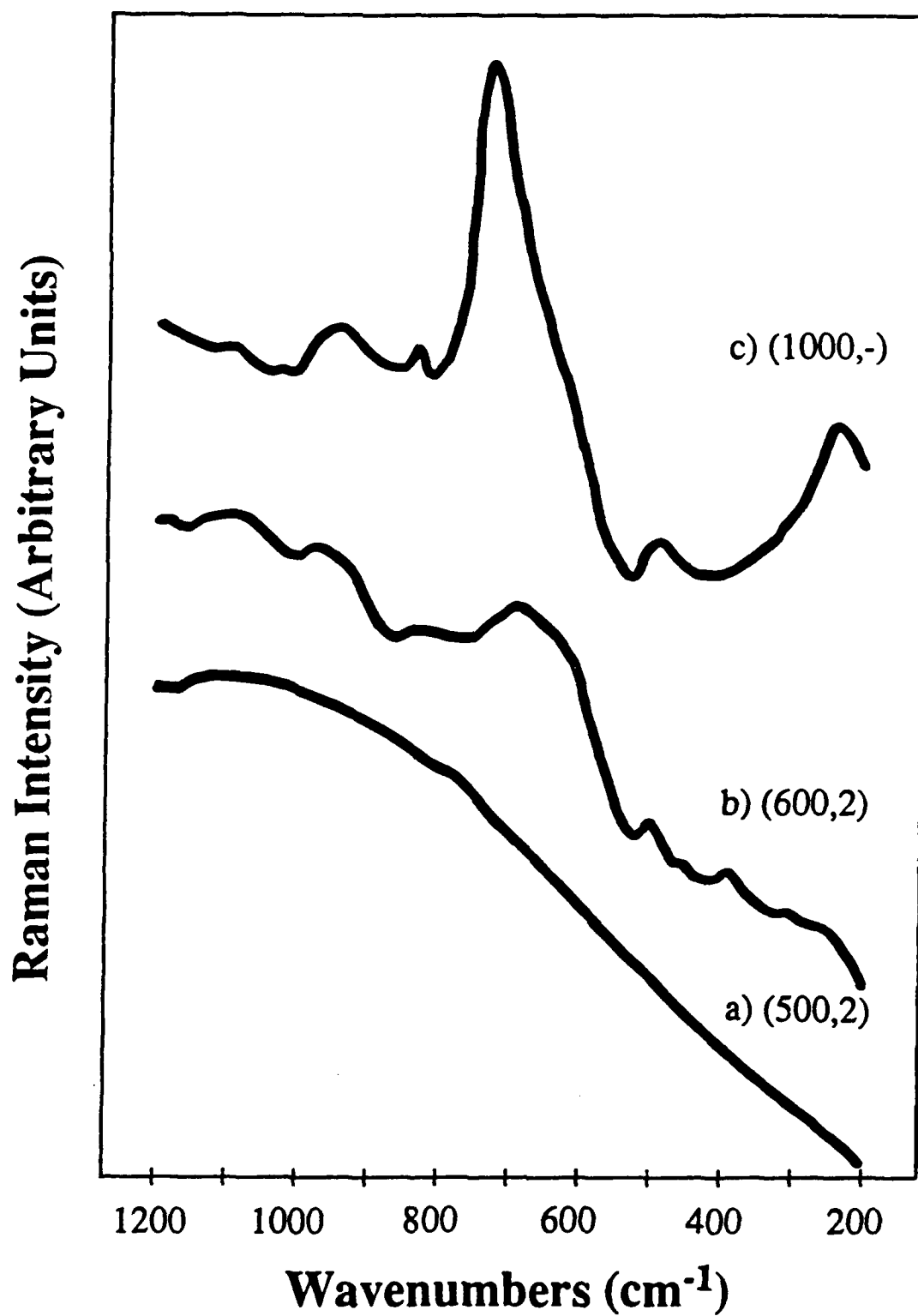
Figure 5-17: LRS SPECTRA OF ALUMINA AEROGEL SUPPORTED NIOBIA
AFTER (600,2): A) A-NA(.05), B) A-NA(.10), AND C) A-NA(.25)
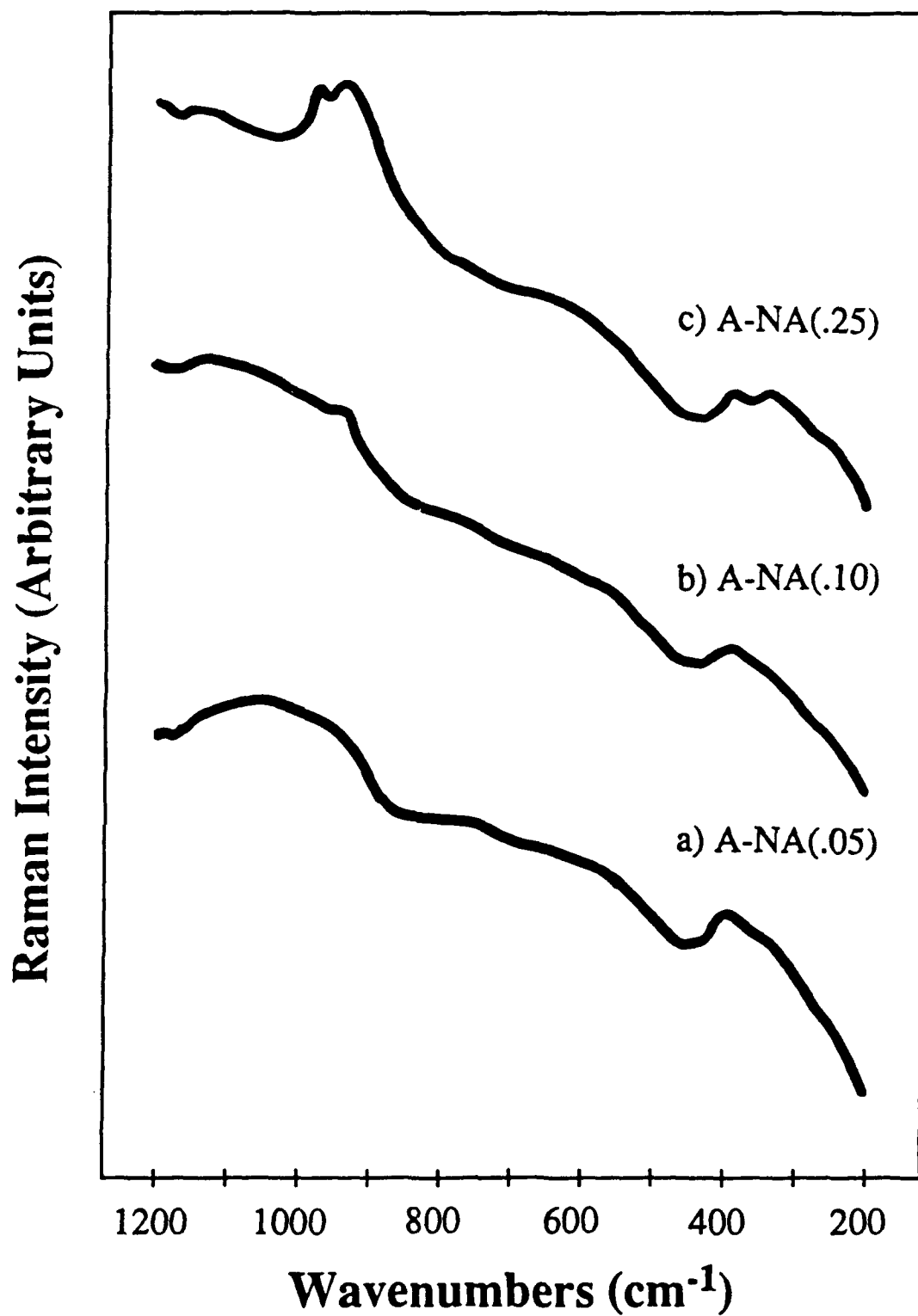
NA(.05) shows no spectral features throughout the entire range. Increasing the loading of niobia to 10% monolayer coverage, A-NA(.10), results in the appearance of a feature around 930 cm^{-1}, and further increase in loading to 25% coverage yields two peaks around 970 cm^{-1} and 935 cm^{-1} corresponding to niobia surface oxide species that are highly distorted and in either a tetrahedral or octahedral environment.[47, 67, 92] Figure 5-18 shows the LRS spectra of A-NA(.25) after various heat treatments. The standard calcination of (500,2) reveals no information about the sample because of the strong fluorescing background, while the (600,2) heat treatment reveals peaks at ~ 970 and 935 cm^{-1} corresponding to highly distorted niobia groups in possession of Nb=O bonds. The vibrations around 630 cm^{-1} indicate the formation of slightly distorted octahedra and the lower vibrations at ~ 340 cm^{-1} are bending modes of Nb-O-Nb groups. After the (1000,-) heat treatment, we have seen that A-NA(.25) undergoes a solid-state reaction to form crystalline NbAlO$_4$ from our earlier XRD studies. This spectrum matches identically to the spectrum for pure NbAlO$_4$.[94] The γ-Al$_2$O$_3$ is Raman inactive and thus does not contribute to the spectrum.[85]

5.2.4.1 In-situ LRS (Dehydrated)

In-situ Raman studies were performed on the (600,2) heat treated samples of A-NS(.10) and A-NA(.25) to provide additional discrimination between surface and bulk functionalities, since moisture has been found to coordinate only to surface functionalities.[188] The *in-situ* LRS spectra of A-NS(.10) (600,2) for hydrated and dehydrated (450 °C, 30 min) species is shown in Figure 5-19. The hydrated silica supported oxide shows a broad peak at ~ 950 cm^{-1}. Upon dehydration this peak splits into two distinct features with the higher frequency located as a sharp peak at ~ 980 cm^{-1} and the lower one at ~ 925 cm^{-1}. The shifts of these peaks and high frequencies of the vibrations indicate coordination of moisture to surface functionalities and possibly highly distorted tetrahedral or octahedral complexes.[67, 94, 188] The fact that there are two high

Figure 5-18: LRS SPECTRA OF A-NA(.25) AFTER HEAT TREATMENT: A) (500,2), B) (600,2), AND C) (1000,-)
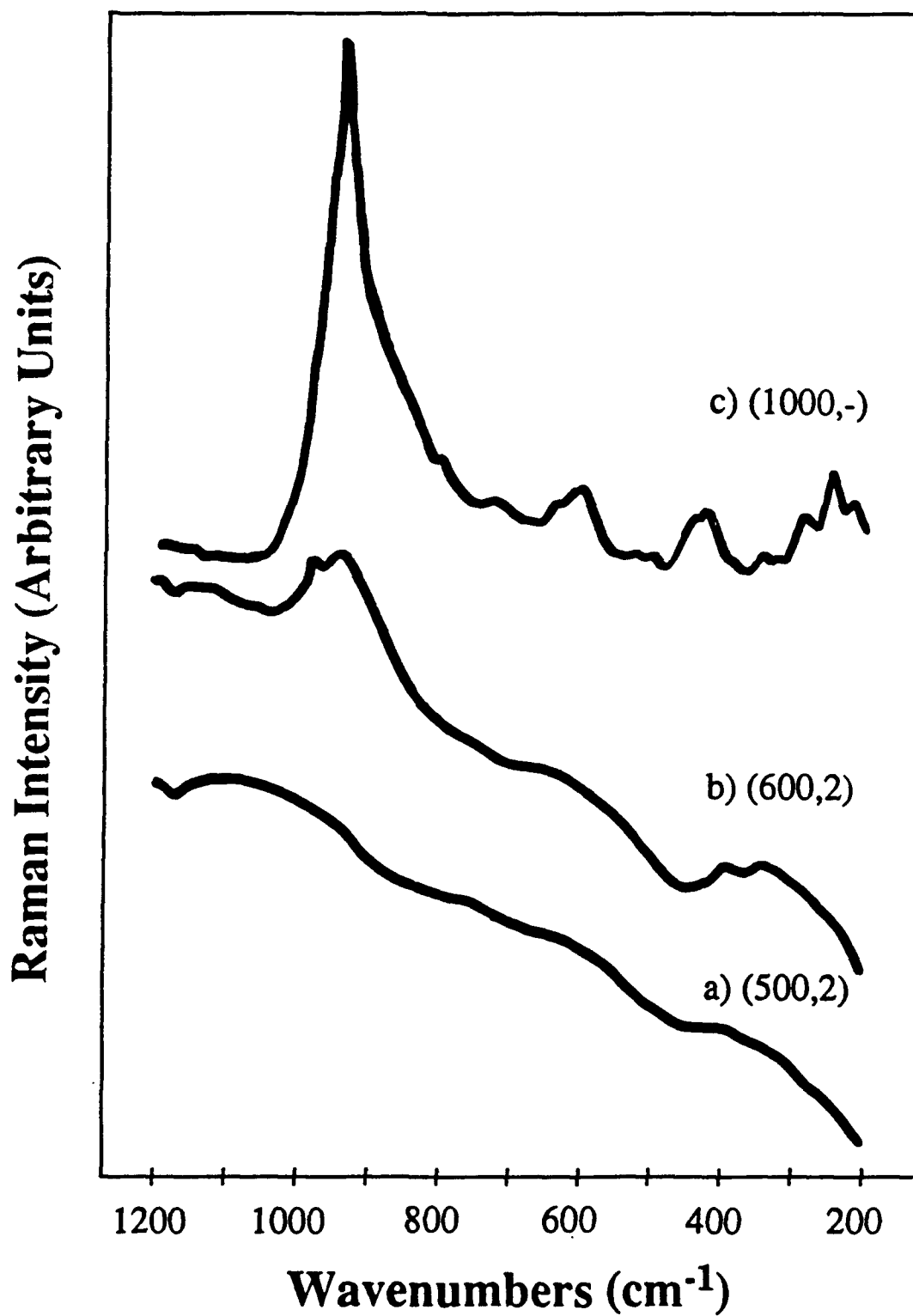
Figure 5-19: IN-SITU LRS SPECTRA OF A-NS(.10) AFTER (600,2): A) HYDRATED AND B) DEHYDRATED (450, 30 min)
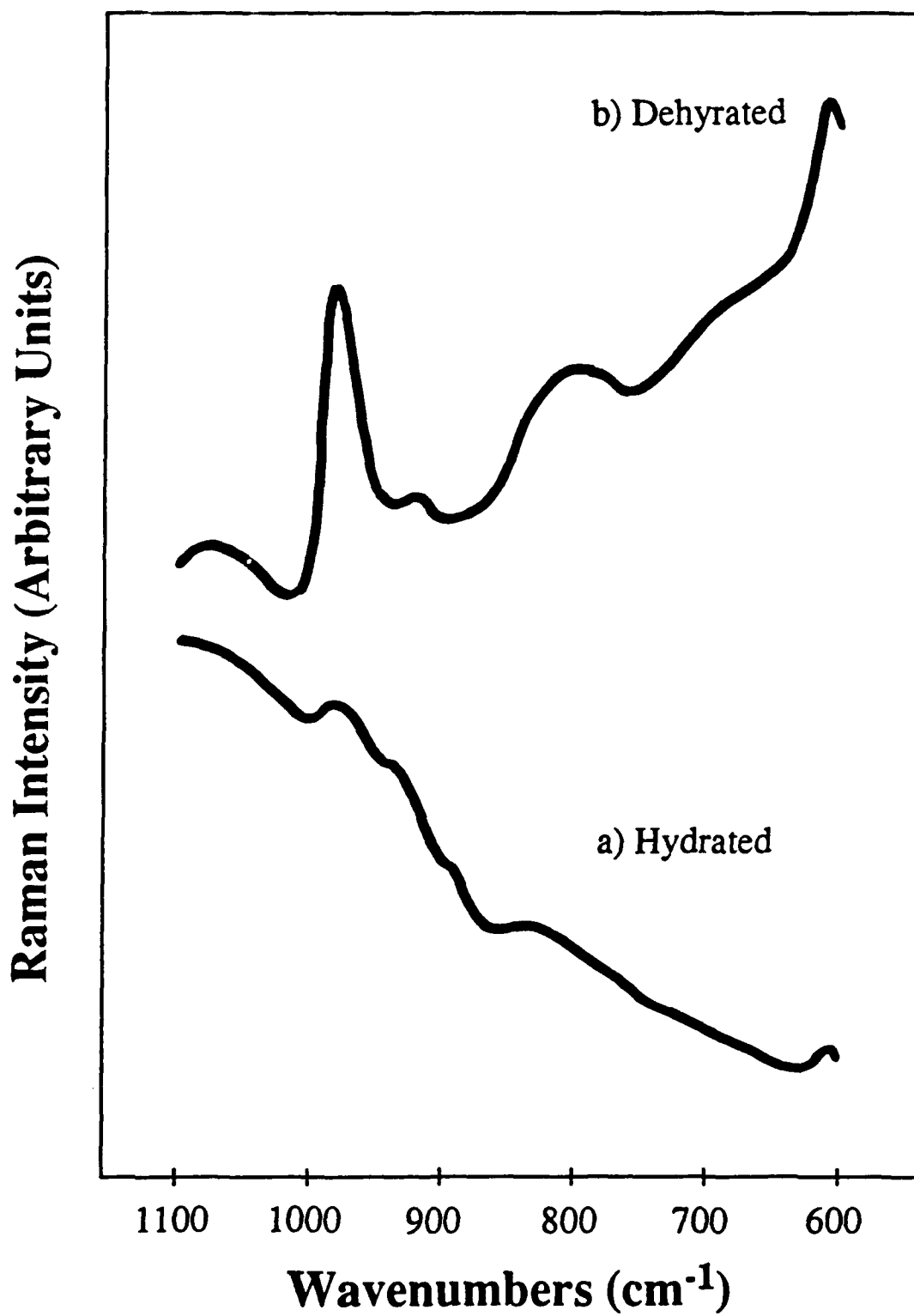
frequency vibrations indicates the possibility of two highly distorted groups on this silica aerogel supported niobia. The broad peaks around 800 and 610 cm^{-1} are characteristic of the silica support.[204] Notice also the absence of peaks at ~ 650 cm^{-1} which would indicate slightly distorted NbO_6 octahedra, thus this technique yields strong evidence that niobia is well dispersed on the silica aerogel at a 10% monolayer coverage. These results are similar to those found by Jehng for a 2 wt.% Nb_2O_5-SiO_2 surface oxide.[98]

Figure 5-20 shows the *in-situ* Raman spectra for A-NA(.25) (600,2) in both hydrated and dehydrated (450 °C, 30 min) conditions. The hydrated alumina supported niobia surface oxide reveals two bands around 970 and 935 cm^{-1} indicating the existence of two highly distorted niobia environments, either tetrahedral (NbO_4) or octahedral (NbO_6). The lower frequency is merely assigned to a longer Nb=O bond that has less distortion and a better distribution of charge throughout its complex. Dehydrating this surface oxide shifts the peaks to ~ 990 and 945 cm^{-1}, respectively. This peak movement is indicative that water is coordinated to the surface species. There are also broad features in the dehydrated Raman spectrum around ~ 650 cm^{-1} that coincide with bands of slightly distorted octahedra as found in a high loading of Nb_2O_5 on Al_2O_3 (19 wt.%).[67] Thus, these *in-situ* Raman results along with the hydrated LRS spectra seem to confirm that both the silica aerogel supported niobia and alumina aerogel supported niobia contain highly distorted groups containing Nb=O bonds. High enough loadings of niobia on the silica and alumina aerogel supports give rise to slightly distorted NbO_6 octahedra, an indication of a decrease in niobia dispersion. This fact is much more apparent on the silica aerogel supported niobia.

5.2.5 Diffuse Reflectance Infrared Spectroscopy (DRIFT)

DRIFT spectra for A-NS(.25) and A-SiO_2 are shown in Figure 5-21, and the subtraction spectra of A-NS(.05), A-NS(.10), and A-NS(.25) minus the background of A-SiO_2 are shown in Figure 5-22. Figure 5-21 shows the complicated nature of the DRIFT spectra and the spectral differences between A-NS(.25) and the background of A-SiO_2.

Figure 5-20: IN-SITU LRS SPECTRA OF A-NA(.25) AFTER (600,2): A) HYDRATED
AND B) DEHYDRATED (450, 30 min)
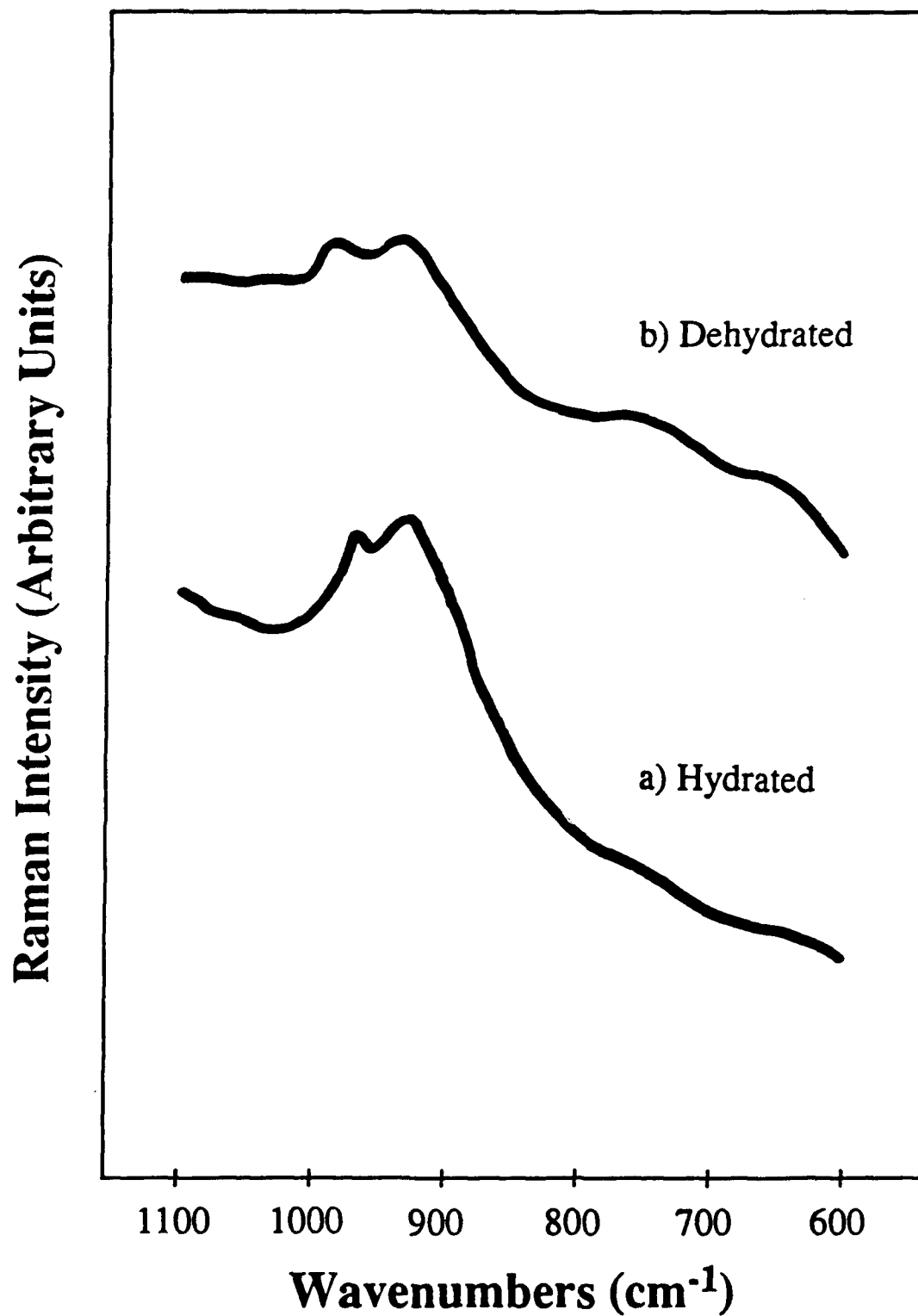
Figure 5-21: DRIFT SPECTRA OF A-NS(.25) AND A-SiO$_2$
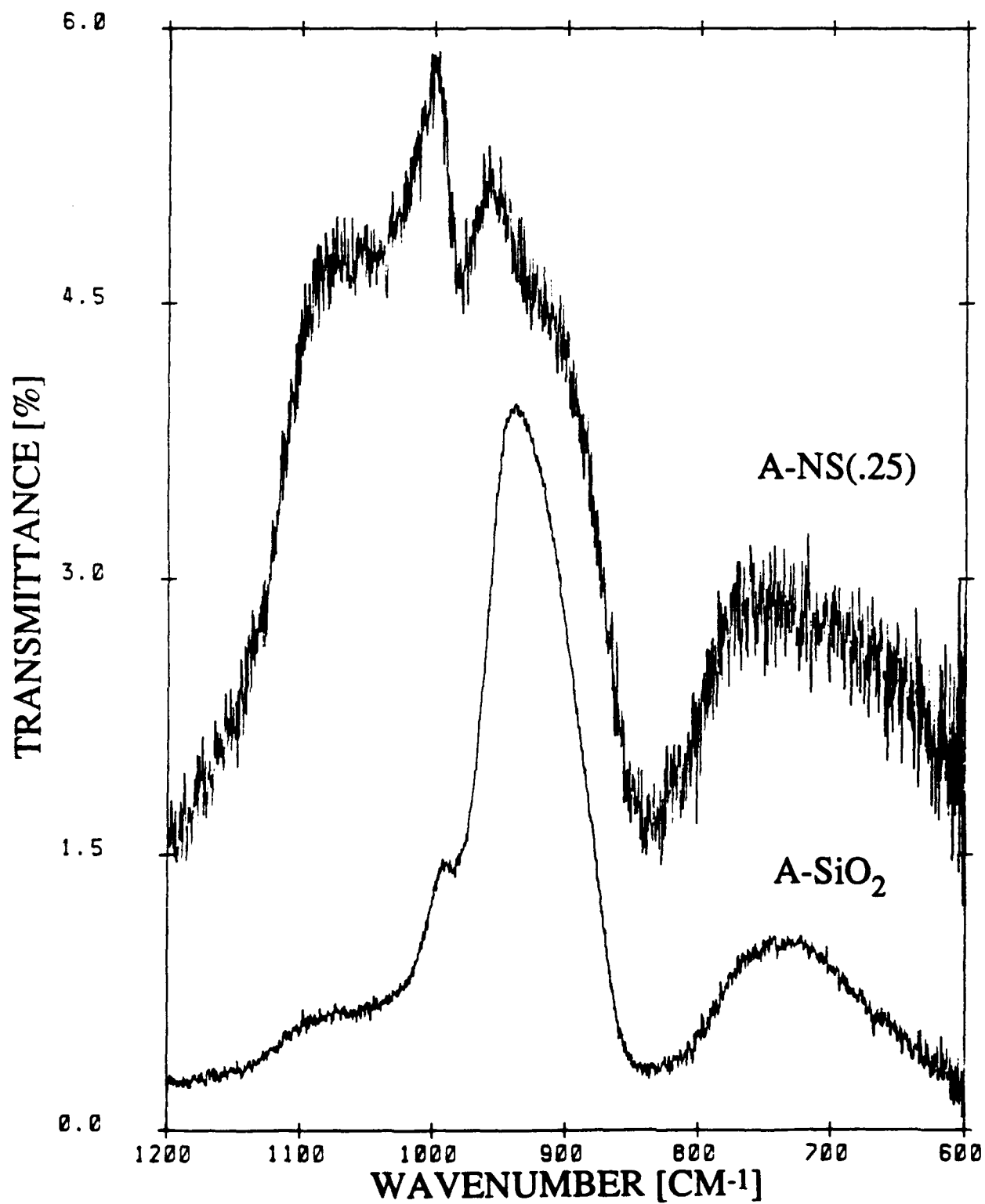
Figure 5-22: DRIFT SUBTRACTION SPECTRA OF A-NS(.25), A-NS(.10), AND A-NS(.05) (TOP TO BOTTOM)
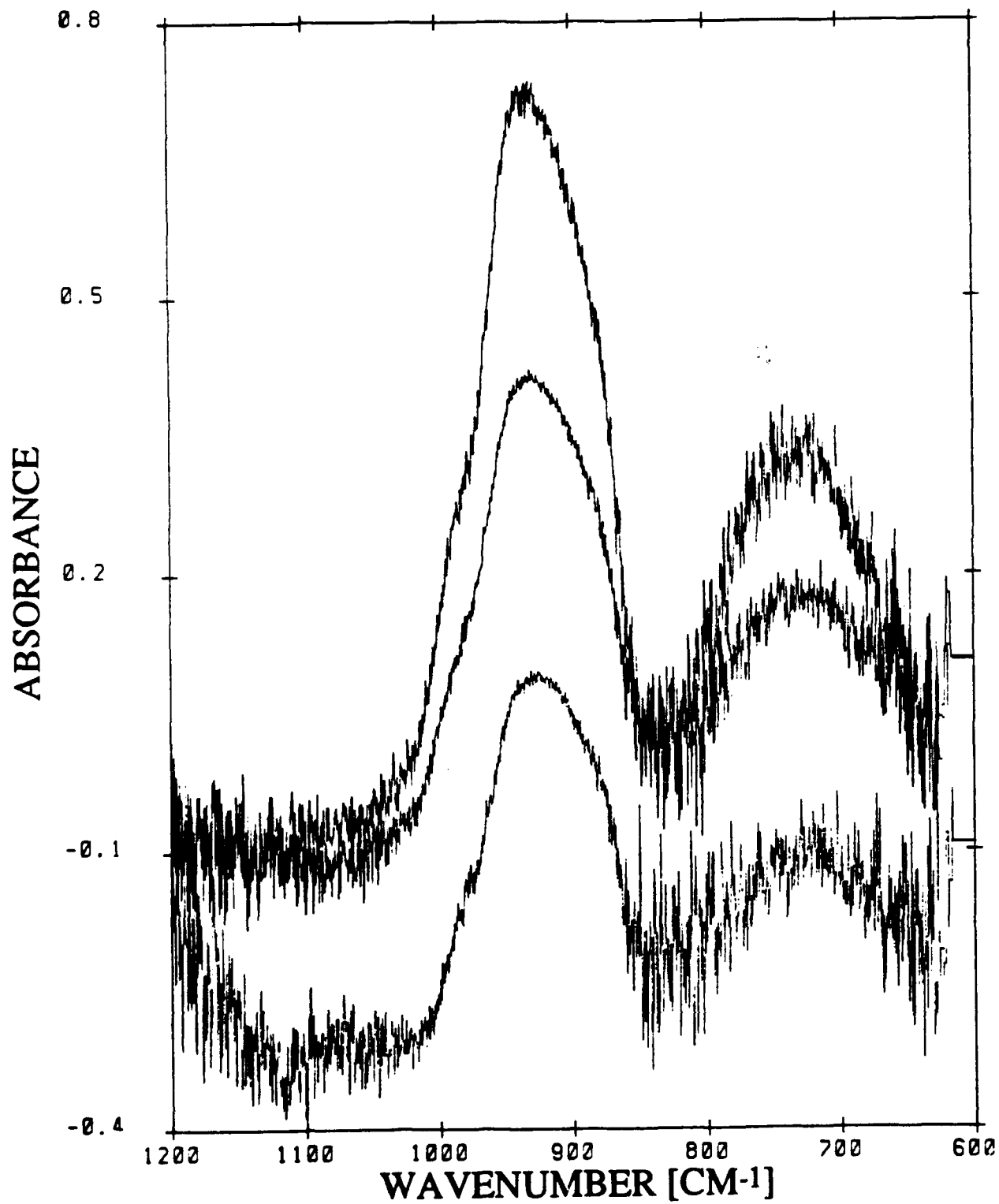
The one main difference of the A-NS(.25) and A-SiO$_2$ spectra is in the region of 900 - 930 cm^{-1}. Interpretation of this peak was based upon the frequency assignments of niobium reference compounds, and was assigned to a niobium oxygen double bond.[205, 206, 207] This peak is more prominent as seen by the subtraction spectra in Figure 5-22. Notice in this figure a broad peak at ~ 740 cm^{-1} is also evident and has been assigned to Nb-O-Nb linkages.[208] The relative ratios of the 920 and 740 cm^{-1} peaks increased with decreasing niobia content on the surface oxides, corresponding to an increased distribution at the lower coverages. The largest increase in the relative ratio was noted for A-NS(.25) to A-NS(.10). The terminal double bond, Nb=O, is indicative of a highly distorted niobia complex that is present as either a tetrahedral or octahedral species; and the appearance, or increase, of the Nb-O-Nb linkages probably results from linking these highly distorted or slightly distorted octahedra into overlayers of niobia on the silica substrate. These results confirm our findings from LRS that these silica aerogel supported oxides do indeed contain terminal Nb=O groups. This same type of study was attempted for the alumina aerogel supported niobia system; however, the strong absorbance of alumina in this region made acquisition of data difficult. Appendix C contains the hydroxyl region from both FTIR and DRIFT studies of these alumina aerogel supported oxides as well as all materials synthesized in this study.

5.3 Chemical Property Characterization of Surface Oxide Aerogels

5.3.1 Acid Strength/Acidity with n-Butylamine Titration

The acid strength and acidity for all of the calcined silica supported surface oxides are shown in Table 5-6 (mmoles/g), and in Table 5-7 (mmoles/g Nb$_2$O$_5$) which also contains the heat treated, (1000,-), samples. Figure 5-23 shows the acidity (mmoles/g) of silica aerogel supported niobia versus acid strength (pKa). Earlier results in Chapter 3 showed that silica is weakly acidic and has an acidity of 0.28 mmoles/g at pKa = +4.8,

Table 5-6: ACID STRENGTH OF SILICA AEROGEL SUPPORTED NIOBIA : ACIDITY (MMOLES/g) VERSUS pKa

	Acidity (mmoles/g)					
	pKa					
Sample	+4.8	+3.3	+1.5	-3.0	-5.6	-8.2
A-NS(.25) (500,2)	0.61	0.42	0.39	0.38	0.32	0.19
A-NS(.10) (500,2)	0.51	0.25	0.22	0.21	0.17	0.067
A-NS(.05) (500,2)	0.41	0.16	0.15	0.13	0.13	0.031
A-NS(.025) (500,2)	0.74	0.11	0.093	0.080	0.074	0.0057

Table 5-7: *ACID STRENGTH OF HEAT TREATED SILICA AEROGEL SUPPORTED NIOBIA : ACIDITY (MMOLES/G Nb_2O_5) VERSUS pKa*

	Acidity (mmoles/g Nb_2O_5)					
	pKa					
Sample	+4.8	+3.3	+1.5	-3.0	-5.6	-8.2
A-NS(.25) (500,2)	2.87	1.99	1.86	1.80	1.50	0.90
A-NS(.25) (1000,-)	2.46	1.23	1.12	0.99	0.89	0.49
A-NS(.10) (500,2)	5.34	2.56	2.33	2.25	1.82	0.70
A-NS(.10) (1000,-)	5.75	1.56	1.53	1.46	1.35	0.64
A-NS(.05) (500,2)	7.91	3.06	2.90	2.56	2.42	0.59
A-NS(.05) (1000,-)	8.85	3.03	2.97	2.69	2.31	0.47
A-NS(.025) (500,2)	24.06	3.52	3.04	2.63	2.44	0.19
A-NS(.025) (1000,-)	17.87	3.43	2.71	2.60	2.09	0.17

Figure 5-23: SILICA AEROGEL SUPPORTED NIOBIA ACIDITY (/G) VS. pKa
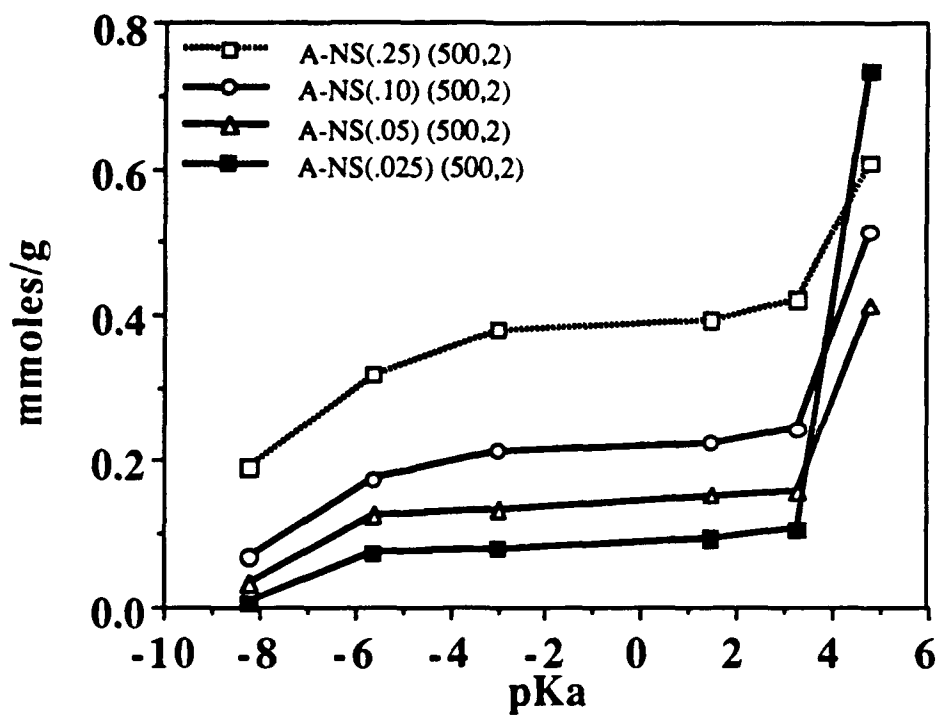
Figure 5-24: SILICA AEROGEL SUPPORTED NIOBIA ACIDITY (/G Nb_2O_5) VS. pKa
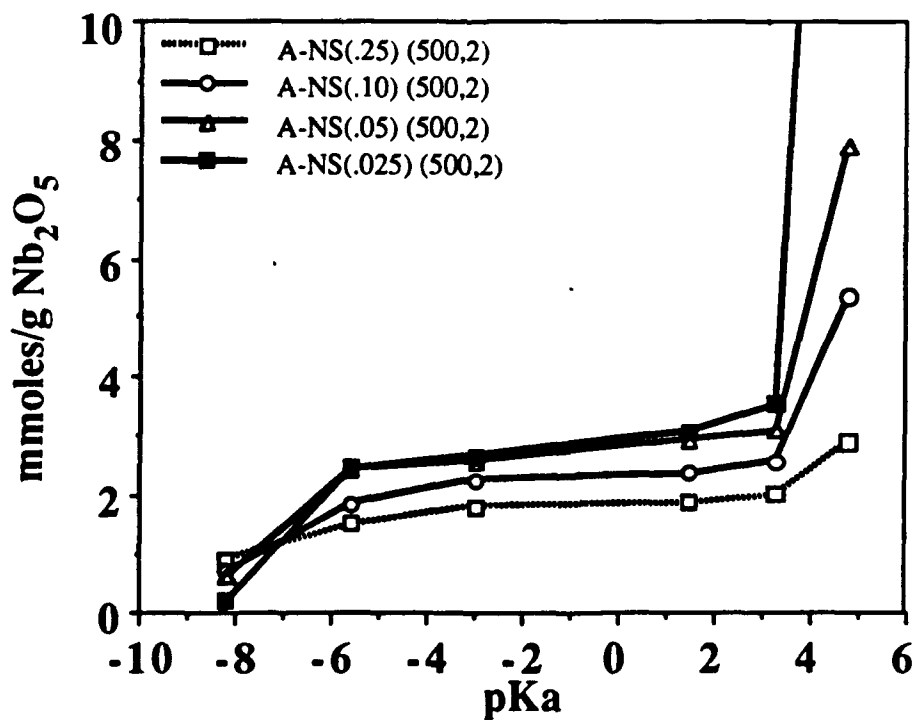
with no higher acid strength in the indicator range. With this in mind it appears that any acidity which is developed by depositing or grafting niobia on the silica aerogel can be attributed entirely to the interaction of niobia with the silica matrix. Figure 5-23 shows what one would expect to see, i.e. the higher the niobia loading the more acidity that is developed. This figure which shows acidity in terms of mmoles/g total sample gives no indication of how well the niobia is distributed on the surface of silica. In order for us to probe this distribution, we need to normalize the acidity with respect to the amount of niobia. Figure 5-24 shows the acidity (mmoles/g Nb_2O_5) versus acid strength for all silica aerogel supported niobia. Notice that as we go down in niobia loading, the normalized acidity across the majority of the acid strength range ($-5.6 \le pKa \le +3.3$) goes up, and levels off around A-NS(.05), a 5% monolayer coverage of niobia on silica. Going to an even lower coverage of 2.5% niobia [A-NS(.025)] gives the same acidity (mmoles/g Nb_2O_5) as the previous 5% coverage. The high acidity seen at the acid strength of pKa = +4.8 is attributed to the silica support and is an artifact of the normalization procedure. At the strongest acid site, pKa = -8.2, there is less acidity, on a per g Nb_2O_5 basis, for both of the well dispersed supported binary oxides of A-NS(.05) and A-NS(.025), over the other silica supported oxides of A-NS(.25) and A-NS(.10). Later pyridine adsorption studies will confirm that the higher coverage of niobia in A-NS(.25) leads to higher acid strengths than the lower coverage counterpart of A-NS(.05).

Figure 5-25 shows the acidity (mmoles/g Nb_2O_5) of the silica aerogel supported niobia after both the standard calcination and a (1000,-) heat treatment. Notice how the acidities of both A-NS(.25) and A-NS(.10) decline dramatically by approximately 40% and 35%, respectively, throughout most of the acid strength range. The A-NS(.05) shows very little decline, if any at all, after a (1000,-) heat treatment and indicates the good dispersion of this silica supported oxide. The lower niobia loading of A-NS(.025) shows this same identical behavior and in fact, lies on top of the acidity curve for A-NS(.05). It has been left off this figure for clarity. The large acidity at pKa = +4.8 can be attributed to

Figure 5-25: SILICA AEROGEL SUPPORTED NIOBIA ACIDITY (/G Nb_2O_5)
CALCINED AND HEAT TREATED (1000,-) VERSUS pKa
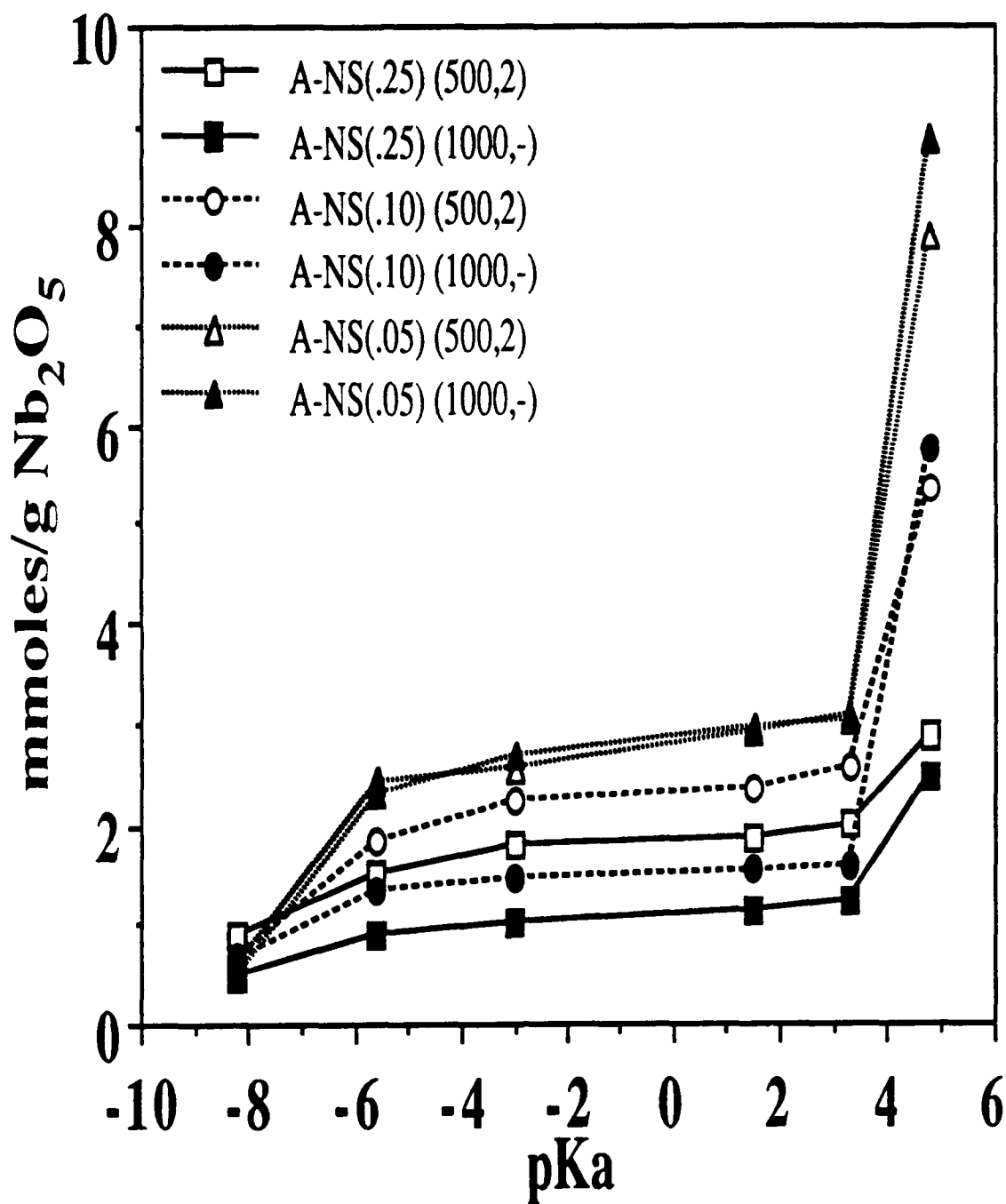
a silica support effect brought on by the normalization procedure, i.e. as the coverage of niobia goes down, more weakly acidic silica is revealed and hence the acidity in this +4.8 range goes up. Also we are dividing or normalizing with respect to Nb_2O_5 and this number is smaller as we go to lower coverages.

Table 5-8 reveals the acidity (mmoles/g) and acid strength for all calcined alumina aerogel supported niobia. Table 5-9 lists the same information as above, but on a per g Nb_2O_5 basis as well as containing the (1000,-) heat treated samples. Figure 5-26 shows the acidity (mmoles/g) of the alumina supported surface oxides versus acid strength. The alumina aerogel showed no acidity throughout the entire acid strength range, therefore any acidity developed in the surface oxides may be attributed to the addition of niobia and the interaction it has with the alumina support. This figure shows that the total acidity on a per g sample basis increases as the loading of niobia is increased, i.e. the more niobia there is on the sample the more acidity that is developed, since the acidity actually stems from the addition of the niobia to the alumina substrate. This figure gives no indication of the distribution of niobia on alumina. This was determined by plotting the normalized acidity (with respect to niobia) versus acid strength, and is shown in Figure 5-27. This figure shows that the acidity (mmoles/g Nb_2O_5) actually increases as one goes down in niobia coverage for the alumina aerogel supported niobia. The normalized acidity goes up from A-NA(.25) to A-NA(.10); however, no further significant increase is noted when we decrease the coverage to the 5% monolayer coverage of A-NA(.05). Therefore, we can conclude from this figure that the 10% monolayer coverage of niobia on the alumina aerogel is well-distributed. Figure 5-28 shows the normalized acidity for the alumina aerogel supported niobia after the standard calcination of (500,2) and the (1000,-) heat treatment. Immediately, one notices the decrease in acidity of A-NA(.25) after (1000,-). This decrease in acidity of ~ 65% of its original calcined acidity throughout the entire range, was attributed to the compound formation of $NbAlO_4$, and was confirmed by XRD and LRS analysis. The lower loadings of A-NA(.10) and A-NA(.05) do not show any

Table 5-8: ACID STRENGTH OF ALUMINA AEROGEL SUPPORTED NIOBIA : ACIDITY (MMOLES/g) VERSUS pKa

	Acidity (mmoles/g)					
	pKa					
Sample	+4.8	+3.3	+1.5	-3.0	-5.6	-8.2
A-NA(.25) (500,2)	0.28	0.24	0.19	0.17	0.15	0.026
A-NA(.10) (500,2)	0.14	0.12	0.097	0.087	0.072	0.020
A-NA(.05) (500,2)	0.071	0.058	0.051	0.045	0.031	0.0095

Table 5-9: ACID STRENGTH OF HEAT TREATED ALUMINA AEROGEL SUPPORTED NIOBIA : ACIDITY (MMOLES/g Nb_2O_5) VERSUS pKa

	Acidity (mmoles/g Nb_2O_5)					
	pKa					
Sample	+4.8	+3.3	+1.5	-3.0	-5.6	-8.2
A-NA(.25) (500,2)	1.67	1.42	1.13	1.00	0.90	0.16
A-NA(.25) (1000,-)	0.53	0.49	0.42	0.33	0.22	0.10
A-NA(.10) (500,2)	1.84	1.62	1.27	1.13	0.94	0.26
A-NA(.10) (1000,-)	2.02	1.41	1.13	0.93	0.65	0.00
A-NA(.05) (500,2)	1.79	1.45	1.28	1.14	0.79	0.24
A-NA(.05) (1000,-)	1.89	1.49	1.36	1.02	0.63	0.00

Figure 5-26: ALUMINA AEROGEL SUPPORTED NIOBIA ACIDITY (/G) VS. pKa
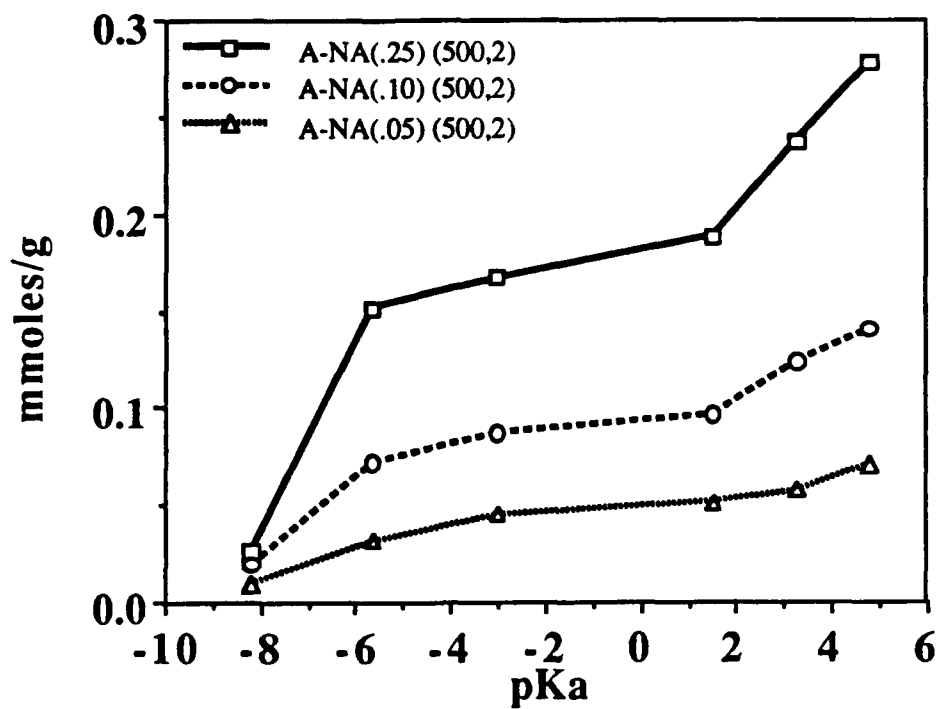
Figure 5-27: ALUMINA AEROGEL SUPPORTED NIOBIA ACIDITY (/G Nb_2O_5) VS. pKa
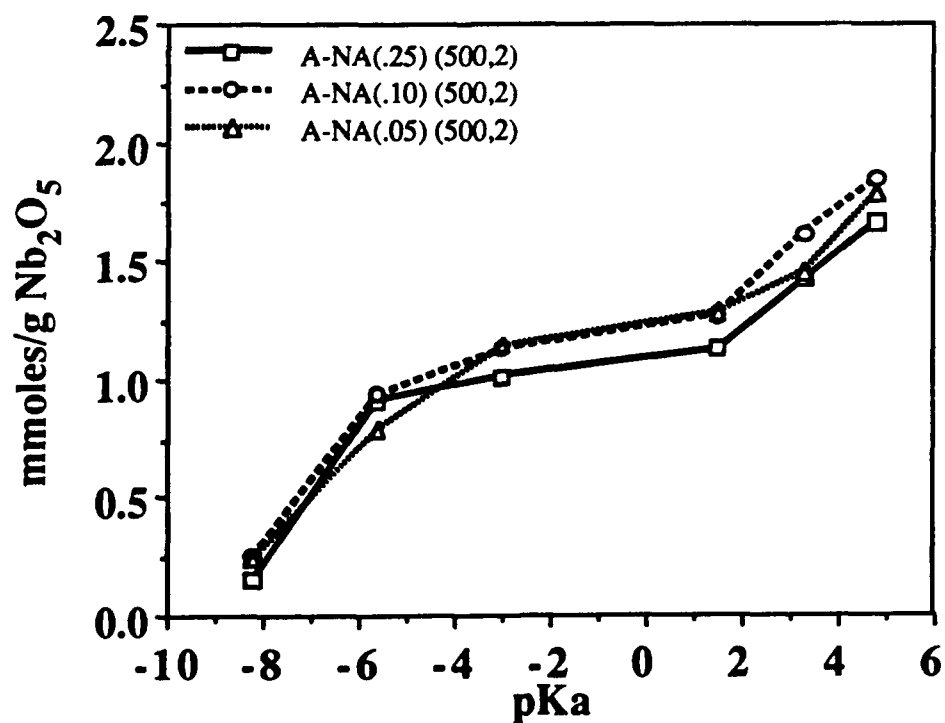
Figure 5-28: ALUMINA AEROGEL SUPPORTED NIOBIA ACIDITY (/G Nb$_2$O$_5$)
CALCINED AND HEAT TREATED (1000,-) VERSUS pKa
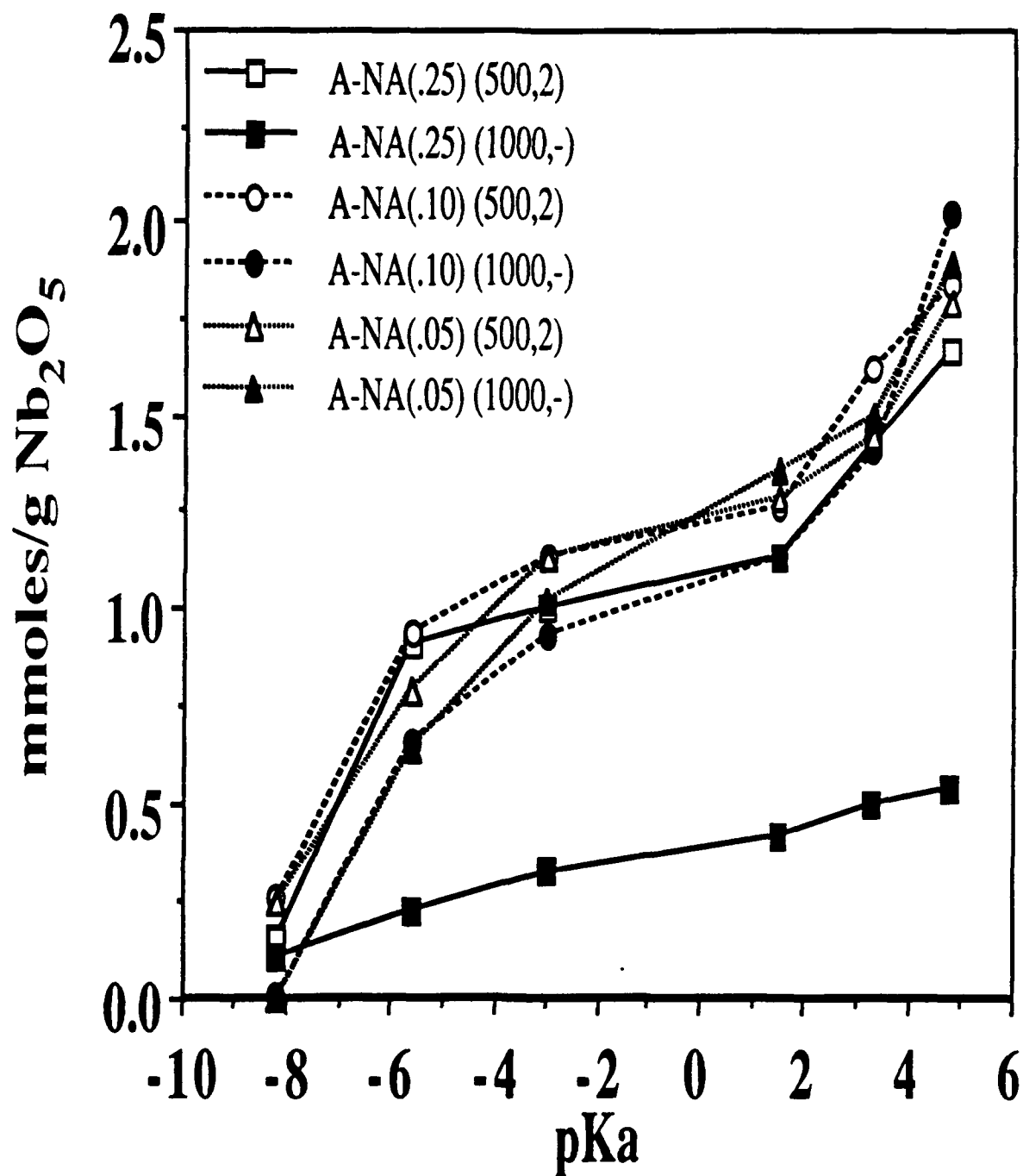
compound formation of NbAlO₄ by XRD and in fact show approximately the same retention in acidity throughout the entire range except at pKa = -8.2 where neither one shows acidity. The fact that these two alumina supported surface oxides do not show a compound formation of NbAlO₄ by XRD is also an indication that both of these samples are well dispersed. Thus, to summarize the results from this section, we have seen that both silica and alumina aerogel supported niobia are acidic binary oxides. The distribution of niobia on these materials is dependent on the supporting oxide and the loading of niobia on these supports. Niobia on the silica aerogel appears well dispersed at A-NS(.05) (5% monolayer coverage) and niobia on the alumina aerogel appears to show good dispersion at A-NA(.10) (10% monolayer coverage).

5.3.2 Superacidity and Basicity

Table 5-10 lists the qualitative measurements of the superacidity and basicity of the silica and alumina aerogel supported niobia after calcination at (500,2) and a (1000,-) heat treatment. A-NS(.25) shows superacidity up to a pKa = -12.40, as well as basic sites at pKa = +9.3. The lower loading of niobia on silica, A-NS(.05), shows superacidity that is qualitatively less than A-NS(.25) as indicated by only the positive acid indication at pKa = -11.35; however, this sample, A-NS(.05), also shows basicity at pKa = +9.3. These results lead to some insight with this system along with the titration results from the last section. The fact that both of these silica aerogel supported oxides show strong basicity is a possible indication of terminal Nb=O bonds. The idea of having a highly distorted group in possession of this Nb=O bond has been proposed by other researchers.[67, 86, 90, 93] On the acidity aspect of these samples, it appears that the higher loading of niobia on the silica aerogel support leads to stronger acid sites. The n-butylamine titration results show that this could be true, due to the fact that the acidity in the well dispersed samples [A-NS(.05) and A-NS(.025)] seemed to be less at the highest acid strength of pKa = -8.2. Since A-NS(.25) was found to be less distributed than A-NS(.05) by LRS and n-butylamine

Table 5-10: SUPERACIDITY AND BASICITY OF HEAT TREATED SUPPORTED NIOBIA AEROGELS

Sample Name	Acid Strength (pKa)			Basic Strength (pKa)	
	-11.35	-12.40	-13.75	+9.3	+15.0
A-NS(0.25) (500,2)	+	+	-	+	-
A-NS(0.25) (1000,-)	+	-	-	+	-
A-NS(0.05) (500,2)	+	-	-	+	-
A-NS(0.05) (1000,-)	-	-	-	+	-
A-NA(0.25) (500,2)	+	+	+	++	+
A-NA(0.25) (1000,-)	+/-	-	-	+	+/-
A-NA(0.10) (500,2)	+	+	+	++	+
A-NA(0.10) (1000,-)	-	-	-	+	+/-

++	(Very Positive Acid or Basic Indication)
+	(Positive Acid or Basic Indication)
+/-	(Positive and/or Negative Indication)
-	(Negative Acid or Basic Indication)

titration, we can conclude that the adjacent units of niobia on the silica surface actually give stronger acid sites upon aggregation. One likely explanation is the fact that by coupling the slightly or highly distorted NbO_6 or NbO_4 groups on the surface of silica, one can more readily delocalize negative charge associated with the acceptance of an electron pair, or with the donation of a proton, as both the niobia surface overlayer as well as the silica support itself help distribute this extra charge. A-NS(.05), being both a well-distributed and dispersed surface oxide, does not have the benefit of the extra distribution of charge over the niobia overlayers, and hence is expected to have a lower acid strength. Upon heat treating both A-NS(.25) and A-NS(.05) to (1000,-) we notice that these materials both have a high basic strength of pKa = +9.3. LRS indicates that A-NS(.25) still possesses highly distorted octahedral or tetrahedral groups as seen by the broad peak at ~ 950 cm^{-1}. We also noticed a shifting of the 725 cm^{-1} peak assigned to slightly distorted NbO_6 octahedra, and this was indexed by XRD as the formation of poorly crystalline TT-Nb_2O_5. The results in Table 5-10 indicate that this sample still possesses superacidity even after (1000,-) as seen by the positive indication at pKa = -11.35. Earlier in Chapter 3 we saw that TT-Nb_2O_5 [A-Nb_2O_5 (600,2)] showed superacidity as well. The A-NS(.05) supported oxide did not show any superacidity, nor did it reveal formation of TT-Nb_2O_5 by XRD. Experiments have not been performed on this sample to determine its bonding environment, but a likely explanation is a change from the highly distorted niobia environment to a less or slightly distorted environment in which little to no charge delocalization can occur.

The alumina aerogel supported niobia in A-NA(.25) and A-NA(.10) are also revealed in Table 5-10 for their superacidity and basicity results. No meaningful information can be extracted after the standard calcination for A-NA(.25) and A-NA(.10) because these results are identical to those found for the pure alumina aerogel (see Table 3-24), i.e. all acidic and basic indicators turned to their positive forms. After the (1000,-) heat treatment, we see that A-NA(.25) shows a positive indication at pKa = +9.3 and

possible indications of higher basic strength (+15.0) and even superacidity (pKa = -11.35). A-NA(.05) shows the same basic characteristics of A-NA(.25); however, it does not show any superacidity in any of the indicators. The aerogel of alumina after a (1000,-) heat treatment showed a basic strength of pKa = +9.3 and no superacidity as seen in Table 3-24, and this oxide was indexed by XRD as γ-Al$_2$O$_3$. A-NA25w after (1000,-) was shown to be neutral to all the indicators, because of the compound formation of NbAlO$_4$. The alumina aerogel supported oxide of A-NA(.25) showed very poorly crystalline NbAlO$_4$, but could possibly have highly distorted niobia or some highly distorted niobia/alumina complex that is giving rise to the slight superacidity and basicity found at pKa = -11.35 and pKa = +15.0, respectively. This sample was shown by n-butylamine titration to have acidity in the highest acid strength range, pKa = -8.2, after the (1000,-) heat treatment. The lower loading of A-NA(.10) after the (1000,-) heat treatment could be explained in the same fashion as above for the silica aerogel supported system; i.e. that there is not enough of the highly distorted niobia or *niobia/alumina complexes around to distribute* and delocalize extra charge associated with donation of a proton or acceptance of an electron pair. The basic indication at pKa = +15.0 is merely a reflection of possible Nb=O groups in the highly distorted octahedra or tetrahedra, that are organizing and restructuring in order to form NbAlO$_4$.

5.3.3 Pyridine Adsorption Studies

5.3.3.1 Heat of Adsorption (ΔH_{ads}): TG Study

Pyridine adsorption experiments were performed to determine the acid strength coverage dependence on a few selected samples of silica and alumina aerogel supported niobia. Table 5-11 lists the pyridine heats of adsorption versus coverage for A-NS(.25) and A-NS(.05) as well as SiO$_2$ and A-Nb$_2$O$_5$ for comparison. Figure 5-29 shows ΔH_{ads} versus coverage for the tabulated results after the standard calcination. The ΔH_{ads} for A-

Table 5-11: ΔH_{ads} VERSUS PYRIDINE COVERAGE FOR SILICA AEROGEL SUPPORTED NIOBIA

Pyridine Coverage (Θ) (Molecules/cm^2 x 10^{13})	ΔH_{ads}(kcal/mol)			
	A-Nb$_2$O$_5$	A-NS(.25)	A-NS(.05)	SiO$_2$
0.8			42.0	
1.0			33.1	12.6
1.3				13.7
1.6			23.6	
1.8				15.0
2.1		51.2		
2.5				15.0
2.7		49.5	24.2	
3.5		37.2		
4.5		32.3	24.0	
5.8		28.7		
7.4	31.1	27.8	24.5	
8.2	32.4			
9.0	33.5			
9.5		27.3		
10.0	33.5			
11.0	32.8			
12.2	31.0	29.7		
13.5	29.6			
14.9	27.2			
16.4	24.1			
18.2	24.3			

Figure 5-29: ΔH_{ads} VERSUS PYRIDINE COVERAGE FOR SILICA AEROGEL SUPPORTED NIOBIA

NS(.05) ranged from 42.0 to 24.5 kcal/mol for coverages of 0.8 to 7.4 x 10^{13} molecules/cm^2. The heats of adsorption for A-NS(.25) ranged from 51.2 to 29.7 kcal/mol for coverages of 2.1 to 12.2 x 10^{13} molecules/cm^2. These values indicate that the higher loading of A-NS(.25) shows heats of adsorptions about 5 to 10 kcal/mol higher at the high and low coverages, respectively, than A-NS(.05). The A-NS(.25) binary surface oxide has the strongest acid strength found in this study. Both of the silica surface oxides had a strong coverage effect which can be described by a Temkin isotherm because of the nearly linear relationship in the heat of adsorption versus coverage. These high acid strengths were confirmed with our superacidity test which showed that the A-NS(.25) was more acidic qualitatively than A-NS(.05). Furthermore, the high acid strength is determined by Nb=O terminal bonds and the ability for the oxide to distribute and delocalize charge over both the doubly bonded oxygen as well as the matrix as a whole.

Heats of adsorption versus pyridine coverage for A-NA(.25), A-NA(.10), A-Al$_2$O$_3$, and A-Nb$_2$O$_5$ are shown in Table 5-12. Figure 5-30 shows ΔH_{ads} versus coverage for the above samples after a standard calcination. One can see that for the alumina aerogel supported oxide at low niobia coverage, A-NA(.10), there does not seem to be a significant difference from the heats of adsorption for the bulk alumina aerogel. Only at the lower coverages could one possibly be able to make a distinction but even these values are close and within a 10% experimental error. The only real differences in acid strength seems to be on the higher loading of niobia, A-NA(.25). The ΔH_{ads} for A-NA(.25) ranged from 29.8 to 24.8 kcal/mol over a coverage of 4.9 to 14.9 x 10^{13} molecules/cm^2, while the ΔH_{ads} for A-NA(.10) ranged only from 26.7 to 21.3 over a pyridine coverage of 4.1 to 13.5 x 10^{13} molecules/cm^2. This corresponds to an average heat of adsorption of nearly 4 kcal/mol higher for A-NA(.25) than for A-NA(.10) over the entire range of pyridine coverage. All data seem to show a linear dependence of ΔH_{ads} with respect to coverage which indicates that the data follow a Temkin isotherm and show significant coverage dependence on the heats of adsorption. The fact that the coverages and heats of adsorption for the alumina

Table 5-12: ΔH_{ads} VERSUS PYRIDINE COVERAGE FOR ALUMINA AEROGEL SUPPORTED NIOBIA

Pyridine Coverage (Θ) (Molecules/cm^2 x 10^{13})	ΔH_{ads}(kcal/mol)			
	A-Nb$_2$O$_5$	A-NA(.25)	A-NA(.10)	A-Al$_2$O$_3$
1.0				
2.0				
3.0				
4.1			26.7	23.6
4.9		29.8	23.8	22.6
6.1		27.1	24.3	23.8
7.4	31.1	26.1	22.4	22.4
8.2	32.4			
9.0		25.4	21.3	22.6
9.5	33.5			
10.0	33.5			
11.0	32.8	25.4	21.1	21.3
12.2	31.0			
13.5	29.6	24.8	21.3	20.4
14.9	27.2	22.9		
16.4	24.1			
18.2	24.3			

Figure 5-30: ΔH_{ads} VERSUS PYRIDINE COVERAGE FOR ALUMINA AEROGEL SUPPORTED NIOBIA
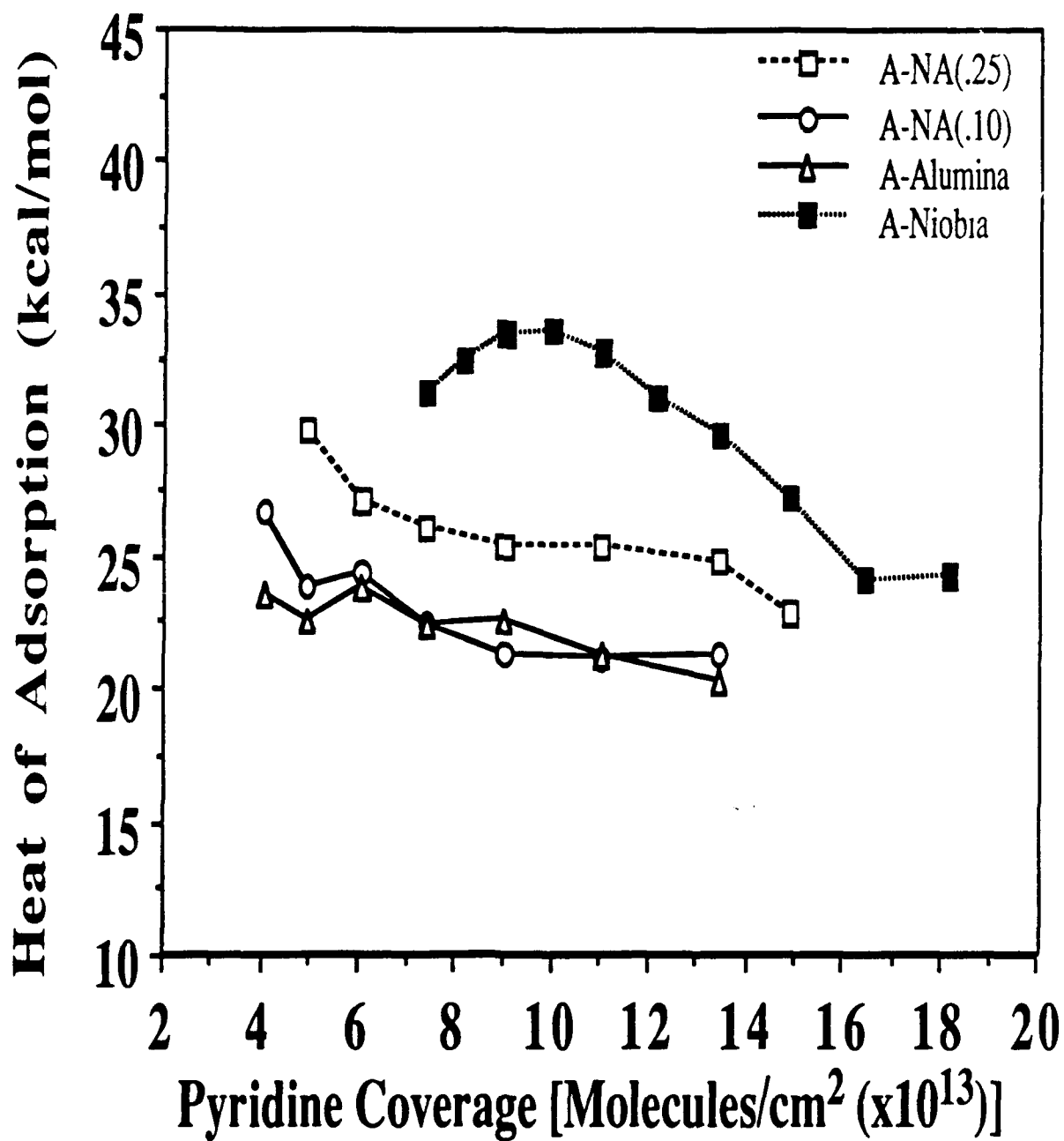
supported oxides do not change drastically from those of bulk alumina, shows that alumina is indeed a very acidic oxide, and has a dominating effect in the acidity of these surface oxides because of the strong interaction between these two materials.

To summarize the heats of adsorption results, it appears that all of the supported surface oxides are quite acidic and do have high acid strengths. The silica aerogel supported niobia samples developed the highest acid strength in this study, but also had the greatest distribution of acid strength. Higher loadings of niobia on silica also increased the acid strength of these binary oxides. The alumina aerogel supported niobia developed high acid strengths at sufficient loadings of niobia on the alumina surface. Low loadings of niobia on alumina, A-NA(.10), revealed acid strengths which are nearly identical to those found in bulk alumina aerogels.

5.3.3.2 Acid Type: FTIR Study

Pyridine adsorption using FTIR was used to examine the vibrational frequencies of the pyridine molecule on the silica and alumina aerogel supported niobia and determine the nature of Lewis or Brønsted acid sites on the oxides. These experiments were used to measure strengths of the Lewis sites by noting shifts in the characteristic frequencies of ~1450 and 1600 cm^{-1}. Relative strengths of the Lewis/Brønsted (L/B) sites were examined as a function of pretreatment temperature, by observing the change in the L/B ratio. This data has been summarized in Table 5-13 for the Lewis acid peak absorption frequencies of the surface oxides as a function of heat treatment, and the L/B ratios are shown in Table 5-14 with the same temperature schedule. Absorption frequencies are shown and discussed in the main text for the 1700 - 1400 cm^{-1} region, while all other hydroxyl region data, 4000 - 2800 cm^{-1}, as well as the low intensity spectra at 300 °C are shown in Appendix C.

Figure 5-31 shows the FTIR spectra of pyridine adsorbed on A-NS(.25). After a 25 °C evacuation 2 strong bands ~ 1595 and 1447 cm^{-1} are noticeable and have been assigned to physisorbed pyridine. These frequencies of the weakly bound pyridine have all

Table 5-13: LEWIS ACID PYRIDINE ABSORPTION FREQUENCIES FOR SURFACE OXIDES

	Lewis Acid Pyridine Absorption Frequencies					
	19b Frequency (cm^{-1})			8a Frequency (cm^{-1})		
Sample	Heat Treatment			Heat Treatment		
	100 °C	200 °C	300 °C	100 °C	200 °C	300 °C
A-NS(.05)	1448.9	1449.7	1449.9	1610.2	1611.7	1612.0
A-NS(.25)	1448.8	1449.4	1449.7	1610.0	1611.4	1611.9
A-Al$_2$O$_3$	1450.1	1452.8	1453.3	1616.0	1621.1	1622.5
A-NA(.05)	1450.6	1452.8	1454.0	1616.3	1621.6	1622.8
A-NA(.25)	1447.5	1449.9	1452.3	1615.1(S)	1621.8(S)	1623.0(S)
				1610.0(S)	1611.7(S)	1612.6(S)

(S), Strong Absorption; (W), Weak Absorption

Table 5-14: LEWIS/BRØNSTED RATIO FOR SURFACE OXIDES

	Lewis/Brønsted Ratio		
Sample	Heat Treatment		
	100 °C	200 °C	300 °C
A-NS(.05)	6.7	10.0	11.8
A-NS(.25)	2.9	3.6	6.5
A-Al$_2$O$_3$	8.4	40.4	675.8
A-NA(.05)	14.3	146.4	227.9
A-NA(.25)	5.6	13.9	45.2

Figure 5-31: FTIR SPECTRA OF PYRIDINE ADSORBED ON A-NS(.25) AFTER
TREATMENTS AT 300, 200, 100, AND 25 °C (TOP TO BOTTOM)
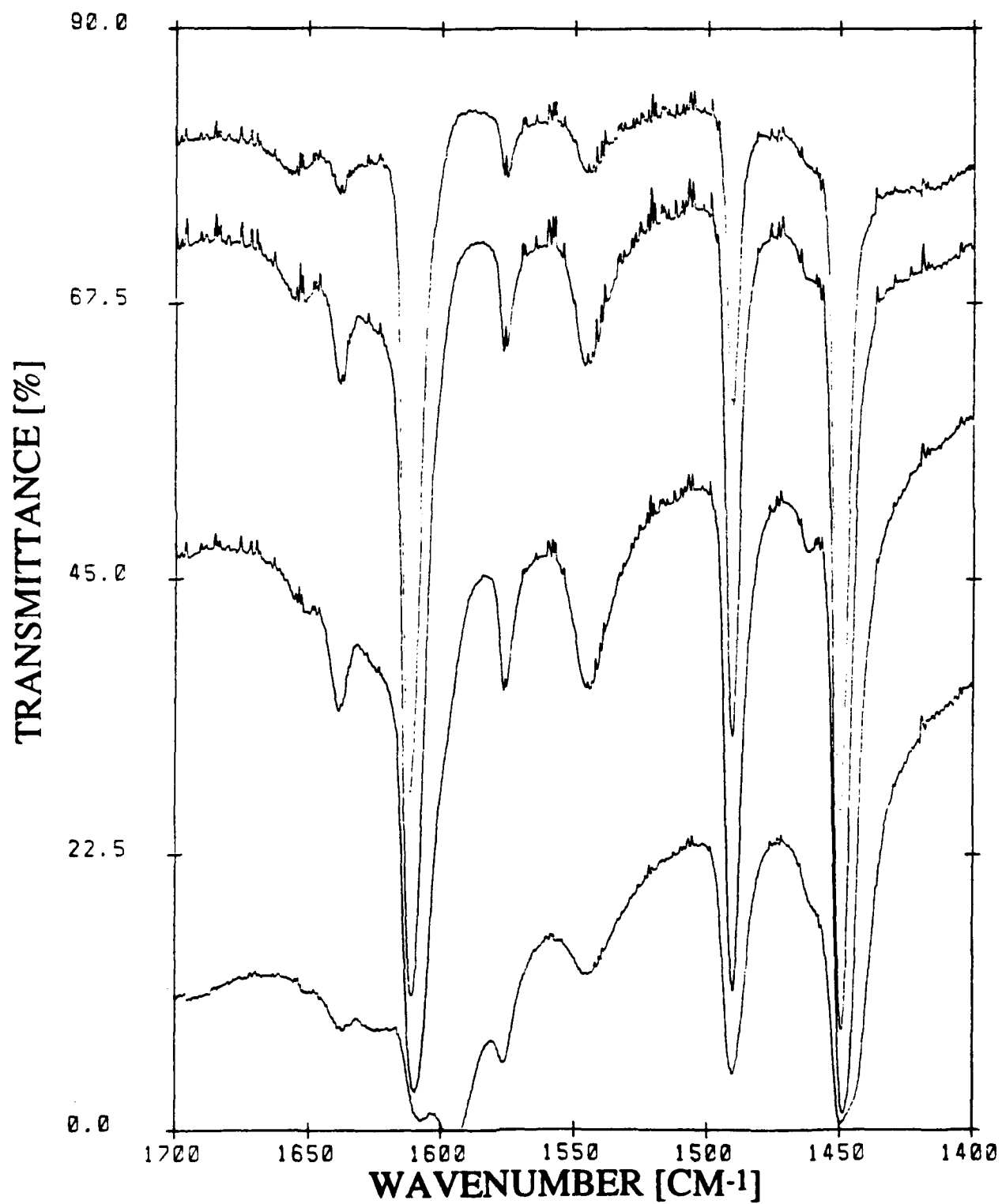
but disappeared after the 100 °C heat treatment and are associated with the silica support. A strong absorption band was seen around 1545 cm^{-1} which is assigned to the characteristic 19b peak of a Brønsted acid. The peak appears to attenuate as the treatment temperature is increased, but a significant portion of this feature remains after the 300 °C heat treatment showing that this sample possesses very strong Brønsted acidity. The heat treatments show a L/B ratio that varies only from ~ 3 to 6 after temperatures of 100 and 300 °C, respectively. These low L/B ratios signify that Brønsted acidity is apparent on this sample and it is strong. Previous results from our group, for a 25% monolayer niobia on a silica support (Davison), also showed strong Brønsted acidity.[88] These earlier findings showed that L/B varied from ~ 7 to 9 over the same temperature range studied. The frequency shifts of the Lewis acid frequencies for A-NS(.25) of approximately 1 cm^{-1} are lower than that found for A-NS25w (~ 1.5 cm^{-1}) and much lower than that found for A-Nb$_2$O$_5$ (~ 3.0 cm^{-1}), which indicates a very narrow distribution of Lewis acid sites on A-NS(.25).

Figure 5-32 shows the FTIR spectra for pyridine adsorption on A-NS(.05). After the room temperature evacuation, strong bands at ~ 1595 and 1445 cm^{-1} are seen and have been assigned to physisorbed pyridine due to the silica substrate. After the 100 °C heat treatment the 1595 cm^{-1} band is still apparent but disappears upon further thermal treatments. As with A-NS(.25), the lower loading of A-NS(.05) shows a fairly strong absorption peak; however, this peak has shifted to a higher frequency of ~ 1546.8 cm^{-1} or about 2 cm^{-1} higher than the peak at ~ 1545.1 cm^{-1} for A-NS(.25). The 1546.8 cm^{-1} peak is severely attenuated on the scale of the figure after higher heat treatments, but an enlarged version of the 300 °C spectrum (shown in Appendix C) shows that there is significant Brønsted acidity with this sample as evidenced by the peak at ~ 1547 cm^{-1}. The L/B ratios after the 100 ° and 300 °C heat treatments vary from ~ 7 to 12, indicating that this sample does indeed possess strong Brønsted acidity. The frequency shifts over the heat treatments of 100 to 300 °C for A-NS(.05) were 0.9 and 1.8 cm^{-1} for the 19b and 8a bands, respectively. This very narrow distribution of Lewis acid sites is also seen for the A-

Figure 5-32: FTIR SPECTRA OF PYRIDINE ADSORBED ON A-NS(.05) AFTER
TREATMENTS AT 300, 200, 100, AND 25 °C (TOP TO BOTTOM)
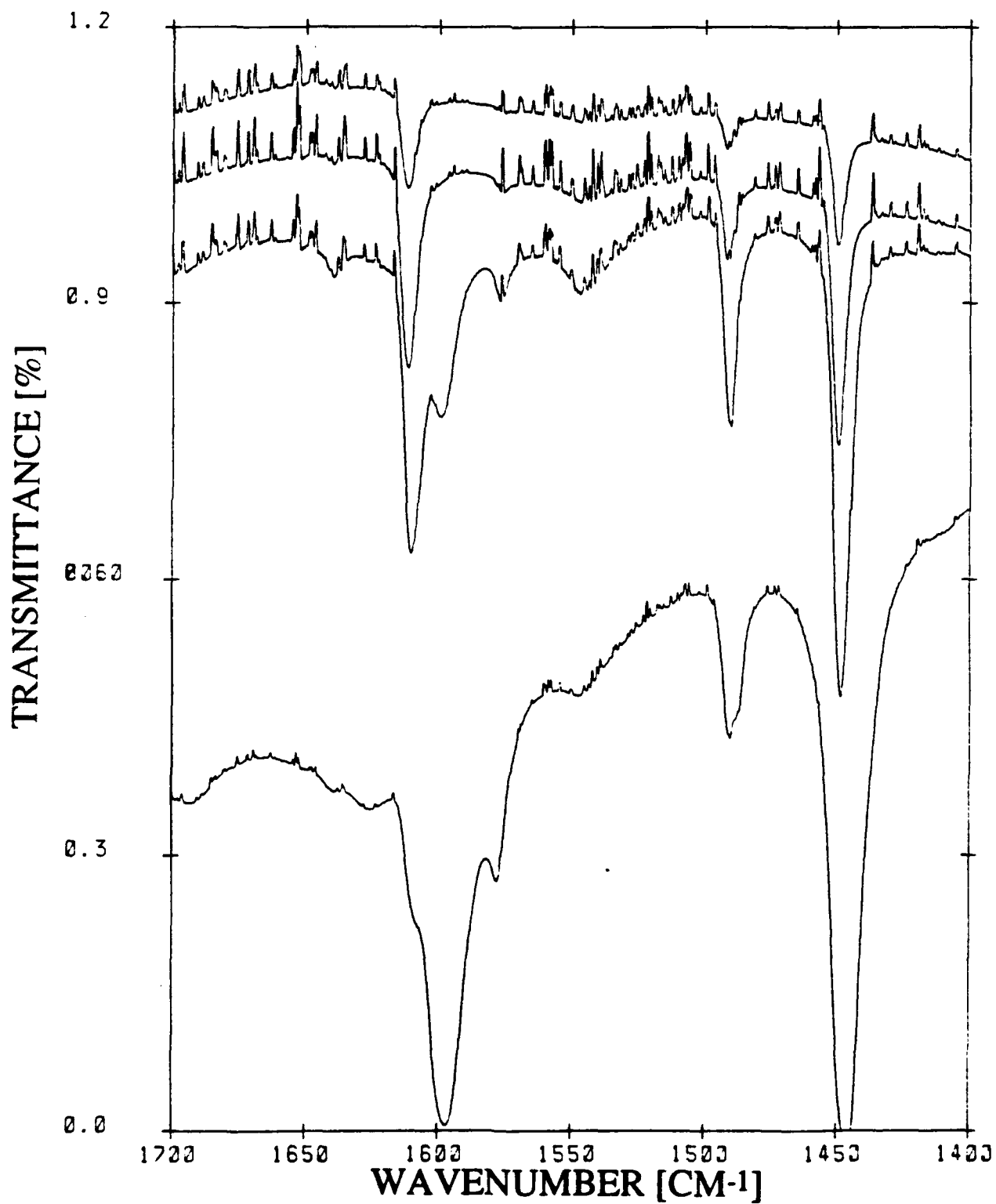
NS(.25) and on an absolute scale, the A-NS(.05) surface oxide shows slightly stronger Lewis acid sites because of the higher frequency of vibration.

Figure 5-33 shows the FTIR spectra for A-NA(.25). After an evacuation at room temperature, strong absorption bands can be seen at ~ 1595 and 1440 cm^{-1} indicative of physisorbed pyridine, and are eliminated upon treatment to 100 °C. One also notices after the 25 °C evacuation the broad Lewis band at ~ 1610 cm^{-1} that will later be seen to form two separate Lewis acid sites. After the 100 °C heat treatment a broad and weak band (as compared to the others) is seen at ~ 1545 cm^{-1} indicative of the 19b peak frequency assigned to a Brønsted acid site. This peak is attenuated at 200 °C and is virtually eliminated at the higher thermal treatment of 300 °C. The L/B ratio for this sample is shown in Table 5-14 and is seen to be 5.6, 13.9, and 45.2 for the heat treatments of 100, 200, and 300 °C, respectively. This identifies A-NA(.25) as having weak Brønsted acidity. This higher loading of niobia on alumina yields interesting spectra in the 1600 - 1630 cm^{-1} region. After the 100 °C heat treatment, there appears a broad peak with a possible doublet at ~ 1615 and 1610 cm^{-1}. This higher frequency peak at ~ 1615 cm^{-1} is attributable to the Lewis acid site on alumina, and the new site at ~ 1610 cm^{-1} can be attributed to the addition of niobia onto the alumina aerogel.[25, 180, 198] This new frequency is possibly due to the highly distorted NbO_6 groups that contain terminal Nb=O, as our previous *in-situ* LRS study showed. The frequency shifts of the 8a frequency band attributed to bulk alumina closely follow those for the alumina aerogel. The 8a Lewis acid frequency shifts are 1615.1 to 1623.0 cm^{-1} (Δ = 7.9 cm^{-1}) for A-NA(.25), and 1616.0 to 1622.5 cm^{-1} (Δ = 6.5 cm^{-1}) for A-Al$_2$O$_3$ after heat treatments of 100 to 300 °C, respectively. Note that the same Lewis band shift attributed to alumina for the niobia/alumina mixed oxide, A-NA25w, was Δ = 7.2 cm^{-1}. This reveals that A-NA(.25) has a broader Lewis acid strength distribution than either the bulk alumina aerogel or the A-NA25w sample. The new 8a Lewis peak shifts identified in A-NA(.25) are 1610.0 to 1612.6 cm^{-1} (Δ = 2.6 cm^{-1}) after the same temperature schedule as above. This large shift

**Figure 5-33:** FTIR SPECTRA OF PYRIDINE ADSORBED ON A-NA(.25) AFTER TREATMENTS AT 300, 200, 100, AND 25 °C (TOP TO BOTTOM)
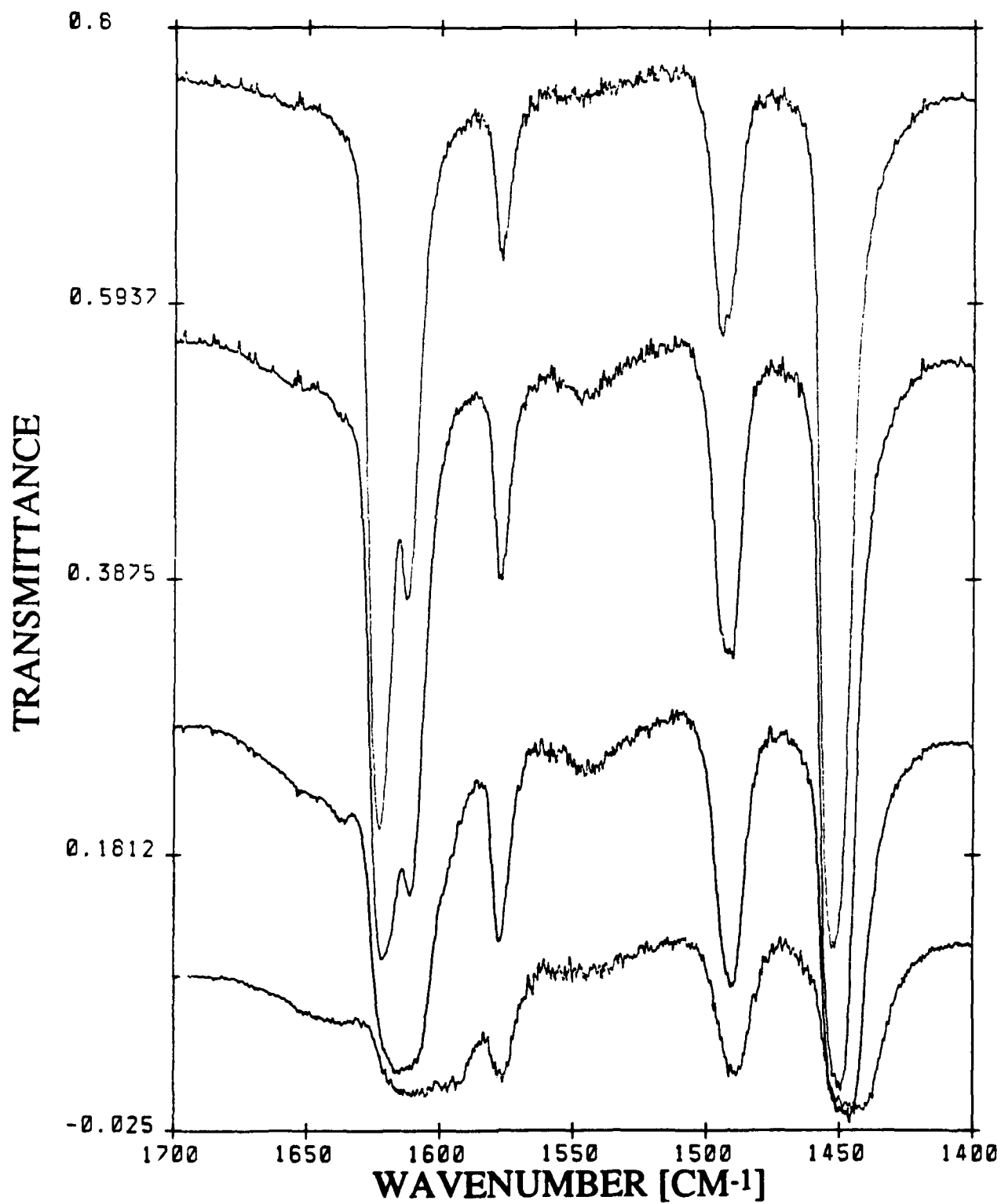
in frequency indicates a distribution of Lewis acid sites for A-NA(.25) that is similar to but slightly less than the frequency band shifts in A-Nb$_2$O$_5$ (Δ = 3.0 cm^{-1}), and the peak assignment in A-NA25w (Δ = 3.5 cm^{-1}). Thus, A-NA(.25) shows a larger distribution of Lewis acid sites and acid strength for the acid sites pertaining to Al$_2$O$_3$ than the bulk alumina aerogel, but a slightly smaller distribution of newly created Lewis sites than the niobia aerogel.

Figure 5-34 shows the FTIR spectra for A-NA(.05). The evacuation at room temperature reveals two peaks at ~ 1595 and 1445 cm^{-1} attributed to physisorbed pyridine. The peaks are virtually eliminated on heat treating to only 100 °C. The appearance of these pyridine adsorption spectra for A-NA(.05) are nearly identical to those for the alumina aerogel (see Figure 3-33). The major distiguishing feature about these two sets of spectra is the absence of a peak at ~ 1545 cm^{-1} attributed to Brønsted acidity. This is revealed in the large L/B ratio for A-NA(.05) of 14.3, 146.4, and 227.9 after heat treatments of 100, 200, and 300 °C. These large ratios indicate that this sample has very little if any Brønsted acidity. The Lewis acid frequency shifts of 1450.6 to 1454.0 cm^{-1} (Δ = 3.4 cm^{-1}) and 1616.3 to 1622.8 cm^{-1} (Δ = 6.5 cm^{-1}) for the 19b and 8a bands, respectively, match up nearly identically for those shifts found on the alumina aerogel, i.e. Δ = 3.2 cm^{-1} (19b) and Δ = 6.5 cm^{-1} (8a). Thus, it appears that the Lewis acid site distributions are the same on both of these samples, but on an absolute scale A-NA(.05) has the higher frequency of vibration for both the 8a and 19b frequency than A-Al$_2$O$_3$, which indicates that this sample should have a slightly higher acid strength. This is exactly what we found from our ΔH_{ads} measurements when we studied the acid strengths of A-NA(.10) and A-Al$_2$O$_3$.

These FTIR pyridine adsorption studies to measure the acidity and relative acid type strengths yielded some very interesting information. First, depositing niobia onto the silica aerogel develops very strong Brønsted acidity for both A-NS(.05) and A-NS(.25) as indicated by the small and nearly constant L/B ratios. This observation of strong Brønsted acid sites is different than that of A-NS25w which showed only weak Brønsted acidity,

Figure 5-34: FTIR SPECTRA OF PYRIDINE ADSORBED ON A-NA(.05) AFTER TREATMENTS AT 300, 200, 100, AND 25 °C (TOP TO BOTTOM)
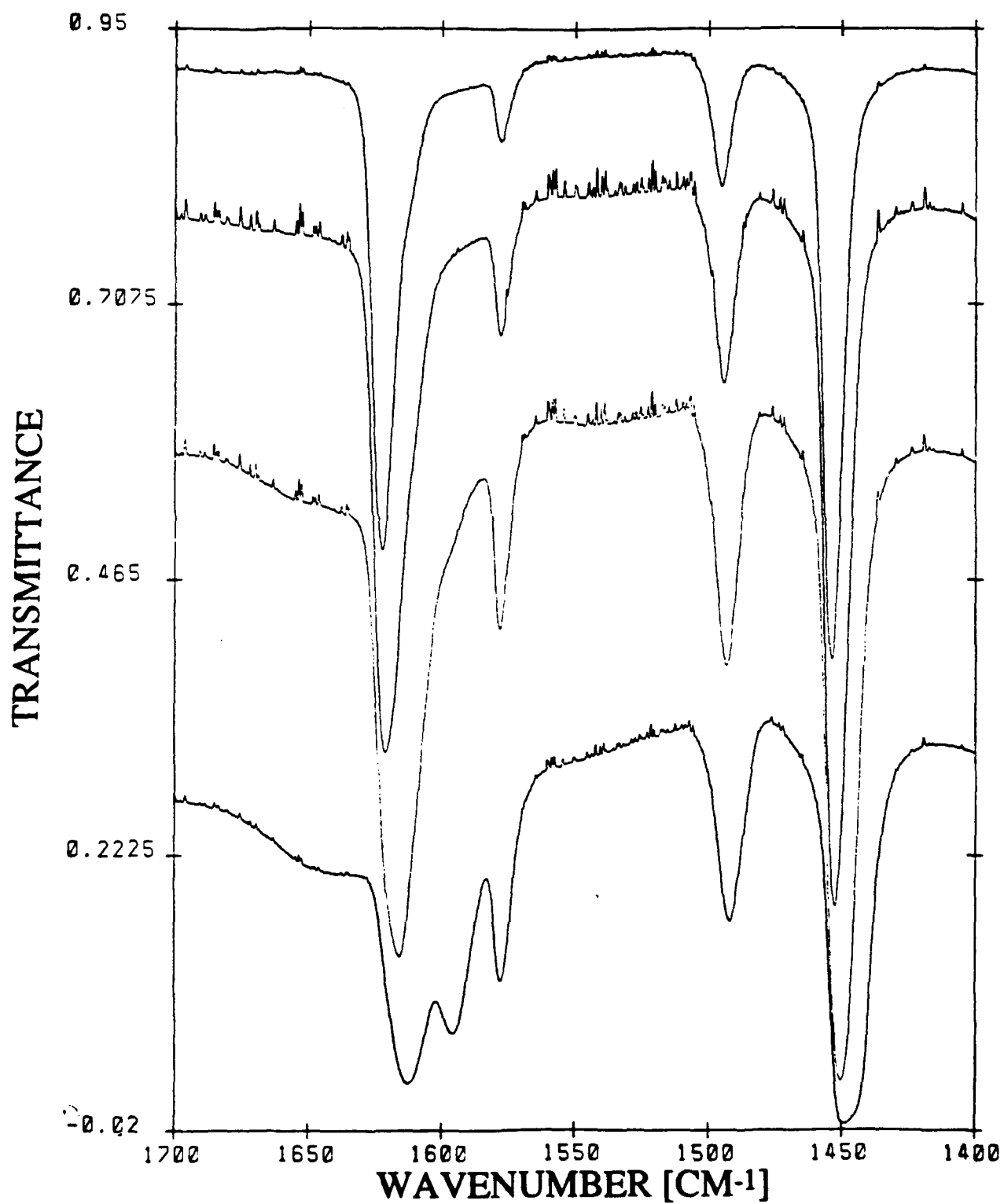
and indicates that the environment of niobia is different when in the mixed oxide or on the surface as a supported oxide. Grafting niobia onto the alumina aerogel also revealed interesting results. The low coverages of niobia on alumina indicate that this surface oxide behaves nearly identical to the alumina aerogel, but A-NA(.05) has a slightly higher acid strength. Also, there are no Brønsted acid sites on this sample unlike the higher niobia loading on alumina. A-NA(.25) has definite Brønsted acidity which is weak and also has a new Lewis acid site that is different than alumina and corresponds to an absorption peak at a lower frequency. These observations indicate that the surface bonding environments of niobia are different for the low and high loadings of niobia on alumina. The observation that the mixed oxide aerogel of A-NA25w has little if any Brønsted acidity, suggests the mixed oxide and surface oxide environments for niobia in these niobia/alumina binary oxides are different.

5.3.4 TG Reduction Studies

Direct reduction studies were performed by heating a supported surface oxide aerogel to 1000 °C at 10 °/min and holding for 2 hrs at 1000 °C in pure flowing hydrogen. A second series of TG reduction experiments was done by first pretreating the sample at 1000 °C, (1000,-) or (1000,2), followed by the reduction procedure using the above temperature schedule. This pretreatment was done to induce crystallization of niobia or compound formation prior to reduction. Two sets of peaks are observed in these reduction studies; those occurring below 400 °C were attributed to water desorption, and those above 600 °C were assigned to the reduction of niobia.

Figure 5-35 shows the direct reduction of silica aerogel supported niobia: A-NS(.05), A-NS(.10), A-NS(.25), and A-Nb$_2$O$_5$ for comparison. The peak temperatures (T_p) for the direct reduction data of silica aerogel supported niobia are listed in Table 5-15. In this figure and table, the first reduction peak corresponds to a temperature of around 750 °C for A-NS(.05) and increases with coverage to ~ 780 °C for A-NS(.25). These peaks

Figure 5-35: TG DIRECT REDUCTION DATA FOR SILICA AEROGEL SUPPORTED NIOBIA: A) Nb₂O₅, B) A-NS(.25), C) A-NS(.10), AND D) A-NS(.05)
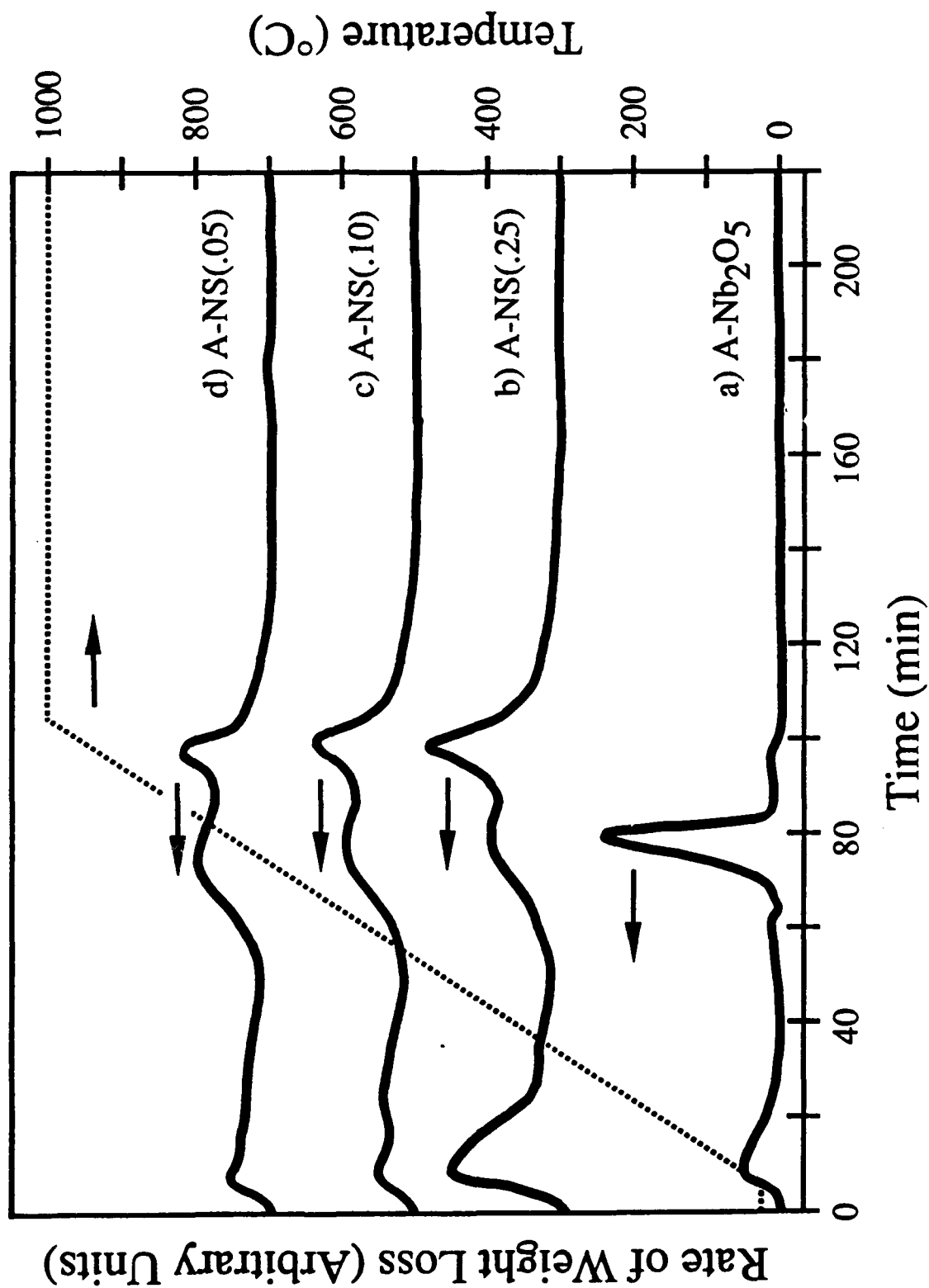
Table 5-15: PEAK TEMPERATURES FOR TG DIRECT REDUCTION DATA OF SILICA AEROGEL SUPPORTED NIOBIA AND A-Nb$_2$O$_5$

Sample	Heat Treatment	Peak Temperature (°C)
A-Nb$_2$O$_5$	(500,2)	797
A-NS(.25)	(500,2)	`79(B*), 989
A-NS(.10)	(500,2)	7`6(B), 989
A-NS(.05)	(500,2)	752(B), 978

* B = Broad

Table 5-16: PEAK TEMPERATURES FOR TG REDUCTION DATA OF HEAT TREATED SILICA AEROGEL SUPPORTED NIOBIA AND A-Nb$_2$O$_5$

Sample	Heat Treatment	Peak Temperature (°C)
A-Nb$_2$O$_5$	(1000,-)	900
A-NS(.25)	(1000,2)	878, 995
A-NS(.10)	(1000,2)	995
A-NS(.05)	(1000,2)	987

match up well with the direct reduction peak for A-Nb$_2$O$_5$ (Tp = 797 °C), and the ease of this reduction could possibly suggest the existence of Nb=O in all of these samples. The second reduction peak at ~ 990 °C corresponds to the reduction temperature for a monolayer of niobia on silica.[76, 88] It becomes sharper and intensifies as we increase coverage to A-NS(.25). This second peak suggests that the interfacial interactions which stabilize niobia from crystallizing in these silica supported niobia systems also makes niobia more difficult to reduce.

Data from these direct reductions are complicated due to the crystallization of niobia during heat treatment, i.e. niobia in A-NS(.25) crystallizes to TT-Nb$_2$O$_5$ when ramped to 1000 °C. In order to eliminate this complication, the silica supported oxides were indirectly reduced by pretreating in helium (1000,2) and then subsequently reducing in the hydrogen environment. These reduction data are shown in Figure 5-36 and the reduction peak temperatures for the sample are listed in Table 5-16. The heat treatment in helium was done *ex-situ*, and therefore the broad peak around 200 °C is attributed to the desorption of water that had adsorbed on the sample surface during transfer. All of the silica supported oxides show a major reduction peak at ~ 995 °C. This peak has shifted slightly from the direct reduction peak at ~ 990 °C, but is attributed to the stabilization of niobia as an overlayer on the silica aerogel support. A-NS(.25) shows a second peak at ~ 880 °C which can be associated with the crystallization of bulk niobia. The reduction of the niobia aerogel is also shown in Figure 5-36 to identify this early peak as being due to the reduction of niobia crystallites. XRD studies showed A-NS(.25) to have TT-Nb$_2$O$_5$ crystallites on the surface which confirm this peak assignment. The collapse of the silica matrix with the (1000,2) pretreatment was attributed to effectively increasing the niobia loading by a factor of 4 and thus leading to this destabilization of niobia. Thus, to summarize the results for silica aerogel supported niobia, it appears that niobia is stabilized as a surface oxide overlayer due to the strong oxide-oxide interaction. High loadings of niobia on silica eventually lead to crystallization of bulk niobia, because the collapse of the silica support leads to a more

Figure 5-36: TG REDUCTION DATA FOR PRETREATED (1000,2) SILICA AEROGEL SUPPORTED NIOBIA: A) Nb_2O_5 (1000,-), B) A-NS(.25), C) A-NS(.10), AND D) A-NS(.05)
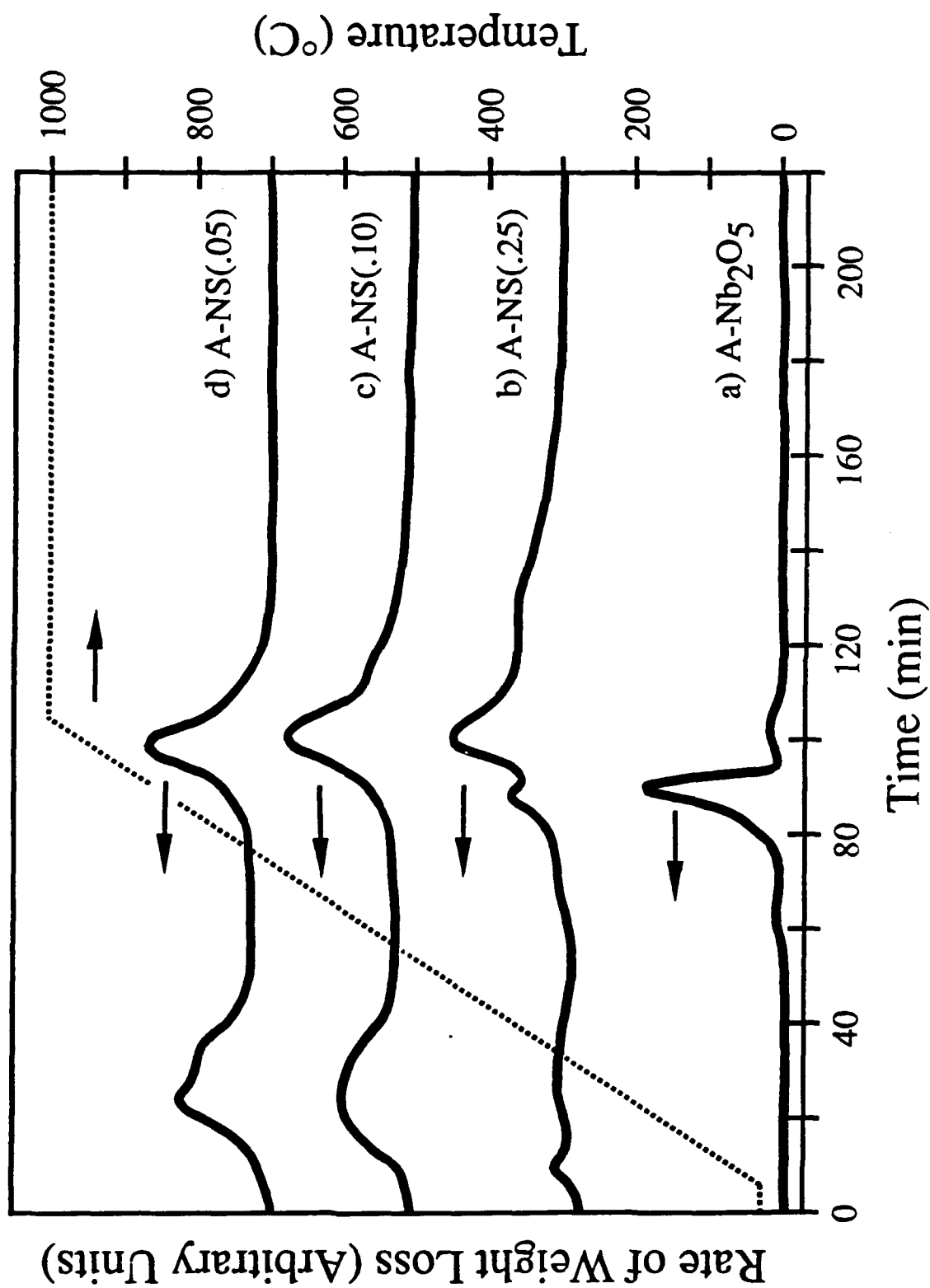
mobile niobia that can be located far enough from a niobia-silica interface so as to be unaffected by the interaction of these two oxides and behave more as a pure bulk niobia.

Figure 5-37 shows the direct reduction scans of alumina aerogel supported niobia: A-NA(.05), A-NA(.10), and A-NA(.25). The peak temperatures for reduction of these alumina supported oxides are compiled in Table 5-17. A-NA(.05) shows a reduction peak at ~ 970 °C, which increases with coverage to ~ 980 °C for A-NA(.10) and ~ 990 °C for A-NA(.25). Another very weak and broad peak at ~ 870 °C is seen for A-NA(.25). This weak peak around ~ 870 °C for A-NA(.25) closely follows the exothermic peak at ~ 860 °C which we have ascribed to the compound formation of $NbAlO_4$, and could possibly be due to the loss in weight from water from this solid-state reaction. No peaks are seen around 800 - 900 °C for the reduction of bulk niobia, and we can attribute this to the very strong interaction of niobia with the alumina aerogel support. The indirect reduction data are shown in Figure 5-38 for the pretreated (1000,-) alumina supported niobia aerogels. Notice that the peak at ~ 870 °C for A-NA(.25) is eliminated confirming that the $NbAlO_4$ compound has been formed and then reduces at ~ 1000 °C. The other alumina supported niobia samples, A-NA(.10) and A-NA(.05), also reduce at ~ 995 °C, slightly lower reduction temperatures than for both A-NA(.25) and A-NA25w which have formed crystalline $NbAlO_4$ compounds. This could be due to the fact that A-NA(.05) and A-NA(.10) remain amorphous, which could mean that either a distorted niobia overlayer has formed on the surface of alumina or these materials are in a highly distorted pre-$NbAlO_4$ compound state. These reduction results show that alumina stabilizes niobia due to the very strong interactions inherent between these two oxides. This oxide interaction is so strong that these materials eventually undergo a solid-state reaction to form $NbAlO_4$ when the loading of niobia on the surface is high enough. Low loadings of niobia on alumina lead to a distorted niobia overlayer even at elevated temperatures.

**Figure 5-37:** TG DIRECT REDUCTION DATA FOR ALUMINA AEROGEL SUPPORTED NIOBIA: A) A-NA(.25), B) A-NA(.10), AND C) A-NA(.05)
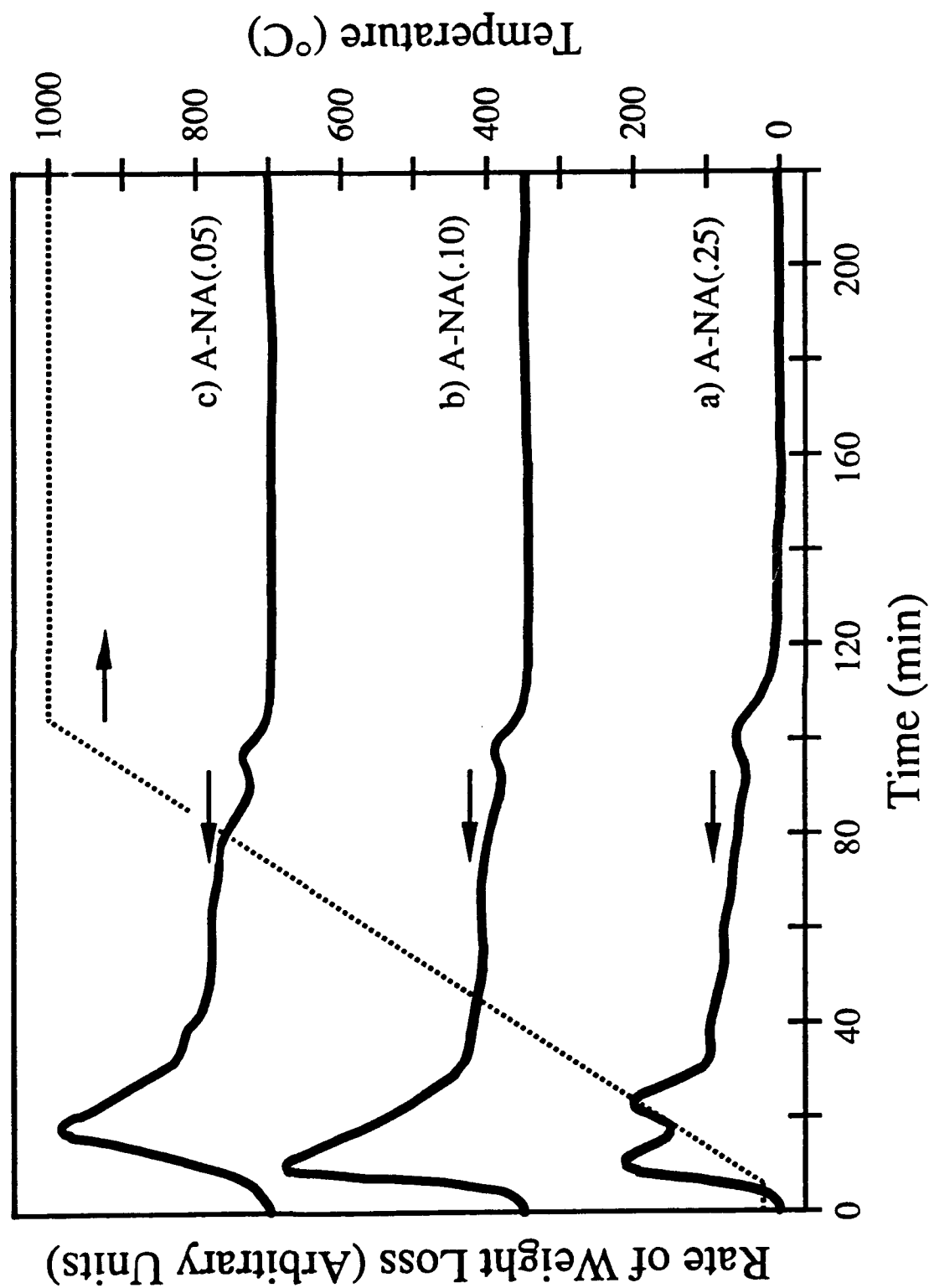
Table 5-17: PEAK TEMPERATURES FOR TG DIRECT REDUCTION DATA OF
ALUMINA AEROGEL SUPPORTED NIOBIA

| Sample	Heat Treatment	Peak Temperature (°C)
A-NA(.25)	(500,2)	868(B*), 990
A-NA(.10)	(500,2)	981
A-NA(.05)	(500,2)	968

* B = Broad

Table 5-18: PEAK TEMPERATURES FOR TG REDUCTION DATA OF HEAT
TREATED ALUMINA AEROGEL SUPPORTED NIOBIA

Sample	Heat Treatment	Peak Temperature (°C)
A-NA(.25)	(1000,-)	1000
A-NA(.10)	(1000,-)	995
A-NA(.05)	(1000,-)	995

Figure 5-38: TG REDUCTION DATA FOR PRETREATED (1000,··) ALUMINA AEROGEL SUPPORTED NIOBIA: A) A-NA(.25), B) A-NA(.10), AND C) A-NA(.05)
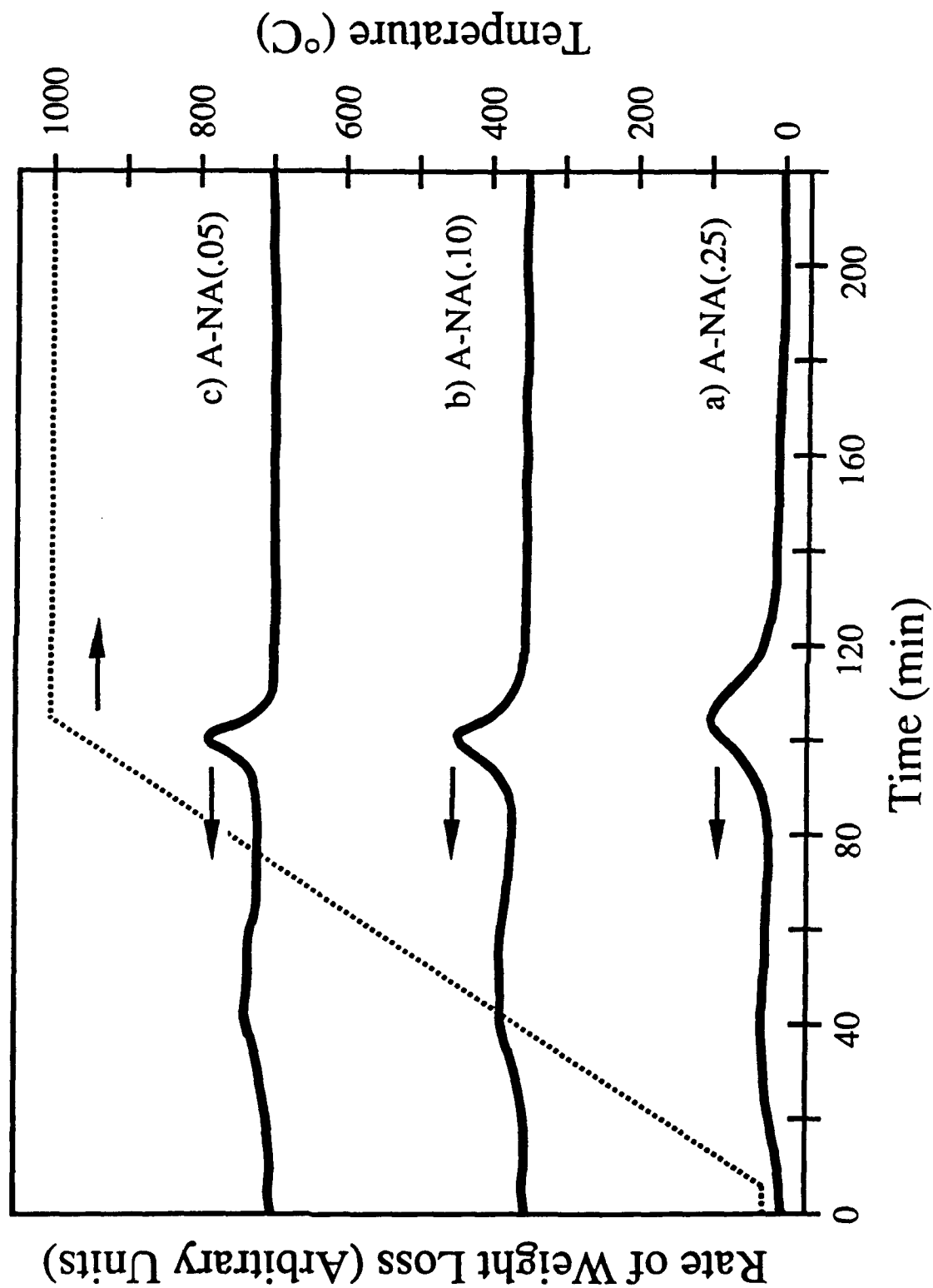
5.3.5 1-Butene Isomerization

1-Butene isomerization is a reaction that has been used to probe the acidity of materials, and makes an ideal choice as a test reaction for the catalytic properties of the supported oxides. Figure 5-39 shows the 1-butene isomerization activity (mol/hr-g) versus time on stream (TOS) for the calcined and heat treated silica aerogel supported niobia. The trend for these materials in both the calcined and heat treated samples is that for the higher loading or content of niobia, the greater the activity of the catalyst on a per gram total sample basis. The steady state isomerization rates are 0.59, 0.24, and 0.14 x 10^{-2} mol/hr-g for the calcined A-NS(.25), A-NS(.10) and A-NS(.05), respectively. These activities and cis-/trans-2-butene ratios of the products are compiled in Table 5-19. The C/T ratios for these above three samples are all around 1 which indicates the reaction is catalyzed by Brønsted acid sites. FTIR studies of pyridine adsorption indicated that these samples do indeed possess Brønsted acidity. After a (1000,-) heat treatment the activity of all silica aerogel supported oxides went up by about a factor of 2 - 3, and is also shown in Figure 5-39. This same large activity increase was seen for A-NS25w in the previous chapter. The A-NS(.25), A-NS(.10), and A-NS(.05) samples had steady-state activities of 1.6, 0.45, and 0.30 x 10^{-2} mol/hr-g after the heat treatment. LRS studies indicated an increased ordering of niobia in A-NS(.25) after (1000,-) by the shift from ~ 680 cm^{-1} (after calcination) to ~ 725 cm^{-1} (after heat treatment) of the peak attributed to slightly distorted NbO$_6$ octahedra. XRD results actually were able to resolve the appearance of very poorly crystalline TT-Nb$_2$O$_5$ for A-NS(.25) after (1000,-). This changing environment for the niobia, from highly distorted complexes to more slightly distorted octahedra, is attributed to the high catalytic activity for 1-butene. The niobia/silica mixed oxide showed similar behavior in that after a (1000,-) heat treatment, this sample was still acidic and possessed weak Brønsted acidity.[88] We would expect to find similar results for the supported oxide of A-NS(.25). The C/T ratio for this sample is 0.04 and is identical to the value of 0.05 found for A-NS25w. These ratios are much smaller than 1, but it has been proposed that

Figure 5-39: 1-BUTENE ISOMERIZATION ACTIVITY (/G) OVER HEAT TREATED SILICA AEROGEL SUPPORTED NIOBIA

Figure 5-40: 1-BUTENE ISOMERIZATION ACTIVITY (/G Nb_2O_5) OVER HEAT TREATED SILICA AEROGEL SUPPORTED NIOBIA
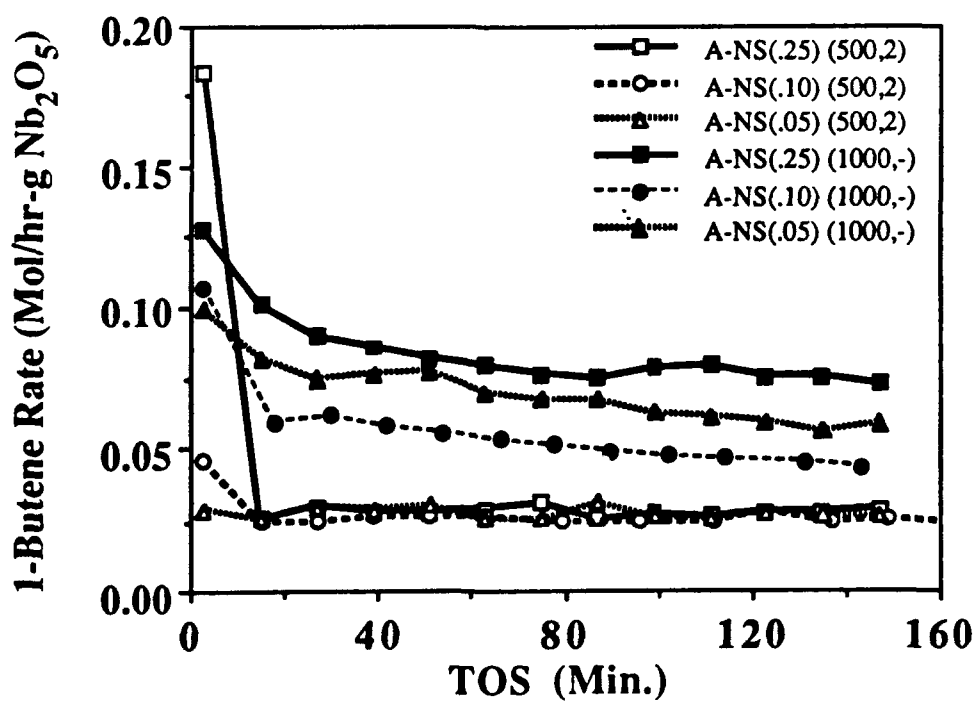
Table 5-19: 1-BUTENE ISOMERIZATION ACTIVITY SURFACE OXIDE AEROGELS (CALCINED)

	Steady-State Activity (mol/hr-) [x100]			
Sample	(/g)	(/g Nb$_2$O$_5$)	(/m^2 x100)	C/T*
A-NS(.25) (500,2)	0.59	2.8	0.098	1.3
A-NS(.10) (500,2)	0.24	2.5	0.032	1.1
A-NS(.05) (500,2)	0.14	2.7	0.020	0.7
A-NA(.25) (500,2)	0.11	0.68	0.024	1.0
A-NA(.10) (500,2)	0.033	0.43	0.0068	0.4
A-NA(.05) (500,2)	0.015	0.38	0.0036	0.1

Table 5-20: 1-BUTENE ISOMERIZATION ACTIVITY HEAT TREATED SURFACE OXIDE AEROGELS

	Steady-State Activity (mol/hr-) [x100]			
Sample	(/g)	(/g Nb$_2$O$_5$)	(/m^2 x100)	C/T*
A-NS(.25) (1000,-)	1.5	7.0	0.48	0.04
A-NS(.10) (1000,-)	0.45	4.6	0.080	0.07
A-NS(.05) (1000,-)	0.30	5.6	0.053	0.07
A-NA(.25) (1000,-)	0.030	0.18	0.023	0.28
A-NA(.10) (1000,-)	0.085	1.1	0.055	1.6
A-NA(.05) (1000,-)	0.039	0.98	0.020	1.1

* C/T = Cis/Trans-2-butene ratio

surface interactions could cause large deviations in this ratio.[203] The lower loadings of niobia on the silica support, A-NS(.10) and A-NS(.05), show increased values in activity after the 1000 °C heat treatment as well as possessing C/T ratios of 0.07. This suggests that these supported oxides behave similarly to A-NS(.25) and show that the niobia overlayer for these samples is also in a distorted (and primarily octahedral) environment that is interacting with the silica aerogel support. XRD studies did not show crystalline TT-Nb_2O_5 until more severe heat treatments (1000,48), which supports the idea that the niobia overlayers for A-NS(0.10) and A-NS(0.05) are distorted and not well ordered.

In order to get an idea of the dispersion of niobia on these silica supported oxides, the activity was normalized with respect to the amount of niobia on the surface, and this is shown in Figure 5-40. It is seen that all calcined (500,2) silica aerogel supported oxides appear to have the same steady-state activity of 2.7 x 10^{-2} mol/hr-g Nb_2O_5. This is not surprising since both A-NS(0.05) and A-NS(0.25) were shown by FTIR to have strong Brønsted acidity that most likely "coked" the surface of the oxide and/or poisoned the reaction down to a low steady-state activity. Note the extremely high initial activity for A-NS(.25) and the much lower steady-state rate attained and stabilized after TOS = 15 minutes. After the 1000 °C heat treatment the isomerization rate increased dramatically for all silica supported oxides as revealed in Figure 5-40 and Table 5-20. This figure shows that the activity increase is likely due to the niobia that is present on the silica aerogel support. The A-NS(.05) and A-NS(.10) supported oxides were XRD amorphous; however, A-NS(.25) revealed TT-Nb_2O_5 crystallites from both XRD and LRS results, but reduction studies also showed that the niobia overlayer on the silica substrate was stabilized by the interaction between these two oxides. This stabilization behavior of niobia by a rigid silica interface is also seen with the mixed oxide aerogel of A-NS25w, hence any activity behavior with the niobia silica mixed oxide would be expected to be pertinent to the silica supported oxide system as well. This is indeed what our findings show. The steady-state activities go up to an average value of ~ 6.0 x 10^{-2} mol/hr-g Nb_2O_5 or an average increase

of about 2 times the calcined activity. Along with this activity increase was a significant decrease in the C/T ratio. These results were seen by A-NS25w too, the calcined activity and heat treated activity were 5.4 and 12.4 x 10^{-2} mol/hr-g Nb_2O_5 and the C/T ratio dropped form 1.2 to 0.05, respectively. These results support the hypothesis that the increase in activity after the heat treatment is due to a restructuring of niobia into a new slightly distorted environment which is stabilized on the silica aerogel support. The fact that the calcined and heat treated steady-state activities are so different lead to the conclusion that niobia is in a different environment after the heat treatment (slightly distorted, Nb-O) than just after the calcination (highly distorted, Nb=O).

The alumina aerogel supported oxides were studied with respect to the 1-butene isomerization reaction and results of the activity (mol/hr-g) versus TOS are shown in Figure 5-41. A-NA(.25) shows the highest activity, 0.11 x 10^{-2} mol/hr-g (see Table 5-19), of all the calcined (500,2) alumina aerogel supported oxides. This sample was also shown to possess very weak Brønsted acidity by FTIR pyridine adsorption experiments which was different from A-NA(.05) which showed little if any Brønsted acidity. For this reason A-NA(.05) shows the lowest activity. A-NA(.10) falls between these two extremes as one would have anticipated. Heat treating A-NA(.25) to (1000,-) was shown by XRD and LRS studies to form $NbAlO_4$ which is known to be inactive towards 1-butene isomerization.[114] Thus, the significant drop in activity was expected for A-NA(.25) upon heat treating. Both of the lower loadings of niobia on the alumina support, A-NA(.05) and A-NA(.10), were shown to increase substantially in activity. Both showed nearly three-fold increases in activity from 0.015 to 0.039 x 10^{-2} mol/hr-g and 0.033 to 0.085 x 10^{-2} mol/hr-g for A-NA(0.05) and A-NA(0.10), respectively. Both of these supported oxides were shown to be XRD amorphous. This change in activity suggests a change in the bonding arrangement of niobia. It appears that the low loading of niobia on alumina transformed from a very strong interacting oxide that had little to no Brønsted acidity, into a material that has weak Brønsted acid sites. This could possibly be explained by a niobia
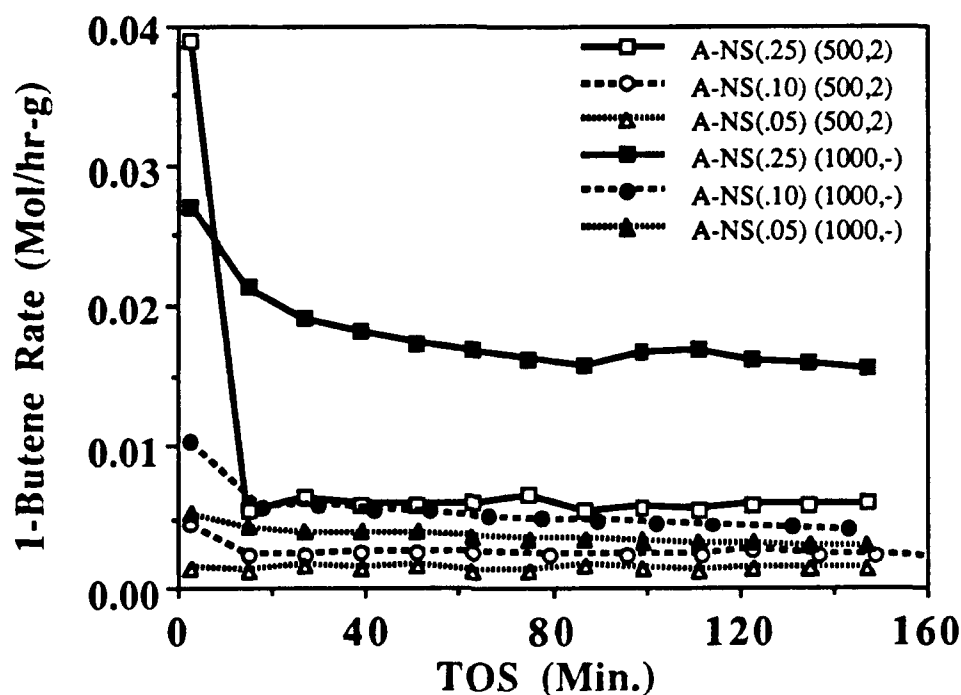
Figure 5-41: 1-BUTENE ISOMERIZATION ACTIVITY (/G) OVER HEAT TREATED ALUMINA AEROGEL SUPPORTED NIOBIA
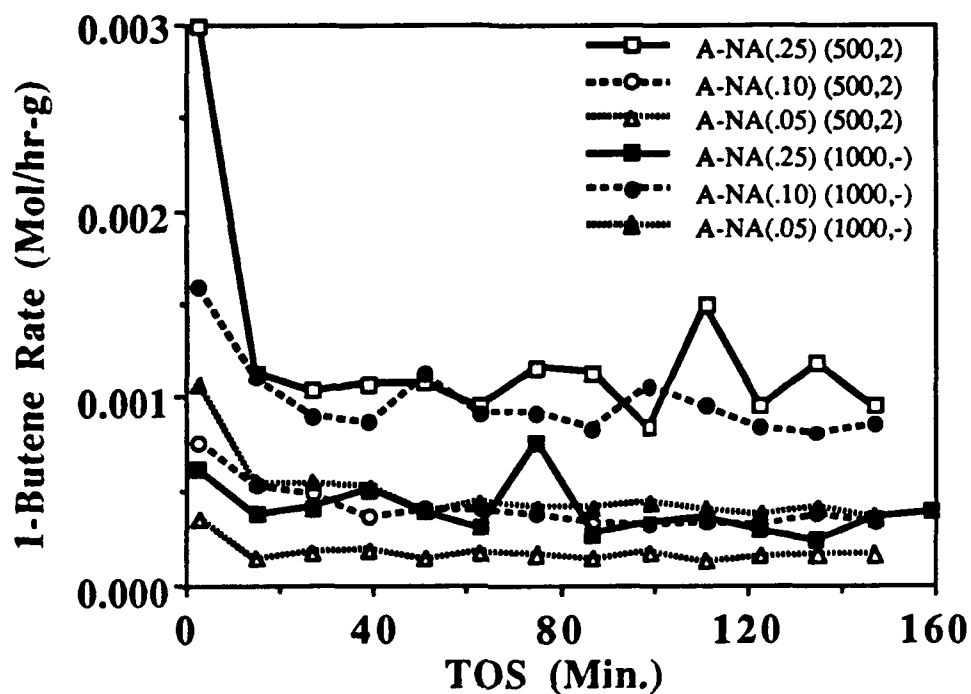
Figure 5-42: 1-BUTENE ISOMERIZATION ACTIVITY (/G Nb_2O_5) OVER HEAT TREATED ALUMINA AEROGEL SUPPORTED NIOBIA
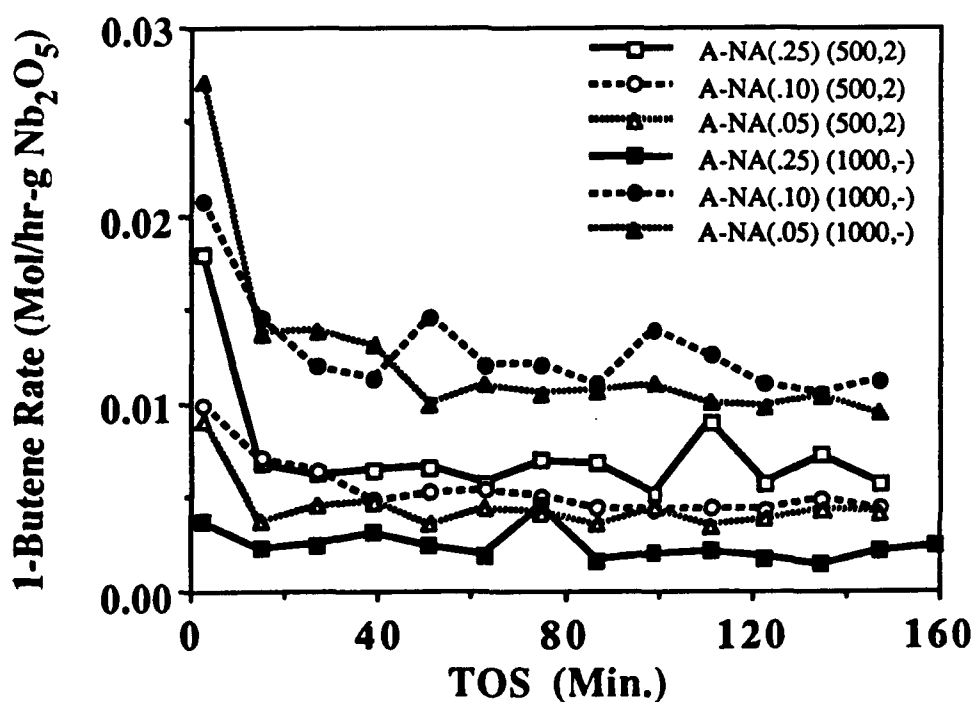
overlayer that is in a distorted environment similar to that found for niobia on silica after the heat treatment. The C/T ratio for A-NA(.05) and A-NA(.10) are 1.1 and 1.6, respectively, which indicates that these samples have Brønsted sites which catalyze the reaction.

The normalized activities for both the calcined and heat treated alumina aerogel supported surface oxides are shown in Figure 5-42. For the calcined alumina supported oxides, A-NA(.25) shows the highest activity, 0.68×10^{-2} mol/hr-g Nb_2O_5. This activity is ~ 65% greater than the other surface oxides which showed little to no Brønsted acidity. After heat treatment to (1000,-) one can see that the activity dramatically decreases due to the formation of the catalytically inactive $NbAlO_4$ compound. The A-NA(.05) and A-NA(.10) surface oxides show a large increase (~ three-fold) in activity from ~ 0.4 to 1.0 x 10^{-2} mol/hr-g Nb_2O_5 that is brought about by the distorted niobia overlayer and the Brønsted acid sites that these supported oxides appear to have developed as a result of this change and is evidenced by their C/T ratio (~ 1).

To summarize this 1-butene isomerization section, we will look at the two supported systems separately. The silica aerogel supported niobia system showed greatly enhanced catalytic activity after (1000,-) than after the standard calcination. The large activity after the heat treatment was attributed to the formation of a distorted niobia overlayer that was stabilized by the silica support. The silica supported samples after calcination had Brønsted sites that were too strong to efficiently catalyze the reaction. Significant "coking" and poisoning effects of the strongest sites were reasons discussed in lowering and achieving a constant activity for the reaction. Despite these "coking" effects, the silica aerogel supported oxides had activities greater than the bulk niobia aerogel after calcination on a per gram Nb_2O_5 basis. The alumina aerogel supported niobia samples only showed significant activity after calcination for A-NA(.25) which was attributed to the weak Brønsted acidity inherent with this material. After the (1000,-) heat treatment, the activity for A-NA(.25) dramatically decreased due to the compound formation of $NbAlO_4$. The A-NA(.05) and A-NA(.10) supported oxides showed enhanced activity for this

reaction after a high temperature heat treatment presumably due to the new bonding environment of the niobia overlayer on alumina. Similar bonding environments for the stabilized niobia on alumina and niobia on silica have been proposed.

5.4 Summary

This chapter presented and discussed results pertaining to the chemical and physical properties of the surface oxide aerogels. It was shown that very high surface area silica and alumina aerogel supported niobia binary oxides could be synthesized. The niobia was found to be dispersed on silica at ~ 5% monolayer coverage, while the alumina showed niobia to be dispersed at a higher coverage of ~ 10% monolayer. With all of the silica supported niobia surface oxides, high acid strength and acidity were found, the origin of which was attributed to highly distorted Nb=O terminal groups. The silica aerogel supported oxides were shown to have strong Brønsted acidity, and the higher loadings of niobia on silica were seen to develop the highest acid strengths. The silica support stabilized the niobia overlayer from crystallizing to bulk Nb_2O_5, because of the rigid niobia-silica interface that is formed upon thermal treatment. Initial 1-butene isomerization activity was high for the calcined silica aerogel supported system, but quickly diminished to a lower steady-state activity from a poisoning effect induced from the strong Brønsted sites. This isomerization rate was increased by a factor of two by allowing the niobia overlayer to orient to a new structure of slightly distorted octahedra stabilized by the silica substrate. The alumina aerogel supported niobia samples were found to have acid strengths at low niobia loadings comparable to the alumina aerogel; however, higher loadings of niobia increased the acid strength while also developing weak Brønsted acidity and new Lewis acid sites. This acid strength and acidity was attributed to the highly distorted niobia groups on the surface of the alumina. The alumina aerogel interacted strongly with the niobia overlayer as evidenced by the dispersion of niobia at a 10% monolayer coverage. This niobia-alumina interaction was so strong that the surface oxides underwent solid-state

reactions to form $NbAlO_4$ at sufficiently high temperatures. 1-Butene isomerization reaction studies confirm the existence of weak Brønsted acidity at the higher loadings of niobia. These isomerization results also show the existence of a stabilized overlayer of niobia on alumina (for low loadings of niobia) that is distorted and reveals the niobia to be in a different bonding environment as shown by the nearly three-fold increase in activity. The results from this chapter on the surface oxide aerogels of niobia will be coupled with the results from the previous chapter on mixed oxide aerogels in order to form a model for these binary oxides which can explain how oxide systems related to the physical and chemical properties of these materials.

Chapter 6

STRUCTURAL AND ACIDIC PROPERTIES

This chapter presents proposed structures for bulk niobia aerogels as well as the binary oxides of niobia-silica and niobia-alumina based upon the experimental data presented in Chapters 3, 4, 5, and the literature review presented in Chapter 1. These molecular structures will then be discussed as to how they relate to their respective acidic properties.

6.1 Acid Strength and Acid Type

There are two types of acid sites found on solid acids. Brønsted acid sites have tendencies to donate protons while Lewis acid sites accept electron pairs because of coordinatively unsaturated cations in the oxide matrix. The distinction between these two sites is important because the catalytic properties of these acid sites can be very different. The acid strength of a solid surface is defined as the ability of the surface to convert an adsorbed neutral base to its conjugate acid.[146] The weaker the base, the stronger the acid must be in order to adsorb it. Often times what dictates the strength of an acid is its ability to delocalize the negative charge that is associated with the acceptance of an electron pair or the donation of a proton. In this fashion, solid acids are very effective since the entire solid oxide matrix is available for the charge distribution. This will be illustrated in the following example for tungsten oxide supported on alumina for both Lewis and Brønsted acids (see Figure 6-1). Analysis of these surface species as acids by Bernholc et al.[12] shows that the

Figure 6-1: TUNGSTA-ALUMINA SURFACE OXIDE: BRØNSTED AND LEWIS ACIDITY

Brønsted Acidity:
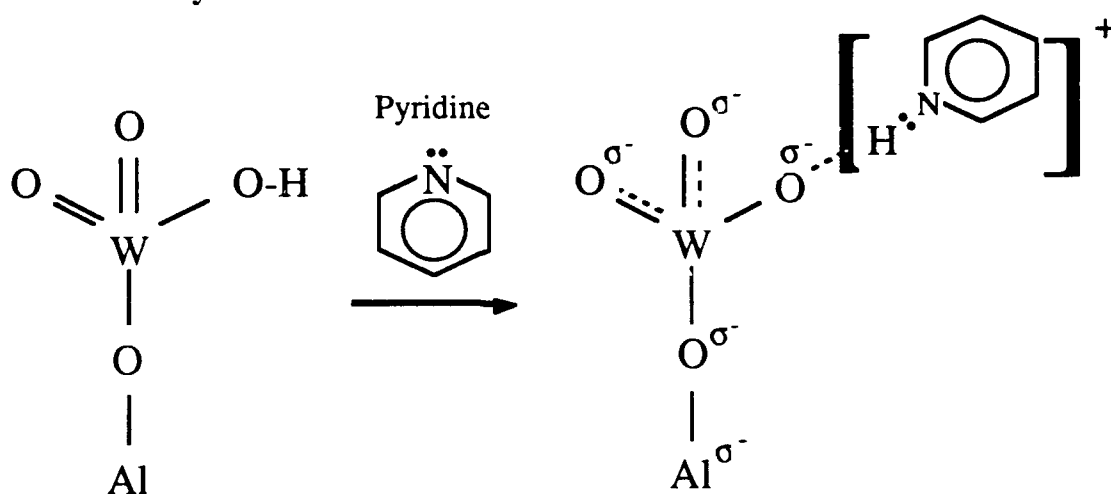
Lewis Acidity
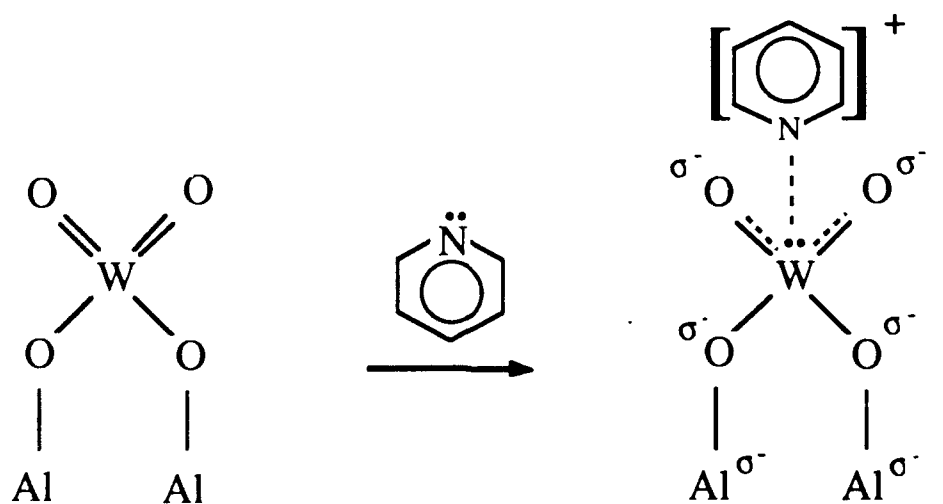
ACID   CONJUGATE BASE

doubly bonded oxygens act to distribute the negative charge associated with the acceptance of an electron pair or donation of a proton as both terminal oxygens have double bond character. The experimental acid strengths of main group elements increase considerably with the number of terminal oxygen atoms, i.e. $Si(OH)_4 \ll PO(OH)_3 \ll SO_2(OH)_2$.[12] The support also plays an "inductive" role by allowing charge distribution to occur into the substrate and delocalize throughout the oxide matrix. This effect is enhanced with an increasing number of surface linkages to the substrate. These ideas will now be used in the following sections to develop structural models based on the chemical property data from the previous chapters.

6.2 Niobia Aerogel Structure

The first structure that we will analyze here is the aerogel of niobia. After a conventional calcination (500,2), LRS results show that this sample has a broad peak centered around 900 cm^{-1}. FTIR and DRIFT spectra indicated that this material also strongly chemisorbed water. This adsorption of water was further confirmed by *in-situ* LRS studies, which showed that water was indeed adsorbed on surface moieties or functionalities as seen by the shift in the broad peak from ~ 900 cm^{-1} to more defined peaks, at about ~ 930 cm^{-1} and ~ 995 cm^{-1}. The two high frequency stretches indicate the possibility of two highly distorted NbO_6 octahedra containing Nb=O bonds, with the lower frequency indicating a longer Nb=O bond.[92] The niobia aerogel also showed high acid strength (~ 34 kcal/mol) and acidity. Pyridine adsorption experiments using FTIR spectroscopy showed that this sample possessed strong Lewis acidity and weak to moderate Brønsted acidity. With these experimental data in mind, and knowing that *in-situ* LRS studies showed a preponderance of Nb=O bonds in this sample as well as a contribution of Nb-O bonds from slightly distorted octahedra sharing edges and corners, we can propose a structure for this niobia aerogel in which the basic building block is a

highly distorted NbO_6 octahedra containing a Nb=O bond (see Figure 6-2). This cage-like octahedral structure looks surprisingly similar to that of $K_8Nb_6O_{19}$, and in fact these two materials share similar LRS spectra with the features for $K_8Nb_6O_{19}$ being sharper than for the amorphous niobia aerogel.[209]

The conventionally prepared niobia samples were indexed by XRD to be the low temperature phase of niobia, TT-Nb_2O_5, unlike the aerogel of niobia which was found to be amorphous after the same heat treatment. A shift in the main LRS stretching modes for the NbO_6 octahedra from ~ 650 cm^{-1} (amorphous) to ~ 680 cm^{-1} (TT-Nb_2O_5) occurred for the conventionally prepared niobia, and indicates a shortening and strengthening of the bond in these materials. *In-situ* LRS studies on the precipitated niobia sample also indicated a lack of peaks at around 995 cm^{-1} or 930 cm^{-1} which have been previously associated with Nb=O bonds contained in highly distorted octahedra. The LRS shift in the NbO_6 feature (650 to 680 cm^{-1}) indicates that the removal of the Nb=O bonds could be shortening the other Nb-O bonds in the NbO_6 octahedra and thus could also be introducing some order in niobia. The conventionally prepared (precipitated) niobia sample showed a much lower acid strength (lower by ~ 10 kcal/mol) when compared with the aerogel of niobia, and this too could be a sign that Nb=O bonds have been removed and replaced with Nb-O bonds. With this in mind we can propose a structure for conventionally prepared niobia, after a (500,2) calcination, in which the basic building block is the slightly distorted NbO_6 octahedra (no Nb=O bonds) as shown in Figure 6-3. The structure that is shown in Figure 6-3 is not a rigid schematic interpretation of TT-Nb_2O_5, but does show some key features that are inherent in the crystalline form of TT-Nb_2O_5, i.e. a lack of niobium-oxygen double bonds and slightly distorted octahedra.

As the aerogel is heat treated to higher temperatures ($\geq$ 600 °C) we notice that the acidity and acid strength of this material decrease. Concommittant with these observations is the lack of LRS features above 900 cm^{-1} which indicates that this material does not possess a significant number of Nb=O bonds. Hence with heat treatment, the niobia

Figure 6-2: PROPOSED MOLECULAR STRUCTURE FOR NIOBIA AEROGEL
AFTER A (500,2) CALCINATION: BASIC BUILDING BLOCK IS A
HIGHLY DISTORTED NbO_6 OCTAHEDRON WITH A Nb=O BOND
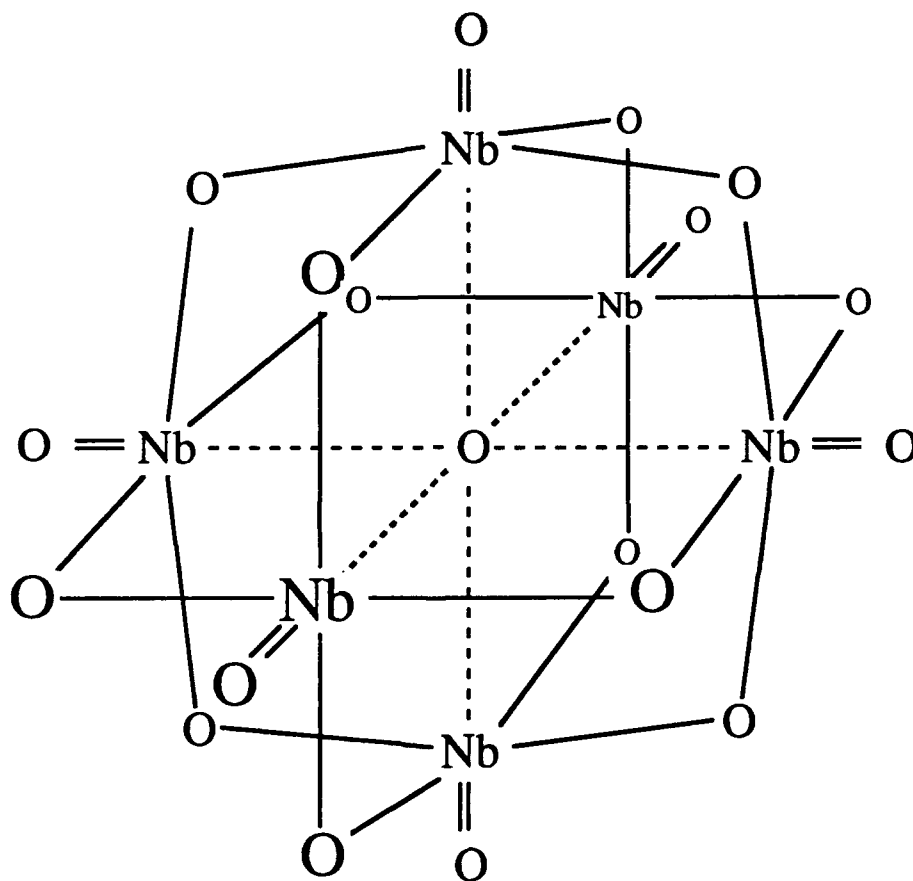
Figure 6-3: PROPOSED MOLECULAR STRUCTURE FOR CONVENTIONALLY PREPARED NIOBIA AFTER A (500,2) CALCINATION: BASIC BUILDING BLOCK IS A SLIGHTLY DISTORTED NbO_6 OCTAHEDRON
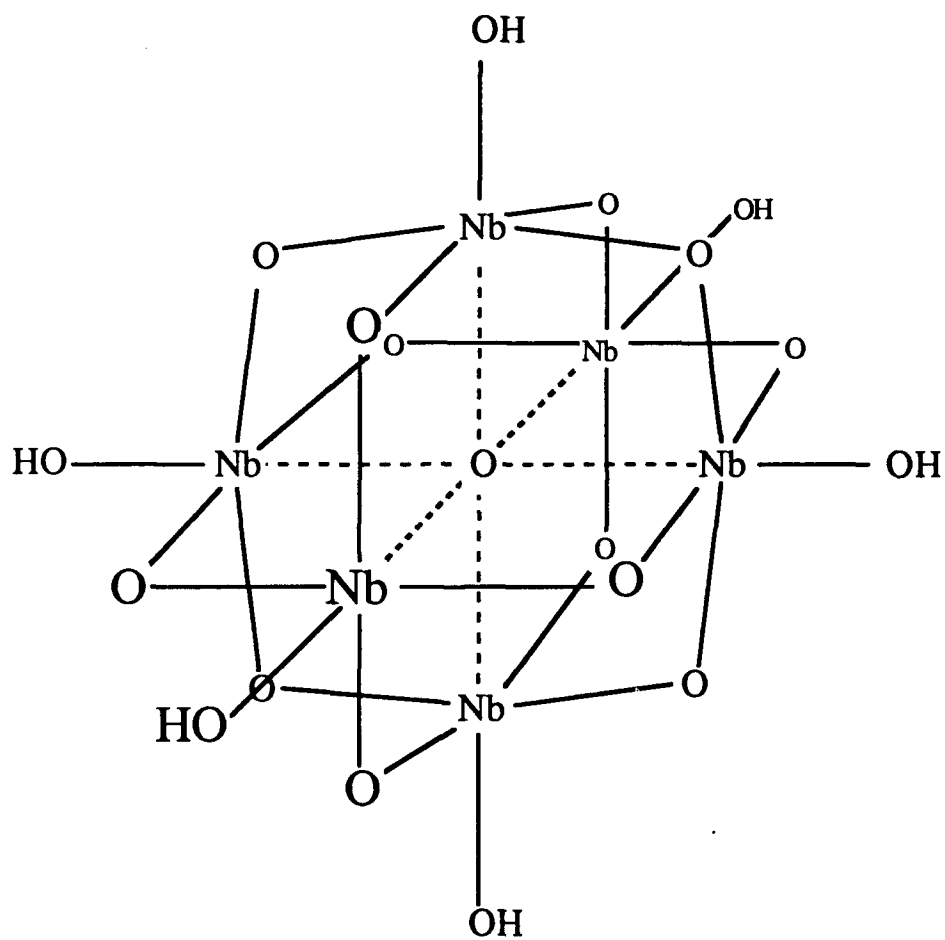
aerogel follows the same course as the conventionally prepared niobia, and indicates that the basic structural unit for the aerogel has changed from a highly distorted NbO_6 octahedron containing a Nb=O bond, to a slightly distorted NbO_6 octahedron which contains no doubly bonded oxygens (see Figure 6-3).

6.3 Niobia-Silica Binary Oxides

The first system that will be discussed is the niobia-silica binary oxides. The mixed oxide aerogel of niobia/silica will be discussed along with proposed structures and will be compared to the silica aerogel supported niobia samples at various coverages to determine similarities or differences in these systems.

6.3.1 Niobia/Silica Mixed Oxide Aerogel

The structural and bonding information for A-NS25w was provided by LRS and *in-situ* LRS measurements. The coordination number of oxygen in niobia is 2.4, which means that the oxygens in niobia primarily have a coordination number of 2, while there are a few oxygen atoms that have a coordination of 3 or even 4. Also, the oxygens in silica have a coordination number of 2, and considering that this is the major oxide in this binary system, we believe that the oxygen coordination around the niobium atom will also be 2. The Si-O bonds in bulk silica are highly covalent and lead to the formation of a preferred tetrahedral structure. The Nb-O bonds on the other hand are less covalent than the Si-O bonds, hence these Nb-O bonds are likely to conform to the rigid tetrahedral silica matrix surrounding the niobium cation. This leads to a structure that is distorted from the preferred octahedral environment for niobia as shown earlier for the conventionally prepared niobia. Indeed LRS indicates that niobia in A-NS25w was definitely not in an octahedral environment and possibly in a highly distorted tetrahedral environment. Applying Pauling's electrostatic bonding rules to niobia in the niobia/silica (tetrahedral environment)

mixed oxide, one sees that a +1 charge builds up around the niobium cation (see Figure 6-4). In order to enforce charge neutrality in this mixed oxide, a Nb=O bond must occur on the oxide surface to counteract this charge imbalance (see Figure 6-4). *In-situ* LRS measurements confirmed the existence of a Nb=O bond, indicative of a highly distorted tetrahedral niobia species since the niobia bonding environment was determined earlier not to be octahedral.[67, 92, 94]

Thus, the basic building block for the mixed oxide aerogel of niobia/silica is a highly distorted tetrahedral niobia species which has a single Nb=O bond, as well as three Nb-O-Si linkages to lock the niobia into the rigid silicia matrix (see Figure 6-5). As discussed previously the doubly bonded oxygen should allow a delocalization of charge to occur over the double bond, and the three Nb-O-Si bonds should allow extra charge distribution to occur throughout the oxide matrix making A-NS25w a strong Lewis acid. Heats of adsorption measurements confirmed this mixed oxide to be a very strong acid. FTIR pyridine adsorption experiments also showed that the niobia/silica mixed oxide does indeed show strong Lewis acidity. The lack of Nb-OH groups adjacent to the Nb=O bond for A-NS25w prevents it from being a strong Brønsted acid. The weak Brønsted acidity that is found in this sample probably occurs from strongly adsorbed water on the Lewis sites or Nb-O-Si linkages. DRIFT and FTIR studies showed that this sample strongly chemisorbed water. We will now focus our attention to the silica aerogel supported niobia system to determine the similarities and differences in these two binary oxides.

6.3.2 Niobia-Silica Supported Oxides

We will first analyze the structure of the lowest coverage niobia surface oxide, A-NS(.05), investigated in this study after calcination at (500,2). LRS results suggest that niobia is present primarily in a tetrahedral bonding environment and DRIFT results confirm the presence of a niobium-oxygen (Nb=O) double bond. *In-situ* LRS studies also show a sharp band around 980 cm^{-1} indicative of a strong interaction between Nb and O and is in

Figure 6-4: POSSIBLE STRUCTURES FOR TETRAHEDRAL NIOBIA IN A-NS25w

Charge Imbalance Around the Niobium Cation Calculated Using Pauling's Electrostatic Valence Rules:

$$\begin{array}{ccccc}
 & | & & | & \\
 & O & & O & +1 \\
 & | & & | & \\
-O-Si&-&O-Nb&-&O- \\
 & | & & | & \\
 & O & & O & \\
 & | & & | &
\end{array}$$

Restructured Surface to Counteract Charge Imbalance:

$$\begin{array}{ccccc}
 & | & & | & \\
 & O & & O & \\
 & | & & | & \\
-O-Si&-&O-Nb&=&O \\
 & | & & | & \\
 & O & & O & \\
 & | & & | &
\end{array}$$
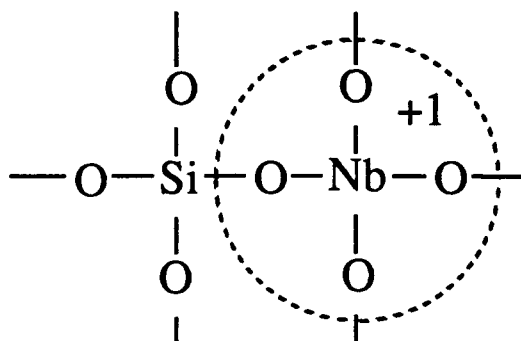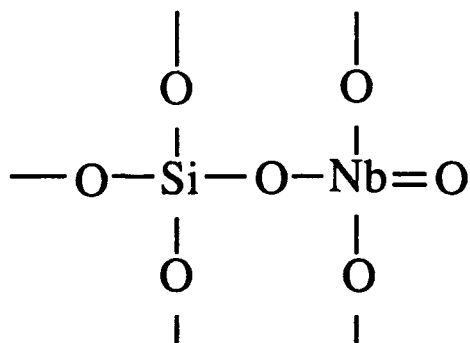
Figure 6-5: PROPOSED MOLECULAR STRUCTURE FOR A-NS25w AFTER A
(500,2) CALCINATION
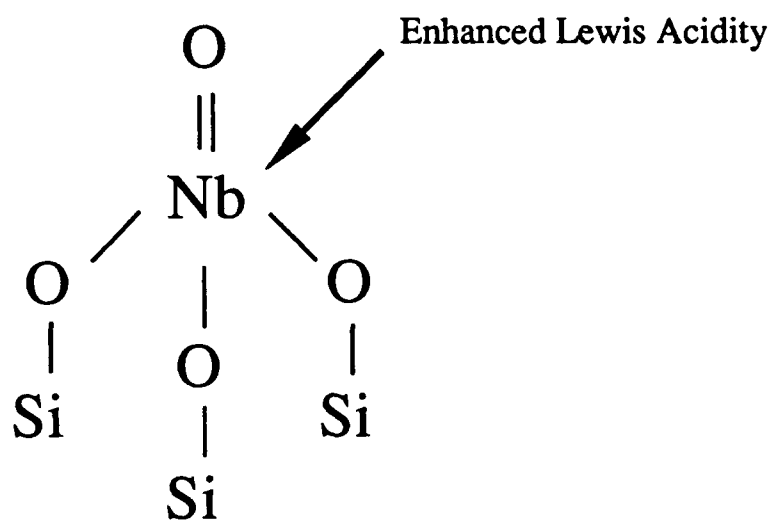
the frequency range of a Nb=O bond. These results confirm the structure for supported niobia presented in the literature and discussed earlier in Chapter 1. The literature suggests that niobia is tetrahedrally coordinated, and is anchored to silica by at least one Nb-O-Si bond with a single Nb=O bond. Quantum mechanical analyses by Kobayashi[93] suggest that the niobia species contains a single double bonded oxygen per niobium atom. The question still remains as to how the niobium cation is grafted to the silica substrate, i.e. how many surface links anchor this species to the surface. Several authors have shown experimentally that alumina is much more reactive than silica with most oxide precursors possibly because of the nearly three-fold concentration of hydroxyl groups on alumina than on silica, 12 OH/nm^2 versus 5 OH/nm^2, respectively.[17, 46, 57] Quantum mechanical calculations by Bernholc et al.[12] suggest that niobia is bonded to alumina via two linkages, thus the lower reactivity of silica makes it likely that the niobia is anchored with only one Nb-O-Si bond per niobium cation. This possible interpretation is also supported by our data, in that the n-butylamine titration results show that niobia is well distributed and dispersed for a higher coverage of niobia on alumina (10% monolayer) than for niobia on silica (5% monolayer). LRS studies also indicate that silica supported niobia easily rearranges to an octahedral environment with thermal treatments as low as 600 °C, while alumina supported niobia does not sinter and rearrange under even more severe thermal treatments.[85] These results indicate that niobia is less mobile on alumina than on silica because of the increased number of linkages to anchor the niobia species and hence is more stable with heat treatment also. Thus, the most likely bonding arrangement for A-NS(.05) will include one Nb-O-Si bond per each niobium atom, one Nb=O bond, and two adjacent hydroxyl groups as shown in Figure 6-6.

Acidity analyses of A-NS(.05) give interesting results which confirm the proposed structure shown in Figure 6-6. As mentioned previously, the niobium-oxygen double bond will distribute the negative charge associated with the donation of a proton or acceptance of an electron pair, and the single surface linkage, Nb-O-Si, acts to distribute

Figure 6-6: PROPOSED MOLECULAR STRUCTURE FOR A-NS(.05) AFTER A
(500,2) CALCINATION
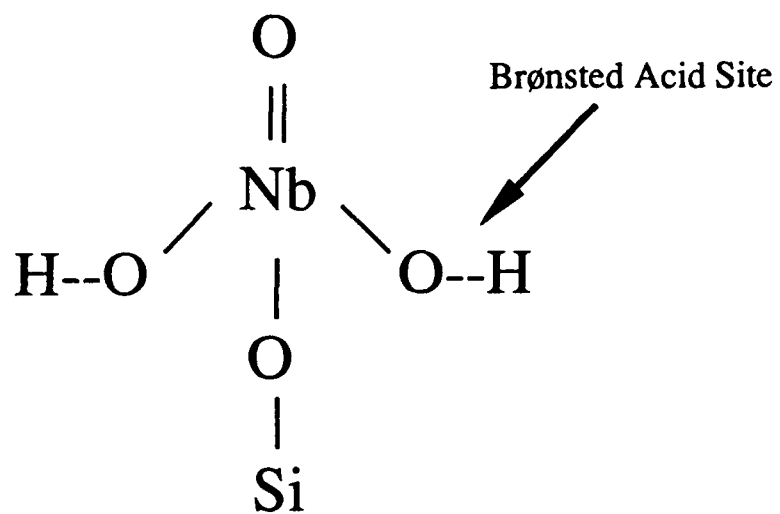
the charge into the supporting oxide matrix. This dispersion of charge into the silica matrix is effective because of the high electronegativity associated with the silicon atom. The hydroxyl groups attached to the niobium atoms adjacent to the Nb=O bond gives A-NS(.05) its high Brønsted acid strength as shown by its nearly constant L/B ratio with thermal treatment. Recall that the proposed structure for A-NS25w did not have any adjacent hydroxyl groups to the doubly-bonded oxygen and that this mixed oxide only showed weak Brønsted acidity unlike A-NS(.05) which has strong Brønsted acidity.

The higher coverage of niobia on silica, A-NS(.25), is more difficult to determine structurally than A-NS(.05) after a (500,2) calcination, because of the presence of both tetrahedral and octahedral niobia. LRS studies on the hydrated form of A-NS(.25) reveal the presence of highly distorted niobia species from a broad peak around ~ 950 cm^{-1} as well as more slightly distorted niobia, shown by the characteristic stretching frequency of ~ 680 cm^{-1} for Nb-O bonds belonging to NbO$_6$ octahedra. DRIFT results show that there is still a significant presence of Nb=O bonds, but the ratio of Nb=O bonds to Nb-O-Nb linkages has decreased with the increased surface coverage of niobia. Literature findings suggest that niobia is present in primarily edge sharing sites and that the average Nb-O bond distance is smaller than that of TT- or T-Nb$_2$O$_5$, thus indicating stronger Nb-O bonds. This is indeed what we found upon higher thermal treatment of this material.

The L/B ratio of Lewis to Brønsted acid sites for the quarter monolayer coverage of niobia on silica, A-NS(.25), is similar to the lower coverage of niobia, A-NS(.05). This suggests that with this supported oxide we also have strong Brønsted acidity, and leads to the conclusion that we have hydroxyl groups adjacent to Nb=O bonds on this niobia species too. Heats of adsorption experiments show that A-NS(.25) has a larger heat of adsorption than with A-NS(.05). This could be due to a two-fold inductive effect of the niobia surface oxide overlayer and the Nb=O bonds, plus the silica support actually yielding a better charge distribution. Recall that A-NS(.05) does not have any other bonds

to link the tetrahedra together and form an overlayer to disperse the charge, unlike A-NS(.25) which has an overlayer of linked highly distorted octahedra.

When A-NS(.25) is synthesized by incipient wetness impregnation, the larger concentration of niobium ethoxide (niobia precursor) causes a steric hindrance to occur on the surface of the silica support. Since the grafting procedure is dependent on the reaction with the hydroxyl groups of the support and this reaction is competitive, the probability of forming only one Nb-O-Si bond per niobium atom is even higher. The increased niobia precursor concentration brings the niobia species closer together on the surface and raises the chance of Nb-O-Nb bonding. These results are reflected in our LRS results mentioned previously. Thus, with all of this in mind we can propose a structure that includes both highly distorted edge sharing NbO_6 octahedra as well as a few tetrahedral niobia, all attached to the silica substrate with one Nb-O-Si bond. A possible structure that includes all of these properties is sketched in Figure 6-7. The basic features of this figure are the islands of edge-sharing highly distorted NbO_6 octahedra containing Nb=O bonds, that are linked to other highly distorted NbO_4 tetrahedra containing Nb=O bonds. This figure shows that there is a smaller percentage of niobia tetrahedra to niobia octahedra in A-NS(.25) than in A-NS(.05), as well as more Nb-O-Nb linkages. These results are all reflected in our DRIFT and LRS studies of these surface oxides. Yoshida et al.[86] have also proposed that higher concentrations of niobia on silica (10 wt.%) also show a highly distorted environment of the niobia species and that the coordination number for the niobium changes from 4 to 6 with this increased coverage while still possessing a Nb=O bond.

6.4 Niobia-Alumina Binary Oxides

The final system investigated in this study is the niobia-alumina binary oxides. The mixed oxide aerogel of niobia/alumina will be first discussed in terms of the proposed

Figure 6-7: PROPOSED MOLECULAR STRUCTURE FOR A-NS(.25) AFTER A (500,2) CALCINATION
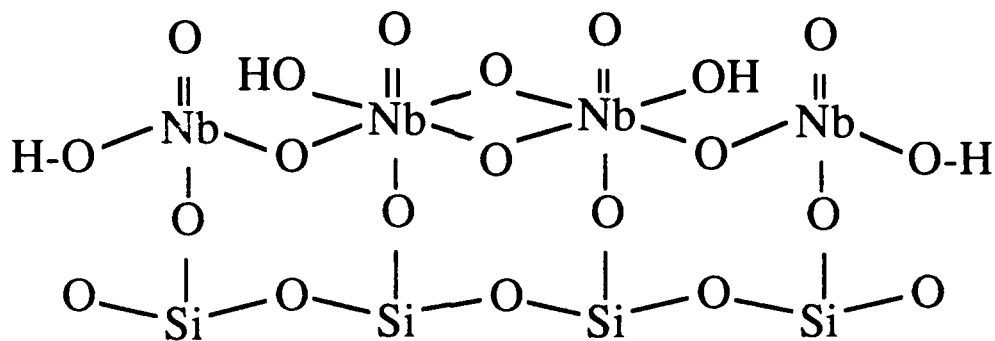
structure of this material and will be compared with the alumina aerogel supported niobia samples at various coverages to determine if these two systems are analogous.

6.4.1 Niobia/Alumina Mixed Oxides

The bonding environment of niobia in A-NA25w was provided by LRS and *in-situ* LRS studies. The coordination around the aluminum cation in bulk alumina can be either 6 or 4 which gives the coordination of the oxygen in this oxide as 4 and 2.7, respectively. The coordination number around the niobium atom in bulk niobia is 6 which gives the oxygen coordination a value of 2.4. Thus, since the aluminum cation can easily fit into an octahedral environment, the preferred bonding environment for niobia, it will be assumed that the niobium cation will also be in an octahedral structure and develop the preferred coordination value of 4 for the oxygens. This is slightly different than the proposed bonding environment for niobia when it is in silica, a much more rigid and covalent oxide than alumina which can develop two possible bonding environments depending on the number of defect sites in the bulk oxide. Our LRS study showed that niobia in A-NA25w was primarily octahedral. Our measurements show this sample, after a heat treatment at (600,2), to have a broad peak around 620 cm^{-1} which is indicative of Nb-O stretches for edge sharing NbO$_6$ octahedra, but there is also a sharper peak about ~ 920 cm^{-1} which is correlated to much stronger niobium-oxygen bonds, Nb=O. The sharpness of this peak could possibly indicate a large concentration of these bonds on the surface because the scattering intensity is so strong. This niobia/alumina mixed oxide also shows broad stretches around 250 cm^{-1} which are indicative of Nb-O-Nb bonds. Thus, these results show that the less rigid alumina allows the niobium cation to assume an octahedral environment that is highly distorted. The (600,2) heat treatment shows that these niobia octahedra begin to aggregate with one another, but the sol-gel chemstry and the normal (500,2) calcination should make the Nb-O-Al bonds linked homogeneously throughout, with little interactions from Nb-O-Nb bonds in the mixed oxide. Applying Pauling's

electrostatic valence rules to niobia in the niobia/alumina (octahedral environment) mixed oxide, one sees that a +2 charge builds up around the niobium cation (see Figure 6-8). In order to counteract this charge imbalance in the mixed oxide, a Nb=O bond must occur on the oxide surface (see Figure 6-8). *In-situ* LRS measurements confirmed the existence of a strong Nb=O bond, indicative of a possibly highly distorted octahedral niobia species.[67,92] Thus, the basic building block for the mixed oxide aerogel of niobia/alumina is a highly distorted NbO_6 octahedral niobia possessing a single Nb=O bond, as well as 5 Nb-O-Al linkages to secure the niobia into the alumina network (see Figure 6-9).

As mentioned previously for the example of tungsta on alumina, the doubly bonded oxygen should allow delocalization of charge over the double bond and the linkages of niobium to aluminum should allow an extra charge distribution to occur through the oxide matrix making A-NA25w a strong Lewis acid. Pyridine adsorption showed that the niobia/alumina mixed oxide does have strong Lewis acidity; however, the highly distorted octahedral niobia species in both bulk niobia as well as A-NA25w do not seem to be as strong as the highly distorted tetrahedral niobia species as found in A-NS25w from heats of adsorption experiments with pyridine. Incorporation of niobia into alumina develops new Lewis acid sites as well as enhancing the Lewis acidity of alumina. No Nb-OH groups, as shown in Figure 6-9 are adjacent to the Nb=O bond in A-NA25w and their absence prevents this mixed oxide from being a Brønsted acid. Even though chemisorbed water was shown to adsorb onto this niobia/alumina binary oxide, the coordinatively unsaturated aluminum and niobium cations bonded the moisture too strongly to facilitate the donation of a proton. The alumina aerogel supported niobia samples will be discussed next to determine similarities and differences in the two niobia-alumina binary oxide systems.

6.4.2 Niobia-Alumina Supported Oxides

A-NA(.05) will be discussed first since this supported oxide had the lowest surface coverage of niobia and was expected to result in an even distribution on the surface of the

Figure 6-8: POSSIBLE STRUCTURES FOR OCTAHEDRAL NIOBIA IN A-NA25w

Charge Imbalance Around the Niobium Cation Calculated
Using Pauling's Electrostatic Valence Rules:
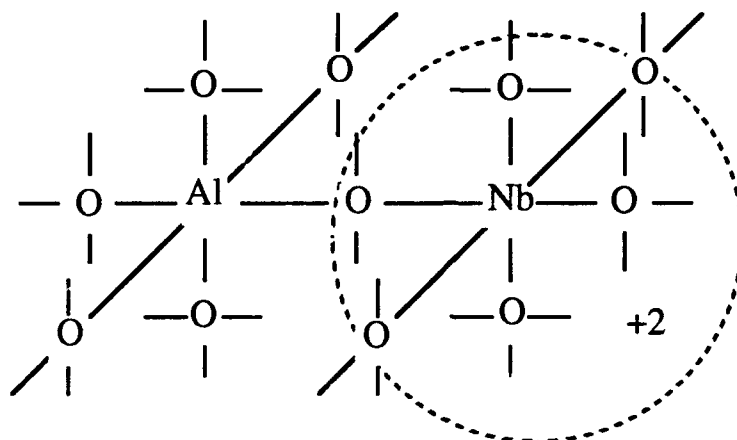
Restructured Surface to Counteract Charge Imbalance:
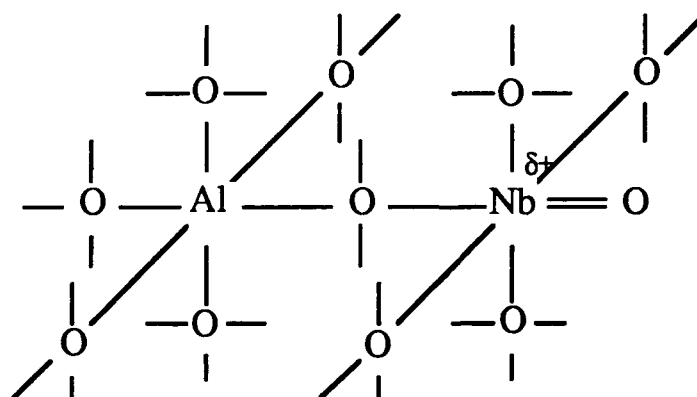
Figure 6-9: PROPOSED MOLECULAR STRUCTURE FOR A-NA25w AFTER A (500,2) CALCINATION
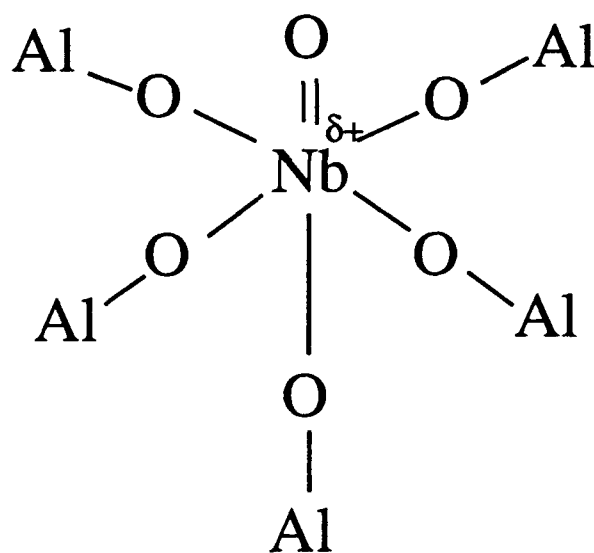
alumina. LRS studies did not yield useful structural information on this A-NA(.05) sample because of the fluorescing problems encountered from the alumina. However, other researchers have found that low coverages of niobia on alumina (1-10 wt.% Nb_2O_5) do show a peak in LRS spectra around ~ 900 cm^{-1} which is characteristic of the symmetric Nb=O stretching modes indicating a highly distorted niobia species. Quantum mechanical calculations by Kobayashi[93] indicated that the stable structure for the niobia species contains a single Nb=O for each niobium atom, and is anchored to the alumina support by one Nb-O-Al linkage. This was the same structure proposed for niobia supported on silica; however, one must realize that this study only assumed one Nb-O-Al bond on all of the proposed structures in order to simplify the calculations. Several authors have demonstrated that alumina is much more reactive than silica with most oxide precursors.[47] In fact, Bernholc et al.[12] performed quantum mechanical calculations using a niobia species that had a single Nb=O bond and was anchored to alumina through two Nb-O-Al linkages. Bernholc's[12] study was performed on samples to show the increased stability and strength of Brønsted acids by the double bonded oxygen in the surface species, but later adsorption studies will show that this A-NA(.05) sample possesses no Brønsted acidity. An interesting study by Hardcastle and Wachs[92] was centered around the determination of bond orders and niobium-oxygen bond distances using Laser Raman Spectroscopy. This study was applied to the dehydrated surface niobate species in niobia supported on alumina. It was found that the Nb^{5+} cation can only accomodate one terminal Nb=O and not two bonds of this strength. Therefore, they assumed a tetrahedral mono-oxo niobia species and performed calculations based on the Nb=O bond stretching frequency for this structure.[92] The calculated bond strengths for the surface linkages of Nb-O-Al were values expected for metal-oxygen-metal linkages of tetrahedral species. Thus, they concluded that a possible surface structure for the alumina supported niobia sample consists of a single Nb=O bond by which the niobium atom (in tetrahedral coordination) is anchored to the alumina support by 3 Nb-O-Al surface linkages as shown in Figure 6-10. This is the same

Figure 6-10: PROPOSED MOLECULAR STRUCTURE FOR A-NA(.05) AFTER A (500,2) CALCINATION
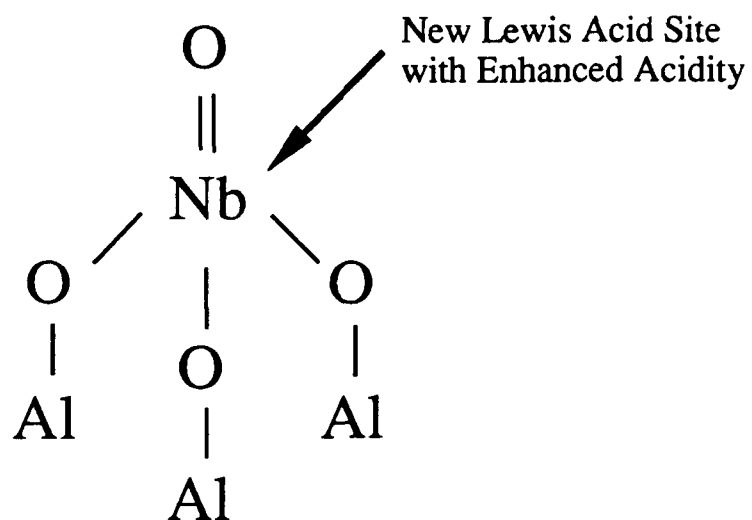
structure we propose for the niobia species on alumina as found in A-NA(.05). Hardcastle and Wachs[92] in their study could also not rule out the possibility that this structure was a highly distorted octahedron containing a Nb=O bond.

Acidity measurements of A-NA(.05) give results which confirm the structure shown in Figure 6-10. The niobia supported on alumina showed an increased stability with a higher coverage of niobia (10 wt.% Nb_2O_5) than the niobia supported on silica (5 wt.% Nb_2O_5) which indicates that niobia is better dispersed on alumina due to a lower mobility from the increased anchoring (3 linkages instead of only 1) to the supporting oxide. FTIR pyridine adsorption experiments showed that A-NA(.05) has very little if any Brønsted acidity as determined by the lack of an absorption peak at 1540 cm^{-1}, and also because the Lewis to Brønsted ratio (L/B) increases from 14.3 to 146.4 to 227.9 with treatment temperatures of 100, 200, and 300 °C, respectively. This is consistent with the proposed model structure since there are no hydroxyl groups adjacent to the Nb=O. Recall that niobia on silica showed a very different L/B ratio with pyridine adsorption which was attributed to Nb-OH groups adjacent to the Nb=O bond in this surface species. In A-NA(.05) there was also a slight shoulder around 1610 cm^{-1} in the FTIR spectrum (see Figure 5-34) which was probably attributed to the incorporation of niobia on alumina, but the concentration of this species was not enough to cause a large signal above the Lewis stretches for the bulk alumina. Heats of adsorption experiments on another low coverage sample, A-NA(.10), showed this sample to have slightly stronger sites than the bulk alumina which can be attributed to the Nb=O bond on the surface of this material. These experiments also showed that the bulk alumina aerogel itself was a moderately strong acid as indicated by the large heat of adsorption. FTIR pyridine adsorption studies also showed that the alumina acid strength is also slightly enhanced by the incorporation of niobia on the surface in A-NA(.05). Thus, although the proposed structures are somewhat different in the mixed oxide of A-NA25w and the surface oxide of A-NA(.05), similarities do exist in that both have Nb=O bonds while possessing no adjacent hydroxyl groups to yield

Brønsted acidity. Both samples also show new Lewis acid sites due to the incorporation of the niobium atom on or in the alumina matrix.

The sample containing a higher coverage of niobia on alumina, A-NA(.25), is slightly more difficult to analyze structurally because of the presence of both tetrahedral and octahedral niobia after the (500,2) calcination. The fact that these structures seem to coexist together leads to similarities that can be drawn between the silica and alumina supported systems. LRS studies on the hydrated form of A-NA(.25) reveal two distinct peaks at ~935 and 970 cm^{-1} corresponding to highly distorted niobia species in possession of Nb=O bonds, while also showing a broad peak at ~ 600 cm^{-1}, characteristic of Nb-O stretches of octahedral niobia, and also peaks around 350 cm^{-1}, characteristic of bending modes for Nb-O-Nb groups. This is similar to what Wachs' group has found for niobia supported on alumina at the higher coverages.[67, 85] Therefore, there appears to be an aggregation of niobia species on the surface of alumina that is changing the coordination of the niobia surface oxide. Hardcastle and Wachs[92] calculated that a highly distorted NbO$_6$ octahedron possessing a single Nb=O is not unlikely as the surface niobia species on alumina.

When A-NA(.25) is synthesized by the grafting procedure of incipient wetness impregnation, the bulkiness of the ethoxide groups in the niobia precursor should minimize the probability of extra linkages to the alumina support, because of the higher concentration and steric problems encountered with the niobium ethoxide precursor. The increased concentration brings niobia species closer together and increases the likelihood of Nb-O-Nb and edge sharing octahedra to bond on the surface of the alumina. This is reflected in the LRS spectrum mentioned earlier, and is similar to the A-NS(.25) supported oxide. Thus, with these results in mind we can propose a surface structure that includes both highly distorted octahedral and tetrahedral niobia species, all attached to the alumina substrate by Nb-O-Al bonds (see Figure 6-11). The main features of this structure are the islands of edge-sharing NbO$_6$ octahedra (highly distorted) that are linked to highly distorted NbO$_4$

Figure 6-11: PROPOSED MOLECULAR STRUCTURE FOR A-NA(.25) AFTER A
(500,2) CALCINATION
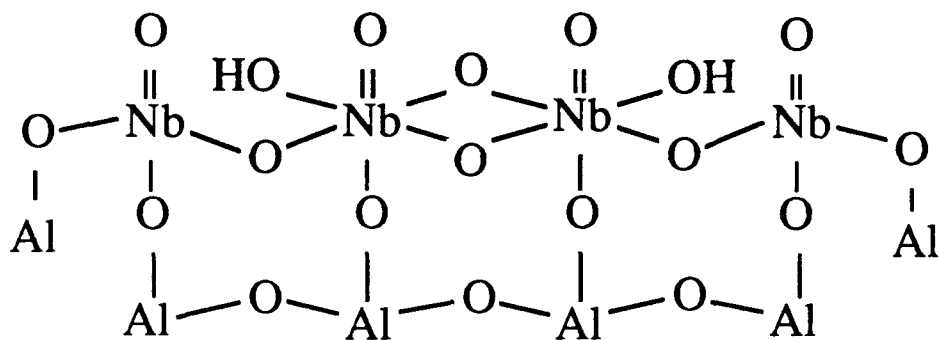
tetrahedra containing Nb=O bonds. Figure 6-11 shows that as the coverage of niobia is increased, the proportion of octahedral niobia to tetrahedral niobia increases as well.

The acidity measurements on this sample confirm the proposed structure for A-NA(.25) shown in Figure 6-11. Pyridine adsorption using FTIR shows a definite peak at ~ 1610 cm^{-1} confirming a new Lewis acid site and is extremely close to the peak on A-Nb$_2$O$_5$. This shows that the peak could possibly be attributed to the niobium cation that has a double bonded oxygen attached to it, similar to the bonding environment found for the niobia aerogel. These FTIR experiments also showed that the L/B ratio varies from 5.6 to 13.9 to 45.2 with increasing heat treatment and indicates that this sample has Brønsted acidity but it is weak. The peak around 1540 cm^{-1} confirms the existence of Brønsted acidity, and this sample was found to be active in 1-butene isomerization, a reaction that is known to be catalyzed by weak Brønsted sites. This sample was also shown to strongly adsorb water by DRIFT and FTIR spectra, and this adsorbed water (possibly on Lewis sites) could be participating as the weak Brønsted acid site. Heat of adsorption experiments on this sample showed that this sample has a much higher acid strength than A-NA(.05) or bulk alumina, and approaches the value for the bulk aerogel of niobia. Thus, this shows that as the niobia species grow as a surface oxide on the alumina substrate, its heat of adsorption approaches that of A-Nb$_2$O$_5$ and it also begins to look structurally similar too, as the tetrahedral niobia species are converted into octahedral species. The enhancement of acid strength for niobia on alumina is very similar to that found for niobia on silica as the coverage of niobia is increased. The reason for this enhanced heat of adsorption capability is the extra charge dispersion that is given by the formed niobia island overlayers.

6.5 Heat Treated Nobia-Silica and Niobia-Alumina Binary Oxides

Both of the niobia-silica binary oxides, A-NS25w and A-NS(.25), showed enhanced activity in 1-butene isomerization after a 1000 °C heat treatment, (1000,-), than

when subjected to the standard (500,2) calcination. Reasons for this enhanced behavior can be explained by developing a structure for these crystallized samples which were both indexed to be very poorly crystalline $TT-Nb_2O_5$. Since these crystalline binary oxides were at the threshold of XRD detectability, their crystallite size is approximately 3 nm. Assuming the crystallites to be spherical with an average Nb-O bond length of 2.0 Å we can calculate that 60% of the niobium atoms are on the surface and 40% are on the interior of the crystallite. Thus, this threshold calculation shows that a considerable number of niobia may be associated with the surface or even possibly a niobia-silica interface. LRS studies indicated large shifts in the range of octahedral Nb-O stretches, which confirm that the majority of the niobia in these crystallites is octahedral. Because the coordination number of each metal cation (niobium and silicon) are unchanged from their respective bulk oxides, interfaces similar to those proposed by Seiyama[151] will be created. Thus, oxygens at a Nb-O-Si interface as in A-NS(.25) (1000,-) and A-NS25w (1000,-) may have a charge build-up of [+5/6 - 2 + 4/4] = -1/6 and thus may participate as Brønsted acid sites. Kataoka and Dumesic's[152] model predicts that this oxygen falls into the correct range of undersaturation in order to participate as a Brønsted acid. It is these sites as well as the other poorly crystalline niobia sites which are responsible for the creation of the weak Brønsted acidity which catalyzes the 1-butene isomerization. A schematic of the niobia-silica binary oxide interface in A-NS25w will be drawn to illustrate the structural orientation that has occurred in these samples (see Figure 6-12). A schematic for the octahedral niobia-silica interface for A-NS(.25) is shown in Figure 6-13. The similar XRD patterns and LRS spectra of both samples confirm the existence of poorly crystalline $TT-Nb_2O_5$ in them. Figures 6-12 and 6-13 show the existence of similar interfaces (Nb-O-Si bonds) as well as octahedral niobia. Both of these bonding environments could possibly yield weak Brønsted acid sites which give these two samples their large and nearly identical isomerization activities. It appears that the niobia species in both of these binary oxides needs to have a sufficiently high temperature in order for the crystallized layers to orient

Figure 6-12: PROPOSED MOLECULAR STRUCTURE FOR OCTAHEDRAL NIOBIA-RIGID SILICA INTERFACE IN A-NS25w

Exposed Nb-O-Si Bond (Brønsted Acid Site)

Niobia-Silica Interface

Crystalline A-NS25w
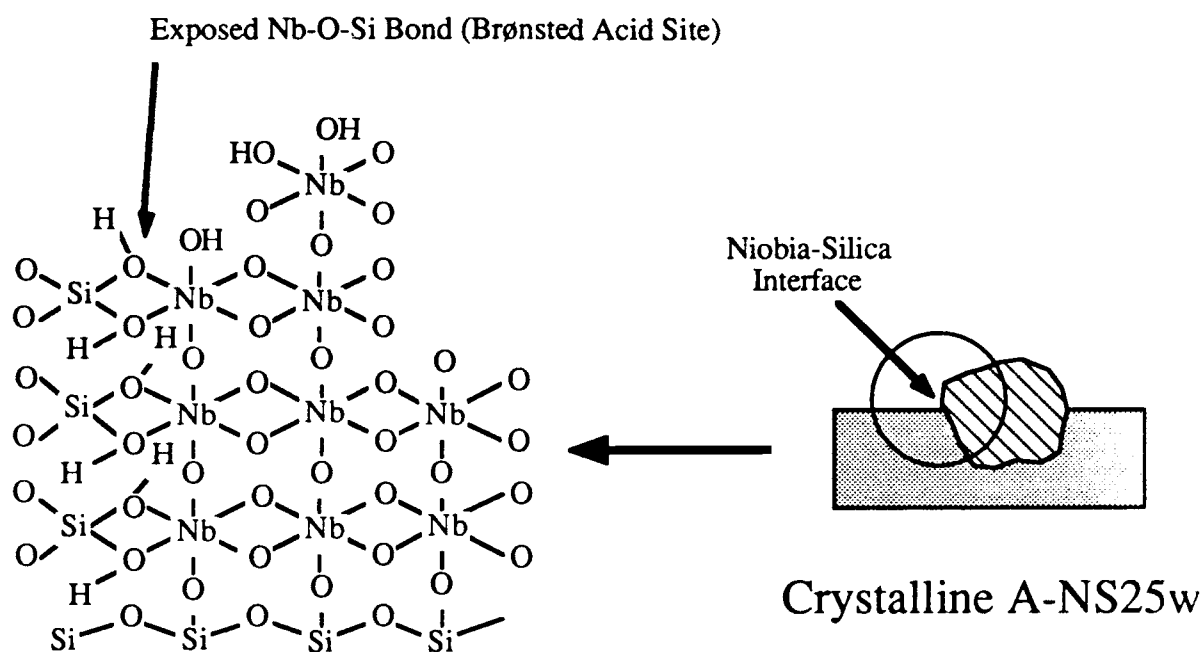
Figure 6-13: PROPOSED MOLECULAR STRUCTURE FOR OCTAHEDRAL NIOBIA-RIGID SILICA INTERFACE IN A-NS(.25)

Niobia-Silica Interface

Crystalline Silica Aerogel Supported Niobia

Exposed Nb-O-Si bond (Brønsted Acid Site)
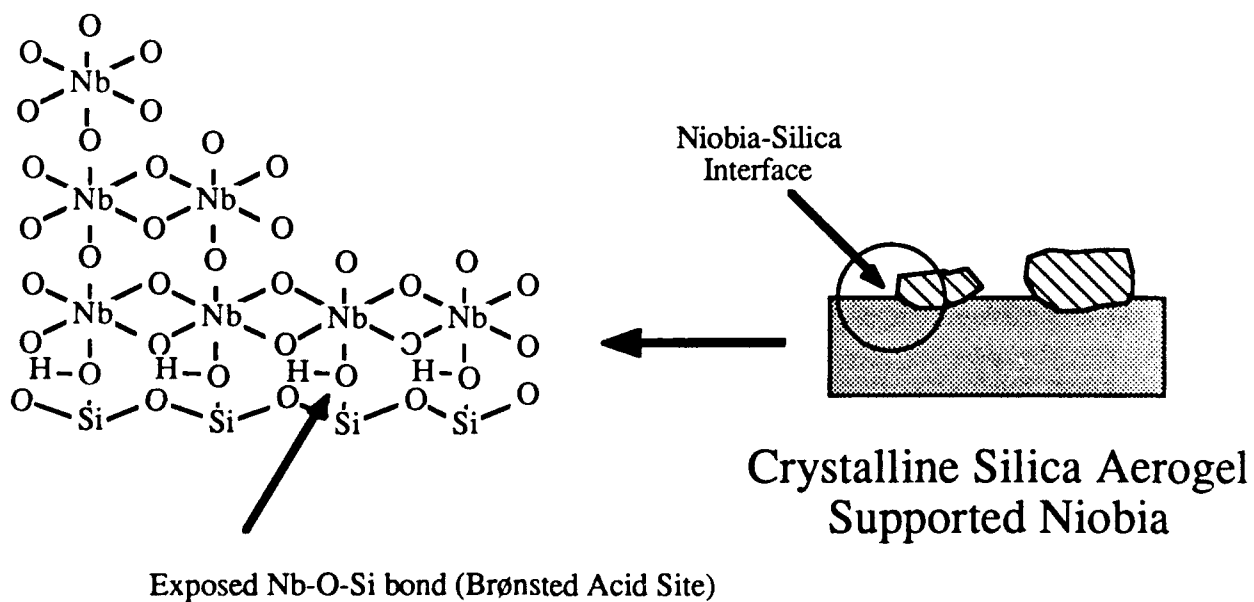
and become distorted when linking with the silica matrix. This orientation of the octahedral niobia with the silica substrate was shown to make niobia stable against reduction as shown in Figures 4-32 and 5-36.

A similar study was attempted for the niobia-alumina binary oxide system; however, due to the complications of the formation of $NbAlO_4$, interpretation of data is difficult. Some general observations will be noted here for completeness. Sufficient loading of niobia on [A-NA(.25)] or in [A-NA25w] the alumina matrix caused the formation of $NbAlO_4$ at (1000,-). A-NA(.05) and A-NA(.10) did not show any detectable formation of $NbAlO_4$, similar to results from other researchers.[85] Wachs[85] attributed the stability of the lower coverages of niobia on alumina to an increase in surface concentration of the niobia overlayer that has not exceeded a monolayer. Once the niobia monolayer coverage is exceeded, a portion of the supported niobia species is not directly interacting with the alumina surface and thus allows the solid-state reactions to occur and form $NbAlO_4$, as shown in A-NA(.25) and A-NA25w. The increased surface concentration of the niobia species on the lower coverages of niobia supported on alumina, A-NA(.05) and A-NA(.10), with heat treatment should allow a restructuring to occur on the surface. Recall that the isomerization activities for these two samples increased dramatically (3-fold) and was thought to be accounted for by a different bonding environment for niobia. The niobia species on these surface oxides is proposed to change from tetrahedral to octahedral niobia by the increased surface coverage induced by the (1000,-) heat treatment and is shown in Figure 6-14. Thus, we would expect to see a similar activity for 1-butene isomerization with these heat treated samples as with the A-NA(.25) (500,2) calcined surface oxide, which is exactly what we have shown in Tables 5-19 and 5-20 and Figures 5-41 and 5-42.

Figure 6-14: PROPOSED MOLECULAR STRUCTURE FOR (1000,-) HEAT
TREATED A-NA(.05) AND A-NA(.10)
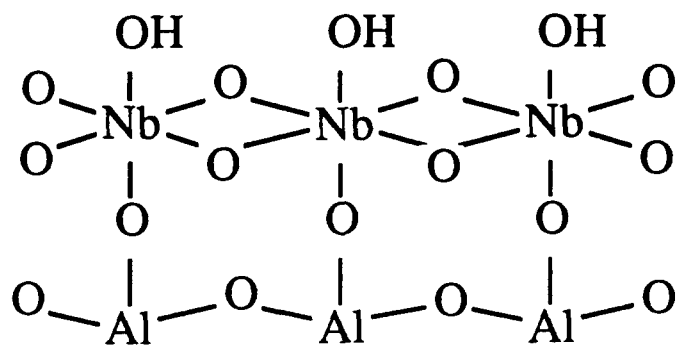
6.6 Summary of Structural-Acidic Properties

The above discussion showed the development of a number of structural-acidic properties relationships that are summarized below.

- Niobium oxygen double bonds in the aerogel of niobia act to form a strong Lewis acid site by the ability to delocalize electrical charge over the Nb=O bond.

- Tetrahedral niobia in possession of a Nb=O bond was shown to have a large acid strength as determined by pyridine adsorption experiments, larger than octahedral niobia with a similar Nb=O bond.

- Nb-OH groups adjacent to a Nb=O bond forms strong Brønsted acid sites, while no adjacent hydroxyl groups to the Nb=O bond show primarily strong Lewis sites.

- Highly distorted niobia surface overlayers as shown in A-NS(.25) are stronger acids than more dispersed surface niobia species as in A-NS(.05) because of the 2-fold distribution of electrical charge both over the island overlayer "inductive effect", and into the oxide matrix.

- Octahedral niobia-rigid silica interfaces can act as weak Brønsted acid sites as well as moderately strong Lewis acids due to the strong distortions induced by the silica matrix.

- Niobia on alumina at high concentrations, forms $NbAlO_4$ at high temperatures, while low niobia coverages show the coordination of the niobia species change from primarily tetrahedral to octahedral and form weak Brønsted acid sites with a high temperature heat treatment of (1000,-).

Chapter 7

SUMMARY AND RECOMMENDATIONS

7.1 Summary

This thesis has clearly shown that the structure of niobia strongly influences its chemical and physical properties. When niobia is placed in or on an oxide matrix such as silica or alumina, different bonding environments are formed which yield unique structures that also possess interesting properties.

We demonstrated the successful synthesis of a niobia aerogel which has the highest surface area ever reported for a 500 °C calcined sample. The aerogel of niobia also possessed a total pore volume and average pore diameter that were significantly larger than more conventionally prepared niobia. These unique physical properties led to the investigation of the structure of the niobia aerogel as well as the chemical properties inherent in this material. It was established from these experiments that the origin of both acid strength and acidity for the niobia aerogel was due to the highly distorted NbO_6 groups containing terminal Nb=O bonds, while the more conventionally prepared niobia samples had acid strength and acidity attributed primarily to slightly distorted NbO_6 octahedra possessing Nb-O bonds. Although the niobia aerogel was initially amorphous after a standard calcination, higher thermal treatments induced a crystallizing behavior similar to that of conventionally prepared niobia. In order to avoid the destabilization, niobia was incorporated in and on silica and alumina aerogels.

The mixed oxide aerogels of A-NS25w and A-NA25w were successfully synthesized and found to have superior physical properties to their more conventionally prepared counterparts. The low concentration of niobia in silica (A-NS25w) was shown to result in tetrahedral niobia. These species contained a doubly bonded oxygen and exhibited high acid strength and acidity. High temperature heat treatments changed the niobium atom environment from highly distorted tetrahedral to primarily octahedral with slightly distorted NbO_6 groups. This structural change resulted in a loss of acid strength, but enhanced the catalytic activity for 1-butene isomerization due to the distorted octahedral-rigid silica interface. A-NA25w, similar to A-NS25w, also possessed a Nb=O bond and had moderate acid strength and acidity. This niobia/alumina mixed oxide aerogel had little to no Brønsted acidity, as determined by pyridine adsorption experiments. High temperature heat treatments showed a formation of slightly distorted NbO_6 groups until a large enough driving force allowed a compound of $NbAlO_4$ to form.

The surface oxide aerogels prepared in this study showed interesting results as well. Low concentration of niobia supported on a silica aerogel resulted in well dispersed tetrahedral niobia species. Increased concentration of niobia to a quarter monolayer resulted in the increased formation of slightly distorted NbO_6 octahedra. Silica aerogel supported niobia exhibited high acid strength and acidity from having Nb=O bonds; the acid strength increased with niobia coverage. The silica supported oxides were also shown to have strong Brønsted acidity and to be effective catalysts for 1-butene isomerization. The alumina aerogel supported niobia samples were found to have moderate acid strength at low loadings of niobia, comparable to the bulk alumina aerogel; however, the higher loading of niobia (quarter monolayer surface oxide) showed a higher acid strength while also developing weak Brønsted acidity and new Lewis acid sites. The acid strength and acidity was attributed to the highly distorted Nb=O species on the surface of alumina. Increased concentration of niobia on the alumina aerogel gradually shows a conversion into slightly distorted NbO_6 as well. The alumina aerogel interacted very strongly with the

niobia overlayer as shown by the high dispersion of niobia at a 10% coverage, while on silica the niobia was dispersed at only a 5% coverage. The niobia-alumina interaction was so strong that solid-state reactions occurred to form $NbAlO_4$ at sufficiently high temperature and concentrations of niobia. Studies of 1-butene isomerization reaction studies confirmed the existence of weak Brønsted acidity at the higher loadings of niobia on alumina.

Niobia either in or on a matrix oxide such as silica or alumina was shown to be stabilized against crystallization and further phase changes to high temperature forms of niobia, as well as being stabilized against reduction. The surface oxides all reduced at a higher temperature than bulk niobia which suggests that the strong interfacial interaction between the two oxides is stabilizing niobia. With large thermal driving forces, high loadings of niobia on silica eventually lead to a destabilization and crystallization of bulk niobia, because the collapse of the silica support leads to a more mobile niobia that can be located far enough away from a stabilized niobia-silica interface so as to be unaffected by the interaction of these two oxides. Without the stabilizing effect of the interface, a high temperature phase of niobia is readily formed, similar to that for bulk niobia.

Thus, to summarize this thesis, a relationship was established between the structure and acidic properties of binary oxides containing niobia through the use of aerogels. This study showed that by careful manipulation of structure, acidic properties could be developed and controlled. By heat treating or using increased concentrations of a second oxide, we were able to form new structures with different properties than those that were untreated. Careful construction of a sample set with well characterized structures and acidic properties also led to a better understanding of the relationships between acidic properties and catalytic reactions.

7.2 Recommendations

This work has laid the foundation for an understanding of the structure-acidity relationship in niobia-containing binary oxides and can be extended to further our knowledge in this area. One promising approach is to apply the same methodology to other systems in order to establish a general trend which will lead to greater understanding and development of predictive models.

Using the ideas developed from this thesis to examine other systems allows for many new possibilities or developments. For example, using silica as the major oxide for the incorporation of oxides such as Ti, V, Zr, Ta, and Mo into a mixed binary oxide matrix should yield interesting results with the formation of extremely strong acid sites. Along these same lines, incorporation of V into an alumina matrix should also yield valuable information because of the lack of compound formation at temperatures below 1000 °C. Another interesting study which could be examined is using an oxide matrix other than silica which is already intrinsically acidic and maintains a covalent structure which is primarily tetrahedral (such as B_2O_3) and incorporating niobia or any of the aforementioned oxides into this matrix. In this fashion one may possibly develop a new line of superacidic binary oxides because of the charge imbalances that would develop as well as the distortions that would be forced onto the substituting oxide in order to accommodate this tetrahedral environment. Another interesting idea is the possibility of using the high surface area niobia aerogel as the supporting oxide for other oxide components to be grafted onto it, such as SiO_2, Al_2O_3, etc. Of course, the choice of any one of these systems depends on the scope of the proposed research, but with the advances and suggestions in this work, the choice of the binary oxide system does not have to be arbitrary or random.

Another approach for further research in this area is the development and refinement of new techniques to better analyze or characterize sample sets. Construction of an *in-situ*

DRIFT cell would be ideal at helping to analyze surface structures on the supported or mixed oxides. Strongly chemisorbed water made most measurements in this area intractable because of the strong absorption of this molecule. A system designed to heat treat the sample up to temperatures of 500 °C with the ability to evacuate the system as well as flow probe molecules to the oxides would make interesting surface sensitive experiments which would reveal more information into the properties of these systems as well. Another interesting experiment would be to probe the strength of specific acid sites in general, i.e. determine the acid strength of Brønsted sites. One could do this experiment by using the same procedures and equipment utilized in his study, except instead of using pyridine, one must use a sterically hindered base such as 2,6-dimethyl pyridine or a probe molecule that is even more sterically hindered like 2,6-di-s-butyl pyridine. Using these molecules would give specific strengths of acid sites using the TG gas adsorption experiment, and could possibly lead to a better understanding of catalytic reactions. The acidity (or number of acid sites) of the oxides, using this sterically hindered probe molecule, could be measured and give an actual distribution of Lewis and Brønsted acid sites and serve as a check to the measured acid strength.

These suggestions should all be useful for further research into this area, but one important step that must be done is to insure that a meaningful sample set is prepared that will allow a determination of how different structures influence the properties of these materials. As was shown in this thesis, it is not only the choice of the oxide components which determine the physical and chemical properties, but also the structure which plays an influential role. This work has shown that similarities do exist between the properties of mixed and supported oxides and that manipulation of various parameters such as oxide concentration or heat treatment can change the structure of an oxide and improve or hinder its catalytic performance. This thesis has offered suggestions to improve understanding of structural-chemical property relationships that should advance the knowledge and application of binary oxides as catalysts.

REFERENCES

1. Tanabe, K., in *Catalytic Science and Technology,* (eds. Anderson, J.R. & Boudart, M.), (Springer-Verlag, New York, 1981), **2**, pp. 231-273.

2. Tanabe, K., *Solid Acids and Bases, Their Catalytic Properties,* (Academic Press, New York, 1970)

3. Chen, J.P., *Synthesis and Characterization of Niobia-Silica and Titania-Silica Mixed Oxides as Catalysts and Supports,* (Carnegie Mellon University, 1986), PhD Thesis dissertation

4. Satterfield, C.N., *Heterogeneous Catalysts in Practice,* (McGraw-Hill Co., New York, 1980)

5. Liu, Y.C., Griffin, G.L., Chan, S.S. & Wachs, I.E., "Photo-Oxidation of Methanol Using MoO_3/TiO_2: Catalyst Structure and Reaction Selectivity", *J. Catal.,* **94**, (1985), pp. 108-119.

6. Wachs, I.E., Saleh, R.Y., Chan, S.S. & Chersich, C.C., "The Interaction of Vanadium Pentoxide with Titania (anatase): Part I. Effect on o-xylene Oxidation to Phthalic Anhydride", *Appl. Catal.,* **15**, (1985), pp. 339-352.

7. Grabowski, R., Grzybowska, B., Haber, J. & Sloczynski, J., *React. Kinet. Catal. Lett.,* **2**, (1975), p. 81.

8. Wainwright, M.S. & Foster, N.R., *Catal. Rev. Sci. Eng.,* **19**, (1979), p. 221.

9. Connell, G. & Dumesic, J.A., "Acidic Properties of Binary Oxide Catalysts I, Møssbauer Spectroscopy and Pyridine Adsorption for Iron Supported Silica", *J. Catal.,* **101**, (1986), pp. 103-113.

10. Connell, G. & Dumesic, J.A., "Acidic Properties of Binary Oxide Catalysts II.", *J. Catal.,* **102**, (1986), pp. 216-233.

11. Connell, G. & Dumesic, J.A., "The Generation of Brønsted and Lewis Acid Sites on the Surface of Silica by Addition of Dopant Cations", *J. Catal.,* **105**, (1987), pp. 285-198.

12. Bernholc, J., Horsley, J.A., Murrell, L.L., Sherman, L.G. & Soled, S., "Brønsted Acid Sites in Transition Metal Oxide Catalysts: Modeling of Structure, Acid Strengths, and Support Effects", *J. Phys. Chem.,* **91**, (1988), pp. 1526-1530.

13. Ibrahim, M. & Bright, N.F.H., "The Binary System $Nb_2O_5-SiO_2$", *J. Amer. Ceram. Soc.,* **45**(5), (1962), pp. 221-222.

14. Layden, G.K., *J. Amer. Ceram. Soc.,* **46**(10), (1963), p. 506.

15. Iler, R.K., *The Colloid Chemistry of Silica and Silicates*, (Cornell Univ. Press, Ithaca, New York, 1955)

16. Iler, R.K., *The Chemistry of Silica*, (John Wiley & Sons, Inc., New York, 1979)

17. Anderson, J.R., *Structure of Metallic Catalysts*, (Academic Press, Inc., New York, 1975)

18. Holtzberg, F., Reisman, A., Berry, M. & Berkenblit, M., "Chemistry of the Group VB Pentoxides VI. The Polymorphism of Nb_2O_5", *J. Am. Chem. Soc.*, **79**, (1957), p. 2039.

19. Sosman, R.R., *The Phases of Silica*, (Rutgers Univ. Press, New Brunswick, N.J., 1965)

20. Yoldas, B.E., "Hydrolysis of Aluminum Alkoxides and Bayerite Conversion", *J. Appl. Chem. Biotechnol.*, **23**(11), (1973), pp. 803-809.

21. Yoldas, B.E., "Alumina Sol Preparation from Alkoxides", *Am. Ceram. Soc. Bull.*, **54**(3), (1975), pp. 289-290.

22. Yoldas, B.E., "Monolithic Glass Formation by Chemical Polymerization", *J. Mat. Sci.*, **14**, (1979), pp. 1843-1849.

23. Yoldas, B.E., "Effect of Variations in Polymerized Oxides on Sintering and Crystalline Transformations", *J. Am. Chem. Soc.*, **65**(8), (1982), pp. 387-393.

24. Teichner, S.J., Nicolaon, G.A., Vicarini, M.A. & Gardes, G.E.E., "Inorganic Oxide Aerogels", *Adv. Colloid Interface Sci.*, **5**, (1976), pp. 245-273.

25. Knøzinger, H. & Ratnasamy, P., "Catalytic Alumina: Surface Models and Characterization of Surface Sites", *Catal. Rev. Sci. Eng.*, **17**(1), (1978), pp. 31-70.

26. Knøzinger, H., "Acidic and Basic Properties of Aluminas in Relation to their Properties as Catalysts and Supports", *Studies in Surface Science and Catalysis*, **20A and B**, (1985), pp. 111-125.

27. Lippens, B.C. & Steggerda, J.J., *Physical and Chemical Aspects of Adsorbents and Catalysts*, (Academic Press, London, 1970), p. 171.

28 Bauer, G., "Die Oxyde des Niobs", *Z. Anorg. Allg. Chem.*, **248**, (1941), p. 1.

29. Schafer, H., Gruehn, R. & Schulte, F., "The Modifications of Niobium Pentoxide", *Agnew. Chem. Internat. Edit.*, **5**, (1966), p. 40.

30. Crawford, E.S. & Anderson, J.S., *Phil. Trans. R. Soc. Lond.*, **A304**, (1982), p. 327.

31. Kato, V.K. & Tamura, S., "Die Kristallstruktur von T-Nb_2O_5", *Acta Cryst.*, **B31**, (1975), p. 673.

32. Tamura, S., "High-Pressure Phase Research on Nb_2O_5", *J. Mat. Sci.*, **7**, (1972), pp. 298-302.

33. Goldschmidt, H.J., "A High-Temperature X-Ray Investigation on Niobium Pentoxide and Some Problems Concerning the Oxidation of Niobium", *J. Inst. Metals,* **87**, (1958/59), p. 235.

34. Forghany, S.K.E. & Anderson, J.S., "Reduction and Polymorxphic Transformation of B-Nb$_2$O$_5$", *J.C.S. Dalton,* **1**, (1981), p. 255.

35. Laves, F., Pelter, W. & Wulf, H., "Die Kristallstruktur von ζ-Nb$_2$O$_5$", *Naturwiss.,* **51**, (1964), p. 633.

36. Grzybowska, B., "Acidic Properties of Mixed Transition Metal Oxides", *Mater. Chem. Physics,* **17**(1-2), (1987), pp. 121-144.

37. Inomata, M., Miyamoto, A., Ui, T., Kobayashi, K. & Murakami, Y., "Activities of V$_2$O$_5$/TiO$_2$ and V$_2$O$_5$/Al$_2$O$_3$ Catalysts for the Reaction of NO and NH$_3$ in the Presence of O$_2$", *Ind. Eng. Chem. Prod. Res. Dev.,* **21**, (1982), pp. 424-428.

38. Murrell, L.L., Grenoble, D.C., Kim, C.J. & Dispensziere, N.C., "Supported Transition Metal Oxides as Acid Cracking Catalysts: Periodic Trends and Their Relationship to Activity and Selectivity", *J. Catal.,* **107**, (1987), pp. 463-470.

39. Rodrigo, L., *et al.,* "A Study of the Dispersion of Molybdenum (IV) Supported on Silica and γ-Alumina", *J. Phys. Chem.,* **90**, (1986), pp. 2690-2696.

40. Kozlowski, R., Pettifer, R.F. & Thomas, J.M., "X-Ray Absorption Fine Structure Investigation of V$_2$O$_5$-TiO$_2$ Catalysts II: The Vanadium Oxide Active Phase", *J. Phys. Chem.,* **87**, (1983), pp. 5176-5181.

41. Eckert, H. & Wachs, I.E., "^{51}V NMR: A New Probe of Structure and Bonding in Catalysts", in *MRS Symp. Proc.,* (eds. Treacy, M., Thomas, J. & White, J.), (1988), **111**, pp. 459-464.

42. Gasior, M. & Machej, T., *J. Catal.,* **83**, (1983), p. 472.

43. Wachs, I.E., Saleh, R.Y., Chan, S.S. & Chersich, C., "Supporting the Catalyst", *Chemtech,* **15**, (1985), pp. 756-761.

44. Roozeboom, F., *et al.,* "Vanadium Oxide Monolayer Catalysts 3: A Raman Spectroscopic and Temperature Programmed Reduction Study of Monolayer and Crystal-Type Vanadia on Various Supports", *J. Phys. Chem.,* **84**, (1980), pp. 2783-2791.

45. Bond, G.C., Zurita, J.P. & Flamerz, S., "Structure and Reactivity of Titania-Supported Oxides Part 2: Characterization of Various Vanadium Oxide on Titania Catalysts by XPS", *App. Catal.,* **27**, (1986), pp. 353-362.

46. Murakami, Y., *et al.,* "Effect of Support and Preparation on the Structure of Vanadium Oxide Catalysts", in *Preparation of Catalysts III,* (Elsevier, New York, 1983), pp. 531-542.

47. Wachs, I.E. & Hardcastle, F.D., "Raman Spectroscopy of Supported Oxides on Al_2O_3, TiO_2, and SiO_2: A Comparative Study", in *Proc. 9th Intern. Congr. Catal.*, (1988), p. 1449.

48. Yoshida, S., Tanaka, T., Nishimura, Y., Mizutani, H. & Funabiki, T., in *Proc. 9th Intern. Cong. Catal.*, (1988), **3**, p. 1473.

49. Medena, J., Stam, C.V., Beer, V.H.J.d., Konings, A.J.A. & Konningsberger, D.C., *J. Catal.*, **36**, (1978), p. 81.

50. Giordano, N., Bart, J.C.J., Vaghi, A., Castellan, A. & Martinotti, G., "Structure and Catalytic Activity of $MoO_3 \cdot Al_2O_3$ Systems I: Solid-State Properties of Oxidized Catalysts", *J. Catal.*, **36**, (1975), p. 81.

51. Hall, W.K. & Lojacono, J., "The Surface Chemistry of Molybdena-Alumina Catalysts", in *Proc. 6th Intern. Congr. Catal.*, (1976), **1**, p. 246.

52. Okamoto, Y., Tomioka, H., Katoh, Y., Imanaka, T. & Teranishi, S., "Surface Structure and Catalytic Activity of MoO_3/Al_2O_3 Catalysts in the Hydrodesulfurization of Thiophene by X-Ray Photoelectron Spectroscopy", *J. Phys. Chem.*, **84**, (1980), pp. 1833-1840.

53. Wang, L. & Hall, W.K., "On the Genesis of Molybdena-Alumina Catalyst", *J. Catal.*, **66**, (1980), pp. 251-255.

54. Brito, J. & Laine, J., "Characterization of Supported MoO_3 by Temperature-Programmed Reduction", *Polyhedron*, **5**, (1986), pp. 179-182.

55. Knøzinger, H. & Jeziorowski, H., "Raman Spectra of Molybdenum Oxide Supported on the Surface of Aluminas", *J. Phys. Chem.*, **82**, (1978), pp. 2002-2005.

56. Che, H., Louis, C. & Tatibouet, J.M., "Influence of Mo-SiO_2 Catalysts Preparation on Molybdenum Coordination and Catalytic Properties", **5**, (1986), pp. 123-128.

57. Stamped, S.R., Chen, Y., Dumesic, J.A., Niu, C. & Jr., C.G.H., "Interactions of Molybdenum Oxide with Various Oxide Supports: Calcination of Mechanical Mixtures", *J. Catal.*, **105**, (1987), pp. 445-454.

58. Leyrer, J., *et al.*, "Structure and Surface Properties of Supported Oxides", *Materials Chem. Phys.*, **13**, (1985), pp. 301-304.

59. Marcinkowska, K., Rodrigo, L., Kaliaguine, S. & Roberge, P.C., "Characterization of Supported Mo(VI)/SiO_2: The Effects of Water Leaching and Support Dehydroxylation", *J. Catal.*, **97**, (1986), pp. 75-84.

60. Arco, M.d., Holgado, M., Martin, C. & Rives, V., "Effect of Thermal Treatments on the Properties of V_2O_5/TiO_2 and MoO_3/TiO_2 Systems", *J. Catal.*, **99**, (1986), pp. 19-27.

61. Zaki, M.I., Vielhaber, B. & Knøzinger, H., "Low-Temperature CO Adsorption and State of Molybdena Supported on Alumina, Titania, Ceria, and Zirconia: An Infrared Spectroscopic Investigation", *J. Phys. Chem.*, **90**, (1986), pp. 3176-3183.

62. Klug, H.P. & Alexander, L.E., *X-Ray Diffraction of Amorphous Materials*, (Wiley, New York, 1974)

63. Ismail, H.M., Theocharis, C.R., Waters, D.N., Zaki, M.I. & Faihm, R.B., "The Nature of Supported-Molybdena Catalysts: Evidence From a Raman and X-Ray Diffraction Investigation of Pyridine Adsorption", *J. Chem. Soc., Faraday Trans. I.*, **83**, (1987), pp. 1601-1608.

64. Kung, H.H., *Transition Metal Oxides: Surface Chemistry and Catalysis*, (Elsevier, New York, 1989)

65. Fransen, T., Berg, P.C.V. & Mars, P., in *First Intern. Symp. on Scientific Bases for the Preparation of Heterogeneous Catalysts*, (Brussels, 1975)

66. Aveston, J., Anacker, E.W. & Johnston, J.S., *Inorg. Chem.*, **3**, (1964), p. 735.

67. Jehng, J.M. & Wachs, I.E., "The Molecular Structures and Reactivity of Supported Niobium Oxide Catalysts", in *Proceedings of the Niobium and Catalysts Symposium at the 1989 International Chemical Congress of Pacific Basin Societies*, (ed. Ko, E.I.), (Elsevier, New York, 1989), **8**, pp. 37-51.

68. Yermakov, Y.I., *Catal. Rev.-Sci. Eng.*, **13**, (1976), pp. 77.

69. Iwasawa, Y., Ichinose, H. & Ogasawara, S., *J. Chem. Soc. Faraday I*, **77**, (1981), p. 1763.

70. Iwasawa, Y. & Yamagishi, M., "New SiO_2-Attached 'Mo-Pair' Catalysts - Preparations, Surface Structures, and Chemical Nature", *J. Catal.*, **82**, (1983), pp. 373-381.

71. Tanaka, T., Nishimura, Y., Kawasaki, S., Funabiki, T. & Yoshida, S., "X-Ray Absorption Spectroscopy (EXAFS/XANES) Evidence for the Preferential Formation of Isolated VO_4 Species on Highly Photoactive V_2O_5/SiO_2 Catalysts", *J. Chem. Soc. Chem. Commun.*, (1987), pp. 506-509.

72. Kijenski, J., Baiker, A., Glinski, M., Dollenmeier, P. & Wokaun, A., "Monolayers and Double Layers of Vanadium Pentoxide on Different Carriers: Preparation, Characterization, and Catalytic Activities", *J. Catal.*, **101**, (1986), pp. 1-11.

73. Sharma, V.K., Wokaum, A. & Baiker, A., "ESR Characterization of V_2O_5 Monolayers and Double Layers Supported on Various Carriers", *J. Phys. Chem.*, **90**, (1986), pp. 2715-2718.

74. Ko, E.I., Bafrali, R., Nuhfer, N.T. & Wagner, N.J., "The Use of Niobia-Silica Surface Phase Oxide in Studying and Varying Metal Support Interactions in Supported Nickel Catalysts", *J. Catal.*, **95**, (1985), pp. 260-270.

75. Weissman, J.G., *Electron Microscopy and Surface Analysis of Niobia-Silica Surface Oxides Using Model Thin Flims*, (Carnegie Mellon University, 1987), PhD Thesis Dissertation

76. Burke, P.A., Weissman, J.G., Ko, E.I. & Wynblatt, P., "Effects of Interfacial Interactions on the Sintering and Reduction of Niobia Supported on Silica", in *Catalysis,* (ed. Wards, J.W.), (Elsevier, Amsterdam, 1987), pp. 457-467.

77. Weissman, J.G., Ko, E.I. & Wynblatt, P., "Summary Abstract: Study of Niobia-Silica Interfacial Phenomena With Model Thin Films", *J. Vac. Sci. Technol. A.,* 5, 4, (1987), p. 1694.

78. Weissman, J.G., Ko, E.I., Wynblatt, P. & Howe, J.M., "High Resolution Electron Microscopy and Image Simulation of TT-, T-, and H-Niobia and Model Silica-Supported Niobium Surface Oxides", *Chem. Mater.,* 1(2), (1989), p. 187.

79. Weissman, J.G., Ko, E.I. & Wynblatt, P., *J. Catal.,* 108, (1987), p. 383.

80. Nishimura, M., Asakura, K. & Iwasawa, Y., "New SiO_2-Supported Niobium Monomer Catalysts for Dehydrogenation of Ethanol", *J. Chem. Soc. Chem. Commun.,* (1986), pp. 1660-1662.

81. Asakura, K. & Iwasawa, Y., "The Surface Structure and Catalytic Properties of One-Atomic Layer Amorphous Niobium Oxide Attached on SiO_2", *Chem. Lett., Chem. Soc. Japan,* (1986), pp. 859-862.

82. Nishimura, M., Asakura, K. & Iwasawa, Y., *Chem. Lett.,* (1986), p. 1457.

83. Iwasawa, Y., "Structures of Acid-Base Design Surfaces and Their Catalysis", in *Proceedings of the International Symposium on Acid-Base Catalysis,* (eds. Tanabe, K., Hattori, H., Yamaguchi, T. & Tanaka, T.), (VCH Publishers, 1988), pp. 42-45.

84. Shirai, M., Ichikuni, N., Asakura, K. & Iwasawa, I., "Preparations and Catalytic Properties of Single, Pair, and Monolayer Niobium Catalysts", in *Catalytic Conversion with Niobium Materials: Niobium and Catalysts Symposium at the 1989 International Chemical Congress of Pacific Basin Societies,* (ed. Ko, E.I.), (Elsevier, New York, 1989), 8, pp. 57-66.

85. Wachs, I.E., Jehng, J.M. & Hardcastle, F.D., "The Interaction of V_2O_5 and Nb_2O_5 with Oxide Surfaces", *Solid State Ionics,* 32/33, (1989), pp. 904-910.

86. Yoshida, S., Nishimura, Y., Tanaka, T., Kanai, H. & Funabiki, T., "The Local Structures and Photo-Catalytic Activity of Supported Niobium Oxide Catalysts", in *Catalytic Conversion with Niobium Materials: Niobium and Catalysts Symposium at the 1989 International Chemical Congress of Pacific Basin Societies,* (ed. Ko, E.I.), (Elsevier, New York, 1989), 8, pp. 67-75.

87. Ko, E.I. & Weissman, J.G., "Structures of Niobium Pentoxide and Their Implications on Chemical Behavior", in *Catalytic Conversion with Niobium Materials: Niobium and Catalysts Symposium at the 1989 International Chemical Congress of Pacific Basin Societies,* (ed. Ko, E.I.), (Elsevier, New York, 1989), 8, pp. 27-36.

88. Burke, P.A., *Relationships Between the Structure and Chemical Properties of Niobia-Silica Binary Oxides*, (Carnegie Mellon University, 1989), Ph.D. Thesis Dissertation

89. Burke, P.A. & Ko, E.I., "The Relationship Between Structure and Acidity in Niobia-Containing Binary Oxides", in *Proceedings of 4th Japan-China-U.S.A. Symposium on Catalysis: Development of Novel Catalysts and Improvement of Catalytic Processes*, (Sapporo, 1989), pp. 24-27.

90. Burke, P.A. & Ko, E.I., "Acidic Properties of Oxides Containing Niobia on Silica and Niobia in Silica", *Submitted to J. Catal.*, (1990)

91. Brown, I.D. & Wu, K.K., *Acta. Cryst.*, **B32**, (1976), pp. 1957.

92. Hardcastle, F.D. & Wachs, I.E., "Determination of Niobium-Oxygen Bond Distances and Bond Orders by Raman Spectroscopy", *Submitted to Solid State Ionics*, (1990)

93. Kobayashi, H., *et al.*, "Quantum Chemical Study of Metal Oxide Catalysts. Structures of Vanadium Oxide and Niobium Oxide Clusters Supported on Silica and Alumina", *J. Phys. Chem.*, **92**, (1988), pp. 2516-2520.

94. Jehng, J.M. & Wachs, I.E., "Structural Chemistry and Raman Spectra of Niobium Oxides", *Submitted to Chem. Mat.*, (1990)

95. Murrell, L.L. & Grenoble, D.C., *Transition Metal Oxide Brønsted Acid Catalysts*, (1983), US Patent #4,415,480

96. Grenoble, D.C., Kim, C.J. & Murrell, L.L., *Method for Preparing a Group IVB, VB, of VIB Metal Oxide on Inorganic Refractory Oxide Support Catalyst and the Product Prepared by Said Method*, (1981), US Patent #4,269,737

97. Ramirez, E.G., *Catalyst for the Preparation of Ethylenimine*, (1982), US Patent #4,337,175

98. Jehng, J.M., (Lehigh University, 1990), Ph.D. Thesis Dissertation

99. Courty, P. & Marcilly, C., "Introduction: Mixed Oxides and Catalysts", in *Preparation of Catalysts*, (eds. Delmon, B., Jacobs, P.A. & Poncelet, G.), (Elsevier, Amsterdam, 1976), pp. 119-146.

100. Levin, E.M., "Phase Equilibria in the System Niobium Pentoxide-Germanium Dioxide", *J. of Res. Nat. Bur. Stnds.*, **70**A(1), (1966), p. 1.

101. Anderson, J.S., *et al.*, "The Structure of Germanium Niobium Oxide, an Inherently Non-Stoichiometric Block Structure", *Proc. R. Soc. Lond. A.*, **346**, (1975), pp. 139-156.

102. Walvekar, S.P. & Halgeri, A.B., "Surface Acidity and Acid Strength of of Some Mixed Oxides Containing TiO_2", *Ind. J. Chem.*, **11**, (1967), pp. 662-665.

103. Itoh, M., Hattori, I. & Tanabe, K., "The Acidic Properties of TiO_2-SiO_2 and Its Catalytic Activities for the Amination of Phenol, the Hydration of Ethylene, and Isomerization of Butenes", *J. Catal.*, **35**, (1974), pp. 225-231.

104. Hattori, H., Itoh, M. & Tanabe, K., "The Nature of Active Sites on TiO_2 and TiO_2/SiO_2 for the Isomerization of Butenes", *Bull. Chem. Soc. Jap.*, **38**, (1975), pp. 172-178.

105. Itoh, M., Hattori, H. & Tanabe, K., "Catalytic Sites on SnO_2 and TiO_2/SnO_2 for the Isomerization of 1-Butene", *J. Catal.*, **43**, (1976), pp. 192-199.

106. Sandstrom, D.R., *et al.*, "Coordination of Ti in TiO_2-SiO_2 Glass by X-Ray Absorption", *J. Non-Cryst. Solids,* **41**, (1980), pp. 201-207.

107. Emili, M., Incoccia, L., Mobilio, S., Fagherazzi, G. & Gugliemi, M., "Structural Investigations of TiO_2-SiO_2 Glassy and Glass-Ceramic Materials Prepared by the Sol-Gel Method", *J. Non-Cryst. Solids,* **74**, (1985), pp. 129-146.

108. Cheng, J.J. & Wang, D.W., "Structural Transformation of the TiO_2-SiO_2 System Gel During Heat Treatment", *J. Non-Cryst. Sol.,* **100**, (1988), pp. 288-291.

109. Greegor, B., Lytle, F.W., Sandstrom, D.R., Wong, J. & Schultz, P., *J. Non-Cryst. Solids,* **55**, (1983), p. 27.

110. Bland, J.L., *Acta Cryst.,* **14**, (1961), p. 875.

111. Evans, D.L., *J. Am. Ceram. Soc.,* **53**, (1970), p. 418.

112. Sivade, A., Bourret, D., Bouaziz, J. & Sempere, R., "Aerogel in the system Nb-Si", in *Revue de Physique Appliquee (J. Phys. Colloq.) of theProceedings of the 2nd International Symposium on Aerogels: ISA2,* (eds. Vacher, R., Phalippou, J., Pelious, J. & Woignier, T.), (Montpelier, France, 1989), **24**, p. C4-79.

113. Toba, M., *et al.*, "Properties of Mixed Oxides Synthesized from Metal Alkoxide Molecules", in *Proceedings of the 4th Japan-USA Symposium on Catalysis: Development of Novel Catalysts and Improvement of Catalytic Processes,* (Sapporo, 1989), pp. 278-279.

114. Maurer, S.M., *Effects of Preparation on the Properties of Niobia-Alumina Binary Oxides,* (Carnegie Mellon University, 1988), Master of Science Thesis

115. Iacobucci, P.A., Cheng, C.P. & Walsh, E.N., *Non-Aged Inorganic Oxide-Containing Aerogels and Their Preparation,* (1986), US Patent #4,619,908

116. Fricke, J., "Aerogels - Highly Tenuous Solids with Fascinating Properties", *J. Non-Cryst. Solids,* **100**, (1988), pp. 169-173.

117. Kistler, S.S., "Coherent Expanded Aerogels", *J. Phys. Chem.,* **36**, (1932), pp. 52-64.

118. Kistler, S.S., *Method of Producing Aerogels,* (1937), US Patent #2,093,454

119. Kistler, S.S., *Method of Making Aerogels*, (1941), US Patent #2,249,767

120. Teichner, S.J. & Nicolaon, G.A., *Method of Preparing Inorganic Aerogels*, (1972), US Patent #3,672,833

121. VonDardel, G., Henning, S.A. & Svensson, L.O.G., *Method of Preparing Silica Aerogels*, (1982), US Patent #4,327,065

122. Hubert-Pfalzgraf, L.G., "Alkoxides as Molecular Precursors for Oxide-Based Inorganic Materials: Opportunities for New Materials", *New Journal of Chemistry*, 11(10), (1987), pp. 663-675.

123. Roy, R., "Ceramics by the Solution-Sol-Gel Route", *Science*, 238, (1987), pp. 1664-1669.

124. Iacobucci, P.A. & Ayen, R.J., "Metal Oxide Aerogel Preparation by Supercritical Extraction", *Rev. Chem. Eng.*, 5(1-4), (1988), pp. 157-198.

125. Armor, J.N., Carlson, E.J. & Zambri, P.M., "Aerogels as Hydrogenation Catalysts", *Appl. Catal.*, 19, (1985), pp. 339-348.

126. Brinker, C.J., Clark, D.E. & Ulrich, D.R., "Better Ceramics Through Chemistry II", in *Mat. Res. Soc.*, (Pittsburgh, Pa., 1986)

127. Hench, L.L. & Ulrich, D.R., *Science of Ceramic Chemical Processing*, (Wiley, New York, 1986)

128. Mehrota, R.C., "Synthesis and Reactions of Metal Alkoxides", *J. Non-Cryst. Solids*, 100, (1988), pp. 1-15.

129. Paulson, B.A., *Use of Sol-Gels in the Application of Ceramic Oxide Thin Films*, (Iowa State University, 1987), Ph.D. Thesis Dissertation

130. Gesser, H.D. & Goswami, P.C., "Aerogels and Related Porous Materials", *Chem. Rev.*, 89, (1989), pp. 765-788.

131. Bradley, D.C., "Polymeric Metal Alkoxides", in *Inorganic Polymers*, (eds. Stone, F. & Graham, W.), (Academic Press, London, 1962), pp. 410-446.

132. Yoldas, B.E., "Hydrolytic Polycondensation of $Si(OC_2H_5)_4$ and Effect of Reaction Parameters", *J. Non-Cryst. Solids*, 83, (1986), pp. 375-390.

133. Fricke, J., "Aerogels", *Scientific American*, 258(5), (1988), pp. 92-97.

134. Nicolaon, G.A. & Teichner, S.J., *Bull. Soc. Chim. France*, 5, (1968), pp. 1900-1906.

135. Nicolaon, G.A. & Teichner, S.J., *Bull. Soc. Chim. France*, 5, (1968), pp. 1906-1911.

136. Tewari, P.H. & Hunt, A.J., (1986), US Patent #4,610,863

137. Tewari, P.H., Hunt, A.J. & Loftus, K.D., *Materials Letters*, **3**, (1985), pp. 363-367.

138. Teichner, S.J., "Aerogels: A Source of Adsorbents, Insulators, Catalysts and Ceramics", in *Revue De Physique Appliquee of the Proceedings of the 2nd International Symposium on Aerogels ISA2*, (Montpelier, France, 1989), p. C4-1.

139. Teichner, S.J., "Aerogels of Inorganic Oxides", in *First International Symposium*, (ed. Fricke, J.), (Springer-Verlag, 1985), **6**, p. 22.

140. Johnson, O., "Acidity and Polymerization Activity of Solid Acid Catalysts", *J. Amer. Chem. Soc.*, **59**, (1955), p. 827.

141. Rodenas, E., Yamaguchi, T., Hattori, H. & Tanabe, K., *J. Catal.*, **69**, (1981), pp. 434-444.

142. Ogasawara, K., Iisuka, T. & Tanabe, K., "Ethylene Hydration Over Niobic Acid Catalysts", *Chem. Lett.*, **1**, (1984), pp. 645-648.

143. Iizuka, T., Ogasawara, K. & Tanabe, K., "Acidic and Catalytic Properties of Niobium Pentoxide", *Bull. Chem. Soc. Japan*, **56**, (1983), pp. 2927-2937.

144. Tanabe, K., "Application of Niobium Oxides as Catalysts", in *Catalytic Conversion with Niobium Materials: Niobium and Catalysts Symposium at the 1989 International Chemical Congress of Pacific Basin Societies*, (ed. Ko, E.I.), (Elsevier, New York, 1989), **8**, pp. 1-11.

145. Hanaoka, T., Takeuchi, K., Matsuzaki, T. & Sugi, Y., "Niobic Acid as a Solid Acid Catalyst for Ring-Opening Reactions of Phenyloxirane", in *Catalytic Conversion with Niobium Materials: Niobium and Catalysts Symposium at the 1989 International Chemical Congress of Pacific Basin Societies*, (ed. Ko, E.I.), (Elsevier, New York, 1989), **8**, pp. 123.

146. Walling, C., "The Acid Strength of Surfaces", *J. Amer. Chem. Soc.*, **72**, (1950), pp. 1164-1168.

147. Forni, L., "Comparison of the Methods for the Determination of Surface Acidity of Solid Catalysts", *Catal. Rev. Sci. Eng.*, **8**(1), (1973), pp. 65-115.

148. Benesi, H.A. & Winquist, B.H.C., *Advances in Catalysis*, (Academic Press, New York, 1978), **27**, p. 98.

149. Pauling, L., *The Nature of the Chemical Bond*, (Cornell Univ. Press, Ithaca, N.Y., 1960)

150. Kung, H.H., "Formation of New Acid Sites in Dilute Solid Oxide Solutions: A Predictive Model", *J. Solid State Chem.*, **52**, (1984), pp. 192-196.

151. Seiyama, T., *Metal Oxides and Their Catalytic Actions*, (Kodansha Scientific, Tokyo, 1978)

152. Kataoka, T. & Dumesic, J.A., "Acidity of Unsupported and Silica-Supported Vanadia, Molybdena, and Titania as Studied by Pyridine Adsorption", *J. Catal.*, **112**, (1988), pp. 66-79.

153. Sargent-Welch Company, *Periodic Table of the Elements,* (Skokie, Illinois, 1980)

154. Autoclave Engineers, *Process Systems Handout #084-1,* (Erie, Pennsylvania, 1983)

155. Smith, J.M. & Ness, H.C.V., *Introduction to Chemical Engineering Thermodynamics, 3rd Ed.,* (McGraw-Hill Co., New York, 1975)

156. Brinker, C.J. & Scherer, G.W., *Sol-Gel Science: The Physics and Chemistry of Sol-Gel Processing,* (Academic Press, Inc., New York, 1990), 1st edition

157. Krol, D.M., Mulder, C.A.M. & Lierop, J.G., "Raman Investigation of Autoclave-Prepared Monolithic Sol-Gels", *J. Non-Cryst. Solids,* **86,** (1986), pp. 241-250.

158. Linsen, B.G. *et al., Physical and Chemical Aspects of Adsorbents and Catalysts,* (Academic Press, New York, 1970), p. 216.

159. Adkins, H., "The Selective Activation of Alumina for Decarboxylation or for Dehydration", *J. Am. Chem. Soc.,* **44,** (1922), pp. 2175-2186.

160. Vicarini, M.A., Nicolaon, G.A. & Teichner, S.J., *Bull. Soc. Chim. Fr.,* **2,** (1970), p. 431.

161. Yoldas, B.E., "A Transparent Porous Alumina", *Am. Chem. Soc. Bull.,* **54,** (1975), pp. 286-288.

162. Quantachrome Corp., *Instruction Manual for the Quantasorb Sorption System,* (Quantachrome Corp., New York, 1981)

163. Wheeler, "Chapter 2", in *Catalysis, Vol. II,* (ed. Emmett, P.H.), (Reinhold Publishing Company, New York, 1955)

164. Ritshcel, M., Opperman, H. & Mattern, N., *Kristall und Technik,* **13**(12), (1978), p. 1421.

165. Terao, N., "Structures des Oxydes de Niobium", *Japan J. Appl. Phys.,* **2,** (1963), p. 156.

166. Terao, M., "Structure des Oxydes de Niobium: Transformation de Structure du Nb_2O_5-γ en Nb_2O_5-α et la Formation du NbO_2", *Japan J. Appl. Phys.,* **4**(1), (1965), pp. 8-15.

167. Waring, J., *JCPDS CARD #27-1003*

168. Waring, J., *JCPDS CARD #26-895*

169. Norin & Nolander, *JCPDS CARD #27-1311*

170. Andersson, *JCPDS CARD #20-804*

171. Moser & Schweiz, *JCPDS CARD #18-911*

172. Rooksby, (1951), *JCPDS CARD #10-425*

173. "α-Al$_2$O$_3$ Diffraction Pattern", *JCPDS CARD #10-173*

174. Burdese & Borlera, (1963), *JCPDS CARD #26-30*

175. Tobias, R.S., "Raman Spectroscopy in Inorganic Chemistry", *J. Chem. Education,* **44**, (1967), pp. 2-8.

176. Delgass, W.N., *et al., Spectroscopy in Heterogeneous Catalysts,* (Academica Press, New York, 1979), pp. 58-60.

177. Colthup, N.B., Daly, L.H. & Wiberley S.E., *Introduction to Infrared and Raman Spectroscopy,* (Academic Press, Inc., New York, 1990), 3rd edition

178. Benesi, H.A., "Acidity of Catalyst Surface II. Amine Titration Using Hammett Indicators", *J. Phys. Chem.,* **61**, (1957), pp. 970-973.

179. Deeba, M. & Hall, W.K., "The Measurement of Catalyst Acidity II: Chemisorption Studies", *Z. Phys. Chem.,* **44**, (1985), p. 85.

180. Parry, E.P., "An Infrared Study of Pyridine Adsorbed on Acidic Solids: Characterization of Surface Acidity", *J. Catal.,* **2**, (1963), pp. 371-379.

181. Basila, M.R. & Kantner, T., "The Nature of the Acidic Sites on Silica-Alumina: A Revaluation of the Relative Absorption Coefficients of Chemisorbed Pyridine", *J. Phys. Chem.,* **70**, (1966), pp. 1681-1682.

182. Ko, E.I. & Maurer, S.M., "Synthesis of Niobium Pentoxide Aerogels", *J. Chem. Soc., Chem. Comm.,* **15**, (1990), pp. 1062-1063.

183. Alquier, C., Vandenborre, M.T. & Henry, M., "Synthesis of Niobium Pentoxide Gels", *J. Non-Cryst. Sol.,* **79**, (1986), pp. 383-395.

184. Vandenborre, M.T., Poumellec, B., Alquier, C. & Livage, J., "EXAFS Study of the Hydrolysis of Niobium Pentaethoxide", *J. Non-Cryst. Solids,* **108**, (1989), pp. 333-337.

185. Izumi, F. & Kodama, H., *Z. Anorg. Allg. Chem.,* **440**, (1978), p. 155.

186. Heurung, G. & Gruehn, R., *Z. Anorg. Allg. Chem.,* **491**, (1982), p. 101.

187. McConnell, A.A., Anderson, J.S. & Rao, C.N.R., "Raman Spectra of Niobium Oxides", *Spectrochimica Acta,* **32A**, (1976), pp. 1067-1076.

188. Chan, S.S., Wachs, I.E., Murrell, L.L., L.Wang & Hall, W.K., *J. Phys. Chem.,* **88**, (1984), pp. 5831-5835.

189. Tanabe, K., *Personal Communication,* (1989)

190. Bourne, K., Cannings, F. & Pitkethy, R., "The Structure and Properties of Acid Sites on a Mixed Oxide System I. Synthesis and Infrared Characterization", *J. Phys. Chem.,* **74**, (1970), pp. 2197-2205.

191. Tanabe, K., *Solid Acid and Base Catalysts,* (GRD, New York, 1934), pp. 231-273.

192. Peri, J.B., "Infrared Spectroscopy in Catalytic Research", *Catal. Sci. Tech.*, **5**, (1983), pp. 141-161.

193. Hightower, J.W. & Hall, W.K., "Tracer Studies of Acid Catalyzed Reactions V: Carbon[14] Kinetic Studies of n-Butene Isomerization Over Alumina and Silica-Alumina Catalysts", *J. Phys. Chem.*, **71**, (1967), pp. 1014-1023.

194. Harris, M.R. & Sing, K., "The Surface Properties of Precipitated Alumina", *J. Appl. Chem.*, **8**, (1958), pp. 586-589.

195. Benesi, H.A., *J. Am. Chem. Soc.*, **78**, (1956), p. 5490.

196. Fowkes, F.M., "Determination of the Interfacial Acid-Base Ineractability of Polymers With the Surface Sites of Metal Oxides", *Polym. Mater. Sci. Eng.*, **53**, (1985)

197. Kiviat, F.E. & Petrakis, L., "Surface Acidity of Transition Metal Modified Aluminas. Infrared and Nuclear Magnetic Resonance Investigation of Adsorbed Pyridine", *J. Phys. Chem.*, **77**(10), (1973), pp. 1232-1239.

198. Segawa, K. & Hall, W.K., "Catalysis and Surface Chemistry III: The Adsorption of Pyridine on Molybdena-Alumina Catalysts", *J. Catal.*, **76**, (1982), pp. 133-143.

199. Huheey, J.E., *Inorganic Chemistry: Principles of Structure and Reactivity*, (Harper and Row, Publishers, New York, 1983), 3rd edition

200. Weissman, J.G., Burke, P.A., Ko, E.I. & Wynblatt, P., "Preparation of Niobia/Silica Mixed Oxide Thin Films", *J. Chem. Soc., Chem. Commun.*, (1989), pp. 329-330.

201. Pederson, B.F., "Crystal Structure of Aluminum Niobium Oxide($NbAlO_4$)", *Acta. Chemica. Scand.*, **16**, (1962), pp. 421-430.

202. Bhide, V. & Husson, E., "Etude de Niobates de Structure GTB Par Absorption Infra-Rouge et Diffusion Raman", *Mat. Res. Bull.*, **15**, (1980), pp. 1339-1344.

203. Goldwasser, J., Engelhardt, J. & Hall, W.K., "The Isomerization and Metathesis of n-Butenes II. Acid-Catalysis on the Fully Oxidized Catalysts", *J. Catal.*, **71**, (1981), pp. 381-388.

204. Tallant, D.R., Bunker, B.C., Brinker, C.J. & Balfe, C.A., in *Better Ceramics Through Chemistry II: Proceedings of the 2nd MRS Symposium on Better Ceramics Through Chemistry*, (eds. Brinker, C.J., D.E.Clark & Ulrich, D.R.), (Mat. Res. Soc., Pittsburgh, PA, 1986), pp. 261-267.

205. Griffith, W.P. & Wickins, T.D., *J. Chem. Soc. (A)*, (1967)

206. Djordjevec, C. & Katovik, V., *J. Chem. Soc. (A)*, (1970)

207. Katovik, V. & Djordjevec, C., *Inorg. Chem.*, **9**, (1970)

208. Prashar, P. & Tandon, J.P., *Z. Naturforsch.*, **25b**, (1970)

209. Farrell, F.J., Maroni, V.A. & Spiro, T.G., *Inorg. Chem.*, **8**(12), (1969), p. 2638.

210. Topoe, N., Pedersen, K. & Derouane, E.G., "Infrared and Temperature-Programmed Desorption Study of the Acidic Properties of ZSM-5 Type Zeolites", *J. Catal.*, **70**, (1981)

211. Messner, A.E., Rosie, D.E. & Argabright, P.A., "Correlation of Thermal Conductivity Cell Response With Molecular Weight and Structure", *Anal. Chem.*, **31**, (1959), pp. 230-233.

APPENDIX

APPENDIX A

SINGLE POINT B.E.T. SURFACE AREA PROGRAM

```
5       REM " BET.BAS BASIC PROGRAM FOR 1 POINT BET SURFACE CALCULATION "
20      N = 6.023 * 10^23
30      R = 82.1
40      ACS = 16.2 * 10^-20
50      INPUT " CALIBRATION GAS VOLUME (CC): ", VC
55      INPUT " MIXED OXIDE ID ----------------: ", ID$
60      INPUT " AMBIENT PRESSURE (mm Hg) --: ", PA
70      INPUT " AMBIENT TEMPERATURE (C) ---: ", TK
80      INPUT " CATALSYT WEIGHT (gm) -------: ", WT
81      INPUT "The number of runs to be calculated: ",RUNS
82      DIM S(RUNS) , ST(RUNS) , A(RUNS) , AC(RUNS)
83      INPUT "the percent of nitrogen : ",PER
90      T = TK + 273.2
100     P0 = PA + 15
110     PN2 = PA * PER/100
120     FOR I = 1 TO RUNS
130     PRINT " AREA OF DESORPTION (COUNTS)  run("; I; "): ";
135     INPUT  A(I)
140     PRINT " AREA OF CALIBRATION (COUNTS) run("; I; "): ";
145     INPUT AC(I)
150     ST(I) = (1-PN2/P0) * (A(I)/AC(I)) * VC * (N * ACS * (PA/760) / (R * T))
160     S(I)  = ST(I) /WT
170     NEXT I
175     PRINT " MIXED OXIDE ID : "; ID$
180     PRINT " PRESSURE(mmHg)   TEMPERATURE(C)   CATALYST WEIGHT(GM)"
190     PRINT USING "     ###.##        "; PA;
192     PRINT USING "       ###.#        "; TK;
194     PRINT USING "     #.####        "' WT
196     PRINT
199     GOTO 240
200     PRINT " RUN #     DESORPTION(COUNTS) CALIBRATION(COUNTS)   M^2     M^2/GM"
210     FOR J = 1 TO RUNS
220     PRINT USING "   ##   "; J;
222     PRINT USING "        ####     "; A(J);
224     PRINT USING "        ####     "; AC(J);
226     PRINT USING " ###.##  "; ST(J);
228     PRINT USING " ###.##  "; S(J)
230     NEXT J
231     PRINT "average surface area is: "
232     PRINT USING " ###.EE "; AVG
233     GOTO 290
239     SUM=0
240     FOR K = 1 TO RUNS
250     SUM = S(K) +SUM
260     NEXT K
270     AVG = SUM/RUNS
280     GOTO 200
290     SYSTEM
```

APPENDIX B

PORE SIZE DISTRIBUTION DATA

This appendix summarizes the physical property data of the materials synthesized in this study. Tables B-1, B-2, and B-3 summarize the physical properties of niobia (also heat treated), bulk and mixed oxides, and niobia aerogels prepared in the solvents of methanol and s-butanol, respectively. Figures B-1 to B-56 show the nitrogen desorption isotherms and pore size distributions for all of the above tabulated samples. I will only briefly discuss each figure contained in this appendix for purposes of completeness.

B.1 Niobia Aerogel and Conventionally Prepared Niobia

Figures B-1/B-2, B-3/B-4, B-5/B-6, and B-7/B-8 show desorption isotherms and pore size distributions for A-Nb$_2$O$_5$, P-Nb$_2$O$_5$, X-Nb$_2$O$_5$, Niobic Acid, respectively, all after a conventional calcination of (500,2). Notice that the aerogel of niobia contains nearly 10 times the pore volume and the pore size is considerably greater as is evident from the large amount of adsorption that occurs at high relative pressures (p/p$_0$ > 0.9). This same behavior in fact is found for every aerogel synthesized in this study, and is of a type II classification according to the original BET classification.[4] The other conventionally prepared samples show type IV isotherms which are characterized by lower adsorption at low pressures and a monotonic increase in adsorption with increasing relative pressure. This indicates that the conventional niobia samples have less microporosity and a broader distribution of larger pores. The difference in scales for the desorption isotherm for the

Table B-1: PHYSICAL PROPERTY DATA OF CALCINED NIOBIA AND HEAT TREATED NIOBIA

Sample	Surface Area (Multi Point)[1]	Avg. Pore Diameter[2]	Total Pore Volume[3]	(Pore Vol.) Med. Pore Diameter(Å)[4]	(Surface Area) Med. Pore Diameter(Å)[5]
A-Nb_2O_5	196.3	260.9	1.28	614.9	77.9
P-Nb_2O_5	85.6	71.5	0.15	84.4	41.7
X-Nb_2O_5	77.0	95.7	0.18	120.0	79.0
Niobic Acid	95.7	54.0	0.13	55.5	21.1
A-Nb_2O_5(600,2)	172.5	119.3	0.51	139.1	67.9
A-Nb_2O_5(800,2)	409.4	81.6	0.83	67.4	46.4
A-Nb_2O_5(1000,-)	512.1	59.2	0.76	61.6	39.1
P-Nb_2O_5(1000,-)	13.1	62.3	0.02	66.9	70.7
Niobic Acid(1000,-)	207.1	54.4	0.28	70.2	34.4

1   Multi-Point B.E.T. Surface Area (m^2/g)

2   Average Pore Diameter , 4V/S, (Å)

3   Total Pore Volume (cm^3/g)

4   Median Pore Diameter Based on Pore Volume (Å)

5   Median Pore Diameter Based on Surface Area (Å)

Table B-2: PHYSICAL PROPERTY DATA OF BULK OXIDE AEROGELS AND MIXED OXIDE AEROGELS

Sample	Surface Area (Multi Point)[1]	Avg. Pore Diameter[2]	Total Pore Volume[3]	(Pore Vol.) Med. Pore Diameter(Å)[4]	(Surface Area) Med. Pore Diameter(Å)[5]
A-Nb$_2$O$_5$	196.3	260.9	1.28	614.9	77.9
P-Nb$_2$O$_5$	85.6	71.5	0.15	84.4	41.7
X-Nb$_2$O$_5$	77.0	95.7	0.18	120.0	79.0
A-Al$_2$O$_3$	552.3	107.9	1.49	163.4	35.5
A-SiO$_2$	989.0	97.2	2.40	161.3	38.57
X-SiO$_2$	1094.8	34.8	0.95	36.8	19.7
A-NS25w	639.8	124.8	2.00	353.8	49.5
A-NA25w	454.1	95.1	1.08	127.8	58.9
NS25w	440.8	43.7	0.48	47.7	32.2
NA25w	339.3	52.7	0.45	56.4	32.4

[1] Multi-Point B.E.T. Surface Area (m^2/g)

[2] Average Pore Diameter, 4V/S, (Å)

[3] Total Pore Volume (cm^3/g)

[4] Median Pore Diameter Based on Pore Volume (Å)

[5] Median Pore Diameter Based on Surface Area (Å)

Table B-3: PHYSICAL PROPERTY DATA OF NIOBIA AEROGELS PREPARED IN MEOH AND S-BUOH SOLVENTS

Sample	Surface Area (Multi Point)[1]	Avg. Pore Diameter[2]	Total Pore Volume[3]	(Pore Vol.) Med. Pore Diameter(Å)[4]	(Surface Area) Med. Pore Diameter(Å)[5]
		MeOH as Solvent			
A-Nb$_2$O$_5$ (.625,5.,0.25)[6]	222.0	121.9	0.68	153.3	93.4
A-Nb$_2$O$_5$ (.50,5.,0.25)	200.4	132.0	0.66	164.8	102.2
A-Nb$_2$O$_5$ (.31,5.,0.25)	215.2	130.6	0.70	168.5	81.2
A-Nb$_2$O$_5$ (.625,10.,0.25)	195.5	166.0	0.81	249.7	105.5
A-Nb$_2$O$_5$ (.50,10.,0.25)	193.9	212.1	1.03	287.3	140.8
A-Nb$_2$O$_5$ (.31,10.,0.25)	218.3	165.7	0.90	210.7	98.6
		s-BuOH as Solvent			
A-Nb$_2$O$_5$ (.625,5.,0.80)	151.4	214.3	0.81	380.6	91.1
A-Nb$_2$O$_5$ (.50,5.,0.80)	132.6	180.5	0.60	264.9	69.3
A-Nb$_2$O$_5$ (.31,5.,0.80)	91.4	166.8	0.38	337.4	63.5
A-Nb$_2$O$_5$ (.625,10.,0.80)	166.1	307.4	1.28	584.4	129.1
A-Nb$_2$O$_5$ (.50,10.,0.80)	196.3	260.9	1.28	614.9	77.9
A-Nb$_2$O$_5$ (.31,10.,0.80)	165.1	394.2	1.63	760.5	114.0

[1] Multi-Point B.E.T. Surface Area (m^2/g)

[2] Average Pore Diameter , 4V/S, (Å)

[3] Total Pore Volume (cm^3/g)

[4] Median Pore Diameter Based on Pore Volume (Å)

[5] Median Pore Diameter Based on Surface Area (Å)

[6] {Conc. Nb^{5+} (mol Nb^{5+}/ml), Water Conc. (mol H_2O/mol Nb^{5+}), Acid Conc. (mol HNO3/mol Nb^{5+})}

393

Figure B-1: NITROGEN DESORPTION ISOTHERM OF A-Nb$_2$O$_5$
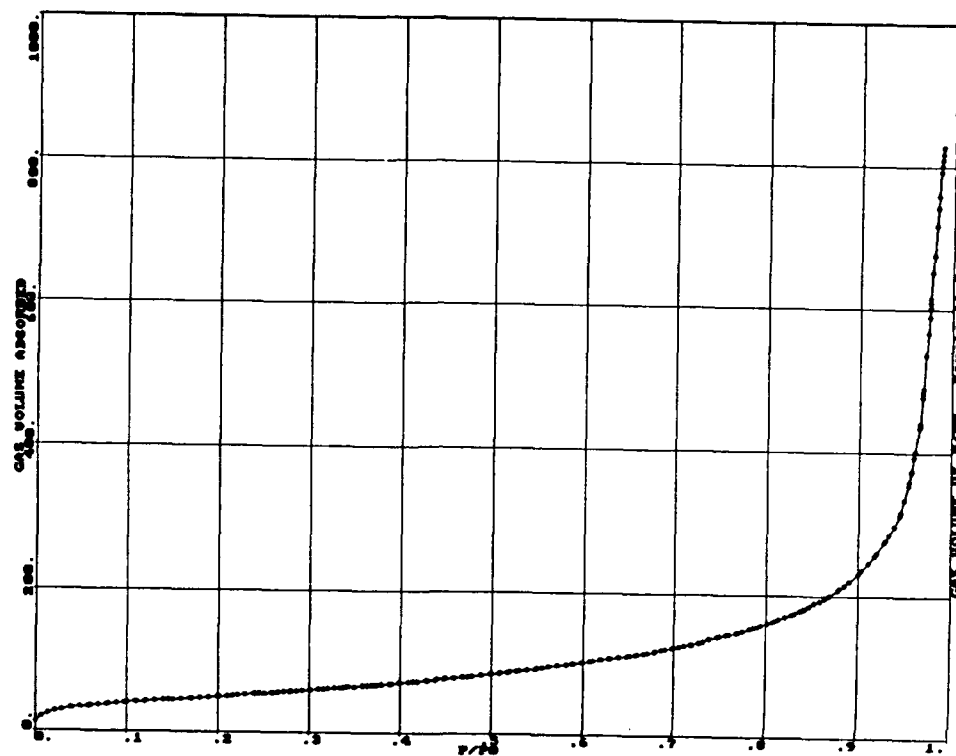
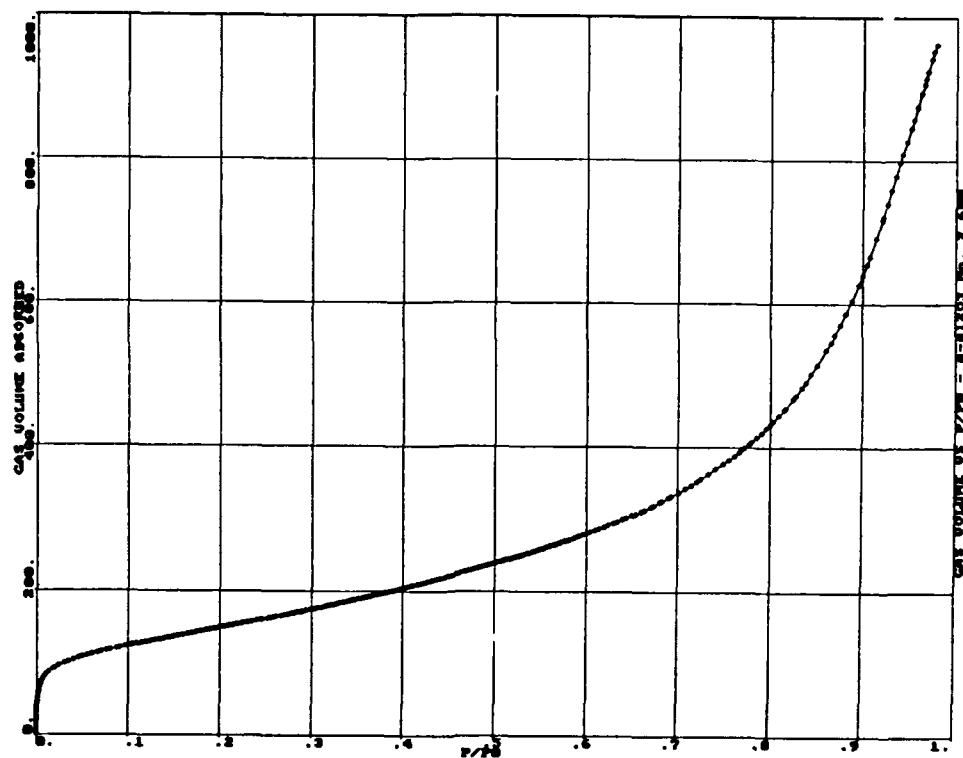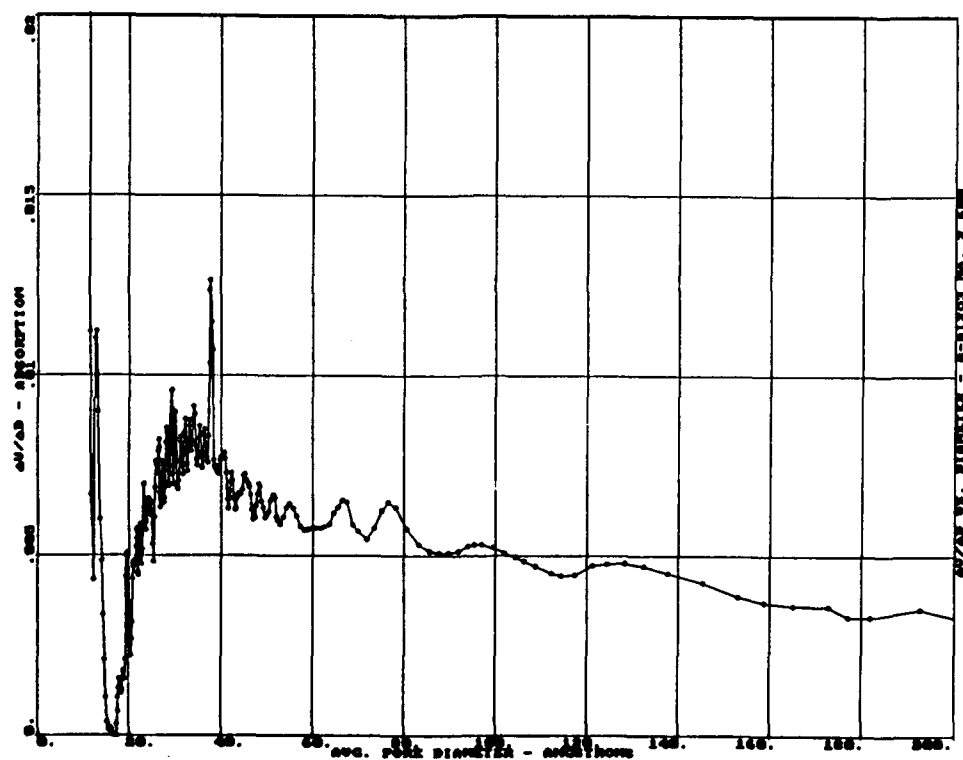**Figure B-2:** PORE SIZE DISTRIBUTION FOR A-Nb$_2$O$_5$ AS DETERMINED BY NITROGEN ADSORPTION
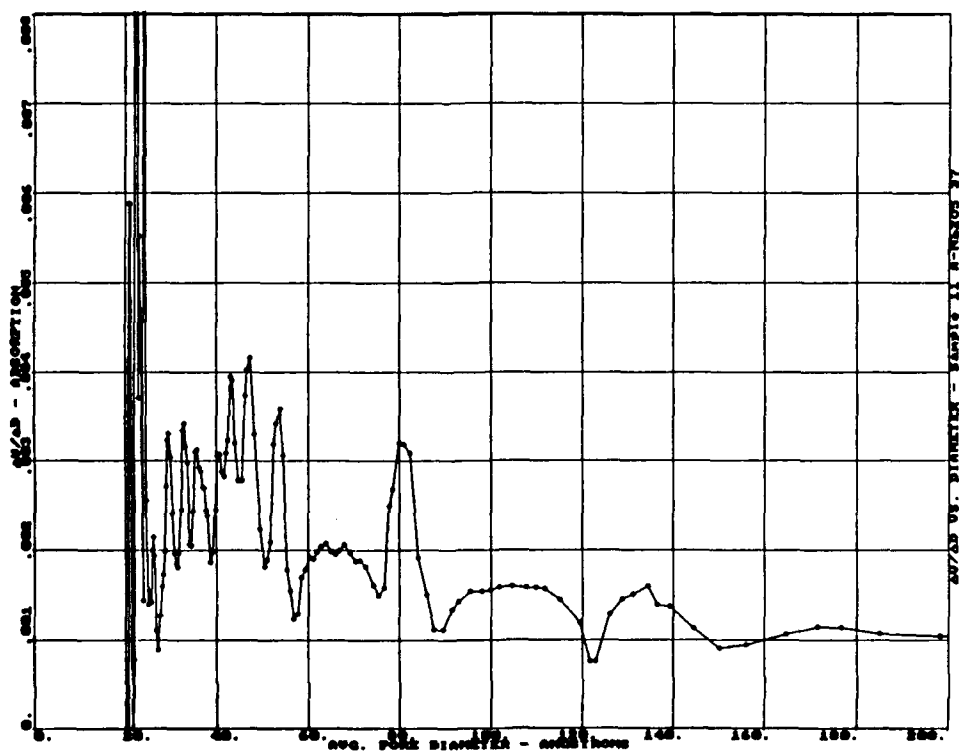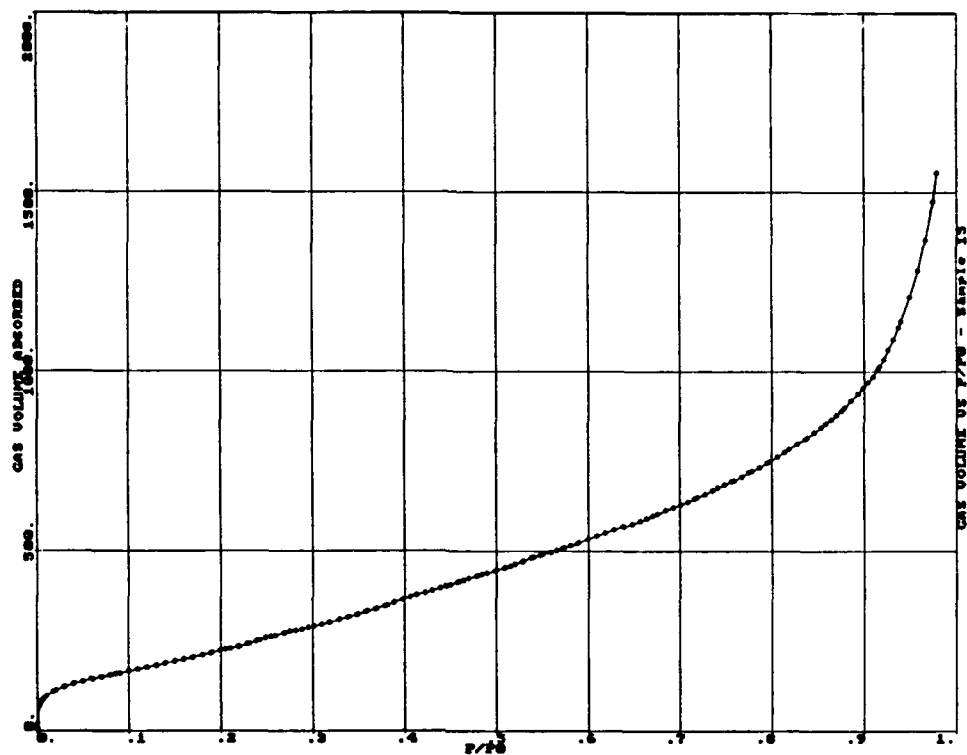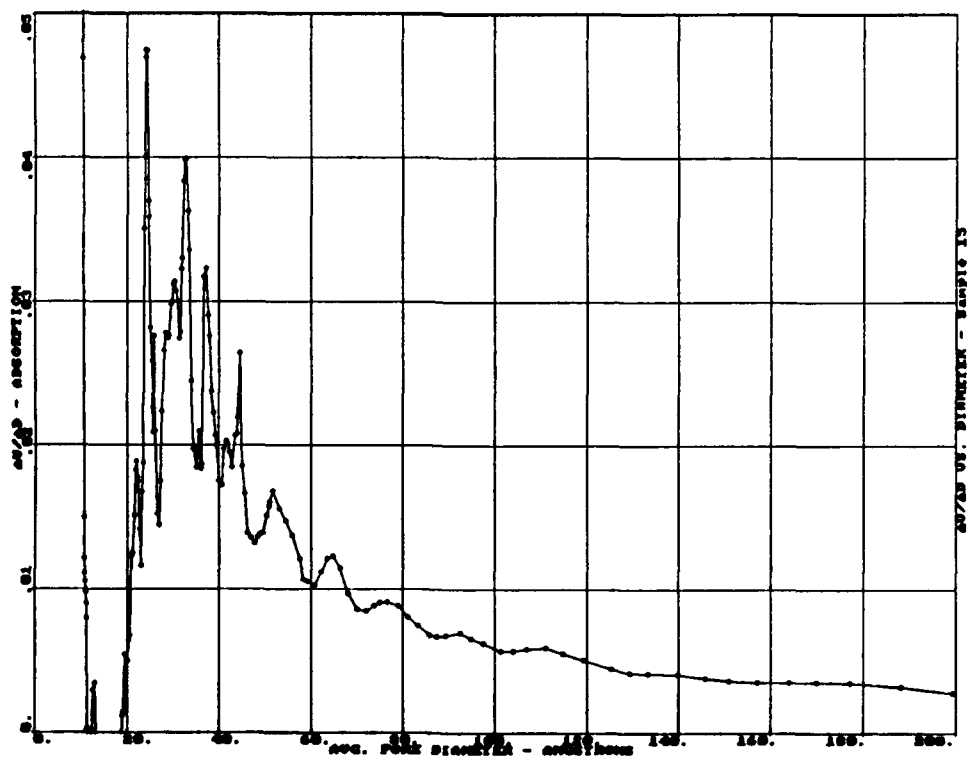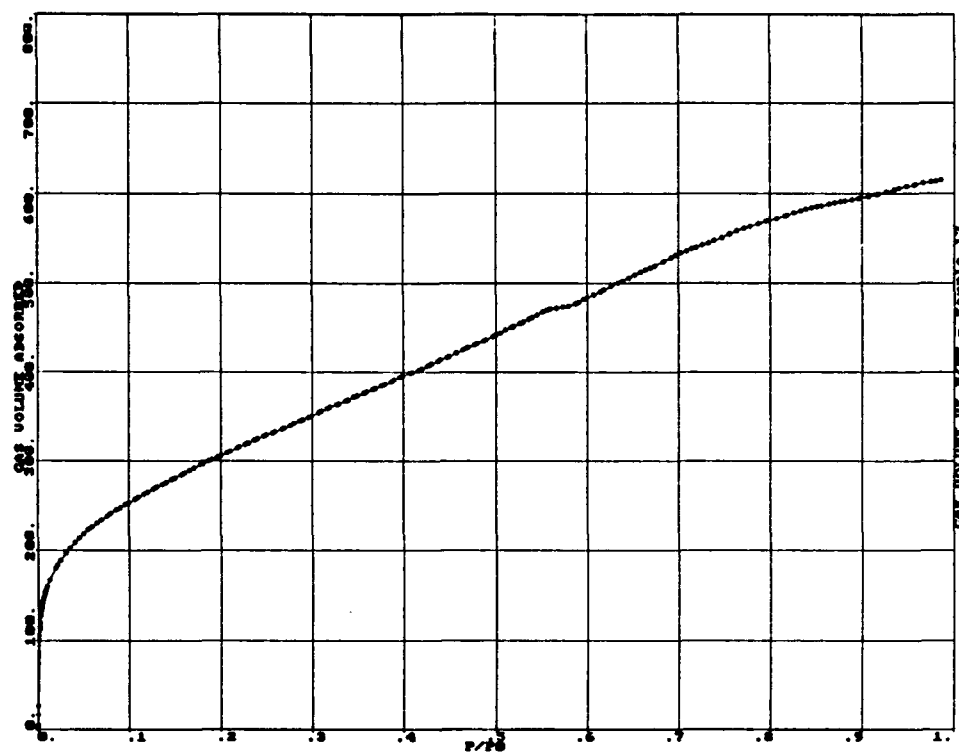
Figure B-3: NITROGEN DESORPTION ISOTHERM OF P-Nb₂O₅
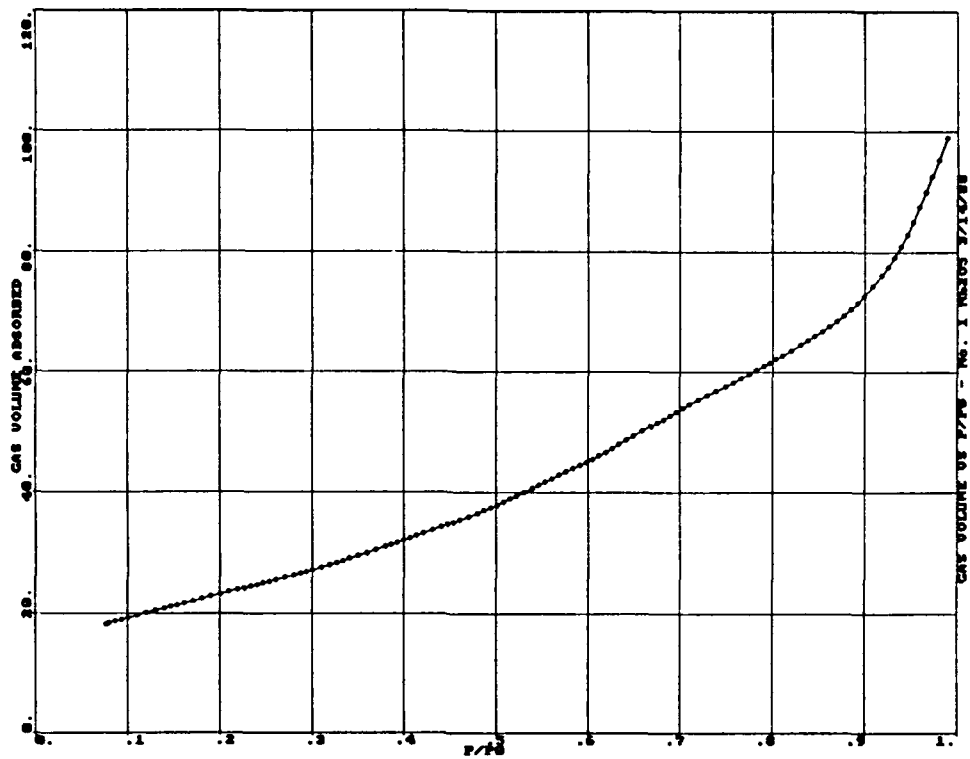
Figure B-4: PORE SIZE DISTRIBUTION FOR P-Nb₂O₅ AS DETERMINED BY NITROGEN ADSORPTION
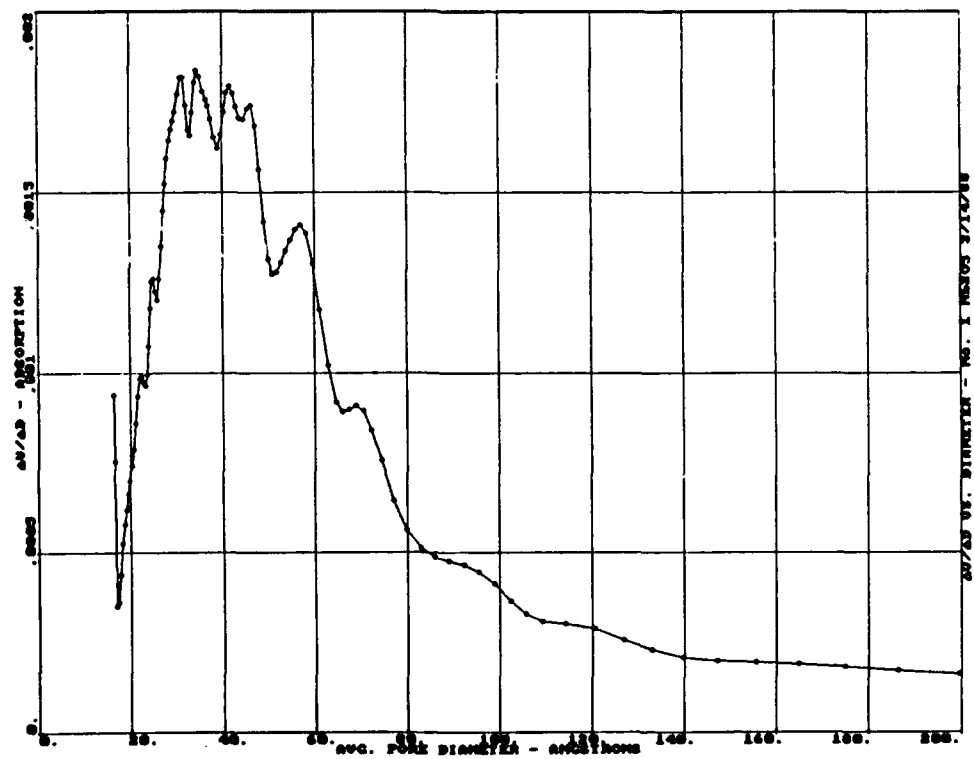
Figure B-5: NITROGEN DESORPTION ISOTHERM OF X-Nb$_2$O$_5$
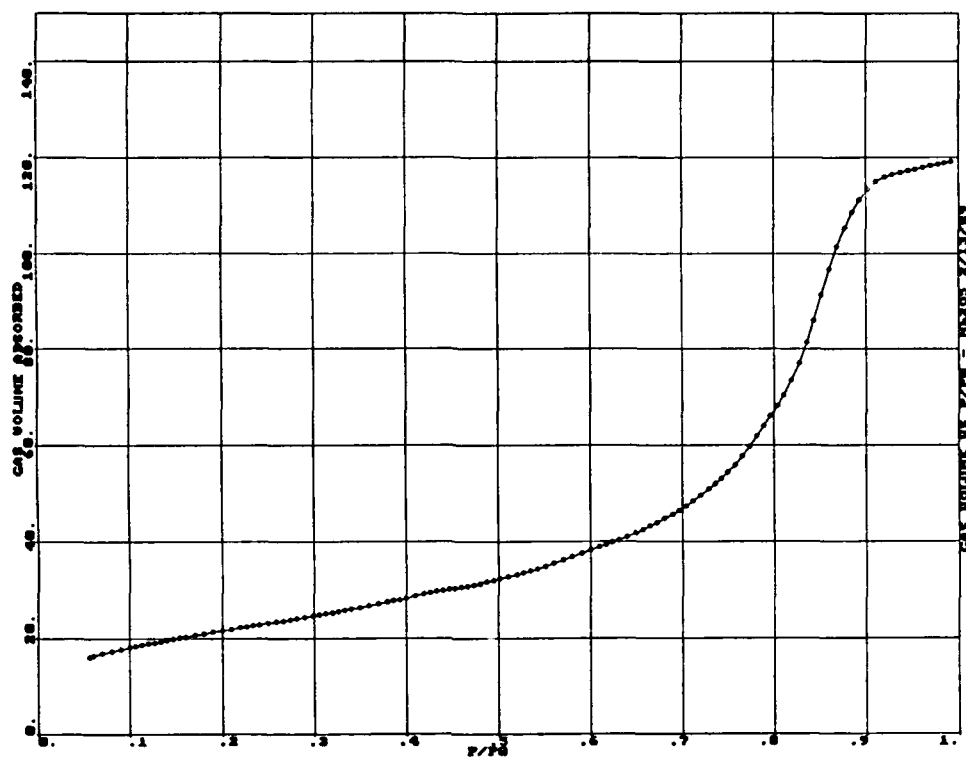
Figure B-6: PORE SIZE DISTRIBUTION FOR X-Nb$_2$O$_5$ AS DETERMINED BY NITROGEN ADSORPTION
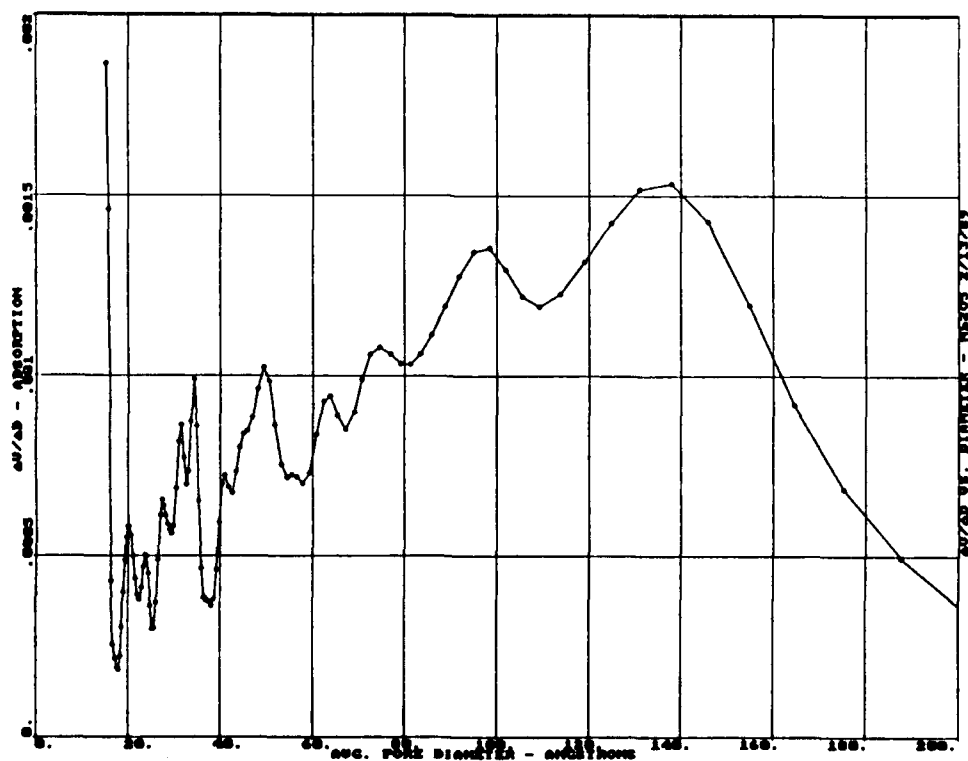
Figure B-7: NITROGEN DESORPTION ISOTHERM OF NIOBIC ACID
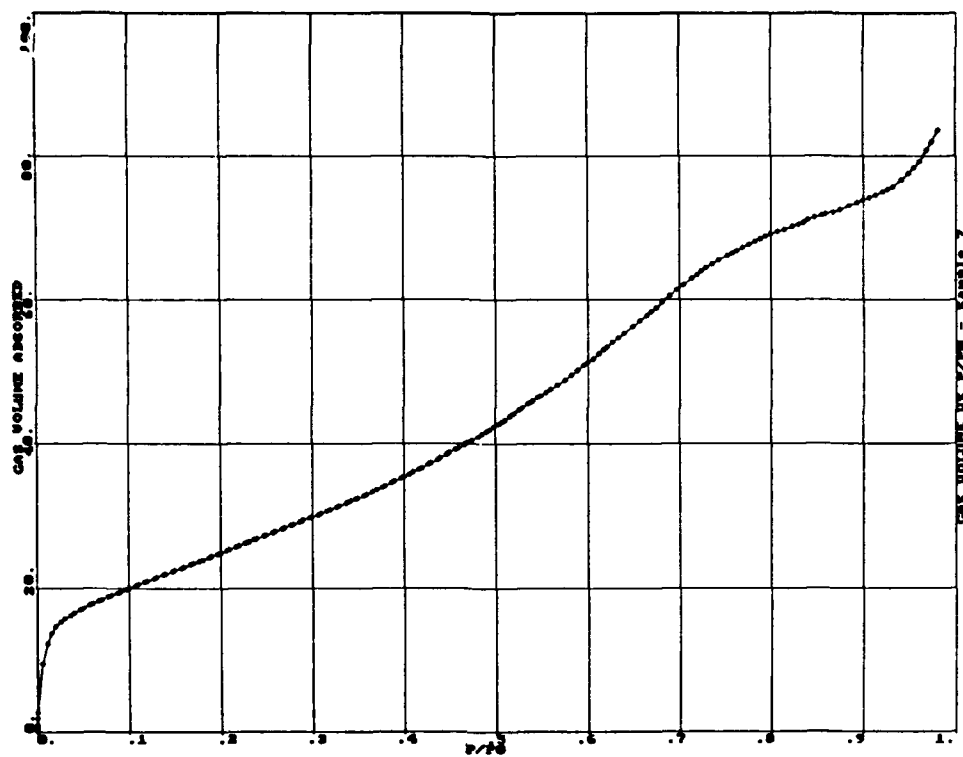
Figure B-8: PORE SIZE DISTRIBUTION FOR NIOBIC ACID AS DETERMINED BY NITROGEN ADSORPTION
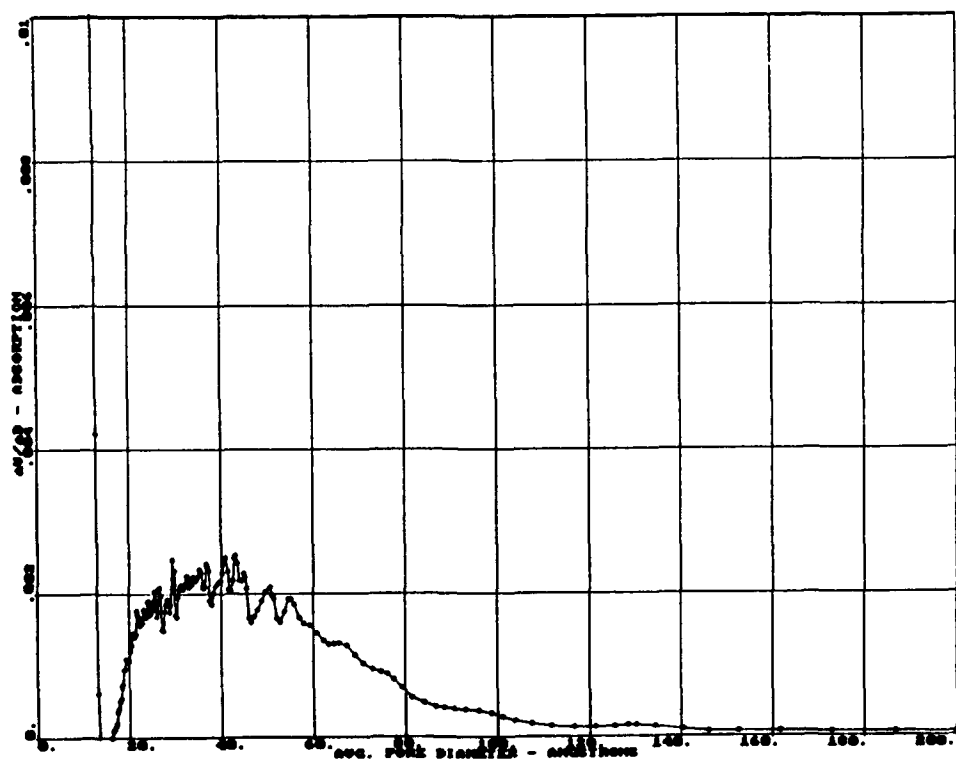
niobia aerogel over the other niobia samples actually indicate that A-Nb_2O_5 should have a fairly broad distribution of larger pores too (mesopores, radii 1.5 to 50 nm). The pore size distributions are shown in Figures B-2, B-4, B-6, and B-8 for A-Nb_2O_5, P-Nb_2O_5, X-Nb_2O_5, and Niobic Acid, respectively. All niobium oxides appear to show a fairly broad distribution of pore sizes; however, the xerogel of niobia shows the largest number of the bigger sized diameter pores (>100 Å). The precipitated niobia and niobic acid samples show a preponderance of pore diameters around 30 - 60 Å while the aerogel appears to have a more even distribution of pore sizes.

B.2 Alumina and Silica Aerogels and Xerogels

The desorption isotherms for the alumina and silica aerogels are shown in Figures B-9 and B-11, respectively. Both aerogels show the type II classification for the isotherms and indicate very high surface area materials as shown by the large volume of nitrogen adsorbed. The pore size distribution for A-Al_2O_3 and A-SiO_2 are shown in Figures B-10 and B-12, respectively. Both oxide aerogels show a broad distribution of pores in the mesopore range; however, the silica aerogel shows an increased number of pores whose diameters are around 30 - 40 Å. This increase in smaller diameter pores probably accounts for the larger surface area found for this aerogel of silica, which is 50% greater than that for the aerogel of alumina. The physical property data for the xerogel of silica is shown in Figures B-13 and B-14. The desorption isotherm in Figure B-13 for this xerogel falls into the type I classification , and indicates a very microporous solid. The volume adsorbed at the lowest partial pressure accounts for nearly half of the total pore volume, which indicates a large number of extremely small pores. This is seen more clearly in the pore size distribution which shows little if any adsorbed volume in pores greater than 100 Å, but we see an enormous amount of adsorption in the pores whose diameters are in the size range of 10 - 20 Å.
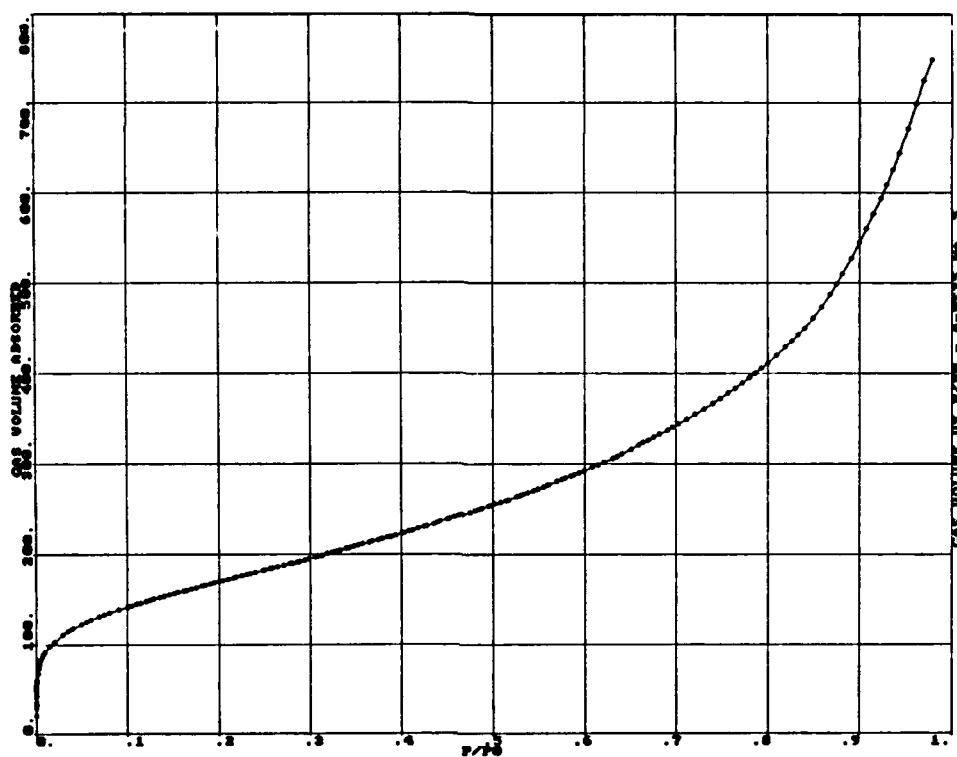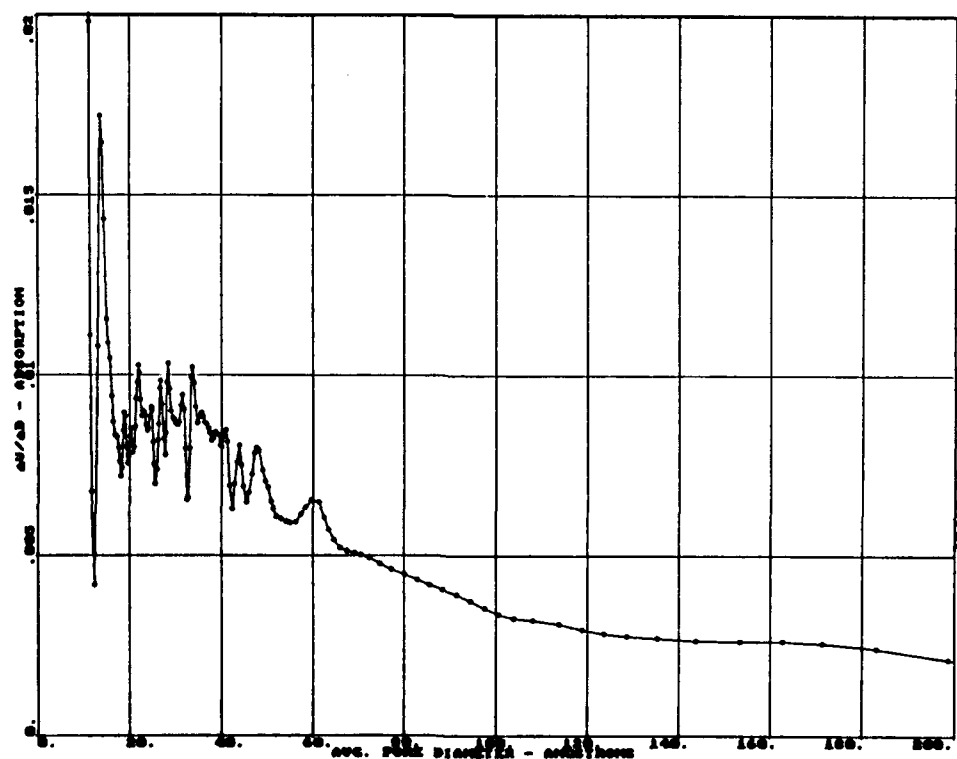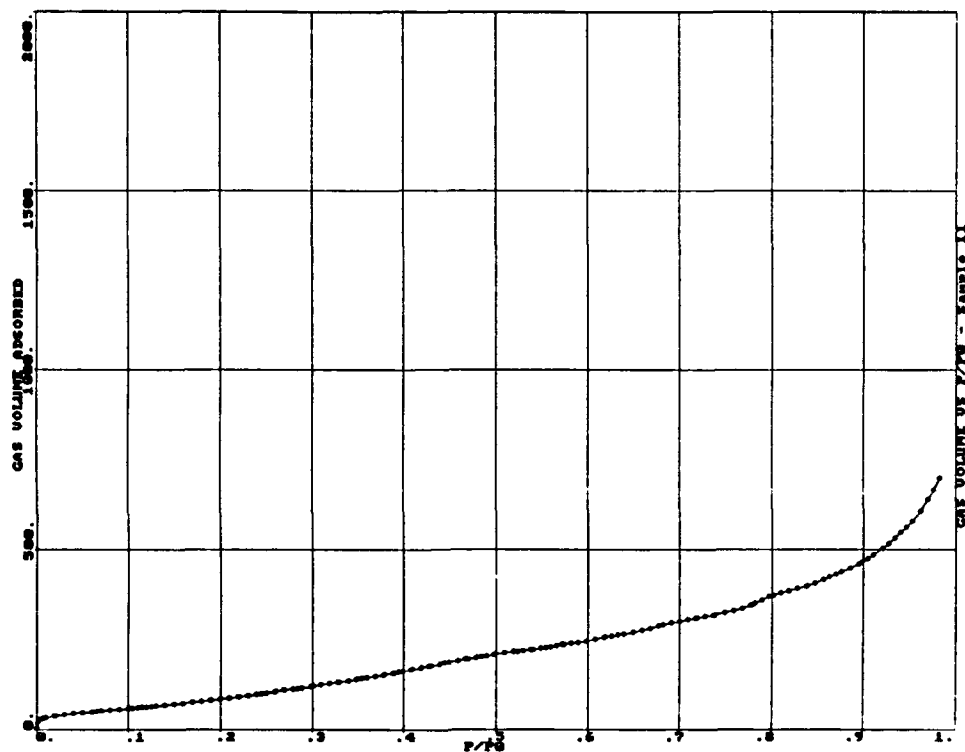
398

Figure B-9: NITROGEN DESORPTION ISOTHERM OF A-Al₂O₃

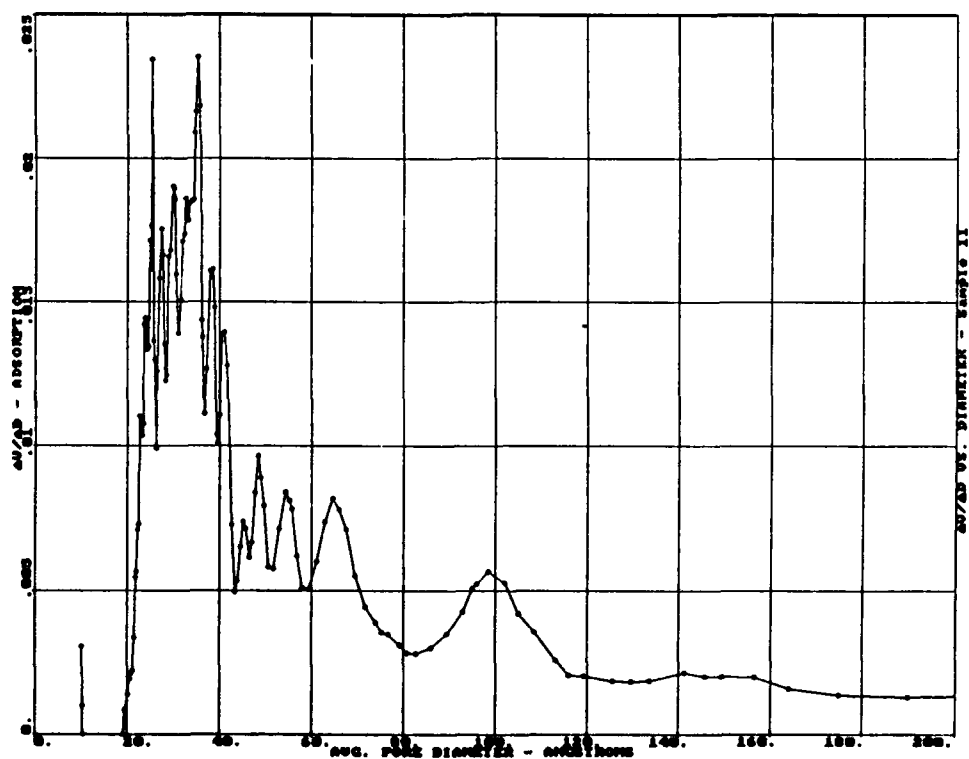**Figure B-10:** PORE SIZE DISTRIBUTION FOR A-Al₂O₃ AS DETERMINED BY
NITROGEN ADSORPTION

Figure B-11: NITROGEN DESORPTION ISOTHERM OF A-SiO$_2$

Figure B-12: PORE SIZE DISTRIBUTION FOR A-SiO$_2$ AS DETERMINED BY NITROGEN ADSORPTION

Figure B-13: NITROGEN DESORPTION ISOTHERM OF X-SiO$_2$

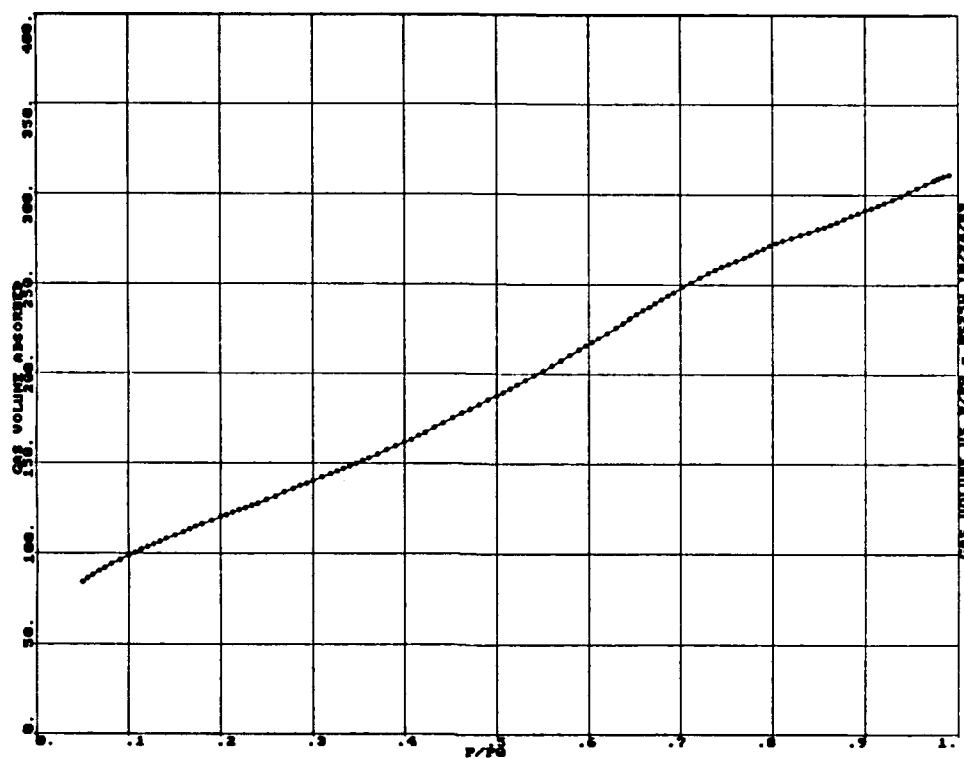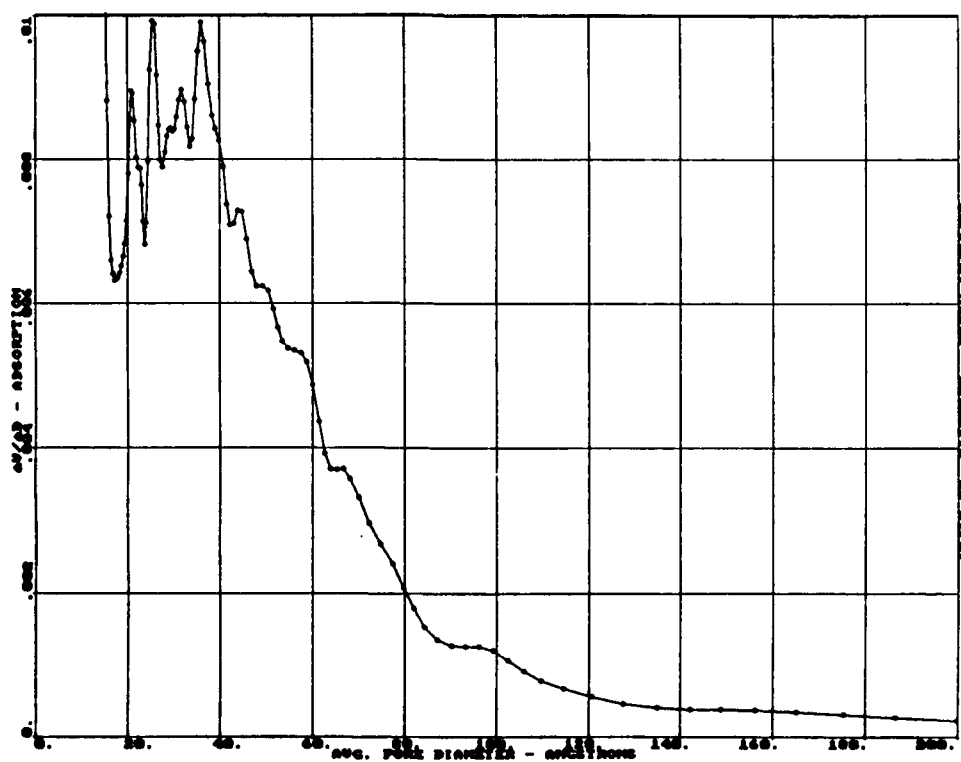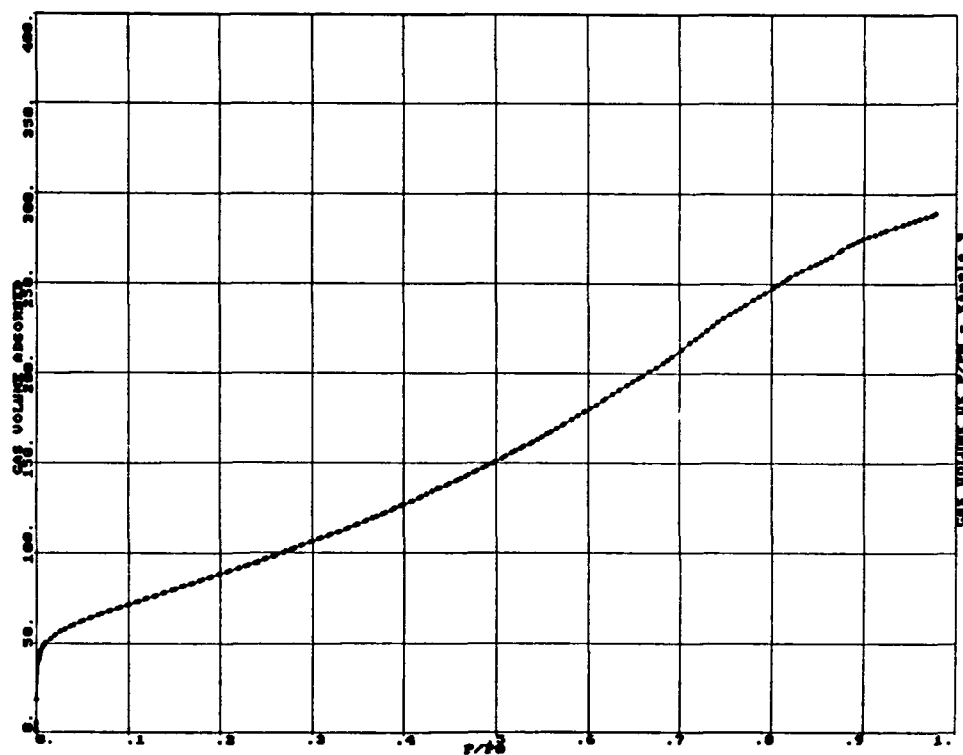
Figure B-14: PORE SIZE DISTRIBUTION FOR X-SiO$_2$ AS DETERMINED BY NITROGEN ADSORPTION
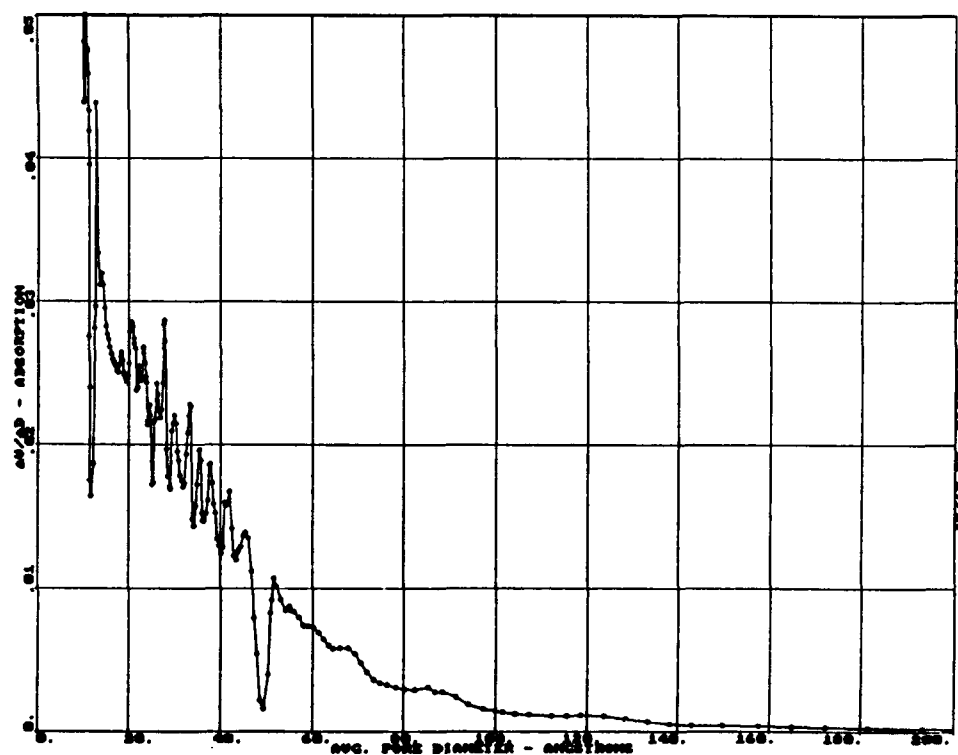
B.3 Niobia/Silica and Niobia/Alumina Mixed Oxide Aerogels

The desorption isotherms for the mixed oxide aerogels of A-NS25w and A-NA25w are shown in Figures B-15 and B-17, respectively. Both of these samples have isotherms which are of the type II classification. The monotonic rise throughout most of the relative pressure range indicates that these samples should have broad pore size distribution, and is confirmed in Figures B-16 and B-18 for A-NS25w and A-NA25w, respectively. However, the A-NA25 mixed oxide has about twice as many pores whose diameters fall in the range of 30 - 40 Å than the other sized pores. The desorption isotherms for the conventionally prepared counterparts to the mixed oxide aerogels are shown in Figures B-19 and B-21 for NS25w and NA25w, respectively. Both of these isotherms are of the type IV classification and yield a wide distribution of pore sizes in these precipitated mixed oxides as shown in Figures B-20 and B-22 for NS25w and NA25w, respectively.

B.4 Heat Treated Niobia Aerogels and Conventionally Prepared Niobia

The desorption isotherms and pore size distributions for the heat treated niobia aerogel samples: A-Nb$_2$O$_5$ (600,2), A-Nb$_2$O$_5$ (800,2), and A-Nb$_2$O$_5$ (1000,-), as well as the heat treated (1000,-) samples of P-Nb$_2$O$_5$ and Niobic Acid are shown in Figures B-23 to B-32, respectively. The accuracy of these samples is questionable because of the small amount of material used in the analysis. Therefore, these data will not be discussed, but are presented here only for measures of completeness.

Figure B-15: NITROGEN DESORPTION ISOTHERM OF A-NS25w

Figure B-16: PORE SIZE DISTRIBUTION FOR A-NS25w AS DETERMINED BY NITROGEN ADSORPTION

Figure B-17: NITROGEN DESORPTION ISOTHERM OF A-NA25w

Figure B-18: PORE SIZE DISTRIBUTION FOR A-NA25w AS DETERMINED BY NITROGEN ADSORPTION

404

Figure B-19: NITROGEN DESORPTION ISOTHERM OF NS25w

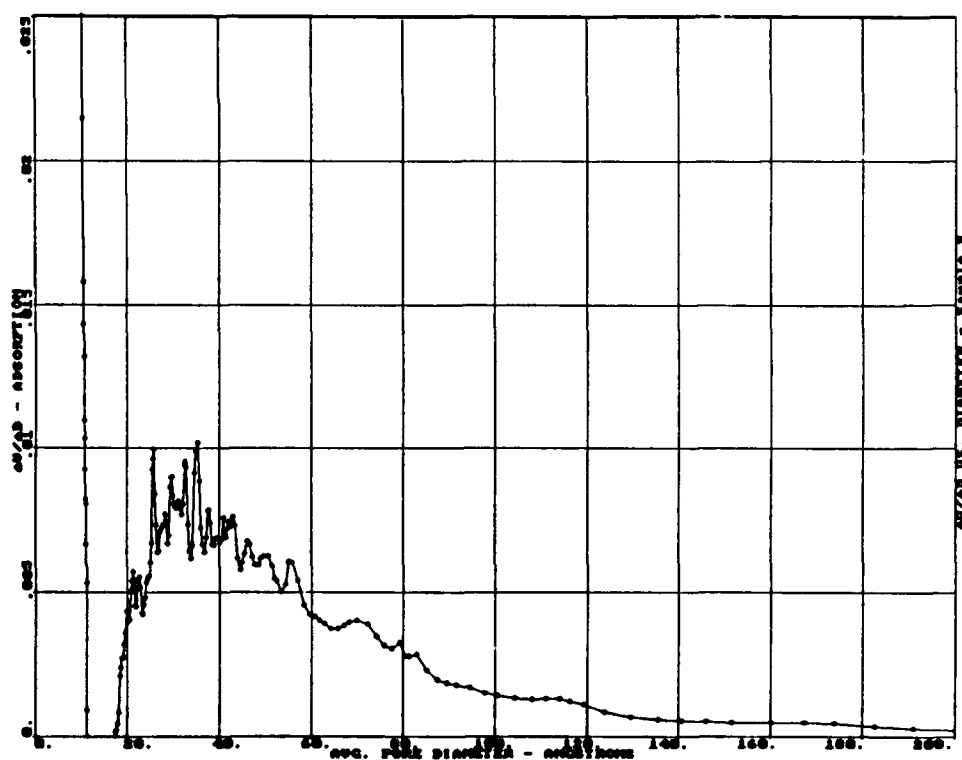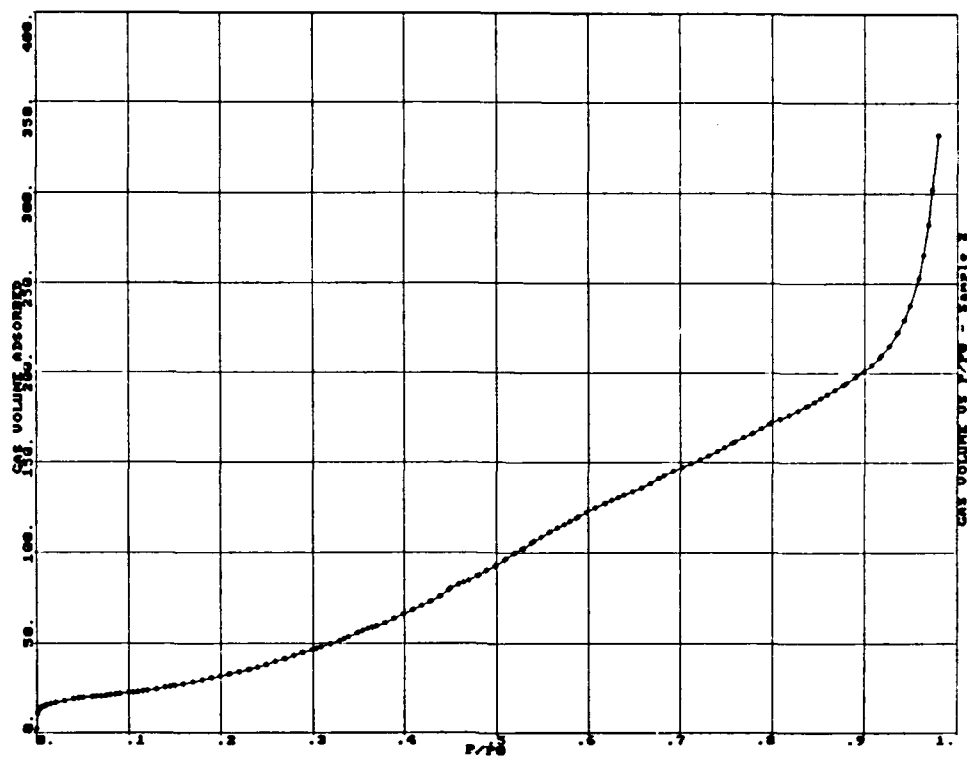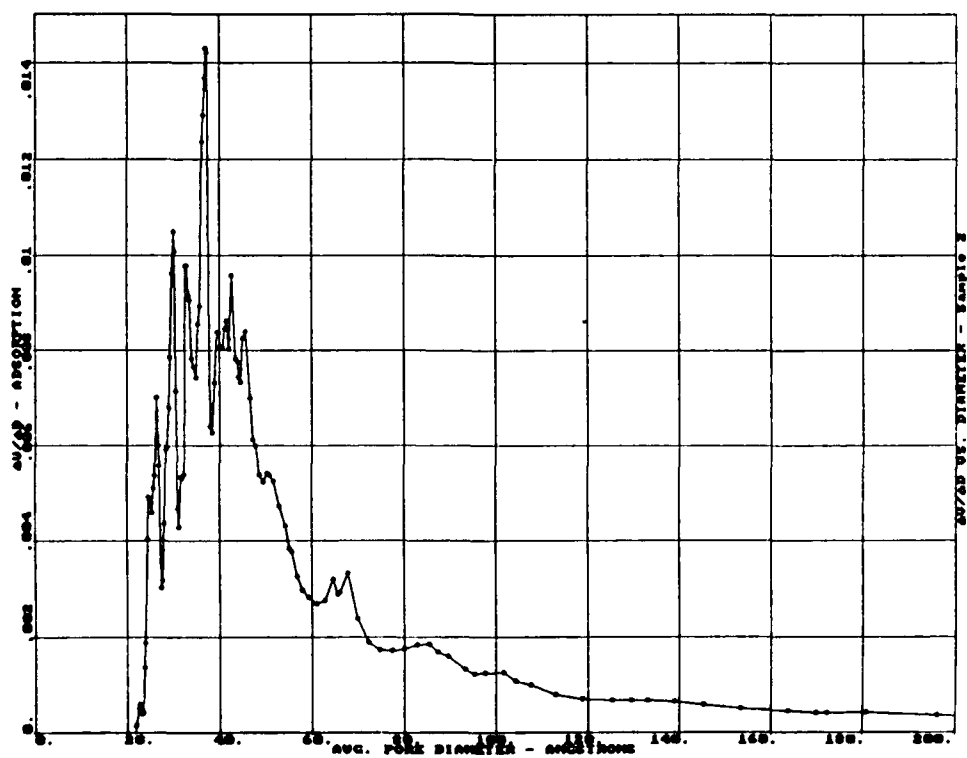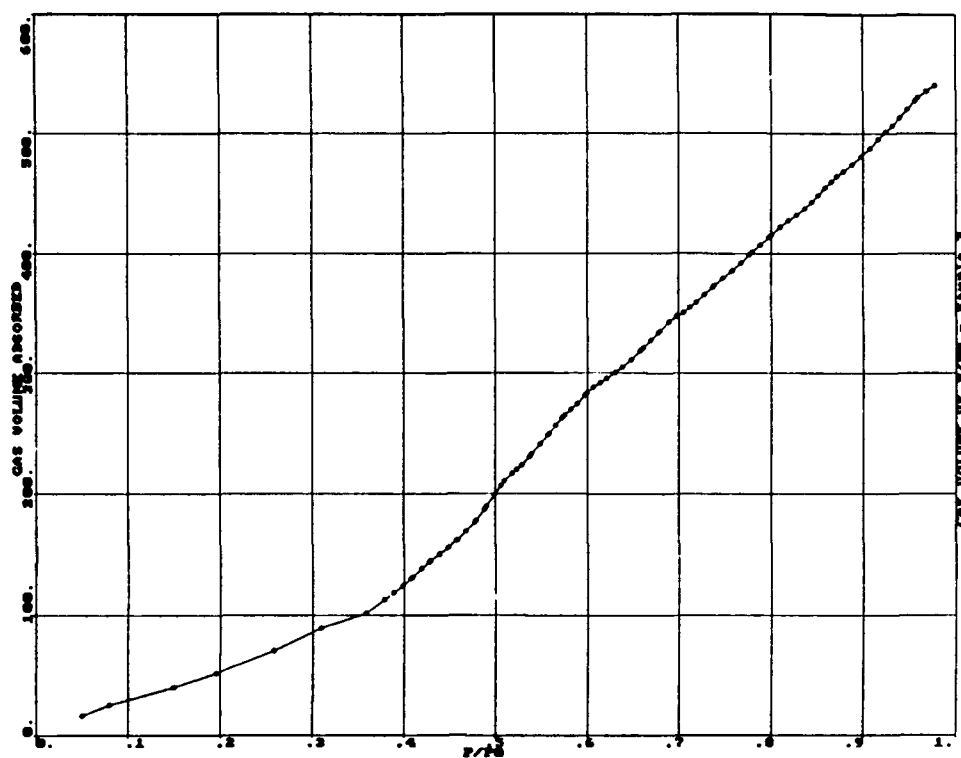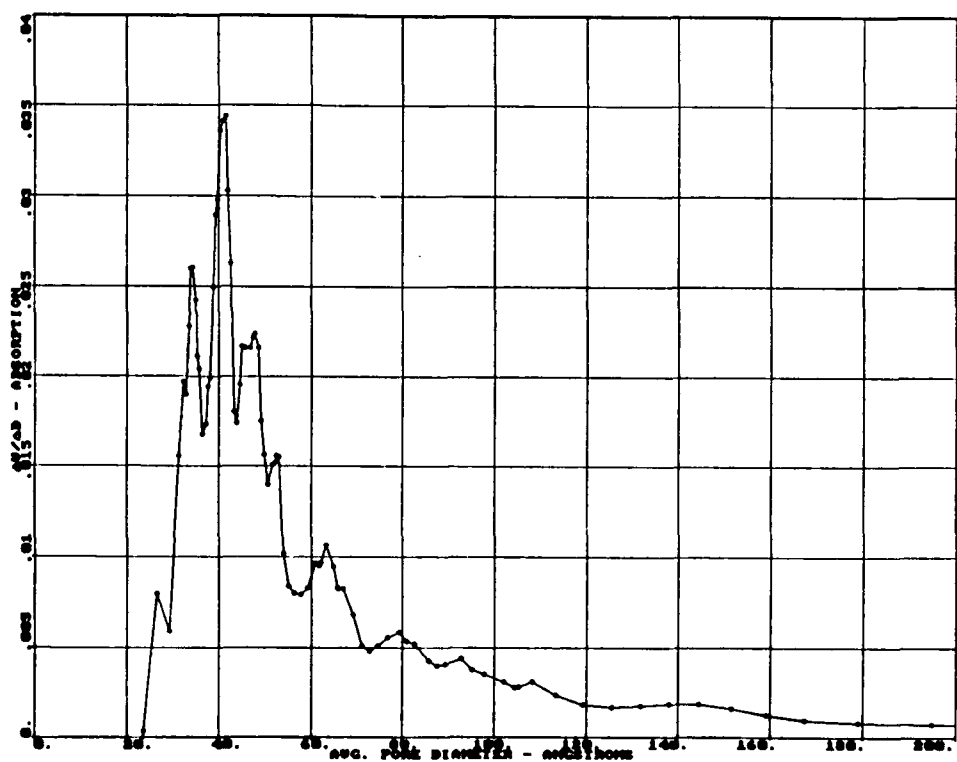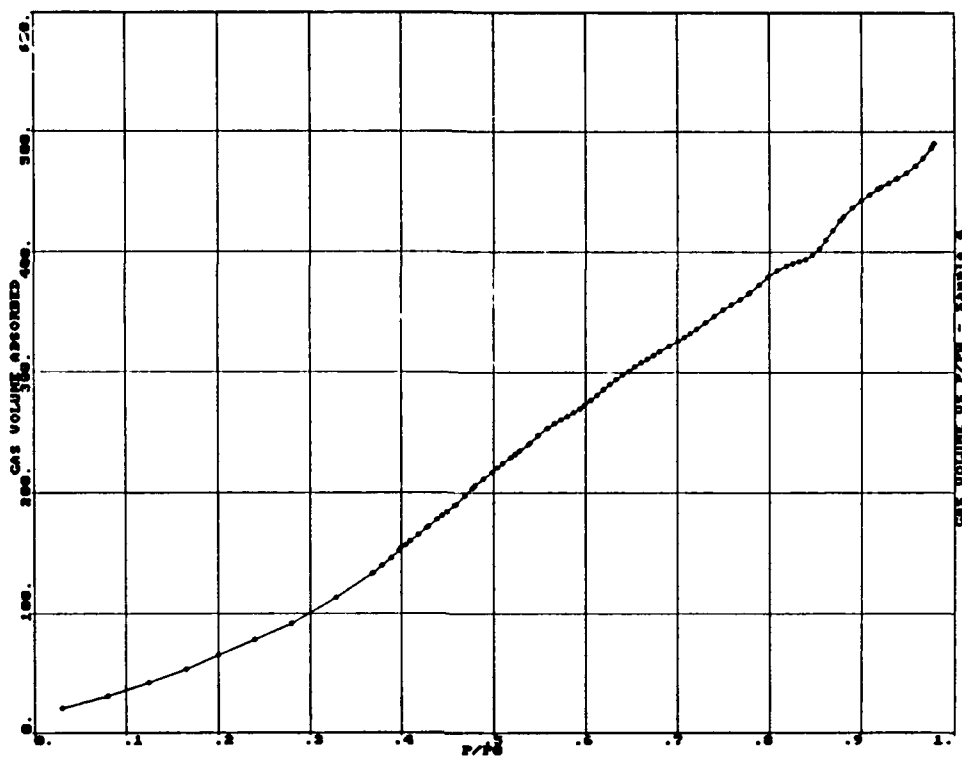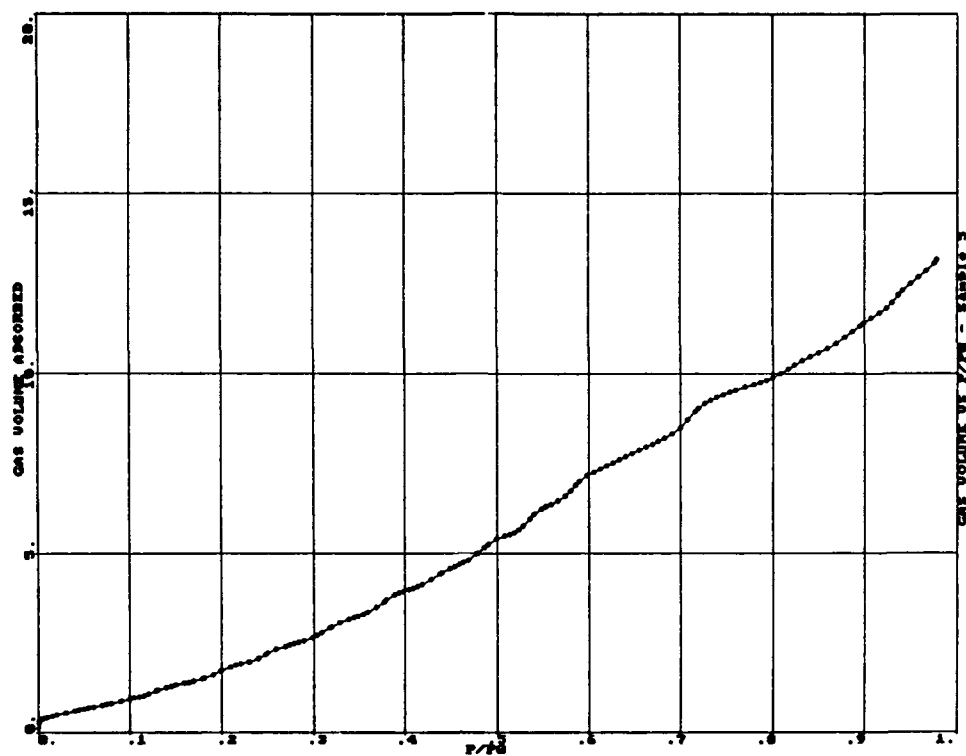**Figure B-20:** PORE SIZE DISTRIBUTION FOR NS25w AS DETERMINED BY NITROGEN ADSORPTION

Figure B-21: NITROGEN DESORPTION ISOTHERM OF NA25w

Figure B-22: PORE SIZE DISTRIBUTION FOR NA25w AS DETERMINED BY NITROGEN ADSORPTION

Figure B-23: NITROGEN DESORPTION ISOTHERM OF A-Nb$_2$O$_5$ (600,2)

Figure B-24: PORE SIZE DISTRIBUTION FOR A-Nb$_2$O$_5$ (600,2) AS DETERMINED BY NITROGEN ADSORPTION

Figure B-25: NITROGEN DESORPTION ISOTHERM OF A-Nb_2O_5 (800,2)

Figure B-26: PORE SIZE DISTRIBUTION FOR A-Nb_2O_5 (800,2) AS DETERMINED BY NITROGEN ADSORPTION

Figure B-27: NITROGEN DESORPTION ISOTHERM OF A-Nb$_2$O$_5$ (1000,-)

Figure B-28: PORE SIZE DISTRIBUTION FOR A-Nb$_2$O$_5$ (1000,-) AS DETERMINED BY NITROGEN ADSORPTION
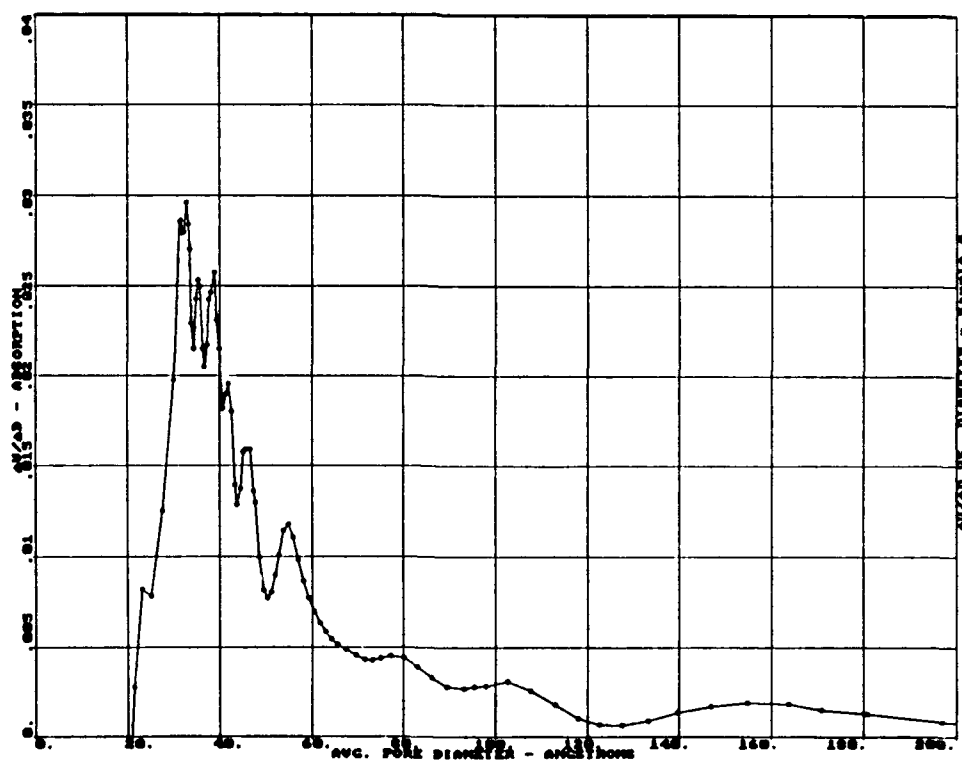
Figure B-29: NITROGEN DESORPTION ISOTHERM OF P-Nb$_2$O$_5$ (1000,-)

Figure B-30: PORE SIZE DISTRIBUTION FOR P-Nb$_2$O$_5$ (1000,-) AS DETERMINED BY NITROGEN ADSORPTION
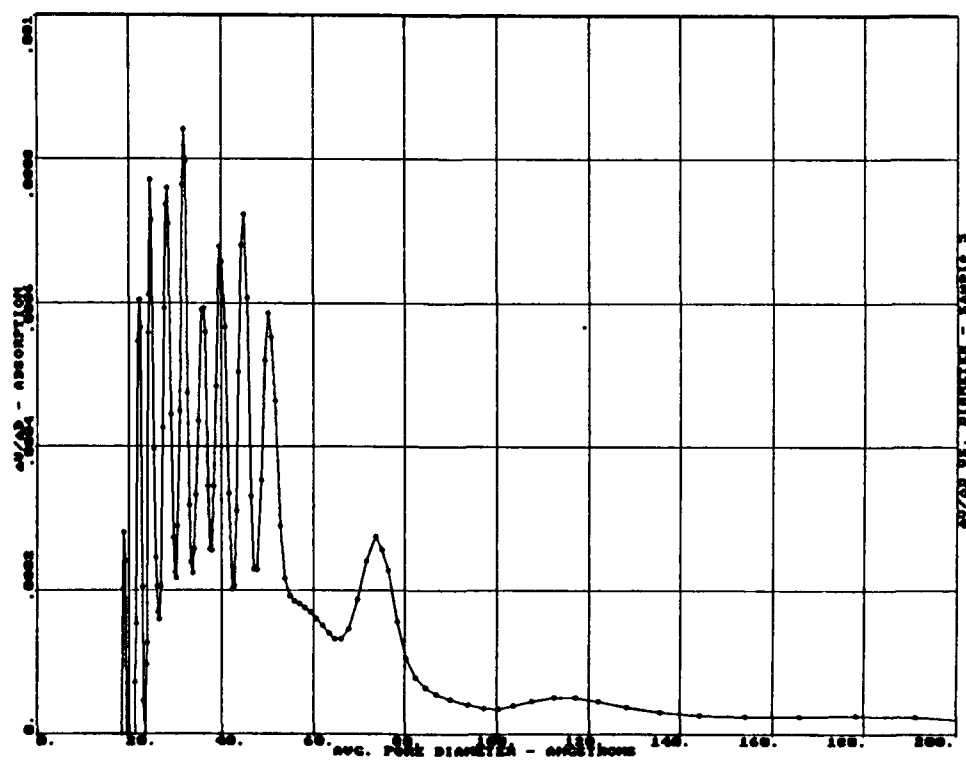
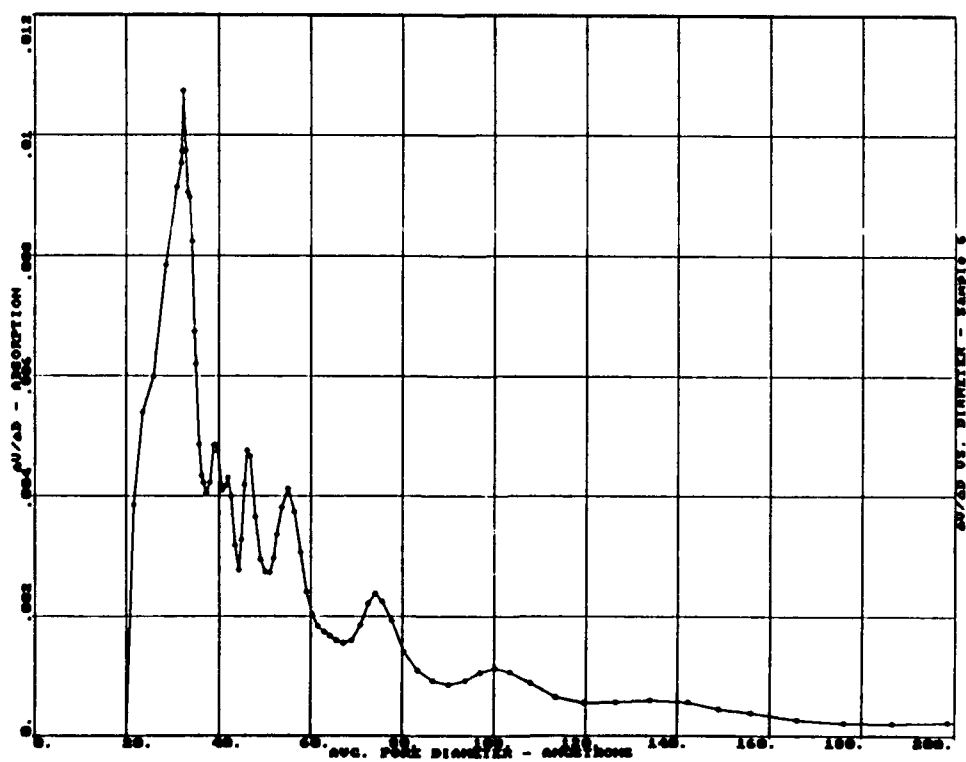**Figure B-31: NITROGEN DESORPTION ISOTHERM OF NIOBIC ACID (1000,-)**
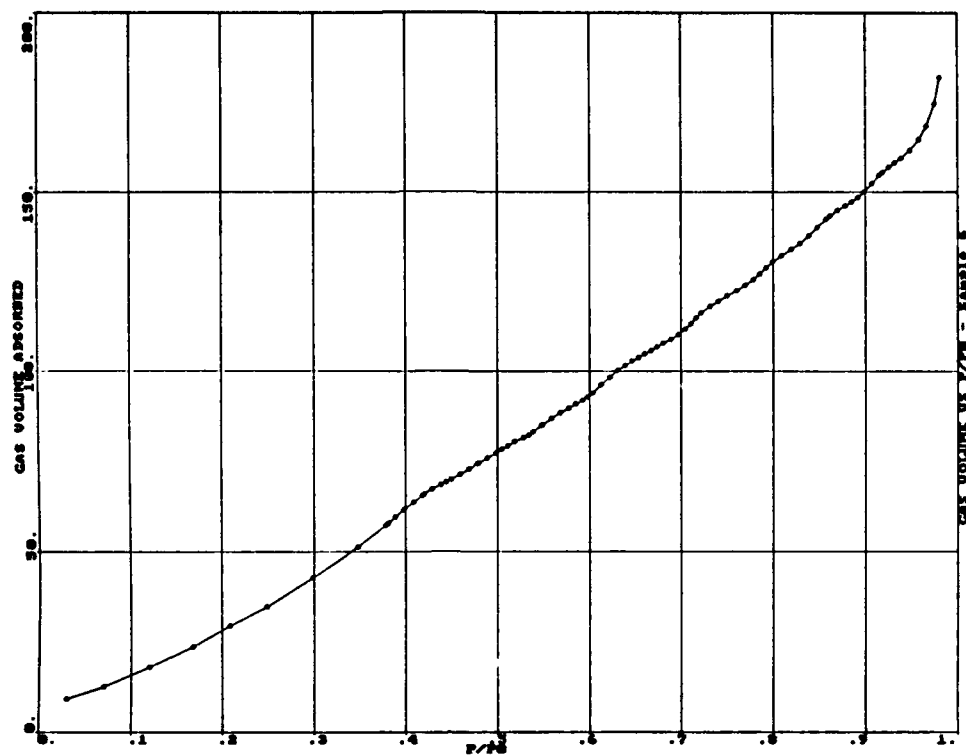
Figure B-32: PORE SIZE DISTRIBUTION FOR NIOBIC ACID (1000,-) AS DETERMINED BY NITROGEN ADSORPTION

B.5 Niobia Aerogels Prepared in Methanol

The desorption isotherms and pore size distribution of the niobia aerogels prepared in methanol (see Table 3-1 and 3-2 for nomenclature in parentheses) are shown in Figures B-33 to B-44. The niobia aerogels prepared in methanol with a water concentration of 5.0 (molar ratio H_2O/Nb^{5+}) are shown in Figures B-33 to B-38, with decreasing niobium ethoxide concentration. All three desorption isotherms are of the type IV classification, and show a wide range of pore sizes as shown in the pore size distribution figures. When the water concentration is doubled for the aerogels of niobia prepared in methanol, the desorption isotherms (see Figures B-39, B-41, and B-43) appear to all change from the classification of type IV to type II isotherms, cons·stent with what we have found for our other synthesized aerogels. The monotonic increase of volume with respect to relative pressure throughout most of the range should yield a wide distribution of pore sizes and is confirmed in Figures B-40, B-42, and B-44, with respect to decreasing niobium ethoxide concentration. These results show that the larger pore volumes and pore sizes are produced when the water ratio is increased to twice the needed stoichiometric amount. The increased pore volume with the increased water ratio could be due to a more complete reaction of all ethoxide groups in the aerogel; however, more work needs to be done in this area.

B.6 Niobia Aerogels Prepared in s-BuOH

The desorption isotherms and pore size distribution of the niobia aerogels prepared in s-butanol (see Table 3-1 and 3-2 for nomenclature) are shown in Figures B-45 to B-56. The niobia aerogels prepared in s-butanol, unlike those prepared in methanol, all show type II classification of desorption isotherms as shown in Figures B-45, B-47, B-49, B-51, B-53, and B-55. Also, similar to all of these isotherms is a linear or monotonic portion throughout most of the relative pressure range which would indicate a very broad

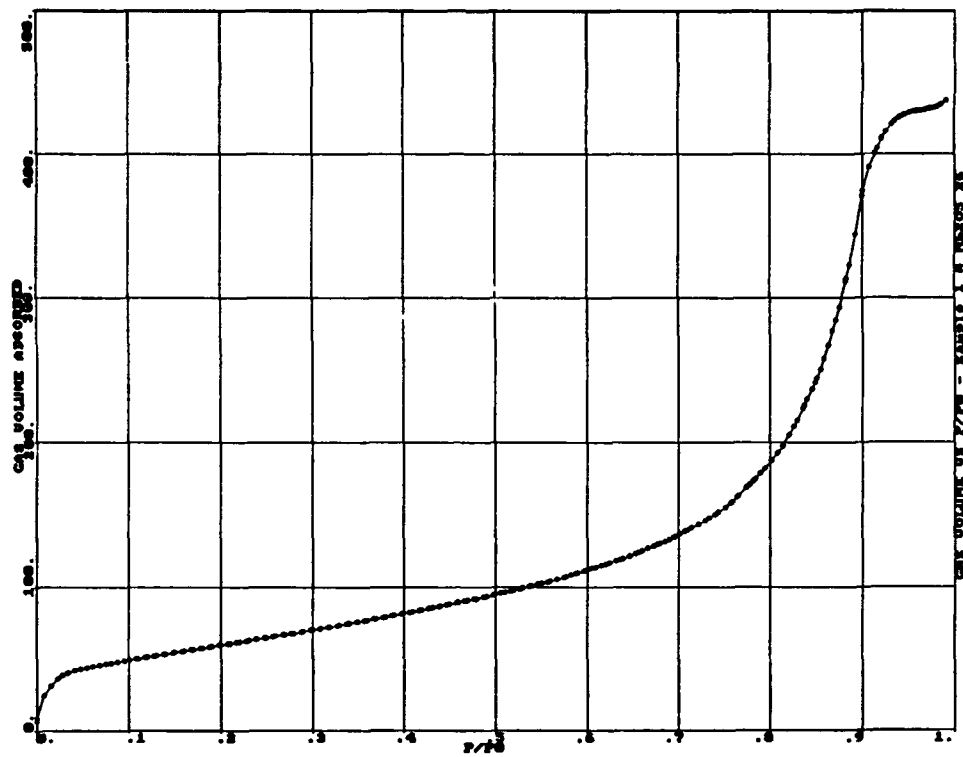**Figure B-33:** NITROGEN DESORPTION ISOTHERM OF A-Nb$_2$O$_5$ (0.625,5.,0.25) WITH MEOH

Figure B-34: PORE SIZE DISTRIBUTION FOR A-Nb$_2$O$_5$ (0.625,5.,0.25) WITH MEOH AS DETERMINED BY NITROGEN ADSORPTION
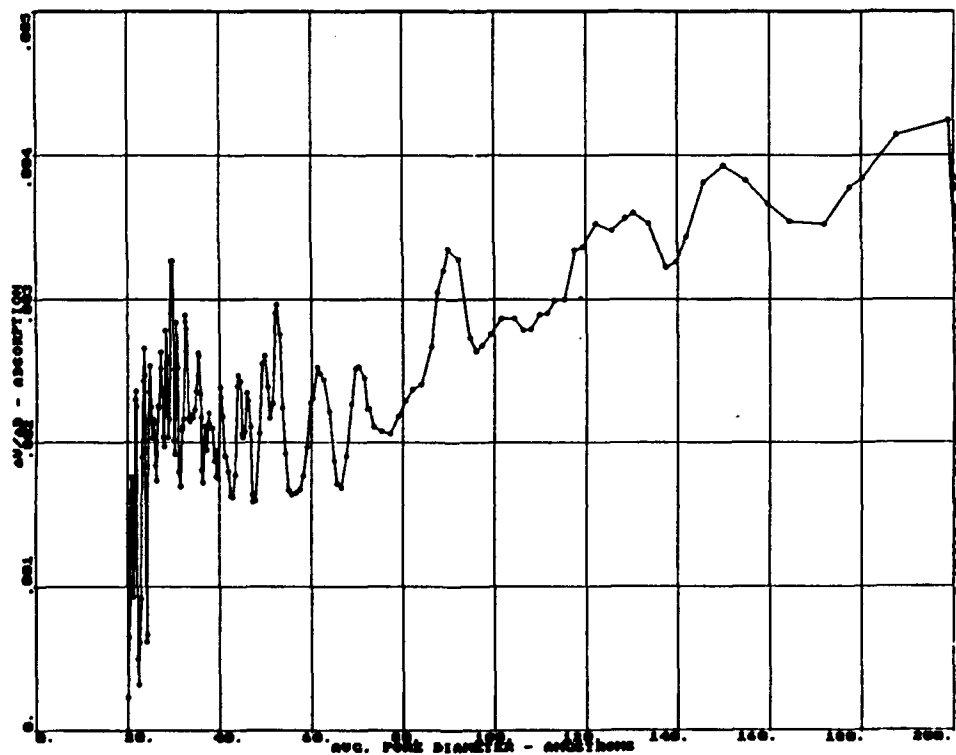
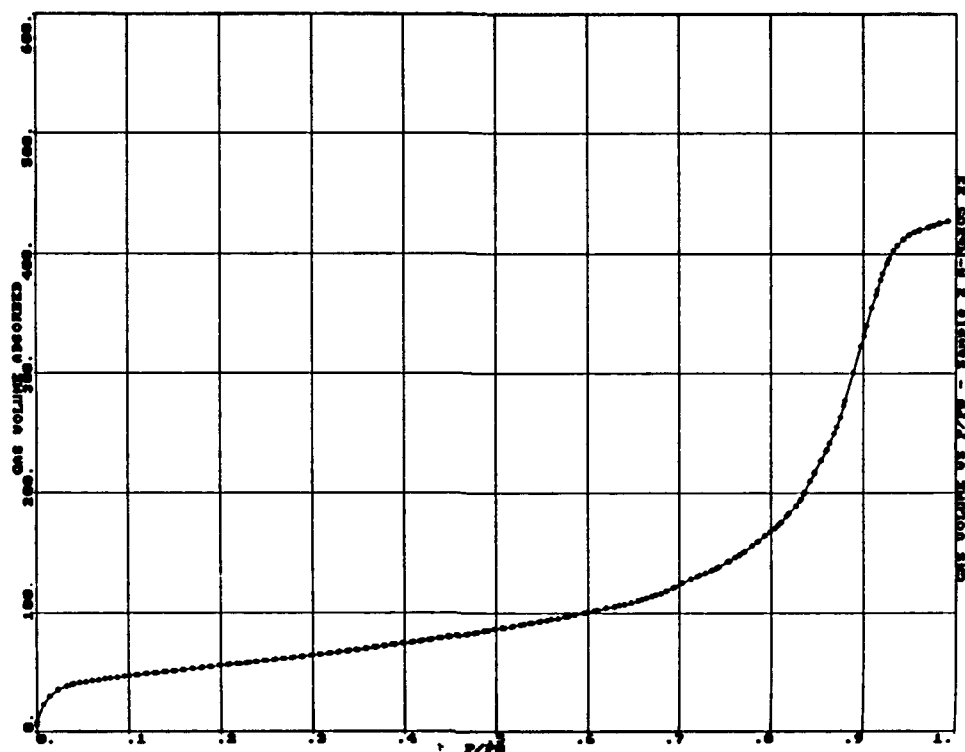**Figure B-35:** NITROGEN DESORPTION ISOTHERM OF A-Nb$_2$O$_5$ (0.50,5.,0.25) WITH MEOH

Figure B-36: PORE SIZE DISTRIBUTION FOR A-Nb$_2$O$_5$ (0.50,5.,0.25) WITH MEOH AS DETERMINED BY NITROGEN ADSORPTION

Figure B-37: NITROGEN DESORPTION ISOTHERM OF A-Nb₂O₅ (0.31,5.,0.25) WITH MEOH
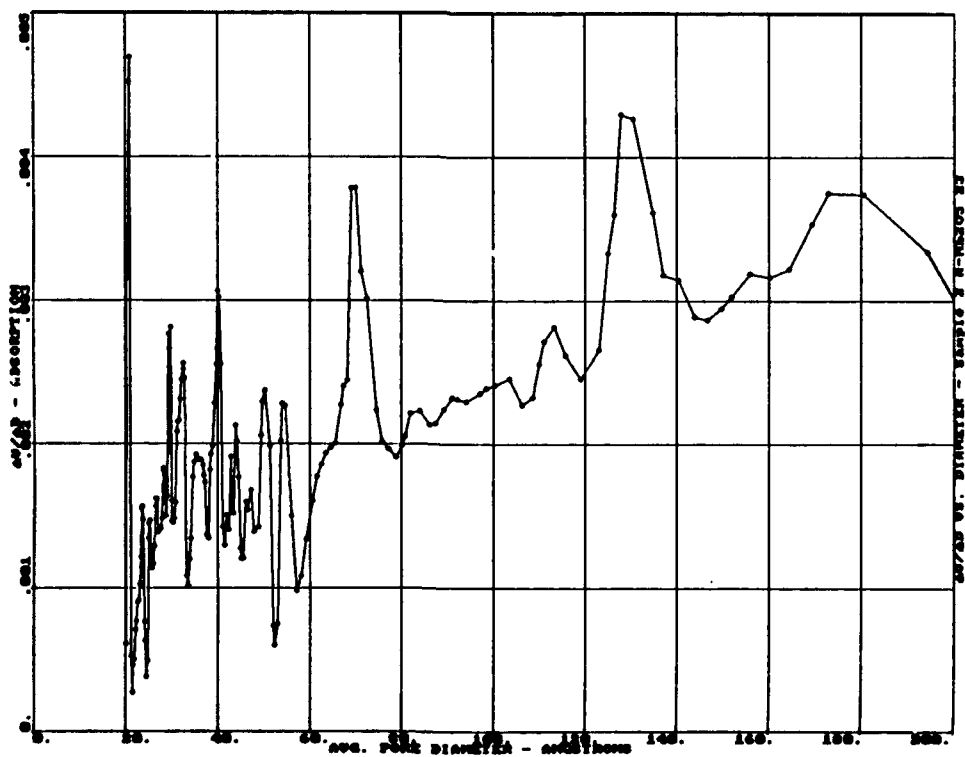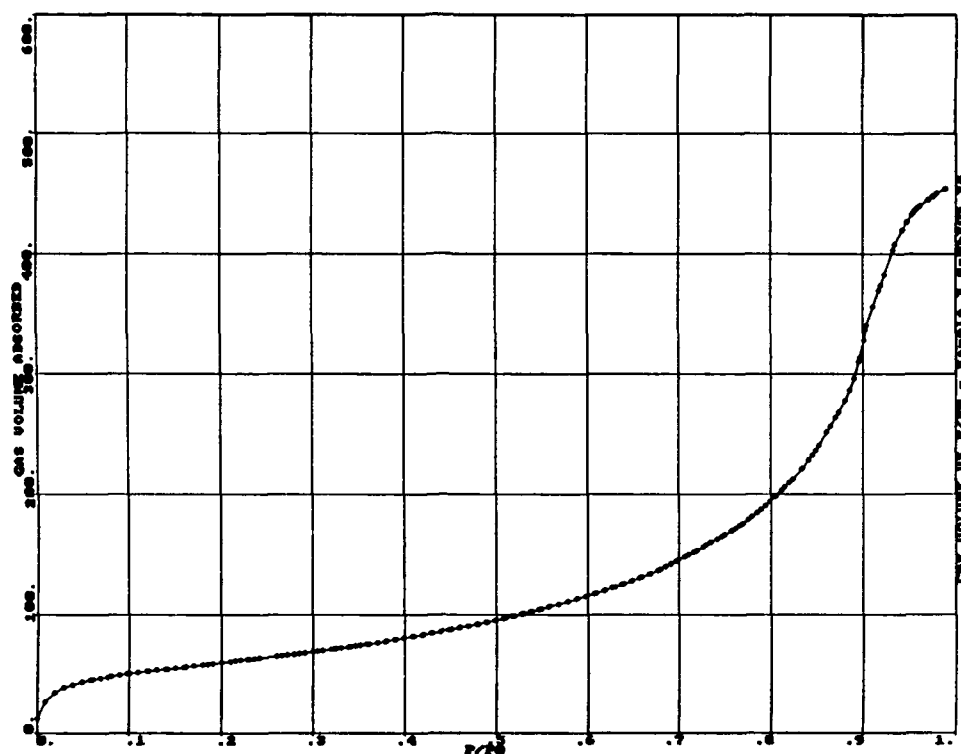
Figure B-37: NITROGEN DESORPTION ISOTHERM OF A-Nb_2O_5 (0.31,5.,0.25) WITH MEOH

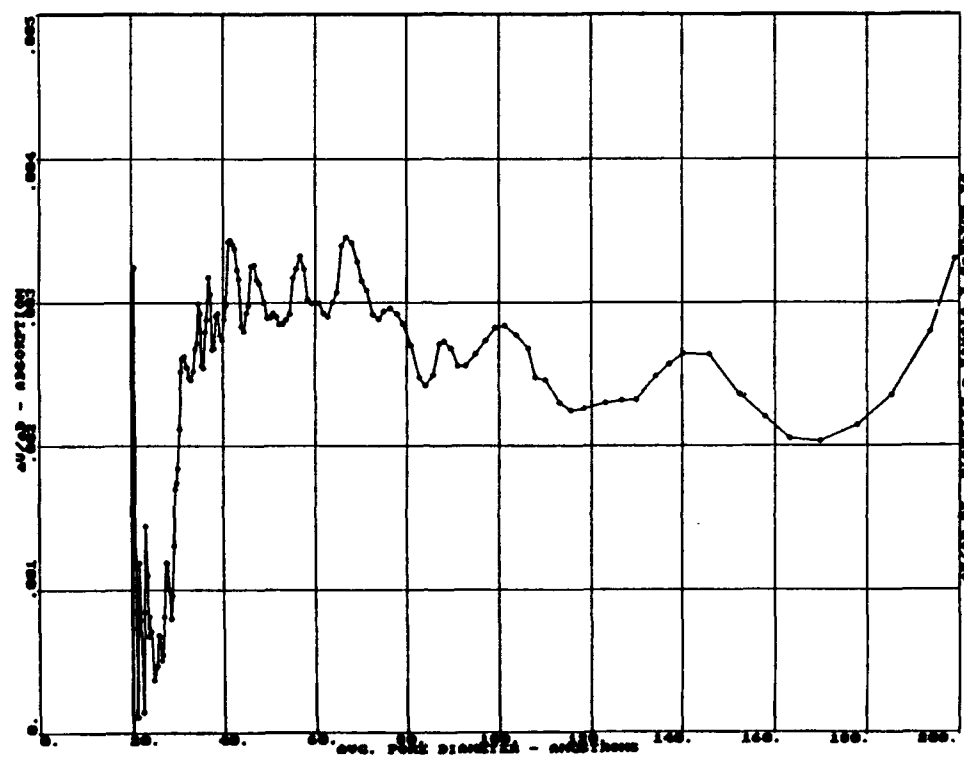Figure B-38: PORE SIZE DISTRIBUTION FOR A-Nb_2O_5 (0.31,5.,0.25) WITH MEOH AS DETERMINED BY NITROGEN ADSORPTION

Figure B-39: NITROGEN DESORPTION ISOTHERM OF A-Nb$_2$O$_5$ (0.625,10.,0.25) WITH MEOH

Figure B-40: PORE SIZE DISTRIBUTION FOR A-Nb$_2$O$_5$ (0.625,10.,0.25) WITH MEOH AS DETERMINED BY NITROGEN ADSORPTION

Figure B-41: NITROGEN DESORPTION ISOTHERM OF A-Nb$_2$O$_5$ (0.50,10.,0.25)
WITH MEOH

Figure B-42: PORE SIZE DISTRIBUTION FOR A-Nb$_2$O$_5$ (0.50,10.,0.25) WITH
MEOH AS DETERMINED BY NITROGEN ADSORPTION

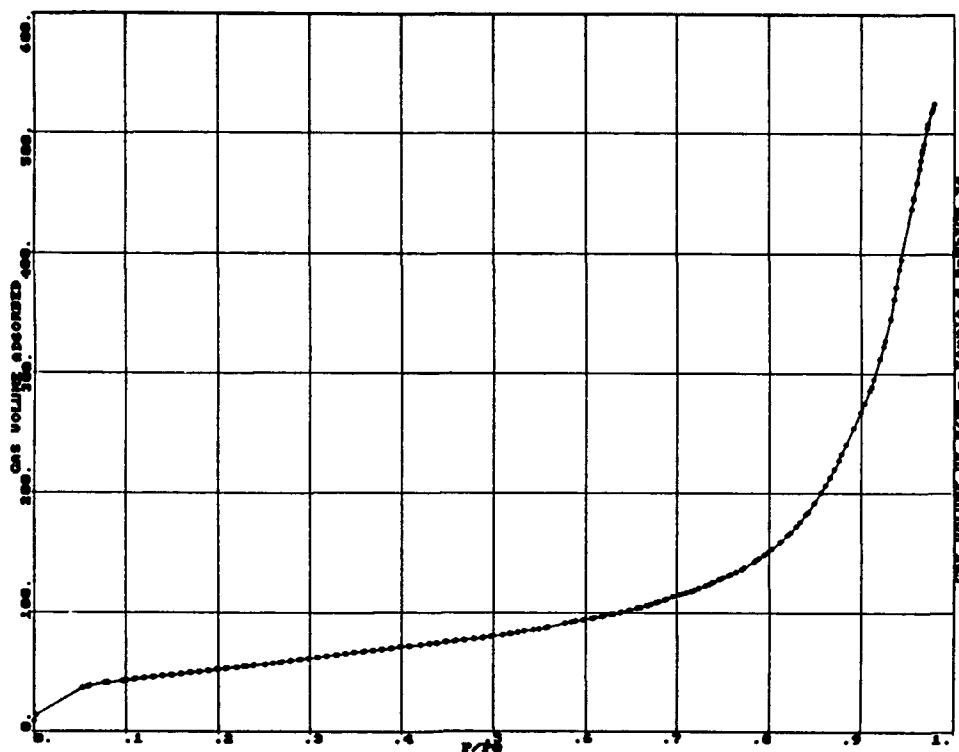**Figure B-43: NITROGEN DESORPTION ISOTHERM OF A-Nb₂O₅ (0.31,10.,0.25)
WITH MEOH**

**Figure B-44: PORE SIZE DISTRIBUTION FOR A-Nb₂O₅ (0.31,10.,0.25) WITH
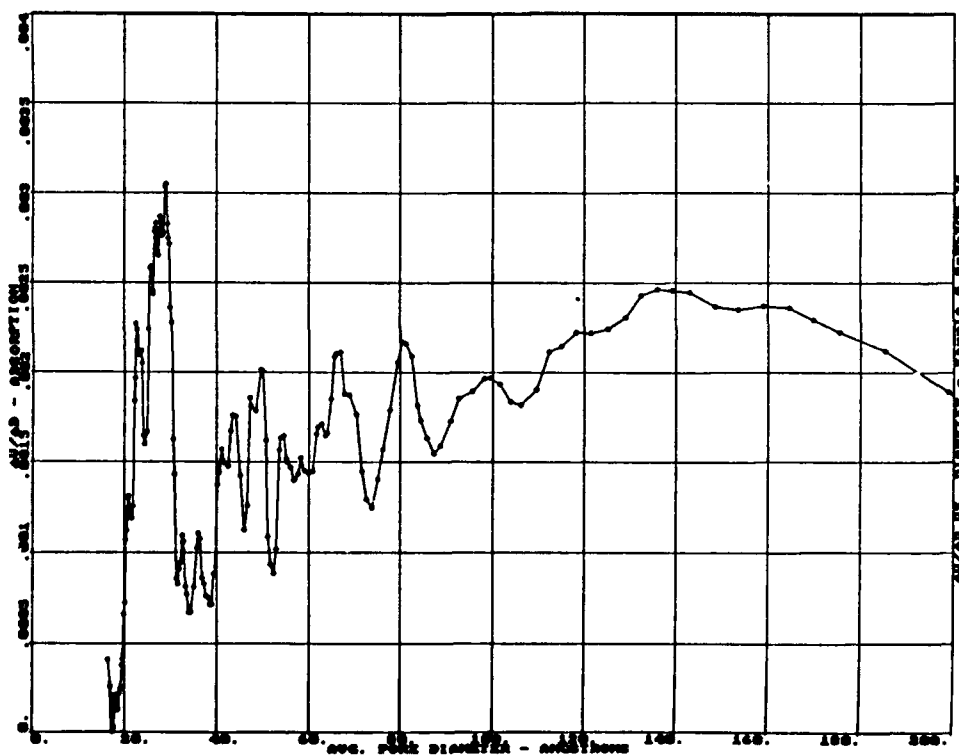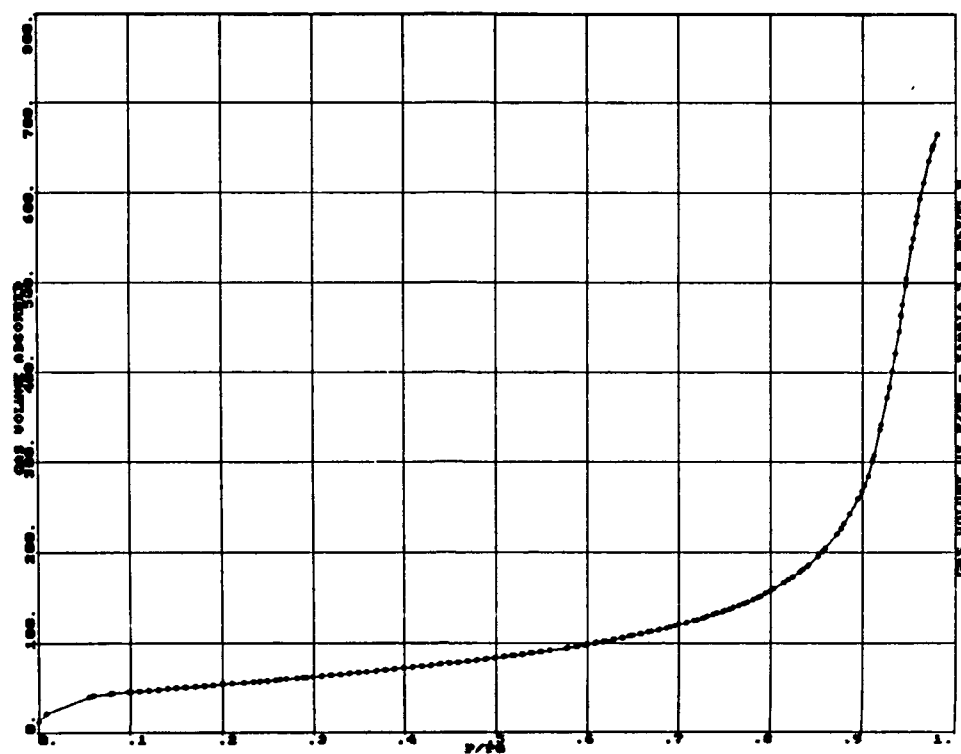MEOH AS DETERMINED BY NITROGEN ADSORPTION**
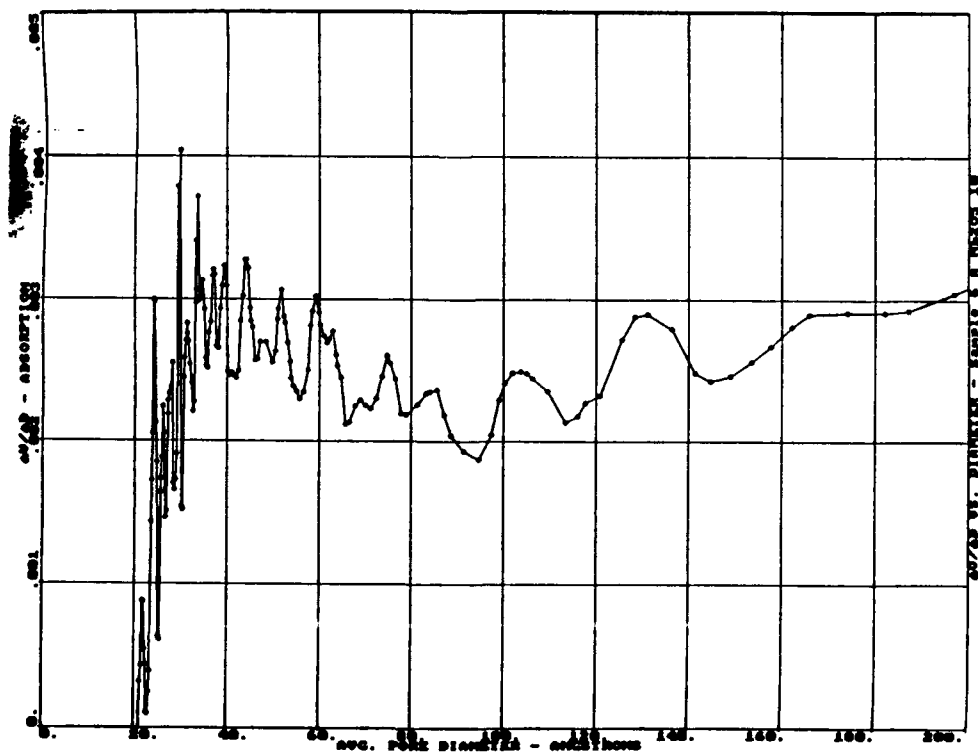
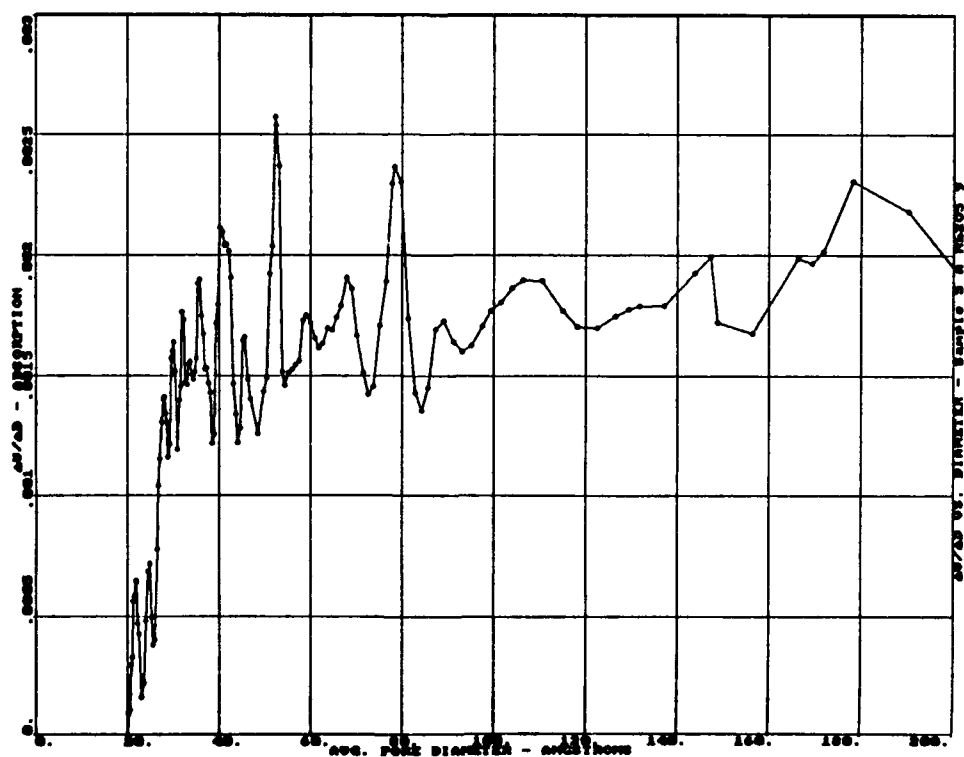

Figure B-45: NITROGEN DESORPTION ISOTHERM OF A-Nb$_2$O$_5$ (0.625,5.,0.80) WITH S-BUOH

Figure B-46: PORE SIZE DISTRIBUTION FOR A-Nb$_2$O$_5$ (0.625,5.,0.80) WITH S-BUOH AS DETERMINED BY NITROGEN ADSORPTION
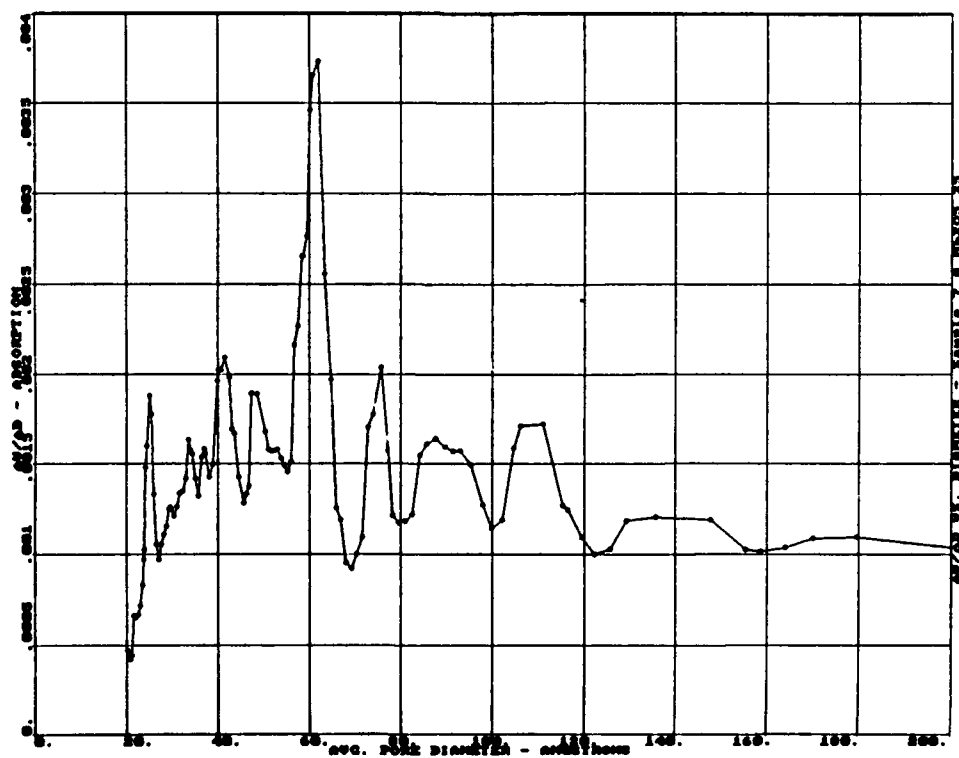
Figure B-47: NITROGEN DESORPTION ISOTHERM OF A-Nb$_2$O$_5$ (0.50,5.,0.80)
WITH S-BUOH
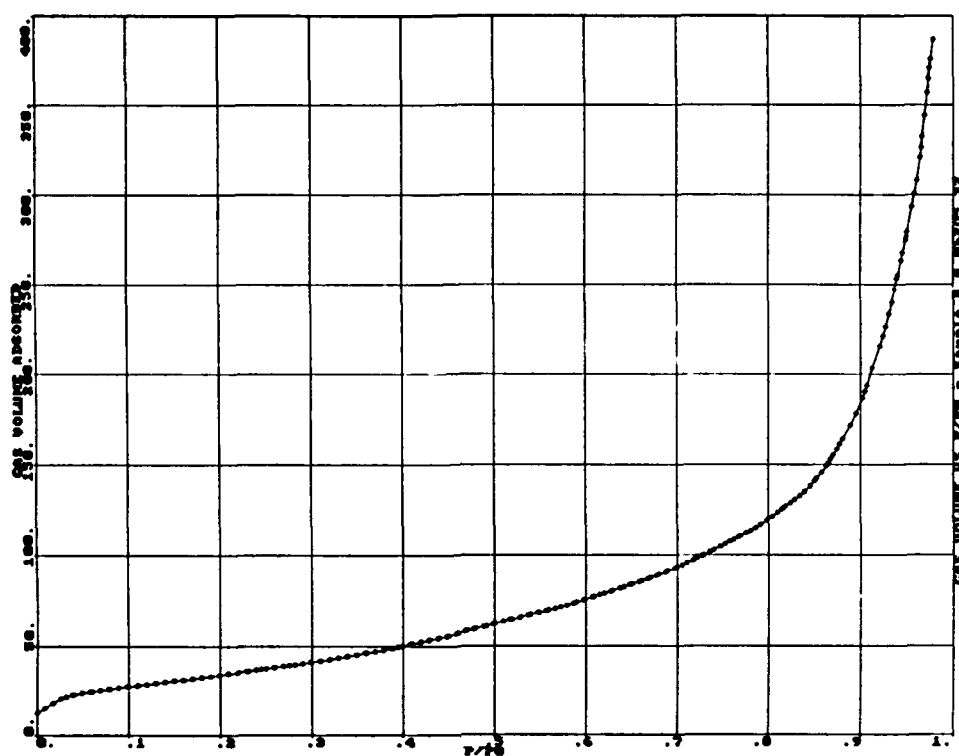
Figure B-48: PORE SIZE DISTRIBUTION FOR A-Nb$_2$O$_5$ (0.50,5.,0.80) WITH S-
BUOH AS DETERMINED BY NITROGEN ADSORPTION

420
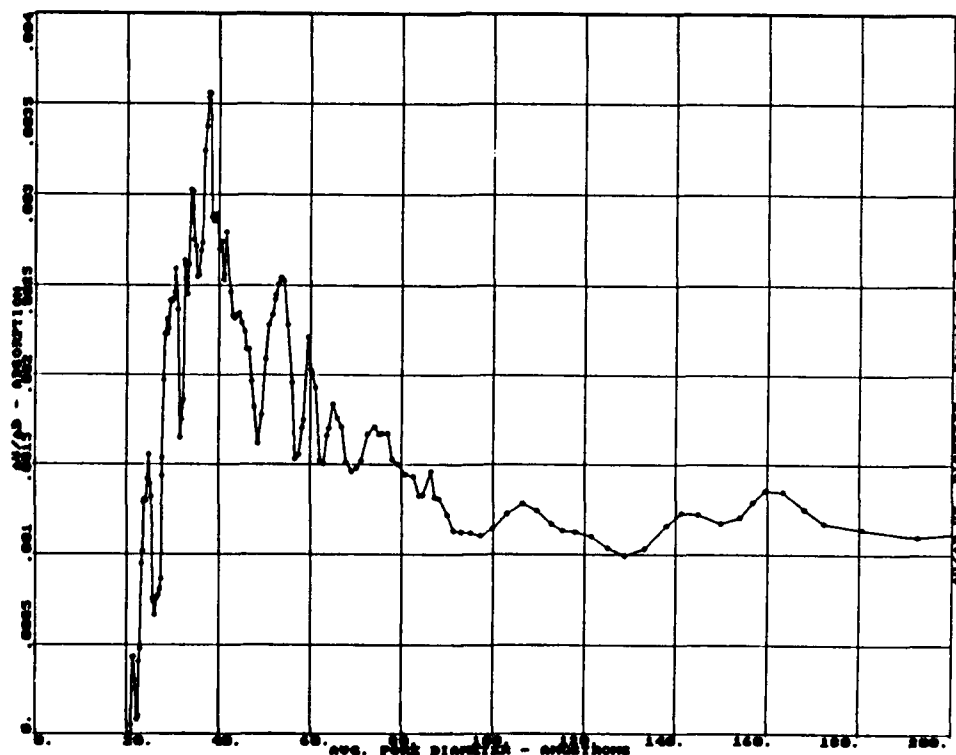
Figure B-49: NITROGEN DESORPTION ISOTHERM OF A-Nb$_2$O$_5$ (0.31,5.,0.80) WITH S-BUOH
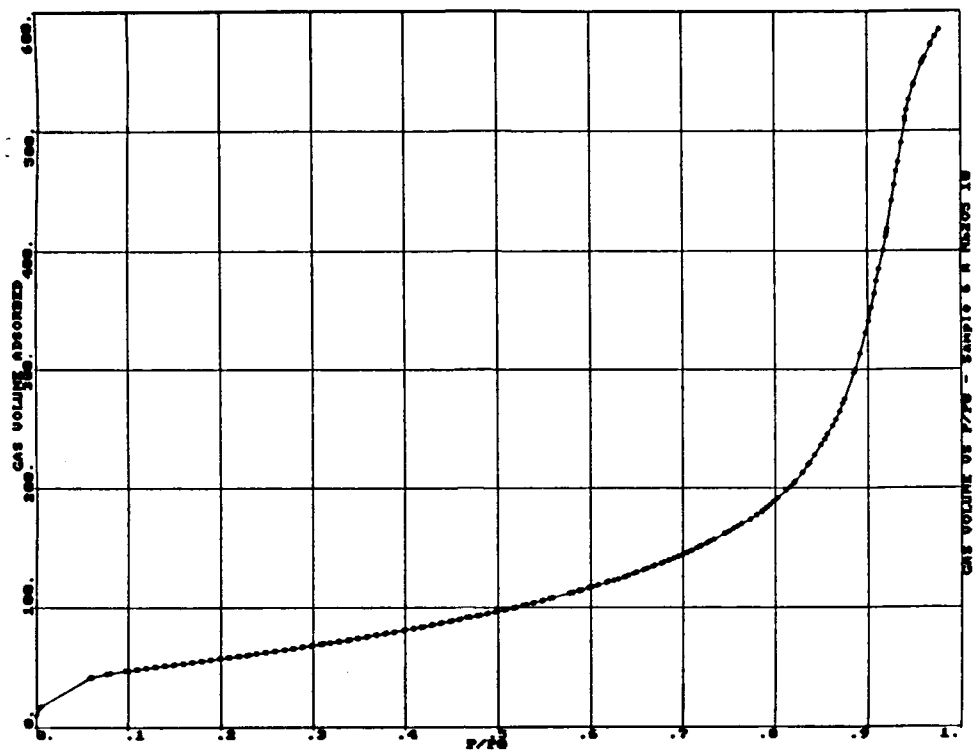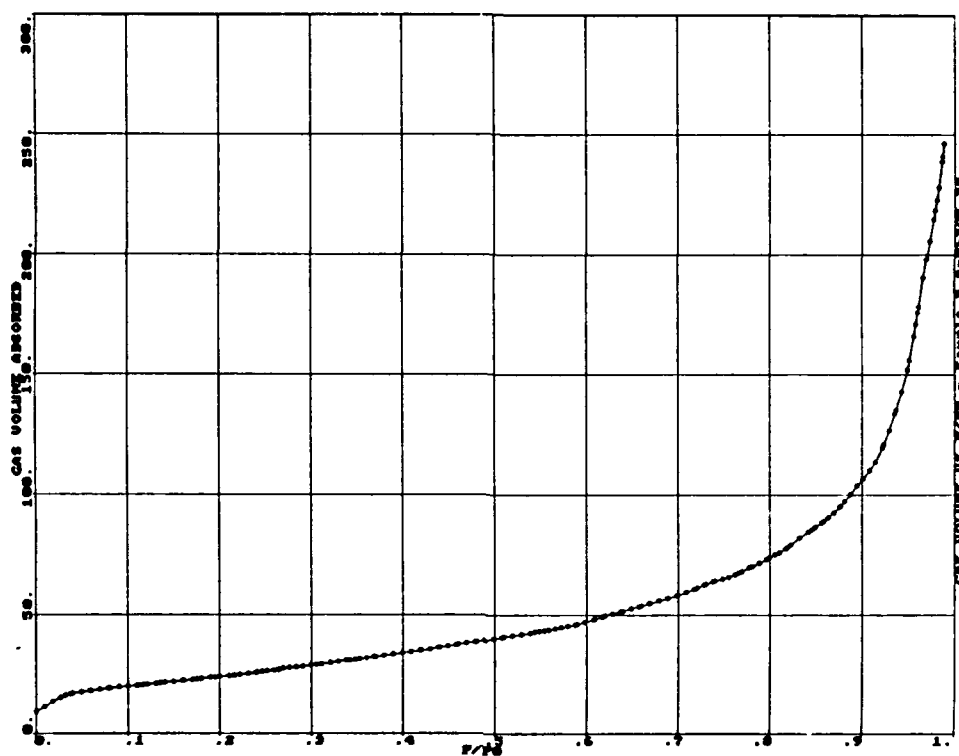

Figure B-50: PORE SIZE DISTRIBUTION FOR A-Nb$_2$O$_5$ (0.31,5.,0.80) WITH S-BUOH AS DETERMINED BY NITROGEN ADSORPTION
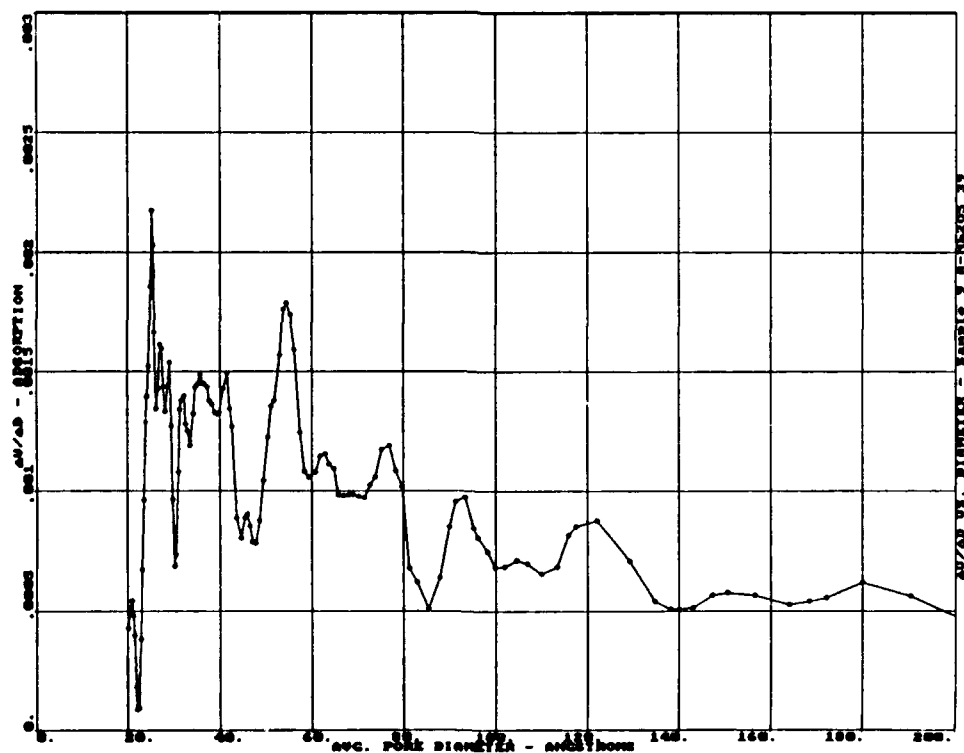
Figure B-51: NITROGEN DESORPTION ISOTHERM OF A-Nb$_2$O$_5$ (0.625,10.,0.80) WITH S-BUOH
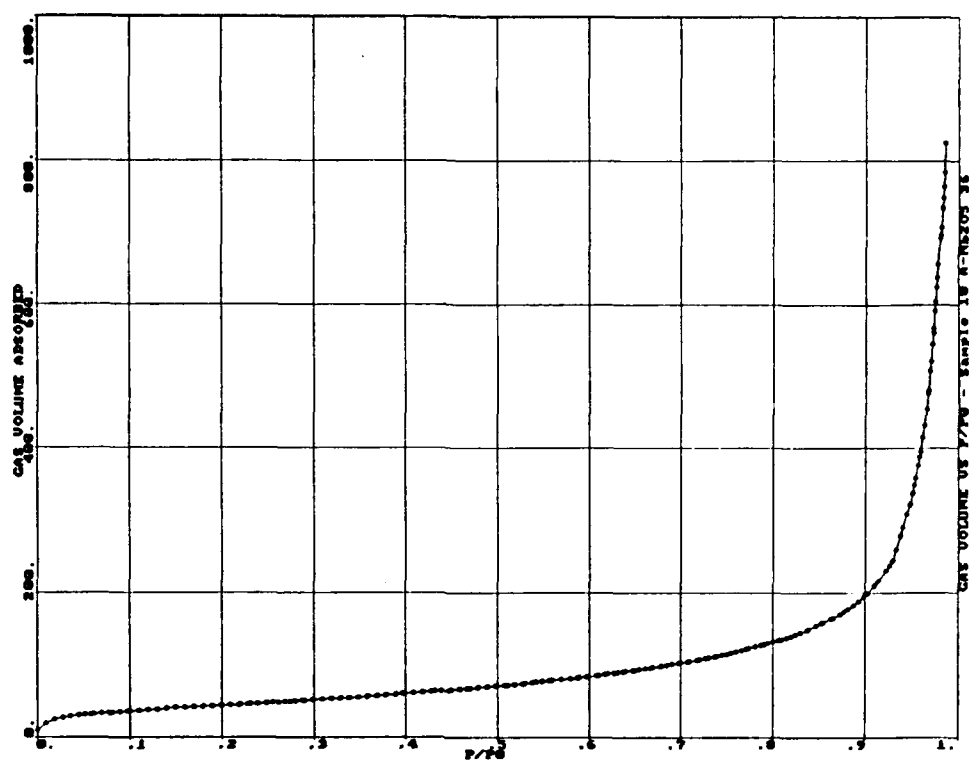
Figure B-52: PORE SIZE DISTRIBUTION FOR A-Nb$_2$O$_5$ (0.625,10.,0.80) WITH S-BUOH AS DETERMINED BY NITROGEN ADSORPTION
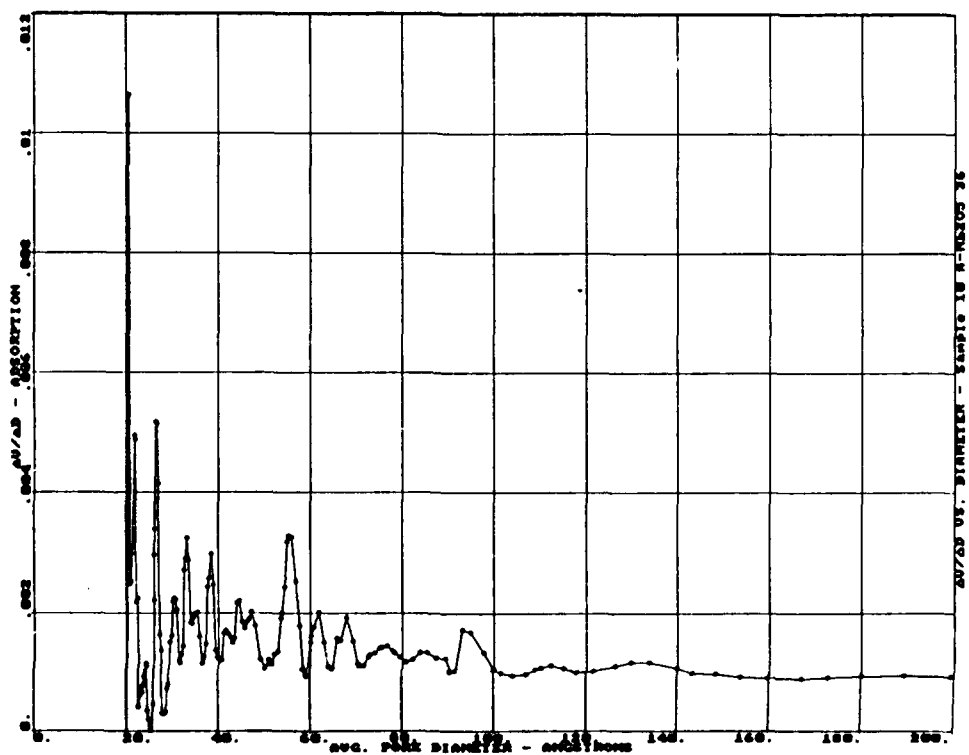
Figure B-53: NITROGEN DESORPTION ISOTHERM OF A-Nb$_2$O$_5$ (0.50,10.,0.80)
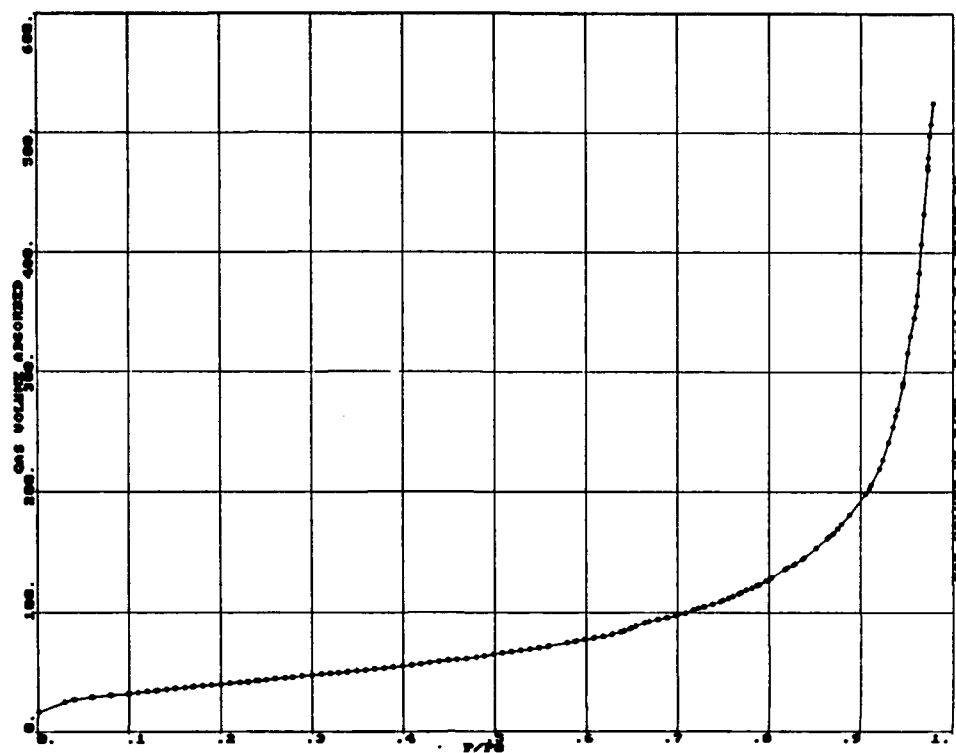WITH S-BUOH
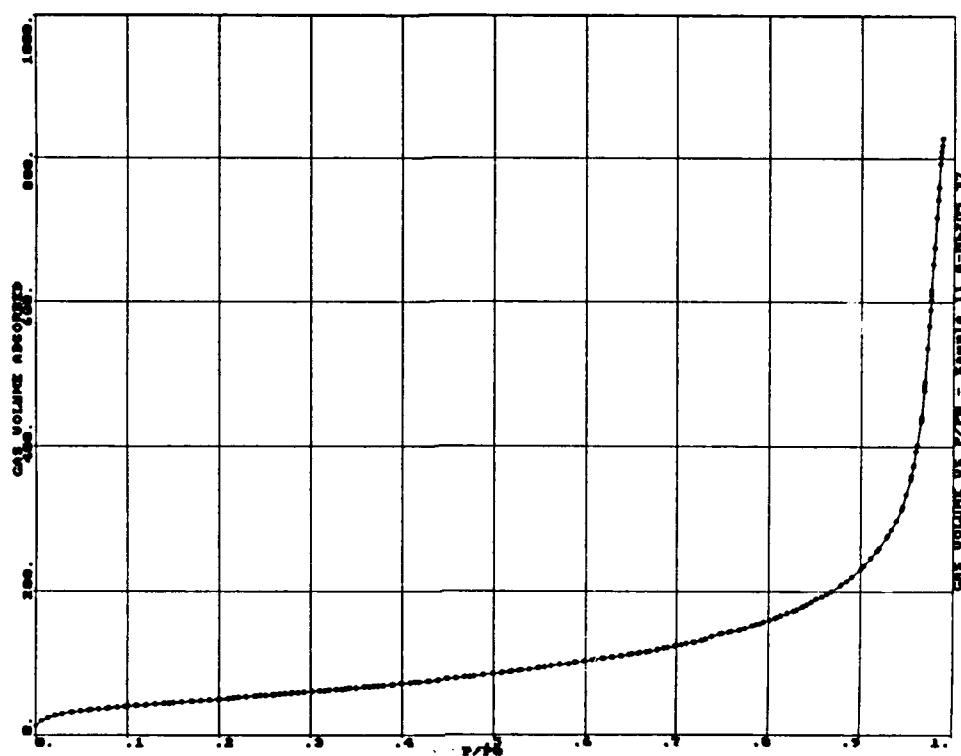
Figure B-54: PORE SIZE DISTRIBUTION FOR A-Nb$_2$O$_5$ (0.50,10.,0.80) WITH S-
BUOH AS DETERMINED BY NITROGEN ADSORPTION
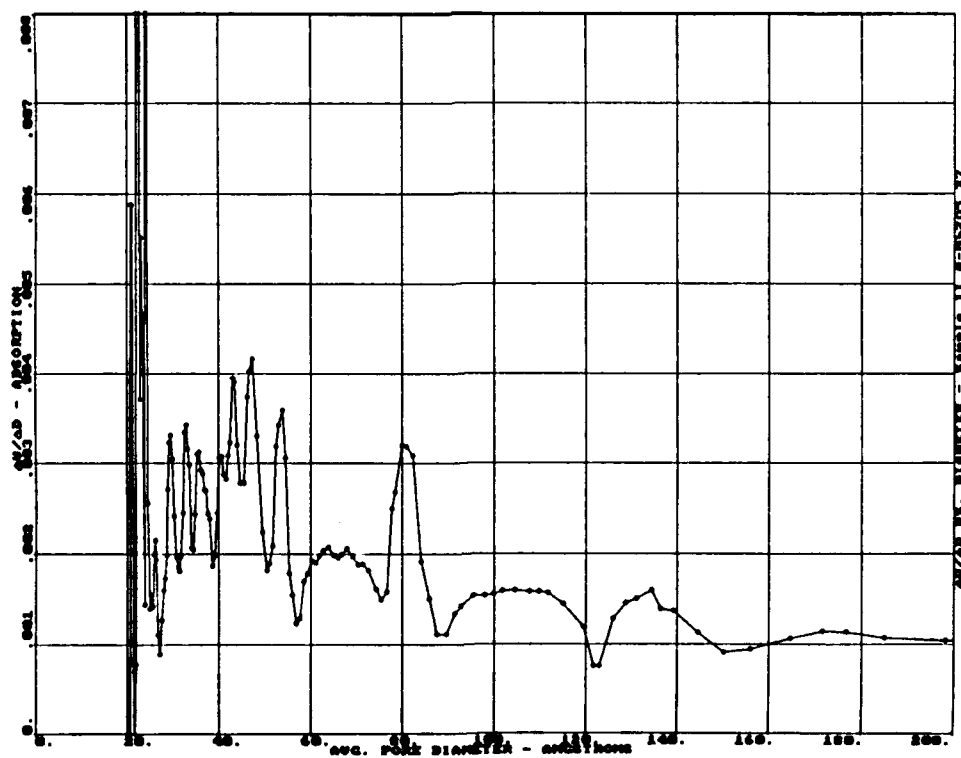
Figure B-55: NITROGEN DESORPTION ISOTHERM OF A-Nb$_2$O$_5$ (0.31,10.,0.80) WITH S-BUOH
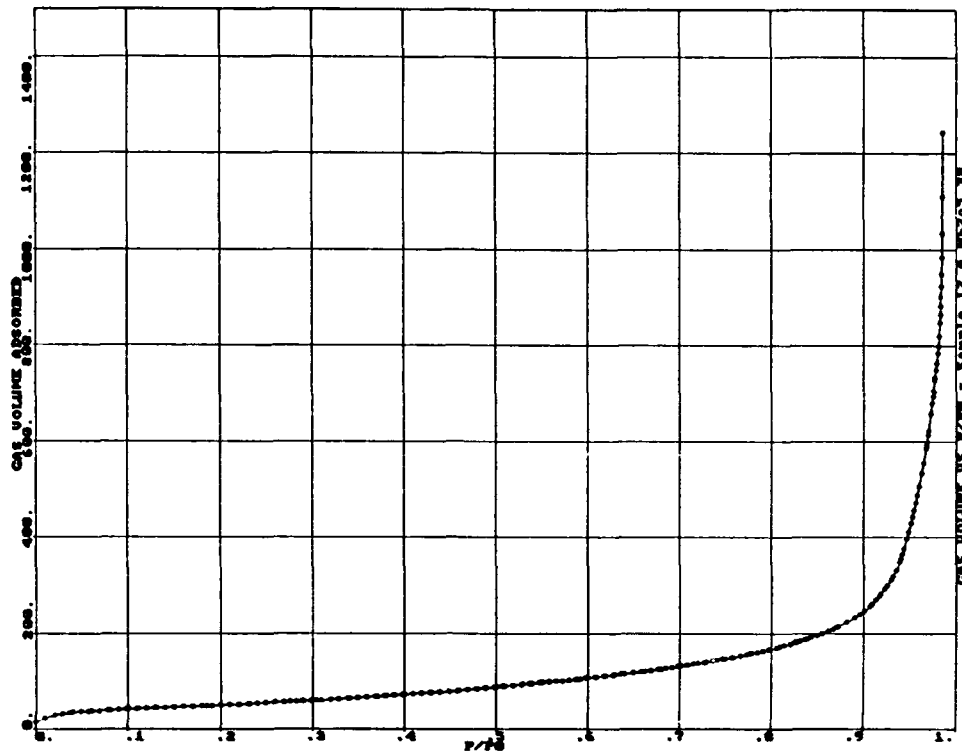
Figure B-56: PORE SIZE DISTRIBUTION FOR A-Nb$_2$O$_5$ (0.31,10.,0.80) WITH S-BUOH AS DETERMINED BY NITROGEN ADSORPTION
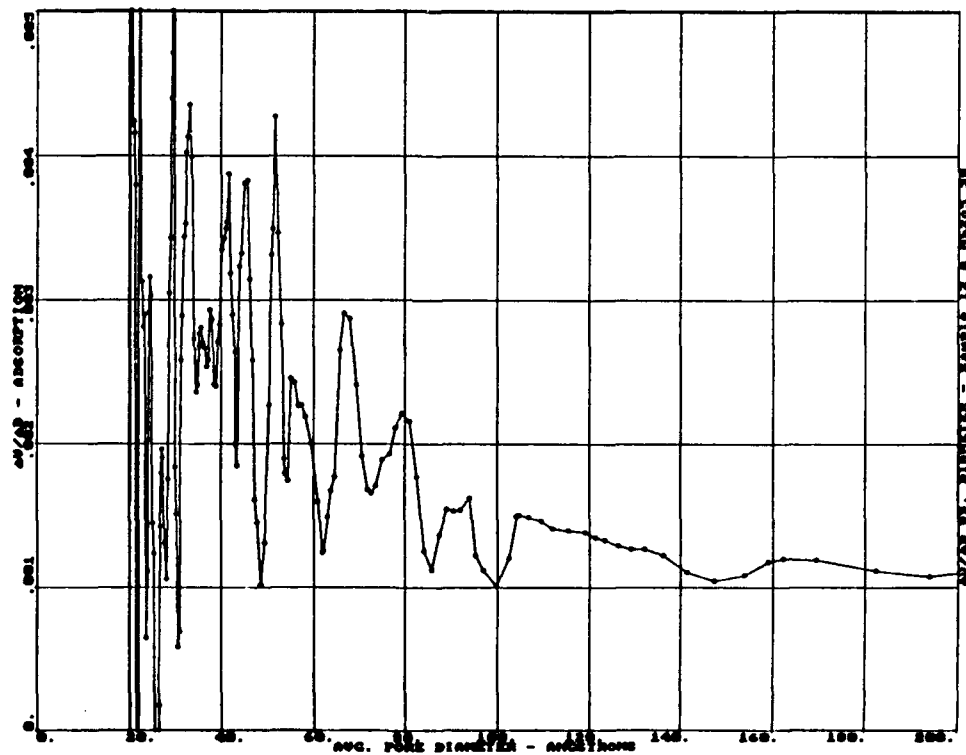
distribution of pore sizes. Indeed this is exactly what is found in all 6 niobia aerogel samples prepared in s-butanol, see Figures B-46, B-48, B-50, B-52, B-54, and B-56. The amount of water does not appear to play a large influential role in the distributions of the pore sizes in the niobia aerogels prepared in s-butanol. This study needs to be expanded upon more fully in order to explore in depth how these various parameters in turn affect the physical properties of the niobia aerogels, and other aerogels in general.

APPENDIX C

FTIR AND DRIFT SPECTRA

This appendix contains FTIR and DRIFT spectra of the hydroxyl region, 4000 - 2800 cm^{-1}, that are not directly incorporated into the main text but relevant to this dissertation. The FTIR hydroxyl region after pyridine adsorption will be discussed to investigate the origin of Brønsted acidity in these samples. The DRIFT spectra after calcination will also be discussed to determine if new hydroxyl groups are formed in the bulk, mixed, and surface oxides in the hydrated state. Also contained in this appendix are FTIR pyridine adsorption spectra in the 1700 - 1400 cm^{-1} range after the 300 °C heat treatment.

C.1 FTIR Pyridine Adsorption Spectra: 1700 - 1400 cm^{-1}

The following figures (Figures C-1 to C-10) show FTIR spectra of pyridine adsorbed on the oxide samples investigated in this study after the 300 °C heat treatment in the range of 1700 - 1400 cm^{-1}. These figures are included because they enlarge the absorption peaks discussed in the main text. The higher temperature evacuations tended to severely attenuate these peaks and because of the large variation of absorptions in the spectra, actual peak determination was difficult without observation of the individual 300 °C spectrum.

Figure C-1: FTIR SPECTRUM OF PYRIDINE ADSORBED ON A-Nb$_2$O$_5$ AFTER HEAT TREATMENT AT 300 °C

Figure C-2: FTIR SPECTRUM OF PYRIDINE ADSORBED ON A-SiO$_2$ AFTER HEAT TREATMENT AT 300 °C

Figure C-3: FTIR SPECTRUM OF PYRIDINE ADSORBED ON A-Al₂O₃ AFTER HEAT TREATMENT AT 300°C

Figure C-4: FTIR SPECTRUM OF PYRIDINE ADSORBED ON A-NS25w AFTER HEAT TREATMENT AT 300 °C

Figure C-5: FTIR SPECTRUM OF PYRIDINE ADSORBED ON A-NA25w AFTER HEAT TREATMENT AT 300 °C
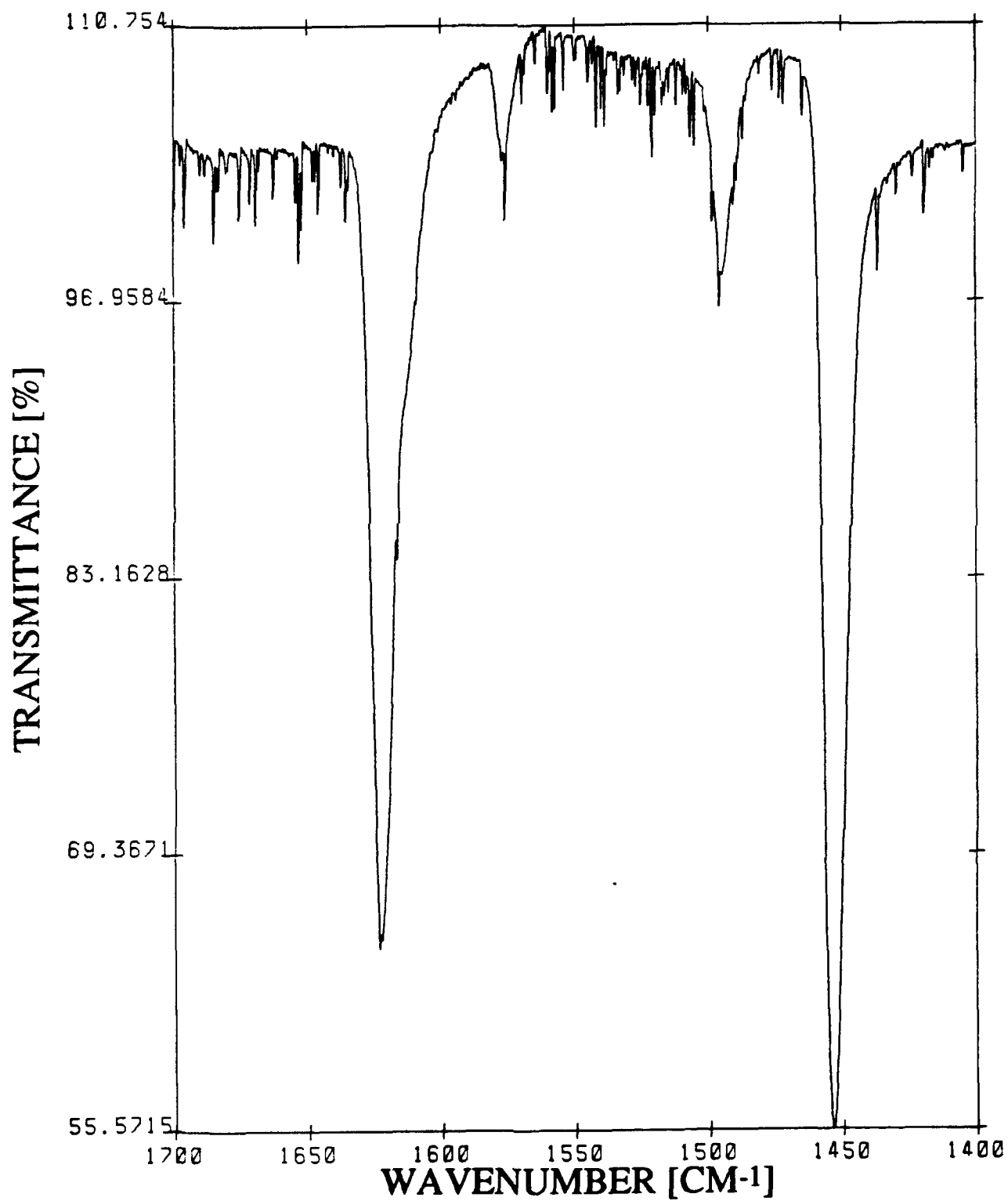
Figure C-6: FTIR SPECTRUM OF PYRIDINE ADSORBED ON NA25w AFTER HEAT TREATMENT AT 300 °C
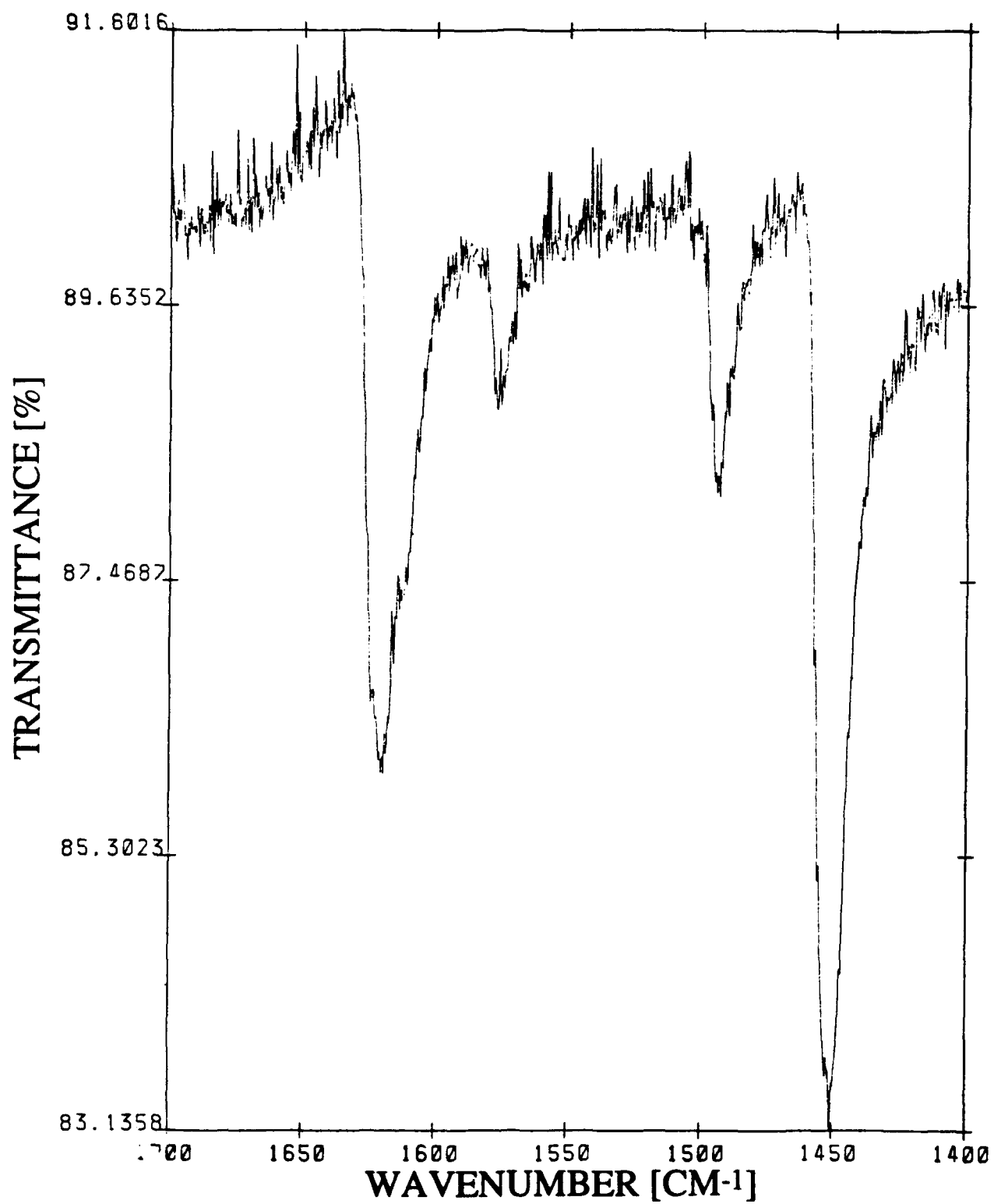
Figure C-7: FTIR SPECTRUM OF PYRIDINE ADSORBED ON A-NS(.05) AFTER HEAT TREATMENT AT 300 °C
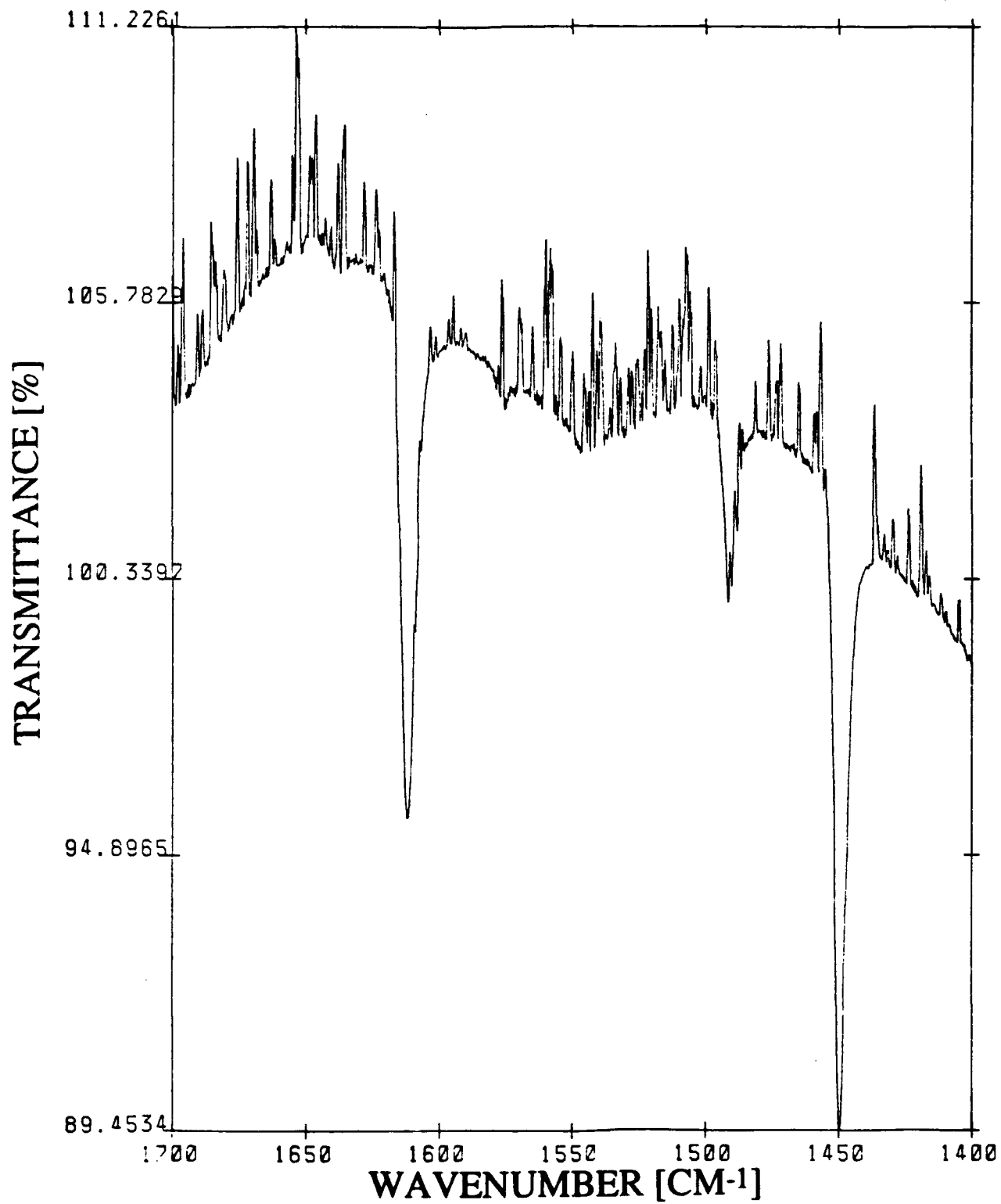
Figure C-8: FTIR SPECTRUM OF PYRIDINE ADSORBED ON A-NS(.25) AFTER HEAT TREATMENT AT 300 °C
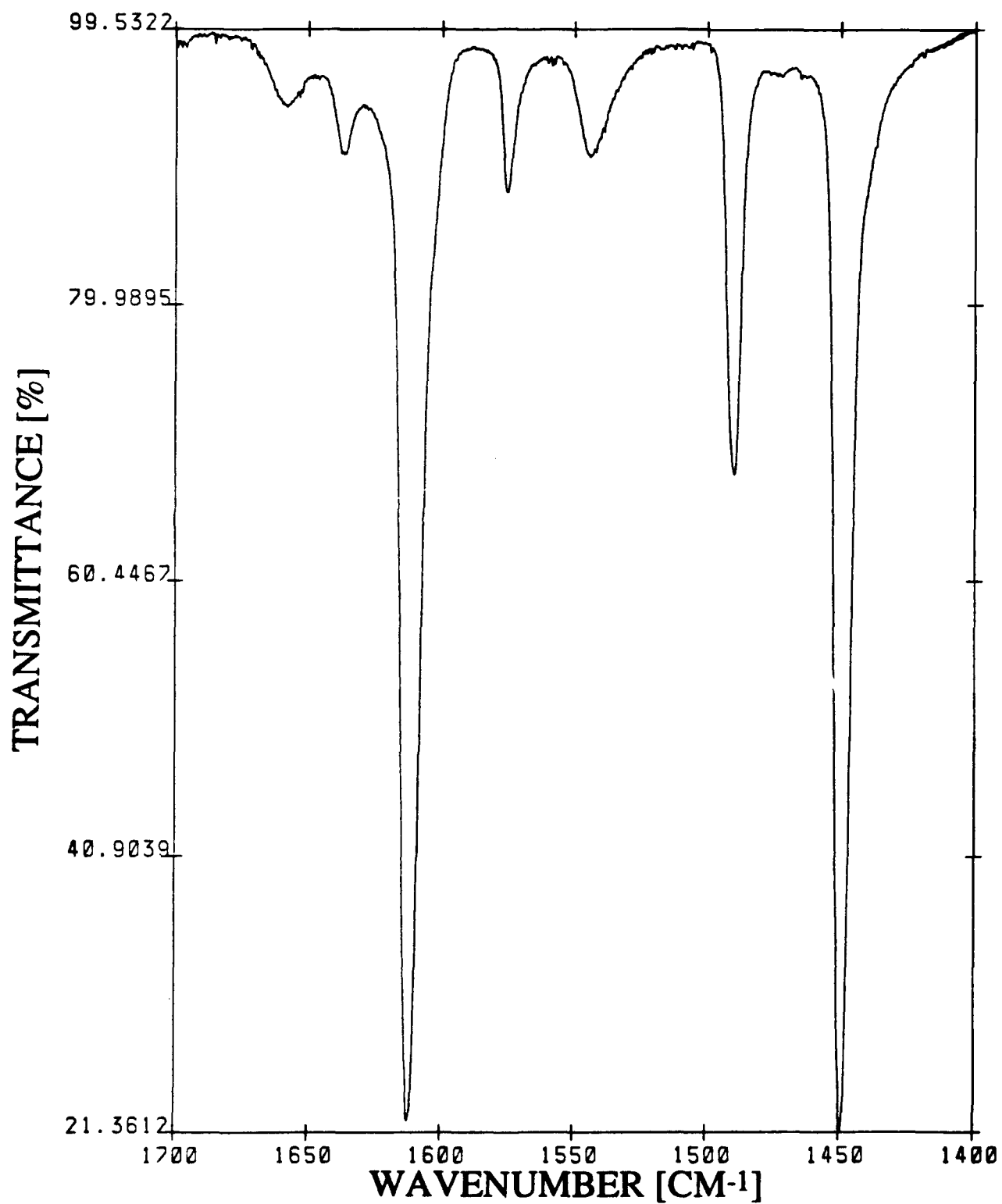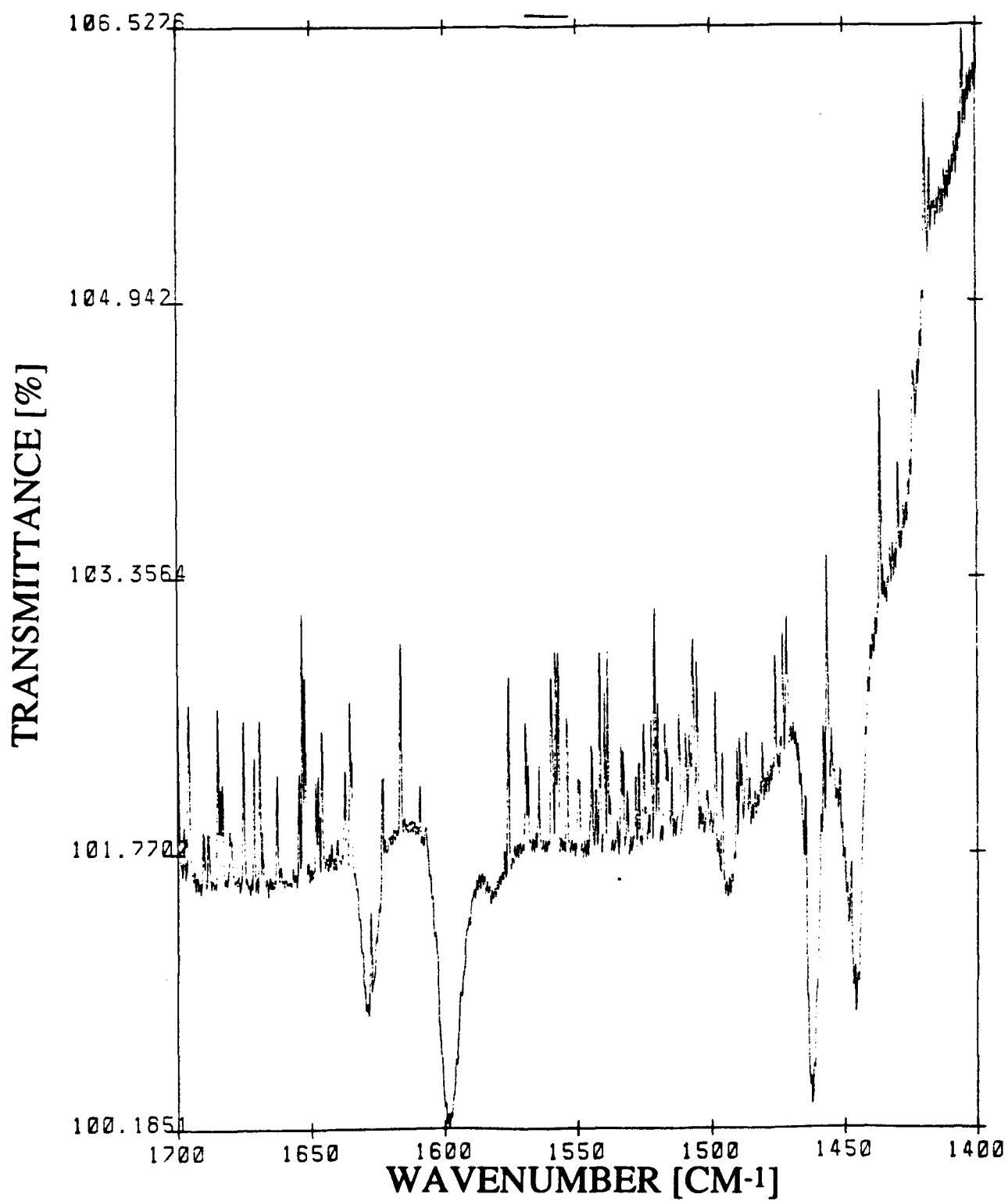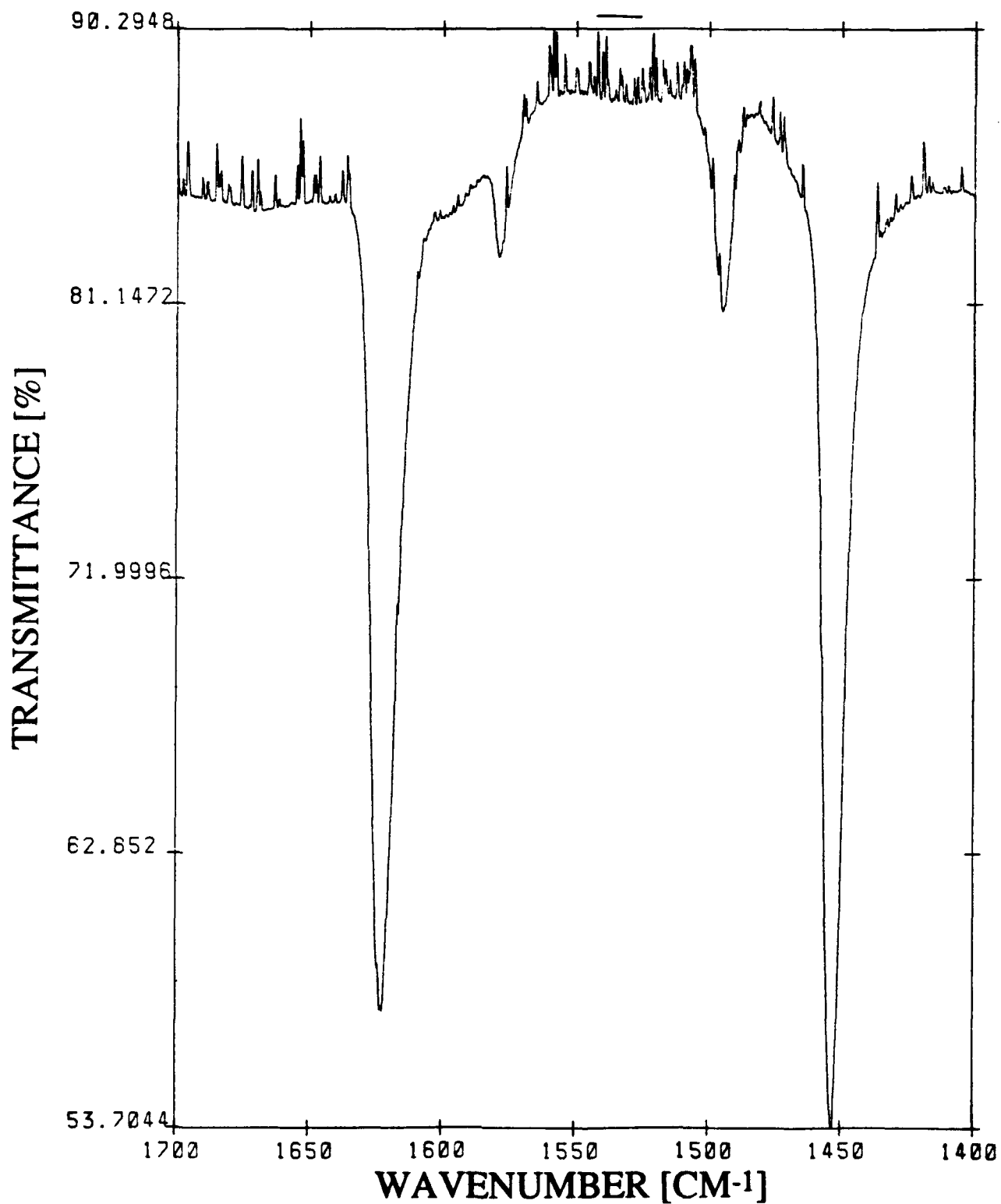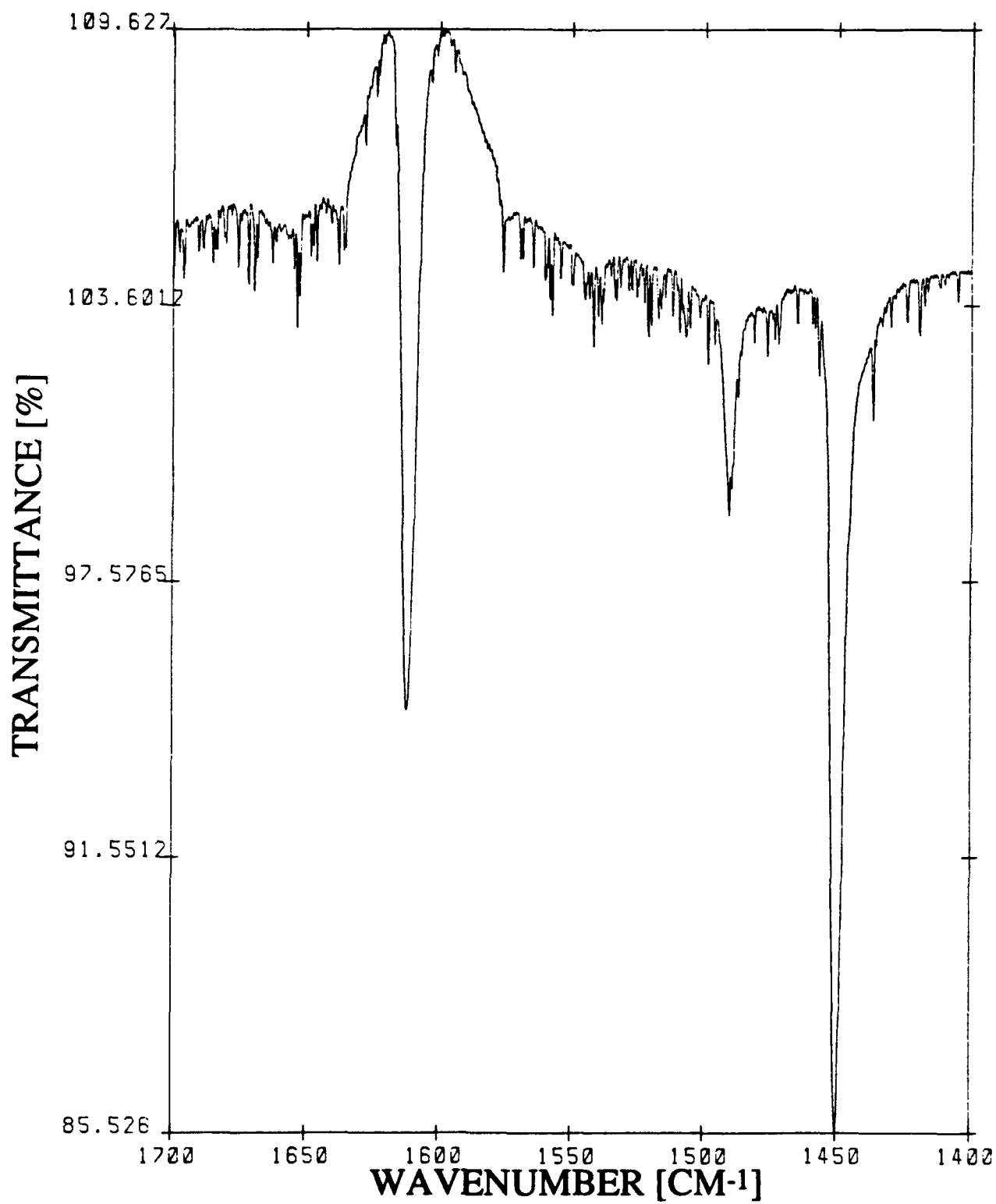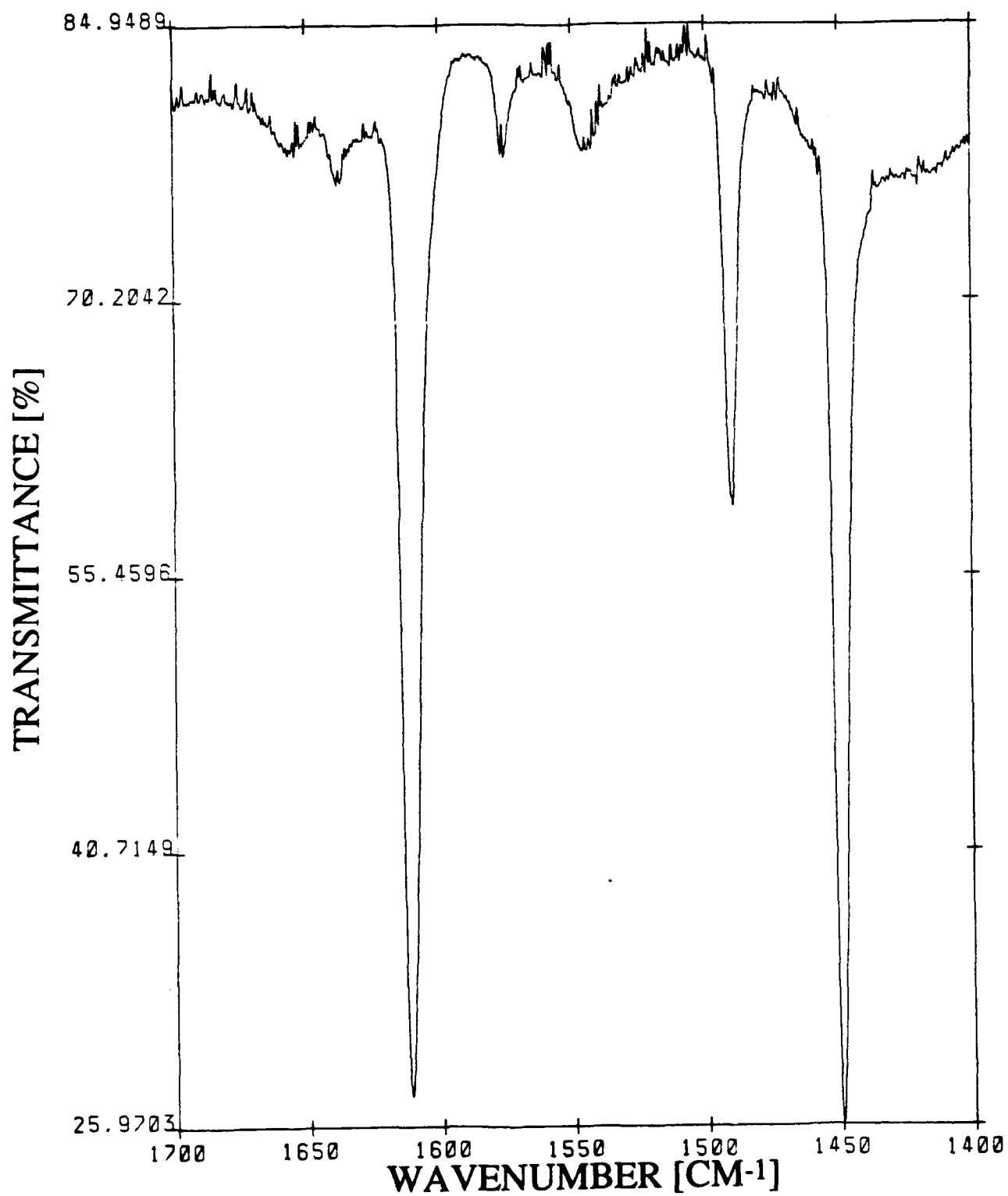
Figure C-9: FTIR SPECTRUM OF PYRIDINE ADSORBED ON A-NA(.05) AFTER
HEAT TREATMENT AT 300 °C
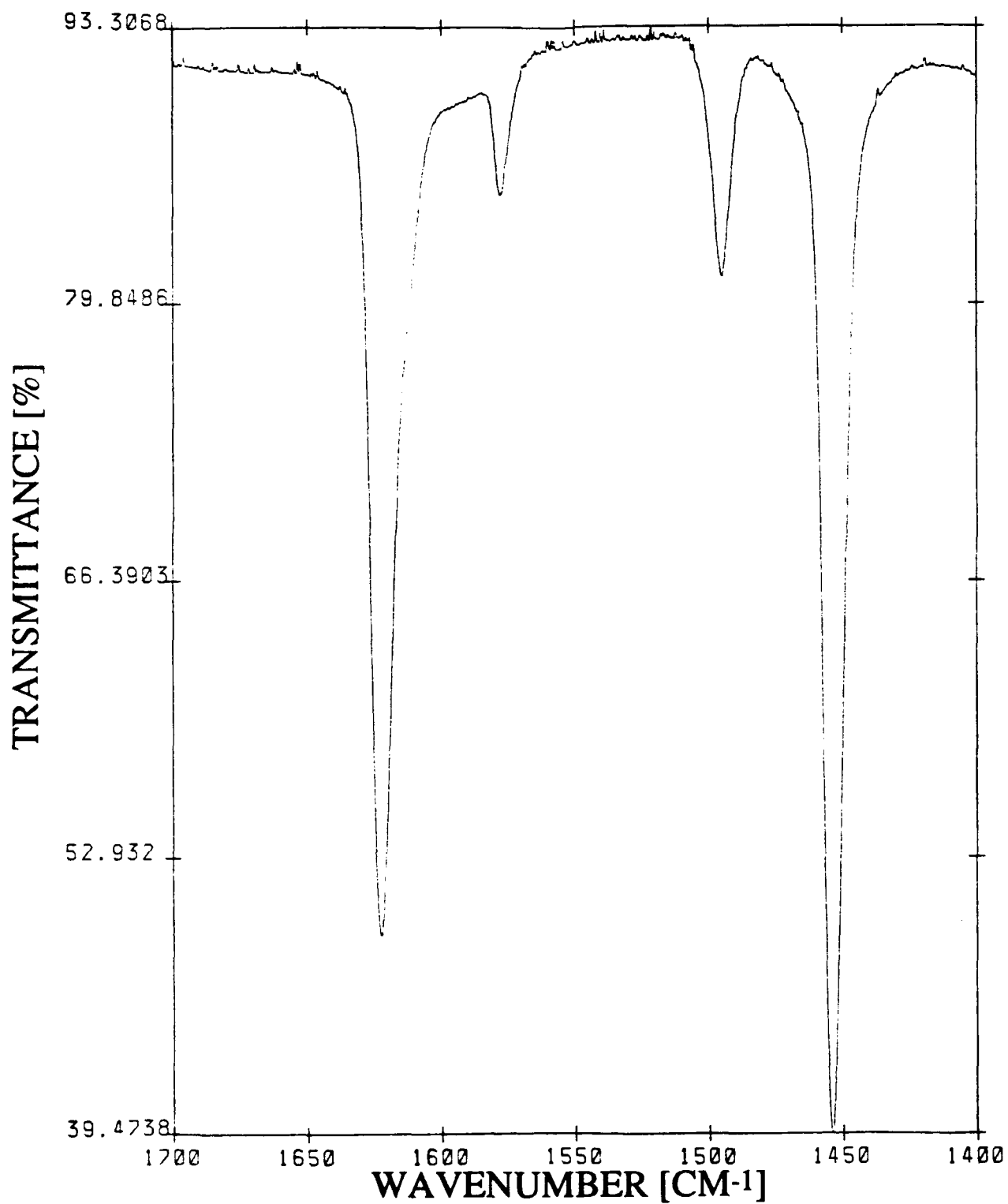
Figure C-10: FTIR SPECTRUM OF PYRIDINE ADSORBED ON A-NA(.25) AFTER HEAT TREATMENT AT 300 °C
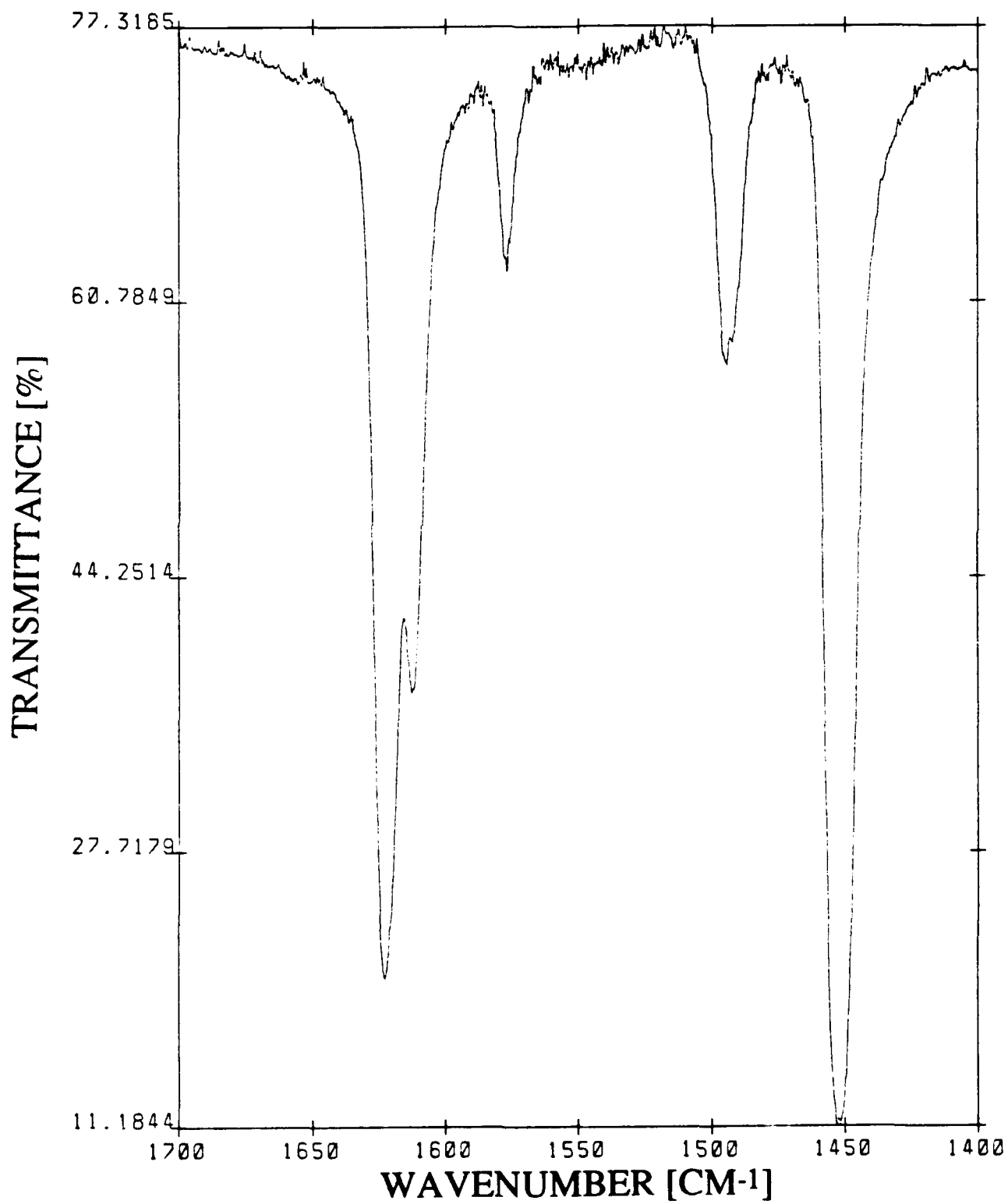
C.2 FTIR Pyridine Adsorption Spectra: 4000 - 2800 cm^{-1}

This section discusses the hydroxyl frequency range of 4000 - 2800 cm^{-1} to examine the -OH groups which participate as Brønsted acid sites in these oxides. The region of 3750 - 3400 cm^{-1} is the stretching frequency range of the O-H group; variation over this region depends on the molecular weight of the metal atom as well as the local environment of the hydroxyl group. The main reason for analyzing this frequency region is to determine and isolate those surface O-H stretching vibrations which can be associated with a Brønsted acid site. The frequency range characteristic of surface hydroxyl groups is 3750 - 3650 cm^{-1}. The frequency region at 3650 - 3600 cm^{-1} may also be attributed to surface hydroxyls, but strongly chemisorbed water also contributes in this region.[192] Hydrogen bonded hydroxyls as well as chemisorbed water contribute in the region of 3600 - 3400 cm^{-1}. The N-H absorption stretches which can be associated with Brønsted acids occur in the range of 3250 - 3070 cm^{-1}.[210]

Each set of pyridine adsorption spectra was observed in the 4000 - 2800 cm^{-1} frequency range over the oxide aerogels. The uppermost spectrum of each sample in these figures is after the *in-situ* pretreatment in vacuum before exposure to any pyridine (blank). The FTIR spectra were recorded after exposure to pyridine, and thermally treated at 25, 100, 200, and 300 °C. These are plotted from bottom to top in the following figures. The transmission FTIR spectra in this region are often noisy due to low throughput of the infrared signal and spectra taken after pyridine exposure and room temperature evacuations were also often opaque, making interpretation of data difficult. Results of the hydroxyl region FTIR pyridine spectra are located in Table C-1.

The first samples to be investigated will be the bulk oxide aerogels: niobia, silica, and alumina. A broad peak at 3716 cm^{-1} as well as a shoulder at 3702 cm^{-1} is observed for the aerogel of niobia as shown in Figure C-11. The 3716 cm^{-1} peak is severely attenuated upon exposure to pyridine with only the peak ~ 3700 cm^{-1} being observed. The N-H

Table C-1: SUMMARY OF FTIR SPECTRA OF ADSORBED PYRIDINE (HYDROXYL REGION): A) BULK AND MIXED OXIDES AND B) SURFACE OXIDES

A) FTIR Spectra Hydroxyl Region of Bulk and Mixed Oxides

Treatment Temp. (°C)	Wavenumbers (cm^{-1})				
	A-Nb$_2$O$_5$	A-SiO$_2$	A-Al$_2$O$_3$	A-NS25w	A-NA25w
Blank	3716	3752	3780,3745,3700	3750,3724	3783,3744,3695(Sh)
25	3696 N-H	3752 N-H	3745,3700 N-H	3747 N-H	
100	3699 N-H	3752 -	3745,3700 N-H	3748,3705(Sh) N-H	3780(Sh),3744 N-H
200	3702 N-H	3752 -	3745,3700 N-H	3750,3720(Sh) N-H	3779,3744,3695(Sh) -
300	3716,3702 N-H	3752 -	3780(Sh),3745,3700 N-H	3750,3724(Sh) -	3779,3744,3695(Sh) -

B) FTIR Spectra Hydroxyl Region of Surface Oxides

Treatment Temp. (°C)	Wavenumbers (cm^{-1})			
	A-NS(.05)	A-NS(.25)	A-NA(.05)	A-NA(.25)
Blank	3752	3752,3700(Sh)	3788,3752,3700(Sh)	3788,3749,3700(Sh)
25	3752,3700(Sh) N-H	3752 -	3745 N-H	3740 -
100	3752,3725(Sh) N-H	3752,3700(Sh) N-H	3745,3700(Sh) N-H	3750,3700(Sh) N-H
200	3752,3730(Sh) N-H	3752,3700(Sh) N-H	3780(Sh),3750,3700(Sh) N-H	3750,3700(Sh) N-H
300	3752,3730(Sh) N-H	3752,3700(Sh) N-H	3780,3752,3700(Sh) N-H	3782,3750,3700(Sh) N-H

N-H = Observed N-H Absorption (Brønsted); - = No Observed N-H Absorption; Sh = Shoulder

Figure C-11: HYDROXYL RANGE FTIR SPECTRA OF PYRIDINE ADSORBED ON A-Nb$_2$O$_5$: BLANK AND AFTER HEAT TREATMENTS AT 300, 200, 100, AND 25 °C (TOP TO BOTTOM)
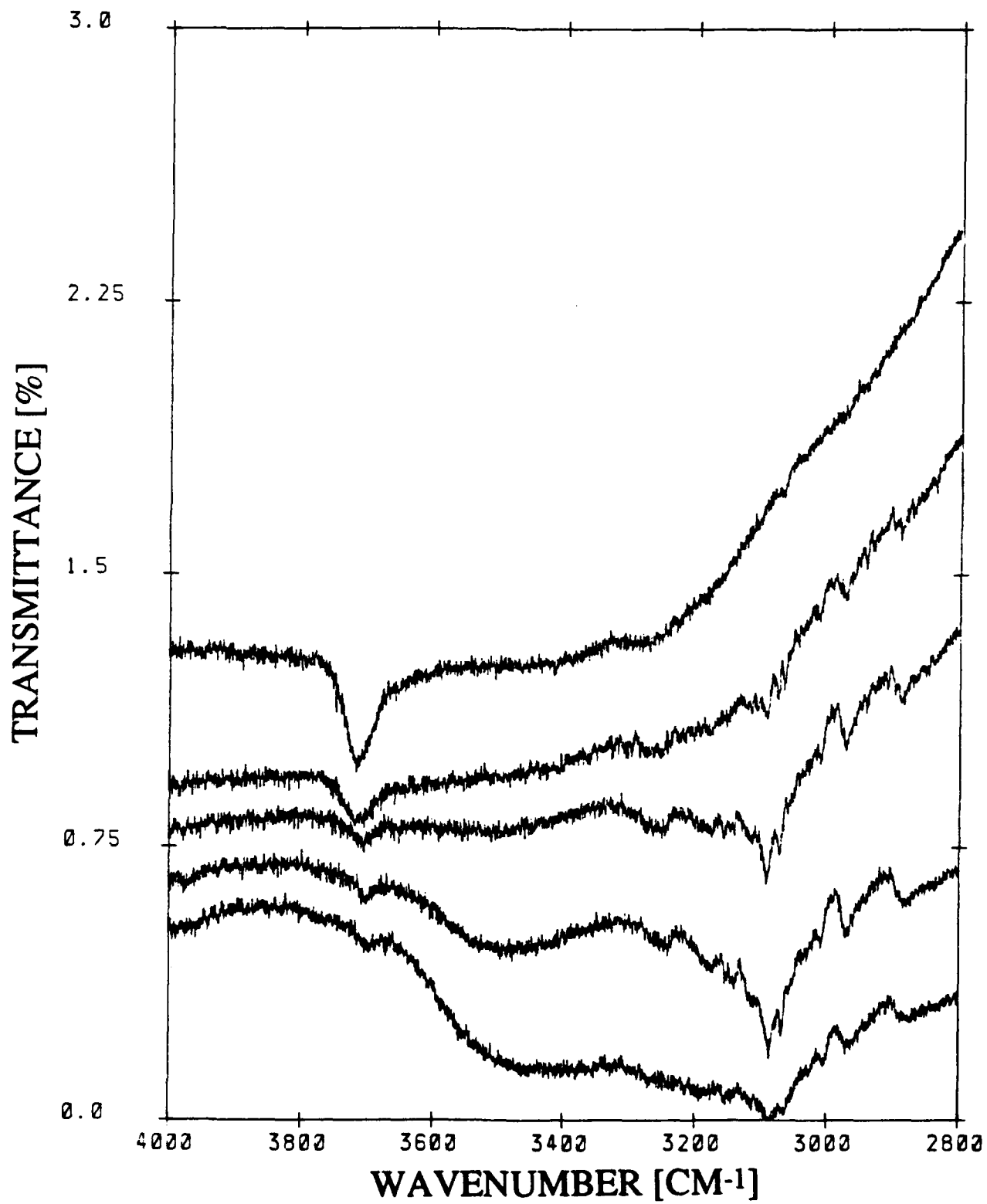
strong absorption peaks are seen at the same time, which indicate the existence of Brønsted acid sites and the possible participation of the 3716 cm^{-1} frequency as the Brønsted acid site for niobia. After all of the heat treatments, there is evidence of Brønsted sites from the absorption occurring in the N-H stretching region; however, these absorption peaks are attenuated with increasing thermal treatments. Concomitant with this attenuation of the N-H peaks is the emergence of the 3716 cm^{-1} peak after the 300 °C heat treatment. Thus, the hydroxyl peak at 3716 cm^{-1} appears to be responsible for the development of the Brønsted acidity in this oxide. There are also a few peaks around 3625 cm^{-1} that are difficult to resolve and which probably belong to adsorbed water. Along with these peaks is a very broad peak from ~ 3400 - 3500 cm^{-1} which is also probably attributable to surface water.

FTIR hydroxyl spectra for aerogels of silica and alumina are shown in Figures C-12 and C-13, respectively. The silica sample shows a single hydroxyl stretch at 3752 cm^{-1} that is stationary throughout all heat treatments. Little evidence of adsorbed pyridine is seen with A-SiO$_2$ except at room temperature where the surface hydroxyl stretch is strongly attenuated and broad absorption from hydrogen bonded pyridine (physisorbed) is seen throughout the entire range making the sample nearly totally opaque. Further heat treating the sample appears to remove nearly all of the pyridine and is confirmed by our FTIR studies on the 1700 - 1400 cm^{-1} region of this sample. A broad peak at ~ 3500 cm^{-1} suggests a possibility of some adsorbed water remaining on the silica aerogel after the pretreatment in vacuum. The FTIR hydroxyl range for the alumina aerogel is shown in Figure C-13. The most complicated aspect of this sample is the hydroxyl region from 3800 - 3600 cm^{-1}. After the pretreatment at 400 °C (blank) there are at least three different hydroxyl stretches: 3780, 3745, and 3700 cm^{-1}. Alumina has been well documented as possessing as many as five different types of hydroxyl groups so the fact that we are able to resolve at least three hydroxyl stretches is not surprising. The pretreated sample also contains a large amount of adsorbed water as shown by the large broad peak in the region 3600 - 3200 cm^{-1}. Thus, longer heating and pumping times are probably necessary in

Figure C-12: HYDROXYL RANGE FTIR SPECTRA OF PYRIDINE ADSORBED
ON A-SiO$_2$: BLANK AND AFTER HEAT TREATMENTS AT 300,
200, 100, AND 25 °C (TOP TO BOTTOM)

Figure C-13: HYDROXYL RANGE FTIR SPECTRA OF PYRIDINE ADSORBED
ON A-Al₂O₃: BLANK AND AFTER HEAT TREATMENTS AT 300,
200, 100, AND 25 °C (TOP TO BOTTOM)
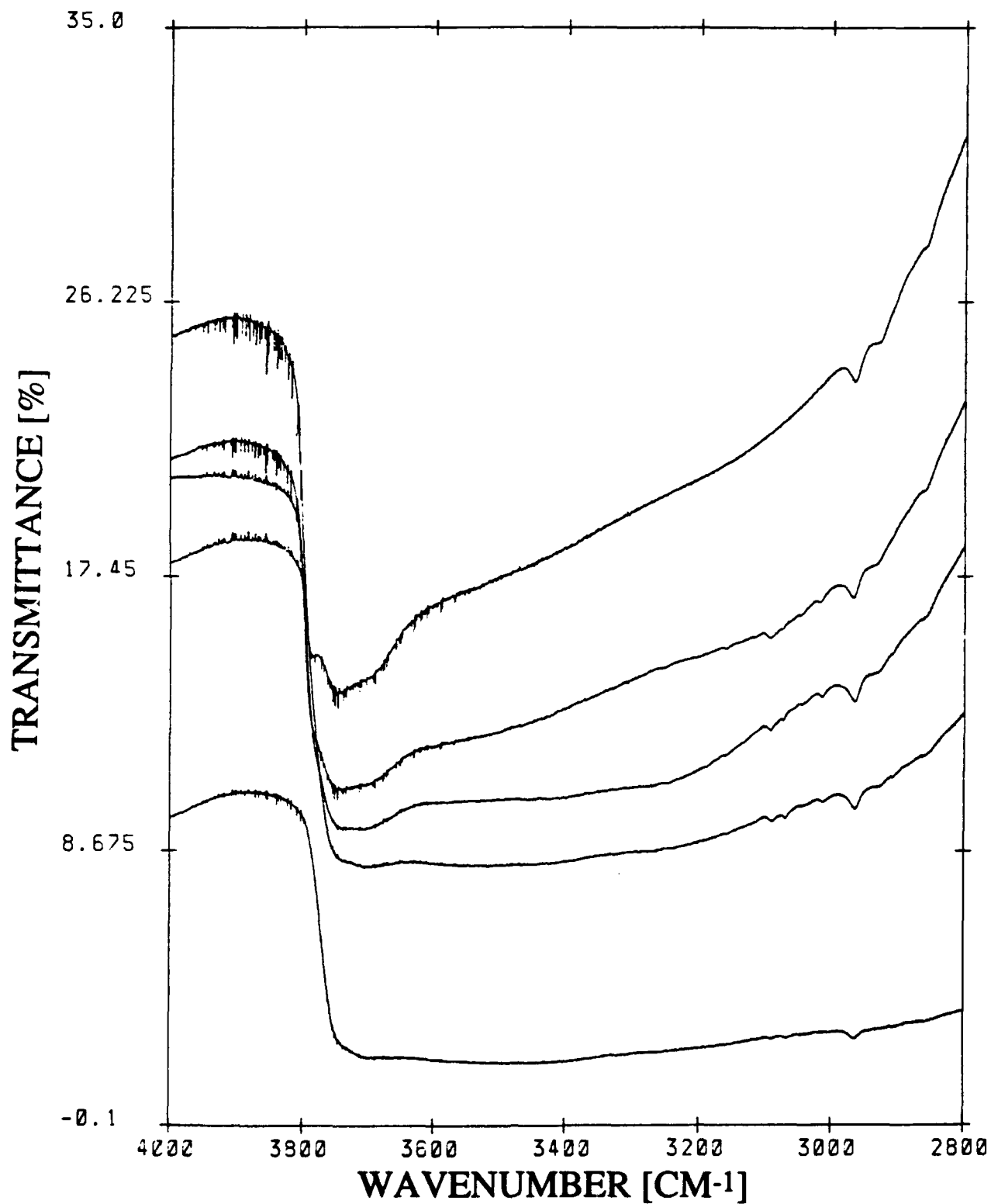
removing this extra water. After exposure to pyridine and evacuating at room temperature the sample is almost totally opaque but hydroxyl stretches at 3745 and 3700 cm^{-1} are apparent. Further thermal treatments to 100 and 200 °C refine these two hydroxyl peaks, and weak N-H absorption peaks are noticed on the sample as well. Further heat treatment to 300 °C attenuates the already weak N-H peaks and a shoulder around 3780 cm^{-1} is formed. The pretreated (blank) sample shows the 3780 cm^{-1} stretch as a definite peak, thus the weak N-H absorption on this sample could possibly be due to the 3780 cm^{-1} hydroxyl stretch which acts as a very weak Brønsted acid site. Recall that this sample showed no peaks at 1540 cm^{-1}, indicative of Brønsted acidity, which means that any N-H stretches on this sample are weak at best and cannot be resolved in the 1700 - 1400 cm^{-1} range.

Results for the mixed oxide aerogels of A-NS25w and A-NA25w are shown in Figures C-14 and C-15, respectively. The pretreated A-NS25w sample (300 °C) shows two hydroxyl stretches at 3750 and 3724 cm^{-1}, plus a large peak centered at ~ 3600 cm^{-1} due to adsorbed water and a few other weak peaks at 3530, 3500, and 3475 cm^{-1} which are also most likely due to strongly chemisorbed water. After the room temperature pyridine exposure, all peaks are severely attenuated as shown by the opacity of the sample; however, the 3750 cm^{-1} hydroxyl stretch is still evident. The thermal treatment at 100 °C reveals a strong N-H stretch at 3085 cm^{-1} as well as a new hydroxyl peak at 3710 cm^{-1} along with the hydroxyl peak attributable to silica at 3750 cm^{-1}. Further heat treatment to 200 °C severely attenuates the N-H stretch and along with the disappearance of this stretch is a shift of the hydroxyl peak to ~ 3720 cm^{-1}. After the 300 °C heat treatment, the N-H peaks have almost completely vanished, along with the development of a shoulder at 3724 cm^{-1}. This peak is apparent in the blank-pretreated sample and suggests that this hydroxyl group is responsible for the weak Brønsted acidity found in this sample. Since this sample also has strongly chemisorbed water as shown after the pretreatment, and the fact that the hydroxyl absorption peak shifts from ~ 3710 to 3724 cm^{-1} after desorbing pyridine, it is possible that the chemisorbed water is functioning as the weak Brønsted acid sites.

Figure C-14: HYDROXYL RANGE FTIR SPECTRA OF PYRIDINE ADSORBED
ON A-NS25w: BLANK AND AFTER HEAT TREATMENTS AT 300,
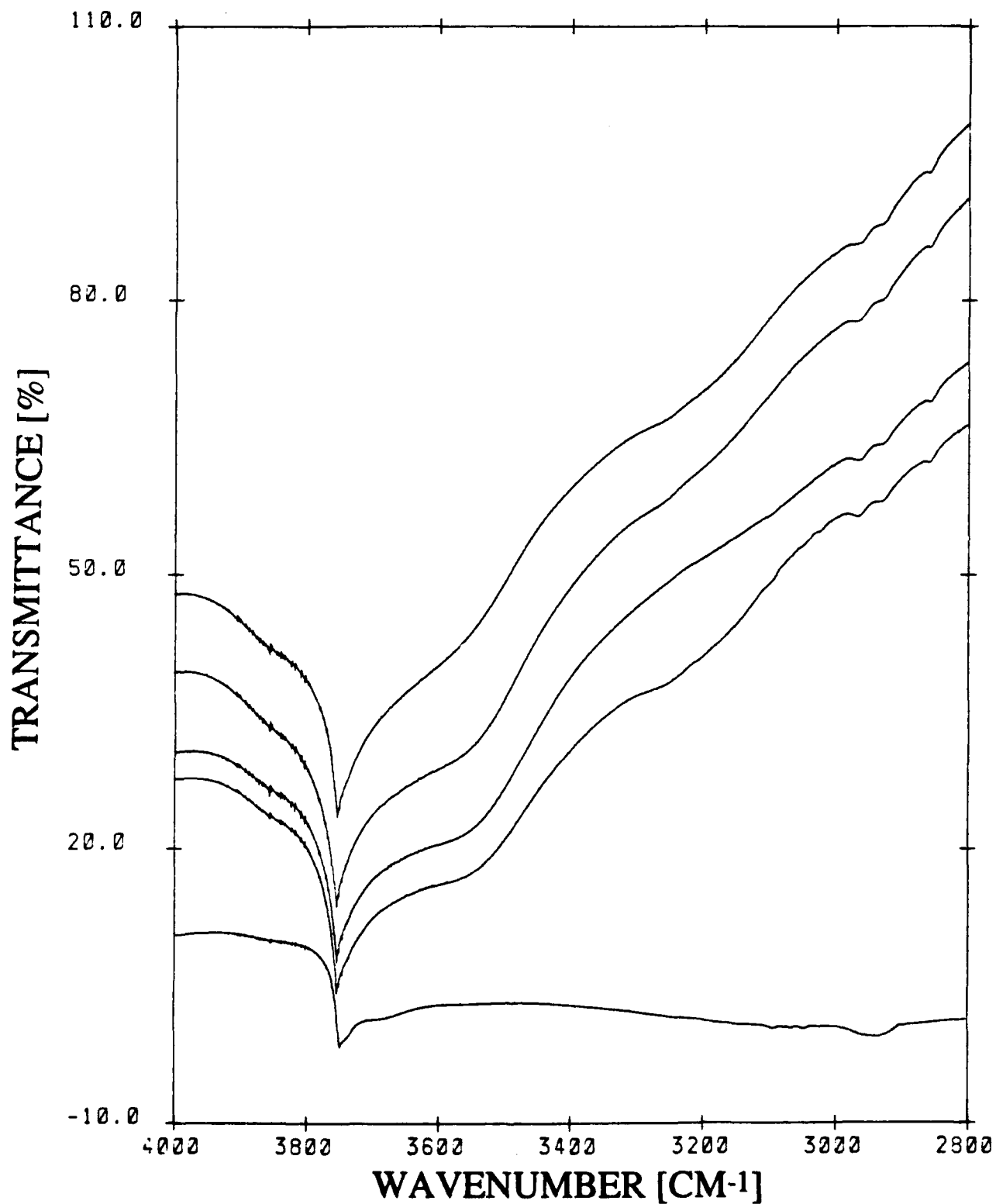200, 100, AND 25 °C (TOP TO BOTTOM)
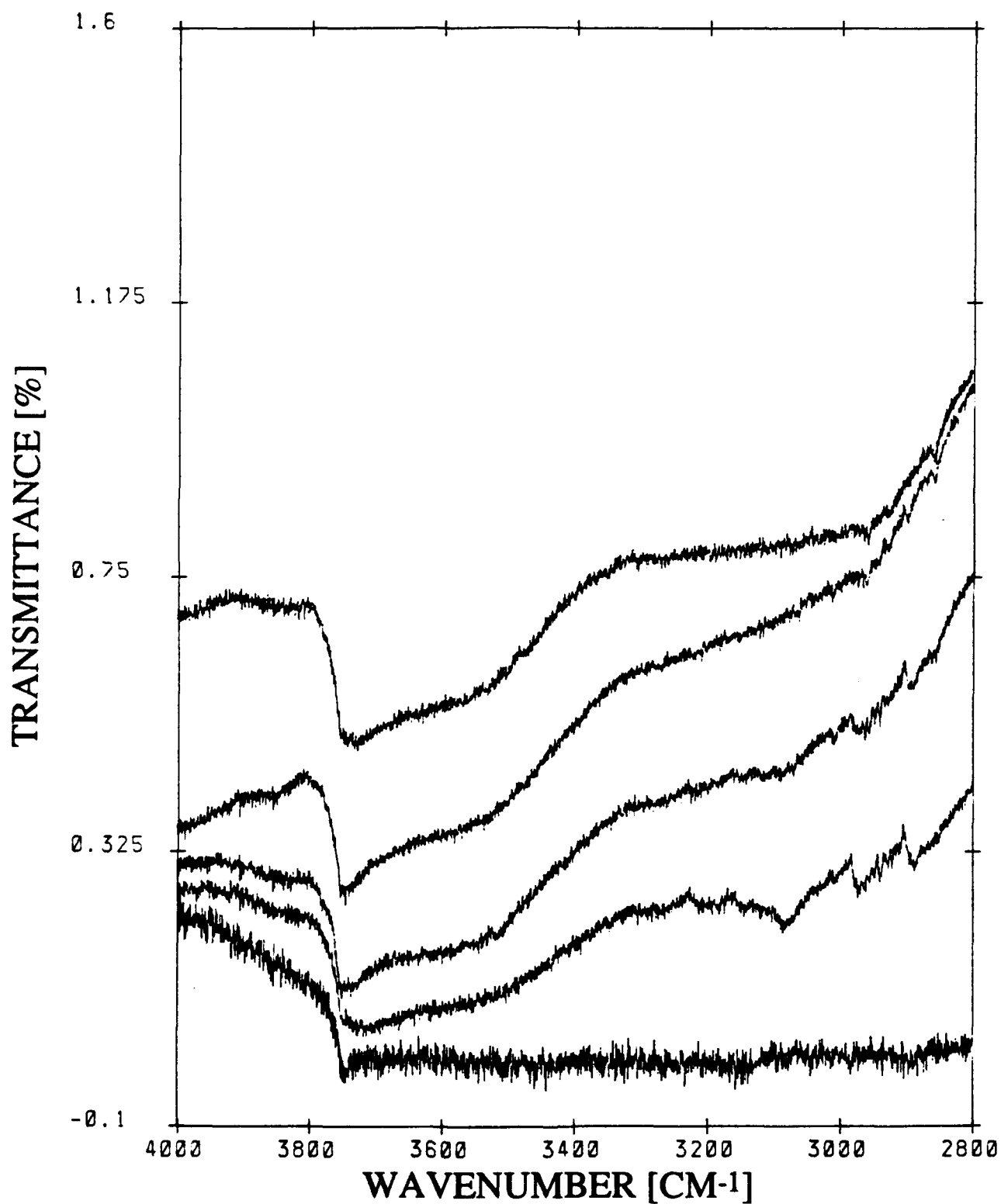
Figure C-15: HYDROXYL RANGE FTIR SPECTRA OF PYRIDINE ADSORBED
ON A-NA25w: BLANK AND AFTER HEAT TREATMENTS AT 300,
200, AND 100 °C (TOP TO BOTTOM)
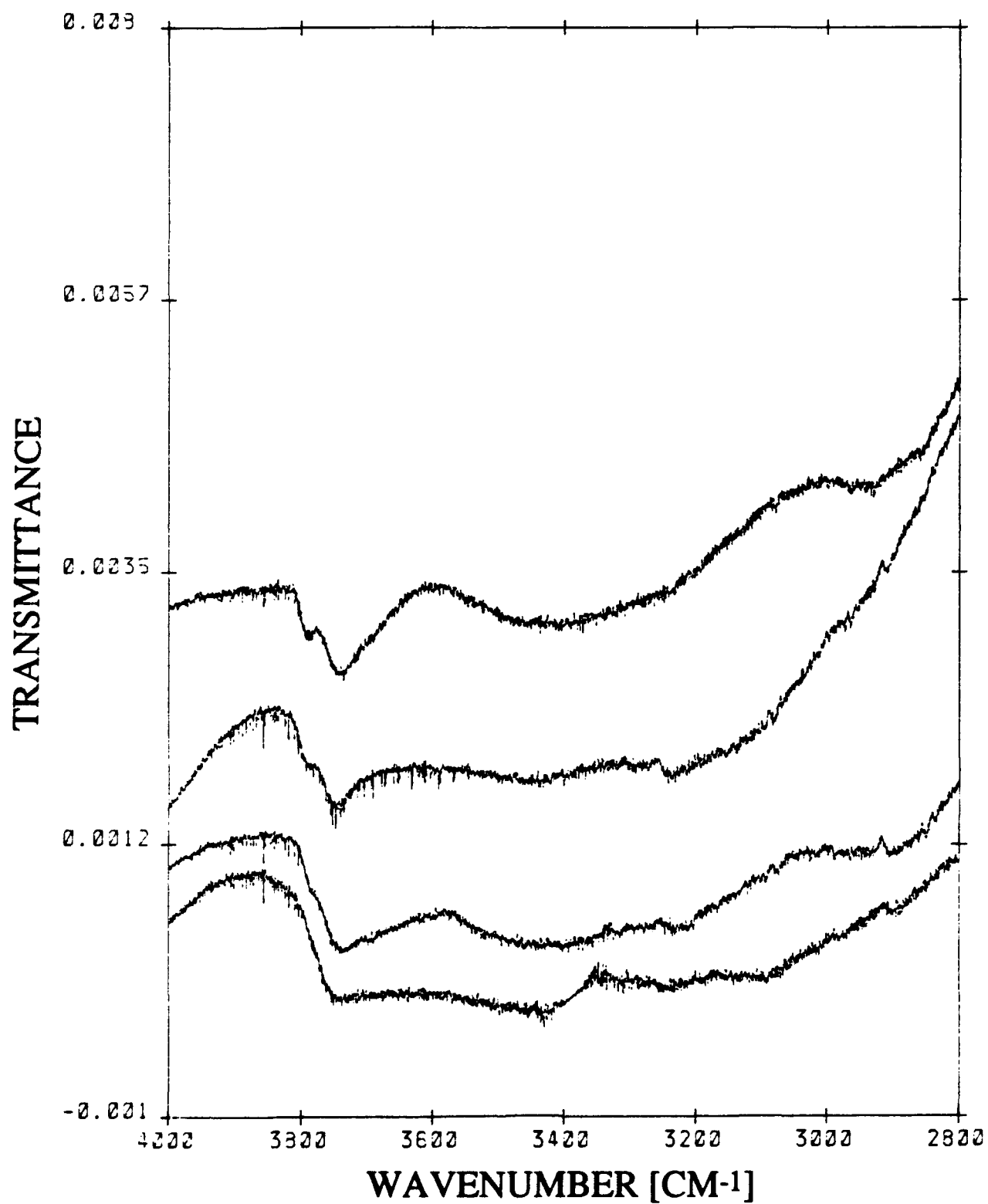
The A-NA25w sample is shown in Figure C-15. The blank pretreated mixed oxide (350 °C) shows two distinct hydroxyl peaks at 3783 and 3744 cm^{-1} as well as a shoulder at 3695 cm^{-1}. These absorption peaks are nearly identical to those found on the bulk alumina aerogel. After pyridine adsorption and heat treating to 100 °C, a very weak N-H absorption peak is evident at 3086 cm^{-1}, and the hydroxyl frequencies observed are 3744 cm^{-1} as well as a shoulder ~ 3780 cm^{-1}. Further heat treatment to 200 °C again shows the absorption at 3744 cm^{-1} and defines the hydroxyl shoulder at 3779 cm^{-1} as well as developing another shoulder at 3695 cm^{-1}. At this 200 °C thermal treatment there is a lack of any N-H absorption peaks as well. Heat treating A-NA25w to 300 °C sharpens the 3779 cm^{-1} peak and the 3774 cm^{-1} peaks while still showing a shoulder at 3695 cm^{-1}. This sample also has water chemisorbed to the surface as shown by the large and broad absorption peak around 3400 cm^{-1}. This niobia/alumina mixed oxide sample behaves similarly to the bulk alumina aerogel, in that it strongly chemisorbs water. This sample showed no peak at 1540 cm^{-1} in the range 1700 - 1400 cm^{-1}, which indicates that this sample had little if any Brønsted acidity and the N-H absorption stretches were extremely weak as determined by this study.

The next samples we looked at were the surface oxides. Figures C-16 and C-17 show the silica aerogel supported niobia samples for A-NS(.05) and A-NS(.25), respectively. On A-NS(.05) we notice that the blank pretreated sample looks nearly identical to that of the bulk silica aerogel (see Figure C-16). In fact, a single hydroxyl peak is seen at 3752 cm^{-1}. Upon adsorption of pyridine at room temperature the sample becomes nearly opaque to the infrared beam but peaks attributable to N-H stretches may be seen. Physisorbed pyridine is also on this sample and probably contributes to the low throughput of the signal. After the 100 °C thermal treatment the N-H peaks are highly visible and there is strong absorption in the region of 3700 - 3500 cm^{-1}, unlike bulk silica which did not readily absorb in this range. A peak at 3752 cm^{-1}, attributable to silica hydroxyl groups, is seen after the 100 °C heat treatment as well as a shoulder which develops at ~ 3725 cm^{-1}, indicative of a possible new hydroxyl group on the surface oxide.

Figure C-16: HYDROXYL RANGE FTIR SPECTRA OF PYRIDINE ADSORBED
ON A-NS(.05): BLANK AND AFTER HEAT TREATMENTS AT 300,
200, 100, AND 25 °C (TOP TO BOTTOM)

Figure C-17: HYDROXYL RANGE FTIR SPECTRA OF PYRIDINE ADSORBED
ON A-NS(.25): BLANK AND AFTER HEAT TREATMENTS AT 300,
200, 100, AND 25 °C (TOP TO BOTTOM)
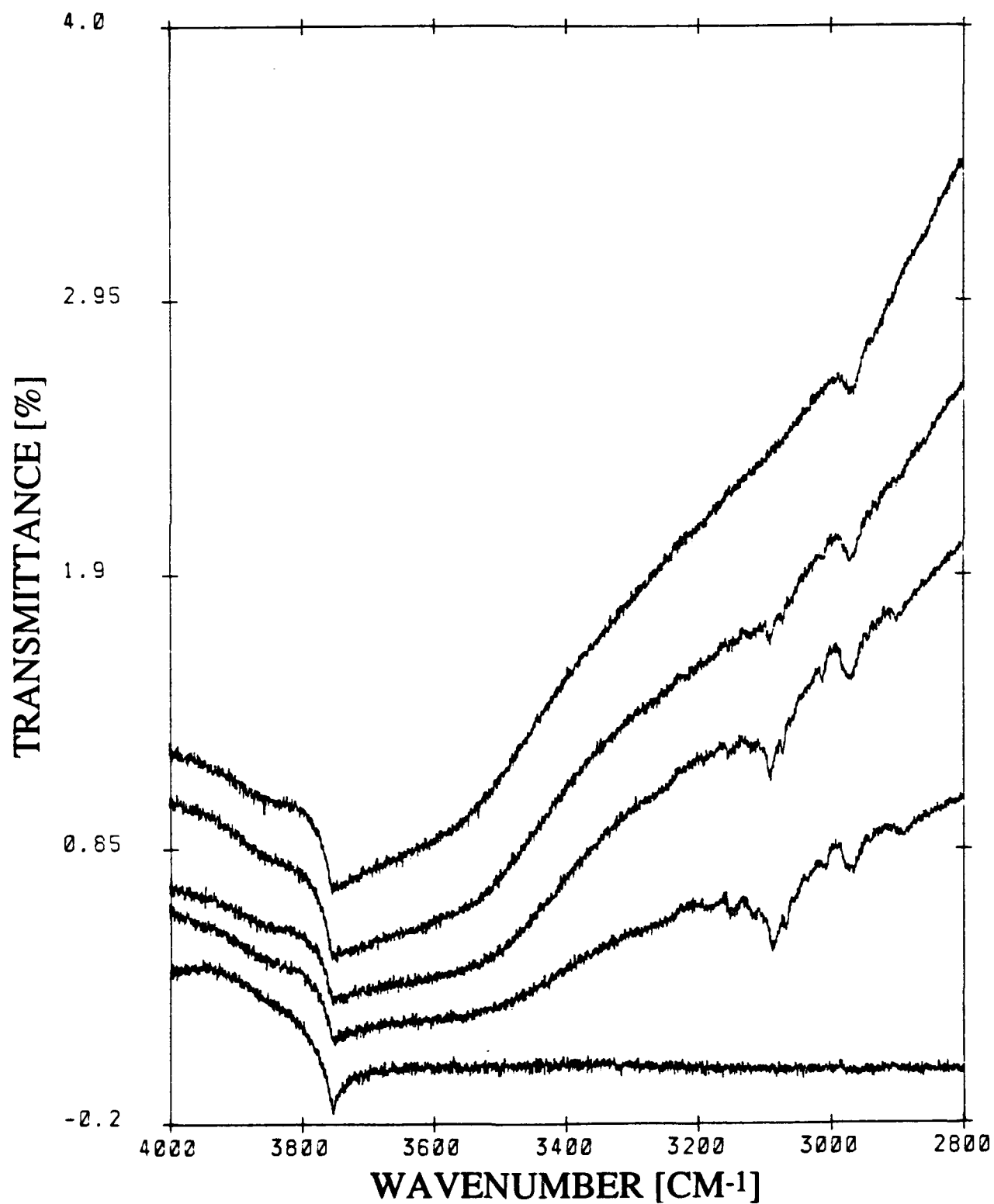
The 200 °C thermal treatment shows N-H absorption peaks, as well as strong absorption in the 3700 - 3500 cm^{-1} range. The new shoulder hydroxyl group appears to have slightly shifted to 3730 cm^{-1}, but the 3752 cm^{-1} peak remains stationary. Even after the 300 °C heat treatment the N-H peaks are present and there is strong absorption in the same range of 3700 - 3500 cm^{-1}. The shoulder hydroxyl peak appears at ~ 3730 cm^{-1} and the silica hydroxyl frequency remains at 3752 cm^{-1}. The fact that such a strong N-H absorption is present even after the 300 °C treatment shows the strength of the Brønsted acid sites on this sample. The disappearance of the absorption peak at ~ 3730 cm^{-1} along with the disappearance of N-H stretches, suggests their possible participation as acid sites. The presence of chemisorbed water is noted on this sample as seen by the broad peak around 3500 cm^{-1}.

Figure C-17 shows the hydroxyl region for pyridine adsorption on A-NS(.25). This sample appears slightly different than A-SiO$_2$ and A-NS(.05), because of the strong absorption around 3700 cm^{-1} without exposure to pyridine. The characteristic peak at 3752 cm^{-1} attributable to silica is present on this sample as well. After exposure to pyridine this sample shows a peak at 3752 cm^{-1} for the hydroxyl region, but is opaque throughout the rest of the entire range making data interpretation difficult. After heat treating to 100 °C, sharp peaks due to N-H absorption are readily seen. Along with this observation we notice a very strong absorption from 3750 - 3500 cm^{-1}. Again, due to the opacity of the sample, analysis of this range is difficult, but we can still observe one hydroxyl peak at 3752 cm^{-1}. After the 200 and 300 °C heat treatments we see an attenuation of the N-H absorption peaks along with appearance of possible hydroxyl groups at a frequency around 3700 cm^{-1}. Exact peak positions are difficult because of the low throughput of the infrared beam; however, the absorption at ~ 3700 cm^{-1} is indicative of possible new hydroxyl peak(s) which are the Brønsted acid sites on this sample. Collectively, the results of the silica aerogel supported niobia samples do confirm tne existence of strong Brønsted acid sites and suggest that new surface -OH groups are created by supporting niobia on silica.

Chemisorbed water was also found in both silica supported surface oxides as indicated by the large broad peak around 3500 cm^{-1}.

The alumina aerogel supported niobia samples are shown in Figures C-18 and C-19 for A-NA(.05) and A-NA(.25), respectively. On A-NA(.05) we notice first that this is similar to, but also different from the bulk alumina aerogel. This sample chemisorbs water as shown by the broad peak around 3500 cm^{-1}. The hydroxyl absorptions appear to be different in A-NA(.05) and A-Al$_2$O$_3$. The main hydroxyl regions for A-NA(.05) are 3788 and 3752 cm^{-1} with a shoulder at 3700 cm^{-1}, while in bulk A-Al$_2$O$_3$ the two main absorptions are 3745 and 3700 cm^{-1} with a shoulder at 3780 cm^{-1}. It appears that the attenuation of the 3700 cm^{-1} peak for A-NA(.05) is due to the preparation of this surface oxide. This hydroxyl group allows the oxygen atom to be the most accessible because of the low frequency of this vibration. The other hydroxyl groups are possibly bound too strongly to react with the niobium alkoxide. After exposure to pyridine at room temperature, weak N-H absorption peaks are observed as well as a broad hydroxyl peak at 3745 cm^{-1}. Heat treating to 100 °C reveals the same hydroxyl peak at 3745 cm^{-1} as well as a shoulder at 3700 cm^{-1} and N-H absorption peaks. Further treatment to 200 and 300 °C shows an attenuation of the N-H absorption peaks while also showing the emergence of the hydroxyl peak at 3780 cm^{-1} and a weak shoulder at 3700 cm^{-1}. This sample was shown earlier in the main text at possessing no Brønsted acidity, therefore, the N-H interactions found in this sample are very weak.

The FTIR pyridine spectra for A-NA(.25) are shown in Figure C-19. This sample strongly chemisorbed water as shown by the broad absorption peak centered around 3500 cm^{-1}. These spectra are similar to those shown for A-NA(.05); however, a stronger absorption at ~ 3700 cm^{-1} is seen with A-NA(.25) possibly due to the formation of a new hydroxyl group on the niobia surface oxide species. The spectra at all treatment temperatures except for 25 °C (due to opaque spectrum) show weak N-H absorption peaks. After the 100 °C heat treatment the hydroxyl peak at 3750 cm^{-1} is seen [similar to A-

Figure C-18: HYDROXYL RANGE FTIR SPECTRA OF PYRIDINE ADSORBED ON A-NA(.05): BLANK AND AFTER HEAT TREATMENTS AT 300, 200, 100, AND 25 °C (TOP TO BOTTOM)
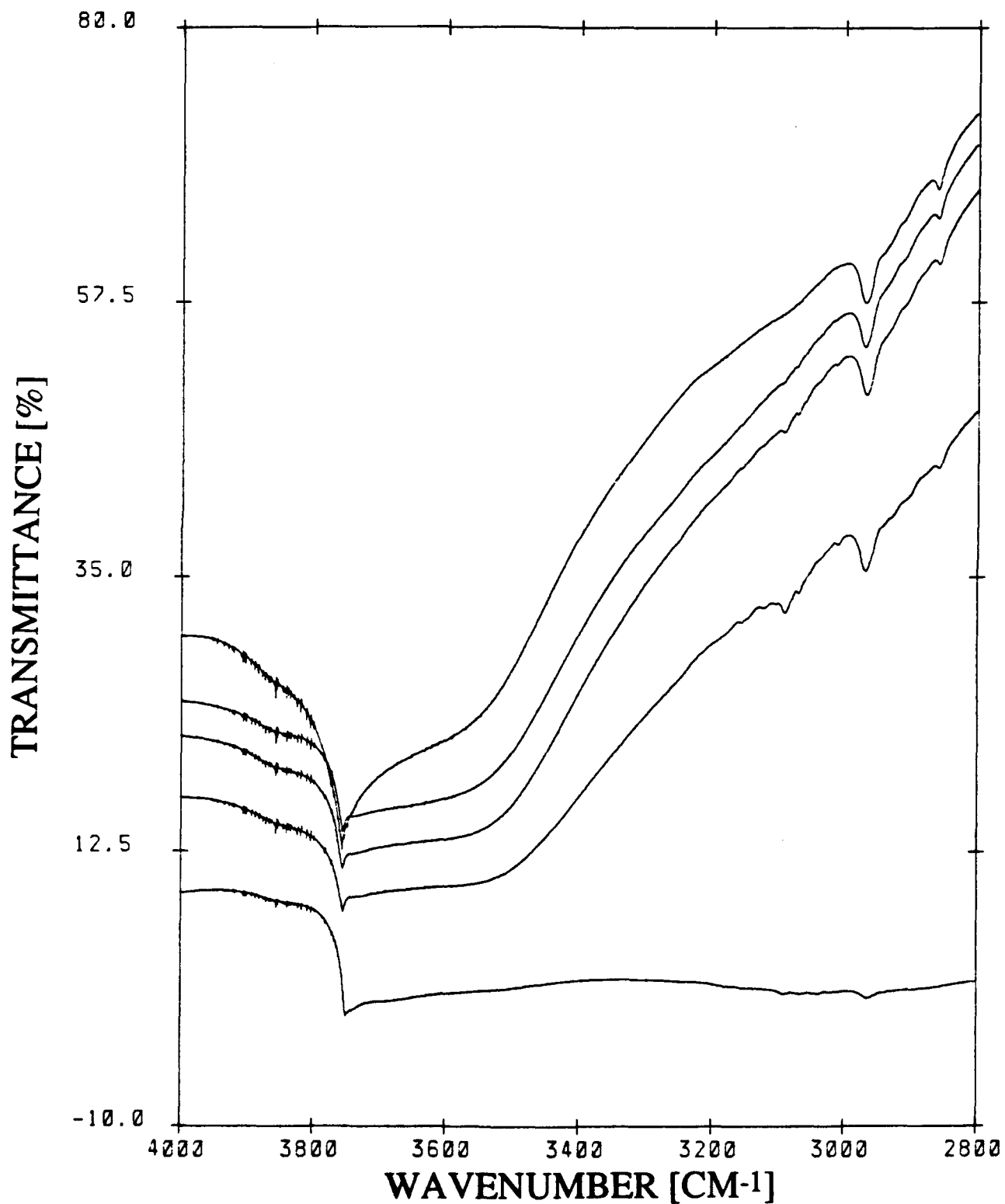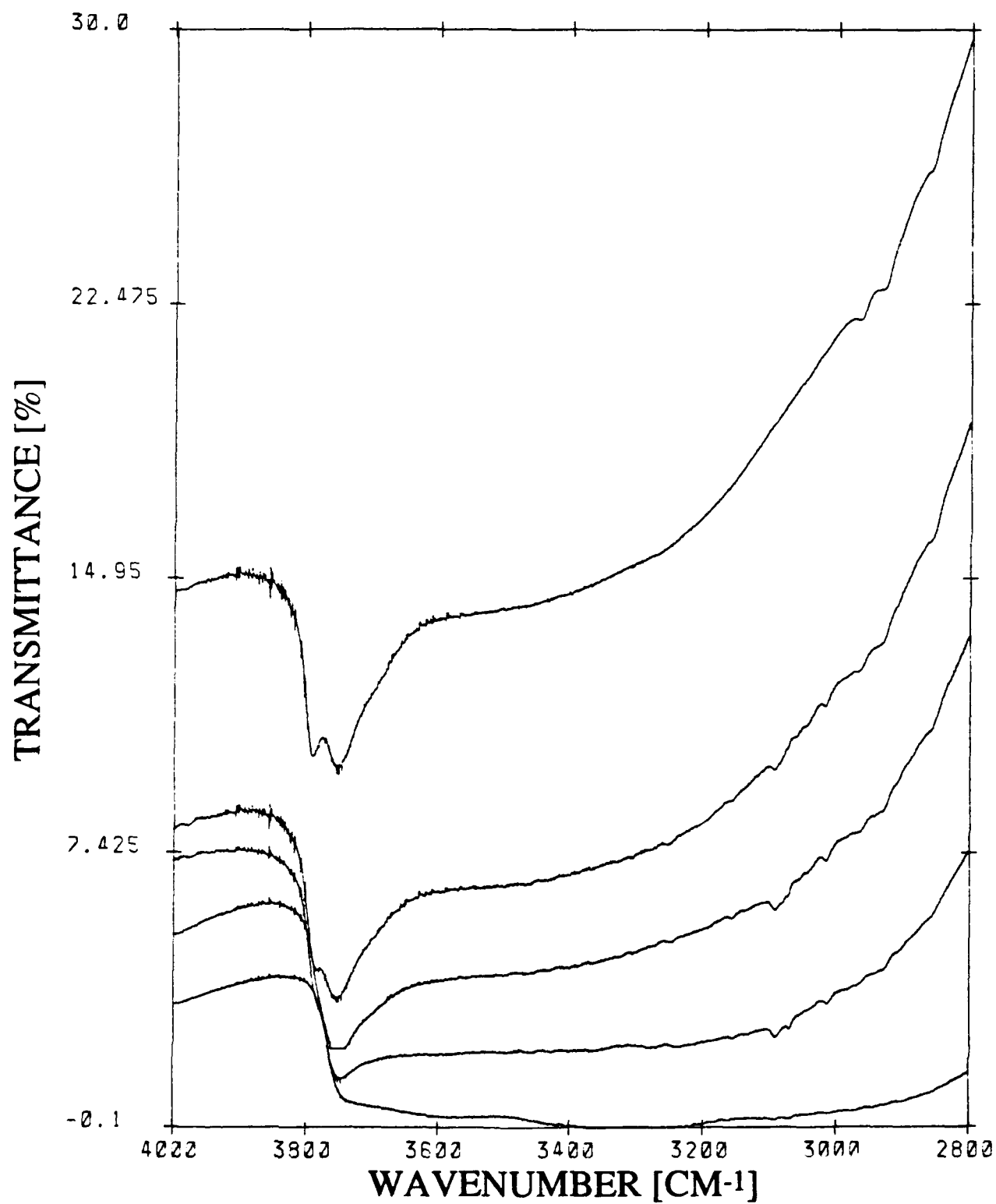
Figure C-19: HYDROXYL RANGE FTIR SPECTRA OF PYRIDINE ADSORBED
ON A-NA(.25): BLANK AND AFTER HEAT TREATMENTS AT 300,
200, 100, AND 25 °C (TOP TO BOTTOM)
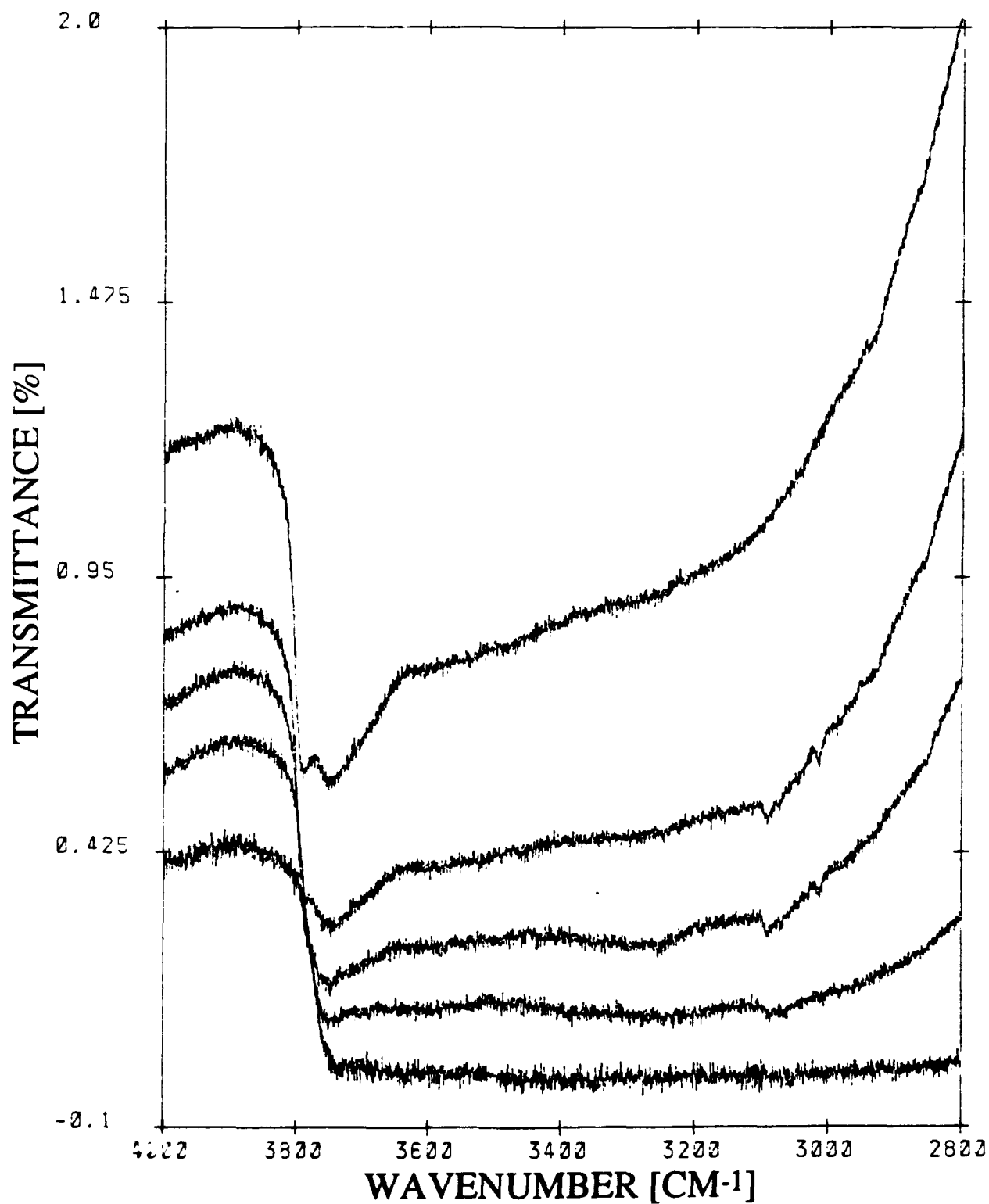
NA(.05)] along with another new hydroxyl group with a strong absorption at 3700 cm^{-1} possibly due to the surface oxide. This new group shows a strong absorption all the way to the 300 °C heat treatment. At this 300 °C treatment a shoulder at 3782 cm^{-1} is also formed, indicating a third hydroxyl group formed on this sample that is similar to those on the bulk alumina aerogel and A-NA(.05). With the A-NA(.25) surface oxide, chemisorbed water is seen with this material which may possibly contribute to the formation of Brønsted acid sites, which were discussed in the main text of this thesis. Although interpretation of this data is difficult, results suggest that supporting niobia on alumina in high enough coverages creates new surface -OH groups which can act as Brønsted acid sites. These studies are hampered by the presence of adsorbed water even after a 400 °C pretreatment which possibly means that longer heating and pumping times are needed to totally rid these samples of adsorbed water.

C.3 DRIFT SPECTRA: 4000 - 2800 cm^{-1}

This section discusses the hydroxyl frequency range of 4000 - 2800 cm^{-1} to examine if any new hydroxyl groups were formed in the newly synthesized oxide aerogels. All samples were calcined the same day and placed into the DRIFT assembly *ex-situ*. The materials were subsequently pumped down in vacuum in the IR assembly for approximately one hour. The experimental apparatus and procedure did not allow us to pretreat the sample *in-situ* as our earlier FTIR measurements, hence these samples will all be at least partially hydrated, although we tried to minimize the amount of hydration that would occur by preparing the sample quickly (~ 1 min exposure to ambient).

The first set of samples that were investigated were the heat treated niobia aerogel samples: A-Nb$_2$O$_5$ (500,2) [A], A-Nb$_2$O$_5$ (600,2) [TT], and A-Nb$_2$O$_5$ (800,2) [T]. The peak frequencies for the heat treated niobia samples are listed in Table C-2(A), and the spectra are shown in Figure C-20. One immediately notices two major differences from the

Table C-2: SUMMARY OF DRIFT HYDROXYL REGION ABSORPTIONS OF: A) HEAT TREATED A-Nb₂O₅, B) BULK AND MIXED OXIDES, AND C) SURFACE OXIDES

A) DRIFT Hydroxyl Region Absorption of Heat Treated A-Nb$_2$O$_5$

Sample	Heat Treatment	Wavenumbers (cm^{-1})
A-Nb$_2$O$_5$	(500,2)	3705,3675
A-Nb$_2$O$_5$	(600,2)	3675
A-Nb$_2$O$_5$	(800,2)	3675

B) DRIFT Hydroxyl Region Absorption of Bulk and Mixed Oxides

Sample	Heat Treatment	Wavenumbers (cm^{-1})
A-Nb$_2$O$_5$	(500,2)	3705,3675
A-SiO$_2$	(500,2)	3752
A-Al$_2$O$_3$	(500,2)	3750
A-NS25w	(500,2)	3749

C) DRIFT Hydroxyl Region Absorption of Surface Oxides

Sample	Heat Treatment	Wavenumbers (cm^{-1})
A-NS(.025)	(500,2)	3752
A-NS(.05)	(500,2)	3752,3710(Sh)
A-NS(.10)	(500,2)	3752,3710(Sh)
A-NS(.25)	(500,2)	3752,3710,3o60(Sh)
A-NA(.05)	(500,2)	3750
A-NA(.25)	(500,2)	3750,3690

Sh = Shoulder

Figure C-20: DRIFT HYDROXYL RANGE SPECTRA FOR HEAT TREATED A-Nb_2O_5: (500,2), (600,2), AND (800,2) (TOP TO BOTTOM)
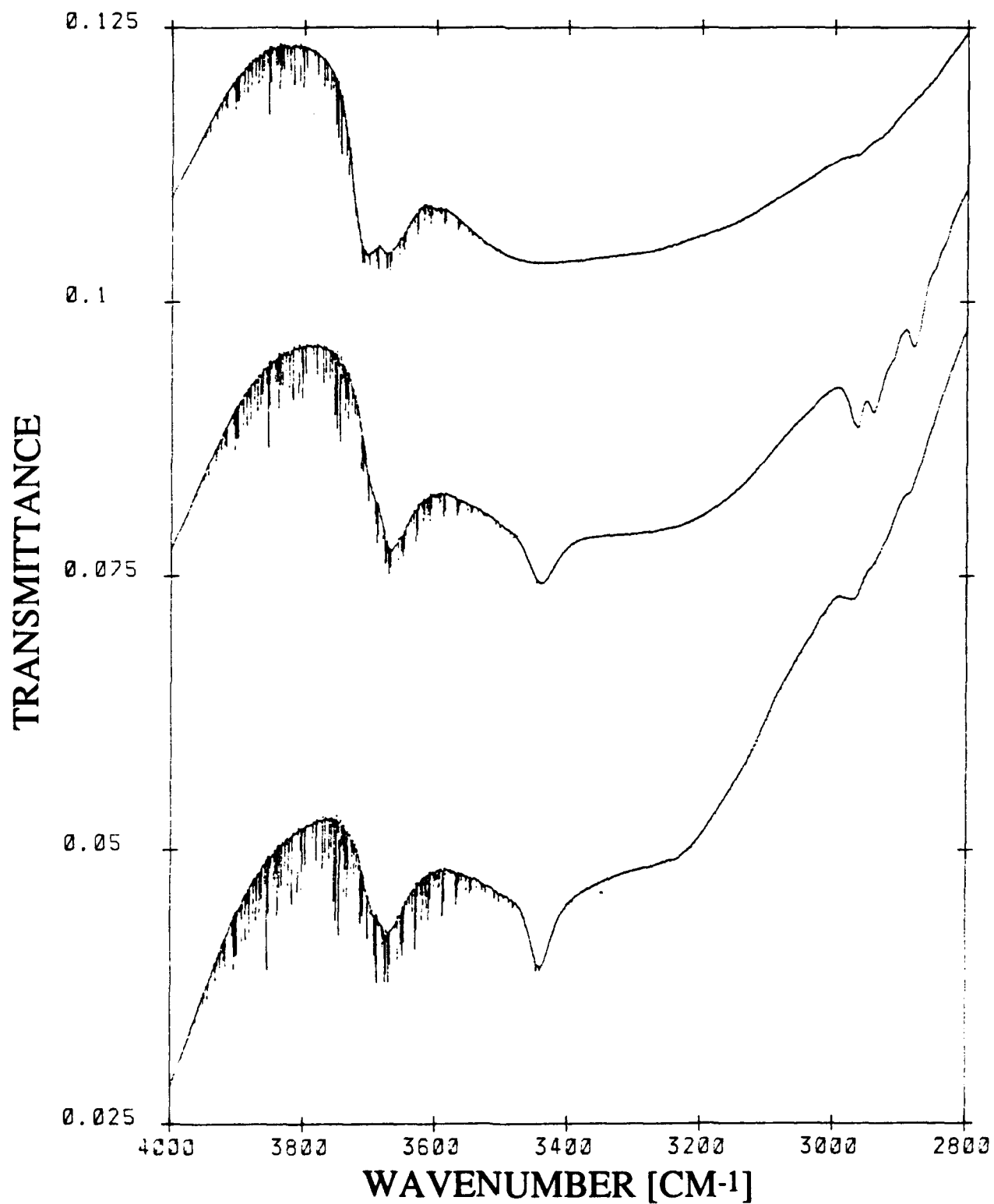
calcined (500,2) niobia aerogel and the other two heat treated, (600,2) and (800,2), niobia aerogels. First of all, A-Nb$_2$O$_5$ (500,2) has two hydroxyl peaks at 3675 and 3705 cm^{-1} while the other two heat treated niobia samples only possess the 3675 cm^{-1} hydroxyl peak. Along with the disappearance of this second hydroxyl peak is the formation of another peak at ~ 3450 cm^{-1}, indicating the presence of strongly adsorbed water. The calcined niobia aerogel has a very broad peak in this same region; however, it is not nearly as sharp as the other heat treated niobia aerogels. The second hydroxyl peak at 3705 cm^{-1} for A-Nb$_2$O$_5$ (500,2) could possibly be attributed to the high acid strength and large amount of Brønsted acidity of this sample, while the other heat treated samples do not show as large an acid strength or acidity. These heat treated niobia aerogels show that different structures influence the surface properties of this material, in particular, the hydroxyl regions and the ability to adsorb water and change the surface characteristics of this material.

The next aerogels investigated with DRIFT were the bulk oxides of niobia, silica and alumina. The hydroxyl region stretching frequencies are summarized in Table C-2(B) and shown in Figure C-21. Again the niobia aerogel (calcined) shows a doublet at 3675 and 3705 cm^{-1} as well as a large broad peak centered around 3450 cm^{-1}. The silica aerogel spectrum is much simpler with only a single peak at 3752 cm^{-1}. This result is identical to the FTIR result of the hydroxyl stretching frequency of silica and shows that physisorbed water does not influence the hydroxyl group for this aerogel. The alumina aerogel has a broad hydroxyl peak around 3750 cm^{-1} and also has a strong and broad absorption throughout the entire range showing that water strongly chemisorbs onto this sample making any peak interpretation difficult. In fact, this alumina aerogel sample shows a DRIFT spectrum similar to that of the FTIR spectrum of pyridine adsorption at room temperature, further confirming that water adsorbs strongly to this sample.

The next aerogel sample investigated was the mixed oxide of A-NS25w. Results of this mixed oxide are summarized in Table C-2(B) and also shown in Figure C-22 along with A-Nb$_2$O$_5$ and A-SiO$_2$ for comparison. A-NS25w has a large amount of chemisorbed

Figure C-21: DRIFT HYDROXYL RANGE SPECTRA FOR CALCINED (500,2): A-Nb_2O_5, A-SiO_2, AND A-Al_2O_3 (TOP TO BOTTOM)
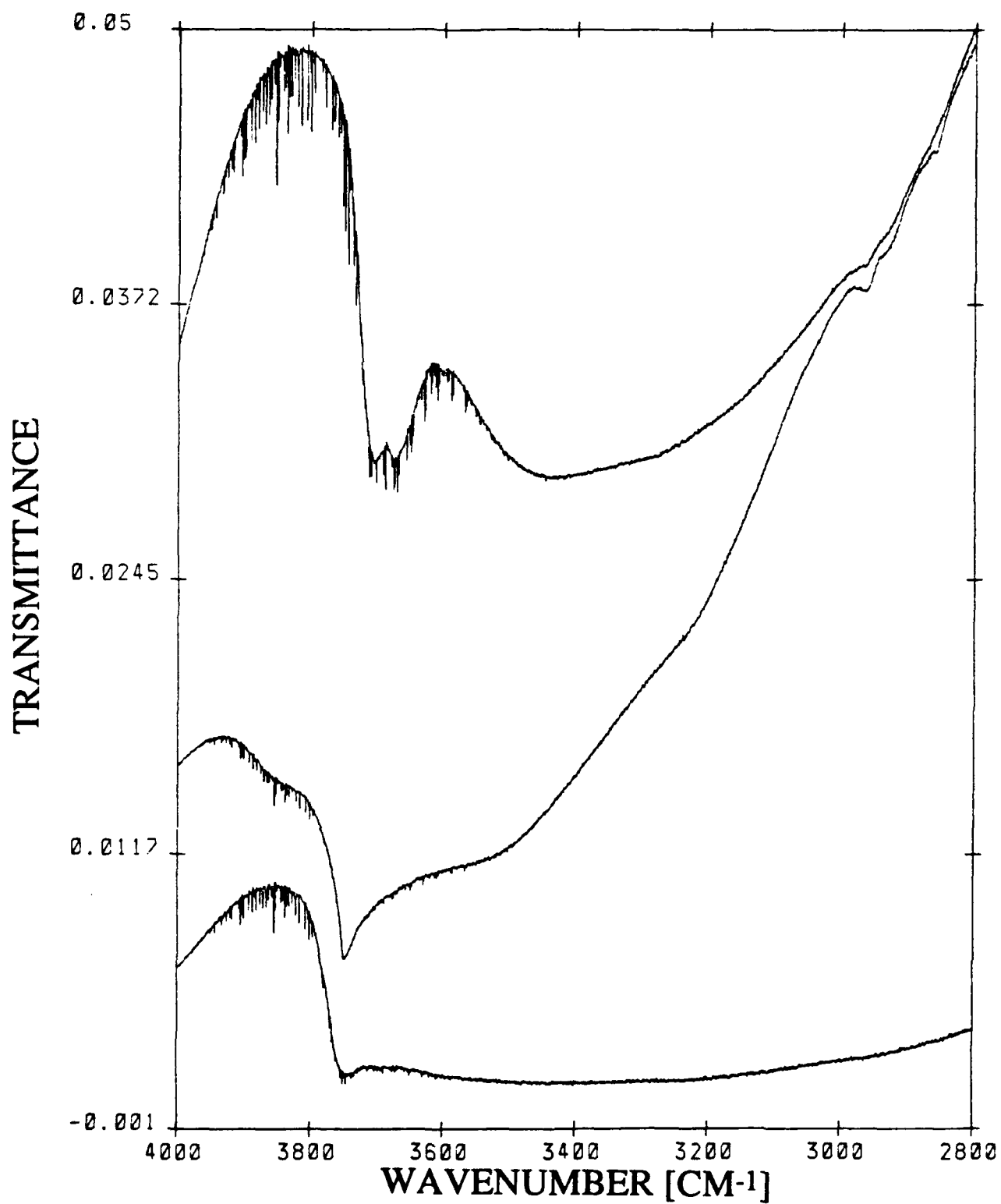
Figure C-22: DRIFT HYDROXYL RANGE SPECTRA FOR CALCINED (500,2): A-Nb$_2$O$_5$, A-NS25w, AND A-SiO$_2$ (TOP TO BOTTOM)
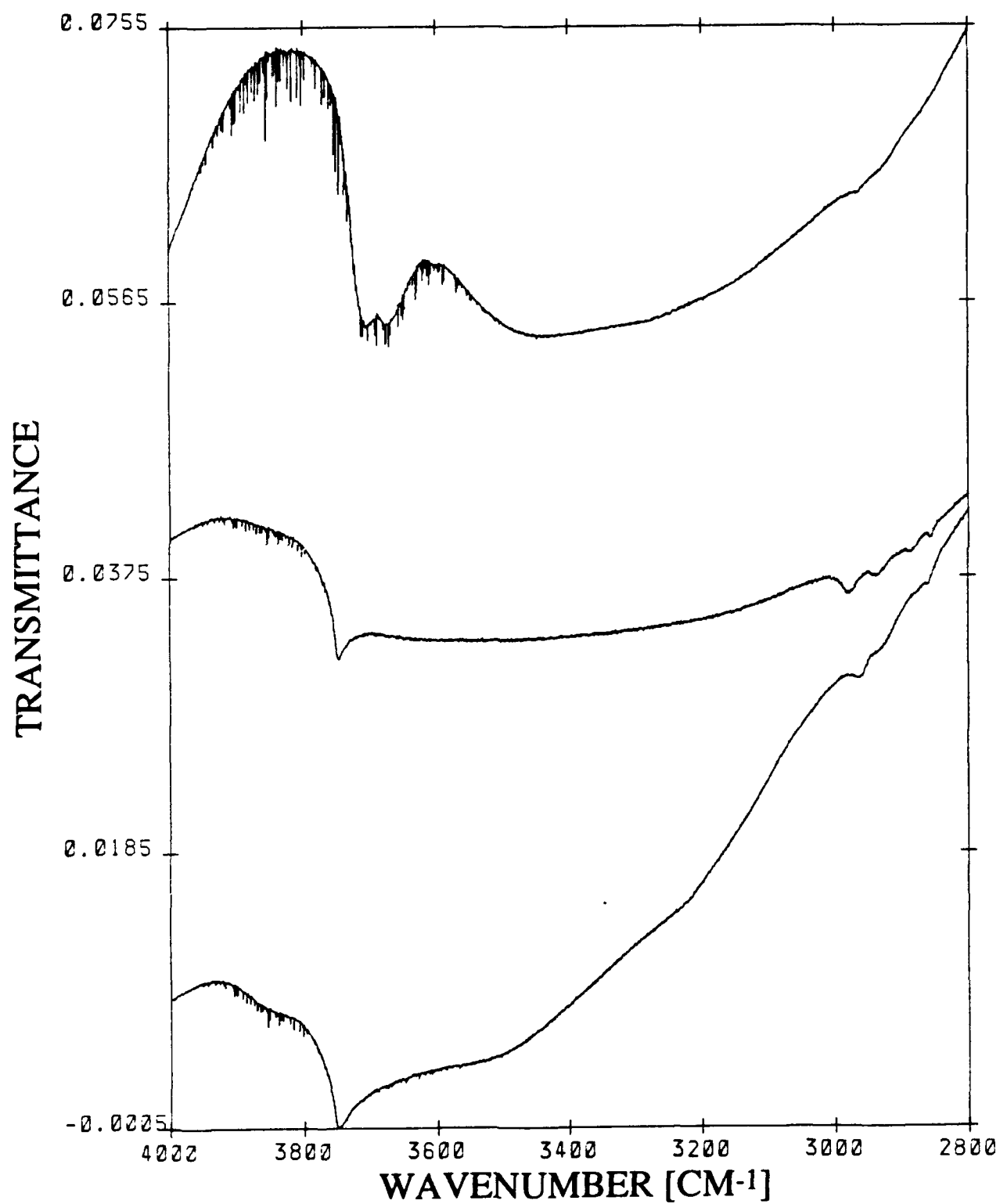
water as shown by the strong absorption throughout the range 3700 to 3000 cm^{-1}. The hydroxyl region shows a single peak at 3749 cm^{-1} which is probably attributed to the large amount of silica found in this oxide, and the second hydroxyl peak observed in the FTIR of this oxide is probably obscured by the strong absorption of chemisorbed water. This is similar to the effect that pyridine was found to have on this mixed oxide.

The silica aerogel supported niobia samples were the next materials examined with DRIFT. The results of this experiment are summarized in Table C-2(C) and Figure C-23. The silica aerogel shows only one hydroxyl peak at 3752 cm^{-1} as discussed earlier. The lowest coverage of niobia sample, A-NS(.025), looks nearly identical to the bulk silica aerogel showing that no new observable hydroxyl stretches are formed. A-NS(.05) has a small shoulder at ~ 3710 cm^{-1}, as well as the 3752 cm^{-1} stretch, indicating the possibility of a newly formed hydroxyl group. This 5% niobia coverage surface oxide also shows a stronger absorption around ~ 3500 cm^{-1} due possibly to chemisorbed water. A-NS(.10) looks nearly identical to A-NS(.05) showing that no drastic changes in the surface property has occurred with increasing the coverage of niobia to 10%. The quarter monolayer sample, A-NS(.25), shows the silica hydroxyl stretch (3752 cm^{-1}) plus the 3710 cm^{-1} shoulder as well as a 3660 cm^{-1} stretch that the other samples do not have. These new hydroxyl stretches may be attributed to a newly formed niobia surface oxide species on the silica aerogel.

Alumina aerogel supported niobia were next investigated with DRIFT. A summary of the hydroxyl region peaks may be found in Table C-2(C), and the spectra are shown in Figure C-24. The alumina aerogel spectrum shows a single hydroxyl absorption peak at 3750 cm^{-1} and strong absorption due to chemisorbed water. A-NA(.05) shows a spectrum nearly identical to bulk alumina; however, it appears that the surface oxide absorbs water more strongly as seen by the sharper peak around ~ 3500 cm^{-1}. The quarter monolayer sample, A-NA(.25), begins to actually show a new peak around 3690 cm^{-1} which can probably be attributed to the new surface oxide phase formed with this sample. This newly

Figure C-23: DRIFT HYDROXYL RANGE SPECTRA FOR CALCINED SILICA AEROGEL SUPPORTED NIOBIA: A-SiO$_2$, A-NS(.025), A-NS(.05), A-NS(.10), AND A-NS(.25) (TOP TO BOTTOM)
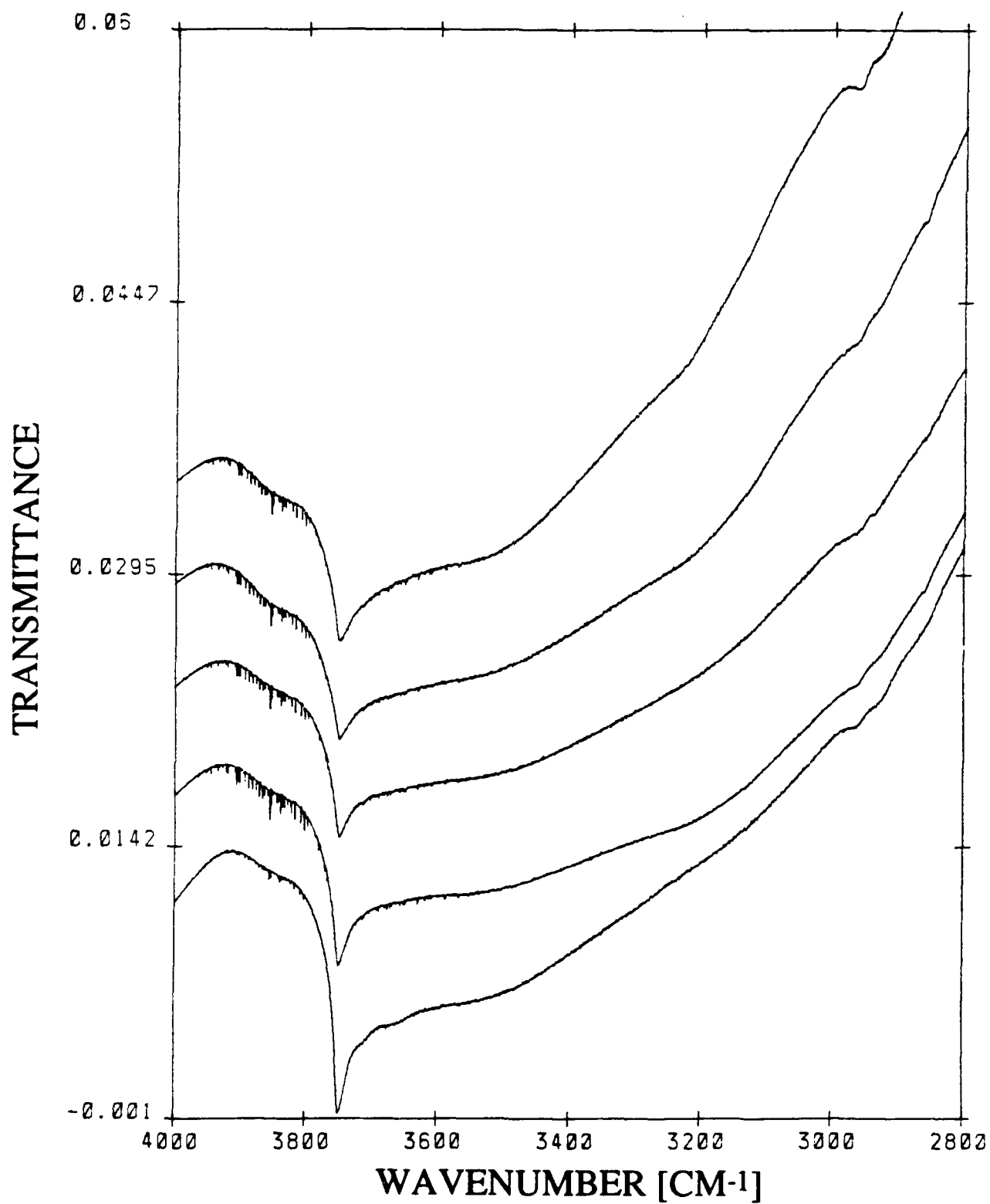
Figure C-24: DRIFT HYDROXYL RANGE SPECTRA FOR CALCINED ALUMINA
AEROGEL SUPPORTED NIOBIA: A-Al$_2$O$_3$, A-NA(.05), AND A-
NA(.25) (TOP TO BOTTOM)
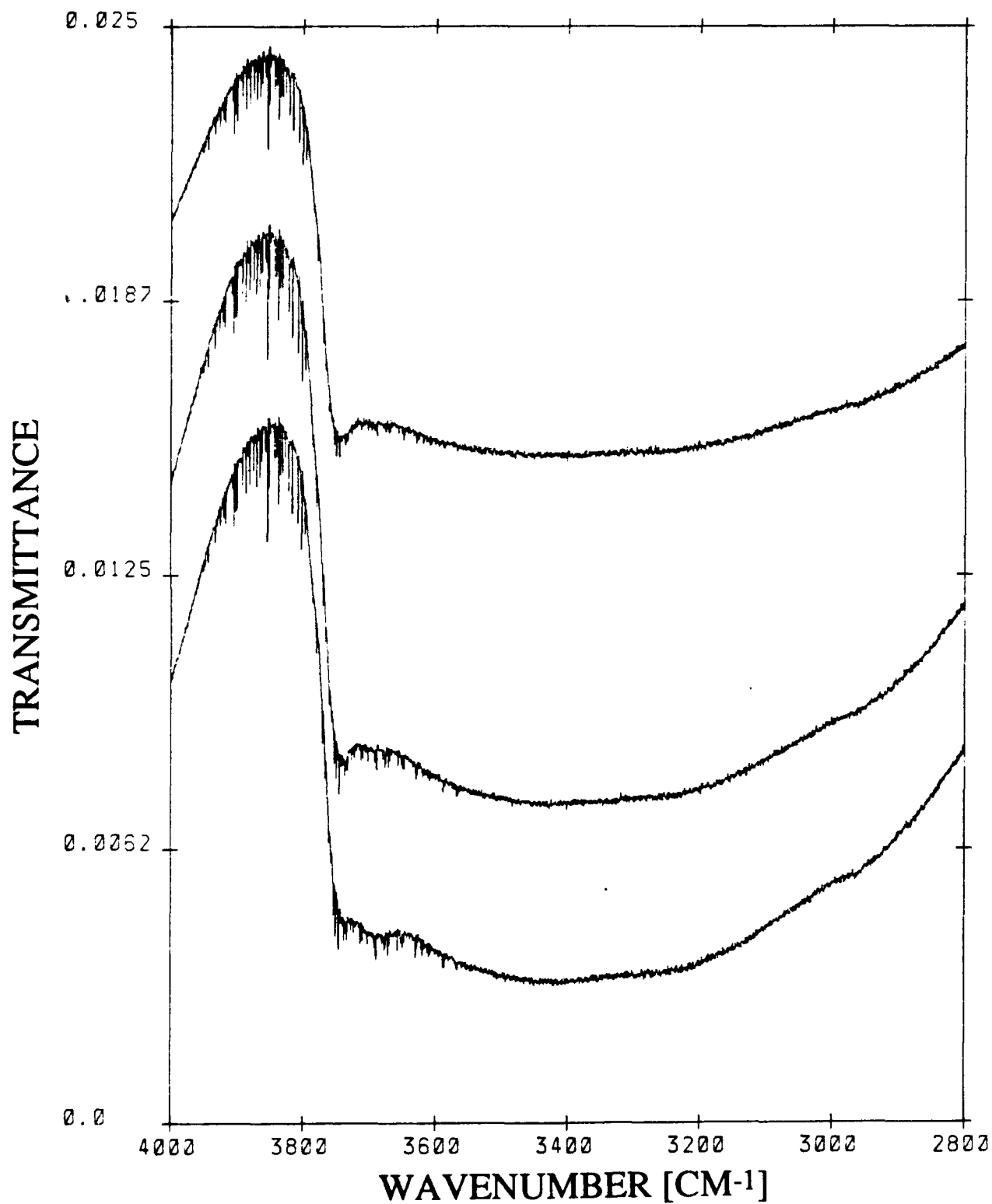
formed hydroxyl group could possibly be attributed to the Brønsted acidity that was found on this sample by pyridine adsorption studies.

This appendix primarily summarizes the hydroxyl region of the oxide aerogels studied and shows the ability of FTIR and DRIFT to determine hydroxyl stretches that contribute to possible Brønsted acidity. It has also been shown how the structure of niobia influences the surface properties of these oxides, in particular the hydroxyl region and the ability to chemisorb surface water.

APPENDIX D

STABILIZATION OF SILICA AND NIOBIA/SILICA MIXED OXIDE AEROGELS

This appendix contains data pertaining to the stability of silica and niobia/silica mixed oxide aerogels with time. This study was performed because of the large decrease in surface area for an aerogel of silica that was supercritically extracted and left uncalcined for a period of 4 months and then calcined at (500,2) after this long waiting period. An attempt was therefore made to understand the underlying mechanism behind this tremendous decrease in surface area from 900 to 500 m^2/g. This appendix will be broken down into two sections, the first will discuss the bulk silica system and the second will discuss the mixed oxide system of niobia/silica.

D.1 Silica Aerogel Stability

The first system studied will be that of silica. There are basically three silica systems that will be discussed in order to explain the surface area decrease phenomenon: silica aerogel (supercritically extracted), silica aerogel(110,3) (supercritically extracted and dried at 110 °C for 3 hrs in a vacuum oven), and silica xerogel (silica sol-gel dried at 110 °C for 3 hrs in a vacuum oven, no supercritical extraction). Data for these three silica samples are shown in Table D-1. This table shows the calcined surface areas and normalized surface areas after a specific period of uncalcined time from the day of preparation. Notice in Table D-1 the large decrease (~ 35%) in surface area for the aerogel of silica over a 69

Table D-1: STABILITY OF SILICA AEROGEL SURFACE AREAS OVER TIME: A) A-SiO$_2$, B) A-SiO$_2$ (110,3) VACUUM OVEN, AND C) X-SiO$_2$

A) A-SiO$_2$ Bulk Oxide

Time (Days)	Surface Area (m^2/g)	Normalized Surface Area
0	820	1.00
1	710	0.87
2	690	0.84
10	640	0.78
69	530	0.65

B) A-SiO$_2$ (110,3) Vacuum Oven

Time (Days)	Surface Area (m^2/g)	Normalized Surface Area
0	830	1.00
1	820	0.99
2	790	0.95
10	810	0.98
69	780	0.94

C) X-SiO$_2$ Bulk Oxide

Time (Days)	Surface Area (m^2/g)	Normalized Surface Area
1	1000	1.00
2	1010	1.01
5	1010	1.01
12	970	0.97
29	1000	1.00
99	920	0.92

day time period. The aerogel of silica that is dried at (110,3) in a vacuum oven after the supercritical extraction shows a considerable stability of surface area with only a 5% decrease over the same time. The silica xerogel also shows an increased stability as shown by the 8% decrease in surface area after 99 days. Figure D-1 shows the total surface area versus uncalcined time for the three silica systems and clearly reveals the large surface area decline for A-SiO$_2$ (silica aerogel). Figure D-2 shows the normalized surface area versus uncalcined time for the same three silica samples. This figure clearly shows the stability effect the vacuum oven has on drying the silica [X-SiO$_2$ and A-SiO$_2$(110,3)] from the regular supercritically extracted silica (A-SiO$_2$).

These three carefully selected systems allow us to make a determination on the possible mechanism involved in this surface area decline. A few general observations must be mentioned before we proceed in our discussion. First, other synthesized aerogels in this study (niobia, alumina, and niobia/alumina) did not show any kind of surface area decline as shown with the silica aerogel containing systems which were prepared using ammonium hydroxide. Secondly, commercial silica (Davison) that has a moderately large surface area (~ 300 m^2/g) does not show any surface area decline even in the presence of water for extended periods of time. Thus, with the above observations we can begin to propose the mechanism for the surface area decline.

It appears that the rate of dissolution of silica is a sign of surface area declination since this process creates larger pores and thus should theoretically lower the surface area. The rate at which silica dissolves in water is complicated and is influenced by a number of factors, but the dissolution process requires the presence of a catalyst.[16] This dissolution of silica in water is a depolymerization of the oxide matrix by a hydrolysis reaction. The catalyst for this hydrolysis reaction is a material which can be chemisorbed, increasing the coordination number of a silicon atom on the surface to more than four (preferably six), and thus weakening the oxygen bonds to the underlying silicon atoms.[16] The hydroxyl ion from the ammonium hydroxide used to synthesize the silica gel is capable of acting as a

Figure D-1: A-SiO$_2$ AND X-SiO$_2$ TOTAL SURFACE AREA STABILITY VERSUS UNCALCINED TIME
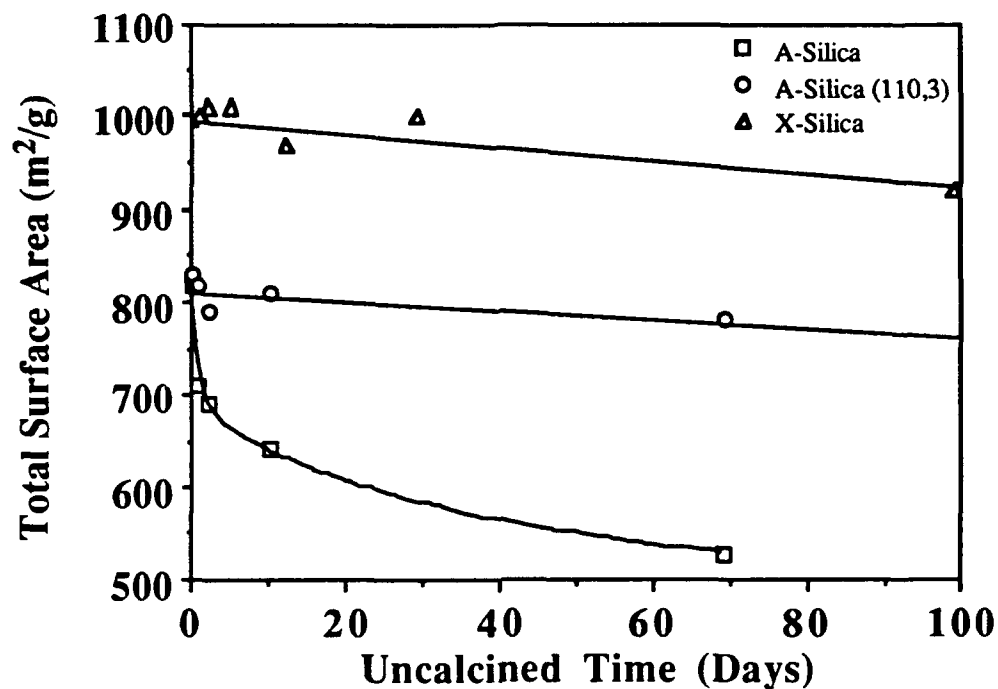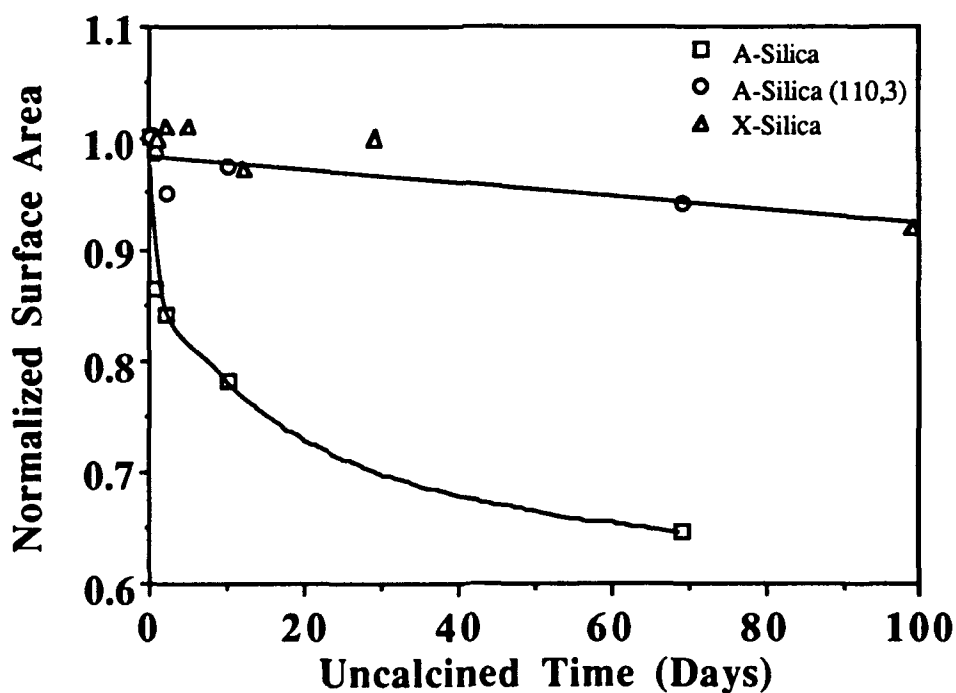

Figure D-2: A-SiO$_2$ AND X-SiO$_2$ NORMALIZED SURFACE AREA STABILITY VERSUS UNCALCINED TIME

strong nucleophile or "catalyst" to bond to the electropositive silicon atom. Since the supercritical extraction process can not efficiently remove the water or ammonium hydroxide from the gel, it can be assumed that these two compounds will be present after the extraction process. Iler[16] goes into a more in-depth discussion of the mechansim of the process for the dissolution of silica in water in the presence of hydroxyl ions. It is beyond the scope of this thesis to totally discuss this process and the reader is encouraged to read more into this subject of silica dissolution. The main points of this mechanism are that the adsorption of the -OH ion causes a silicon atom to go into solution as a silicate ion and eventually hydrolyzes to soluble silica, $Si(OH)_4$. This process is repeated to open the pores of the silica and effectively lower the surface area. The vacuum oven treatment on the two silica samples eliminates the water and the ammonium hydroxide thus preserving and retaining the large surface areas for these two materials. The size of the particles of silica has also been shown to be a factor in the dissolution of silica. The larger the surface area of the silica, the smaller the particle size that comprises the sample which increases the rate of dissolution of this sample. Therefore, the high surface area aerogels of silica prepared in this study will be expected to be more effected than lower surface area samples.

D.2 Niobia/Silica Mixed Oxide Aerogel Stability

The niobia/silica mixed oxide (A-NS25w) experienced a similar surface area decline as the bulk silica aerogel as shown in Table D-2. Also shown in this table is A-NS25w after being dried at 110 °C for 3 hrs in a vacuum oven. Similar to the results for the oven dried aerogel of silica, the A-NS25w (110,3) sample showed a surface area stabilization after 128 days. These niobia/silica mixed oxide results are shown in Figures D-3 and D-4 for the total surface area and normalized surface area versus uncalcined time, respectively. Figure D-5 shows the stability of the aerogels of silica and niobia/silica as well as their oven dried counterparts. Notice in this figure, as shown by the dashed line, that the

Table D-2: STABILITY OF NIOBIA/SILICA MIXED OXIDE AEROGEL SURFACE
AREAS OVER TIME: A) A-NS25w AND B) A-NS25w (110,3)
VACUUM OVEN

A) A-NS25w Mixed Oxide

Time (Days)	Surface Area (m^2/g)	Normalized Surface Area
0	670	1.00
1	625	0.93
2	575	0.86
3	570	0.85
64	530	0.79

B) A-NS25w (110,3) Vacuum Oven

Time (Days)	Surface Area (m^2/g)	Normalized Surface Area
1	615	1.00
2	620	1.01
3	640	1.04
67	600	0.98
128	620	1.01

Figure D-3: A-NS25w TOTAL SURFACE AREA STABILITY VERSUS
UNCALCINED TIME
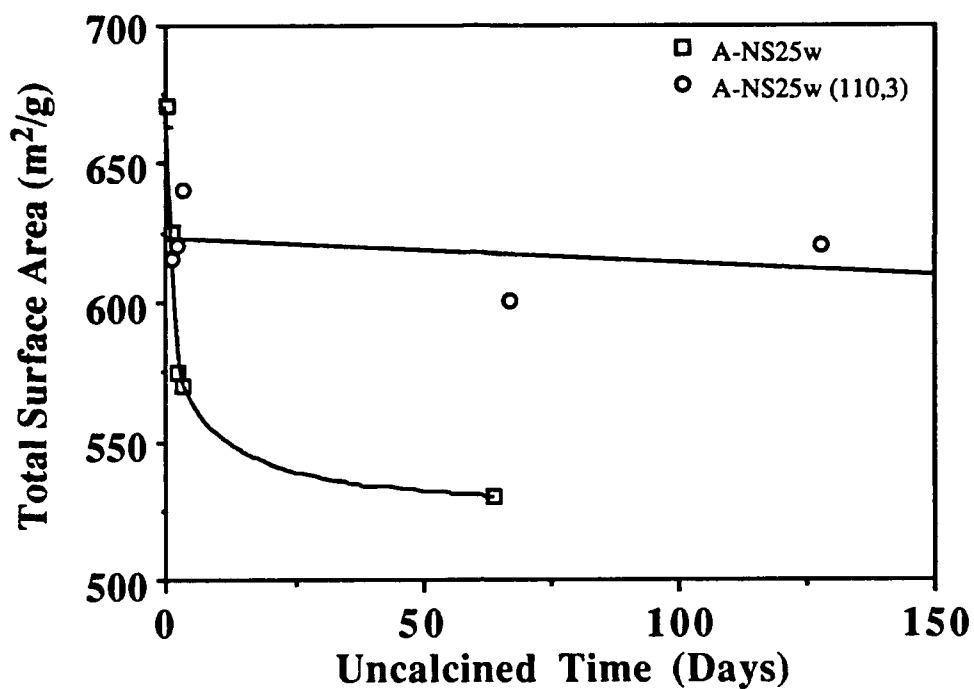
Figure D-4: A-NS25w NORMALIZED SURFACE AREA STABILITY VERSUS
UNCALCINED TIME
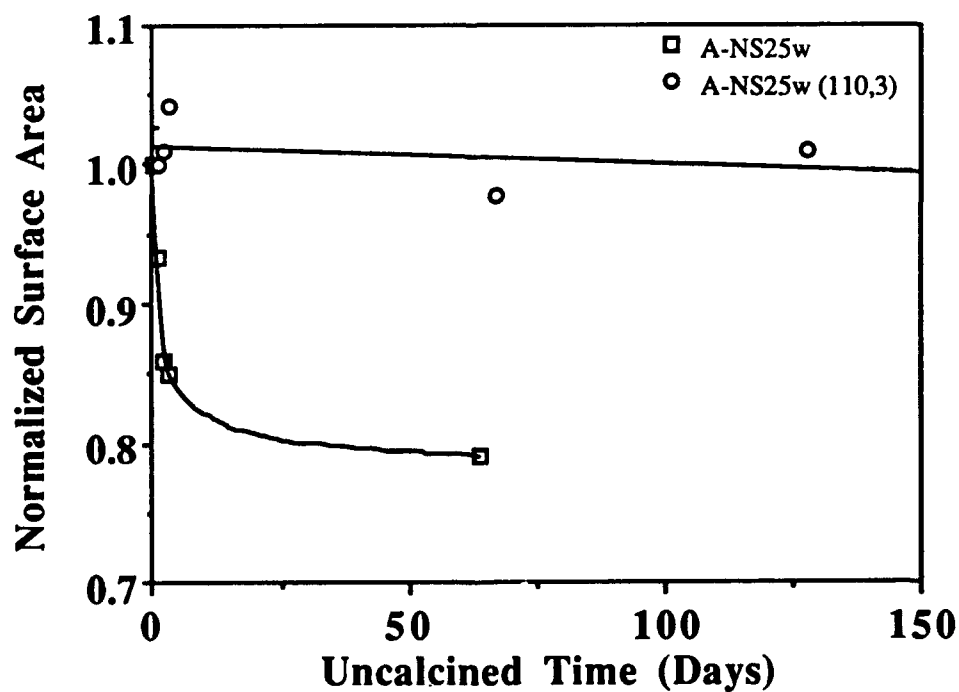
Figure D-5: A-NS25w TOTAL SURFACE AREA STABILITY VERSUS
UNCALCINED TIME
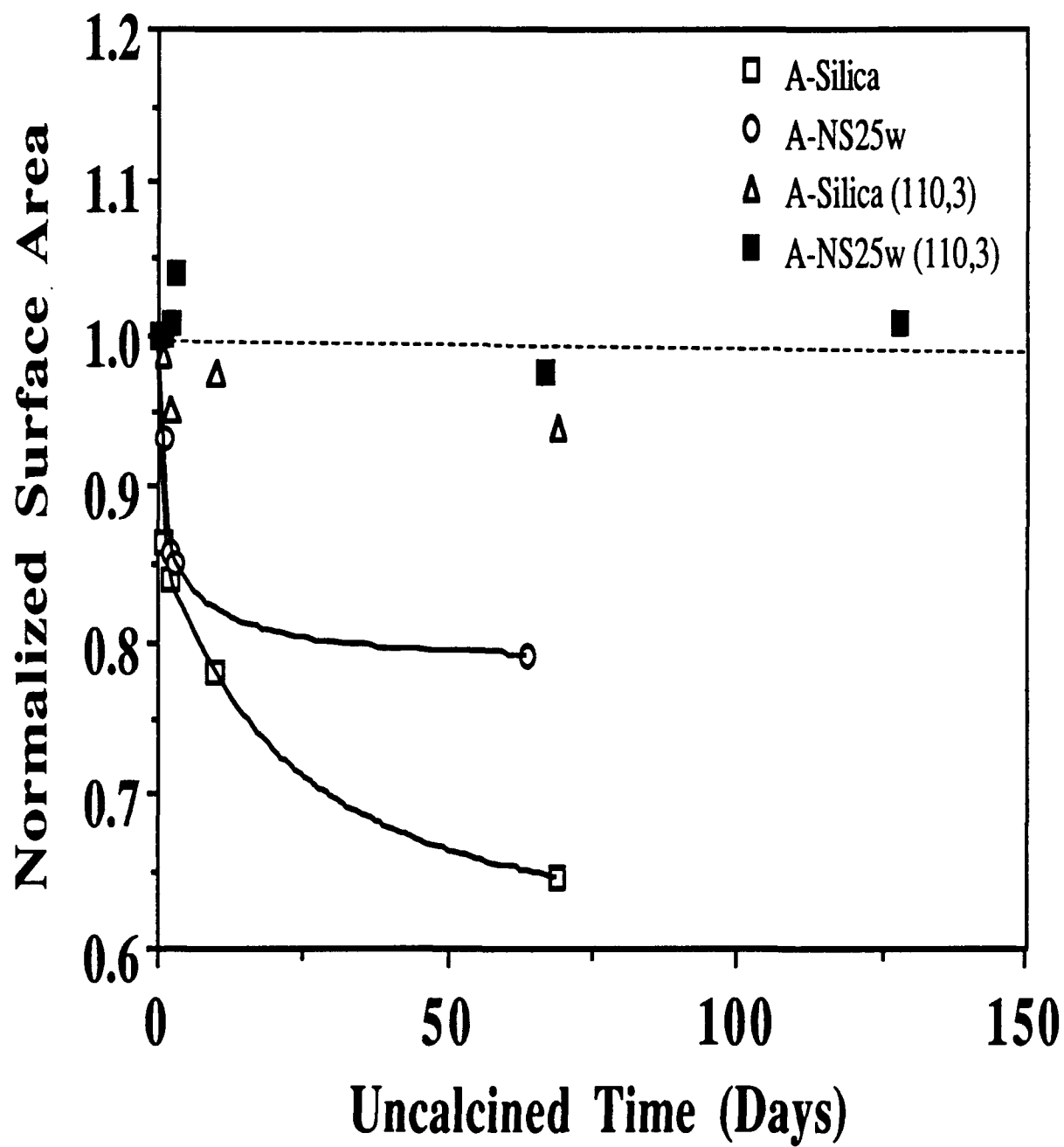
surface areas of the oven treated aerogel samples are nearly constant, while the untreated aerogels show a significant decline with time. An important observation in this figure is the fact that the niobia/silica mixed oxide aerogel does not lose its surface area at nearly the same rate as the bulk silica aerogel. This could be due to a stabilizing influence imparted by the incorporation of niobia into the silica matrix. Recall that the niobia/silica mixed oxide aerogel was prepared in a similar fashion as the silica aerogel with the incorporation of ammonium hydroxide to gel the sample in the sol-gel synthesis. Thus, a similar mechanism is proposed to explain the surface area decline of A-NS25w as was discussed for the surface area loss of A-SiO$_2$. All oxide aerogels prepared in this thesis were synthesized and calcined in one 12-hr day in order to avoid the aforementioned phenomena.

APPENDIX E

1-BUTENE ISOMERIZATION

Operating Conditions for GC and Integrator:

(I.) Relative Thermal Response Data and Retention Time:[211]

COMPOUND	RELATIVE RESPONSE/MOLE	RETENTION TIME (min)
1-Butene	81	6.01 ± 0.05
cis-2-Butene	85	9.01 ± 0.08
trans-2-Butene	87	10.29 ± 0.09

(II.) GC Operating Conditions:

He Gas Flow Rates:
- Channel A : 25.5 ml/min
- Channel B : 80.5 ml/min
- Detector Current : 130 mA
- Attenuation : 1
- Detector : TC
- Injector Temperature : 313 K
- Detector Temperature : 313 K
- Oven Temperature : 313 K
- On Line Sampling Time : 10 sec

(III.) Integrator Settings:

Model: HP 3390A Analysis Programs:

Normal Detection Program

```
RUN PRMTRS
ZERO      =  10
ATTN 2↑   =  0
CHT SP    =  1.0
PK WD     =  0.20
THRSH     =  -1
AR REJ    =  0
TIME TBL
4.00   PK WD    =  0.80
4.00   ZERO     =  10
4.00   ATT 2↑   =  3
6.80   ZERO     =  10
6.80   ATTN 2↑  =  0
11.0   STOP
```

Sensitive Detection Program

```
RUN PRMTS
ZERO      =  10
ATTN 2↑   =  0
CHT SP    =  1.0
PK WD     =  0.2
THRSH     =  -1
AR REJ    =  0
TIME TBL
4.00   PK WD    =  0.80
4.00   ZERO     =  10
4.00   ATTN 2↑  =  3
6.80   ZERO     =  10
6.80   ATTN 2↑  =  -3
6.80   THRSH    =  -6
6.80   PK WD    =  0.64
11.0   STOP
```

1-BUTENE ISOMERIZATION PROGRAM

```
10   REM "C4H8.BAS" BASIC PROGRAM FOR 1-C4H8 ISOMERIZATION
20   REM INPUT:   CATWT  =  CATALYST WEIGHT (GM)
30   REM           TR     =  REACTION TEMPERATURE (C)
40   REM           CATID  =  CATALYST ID
50   REM           HEFLOW =  He FLOW RATE (SCCM)
60   REM           C4FLOW =  1-C4H8 FLOW RATE (SCCM)
70   REM           TIME(I)=  REACTION TIME (MIN) AT POINT I
80   REM OUTPUT:  "C4H8.DAT" TIME(I), CONVERSION(I), REACTION RATE(I)
90   REM           MOL% (I), CIS/TRANS RATIO(I)
100  REM OTHERS:  A1(I)  =  AREA OF 1-C4H8 AT POINT I
110  REM           A2(I)  =  AREA OF ISO-C4H8 AT POINT 1
120  REM           A3(I)  =  AREA OF CIS-C4H8 AT POINT 1
130  REM           A4(I)  =  AREA OF TRANS-C4H8 AT POINT 1
140  REM           WTi(I) =  WEIGHT FRACTION OF i
150  REM           Xi(I)  =  MOLE PERCENT OF i
160  REM           RATIO(I)= CIS/TRANS RATIO AT POINT I
170  REM           I      =  POINTS OF DATA IN REACTION
180  DIM TIME(20), A1(20), A2(20), A3(20), A4(20), WT1(20), WT2(20)
190  DIM WT3(20), WT4(20), X1(20), X2(20), X3(20), X4(20)
200  DIM RATIO(20), CONVR(20), RATE(20), NH3(20), RATEM(20)
210  INPUT " DATE          : ",TODAT$
220  INPUT " CATALYST ID: ",CATID$
230  INPUT " CATALYST WEIGHT(GM)      : ",CATWT
235  INPUT " SURFACE AREA (m**2/g)    : ",SA
240  INPUT " REACTION TEMP(C)         : ",TR
250  INPUT " He FLOW RATE(SCCM)       : ",HEFLOW
260  INPUT " 1-C4H8 FLOW RATE(SCCM) : ",C4FLOW
280  INPUT " WOULD YOU LIKE TO LOAD BATCH DATA (Y/N) ";CH1$
290  IF CH1$ = "n" OR CH1$ = "N" THEN 410
295  INPUT "FILENAME-->",AME$
300  OPEN AME$ FOR INPUT AS #1
305  M=4
310  NUM = 1
320  WHILE M>0
330  INPUT #1, TIME(NUM)
340  INPUT #1, NH3(NUM)
350  INPUT #1, A1(NUM)
355  A2(NUM) = 0
360  INPUT #1, A3(NUM)
370  INPUT #1, A4(NUM)
380  PRINT TIME(NUM); NH3(NUM); A1(NUM) ; A2(NUM); A3(NUM); A4(NUM)
385  NUM = NUM + 1
390  IF EOF(1) THEN M= 0
395  WEND
400  CLOSE #1
402  N = NUM - 1
405  GOTO 525
407  INPUT " DATA POINTS      : ",N
410  FOR I= 1 TO N
420  PRINT
430  PRINT " TIME ON STREAM(MIN)    AT POINT(";I;") = ";
440  INPUT    TIME(I)
450  PRINT " AREA OF 1-C4H8         AT POINT(";I;") = ";
460  INPUT    A1(I)
470  A2(I) = 0
```

```
480 PRINT " AREA OF CIS-C4H8      AT POINT(";I;") = ";
490 INPUT A3(I)
500 PRINT " AREA OF TRANS-C4H8    AT POINT(";I;") = ";
510 INPUT A4(I)
520 NEXT I
525 INPUT "OUTPUT FILENAME-->",AMEOUT$
530 OPEN AMEOUT$ FOR OUTPUT AS #2
540 PRINT #2"===================================================="
550 PRINT #2,
560 PRINT #2,"DATE             : ";TODAT$
565 PRINT #2,"CATALYST NAME    : ";CATID$
570 PRINT #2,"CATALYST WEITHT (GM) :";CATWT
572 PRINT #2,"SURFACE AREA M**2/GM :";SA
575 PRINT #2,"REACTION TEMP(C)     :";TR
580 PRINT #2,"He FLOW RATE(SCCM)   :";HEFLOW
590 PRINT #2," 1-C4H8 FLOW RATE(SCCM):";C4FLOW
600 PRINT #2,
610 PRINT #2,"          TOS           1-C4 RATE            MOL%      CIS/TRANS"
620 PRINT #2,"POINT (MIN) CONVR  MOL/HR/GM MOL/HR/M2*100 CIS-C4 TRANS-C4 RATIO"
630 PRINT #2,"----- ----- -----  --------- ------------- ====== ======== ====="
640 FOR I= 1 TO N
650 WT1(I) = A1(I)/(A1(I)+1.0123*A2(I)+1.0494*A3(I)+1.0741*A4(I))
660 WT2(I) = 1.012*A2(I)/(A1(I)+1.012*A2(I)+1.049*A3(I)+1.074*A4(I))
670 WT3(I) = 1.049*A3(I)/(A1(I)+1.012*A2(I)+1.049*A3(I)+1.074*A4(I))
680 WT4(I) = 1.074*A4(I)/(A1(I)+1.012*A2(I)+1.049*A3(I)+1.074*A4(I))
690 X1(I) = WT1(I)*100
700 X2(I) = WT2(I)*100
710 X3(I) = WT3(I)*100
720 X4(I) = WT4(I)*100
730 RATIO(I) = WT3(I)/WT4(I)
740 CONVR(I) = (WT2(I)+WT3(I)+WT4(I)/(WT1(I)+WT2(I)+WT3(I)+WT4(I))
750 RATE(I) = C4FLOW*60*CONVR(I)/(22400*CATWT)
752 RATEM(I) = RATE(I)*100/SA
755 PRINT #2, USING" ##   ";I;
760 PRINT #2, USING"###.#   ";TIME(I);
770 PRINT #2, USING"#.####";CONVR(I);
780 PRINT #2, USING" ##.###### ";RATE(I);
790 PRINT #2, USING" ##.###### ";RATEM(I);
800 PRINT #2, USING"   ##.## ";X3(I);
810 PRINT #2, USING"  ##.##'X4(I);
820 PRINT #2, USING"  ##.## ";RATION(I)
830 NEXT I
840 PRINT #2,
850 PRINT #2,"---------------------------------------------------------------"
860 PRINT #2,"         TOS   NH3          AREA (COUNTS)"
870 PRINT #2,"POINT (MIN) (ML)   1-C4   ISO-C4   CIS-C   TRANS-C4"
880 PRINT #2,"----- ----- ----   ======  ======  ======  ========"
890 FOR I = 1 TO N
895 PRINT #2, USING" ##    ";I;
900 PRINT #2, USING"###.#    ";TIME(I);
910 PRINT #2, USING" #.## ";NH3(I);
915 PRINT #2, USING"#######   ";A1(I);A2(I);A3(I);A4(I)
920 NEXT I
930 PRINT #2,"===================================================="
940 PRINT #2,
950 CLOSE #2
960 INPUT " WOULD YOU LIKE TO MAKE A PLOT FILE (Y/N) ";CH2$
970 IF CH2$ = "n" OR CH2$ = "N" THEN 995
975 INPUT "FILENAME-->",AME$
976 OPEN AME$ FOR OUTPUT AS #2
```

```
980 FOR I= 1 TO N
982 PRINT #2, USING" ###.#  ";TIME(I);
984 PRINT #2, USING" ##.######  ";RATE(I);
986 PRINT #2, USING" ##.######  ";RATEM(I)
990 NEXT I
992 CLOSE #2
995 SYSTEM
```

APPENDIX F

PYRIDINE ADSORPTION

FTIR Sample Calculations of Lewis/Brønsted Ratios:

The extinction coefficients for Lewis acid sites, ε^L, were calculated using the integrated 1450 and 1490 cm^{-1} peak areas, A_{1450} and A_{1490}, respectively, for a sample that was free of Brønsted acid sites.[88]

$$A_{1490}/A_{1450} = \varepsilon^L_{1490}/\varepsilon^L_{1450} = C = 0.205 \tag{F.1}$$

The aerogel of alumina in this study was also shown to possess little to no Brønsted acidity and doing a calculation of the ratio of the extinction coefficients to check this value yields the following value for C:

$$A_{1490}/A_{1450} = 1.5375/7.434 = C = 0.207 \tag{F.2}$$

which is close to the value found above and used in this thesis, as well as the literature value of C (0.25). The equation developed by Basila and Kantner[181] used to calculate the Lewis/Brønsted ratios found in this thesis is found below:

$$\frac{[LPY]}{[BPY]} = \frac{6.0 \cdot C \cdot A_{1450}}{A_{1490} - C \cdot A_{1450}} \tag{F.3}$$

For A-Nb$_2$O$_5$ after a 100 °C treatment as sample calculation we find that:

$$A_{1450} = 11.016$$
$$A_{1490} = 6.365$$

$$L/B = 7.7$$

TG PYRIDINE ADSORPTION PROGRAM

```
C
C
C       THIS PROGRAM IS USED TO PROCESS PYRIDINE ADSORPTION DATA
C
C       THE PROGRAMS FUNCTION IS TO CONVERT RAW TGA DATA INTO DATA
C       SUITABLE FOR PLOTING MOLECULES/M2 X 10(13) VERUS 1/T FOR
C       A CONSTANT PRESSURE OF PYRIDINE.
C
C       8/14/90    SCOTT M. MAURER
C
C       T(I)=TEMPERATURE(CELCIUS)      SW(I)=SCALE WGT(-10 - +10)
C       OFFSET=ANY VALUE ADDED TO SCALE TO MAKE USING CHART RECORDER EASIER
C       STARTWGT=WEIGTH OF SAMLE FREE OF ADSORBED BASE
C       SUPP=SUPPRESSION                SCALE=TGA WGT. SCALE
C       PRESS=CONVERTS PYRIDINE BATH TEMP TO PRESSURE (ANTOINE'S EQUATION)
C
C       AN ENTIRE SECTION IS DEVOTED TO PROVIDING AN ACCURATE ZERO
C
        DIMENSION T(100),SW(100)
        CHARACTER*64 FNAME
        CHARACTER*64 FSAMPLE
        WRITE(*,'(A\)')' PYRIDINE BATH TEMP [C]?'
        READ(*,45)TPRESS
        WRITE(*,45)TPRESS
        WRITE(*,'(A\)')' SURFACE AREA [M2/G]?'
        READ(*,45)SA
        WRITE(*,45)SA
        WRITE(*,'(A\)')' SUPPRESION?'
        READ(*,45)SUPP
        WRITE(*,45)SUPP
        WRITE(*,'(A\)')' SCALE?'
        READ(*,45)SCALE
        WRITE(*,45)SCALE
        WRITE(*,'(A\)')' START WEIGHT [MG]?'
        READ(*,45)SWGT
        WRITE(*,45)SWGT
        WRITE(*,'(A\)')' SCALE OFFSET (WHAT DID YOU ADD)?'
        READ(*,45)SOFF
        WRITE(*,45)SOFF
        CALOFF = 1.00
        WRITE(*,'(A\)')' CALIBRATION ERROR FACTOR? (DIVID BY)?'
        READ(*,45)CALOFF
        WRITE(*,45)CALOFF
        WRITE(*,'(A\)')' USE A ZERO/BLANK BASELINE, TYPE 1?'
        READ(*,48)NCHECK
        IF(NCHECK.NE.1)GOTO 3
        WRITE(*,'(A\)')' PYRID B.T.=?,TYPE#: (P56)+28C=0, (P30)+1.3C=1'
        WRITE(*,50)
        READ(*,48)NZERO
C
C       ZEROS REDONE 7/29/88 WITH 28C=#56, 1.3C=#30, -14.7C=#39, -30.3=#42
C       (ZEROS ARE A FUNCTION OF PYRIDINE BUBBLER FLUID HEIGHT AND
C       TEMPERATURE-COMPLEX).
C
```

```
      IF(NZERO.EQ.0)THEN
      AZ=-.60882
      AMZ=.002669
      ELSEIF(NZERO.EQ.1)THEN
      AZ=1.335205
      AMZ=-1.39849
      ELSEIF(NZERO.EQ.2)THEN
      AZ=-1.10765
      AMZ=0.003571
      ELSEIF(NZERO.EQ.3)THEN
      AZ=1.227369
      AMZ=-2.25538
      ELSEIF(NZERO.EQ.4)THEN
      AZ=1.010458
      AMZ=-1.97637
      ELSEIF(NZERO.EQ.5)THEN
      AZ=-.6612
      AMZ=0.002518
      ELSEIF(NZERO.EQ.6)THEN
      AZ=-.41671
      AMZ=0.003491
      ELSEIF(NZERO.EQ.7)THEN
      AZ=3.100006
      AMZ=-1.52862
      ELSEIF(NZERO.EQ.8)THEN
      AZ=-1.38368
      AMZ=1.211246
      ELSEIF(NZERO.EQ.9)THEN
      AZ=-2.35643
      AMZ=1.84224
      ENDIF
    3 CONTINUE
      write(*,45)AZ
C
C     READING AND CREATING FILES
C
      WRITE(*,'(A\)')' INPUT FILE NAME?'
      READ(*,'(A)')FNAME
      OPEN( 7,FILE=FNAME)
      WRITE(*,'(A\)')' OUTPUT FILE NAME?'
      READ(*,'(A)')FSAMPLE
      OPEN( 4,FILE=FSAMPLE,STATUS='NEW')
      DO 5 I=1,100
      READ(7,46,END=6)T(I),SW(I)
      WRITE(*,49)T(I),SW(I)
      N=I
    5 CONTINUE
    6 CONTINUE
C
C     MESSING WITH DATA
C
      TPRESS = 16.091-(3095.13/(TPRESS+212))
      TPRESS = EXP(TPRESS)
C
C     THIS SECTION CREATES THE ZERO BASED ON FITTED EQUATIONS FOR THE
C     ZERO DATA USING LOTUS
C
      DO 15 I=1,N
      IF(NZERO.EQ.0)THEN
       SZWGT=(1.0-EXP(AZ+AMZ*T(I)))*.02/CALOFF
```

```fortran
        T(I)=1000.0/(T(I)+273.15)
      ELSEIF(NZERO.EQ.1)THEN
       T(I)=1000.0/(T(I)+273.15)
       SZWGT=(2-EXP(AMZ*ALOG(T(I)+AZ)))*.02/CALOFF
      ELSEIF(NZERO.EQ.2)THEN
       SZWGT=(1.0-EXP(AZ+AMZ*T(I)))*.02/CALOFF
       T(I)=1000.0/(T(I)+273.15)
      ELSEIF(NZERO.EQ.3)THEN
       T(I)=1000.0/(T(I)+273.15)
       SZWGT=(1.0-EXP(AZ+AMZ*ALOG(T(I))))*.02/CALOFF
      ELSEIF(NZERO.EQ.4)THEN
       T(I)=1000.0/(T(I)+273.15)
       SZWGT=(1-EXP(AMZ*ALOG(T(I))+AZ))*.02/CALOFF
      ELSEIF(NZERO.EQ.5)THEN
       SZWGT=(0.84-EXP(AMZ*T(I)+AZ))*.02/CALOFF
       T(I)=1000.0/(T(I)+273.15)
      ELSEIF(NZERO.EQ.6)THEN
       SZWGT=(2.0-EXP(AMZ*T(I)+AZ))*.01/CALOFF
       T(I)=1000.0/(T(I)+273.15)
      ELSEIF(NZERO.EQ.7)THEN
       T(I)=1000.0/(T(I)+273.15)
       SZWGT=(1.0-EXP(AMZ*T(I)+AZ))*.01/CALOFF
      ELSEIF(NZERO.EQ.8)THEN
       T(I)=1000.0/(T(I)+273.15)
       SZWGT=ALOG(AZ+AMZ*T(I))*.01/CALOFF
      ELSEIF(NZERO.EQ.9)THEN
       T(I)=1000.0/(T(I)+273.15)
       SZWGT=ALOG(AZ+AMZ*T(I))*.01/CALOFF
      ELSE
       T(I)=1000.0/(T(I)+273.15)
      ENDIF
C
C     THIS SECTION COMPUTES THE COVERAGES USING THE ZEROS FOR A BASELINE
C
      SW(I)=((SW(I)-SOFF)*SCALE/10.0+SUPP-SWGT-SZWGT)/CALOFF
      SW(I)=SW(I)/(SWGT*SA)*7.61315E+4
   15 CONTINUE
      WRITE(4,47)T(1),SW(1),TPRESS
      WRITE(4,46)(T(I),SW(I),I=2,N)
   45 FORMAT(F12.4)
   46 FORMAT(F7.3,F12.4)
   47 FORMAT(F7.3,F12.4,F8.2)
   48 FORMAT(I2)
   49 FORMAT(1X,F7.3,F12.4)
   50 FORMAT(/,21X,'(P39)-14.7C=2,  (P63)-16.4C=3',/,21X,
     $'(P79)-18.5C=7,  (P42)-30.3C=4,',/,21X,
     $'(P60)-34.7C=5,  (P71)-32.0C=6,',/,21X,
     $'(P82)-36.8C=8,  (P87)-33.2C=9,')
      CLOSE(7)
      CLOSE(4)
      STOP
      END
```